BioMed Research International

Chemo-radiotherapy for Multimodality Treatment of Tumours

Lead Guest Editor: Qiang Liu
Guest Editors: Bing Wang and Ning Cao

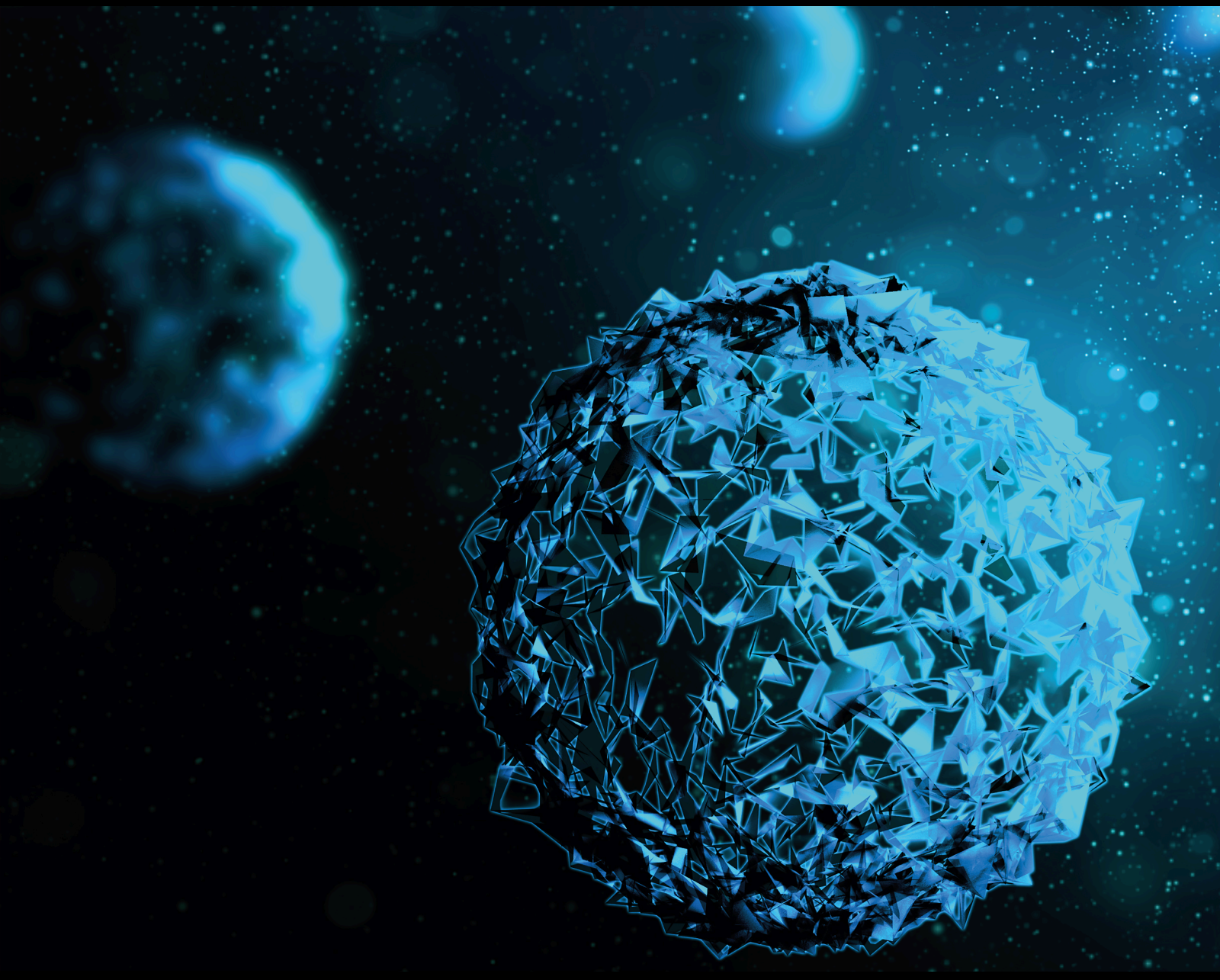

Chemo-radiotherapy for Multimodality Treatment of Tumours

BioMed Research International

Chemo-radiotherapy for Multimodality Treatment of Tumours

Lead Guest Editor: Qiang Liu
Guest Editors: Bing Wang and Ning Cao

Section Editors

Penny A. Asbell, USA
David Bernardo, Spain
Gerald Brandacher, USA
Kim Bridle, Australia
Laura Chronopoulou, Italy
Gerald A. Colvin, USA
Aaron S. Dumont, USA
Pierfrancesco Franco, Italy
Raj P. Kandpal, USA
Fabrizio Montecucco, Italy
Mangesh S. Pednekar, India
Letterio S. Politi, USA
Jinsong Ren, China
William B. Rodgers, USA
Harry W. Schroeder, USA
Andrea Scribante, Italy
Germán Vicente-Rodriguez, Spain
Momiao Xiong, USA
Hui Zhang, China

Academic Editors

Oncology

Fawzy A.S., Australia
Gitana Maria Aceto, Italy
Amedeo Amedei, Italy
Aziz ur Rehman Aziz, China
Riadh Badraoui, Tunisia
Stergios Boussios, Greece
Alberto Briganti, Italy
Franco M. Buonaguro, Italy
Xianbin Cai, Japan
Melchiorre Cervello, Italy
Winson Cheung, Canada
Somchai Chutipongtanate, Thailand
Kate Cooper, USA
Enoc Mariano Cortes-Malagon, Mexico
Alessandro De Vita, Italy
Hassan, El-Abid, Morocco
Yujiang Fang, USA
Zhien Feng, China
Stefano Gambardella, Italy
Dian Gao, China
Piotr Gas, Poland
Nebu Abraham George, India
Xin-yuan Guan, Hong Kong
Hirotaka Iwase, Japan
Arumugam R. Jayakumar, USA
Mitomu Kioi, Japan
Krzysztof Ksiazek, Poland
Yuan Li, China
Anna Licata, Italy
Wey-Ran Lin, Taiwan
César López-Camarillo, Mexico
João F Mota, Brazil
Rakesh Sathish Nair, USA
Peter J. Oefner, Germany
Mana Oloomi, Iran
Vera Panzarella, Italy
Pierpaolo Pastina, Italy
Georgios G. Pissas, Greece
Kyoung-Ho Pyo, Republic of Korea
Giandomenico Roviello, Italy
Daniele Santini, Italy
Wen Shi, USA
Krzysztof Siemianowicz, Poland
Henrique César Santejo Silveira, Brazil
Himangshu Sonowal, USA
Maurizio Soresi, Italy
Kenichi Suda, Japan
Farzad Taghizadeh-Hesary, Iran
Seyithan Taysi, Turkey
Fernando Toshio Ogata, Sweden
Abhishek Tyagi, USA
Marco A. Velasco-Velázquez, Mexico
Thirunavukkarasu Velusamy, India
Navin Viswakarma, USA
Ya-Wen Wang, China
Hushan Yang, USA
Zongguo Yang, China
Hui Yu, USA
Baotong Zhang, USA
Yi Zhang, China

Eugenio Zoni, Switzerland

Contents

Hindawi
BioMed Research International
Volume 2021, Article ID 7453500, 12 pages
https://doi.org/10.1155/2021/7453500

Research Article

COL3A1 and Its Related Molecules as Potential Biomarkers in the Development of Human Ewing's Sarcoma

Min Tang,[1] Peiqing Liu,[2] Xiaoke Wu,[2] Jie Gong,[2] Jiacheng Weng,[2] Guangyu Gao,[2] Yulong Liu,[2,3,4] and Lei Gan[2]

[1]*Department of Radiotherapy and Oncology, First People's Hospital of Kunshan, Kunshan, Jiangsu Province, China*
[2]*Department of Oncology, The Second Affiliated Hospital of Soochow University, Suzhou 215004, China*
[3]*State Key Laboratory of Radiation Medicine and Protection, School of Radiation Medicine and Protection, Soochow University, Suzhou 215123, China*
[4]*Collaborative Innovation Center of Radiological Medicine of Jiangsu Higher Education Institutions, Suzhou 215123, China*

Correspondence should be addressed to Lei Gan; ganlei19870810@163.com

Received 25 August 2021; Accepted 20 October 2021; Published 22 December 2021

Academic Editor: Qiang Liu

Background. Ewing's sarcoma (ES) is the most common malignant primary bone tumor in children and adolescents. This study is aimed at developing new prognostic markers and building a microRNA-mRNA network in the development of ES. *Method*. GSE80201 and GSE39262 were downloaded from the Gene Expression Omnibus (GEO) database. Bioinformatics analysis was used to download and process data. The coexpression of differentially expressed microRNAs (DEMs) and genes (DEGs) was selected by using R software. The FunRich database was utilized to perform cellular component (CC), molecular function (MF), and biological process (BP) enrichment analysis. Cytoscape and ClueGO were used to perform Kyoto Encyclopedia of Genes and Genomes (KEGG) enrichment analysis and construct the mRNA-microRNA network. The Kaplan-Meier Plotter was used to perform prognosis analysis between the expression level of genes we selected and overall survival (OS) of patients with ES. Univariate analysis and multivariate analysis were carried out to research the prognostic value of identified mRNA expression in ES according to TCGA database. *Results*. By using bioinformatics analysis, 10 DEMs and 5 target mRNAs were identified. Based on the KmPlot software, COL1A2, COL3A1, and TGFBI were significantly related to the OS of patients with ES. High COL3A1 mRNA expression was correlated with distant metastasis, margin status, and poor overall survival of ES. Besides, multivariate analysis indicated that COL3A1 was an independent risk factor for ES patients. *Conclusions*. In conclusion, our results suggest that COL3A1 and its related molecules may be a potential diagnostic and prognostic biomarker for patients with ES.

1. Background

Ewing's sarcoma (ES) is thought to originate from mesenchymal stem cells in pediatric patients [1]. It is the second most common osteosarcoma in pediatric patients and young people [2]. ES can appear as conventional ES or extraosseous ES and is now classified as undifferentiated small round cell sarcoma of bone and soft tissue [3]. The incidence age of the disease is 10~15 years old. Boys are more common than girls. This kind of tumor has high malignancy, easy recurrence, and poor prognosis. Bone ES often occurs in the ilium, femur, humerus, fibula, and tibia. When invading long tubular bone, it mostly occurs in the shaft. Compared with bone ES, extraosseous Ewing sarcoma (EES) occurred mainly in the trunk and central axis [4]. At present, the treatment methods of ES are multidisciplinary comprehensive treatment strategies such as chemotherapy, surgery, and radiotherapy. The multidisciplinary team should also include nursing, nutrition, psychology, and rehabilitation disciplines [5]. With the in-depth study of the occurrence, development, and metastasis mechanism of Ewing sarcoma, the molecular targeted therapy of Ewing sarcoma has gradually become a new research hotspot. At present, it mainly focuses on targeted silencing of EWS/FLI-1 fusion gene, targeted blocking of insulin-like factor receptor,

targeted inhibition of receptor tyrosine kinase, antiangiogenesis, and so on [6]. The study of new therapeutic targets is of great significance for the treatment of Ewing sarcoma.

miRNA is a kind of noncoding single-stranded RNA with a length of 18~25 nucleotides. It not only plays a very important role in gene expression regulation but also plays an important role in many biological processes such as cell proliferation, differentiation, apoptosis, and hematopoiesis [7]. A large number of studies have shown that the expression level of miRNA is closely related to the occurrence and development of many kinds of tumors. The monitoring of miRNA expression level is of great significance in the early diagnosis and prognosis of diseases [8]. In particular, Zhai et al. found that microRNA-181 is a potential molecular biomarker in the clinical management of glioblastoma and is associated with poor prognosis in patients [9]. Zhou et al. reported that microRNA-134-mediated direct downregulation of laminin subunit gamma 2 inhibits migration and invasion of cancer stem cells in oral squamous cell carcinoma by suppressing the PI3K-Akt signaling pathway [10]. Jiang et al. also reported that miR-24 was significantly suppressed in gastric cancer tissues; it can inhibit the proliferation, migration, and invasion and enhances chemosensitivity of human gastric carcinoma by targeting DND microRNA-mediated repression inhibitor 1. Besides, it may be an important therapeutic target for the treatment of gastric carcinoma [10].

In this article, microarray data from the GEO database and ES clinical sample information in TCGA database were used for identifying differently expressed microRNAs (DEMs) between normal tissues and ES tissues. By using a variety of mRNA and microRNA-related functional databases and performing verification experiments, several genes associated with the development of ES and subsequent pathways were identified.

2. Methods

2.1. Microarray Data. The GEO database, with the full name Gene Expression Omnibus, is a gene expression database created and maintained by the National Biotechnology Information Center (NCBI). It was founded in 2000 and contains high-throughput gene expression data submitted by research institutions around the world. In our article, gene expression profile data (GSE80201 and GSE39262) were obtained from GEO.

GSE80201 had biopsies from 20 ES patients using paraffin-embedded tissues and normal human mesenchymal stromal cells as controls. MicroRNA expression profiling analysis of these samples was performed on miRXplore TM Microarray (968) (GPL17603). Dataset GSE149507 includes 46 sarcoma cell lines and 5 primary cell lines. Gene expression profiling was performed on Affymetrix Human Genome U133A Array (GPL96).

2.2. Differentially Expressed miRNA Analysis. GEO2R, an R-associated web application, was applied to filter DEMs between normal tissues and ES tissues. We also used R software to analyze two sets of data. $p < 0.05$ and $|\log FC| \geqslant 2$ were considered as cutoff criterion.

2.3. Gene Ontology and Pathway Enrichment Analysis. The FunRich database is an online database. Users can upload miRNA and mRNA online for target gene prediction, gene enrichment analysis, and pathway correlation analysis. At the same time, they can also convert ID online and present the results in various forms of pictures. In addition to the annotation of the function of genes, we also know that genes will participate in various pathways of the human body. The database based on human pathways is the pathway-related database. KEGG is a kind of path-related database. Cytoscape software and ClueGO were used to perform this study and build a microRNA-mRNA network. ClueGO: deciphering and enriching go and pathways can visually summarize similar processes or pathways, mainly GO and KEGG, and the author can set his threshold to dynamically change the network. ClueGO has two main features: (1) according to the gene list, it can be used for the visualization of terms and (2) the comparison of the functional interpretation of the two clusters. Based on the above software, the results of data processing are presented in the form of a network diagram.

2.4. Prediction of miRNA Target Genes and miRNA-mRNA Regulatory Network. miRNA is differentially expressed in a variety of tumors compared with normal tissues. Its mechanisms include miRNA is located in the cancer-related genomic region (CAGR), epigenetic regulation of miRNA expression, and developmental abnormalities of miRNA processing genes and proteins. These mechanisms enable miRNA not only to induce cancer but also to inhibit tumorigenesis. Differentially expressed microRNAs were uploaded to the FunRich software to obtain target mRNAs. Besides, GSE39262 was analyzed by using R software. According to the prediction results of target genes in FunRich software and the DEGs of GSE39262, the coexpressed genes between the two results were identified, and the regulatory network was built by using Cytoscape.

2.5. Analysis of the Relationship between the Expression Level of mRNAs and Prognosis of Patients with ES. KmPlot is an online tool for survival analysis. It was originally designed to analyze the survival of miRNA in liver cancer. It can collect miRNA expression profile data related to liver cancer from large databases such as TCGA and GEO, sort out the reported survival-related biomarker miRNAs from the literature for survival analysis, and further screen biomarker miRNAs by integrating the results of Cox regression and differential expression. Later, it was further expanded on this basis. At present, it supports the survival analysis of 21 tumor types, including miRNA and mRNA. In this study, patients with ES were divided into two groups. By inputting the mRNAs we screened into the website, we can get the corresponding survival curve.

2.6. Gene Expression and Clinical Characteristics in TCGA. The associated statistics offered by TCGA are open and do not need the approval of the local ethics committee. The

data of 1145 patients with small cell lung cancer were obtained from TCGA database. COL1A2, COL3A1, and TGFBI mRNA level, clinicopathological data, and general data of patients with ES were collected.

3. Results

3.1. Identification of the DEGs and DEMs between ES Samples and Normal Samples. GEO2R was utilized to analyze the microRNA and target gene expression profiles from the GSE80201 and GSE39262. According to the cutoff criteria ($p < 0.05$ and $|\log_2 FC| \geq 2$), 82 DEMs including miRNA-181b, miRNA-29A, miRNA-223, miRNA-21, miRNA-29B, miRNA-181A, miRNA-30B, and miRNA-1248 and 74 DEGs were identified (Figure 1).

3.2. Gene Ontology Enrichment Analysis. Transcription factor enrichment analysis was conducted by using FunRich software, and the result is shown in Figure 2(a). To further learn about the mechanisms of identified microRNAs, it was also used to perform Gene Ontology enrichment analysis. The pictures demonstrated that DE-microRNAs were most enriched in the regulation of nucleobase, nucleoside, regulation of translation, extracellular matrix, Golgi apparatus, cyclin-dependent protein kinase holoenzyme complex, extracellular matrix structural constituent, transcription factor activity, and GTPase activity (Figure 2(b)). Furthermore, Cytoscape and ClueGO were used to conduct KEGG pathway enrichment analysis. These selected microRNAs were mainly enriched in 8 pathways: p53 signaling pathway, ECM-receptor interaction, autophagy, DNA replication, base excision repair, complement and coagulation cascades, homologous recombination, and nucleotide excision repair (Figure 3).

3.3. microRNA-mRNA Regulatory Network. Based on FunRich software, 2000 target genes were downloaded and 7 of them were differentially expressed in GSE39262 (DBF4, CEP55, FBN1, COL1A2, COL3A1, TGFBI, and COL6A3) (Figure 4). According to the relationship between them, 5 essential miRNA-mRNA pairs (microRNA-29a, microRNA-21, FBN1, COL1A2, COL3A1, TGFBI, and COL6A3) were selected which were identified for further study (Figure 5).

3.4. Analysis of the Gene Expression and Their Relationships with ES Prognosis. KmPlot was utilized to research the survival of patients with ES. By submitting the 5 genes we selected, survival curves were obtained. The results indicated that COL1A2, COL3A1, and TGFBI (Figure 6) were significantly related to the prognosis of patients with ES. However, the expression level of FBN1 and COL6A3 may have no significant association with OS.

3.5. Correlation between Clinical Characteristics and COL1A2, COL3A1, and TGFBI mRNA Expression of ES. Clinical and gene expression data of 101 ES were obtained from TCGA database, including metastasis stage, tumor region, age stage, gender stage, and race stage. We found that the expression level of TGFB1 was not associated with metastasis stage, tumor region, age stage, gender stage, and race stage ($p > 0.01$) (Table 1). Besides, relationships between clinical characteristics and TGFB1 expression level in ES were researched. The univariate analysis revealed that the metastasis stage was related to overall survival. However, higher TGFB1 mRNA expression, tumor region, age stage, gender stage, and primary site progression were not related to overall survival. Multivariate analysis also indicated that only the metastasis stage was an independent risk factor for OS in ES (Table 2). Our results also demonstrated that the expression level of COL1A2 was not associated with metastasis stage, tumor region, age stage, gender stage, and race stage ($p > 0.01$) (Table 3). Besides, correlations between clinical characteristics and COL1A2 expression in ES were researched. The univariate analysis revealed that the metastasis stage was related to overall survival. However, higher COL1A2 mRNA expression, tumor region, age stage, gender stage, and primary site progression were not correlated with overall survival. Multivariate analysis also showed that only the metastasis stage was an independent risk factor for overall survival in ES (Table 4). We also found that the expression level of COL3A1 was not associated with metastasis stage, tumor region, age stage, gender stage, and race stage ($p > 0.01$) (Table 5). Besides, correlations between clinical characteristics and COL3A1 expression in ES were researched. The univariate analysis revealed that metastasis stage and COL3A1 expression level are related to overall survival. However, tumor region, age stage, gender stage, and primary site progression were not related to overall survival. Multivariate analysis also indicated that COL3A1 expression level and metastasis stage were an independent risk factor for OS in ES (Table 6).

4. Discussion

Up to the present, cancer has become the first-rate killer in the world. Despite tremendous efforts being made to ameliorate tumor treatment, cancer cases are increasing every year [11, 12]. In our article, GSE80201 and GSE39262 were downloaded from the GEO database. 82 DEMs including microRNA-181b, microRNA-29A, microRNA-223, microRNA-21, microRNA-29B, microRNA-181A, microRNA-30B, and microRNA-1248 and 74 DEGs were identified. To further understand the mechanisms of the 5 microRNAs in ES, we used FunRich for the next research. GO and KEGG analysis showed that these microRNAs were primarily related to the regulation of nucleobase, nucleoside, regulation of translation, extracellular matrix, Golgi apparatus, cyclin-dependent protein kinase holoenzyme complex, extracellular matrix structural constituent, transcription factor activity, and GTPase activity. This is consistent with the recognition that lysosomes and nucleus play a key role in several human diseases, such as cancer, obesity, neurodegenerative diseases, and infection [13]. As for transporter activity, it is involved in various tumor metastases, targeting lactate transporters and drugs to treat cancer and may serve as an opportunity to develop new therapies for inflammation and cancer [14, 15]. Besides, KEGG

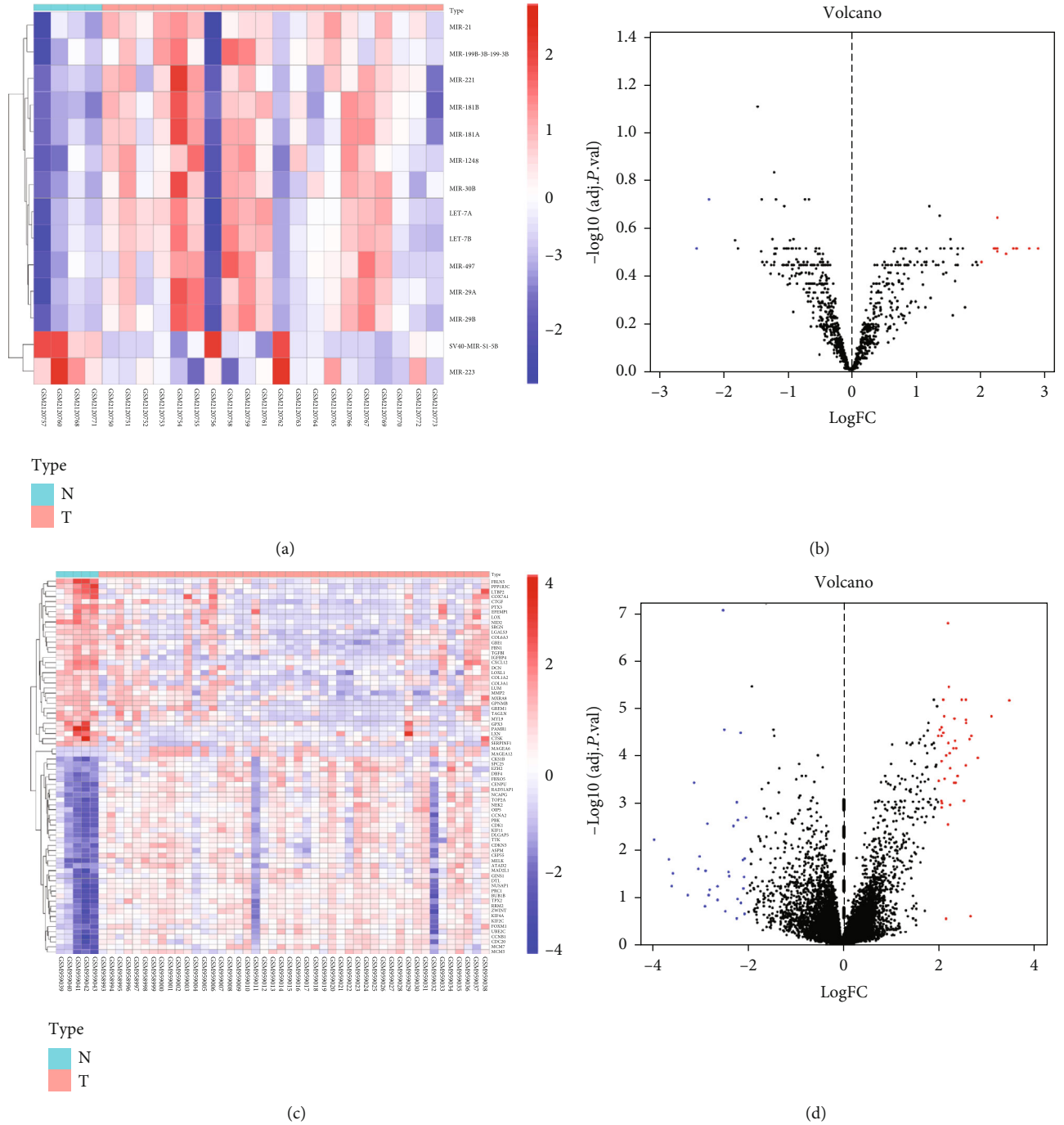

Figure 1: Heat map and volcano map of differentially expressed genes of GSE80201 and GSE39262. (a) Heat map of DEGs in GSE80201. (b) Volcano map of DEGs in GSE80201. (c) Heat map of DEGs in GSE39262. (d) Volcano map of DEGs in GSE39262. Red dots represent upregulated genes, and blue dots represent downregulated genes.

research indicated that these genes were mainly enriched in 8 pathways including p53 signaling pathway, ECM-receptor interaction, autophagy, DNA replication, base excision repair, complement and coagulation cascades, homologous recombination, and nucleotide excision repair, which were shown to affect migration and proliferation [16]. In many human tumors, p53 function is destroyed by p53 gene mutation and other mechanisms, including the amplification and/or overexpression of p53 negative regulators (such as murine double minute 2 and murine double minute 4), which is a prerequisite for the occurrence and/or progression of many human tumors [17, 18]. To ensure the proper function of p53 in regulating many basic cellular processes, p53 protein level and activity are strictly regulated in cells. Under nonstress conditions, p53 protein in normal cells is usually maintained at a low level, but the half-life of p53 protein increases significantly, resulting in various stress signals (such as DNA

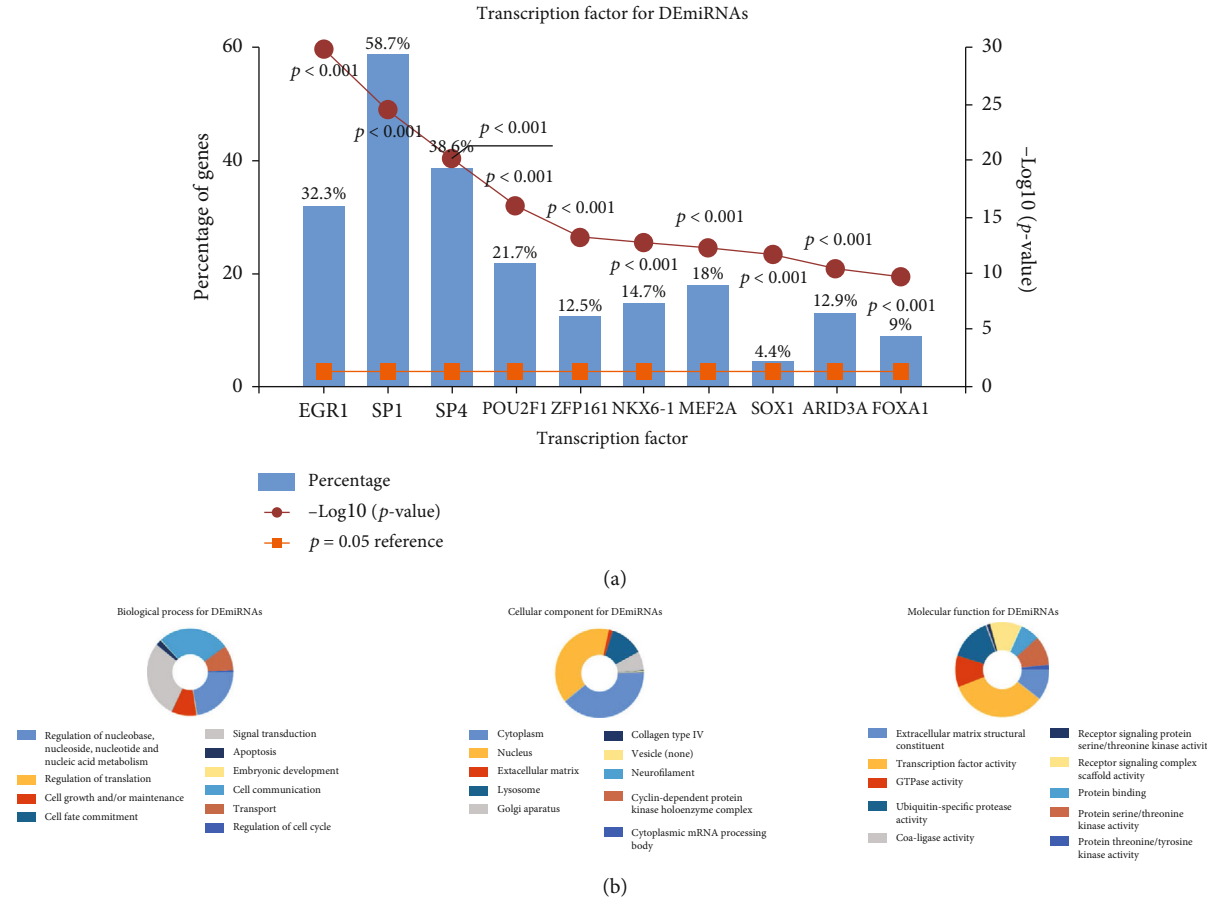

Figure 2: Gene Ontology enrichment. (a) Identification of the potential transcription factors of DEMs by FunRich software. (b) The top 10 of biological process, cellular component, and molecular function of the target genes of miRNAs.

damage, hypoxia, nutritional deficiency, and oncogene activation) inside and outside cells. Once activated, p53 binds to the p53 response element in the target gene and regulates its expression in a transcriptional manner [19]. The expression of endogenous p53 is silent in different kinds of tumors. Polyphenols from various dietary sources, including luteolin, quercetin, and epigallocatechin-3 gallate, can increase the expression of p53 in several tumor cell lines through different mechanisms. Polyphenols can stabilize p53 protein by p53 phosphorylation, p53 acetylation, and reducing oxidative stress. Previous articles also linked p53 mutation with chemotherapy resistance, and polyphenols overcome the chemotherapy resistance of tumor cells by increasing the expression of p53 [20, 21]. As for extracellular matrix-receptor interaction, it was also the most differentially expressed gene-enriched signaling pathway. Its pathway-related genes play a key role in the process of tumor abscission, adhesion, degradation, movement, and proliferation. The role of the extracellular matrix in other tumors has been demonstrated. The extracellular matrix is upregulated in prostate carcinoma [22] and takes part in the development of cancer invasion and metastasis in gastric carcinoma [23]. Besides, the colorectal cancer extracellular matrix can promote the occurrence of epithelial-mesenchymal transformation (EMT) [24]. Glioblastoma is the most common adult brain cancer. The pathological features were abnormal neovascularization and diffuse infiltration of cancer cells. The relationship between ECM and glioblastoma microenvironment is very vital in this development [25]. By utilizing FunRich software, 2000 potential target mRNAs were downloaded and 7 of them were differentially expressed in GSE39262 (DBF4, CEP55, FBN1, COL1A2, COL3A1, TGFBI, and COL6A3). According to the relationship between them, 5 essential miRNA-mRNA pairs (microRNA-29a, microRNA-21, FBN1, COL1A2, COL3A1, TGFBI, and COL6A3) were selected.

The human miRNA-29 family has 3 members including microRNA-29a, microRNA-29b, and microRNA-29c. Among the members of the microRNA-29 family, microRNA-29a was firstly found by Rauhut [26]. Researches about microRNA expression in cancer tissues or cell lines showed that microRNA-29 was downregulated in most carcinomas and upregulated in a few carcinomas. The abnormal expression of microRNA-29 and the carcinogenic or antitumor function of microRNA-29 have been widely studied in many kinds of carcinomas [27–30]. A previous study reported that the microRNA-29 family (microRNA-29a, microRNA-29b, and microRNA-29c) inhibited several proteins related to invasion and

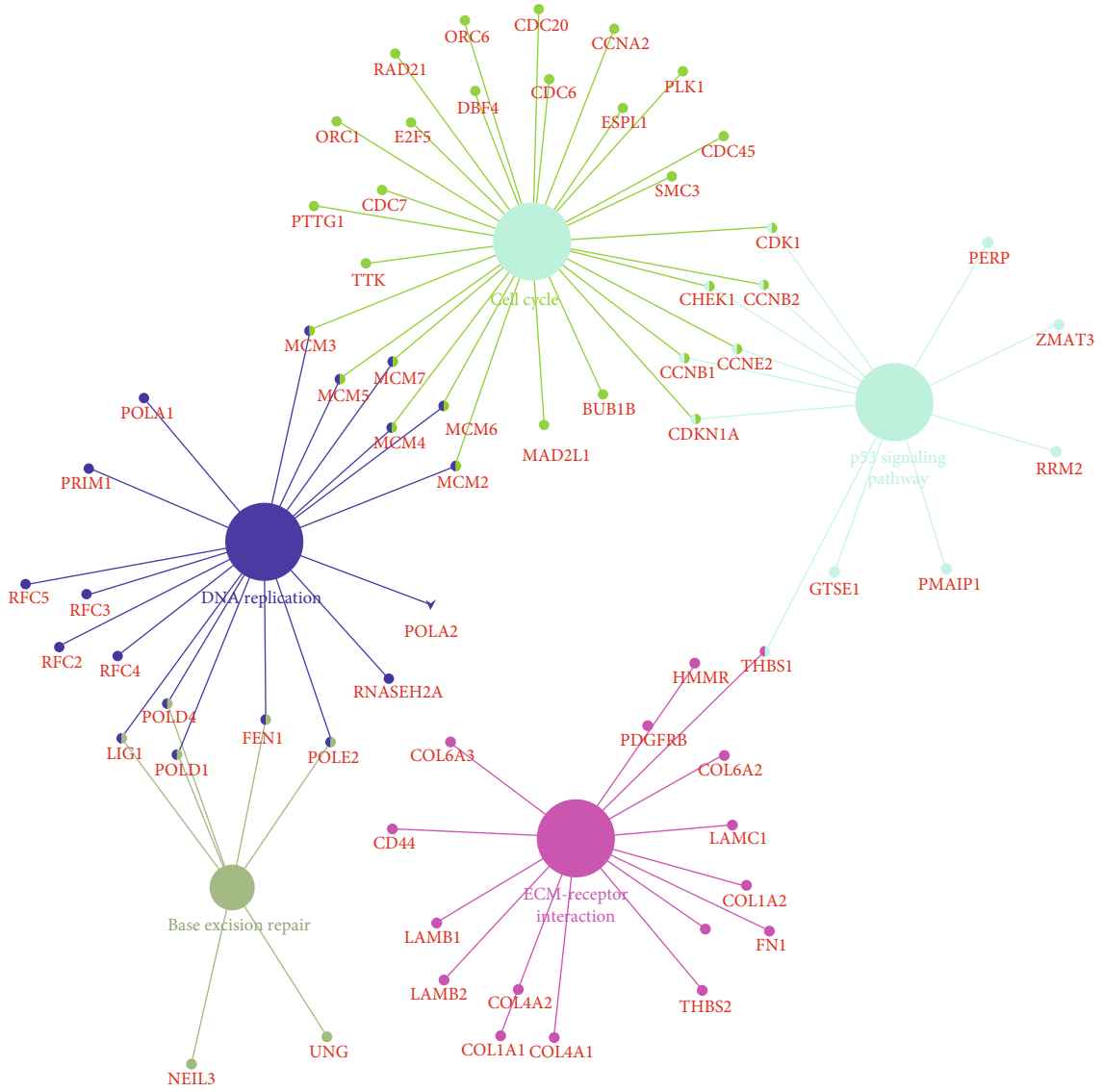

Figure 3: KEGG pathway enrichment analysis of potential target mRNAs.

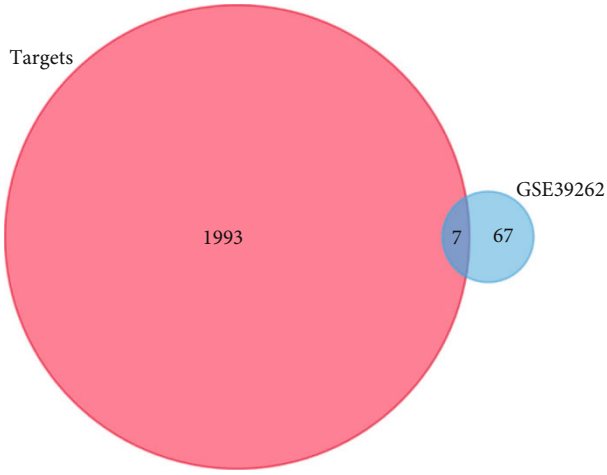

Figure 4: Venn diagram of GSE80201 and GSE39262.

metastasis of lung carcinoma. In the nervous system, microRNA-29 was discovered to be downregulated in nervous system tumors such as glioblastoma and neuroblastoma [31, 32]. Besides, in the musculoskeletal system, microRNA-29 was discovered downregulated in osteoblast tumors. microRNA-29a induces osteoblast apoptosis by silencing B cell lymphoma-2 and myeloid cell leukemia 1 and inducing E2F transcription factor 1 and E2F transcription factor 3 expression [33].

miRNA-21 is a member of the miRNA family and encoded by the MIR21 gene on human chromosome 17q23.2. Mature microRNA-21 is formed from endogenous noncoding RNA molecules of about 22 nucleotides and integrated into RNA-induced silencing complex, which binds to 3′-untranslated regions of different genes by incomplete base pairing with microRNA. The expression level of microRNA-21 is overexpressed in plenty of solid tumors, including lung carcinoma, colorectal

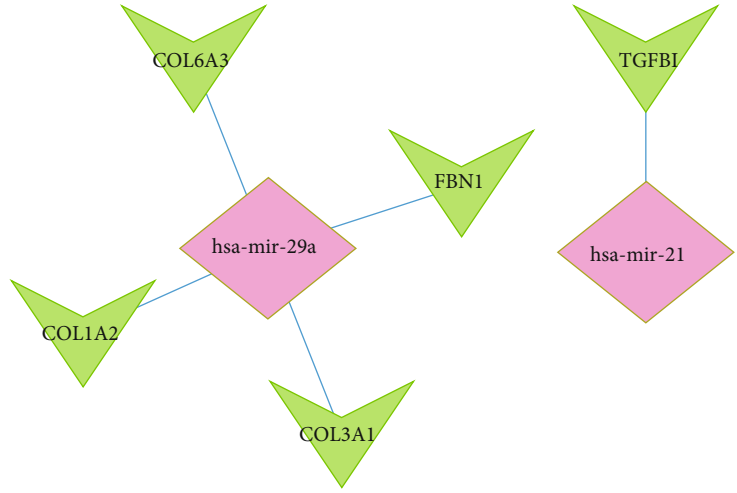

Figure 5: Identified target mRNAs and miRNA-mRNA regulatory network.

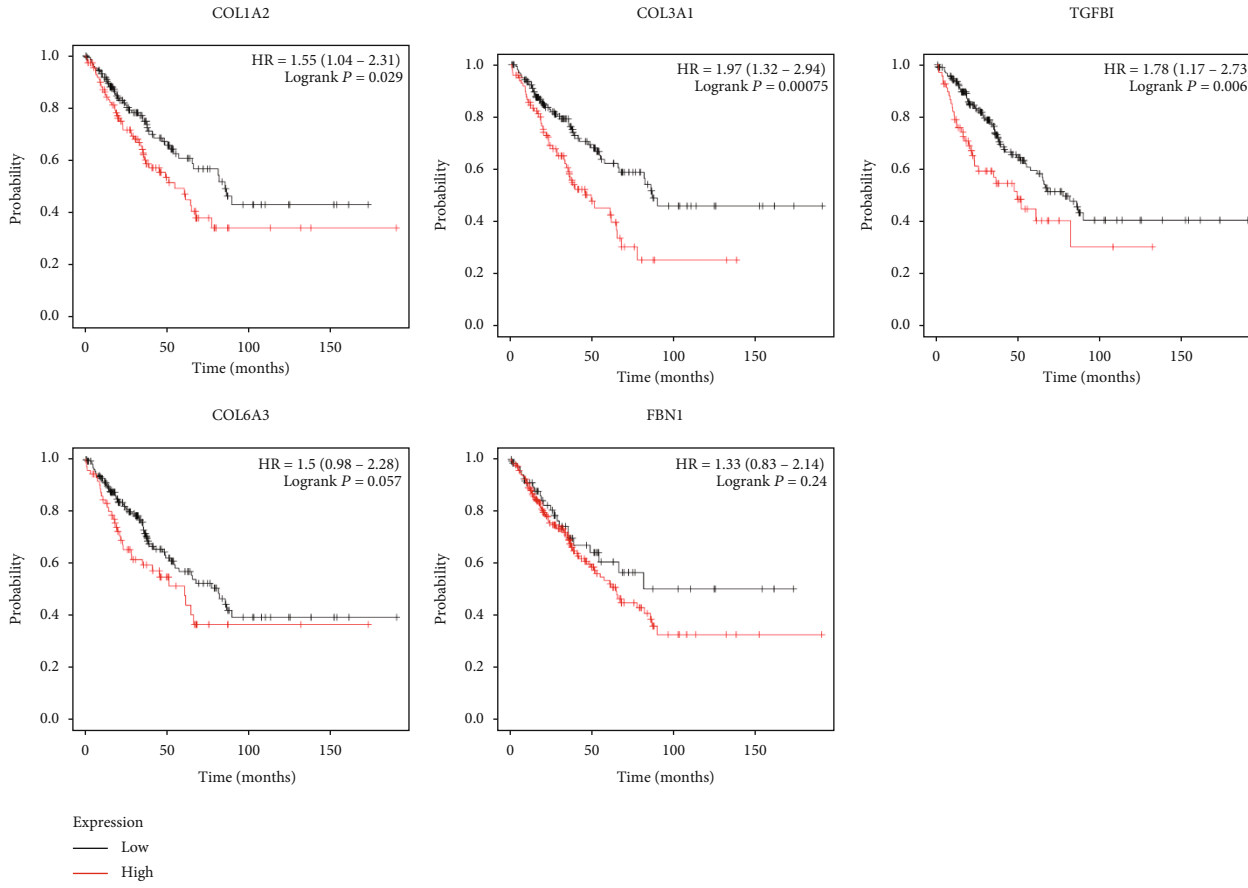

Figure 6: The association between the expression level of selected target mRNAs and Ewing sarcoma prognosis.

carcinoma, and gastric carcinoma [34–36]. In addition, previous researches have shown that microRNA-21 is also overexpressed in immune cells, promoting immune-related inflammatory diseases and taking part in the pathogenesis of autoimmune diseases [37].

KmPlot was utilized to study the OS of patients with ES. By submitting the 5 genes we selected, 5 survival curves were obtained. The results showed that COL1A2, COL3A1, and TGFBI were significantly related to the prognosis of patients with ES. Besides, correlations between clinical characteristics and COL1A2, COL3A1, and TGFBI expression in ES were researched. The univariate analysis revealed that the metastasis stage was related to overall survival. We also found that the expression level

Table 1: Relationship between the expression level of TGFB1 and clinical characteristics in ES.

Characteristic	Low expression of TGFBI	High expression of TGFBI	*p*
n	50	51	
Metastasis, *n* (%)			0.686
No	39 (38.6%)	37 (36.6%)	
Yes	11 (10.9%)	14 (13.9%)	
Tumor region, *n* (%)			1.000
Distal	18 (28.1%)	18 (28.1%)	
Other	2 (3.1%)	1 (1.6%)	
Proximal	12 (18.8%)	13 (20.3%)	
Proximal and distal	0 (0%)	0 (0%)	
Age, *n* (%)			1.000
<18	39 (38.6%)	39 (38.6%)	
≥18	11 (10.9%)	12 (11.9%)	
Gender, *n* (%)			0.372
Female	23 (22.8%)	18 (17.8%)	
Male	27 (26.7%)	33 (32.7%)	
Race, *n* (%)			
American Indian or Alaska Native	0 (0%)	1 (1.3%)	
Asian	3 (3.9%)	4 (5.3%)	
Black or African American	5 (6.6%)	5 (6.6%)	
Native Hawaiian or other Pacific Islander	0 (0%)	0 (0%)	
White	28 (36.8%)	30 (39.5%)	
Age, median (IQR)	15.27 (12.35, 17.69)	15.06 (12.63, 17.77)	0.989

Table 2: Relationship between overall survival and the expression level of TGFB1 researched by univariate and multivariate Cox regression.

Characteristics	Total (*N*)	Univariate analysis		Multivariate analysis	
		Hazard ratio (95% CI)	*p* value	Hazard ratio (95% CI)	*p* value
Metastasis (yes vs. no)	99	3.679 (1.964-6.892)	**<0.001**	3.459 (1.438-8.318)	**0.006**
Tumor region (other and proximal and proximal and distal vs. distal)	63	0.473 (0.198-1.127)	0.091	0.547 (0.226-1.321)	0.180
Age (≥18 vs. <18)	99	0.732 (0.325-1.653)	0.454		
TGFBI (high vs. low)	99	0.566 (0.304-1.055)	0.073	0.552 (0.245-1.246)	0.153
Primary site progression (yes vs. no)	50	1.769 (0.864-3.626)	0.119		
Gender (male vs. female)	99	0.976 (0.520-1.832)	0.940		

of COL3A1 was not associated with metastasis stage, tumor region, age stage, gender stage, and race stage ($p > 0.01$). Besides, correlations between clinical characteristics and COL3A1 expression in ES were researched. The univariate analysis revealed that metastasis stage and COL3A1 expression level are related to overall survival. However, tumor region, age stage, gender stage, and primary site progression were not correlated with overall survival (Table 3). Multivariate analysis also showed that COL3A1 expression level and metastasis stage were an independent risk factor for overall survival in ES.

COL3A1 (collagen type III alpha 1) is an important extracellular matrix protein that was found in 1971 [38]. Type III collagen has many important physiological functions. It is revealed that abnormal overexpression of collagen type III alpha 1 happens in some different types of tumors [39–42]. For example, collagen type III alpha 1 overexpression is associated with poor survival and may be a potential biomarker for early diagnosis of ovarian carcinoma [39]. Engqvist et al. indicated that collagen type III alpha 1 was overexpressed in brain tumors at different stages [40]. Besides, the expression level of COL3A1 can predict the efficacy of neoadjuvant therapy in rectal carcinoma [41]. A previous study also reported that it was differently expressed in a variety of tumors, and its expression is related to tumor immune microenvironment and pan-cancer prognosis. Moreover, it was expected to be further studied as a marker in malignant tumor prognosis

Table 3: Relationship between the expression level of COL1A2 and clinical characteristics in ES.

Characteristic	Low expression of COL1A2	High expression of COL1A2	*p*
n	50	51	
Metastasis, *n* (%)			1.000
No	38 (37.6%)	38 (37.6%)	
Yes	12 (11.9%)	13 (12.9%)	
Tumor region, *n* (%)			0.360
Distal	18 (28.1%)	18 (28.1%)	
Other	3 (4.7%)	0 (0%)	
Proximal	13 (20.3%)	12 (18.8%)	
Proximal and distal	0 (0%)	0 (0%)	
Age, *n* (%)			0.139
<18	35 (34.7%)	43 (42.6%)	
≥18	15 (14.9%)	8 (7.9%)	
Gender, *n* (%)			0.626
Female	22 (21.8%)	19 (18.8%)	
Male	28 (27.7%)	32 (31.7%)	
Race, *n* (%)			
American Indian or Alaska Native	1 (1.3%)	0 (0%)	
Asian	5 (6.6%)	2 (2.6%)	
Black or African American	6 (7.9%)	4 (5.3%)	
Native Hawaiian or other Pacific Islander	0 (0%)	0 (0%)	
White	26 (34.2%)	32 (42.1%)	
Age, median (IQR)	15.52 (12.76, 18.8)	13.87 (11.87, 16.65)	0.111

Table 4: Relationship between overall survival and the expression level of COL1A2 researched by univariate and multivariate Cox regression.

Characteristics	Total (*N*)	Univariate analysis		Multivariate analysis	
		Hazard ratio (95% CI)	*p* value	Hazard ratio (95% CI)	*p* value
Metastasis (yes vs. no)	99	3.679 (1.964-6.892)	**<0.001**	2.871 (1.253-6.578)	**0.013**
Tumor region (other and proximal and proximal and distal vs. distal)	63	0.473 (0.198-1.127)	0.091	0.518 (0.216-1.241)	0.140
Age (≥18 vs. <18)	99	0.732 (0.325-1.653)	0.454		
COL1A2 (high vs. low)	99	1.026 (0.554-1.900)	0.935		
Gender (male vs. female)	99	0.976 (0.520-1.832)	0.940		
Primary site progression (yes vs. no)	50	1.769 (0.864-3.626)	0.119		

and associated tumor immunotherapy [43]. In breast cancer, it was found that methyltransferase-like 3 could target COL3A1 in triple-negative breast cancer cell lines. Methyltransferase-like 3 could suppress the expression of COL3A1 by upregulating its m6A methylation, ultimately inhibiting the metastasis of triple-negative breast cancer cells [44]. In osteosarcoma, it was found that the microRNA-29 family may play a tumor inhibitory role in controlling methotrexate resistance and apoptosis by targeting COL3A1 or MCL1 apoptosis regulators. The development of drugs targeting the microRNA-29 family may provide a new treatment method to overcome the cytotoxicity and drug resistance of osteosarcoma induced by high-dose methotrexate [45].

In recent years, the role of microRNA and its target genes in tumorigenesis and development has been widely studied. Many reports have shown that changes in microRNA and mRNA expression have been found in initial and developing cancers. It is very important to clarify the role of microRNA and mRNA in various human cancers, because the regulation of gene expression may be a new choice for cancer treatment. Our research demonstrated that microRNA-29a and its target gene COL3A1 were involved in the development of ES by several signaling pathways and had prognostic worth. Therefore, overexpression of microRNA-29a or suppression of COL3A1 may have potential therapeutic values in ES patients with metastasis.

Table 5: Relationship between the expression level of COL3A1 and clinical characteristics in ES.

Characteristic	Low expression of COL3A1	High expression of COL3A1	*p*
n	50	51	
Metastasis, *n* (%)			0.686
No	39 (38.6%)	37 (36.6%)	
Yes	11 (10.9%)	14 (13.9%)	
Tumor region, *n* (%)			0.920
Distal	19 (29.7%)	17 (26.6%)	
Other	1 (1.6%)	2 (3.1%)	
Proximal	13 (20.3%)	12 (18.8%)	
Proximal and distal	0 (0%)	0 (0%)	
Age, *n* (%)			0.371
<18	41 (40.6%)	37 (36.6%)	
≥18	9 (8.9%)	14 (13.9%)	
Gender, *n* (%)			0.089
Female	25 (24.8%)	16 (15.8%)	
Male	25 (24.8%)	35 (34.7%)	
Race, *n* (%)			
American Indian or Alaska Native	0 (0%)	1 (1.3%)	
Asian	3 (3.9%)	4 (5.3%)	
Black or African American	3 (3.9%)	7 (9.2%)	
Native Hawaiian or other Pacific Islander	0 (0%)	0 (0%)	
White	31 (40.8%)	27 (35.5%)	
Age, median (IQR)	15.12 (12.62, 17.33)	15.1 (12.12, 18.41)	0.973

Table 6: Relationship between overall survival and the expression level of COL3A1 researched by univariate and multivariate Cox regression.

Characteristics	Total (*N*)	Univariate analysis		Multivariate analysis	
		Hazard ratio (95% CI)	*p* value	Hazard ratio (95% CI)	*p* value
Metastasis (yes vs. no)	99	3.679 (1.964-6.892)	**<0.001**	3.322 (1.419-7.774)	**0.006**
Tumor region (other and proximal and proximal and distal vs. distal)	63	0.473 (0.198-1.127)	0.091	0.507 (0.212-1.214)	0.127
Age (≥18 vs. <18)	99	0.732 (0.325-1.653)	0.454		
COL3A1 (high vs. low)	99	0.512 (0.273-0.960)	**0.037**	0.522 (0.234-0.865)	**0.002**
Gender (male vs. female)	99	0.976 (0.520-1.832)	0.940		
Primary site progression (yes vs. no)	50	1.769 (0.864-3.626)	0.119		

5. Conclusion

Our study concluded certain mechanisms for the development of ES. Plenty of differentially expressed mRNAs and miRNAs were identified between ES cells and osteoblasts cells. Also, microRNA-29a and its target gene COL3A1 were identified as potential markers of ES. However, these conclusions need further experiments to prove.

Data Availability

The datasets used and/or analyzed during the current study are available from the corresponding author on reasonable request.

Consent

Consent is not applicable.

Conflicts of Interest

The authors have declared that no competing interest exists.

Authors' Contributions

Min Tang contributed to the conception of the present study and completed the draft of the manuscript. All authors participated in the design of the study and conducted the research. Xiaoke Wu processed and analyzed the data from

the dataset. Min Tang, Peiqing Liu, and Xiaoke Wu contributed equally to this work.

Acknowledgments

This work was supported by the National Natural Science Foundation of China (Grant No. 81803553) and the National Natural Science Foundation Preresearch Program of China (SDFEYGJ1608).

References

[1] N. Riggi, L. Cironi, P. Provero et al., "Development of Ewing's sarcoma from primary bone marrow-derived mesenchymal progenitor cells," *Cancer Research*, vol. 65, no. 24, pp. 11459–11468, 2005.

[2] S. S. Desai and N. A. Jambhekar, "Pathology of Ewing's sarcoma/PNET: current opinion and emerging concepts," *Indian journal of orthopaedics*, vol. 44, no. 4, pp. 363–368, 2010.

[3] M. E. Kallen and J. L. Hornick, "The 2020 WHO classification," *The American Journal of Surgical Pathology*, vol. 45, no. 1, pp. e1–e23, 2021.

[4] J. M. Simon and N. C. Gomez, "Epigenetic analysis in Ewing sarcoma," *Methods in Molecular Biology*, vol. 2226, pp. 285–302, 2021.

[5] H. Uezono, D. J. Indelicato, R. L. Rotondo et al., "Treatment outcomes after proton therapy for Ewing sarcoma of the pelvis," *International Journal of Radiation Oncology • Biology • Physics*, vol. 107, no. 5, pp. 974–981, 2020.

[6] B. R. Eaton, L. Claude, D. J. Indelicato et al., "Ewing sarcoma," *Pediatric Blood & Cancer*, vol. 68, article e28355, Supplement 2, 2021.

[7] G. Gao, X. Shi, and J. Shen, "HS3ST2 and its related molecules as potential biomarkers for predicting lymph node metastasis in patients with colorectal cancer," *Oncotargets and Therapy*, vol. 14, pp. 3881–3894, 2021.

[8] X. Wang, G. Gao, Z. Chen et al., "Identification of the miRNA signature and key genes in colorectal cancer lymph node metastasis," *Cancer Cell International*, vol. 21, no. 1, p. 358, 2021.

[9] F. Zhai, X. Chen, Q. He et al., "MicroRNA-181 inhibits glioblastoma cell growth by directly targeting CCL8," *Oncology Letters*, vol. 18, no. 2, pp. 1922–1930, 2019.

[10] Y. M. Zhou, Y. L. Yao, W. Liu, X. M. Shen, L. J. Shi, and L. Wu, "MicroRNA-134 inhibits tumor stem cell migration and invasion in oral squamous cell carcinomas via down-regulation of PI3K-Akt signaling pathway by inhibiting LAMC2 expression," *Cancer Biomarkers*, vol. 29, no. 1, pp. 51–67, 2020.

[11] W. Jiang, K. Meng, G. Sheng, and T. Yang, "MicroRNA-24 inhibits the proliferation, migration and invasion and enhances chemosensitivity of human gastric cancer by targeting DND1," *Journal of BUON*, vol. 25, no. 2, pp. 1001–1006, 2020.

[12] E. Laconi, F. Marongiu, and J. DeGregori, "Cancer as a disease of old age: changing mutational and microenvironmental landscapes," *British Journal of Cancer*, vol. 122, no. 7, pp. 943–952, 2020.

[13] M. S. Y. Thong, C. J. F. van Noorden, K. Steindorf, and V. Arndt, "Cancer-related fatigue: causes and current treatment options," *Current Treatment Options in Oncology*, vol. 21, no. 2, p. 17, 2020.

[14] A. Ballabio, "The awesome lysosome," *EMBO Molecular Medicine*, vol. 8, no. 2, pp. 73–76, 2016.

[15] V. Pucino, D. Cucchi, and C. Mauro, "Lactate transporters as therapeutic targets in cancer and inflammatory diseases," *Expert Opinion on Therapeutic Targets*, vol. 22, no. 9, pp. 735–743, 2018.

[16] V. L. Payen, M. Y. Hsu, K. S. Rädecke et al., "Monocarboxylate transporter MCT1 promotes tumor metastasis independently of its activity as a lactate transporter," *Cancer Research*, vol. 77, no. 20, pp. 5591–5601, 2017.

[17] L. Galli and G. Marcelli, "Water-electrolyte balances in urological surgery," *Archivio Italiano di Urologia e Nefrologia*, vol. 41, no. 3, pp. 199–217, 1968.

[18] G. W. Yee, C. Naasz, L. Hatle, R. Pipkin, and I. Schnittger, "Doppler diagnosis of left ventricle to coronary sinus fistula: an unusual complication of mitral valve replacement," *Journal of the American Society of Echocardiography*, vol. 1, no. 6, pp. 458–462, 1988.

[19] A. J. Levine, "The many faces of p53: something for everyone," *Journal of Molecular Cell Biology*, vol. 11, no. 7, pp. 524–530, 2019.

[20] J. Liu, C. Zhang, W. Hu, and Z. Feng, "Tumor suppressor p53 and its mutants in cancer metabolism," *Cancer Letter*, vol. 356, no. 2, pp. 197–203, 2015.

[21] M. J. Duffy, N. C. Synnott, and J. Crown, "Mutant p53 in breast cancer: potential as a therapeutic target and biomarker," *Breast Cancer Research and Treatment*, vol. 170, no. 2, pp. 213–219, 2018.

[22] B. E. Kennedy, T. Sharif, E. Martell et al., "NAD^+ salvage pathway in cancer metabolism and therapy," *Pharmacological Research*, vol. 114, pp. 274–283, 2016.

[23] M. K. Andersen, K. Rise, G. F. Giskeødegård et al., "Integrative metabolic and transcriptomic profiling of prostate cancer tissue containing reactive stroma," *Scientific Reports*, vol. 8, no. 1, article 14269, 2018.

[24] P. Yan, Y. He, K. Xie, S. Kong, and W. Zhao, "*In silico* analyses for potential key genes associated with gastric cancer," *PeerJ*, vol. 6, article e6092, 2018.

[25] N. N. Rahbari, D. Kedrin, J. Incio et al., "Anti-VEGF therapy induces ECM remodeling and mechanical barriers to therapy in colorectal cancer liver metastases," *Science Translational Medicine*, vol. 8, no. 360, p. 360ra135, 2016.

[26] X. Cui, R. T. Morales, W. Qian et al., "Hacking macrophage-associated immunosuppression for regulating glioblastoma angiogenesis," *Biomaterials*, vol. 161, pp. 164–178, 2018.

[27] M. Lagos-Quintana, R. Rauhut, W. Lendeckel, and T. Tuschl, "Identification of novel genes coding for small expressed RNAs," *Science*, vol. 294, no. 5543, pp. 853–858, 2001.

[28] N. Yanaihara, N. Caplen, E. Bowman et al., "Unique microRNA molecular profiles in lung cancer diagnosis and prognosis," *Cancer Cell*, vol. 9, no. 3, pp. 189–198, 2006.

[29] M. Fabbri, R. Garzon, A. Cimmino et al., "MicroRNA-29 family reverts aberrant methylation in lung cancer by targeting DNA methyltransferases 3A and 3B," *Proceedings of the National Academy of Sciences of the United States of America*, vol. 104, no. 40, pp. 15805–15810, 2007.

[30] X. Z. Meng, T. S. Zheng, X. Chen et al., "microRNA expression alteration after arsenic trioxide treatment in HepG-2 cells,"

Journal of Gastroenterology and Hepatology, vol. 26, no. 1, pp. 186–193, 2011.

[31] Y. Xiong, J. H. Fang, J. P. Yun et al., "Effects of microRNA-29 on apoptosis, tumorigenicity, and prognosis of hepatocellular carcinoma," *Hepatology*, vol. 51, no. 3, pp. 836–845, 2010.

[32] M. A. Cortez, M. S. Nicoloso, M. Shimizu et al., "*miR-29b* and *miR-125a* regulate podoplanin and suppress invasion in glioblastoma," *Genes, Chromosomes & Cancer*, vol. 49, no. 11, pp. 981–990, 2010.

[33] H. Xu, I. Y. Cheung, H. F. Guo, and N. K. Cheung, "MicroRNA miR-29 modulates expression of immunoinhibitory molecule B7-H3: potential implications for immune based therapy of human solid tumors," *Cancer Research*, vol. 69, no. 15, pp. 6275–6281, 2009.

[34] W. Zhang, J. X. Qian, H. L. Yi et al., "The microRNA-29 plays a central role in osteosarcoma pathogenesis and progression," *Molekuliarnaia Biologiia (Mosk)*, vol. 46, no. 4, pp. 557–562, 2012.

[35] Z. Chen, H. Liu, W. Jin, Z. Ding, S. Zheng, and Y. Yu, "Tissue microRNA-21 expression predicted recurrence and poor survival in patients with colorectal cancer - a meta-analysis," *Oncotargets and Therapy*, vol. 9, pp. 2615–2624, 2016.

[36] S. Jiang, R. Wang, H. Yan, L. Jin, X. Dou, and D. Chen, "MicroRNA-21 modulates radiation resistance through upregulation of hypoxia-inducible factor-1α-promoted glycolysis in non-small cell lung cancer cells," *Molecular Medicine Reports*, vol. 13, no. 5, pp. 4101–4107, 2016.

[37] J. Yan, T. Liu, X. Zhou, Y. Dang, C. Yin, and G. Zhang, "FZD6, targeted by miR-21, represses gastric cancer cell proliferation and migration via activating non-canonical wnt pathway," *American Journal of Translational Research*, vol. 8, no. 5, pp. 2354–2364, 2016.

[38] M. Husakova, "MicroRNAs in the key events of systemic lupus erythematosus pathogenesis," *Biomedical Papers of the Medical Faculty of the University Palacky, Olomouc, Czech Republic*, vol. 160, no. 3, pp. 327–342, 2016.

[39] E. J. Miller, E. H. Epstein Jr., and K. A. Piez, "Identification of three genetically distinct collagens by cyanogen bromide cleavage of insoluble human skin and cartilage collagen," *Biochemical and Biophysical Research Communications*, vol. 42, no. 6, pp. 1024–1029, 1971.

[40] H. Engqvist, T. Z. Parris, A. Kovács et al., "Immunohistochemical validation of COL3A1, GPR158 and PITHD1 as prognostic biomarkers in early-stage ovarian carcinomas," *BMC Cancer*, vol. 19, no. 1, p. 928, 2019.

[41] Y. Liu, E. B. Carson-Walter, A. Cooper, B. N. Winans, M. D. Johnson, and K. A. Walter, "Vascular gene expression patterns are conserved in primary and metastatic brain tumors," *Journal of Neuro-Oncology*, vol. 99, no. 1, pp. 13–24, 2010.

[42] S. Gonçalves-Ribeiro, R. Sanz-Pamplona, A. Vidal et al., "Prediction of pathological response to neoadjuvant treatment in rectal cancer with a two-protein immunohistochemical score derived from stromal gene- profiling," *Annals of Oncology*, vol. 28, no. 9, pp. 2160–2168, 2017.

[43] Y. Shi, C. Zheng, Y. Jin et al., "Reduced expression of *METTL3* promotes metastasis of triple-negative breast cancer by m6A methylation-mediated *COL3A1* up-regulation," *Frontiers in Oncology*, vol. 10, p. 1126, 2020.

[44] H. Zhang, C. Ding, Y. Li et al., "Data mining-based study of collagen type III alpha 1 (COL3A1) prognostic value and immune exploration in pan-cancer," *Bioengineered*, vol. 12, no. 1, pp. 3634–3646, 2021.

[45] W. Xu, Z. Li, X. Zhu, R. Xu, and Y. Xu, "miR-29 family inhibits resistance to methotrexate and promotes cell apoptosis by targeting COL3A1 and MCL1 in osteosarcoma," *Medical Science Monitor*, vol. 24, pp. 8812–8821, 2018.

Hindawi
BioMed Research International
Volume 2021, Article ID 2888393, 12 pages
https://doi.org/10.1155/2021/2888393

Research Article

Mitigation of Iron Irradiation-Induced Genotoxicity and Genomic Instability by Postexposure Dietary Restriction in Mice

Bing Wang[1], **Takanori Katsube**[1], **Kaoru Tanaka**[1], **Masahiro Murakami**[1], **and Mitsuru Nenoi**[2]

[1]*Dietary Effects Research Group, Department of Radiation Effects Research, National Institute of Radiological Sciences, Quantum Life and Medical Science Directorate, National Institutes for Quantum and Radiological Science and Technology, Chiba, Japan*
[2]*Human Resources Development Center, Quantum Life and Medical Science Directorate, National Institutes for Quantum and Radiological Science and Technology, Chiba, Japan*

Correspondence should be addressed to Bing Wang; wang.bing@qst.go.jp and Mitsuru Nenoi; nenoi.mitsuru@qst.go.jp

Received 30 August 2021; Accepted 5 November 2021; Published 25 November 2021

Academic Editor: Syed Sameer Aga

Background and Purpose. Postexposure onset of dietary restriction (DR) is expected to provide therapeutic nutritional approaches to reduce health risk from exposure to ionizing radiation (IR) due to such as manned space exploration, radiotherapy, or nuclear accidents as IR could alleviate radiocarcinogenesis in animal models. However, the underlying mechanisms remain largely unknown. This study is aimed at investigating the effect from postexposure onset of DR on genotoxicity and genomic instability (GI) induced by total body irradiation (TBI) in mice. *Materials and Methods*. Mice were exposed to 2.0 Gy of accelerated iron particles with an initial energy of 500 MeV/nucleon and a linear energy transfer (LET) value of about 200 keV/μm. After TBI, mice were either allowed to free access to a standard laboratory chow or treated under DR (25% cut in diet). Using micronucleus frequency (MNF) in bone marrow erythrocytes, induction of acute genotoxicity and GI in the hematopoietic system was, respectively, determined 1 and 2 months after TBI. *Results and Conclusions*. TBI alone caused a significant increase in MNF while DR alone did not markedly influence the MNF. DR induced a significant decrease in MNF compared to the treatment by TBI alone. Results demonstrated that postexposure onset of DR could relieve the elevated MNF induced by TBI with high-LET iron particles. These findings indicated that reduction in acute genotoxicity and late GI may be at least a part of the mechanisms underlying decreased radiocarcinogenesis by DR.

1. Introduction

Ionizing radiation (IR) as a carcinogen could induce genotoxicity, genomic instability (GI), and cancer. GI is an increased tendency to alterations in the genome and an important initiating and central event in carcinogenesis [1]. GI could be provoked by a variety of endogenous and exogenous insults including IR, and GI could be modified by lifestyle factors such as diet [2–6]. Characterized by various endpoints such as chromosomal rearrangements and aberrations, micronucleus formation, and gene mutation, IR-induced genotoxicity and GI have a big impact on radiocarcinogenesis. IR-induced GI is the driving force responsible for radiocarcinogenesis [1, 7–10]. Radiocarcinogenesis is the most concerned long-term health consequences. As humans are unavoidably exposed to high linear energy transfer (LET) IR in some circumstances such as hadrontherapy and manned space activities, limiting cancer risk from exposure to high-LET IR is of great public concern [11, 12].

Many factors could modify IR-induced biological effects including carcinogenesis, such as intervention of dietary and lifestyle-related factors. Studies show clearly that certain cancers are primarily dependent on dietary habits [13, 14], and dietary and lifestyle-related factors could influence health in many species, playing key roles in modulating the risk of developing cancer. It is known that dietary restriction (DR), i.e., restriction of either calories or macronutrients and fasting, could increase mean lifespan by decelerating aging

rate and inhibiting tumor formation in a variety of species [15–17]. DR could decrease both spontaneous and chemical carcinogen-induced tumors in rodents and nonhuman primates [18–20]. DR could act synergistically with other treatments [21] and decrease significantly the incidence of both spontaneous and induced neoplasms in experimental carcinogenesis [21–26]. For prevention of radiocarcinogenesis, the early pioneer studies show that food or caloric restriction could decrease dramatically low LET gamma- or X-ray-induced solid tumors and/or leukemia in mice and rats [27–29]. DR could not only protect acute IR-induced damage and promote early regeneration [30] but also suppress residual genotoxic damage [31] and development of cancer including its initiation, progression, and metastasis [22]. Preexposure onset of caloric restriction could extend latency of myeloid leukemia and prevent radiation-induced myeloid leukemia and life shortening in mice [32–34]. Furthermore, postexposure onset of DR during the tumor promotion/progression phase could still be a valuable strategy in extending lifespan, reducing frequencies of radiocarcinogenesis for myeloid leukemia [35] and late-occurring tumor [36] and suppressing the size and progression of intestinal tumors [37]. All these findings demonstrate that DR including postexposure onset of DR could generally prevent incidence of radiocarcinogenesis in experimental models. On the other hand, the mechanisms underlying postexposure onset DR-induced reduction of radiocarcinogenesis are still largely unknown. A few of studies in mouse models show that suppression of radiocarcinogenesis could be attributed to the reduced IR-induced mutations [38, 39]. In this work, the impact of postexposure onset of DR on high-LET IR-induced acute genotoxicity and late GI was investigated in a mouse model measured as micronucleus erythrocytes in the bone marrow. We demonstrated that postexposure onset of DR could efficiently reduce acute genotoxicity and late GI in the erythrocytes in the bone marrow without significant change in peripheral blood hemogram. Our findings suggested that DR could activate mechanisms consequently resulting in suppression of IR-induced genotoxicity and GI.

Micronucleus formation resulted from DNA damage and defects in mitosis. It could serve as an index of genotoxicity and chromosomal instability [40]. Micronucleus is a highly accepted biomarker for the detection and quantification of GI to predict cancer risk and identify high risk individuals, and the micronucleus test is one of the most widely used assays to evaluate GI in different tissues [6, 41–46]. In this work, the impact from postexposure onset of DR (25% cut in diet) on genotoxicity and GI induced by high-LET iron irradiation was investigated in a mouse model measured as changes in the micronucleus frequency (MNF) in bone marrow erythrocytes, respectively, 1 and 2 months after total body irradiation (TBI). Results demonstrated that postexposure onset of DR could relieve the elevated MNF induced by high-LET iron irradiation.

2. Materials and Methods

2.1. Animals. Seven-week-old C57BL/6J Jms strain female mice were purchased from SLC, Inc. (Japan). To avoid possible effects from the developmental condition of the animals, any mouse with a significantly different body weight, namely, more or less than the mean ± 2 standard deviation (SD) of all the animals upon arrival, was omitted from this study. The selected mice were randomly assigned to 2 experimental groups as either the nonirradiated group or the irradiated group. All animals were maintained in a conventional animal facility under a 12 h light-12 h dark photoperiod, controlled temperature (23 ± 2°C), and humidity (50 ± 10 %); housed in autoclaved aluminum cages (one mouse per cage) with sterilized wood chips; and allowed access to a standard laboratory chow MB-1 (Funabashi Farm Co., Japan) and acidified water (pH = 3.0 ± 0.2) *ad libitum*. Ingredients of the diet MB-1 contained 24.2% crude protein, 4.4% crude fat, and 54.4% carbohydrate. The metabolizable energy was 354.0 kcal/100 g. The mice were acclimatized to the laboratory conditions for 1 week before use. The mice at postnatal 8 weeks old in the irradiated group were irradiated with iron particles. Then, the animals in each of the experimental groups were further divided into 2 subgroups, namely, the Control group (Control, without radiation exposure and DR), the DR group (DR, receiving the 25% cut in diet), the exposure group (2.0 Gy, receiving a total body exposure to iron particles at a dose of 2.0 Gy), and the exposure plus DR group (2.0 Gy + DR, receiving a total body exposure to iron particles at a dose of 2.0 Gy plus the 25% cut in diet). The animals under DR were given daily (around 9:30 am) 75% of the amount (weight in gram) of the chow consumed by the animals that were allowed to free access to the diet. The mean amount of chow consumed per mouse allowed free access to the diet was 2.92 g per day; each of the mice under the 25% cut in diet was given daily 2.19 g of the chow. Thus, the weekly metabolizable energy was 72.36 kcal and 54.27 kcal, respectively, for each of the mice without DR and under DR. All animals were allowed access to the acidified water *ad libitum*. Based on our previous studies and preliminary trials, in the present study, 20-24 mice were used in each experimental subgroup.

All experimental protocols (Experimental Animal Research Plan No. 09-1049-1, No. 09-1042 and No. 17-2006) involving mice mentioned above and descripted in the irradiation section were reviewed and approved by The Institutional Animal Care and Use Committee of the National Institute of Radiological Sciences, National Institutes for Quantum and Radiological Science and Technology. The experiments were performed in strict accordance with the Institutional Guidelines for the Care and Use of Laboratory Animals.

2.2. Irradiation. Iron particles were generated and accelerated by a synchrotron, the Heavy Ion Medical Accelerator in Chiba (HIMAC), Japan. The monoenergetic iron beams having 500 MeV/nucleon of initial energy were expanded by wobbler magnets to a 10 cm irradiation field with homogeneous irradiation dose. Animals were irradiated at the entrance (plateau) region of the iron beams. The dose-averaged LET value of iron particles calculated by the Monte-Carlo simulation was 200 ± 20 KeV/μm. TBI with 2.0 Gy was performed at a dose rate about 1.0-2.0 Gy/min.

For TBI, the mice were held in a special Lucite columnar container, which was with an outer diameter of 10 cm and 3 individual cells of the same size (each mouse in each cell). The mice were in an air-breathing condition (there were six holes 5 mm in diameter in the wall of each cell). The containers were set on the beam track, and the focused 10 cm diameter iron beam was delivered to the animals at room temperature without anesthesia.

2.3. Micronucleus Test. The micronucleus test has been extensively used in a variety of exploratory and mechanistic studies aiming to explore the mechanisms underlying genotoxicity. Due to its simplicity and readiness, this test could be applied to a variety of cell types. An increase in the micronucleus frequency in treated animals is an indication of induced chromosome damage. A bone marrow erythrocyte micronucleus test was carried out according to our previous study [31]. Induction of micronucleus erythrocytes in bone marrow by TBI was used as an index to evaluate radiation-induced acute genotoxicity and late GI, depending on early and late timing of measurement after exposure. Mice were sacrificed by CO_2 asphyxiation 1 or 2 months after TBI. Bone marrow was collected from both femurs. Then, bone marrow smears were prepared and processed for the enumeration of micronucleated polychromatic erythrocytes (MNPCEs) and micronucleated normochromatic erythrocytes (MNNCEs). The slides were coded to avoid observer bias. The micronuclei were scored using a light microscope at a magnification of 1000x. At least 5000 PCEs and 5000 NCEs per mouse were counted, and the data for each experimental point were from at least 6 mice.

2.4. Physiological Endpoints. Physiological conditions were comparatively studied in mice that were allowed free access to the diet and being under DR. The assessments included evaluating changes in body mass and measurements of peripheral hemogram. For monitoring body weight gain, all the animals were weighed weekly from onset of DR at postnatal age 8 weeks (immediately after TBI) to the end of experiment at postnatal age 17 weeks (2 months after TBI). The body weight gain data for each experimental subgroup were from at least 10 mice. For the analysis of hemogram, animals were anesthetized by CO_2 inhalation 1 or 2 months after TBI. The peripheral blood was collected from a femoral artery with a heparinized syringe in vacutainer blood collection tubes containing EDTA (Venoject II, Terumo Co., Japan), and the animals were killed by cervical dislocation. For the analysis of hemogram, blood samples were immediately subjected to a differential blood cell count and hemoglobin concentration measurement using a blood cell differential automatic analyzer (SYSMEX K-4500, Sysmex Corporation, Japan). The data for each experimental subgroup were from at least 6 mice.

2.5. Statistical Analysis. Statistical evaluation of the data was done with the chi-squared test for the micronucleus test and Student's t-test the other endpoints. The statistical significance was assigned to $P < 0.05$.

3. Results

3.1. Body Weight Gain. As an important index, changes in body mass were assessed to evaluate physiological effects from TBI and DR (Figure 1). Although a tendency for body weight gain was observed in animals in both the Control group and the 2.0 Gy group, in the 2.0 Gy group, the body weight gain decreased markedly than that in the Control group. On the other hand, significant reduction of body weight gain in the DR group and the 2.0 Gy + DR group was observed regardless of TBI. Body mass measurements of animals under DR pointed to a general significantly lower body weight gain after onset of DR until the end of the experiment compared to that of animals without DR. In addition, animals under DR have no significant difference in physiological appearance compared to their counterparts and no mortality occurred throughout the whole monitoring period. Results indicate that DR has a big impact on body weight gain in mice during the whole period of diet regimen in our experimental setup.

3.2. Peripheral Blood Hemogram. Alterations in the hematopoietic system measured as changes in peripheral blood hemogram were also studied to evaluate physiological effects (Figure 2). In general, DR alone did not induce any marked effects on all the parameters (Figure 2) while TBI alone significantly reduced the white blood cell count 1 and 2 months after exposure regardless of DR (Figure 2(a)). Though some alterations were detectable, no statistical significance was found in red blood cell count, hemoglobin concentration, and blood platelet count in animals from the groups treated with TBI, DR, or both, when compared to the Control group (Figures 2(b)-2(d)). These data clearly indicate that there is no significant alteration in peripheral blood hemogram in animals under DR compared to their counterparts without DR. On the other hand, TBI alone could induce significantly detrimental effects on the hematopoietic system measured as the persistent markedly lower white blood cell count in peripheral blood.

3.2.1. Micronucleus Frequency. Induction of micronuclei measured as MNF in PCEs (Figure 3(a)) and NCEs (Figure 3(b)) was used to evaluate acute genotoxicity at 1 month after TBI and late GI at 2 months after TBI. In general, TBI alone could significantly increase the MNF in both PCEs and NCEs, namely, for MNF in PCEs in the 2.0 Gy group; it was $2.10 \pm 0.33‰$ and $2.50 \pm 0.43‰$, respectively, at 1 and 2 months after TBI while in the Control group it was $0.51 \pm 0.08‰$ and $0.57 \pm 0.08‰$; and for MNF in NCEs in the 2.0 Gy group, it was $1.70 \pm 0.32‰$ and $1.80 \pm 0.33‰$, respectively, at 1 and 2 months after TBI while in the Control group it was $0.48 \pm 0.17‰$ and $0.52 \pm 0.18‰$. On the other hand, although DR alone did not markedly change the MNF in the nonirradiated animals in the Control group, namely, for MNF in PCEs in the DR group, it was $0.50 \pm 0.09‰$ and $0.53 \pm 0.09‰$, respectively, at 1 and 2 months; and for MNF in NCEs in the DR group, it was $0.49 \pm 0.19‰$ and $0.50 \pm 0.19‰$. DR had a significantly inhibitory effect on induction of micronuclei by TBI, showing

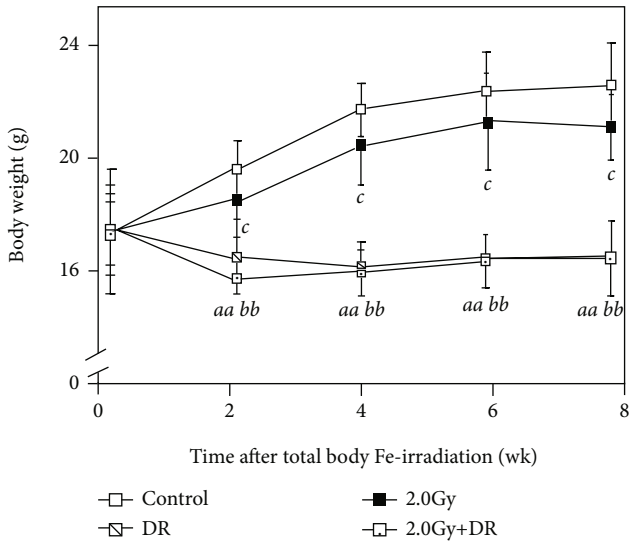

Figure 1: Effects of TBI and DR on body weight gain in mice. Body weight in grams (g) is presented as the mean ± SD. The solid line with open, solid, striped, and dotted boxes, respectively, stands for the Control group, the DR group, the 2.0 Gy group, and the 2.0 Gy + DR group. Letters *aa* and *bb* indicate statistically significant difference at $P < 0.01$ between the Control group and the 2.0 Gy group and between the DR group and the 2.0 Gy + DR group, respectively. Letter *c* stands for statistically significant difference at $P < 0.05$ between the Control group and the DR group.

significantly decreased MNF in both PCEs and NCEs in the animals of the 2.0 Gy + DR group (for MNF in PCEs, it was $1.50 \pm 0.51‰$ and $1.97 \pm 0.72‰$, respectively, at 1 and 2 months; and for MNF in NCEs, it was $1.10 \pm 0.34‰$ and $1.25 \pm 0.23‰$) when compared to that in the 2.0 Gy group. Results clearly demonstrate that postexposure DR could relieve genotoxicity and GI caused by TBI with high-LET iron particles.

3.2.2. Bone Marrow Proliferation. The percentage of PCEs to the sum of PCEs and NCEs, as an indicator for evaluating bone marrow cell proliferation condition, was assessed 1 and 2 months after TBI (Figure 3(c)). Proliferation in the animals after TBI (the 2.0 Gy group and the 2.0 Gy + DR group) was significantly inhibited manifesting as much lower percentages compared to that in the nonirradiated animals (the Control group and the DR group). On the other hand, all animals under DR regimen showed markedly decreased percentage when compared to their nonirradiated counterparts. Moreover, the percentages in the 2.0 Gy + DR group were significantly lower than that in the 2.0 Gy group 1 and 2 months after TBI. These findings indicate that either TBI or DR could decrease the proliferation of bone marrow cells, and concurrent exposure to both TBI and DR could further increase the inhibitory effect.

4. Discussion

Radiocarcinogenesis is one of the key concerns for medical, occupational, environmental, or accidental exposures to IR [47]. For example, exposure to high-LET IR during manned deep-space activities would increase unavoidably radiation health risk [12], and modern radiotherapy (RT) including high-precision hadrontherapy could control and cure efficiently cancers with high-LET IR while it still inevitably leads to increased mutation and secondary malignancy risk [11, 48]. Therefore, new methods for mitigating this adverse effect to limit cancer risk are urgently needed [11, 12]. GI is the earliest step and critical early event [1, 49–52], being central to carcinogenesis associating with cancer initiation and augmenting cancer progression [53–58]. It is the driving force responsible for radiocarcinogenesis [7–9]. In this work, we demonstrated that postexposure onset of DR could efficiently reduce acute genotoxicity and late GI measured as significantly decreased MNFs in PCEs and NCEs. Our findings suggested that DR could activate mechanisms consequently resulting in suppression of radiation-induced genotoxicity and GI.

Since the early work by Moreschi and McCay et al. [59, 60], the rapidly growing body of evidence on the effects from dietary intervention has shown that diet intervention has a great impact on health, pointing to a multitude of benefits affecting numerous physiological systems [61]. Diet intervention also elicits a variety of immediate and long-term physiological effects, in particular, beneficial effects on numerous diseases including cancer in experimental models [22]. Effects of DR depend on many factors including the restriction extent, dietary composition, and restriction onset timing. Mild DR (25% cut in diet) was considered adaptive and innocuous as DR at this level it was associated with increased longevity and decreased disease incidence in rodent models [62]. In a comprehensive study on the effects from various levels of food reduction on a wide range of toxicological parameters in rats, it also demonstrated that mild DR daily was dietary-optimized as a nutritionally appropriate and well-controlled animal model in conducting toxicity studies [63]. Based on a series of trials on the level of food reduction from 25% (mild DR) and 50% (moderate DR) to 75% (severe DR) of diet cut in the experimental conditions in our facilities, we also confirmed that mild DR was the dietary-optimized condition, and mild DR (25% cut in diet) was finally applied to the present study. Interestingly, in a series of investigations in rats and mice receiving DR, in the animals feed in amounts that limited the mean body weight to approximately 85% of the controls fed *ad libitum*, it was found that DR increased survival rates and decreased the incidences of chemical carcinogen-induced neoplasms and nonneoplastic lesions at a variety of sites [64]. In the present study, the extent of DR-induced body weight decrease was comparable to this work [64]. On the other hand, DR is effective on tumor initiation and more effective on tumor promotion phase [15, 65, 66]. In an analysis using a multistage carcinogenesis model [67] to the data obtained in a mouse lifespan study following postexposure onset of DR [36], it was shown that DR could offset both spontaneous and IR-induced carcinogenesis, and there is little or no interaction between the detrimental effects of IR and the beneficial effects of DR. DR could delay the onset of the tumors by overarchingly altering all the steps (i.e., decrease in the mutation rate) or a particular step necessary for

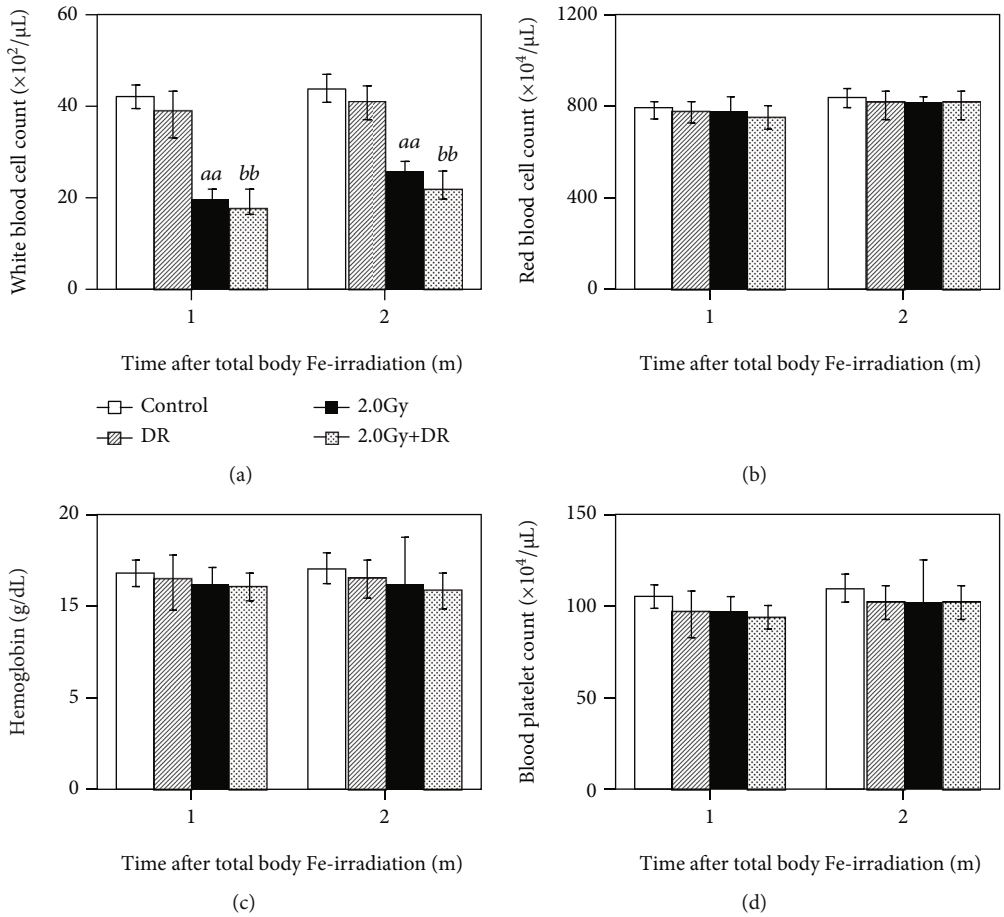

FIGURE 2: Effects of TBI and DR on peripheral blood hemogram in mice. (a) White blood cell count, (b) red blood cell count, (c) hemoglobin concentration, and (d) blood platelet count were measured 1 and 2 months after TBI. Cell count or hemoglobin concentration is presented as the mean ± SD. The open, solid, striped, and dotted bar stands for the Control group, the DR group, the 2.0 Gy Group, and the 2.0 Gy + DR group, respectively. Letters *aa* and *bb*, respectively, indicate statistically significant differences at $P < 0.01$ between the Control group and the 2.0 Gy group and between the DR group and the 2.0 Gy + DR group.

carcinogenesis [38]. In the present work, we confirmed that postexposure onset of DR could also efficiently reduce IR-induced GI measured as decreased MNF.

The mechanisms underlying suppression by DR of radiocarcinogenesis including GI investigated in the present work are still largely unknown. Increased resistance to oxidative stress and enhanced DNA repair are possible mechanisms. It is known that exposure to high-LET iron significantly increased the oxidative stress (i.e., reactive oxygen species (ROS)) in the irradiated animals [68, 69]. Dietary intervention shows potential health benefits in humans and animals [70] as one of the means to minimize health risk from exposure to IR via increasing endogenous antioxidative protection [71, 72]. Studies showed that DR could lead to the reduction of oxidative damage to macromolecules [73], modulation of oxidative DNA damage, and enhancement of DNA repair via affection of adrenal metabolism, insulin metabolism, and various aspects of gene expression [16, 74]. DR could also decrease IR-induced mutation frequencies via suppression of oxidative stress in a radiocarcinogenesis model in mice [39]. Through a process known as mitohormesis, a retrograde response, DR could increase formation of ROS within the mitochondria. This could cause an adaptive response that culminates in subsequently increased stress resistance and ultimately lead to a long-term reduction of oxidative stress [75]. DR could further activate expression of endogenous antioxidant genes to produce ROS-eliminating enzymes and increase activities of antioxidant enzymes including superoxide dismutase, catalase, glutathione peroxidase, and paraoxonase [76, 77]. DR could also decrease oxidative protein modification and sensitivity of membranes to lipid peroxidation in association with a reprogramming of the respiratory chain complexes and apoptosis-inducing factor content [78] in experimental animal models. In addition, reduction (25% cut) in caloric intake could rapidly reduce and then sustain oxidative stress in humans [79].

In addition to DR-induced resistance to oxidative stress, postexposure DR-induced decrease in IR-induced genotoxicity and GI may be through shifting metabolism to less cell differentiation and proliferation and enhanced elimination of abnormal cells [80, 81]. Increased cell proliferation is associated with GI [82]. DR could decrease circulating levels of growth factors, anabolic hormones, inflammatory cytokines, and oxidative stress markers associated with various

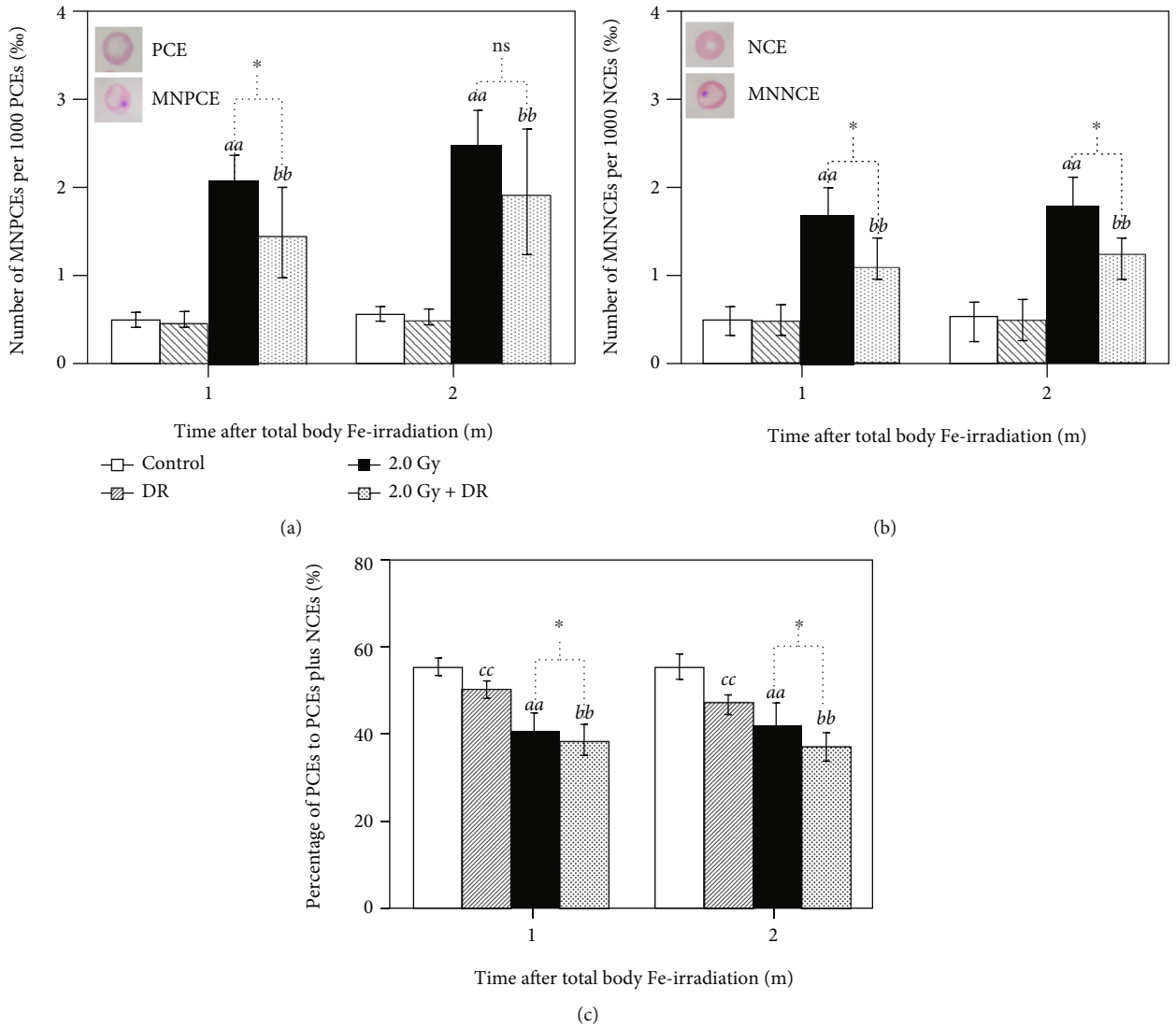

Figure 3: Effects of TBI and DR on induction of MNF and proliferation of bone marrow erythrocytes in the femur in mice. (a) The permillages (‰) of MNPCEs per 1000 PCEs and (b) MNNCEs per 1000 NCEs were used to measure MNF, and (c) the percentage (%) of PCEs to the sum of PCEs and NCEs as the indicator for proliferation. Letters *aa*, *bb*, and *cc*, respectively, indicate statistically significant difference at $P < 0.01$ between the Control group and the 2.0 Gy group, between the DR group and the 2.0 Gy + DR group, and between the Control group and the DR group. One asterisk (∗) stands for statistically significant difference at $P < 0.05$ between the 2.0 Gy group and the 2.0 Gy + DR group.

malignancies, exerting multiple suppressive effects on both target cells and microenvironments during carcinogenesis [83]. It is well known that dietary intervention was a regulator of stem cell behavior [84]. DR was able to restrict increase in hematopoietic stem and progenitor cells and formation of myeloid colony in mouse bone marrow [85]. Even a diet limited only in protein (4% cut by weight) for 3 weeks could markedly reduce hemopoietic stem cells in mice [86]. In the present work, our results clearly showed that DR could result in inhibition of erythrocytogenesis measured as decrease in the percentage of PCEs to the sum of PCEs and NCEs in the bone marrow in mice (Figure 3(c)). DR could also inhibit cell proliferation in spleen and thymus in mice [87]. Studies show that DR could induce memory T cell accumulation in bone marrow associating with enhanced protection against infections and tumors [88]. It was reported that calorie restriction (33% cut) could reduce cell proliferation in several tissues and cell populations including T cells within 2 weeks in mice that were of the same strain, sex, and age as used in the present work. This effect was potent and rapid and mediated anticarcinogenic effects [89]. It was also shown that moderate caloric restriction could contribute to slow down in aging and to prevent chronic diseases [90]. In murine models, studies showed that DR-induced delayed aging and retarded tumor development were attributed to induction of apoptosis to selectively eliminate preneoplastic and superfluous cells that negatively affected normal function and promote cell transformation [91]. Through metabolic energy modulation, DR could enhance autophagy [92].

There is a complex interplay among the diet, gastrointestinal microbiota, and health. One of the possible mechanisms underlying postexposure DR-induced mitigative effect on IR-induced genotoxicity and GI might be attributed to the DR-induced alterations in the mouse gastrointestinal microbiota. Diet is a key determinant of the microbiota diversity, composition, stability, activity, and function of gut. Gastrointestinal microbiota has a symbiotic relationship with the host and is involved in maintaining gastrointestinal homeostasis through its impact on nutrient metabolism, energy balance, gut barrier, inflammation, microenvironment, and immune and stress response [93–97]. The gastrointestinal microbiome plays a critical role in competitive pathogen exclusion and immune development. By influencing the immune system of the host, studies show that dietary intervention could change the composition or functions of the microbiota to confer health benefits including cancer prevention and treatment [93, 98–101]. Radiation exposure could disrupt the gut-brain axis [102]. On the other hand, diet contents and quantity could play a pivotal role in modifying susceptibility to IR exposure including both acute and late effects of radiation in animal models. As a therapeutic modality in various clinical contexts, gastrointestinal microbiota manipulation through dietary intervention is expected to maximize the response to treatment and minimize adverse effects by reducing radiation injury and improving the health in the treatment of accidental radiation exposure and restoration of human health from cancer RT [103–106].

Dietary and lifestyle factors are considered causes of cancer and targets for cancer prevention as well. As lifestyle and environmental factors could affect cancer initiation, promotion, and progression, radiocarcinogenesis could be preventable by intervention of lifestyle and environmental factors [83]. A healthy lifestyle (including but not limited to keeping a healthy diet and maintaining a healthy weight) is a simply efficient strategy for cancer prevention and reduction in cancer morbidity and mortality, and thus, dietary intervention should be given priority for cancer prevention [107–113], increasing resistance to chemotherapy and RT in normal cells and reducing certain side effects of cytotoxic therapy [114] and limiting tumor growth [115, 116]. We propose that a combination of DR and other cancer treatments (i.e., chemotherapy and RT) represents a potential strategy to increase the treatment efficacy and prevent IR risk in humans. In addition to the possible mechanisms discussed, there are still many questions to consider in further studies; for examples, how long does DR need to be imposed to be effective and what role does dietary composition play [117]? Further investigation is warranted to characterize the mitigative effects on IR-induced genotoxicity and GI by postexposure onset of DR and to explore the exact underlying mechanisms. Although challenges and remaining unknowns persist and need in-depth exploration, it is clear that multiple approaches can be applied simultaneously to obtain integrated results.

IR is widely used in a variety of fields such as applications in industry, agriculture, medicine, life science, and research. Simultaneously, IR also presents a potential health risk by causing health consequences including cancer. With the advances in hadrontherapy development and space exploration, humans now encounter increasing exposure to high-LET IR. Radiation protection is defined as the protection of people from harmful effects due to exposure to IR and the means for achieving this goal. Avoidance or reduction of exposure dose using the simple protective measures of time, distance and shielding is fundamental. Being different from the existing exposure mainly due to naturally occurring radioactive materials that exist in the environment and the planned exposure such as in occupational and therapeutical situations where radiation protection could be planned in advance, emergency exposure usually occurs in unexpected situations such as emergency nuclear events and thus requires urgent protective actions. Nowadays, research on radiation protection marks an exciting new era with novel endeavor and achievement of applications. The time comes to conceive a timely concept for radiation protection to further include multimodality treatments with multidisciplinary management to increase radioresistance and/or decrease radiosusceptibility, to prevent, mitigate, and treat radiation damage and reduce radiation health risk in both the individual and the group. A new concept "proactive radiation protection" has been proposed, which is conceived as vigorously implementing what we already know from transdisciplinary research in preventing radiation damage and reducing radiation health risk to proactively achieve radiation protection potential through medical intervention [118]. For example, cancer treatment will not be successfully accomplished devoid of multimodality treatments including proactive radiation protection. Cancer RT advanced in both methodology and biology is the chief nonsurgical method to control cancer while one of its major drawbacks is the development of secondary malignancies. To surmount this side effect, it needs to brace every nerve for a supreme effort. Multimodality treatments include not only therapeutic administration of radiation and pharmaceutical agents such as tissue-specific radiosensitizers and radioprotectors [11, 119–121] but also prospective application of gene therapy (i.e., to modulate target gene splicing or aberrant splicing isoforms) [122], induction of hormesis and adaptive response [123, 124], lifestyle intervention (including but not limited to such as dietary and nutritional interventions and administration of DR mimetic drugs) [114, 125, 126], psychiatric management [127], and other components such as public health issues. Among the treatments, dietary intervention as one of the adjuvant therapies is with a high acceptability and feasibility [128]. A big impact from DR on the health consequences of the cancer patient receiving RT is expected [129]. Postexposure onset of DR is within the scope of proactive radiation protection. Elucidation of the underlying mechanisms would be expected to connect to a pharmaceutical treatment, which would be easier to be emotionally acceptable and clinically practical.

5. Conclusion

Exposure of mice to TBI from high-LET iron particles caused a significant increase in MNF in bone marrow

erythrocytes. Postexposure DR alone did not markedly influence the MNF in the nonirradiated mice but induced a significant decrease in MNF in the exposed animals when compared to that exposed to TBI alone. Postexposure onset of DR could relieve the elevated MNF induced by TBI, which is expected as one of the proactive strategies to prevent radiocarcinogenesis and achieve maximum benefit for the cancer patients receiving RT and the exposed victims in nuclear accidents. Reduction in acute genotoxicity and late GI may be at least a part of the mechanisms underlying decreased radiocarcinogenesis by DR.

Abbreviations

DR: Dietary restriction
GI: Genomic instability
HIMAC: The Heavy Ion Medical Accelerator in Chiba
IR: Ionizing radiation
LET: Linear energy transfer
MNF: Micronucleus frequency
MNNCE: Micronucleated normochromatic erythrocyte
MNPCE: Micronucleated polychromatic erythrocyte
RT: Radiotherapy
SD: Standard deviation
TBI: Total body irradiation.

Data Availability

Data supporting the findings of the present study are available within the article.

Disclosure

An earlier version of this work was presented as a poster at The 63rd Annual Meeting of The Japanese Radiation Research Society, 2020.

Conflicts of Interest

The authors declare no conflict of interest with respect to the research, authorship, and publication of this paper.

Authors' Contributions

Bing Wang and Mitsuru Nenoi conceived and implemented the research. Bing Wang, Takanori Katsube, Kaoru Tanaka, and Masahiro Murakami performed the experiments. Bing Wang and Kaoru Tanaka processed the experimental data and performed the analysis. Bing Wang drafted the manuscript, Kaoru Tanaka and Masahiro Murakami provided critical feedback, Takanori Katsube and Mitsuru Nenoi helped shape the final version, and all authors approved the submitted version. Bing Wang and Takanori Katsube contributed equally to this work.

Acknowledgments

This work was partially supported by the Ministry of Education, Culture, Sports, Science and Technology Grant-in-Aid for Scientific Research on Innovative Areas, "Living in Space" (Grant numbers 15H05944 and 15H05935), and three Research Project Grants (numbers 14J286, 16J295, and 20J327) for Cooperative Research using HIMAC, Japan. The authors wish to thank Ms. Hiromi Arai, Mr. Sadao Hirobe, Ms. Mikiko Nakajima, Ms. Chianing Hsieh, and Ms. Yasuko Morimoto for their expert technical assistance and administrative support. All authors would like to express their profound gratitude to their families for the understanding and encouragement essential to successfully complete this work during the COVID-19 pandemic time. This article is dedicated to late Dr. Akihiro Shima, professor emeritus, The University of Tokyo, Japan, for his continual encouragement to carry out the mechanism study on radiation-induced biological effects.

References

[1] M. W. Schmitt, M. J. Prindle, and L. A. Loeb, "Implications of genetic heterogeneity in cancer," *Annals of the New York Academy of Sciences*, vol. 1267, no. 1, pp. 110–116, 2012.

[2] T. Sugimura, "Cancer prevention: past, present, future," *Mutation Research*, vol. 402, no. 1-2, pp. 7–14, 1998.

[3] T. Abbas, M. A. Keaton, and A. Dutta, "Genomic instability in cancer," *Cold Spring Harbor Perspectives in Biology*, vol. 5, no. 3, article a012914, 2013.

[4] P. A. Jeggo, L. H. Pearl, and A. M. Carr, "DNA repair, genome stability and cancer: a historical perspective," *Nature Reviews Cancer*, vol. 16, no. 1, pp. 35–42, 2016.

[5] J. J. Moon, A. Lu, and C. Moon, "Role of genomic instability in human carcinogenesis," *Experimental Biology and Medicine*, vol. 244, no. 3, pp. 227–240, 2019.

[6] O. Torres-Bugarín, E. Garcia-Arellano, K. Onel Salas-Cordero, and L. D. Molina-Noyola, "Micronuclei and nuclear abnormalities as bioindicators of gene instability vulnerability," *Austin Journal of Pathology & Laboratory Medicine*, vol. 6, no. 1, 2019.

[7] W. F. Morgan, J. P. Day, M. I. Kaplan, E. M. McGhee, and C. L. Limoli, "Genomic instability induced by ionizing radiation," *Radiation Research*, vol. 146, no. 3, pp. 247–258, 1996.

[8] C. L. Limoli, B. Ponnaiya, J. J. Corcoran et al., "Genomic instability induced by high and low let ionizing radiation," *Advances in Space Research*, vol. 25, no. 10, pp. 2107–2117, 2000.

[9] L. E. Smith, S. Nagar, G. J. Kim, and W. F. Morgan, "Radiation-induced genomic instability: radiation quality and dose response," *Health Physics*, vol. 85, no. 1, pp. 23–29, 2003.

[10] L. Huang, A. R. Snyder, and W. F. Morgan, "Radiation-induced genomic instability and its implications for radiation carcinogenesis," *Oncogene*, vol. 22, no. 37, pp. 5848–5854, 2003.

[11] G. Mohan, T. P. Ayisha Hamna, A. J. Jijo, K. M. Saradha Devi, A. Narayanasamy, and B. Vellingiri, "Recent advances in radiotherapy and its associated side effects in cancer - a review," *The Journal of Basic and Applied Zoology*, vol. 80, no. 1, p. 14, 2019.

[12] S. Furukawa, A. Nagamatsu, M. Nenoi et al., "Space Radiation Biology for "Living in Space"," *BioMed Research International*, vol. 2020, Article ID 4703286, 25 pages, 2020.

[13] G. De Pergola and F. Silvestris, "Obesity as a major risk factor for cancer," *Journal of Obesity*, vol. 2013, Article ID 291546, 11 pages, 2013.

[14] J. Kerr, C. Anderson, and S. M. Lippman, "Physical activity, sedentary behaviour, diet, and cancer: an update and emerging new evidence," *The Lancet Oncology*, vol. 18, no. 8, pp. e457–e471, 2017.

[15] D. Kritchevsky and D. M. Klurfeld, "Influence of caloric intake on experimental carcinogenesis: a review," *Advances in Experimental Medicine and Biology*, vol. 206, pp. 55–68, 1986.

[16] D. Kritchevsky, "Caloric restriction and experimental carcinogenesis," *Hybridoma and Hybridomics*, vol. 21, no. 2, pp. 147–151, 2002.

[17] R. B. McDonald and J. J. Ramsey, "Honoring Clive McCay and 75 years of calorie restriction research," *The Journal of Nutrition*, vol. 140, no. 7, pp. 1205–1210, 2010.

[18] A. Tannenbaum and H. Silverstone, "The influence of the degree of caloric restriction on the formation of skin tumors and hepatomas in mice," *Cancer Research*, vol. 9, no. 12, pp. 724–727, 1949.

[19] M. J. Tucker, "The effect of long-term food restriction on tumours in rodents," *International Journal of Cancer*, vol. 23, no. 6, pp. 803–807, 1979.

[20] J. R. Speakman, S. E. Mitchell, and M. Mazidi, "Calories or protein? The effect of dietary restriction on lifespan in rodents is explained by calories alone," *Experimental Gerontology*, vol. 86, pp. 28–38, 2016.

[21] R. J. Klement and M. K. Fink, "Dietary and pharmacological modification of the insulin/IGF-1 system: exploiting the full repertoire against cancer," *Oncogene*, vol. 5, no. 2, article e193, 2016.

[22] M. Lv, X. Zhu, H. Wang, F. Wang, and W. Guan, "Roles of caloric restriction, ketogenic diet and intermittent fasting during initiation, progression and metastasis of cancer in animal models: a systematic review and meta-analysis," *PLoS One*, vol. 9, no. 12, article e115147, 2014.

[23] I. Sivertsen and W. H. Hastings, "A preliminary report on the influence of food and function on the incidence of mammary gland tumor in "A" stock albino mice," *Minnesota Medicine*, vol. 21, pp. 873–875, 1938.

[24] L. Fontana, L. Partridge, and V. D. Longo, "Extending healthy life span—from yeast to humans," *Science*, vol. 328, no. 5976, pp. 321–326, 2010.

[25] S. D. Hursting, S. M. Dunlap, N. A. Ford, M. J. Hursting, and L. M. Lashinger, "Calorie restriction and cancer prevention: a mechanistic perspective," *Cancer & Metabolism*, vol. 1, no. 1, p. 10, 2013.

[26] A. Nencioni, I. Caffa, S. Cortellino, and V. D. Longo, "Fasting and cancer: molecular mechanisms and clinical application," *Nature Reviews Cancer*, vol. 18, no. 11, pp. 707–719, 2018.

[27] L. Gross and Y. Dreyfuss, "Reduction in the incidence of radiation-induced tumors in rats after restriction of food intake," *Proceedings of the National Academy of Sciences of the United States of America*, vol. 81, no. 23, pp. 7596–7598, 1984.

[28] L. Gross and Y. Dreyfuss, "Inhibition of the development of radiation-induced leukemia in mice by reduction of food intake," *Proceedings of the National Academy of Sciences of the United States of America*, vol. 83, no. 20, pp. 7928–7931, 1986.

[29] L. Gross, "Inhibition of the development of tumors or leukemia in mice and rats after reduction of food intake. Possible implications for humans," *Cancer*, vol. 62, no. 8, pp. 1463–1465, 1988.

[30] M. de la Cruz Bonilla, "Fasting reduces intestinal radiotoxicity enabling dose-escalated radiotherapy for pancreatic cancer," *The University of Texas MD Anderson Cancer Center UTHealth Graduate School of Biomedical Sciences Dissertations and Theses*, vol. 969, 2019.

[31] B. Wang, K. Tanaka, T. Katsube et al., "Reduced high-dose radiation-induced residual genotoxic damage by induction of radioadaptive response and prophylactic mild dietary restriction in mice," *Dose Response*, vol. 19, no. 1, 2021.

[32] K. Yoshida, T. Inoue, Y. Hirabayashi, T. Matsumura, K. Nemoto, and T. Sado, "Radiation-induced myeloid leukemia in mice under calorie restriction," *Leukemia*, vol. 11, pp. 410–412, 1997.

[33] K. Yoshida, Y. Hirabayashi, and T. Inoue, "Calorie restriction reduces the incidence of radiation-induced myeloid leukaemia," *IARC Scientific Publications*, vol. 156, pp. 553–555, 2002.

[34] K. Yoshida, Y. Hirabayashi, F. Watanabe, T. Sado, and T. Inoue, "Caloric restriction prevents radiation-induced myeloid leukemia in C3H/HeMs mice and inversely increases incidence of tumor-free death: implications in changes in number of hemopoietic progenitor cells," *Experimental Hematology*, vol. 34, no. 3, pp. 274–283, 2006.

[35] K. Yoshida, T. Inoue, K. Nojima, Y. Hirabayashi, and T. Sado, "Calorie restriction reduces the incidence of myeloid leukemia induced by a single whole-body radiation in C3H/He mice," *Proceedings of the National Academy of Sciences of the United States of America*, vol. 94, no. 6, pp. 2615–2619, 1997.

[36] Y. Shang, S. Kakinuma, K. Yamauchi et al., "Cancer prevention by adult-onset calorie restriction after infant exposure to ionizing radiation in B6C3F1 male mice," *International Journal of Cancer*, vol. 135, no. 5, pp. 1038–1047, 2014.

[37] T. Morioka, S. Yamazaki, H. Yanagihara, M. Sunaoshi, M. Kaminishi, and S. Kakinuma, "Calorie restriction suppresses the progression of radiation-induced intestinal tumours in C3B6F1ApcMin/+Mice," *Anticancer Research*, vol. 41, no. 3, pp. 1365–1375, 2021.

[38] S. Tani, B. J. Blyth, Y. Shang, T. Morioka, S. Kakinuma, and Y. Shimada, "A multi-stage carcinogenesis model to investigate caloric restriction as a potential tool for post-irradiation mitigation of cancer risk," *Journal of Cancer Prevention*, vol. 21, no. 2, pp. 115–120, 2016.

[39] S. Kakomi, T. Nakayama, Y. Shang et al., "The effects of short-term calorie restriction on mutations in the spleen cells of infant-irradiated mice," *Journal of Radiation Research*, vol. 61, no. 2, pp. 187–196, 2020.

[40] M. Fenech, M. Kirsch-Volders, A. T. Natarajan et al., "Molecular mechanisms of micronucleus, nucleoplasmic bridge and nuclear bud formation in mammalian and human cells," *Mutagenesis*, vol. 26, no. 1, pp. 125–132, 2011.

[41] A. Imle, B. Polzer, S. Alexander, C. A. Klein, and P. Friedl, "Genomic instability of micronucleated cells revealed by single-cell comparative genomic hybridization," *Cytometry Part A*, vol. 75, no. 7, pp. 562–568, 2009.

[42] S. Burgaz, E. Coskun, G. C. Demircigil et al., "Micronucleus frequencies in lymphocytes and buccal epithelial cells from patients having head and neck cancer and their first-degree relatives," *Mutagenesis*, vol. 26, no. 2, pp. 351–356, 2011.

[43] W. Jdey, S. Thierry, T. Popova, S. Marc-Henri, and M. Dutreix, "Micronuclei frequency in tumors is a predictive biomarker for genetic instability and sensitivity to the DNA

repair inhibitor AsiDNA," *Cancer Research*, vol. 77, no. 16, pp. 4207–4216, 2017.

[44] A. Podrimaj-Bytyqi, A. Borovečki, Q. Selimi, S. Manxhuka-Kerliu, G. Gashi, and I. R. Elezaj, "The frequencies of micronuclei, nucleoplasmic bridges and nuclear buds as biomarkers of genomic instability in patients with urothelial cell carcinoma," *Scientific Reports*, vol. 8, no. 1, p. 17873, 2018.

[45] C. J. Ye, Z. Sharpe, S. Alemara et al., "Micronuclei and genome chaos: changing the system inheritance," *Genes*, vol. 10, no. 5, p. 366, 2019.

[46] B. Laffon, S. Bonassi, S. Costa, and V. Valdiglesias, "Genomic instability as a main driving factor of unsuccessful ageing: potential for translating the use of micronuclei into clinical practice," *Mutation Research*, vol. 787, article 108359, 2021.

[47] M. Sowa, B. J. Arthurs, B. J. Estes, and W. F. Morgan, "Effects of ionizing radiation on cellular structures, induced instability and carcinogenesis," *Experientia Supplementum*, vol. 96, pp. 293–301, 2006.

[48] E. K. Balcer-Kubiczek and J. G. Eley, "Secondary malignancies in the era of high-precision radiation therapy," *Critical Review in Oncogenesis*, vol. 23, no. 1-2, pp. 93–112, 2018.

[49] L. Sabatier, J. Lebeau, and B. Dutrillaux, "Radiation-induced carcinogenesis: individual sensitivity and genomic instability," *Radiation and Environmental Biophysics*, vol. 34, no. 4, pp. 229–232, 1995.

[50] R. L. Ullrich and B. Ponnaiya, "Radiation-induced instability and its relation to radiation carcinogenesis," *International Journal of Radiation Biology*, vol. 74, no. 6, pp. 747–754, 1998.

[51] G. S. Charames and B. Bapat, "Genomic instability and cancer," *Current Molecular Medicine*, vol. 3, no. 7, pp. 589–596, 2003.

[52] K. Suzuki, M. Ojima, S. Kodama, and M. Watanabe, "Radiation-induced DNA damage and delayed induced genomic instability," *Oncogene*, vol. 22, no. 45, pp. 6988–6993, 2003.

[53] N. L. Komarova, "Genomic instability in cancer: biological and mathematical approaches," *Cell Cycle*, vol. 3, no. 8, pp. 1081–1085, 2004.

[54] S. Negrini, V. G. Gorgoulis, and T. D. Halazonetis, "Genomic instability – an evolving hallmark of cancer," *Nature Reviews Molecular Cell Biology*, vol. 11, no. 3, pp. 220–228, 2010.

[55] E. J. Fox, M. J. Prindle, and L. A. Loeb, "Do mutator mutations fuel tumorigenesis?," *Cancer Metastasis Reviews*, vol. 32, no. 3&4, pp. 353–361, 2013.

[56] Y. Yao and W. Dai, "Genomic instability and cancer," *Journal of Carcinogenesis & Mutagenesis*, vol. 5, no. 2, 2014.

[57] L. R. Ferguson, H. Chen, A. R. Collins et al., "Genomic instability in human cancer: molecular insights and opportunities for therapeutic attack and prevention through diet and nutrition," *Seminars in Cancer Biology*, vol. 35, Supplement, pp. S5–S24, 2015.

[58] S. F. Bakhoum and D. A. Landau, "Chromosomal instability as a driver of tumor heterogeneity and evolution," *Cold Spring Harbor Perspectives in Medicine*, vol. 7, no. 6, article a029611, 2017.

[59] C. Moreschi, "Beziehung zwischen ernahrung and tumorwachstum," *ZImmunitatsforsch*, vol. 2, pp. 651–675, 1909.

[60] C. M. McCay, M. F. Crowell, and L. A. Maynard, "The effect of retarded growth upon the length of life span and upon the ultimate body size," *The Journal of Nutrition*, vol. 10, no. 1, pp. 63–79, 1935.

[61] S. Valayer, D. Kim, A. Fogtman et al., "The potential of fasting and caloric restriction to mitigate radiation damage - a systematic review," *Frontiers in Nutrition*, vol. 7, 2020.

[62] S. Levin, D. Semler, and Z. Ruben, "Effects of two weeks of feed restriction on some common toxicologic parameters in Sprague-Dawley rats," *Toxicological Pathology*, vol. 21, no. 1, pp. 1–14, 1993.

[63] T. Moriyama, S. Tsujioka, T. Ohira et al., "Effects of reduced food intake on toxicity study parameters in rats," *The Journal of Toxicological Sciences*, vol. 33, no. 5, pp. 537–547, 2008.

[64] National Toxicology Program, "Effect of dietary restriction on toxicology and carcinogenesis studies in F344/N rats and B6C3F1 mice," *National Toxicology Program Technical Repots Series*, vol. 461, pp. 1–414, 1997.

[65] D. F. Birt, J. C. Pelling, L. T. White, K. Dimitroff, and T. Barnett, "Influence of diet and calorie restriction on the initiation and promotion of skin carcinogenesis in the SENCAR mouse model," *Cancer Research*, vol. 51, no. 7, pp. 1851–1854, 1991.

[66] D. F. Birt, H. J. Pinch, T. Barnett, A. Phan, and K. Dimitroff, "Inhibition of skin tumor promotion by restriction of fat and carbohydrate calories in SENCAR mice," *Cancer Research*, vol. 53, no. 1, pp. 27–31, 1993.

[67] P. Armitage and R. Doll, "The age distribution of cancer and a multi-stage theory of carcinogenesis," *British Journal of Cancer*, vol. 8, no. 1, pp. 1–12, 1954.

[68] J. Guan, X. S. Wan, Z. Zhou et al., "Effects of dietary supplements on space radiation-induced oxidative stress in Sprague-Dawley rats," *Radiation Research*, vol. 162, no. 5, pp. 572–579, 2004.

[69] M. Li, G. Gonon, M. Buonanno et al., "Health risks of space exploration: targeted and nontargeted oxidative injury by high-charge and high-energy particles," *Antioxidants & Redox Signaling*, vol. 20, no. 9, pp. 1501–1523, 2014.

[70] J. F. Trepanowski, R. E. Canale, K. E. Marshall, M. M. Kabir, and R. J. Bloomer, "Impact of caloric and dietary restriction regimens on markers of health and longevity in humans and animals: a summary of available findings," *Nutrition Journal*, vol. 10, no. 1, p. 107, 2011.

[71] A. R. Kennedy, "Biological effects of space radiation and development of effective countermeasures," *Life Sciences in Space Research*, vol. 1, pp. 10–43, 2014.

[72] B. Poljsak, "Strategies for reducing or preventing the generation of oxidative stress," *Oxidative Medicine and Cellular Longevity*, vol. 2011, Article ID 194586, 15 pages, 2011.

[73] M. E. Walsh, Y. Shi, and H. Van Remmen, "The effects of dietary restriction on oxidative stress in rodents," *Free Radical Biology & Medicine*, vol. 66, pp. 88–99, 2014.

[74] T. W. Rhoads, M. S. Burhans, V. B. Chen et al., "Caloric restriction engages hepatic RNA processing mechanisms in rhesus monkeys," *Cell Metabolism*, vol. 27, no. 3, pp. 677–688.e5, 2018.

[75] M. Ristow and K. Zarse, "How increased oxidative stress promotes longevity and metabolic health: the concept of mitochondrial hormesis (mitohormesis)," *Experimental Gerontology*, vol. 45, no. 6, pp. 410–418, 2010.

[76] J. Skrha, "Chapter 8 Effect of caloric restriction on oxidative markers," *Advances in Clinical Chemistry*, vol. 47, pp. 223–247, 2009.

[77] S. Kasai, S. Shimizu, Y. Tatara, J. Mimura, and K. Itoh, "Regulation of Nrf2 by mitochondrial reactive oxygen species in

physiology and pathology," *Biomolecules*, vol. 10, no. 2, p. 320, 2020.

[78] J. Gómez, P. Caro, A. Naudí, M. Portero-Otin, R. Pamplona, and G. Barja, "Effect of 8.5% and 25% caloric restriction on mitochondrial free radical production and oxidative stress in rat liver," *Biogerontology*, vol. 8, no. 5, pp. 555–566, 2007.

[79] M. S. Buchowski, N. Hongu, S. Acra, L. Wang, J. Warolin, and L. J. Roberts II, "Effect of modest caloric restriction on oxidative stress in women, a randomized trial," *PLoS One*, vol. 7, no. 10, article e47079, 2012.

[80] Y. Zhu, Y. Yan, D. R. Gius, and A. Vassilopoulos, "Metabolic regulation of sirtuins upon fasting and the implication for cancer," *Current Opinion in Oncology*, vol. 25, no. 6, pp. 630–636, 2013.

[81] S. de Groot, H. Pijl, J. J. M. van der Hoeven, and J. R. Kroep, "Effects of short-term fasting on cancer treatment," *Journal of Experimental & Clinical Cancer Research*, vol. 38, no. 1, p. 209, 2019.

[82] H. Stopper, E. Schmitt, C. Gregor, S. O. Mueller, and W. H. Fischer, "Increased cell proliferation is associated with genomic instability: elevated micronuclei frequencies in estradiol-treated human ovarian cancer cells," *Mutagenesis*, vol. 18, no. 3, pp. 243–247, 2003.

[83] V. D. Longo and L. Fontana, "Calorie restriction and cancer prevention: metabolic and molecular mechanisms," *Trends in Pharmacological Sciences*, vol. 31, no. 2, pp. 89–98, 2010.

[84] J. S. S. Novak, S. C. Baksh, and E. Fuchs, "Dietary interventions as regulators of stem cell behavior in homeostasis and disease," *Genes & Development*, vol. 35, no. 3-4, pp. 199–211, 2021.

[85] N. Al-Ajmi, G. Saretzki, C. Miles, and I. Spyridopoulos, "Dietary restriction ameliorates haematopoietic ageing independent of telomerase, whilst lack of telomerase and short telomeres exacerbates the ageing phenotype," *Experimental Gerontology*, vol. 58, pp. 113–119, 2014.

[86] R. G. Bell, L. A. Hazell, and J. W. Sheridan, "The influence of dietary protein deficiency on haemopoietic cells in the mouse," *Cell and Tissue Kinetics*, vol. 9, no. 4, pp. 305–311, 1976.

[87] M. H. Lu, W. G. Hinson, A. Turturro, W. G. Sheldon, and R. W. Hart, "Cell proliferation by cell cycle analysis in young and old dietary restricted mice," *Mechanisms of Ageing and Development*, vol. 68, no. 1–3, pp. 151–162, 1993.

[88] N. Collins, S.-J. Han, M. Enamorado et al., "The bone marrow protects and optimizes immunological memory during dietary restriction," *Cell*, vol. 178, no. 5, pp. 1088–1101.e15, 2019.

[89] E. A. Hsieh, C. M. Chai, and M. K. Hellerstein, "Effects of caloric restriction on cell proliferation in several tissues in mice: role of intermittent feeding," *American Journal of Physiology-Endocrinology and Metabolism*, vol. 288, no. 5, pp. E965–E972, 2005.

[90] N. Kozak and M. Krośniak, "The influence of dietary restrictions and malnutrition on morphological construction of bone marrow," *International Journal of Food Sciences and Nutrition*, vol. 1, no. 1, p. 1001, 2019.

[91] S. J. James, L. Muskhelishvili, D. W. Gaylor, A. Turturro, and R. Hart, "Upregulation of apoptosis with dietary restriction: implications for carcinogenesis and aging," *Environmental Health Perspectives*, vol. 106, Supplement 1, pp. 307–312, 1998.

[92] A. J. Cozzo, M. F. Coleman, J. B. Pearce, A. J. Pfeil, S. K. Etigunta, and S. D. Hursting, "Dietary energy modulation and autophagy: exploiting metabolic vulnerabilities to starve cancer," *Frontiers in Cell and Development Biology*, vol. 8, article 590192, 2020.

[93] S. E. Power, P. W. O'Toole, C. Stanton, R. P. Ross, and G. F. Fitzgerald, "Intestinal microbiota, diet and health," *The British Journal of Nutrition*, vol. 111, no. 3, pp. 387–402, 2014.

[94] C. L. Boulangé, A. L. Neves, J. Chilloux, J. K. Nicholson, and M. E. Dumas, "Impact of the gut microbiota on inflammation, obesity, and metabolic disease," *Genome Medicine*, vol. 8, no. 1, p. 42, 2016.

[95] C. N. Heiss and L. E. Olofsson, "Gut microbiota-dependent modulation of energy metabolism," *Journal of Innate Immunity*, vol. 10, no. 3, pp. 163–171, 2018.

[96] D. Lettieri-Barbato and K. Aquilano, "Pushing the limits of cancer therapy: the nutrient game," *Frontiers in Oncology*, vol. 8, p. 148, 2018.

[97] P. C. Barko, M. A. McMichael, K. S. Swanson, and D. A. Williams, "The gastrointestinal microbiome: a review," *Journal of Veterinary Internal Medicine*, vol. 32, no. 1, pp. 9–25, 2018.

[98] N. Zmora, J. Suez, and E. Elinav, "You are what you eat: diet, health and the gut microbiota," *Nature Reviews Gastroenterology & Hepatology*, vol. 16, no. 1, pp. 35–56, 2019.

[99] R. J. Klement and V. Pazienza, "Impact of different types of diet on gut microbiota profiles and cancer prevention and treatment," *Medicina (Kaunas, Lithuania)*, vol. 55, no. 4, p. 84, 2019.

[100] E. Rinninella, M. Cintoni, P. Raoul et al., "Gut microbiota during dietary restrictions: new insights in non-communicable diseases," *Microorganisms*, vol. 8, no. 8, p. 1140, 2020.

[101] J. Wu, K. Wang, X. Wang, Y. Pang, and C. Jiang, "The role of the gut microbiome and its metabolites in metabolic diseases," *Protein & Cell*, vol. 12, no. 5, pp. 360–373, 2021.

[102] C. B. Jones, C. M. Davis, and K. S. Sfanos, "The potential effects of radiation on the gut-brain axis," *Radiation Research*, vol. 193, no. 3, pp. 209–222, 2020.

[103] E. R. Leeming, A. J. Johnson, T. D. Spector, and C. I. Le Roy, "Effect of diet on the gut microbiota: rethinking intervention duration," *Nutrients*, vol. 11, no. 12, p. 2862, 2019.

[104] M. Tonneau, A. Elkrief, D. Pasquier et al., "The role of the gut microbiome on radiation therapy efficacy and gastrointestinal complications: a systematic review," *Radiotherapy and Oncology*, vol. 156, pp. 1–9, 2021.

[105] A. Mao, C. Sun, T. Katsube, and B. Wang, "A minireview on gastrointestinal microbiota and radiosusceptibility," *Dose Response*, vol. 18, no. 4, 2020.

[106] J. Liu, C. Liu, and J. Yue, "Radiotherapy and the gut microbiome: facts and fiction," *Radiation Oncology*, vol. 16, no. 1, 2021.

[107] G. A. Colditz, K. Y. Wolin, and S. Gehlert, "Applying what we know to accelerate cancer prevention," *Science Translational Medicine*, vol. 4, no. 127, 2012.

[108] V. A. Katzke, R. Kaaks, and T. Kühn, "Lifestyle and cancer risk," *Cancer Journal*, vol. 21, no. 2, pp. 104–110, 2015.

[109] K. Basen-Engquist, P. Brown, A. M. Coletta, M. Savage, K. C. Maresso, and E. Hawk, *22- Lifestyle and Cancer Prevention*, J. E. Niederhuber, J. O. Armitage, M. B. Kastan, J. H. Doroshow, and J. E. Tepper, Eds., in Abeloff's Clinical Oncology, Elsevier, Sixth Edition edition, 2020.

[110] Y.-B. Zhang, X.-F. Pan, J. Chen et al., "Combined lifestyle factors, incident cancer, and cancer mortality: a systematic review and meta-analysis of prospective cohort studies," *British Journal of Cancer*, vol. 122, no. 7, pp. 1085–1093, 2020.

[111] S. Brandhorst and V. D. Longo, "Fasting and caloric restriction in cancer prevention and treatment," *Recent Results in Cancer Research*, vol. 207, pp. 241–266, 2016.

[112] M. C. L. Phillips, "Fasting as a therapy in neurological disease," *Nutrients*, vol. 11, no. 10, p. 2501, 2019.

[113] M. V. Deligiorgi, C. Liapi, and D. T. Trafalis, "How far are we from prescribing fasting as anticancer medicine?," *International Journal of Molecular Sciences*, vol. 21, no. 23, p. 9175, 2020.

[114] C. H. O'Flanagan, L. A. Smith, S. B. McDonell, and S. D. Hursting, "When less may be more: calorie restriction and response to cancer therapy," *BMC Medicine*, vol. 15, no. 1, p. 106, 2017.

[115] E. C. Woolf, N. Syed, and A. C. Scheck, "Tumor metabolism, the ketogenic diet and β-hydroxybutyrate: novel approaches to adjuvant brain tumor therapy," *Frontiers in Molecular Neuroscience*, vol. 9, p. 122, 2016.

[116] E. Shingler, R. Perry, A. Mitchell et al., "Dietary restriction during the treatment of cancer: results of a systematic scoping review," *BMC Cancer*, vol. 19, no. 1, p. 811, 2019.

[117] D. K. Ingram and R. de Cabo, "Calorie restriction in rodents: caveats to consider," *Ageing Research Reviews*, vol. 39, pp. 15–28, 2017.

[118] A. Morita, *On Proactive Radiation Protection*, 2020, https://otsucle.jp/cf/project/2904.html.

[119] G. van Niekerk, S. M. Hattingh, and A.-M. Engelbrecht, "Enhanced therapeutic efficacy in cancer patients by short-term fasting: the autophagy connection," *Frontiers in Oncology*, vol. 6, 2016.

[120] F. Mohd Saaya, T. Katsube, Y. Xie, K. Tanaka, K. Fujita, and B. Wang, "Research and development of radioprotective agents: a mini-review," *International Journal of Radiology*, vol. 4, no. 2, pp. 128–138, 2017.

[121] S. Ochi, Y. Nishiyama, and A. Morita, "Development of p53-targeting drugs that increase radioresistance in normal tissues," *The Journal of Medical Investigation*, vol. 66, no. 3.4, pp. 219–223, 2019.

[122] C. Di, Q. Z. Syafrizayanti, Y. Chen et al., "Function, clinical application, and strategies of pre-mRNA splicing in cancer," *Cell Death & Differentiation*, vol. 26, no. 7, pp. 1181–1194, 2019.

[123] J. Cui, G. Yang, Z. Pan et al., "Hormetic response to low-dose radiation: focus on the immune system and its clinical implications," *International Journal of Molecular Sciences*, vol. 18, no. 2, p. 280, 2017.

[124] M. Nenoi, B. Wang, and G. Vares, "In vivo radioadaptive response," *Human and Experimental Toxicology*, vol. 34, no. 3, pp. 272–283, 2015.

[125] C. Hertel, A. Harandi, C. P. Connery, and D. Papadopoulos, "Nutritional intervention in high-risk patients receiving radiation for a broad spectrum of tumor types," *Journal of Clinical Oncology*, vol. 35, 8_suppl, pp. 203–203, 2017.

[126] C. M. Wright, A. A. Shastri, E. Bongiorno, A. Palagani, U. Rodeck, and N. L. Simone, "Is host metabolism the missing link to improving cancer outcomes?," *Cancers*, vol. 12, no. 9, p. 2338, 2020.

[127] B. Wang, T. Katsube, N. Begum, and M. Nenoi, "Revisiting the health effects of psychological stress—its influence on susceptibility to ionizing radiation: a mini-review," *Journal of Radiation Research*, vol. 57, no. 4, pp. 325–335, 2016.

[128] A. Gray, B. N. Dang, T. B. Moore, R. Clemens, and P. Pressman, "A review of nutrition and dietary interventions in oncology," *SAGE Open Medicine*, vol. 8, article 205031212092687, 2020.

[129] R. J. Klement and C. E. Champ, "Calories, carbohydrates, and cancer therapy with radiation: exploiting the five R's through dietary manipulation," *Cancer Metastasis Reviews*, vol. 33, no. 1, pp. 217–229, 2014.

Hindawi
BioMed Research International
Volume 2021, Article ID 6840642, 12 pages
https://doi.org/10.1155/2021/6840642

Research Article

Downregulation of Rap1GAP Expression Activates the TGF-β/Smad3 Pathway to Inhibit the Expression of Sodium/Iodine Transporter in Papillary Thyroid Carcinoma Cells

Zheng Yan,[1] Wang Yangyanqiu,[2] Han Shuwen,[3] Mao Jing,[2] Liao Haihong,[3] Chen Gong,[4] Jin Yin,[5] Zhou Qing,[6] and Gao Weili[7]

[1]*Department of Pathology, Affiliated Huzhou Hospital Zhejiang University, Affiliated Central Hospital Huzhou University, No. 1558, Sanhuan North Road, Wuxing District, Huzhou, Zhejiang Province, China 313000*
[2]*Graduate of Affiliated Huzhou Hospital Zhejiang University, Affiliated Central Hospital HuZhou University, No. 1558, Sanhuan North Road, Wuxing District, Huzhou, Zhejiang Province, China 313000*
[3]*Department of Oncology, Affiliated Huzhou Hospital Zhejiang University, Affiliated Central Hospital Huzhou University, No. 1558, Sanhuan North Road, Wuxing District, Huzhou, Zhejiang Province, China*
[4]*Department of Laboratory Medicine, Huzhou Central Hospital, Affiliated Central Hospital HuZhou University, No. 1558, Sanhuan North Road, Wuxing District, Huzhou, Zhejiang Province, China 313000*
[5]*Department of Nursing, Huzhou Central Hospital, Affiliated Central Hospital Huzhou University, No. 1558, Sanhuan North Road, Wuxing District, Huzhou, Zhejiang Province, China 313000*
[6]*Department of Thyroid Surgery, Huzhou Central Hospital, Affiliated Central Hospital Huzhou University, No. 1558, Sanhuan North Road, Wuxing District, Huzhou, Zhejiang Province, China 313000*
[7]*Undergraduate School of Clinic Medicine, Huzhou University, No. 1 Bachelor Road, Huzhou, Zhejiang Province, China 313000*

Correspondence should be addressed to Gao Weili; gaoweili2019@163.com

Received 29 July 2021; Revised 19 October 2021; Accepted 22 October 2021; Published 18 November 2021

Academic Editor: Qiang Liu

Objective. Rap1GAP is considered a tumor suppressor gene, but its regulatory mechanism in papillary thyroid cancer (PTC) has not been clearly elucidated. The aim of this study was to explore whether the regulation between Rap1GAP and sodium/iodine transporter (NIS) in tumorigenesis of PTC is mediated by TGF-β1. *Methods*. Western blotting (WB) and quantitative reverse-transcription polymerase chain reaction were performed to analyze the relationships between TGF-β1 concentration and NIS expression. After transfecting BCPAP cells with siRNAs, the Rap1GAP interference model was successfully established. Then, the expression and nuclear localization of TGF-β1 and pathway-related proteins were detected. Flow cytometry was applied to analyze cell apoptosis and cycle. WB was performed to detect apoptotic-related proteins. Wound healing and transwell assays were used to measure cell migration and invasion. EDU was performed to detect cell proliferative activity. *Results*. The results suggested that TGF-β1 could significantly inhibit the expression of NIS in both mRNA and protein levels. In BCPAP cells transfected with siRNA-Rap1GAP, the expression levels of TGF-β1, Foxp3, and p-Smad3 were significantly increased. By applying immunofluorescence assay, the nuclear localizations of TβR-1 and p-Smad3 were found to be activated. Moreover, anti-TGF-β1 can reverse the decrease in NIS expression caused by downregulation of Rap1GAP. Additionally, the knockdown of Rap1GAP could alter the cell apoptosis, cycle, migration, invasion, and proliferation of BCPAP. *Conclusion*. The downregulation of Rap1GAP expression can activate the TGF-β/Smad3 pathway to inhibit NIS expression and alter the tumor cell functions of PTC.

1. Introduction

Papillary thyroid cancer (PTC) is the most common histological type of differentiated thyroid malignancies, accounting for about 85% of all pathologic types [1, 2]. The extensive application of ultrasound screening and ultrasound-guided fine needle biopsy has promoted the detection and diagnosis of PTC [3, 4]. Currently, treatments for PTC include surgery, thyroid hormone suppression, iodine-131 therapy, and adjuvant radiation therapy [5]. Although PTC is a low-grade malignancy with a good prognosis, there are still approximately 10-15% of cases showing tumor heterogeneity and aggressive variation along with unique clinical, pathological, and molecular characteristics [6]. These histological variations are associated with tumor recurrence, metastasis, therapeutic resistance, and radioiodine resistance and may eventually lead to lower survival rates [7]. Large-scale genomic characterization studies of PTC have revealed the key role of genetic alterations in the oncogenesis of this disease [8]. In particular, BRAFV600E and RAS are believed to be major signaling drivers, and about 50% of PTC cases carry BRAFV600E mutations [9]. However, the cancerization of PTC is a complex biological process characterized by a variety of molecular abnormalities. Therefore, decoding the molecular mechanisms related to the pathogenesis of PTC may help to identify new therapeutic targets.

Rap1 GTPase-activating protein (Rap1GAP) locates on chromosome 1p36.1-p35 and encodes a protein with the molecular weight of 73 kDa [10]. Rap1GAP regulates the specific GAP activity for Rap1 and is known as a tumor suppressor gene and plays a key role in human tumor progression including thyroid cancer [11]. Previous studies have found the deficiency expression of Rap1GAP in PTC, and the deletion of Rap1GAP allele was detected in about 20% of PTC cases [12, 13]. Studies on the upstream regulatory mechanisms revealed that miR-3121-3p could mediate the expression of Rap1GAP and affect the proliferation and metastasis of PTC cells by regulating the MAPK signaling pathway [14]. However, limited reports failed to fully explain the regulatory mechanism of Rap1GAP in PTC.

Sodium iodide symporter (NIS), a transmembrane glycoprotein, mediates the movement of active iodine in the thyroid gland and other tissues, and the expression of NIS can be selectively enhanced in thyroid cells by thyroid-stimulating hormone (TSH) [15, 16]. It has been reported that BRAFV600E mutation in PTC is related to expression changes of Rap1GAP, while the inhibition of BRAFV600E mutation can restore the expression of NIS in PTC cells, thereby illustrating the potential regulatory relationships between Rap1GAP and NIS in PTC development [13, 17]. Notably, the expression of NIS and its targeting localization on the plasma membrane of thyroid cells are not only regulated by TSH and iodine but also closely related to the concentration of transforming growth factor beta1 (TGF-β1) [18]. It has been shown that NIS expression level is decreased in tumor cells treated with TGF-β1 and NIS may be regulated by TGF-β1 [19, 20]. However, whether the regulation mechanism of Rap1GAP on NIS in PTC is mediated by TGF-β1 and related signaling pathway has not been elucidated.

Combined with the above findings, this study speculated that Rap1GAP regulates the expression of NIS by mediating TGF-β1 and its signaling pathway in PTC. To further investigate the hypothesis, we experimentally explored the expression relationship between Rap1Gap, TGF-β1, and NIS in PTC cells. Subsequently, siRNAs were applied to silence the expression of Rap1GAP, and functional changes of transfected PTC cells including the cell apoptosis, cell cycle, migration, and invasion, as well as expression and localization changes of TGF-β1 and TGF-β/Smad3 pathway proteins, were detected. Our study proposed a new regulatory axis of Rap1GAP in inhibiting PTC progression and provided theoretical basis to discovery novel therapeutic targets for disease.

2. Methods

2.1. Cell Lines and Cell Culture. BCPAP cells provided by KeyGen BioTECH Co., Ltd. (Nanjing, China), were human thyroid carcinoma papillary cells. They were isolated from a 76-year-old woman with metastatic papillary thyroid tumor in 1992. Based on their growth characteristics, they were cultured in a 90% RPMI1640 culture medium supplemented with 10% fetal bovine serum (FBS). The cells were then grown in an incubator with saturated humidity and 5% CO_2 at 37°C. They usually grow into adherent cells, and their shapes are usually fusiform or round in shape. Cells in a logarithmic growth phase were extracted for subsequent experiments.

2.2. Quantitative Reverse-Transcription Polymerase Chain Reaction (qRT-PCR) Analysis. The total RNA was extracted from BCPAP using the TRIzol (15596-026, Invitrogen, USA). After reverse transcriptional reaction, cDNA was quantified by the Step one plus Real time-PCR system (ABI, USA) by following the standard procedures of One Step TB Green™ PrimeScript™ RT-PCR Kit II (RR086B, TaKaRa, Japan). The primers were designed by Primer6, synthesized by KeyGen BioTECH Co., Ltd., and purified by polyacrylamide gel electrophoresis (PAGE). The gene accession number and sequences of primers used in the present study are shown in Table 1. The mRNA expression level was normalized against GAPDH.

2.3. Western Blotting (WB) Analysis. The total protein was obtained using extraction kit (KGP250, KeyGen BioTECH, Nanjing, China), followed by the quantification using BCA protein concentration detection kit (KGA902, KeyGen BioTECH, Nanjing, China). By applying gel preparation kit (KGP113, KeyGen BioTECH, Nanjing, China), sodium dodecyl sulfate- (SDS-) PAGE was conducted followed by the membrane transfer. Thereafter, WB was performed, using anti-NIS (24324-1-AP, Proteintech Group, Inc., China), anti-Rap1GAP (ab32373, Abcam, UK), anti-TGF-β1 (ab215715, Abcam, UK), anti-Foxp3 (bs10211R, Bioss, China), anti-TβR1 (bs0638R, Bioss, China), anti-p-Smad3 (ab52903, Abcam, UK), anti-Smad3 (ab40854, Abcam,

Table 1: Gene accession number and sequences of primers.

Gene	Gene accession	Sequences of primers
NIS	NM_000453	Forward: CCTCTGCTGGTGCTGGACATCT Reverse: TGCTGGTGGATGCTGTGCTGAG
Rap1GAP	NM_001388273 XM_017001977	Forward: GGCGACGAGGACAAGATGGAGA Reverse: TGGCTGGTGGACACGGTGTT
TGF-β1	NM_000660	Forward: AGGACCTCGGCTGGAAGTGGAT Reverse: AGGACCTTGCTGTACTGCGTGT
GAPDH	NM_000453	Forward: CAAATTCCATGGCACCGTCA Reverse: AGCATCGCCCCACTTGATTT

UK), anti-bcl-2 (ab182858, Abcam, UK), and anti-Bax (ab182733, Abcam, UK) with dilution rates of 1 : 1000, 1 : 10000, 1 : 1000, 1 : 1000, 1 : 1000, 1 : 2000, 1 : 1000, 1 : 2000, and 1 : 2000, respectively. After incubation with the secondary antibody, the membrane was colorized and imaged using G: BOX chemiXR5 (syngene, UK).

2.4. Retroviral Construction Infection and Transfection. To downregulate the expression of Rap1GAP, three siRNA plasmids synthesized by KeyGen BioTECH Co., Ltd. (Nanjing, China), were transfected into BCPAP using Lipofectamine 3000 (L3000015, Invitrogen, USA). The sequences were listed as follows: siRNA-Rap1GAP-1-F—GCUACAAGG CAGAGAAGUUTT; siRNA-Rap1GAP-1-R—AACUUC UCUGCCUUGUAGCTT; siRNA-Rap1GAP-2-F—AGGU GAAGCUCGAGUGCAATT; siRNA-Rap1GAP-2-R: UUGCACUCGAGCUUCACCUTT; siRNA-Rap1GAP-3-F—GCAAGGAGCAUUUCAAUUATT; and siRNA-Rap1-GAP-3-R—UAAUUGAAAUGCUCCUUGCTT. After 24 and 48 hours of transfection, qRT-PCR was used to verify the expression of Rap1GAP (compared with the blank and negative control (NC) groups). These verified cells were used for further experiments.

2.5. Enzyme-Linked Immunosorbent Assay (ELISA). BCPAP cells were cultivated at an appropriate density, and a cell culture supernatant was collected for ELISA with references to the instructions of human TGF-β1 ELISA kit (KGEHC107b, KeyGen BioTECH, Nanjing, China). Then, the absorbance of each sample was measured by a microplate reader (SpectraMax M3, MD, USA), and the concentration of TGF-β1 was calculated according to the standard curve.

2.6. Immunofluorescence Analysis. After drying naturally, BCPAP cells were immersed in 4% paraformaldehyde fixation solution to improve the cell permeability. Then, BCPAP was coincubated with anti-TβR1 (bs0638R, Bioss, China) and anti-p-Smad3 (ab52903, Abcam, UK) with a dilution rate of 1 : 100 for 2 hours. Followed by exposing to fluorescent dye-conjugated secondary antibody (TRITC) diluted at 1 : 100, BCPAP was mounted with DAPI. The expression of target protein was observed and recorded by a laser scanning confocal microscope (710, Zeiss, Germany).

2.7. Cell Apoptosis Assay. A flow cytometer (FACSCalibur, Becton-Dickinson, USA) was employed for cell apoptosis assay using Annexin V-APC/7-AAD Apoptosis Assays Kit (KGA1024, KeyGen BioTECH, Nanjing, China). For cell cycle analysis, a PI single staining method was implemented followed by the flow cytometry analysis using Cell Cycle Assay Kit (KGA511, KeyGen BioTECH, Nanjing, China).

2.8. Cell Migration and Invasion Assay. Cell migration was measured by wound healing assay, while cell invasion was detected by transwell assay. BCPAP cells at the logarithmic growth phase were digested and inoculated into a six-well plate (3516, Corning Incorporated, USA). For invasion assay, cells were seeded into the upper chamber with or without Matrigel (356234, BD, USA) after 48 h transfection, and the lower chamber was placed into culture medium with 20% FBS. Followed by 24 h incubation, transwell was removed and cells were dried for staining with crystal violet (C3886, Sigma, USA). Then, cells were recorded with a magnification of 200x and finally counted. For migration assay, BCPAP cells were transfected with lentivirus and a negative control group was set. Subsequently, cultured cells were evenly lined with a sterile spear tip and continued to grow for 24 hours. Finally, cells were photographed under a 100x magnification microscope (IX51, OLYMPUS, Japan), and the migration distance was measured.

2.9. Cell Proliferation Assay. Cell proliferation was detected by EDU assay. The cell suspension was added to the 96-well cell culture plate and cultured in a 5% CO_2 incubator at 37°C for 24 h and cleaned twice with PBS. Edu culture was added, then discarded, and cleaned twice. Each well was treated with cell fixative solution, glycine, PBS, 1×Apollo® staining reaction solution, osmotic agent (0.5% TRiton X-100 PBS), and 1×Hoechst 33342 reaction solution and monitored by high content cell imaging system (MD).

2.10. Animal Assay. Ten 4-week-old female BALB/C nude mice (SCXK (Shanghai) 2017-0005) were provided by Shanghai Slack Laboratory Animal Co., Ltd. Animals were fed in the room temperature of 20~26°C (diurnal temperature variation ≤ 4°C), relative humidity of 40~70%, 12 hours of an alternating light and dark (7 o'clock lights on, 19 o'clock lights off) environment. The mice were randomly divided into two groups. The cell suspension concentration of BCPAP cells and BCPAP cells that downregulated the expression of Rap1GAP was 1×10^7/mL, and 0.1 mL of each cell suspension was inoculated into the left

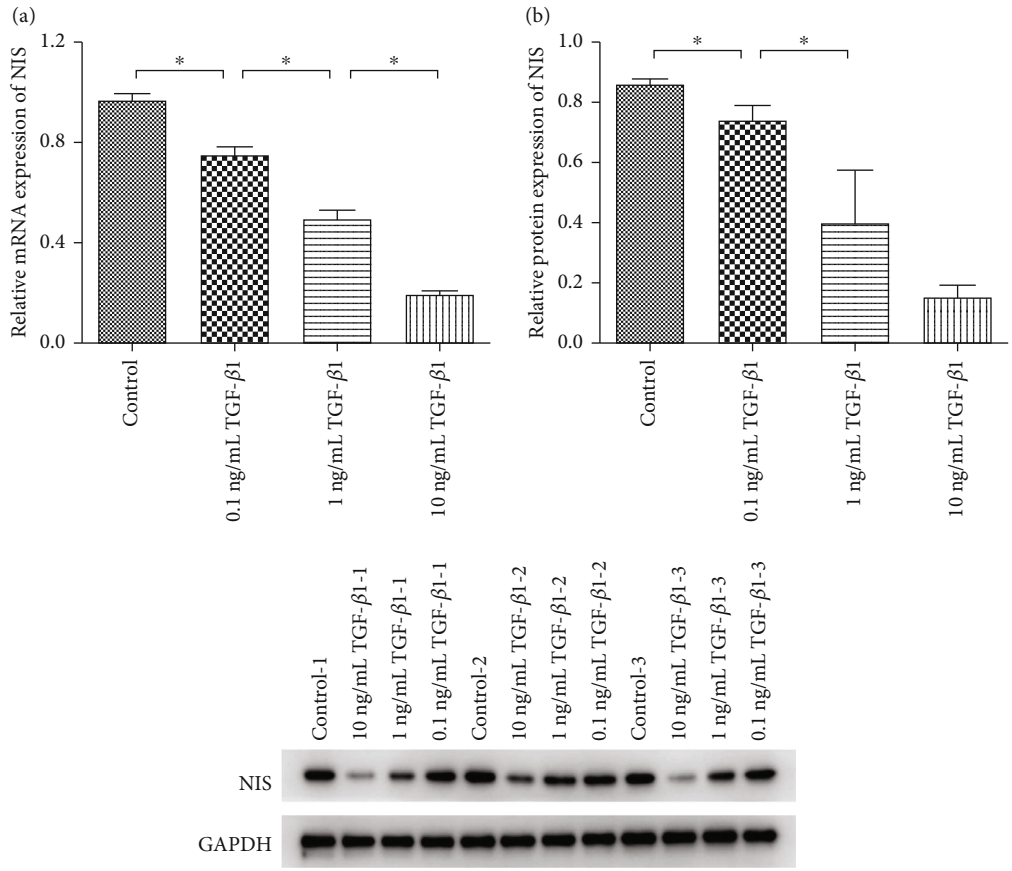

Figure 1: The expression of NIS detected by qRT-PCR (a) and WB (b) (*$p < 0.05$ compared between two groups). Independent experiments were conducted in triplicates.

thyroid lobe of nude mice of the two groups. Two weeks later, the nude mice were sacrificed. The tumor was surgically removed and weighed. An oil gauge caliper was used to measure tumor diameter.

2.11. Statistical Analysis. GEL-PRO32 software was used to analyze the gray scale of WB results. All data was expressed as means ± standard deviation (SD) of at least triplicate and was processed by GraphPad Prism 5 (GraphPad, USA). Differences between two groups were analyzed by a t-test. Two-tailed $p < 0.05$ was set as statistical significance.

3. Result

3.1. TGF-β1 Inhibits the Expression of NIS in BCPAP. To explore whether the expression level of NIS was affected by TGF-β1 in PTC, qRT-PCR and WB were carried out on BCPAP. Cells were grouped as BCPAP, BCPAP + 0.1 ng/mL TGF-β1, BCPAP + 1 ng/mL TGF-β1, and BCPAP + 10 ng/mL TGF-β1, and the experiment was set up with three replicates in each groups. The results (Figures 1(a) and 1(b)) suggested that the expressions of NIS in both mRNA and protein levels were significantly decreased with the increase of TGF-β1 concentration ($p < 0.05$). This finding suggested that TGF-β1 could inhibit the expression of NIS in BCPAP.

3.2. Downregulation of Rap1GAP Activates TGF-β/Smad3 Pathway in BCPAP. In order to investigate the regulatory relationship between Rap1GAP and TGF-β1, three siRNAs of Rap1GAP plasmid were constructed and then transfected into BCPAP. The results of qRT-PCR showed that siRNA-Rap1GAP-2 had the highest knockdown efficiencies among all three siRNAs with $p < 0.001$ (Figure 2(a)). With the downregulation of Rap1GAP, the mRNA expression of TGF-β1 was found to be significantly increased (Figure 2(b)). Therefore, we further detected the expression of key proteins involved in TGF-β/Smad3 pathways by WB. As shown in Figure 2(c), the knockdown of Rap1GAP can significantly increase the expression of TGF-β1, Foxp3 and p-Smad3 ($p < 0.001$). However, the expression levels of TβR-1 and Smad3 were not significantly changed. The increased expression of TGF-β1 in the siRNA-Rap1GAP group was also verified by ELISA (Figure 2(d), $p < 0.001$). Moreover, NIS was found to be downregulated and expressed in BCPAP infected with siRNA-Rap1GAP, which could be further reversed by anti-TGF-β1 (Figure 2(e), $p < 0.01$). The above findings illustrated that downregulation of Rap1GAP can activate the TGF-β/Smad3 pathway in BCPAP, and anti-TGF-β1 can rescue the downregulation of NIS expression caused by siRNA-Rap1GAP.

We further detected the plasma membrane localization of TGF-β1 and p-Smad3 in BCPAP transfected with

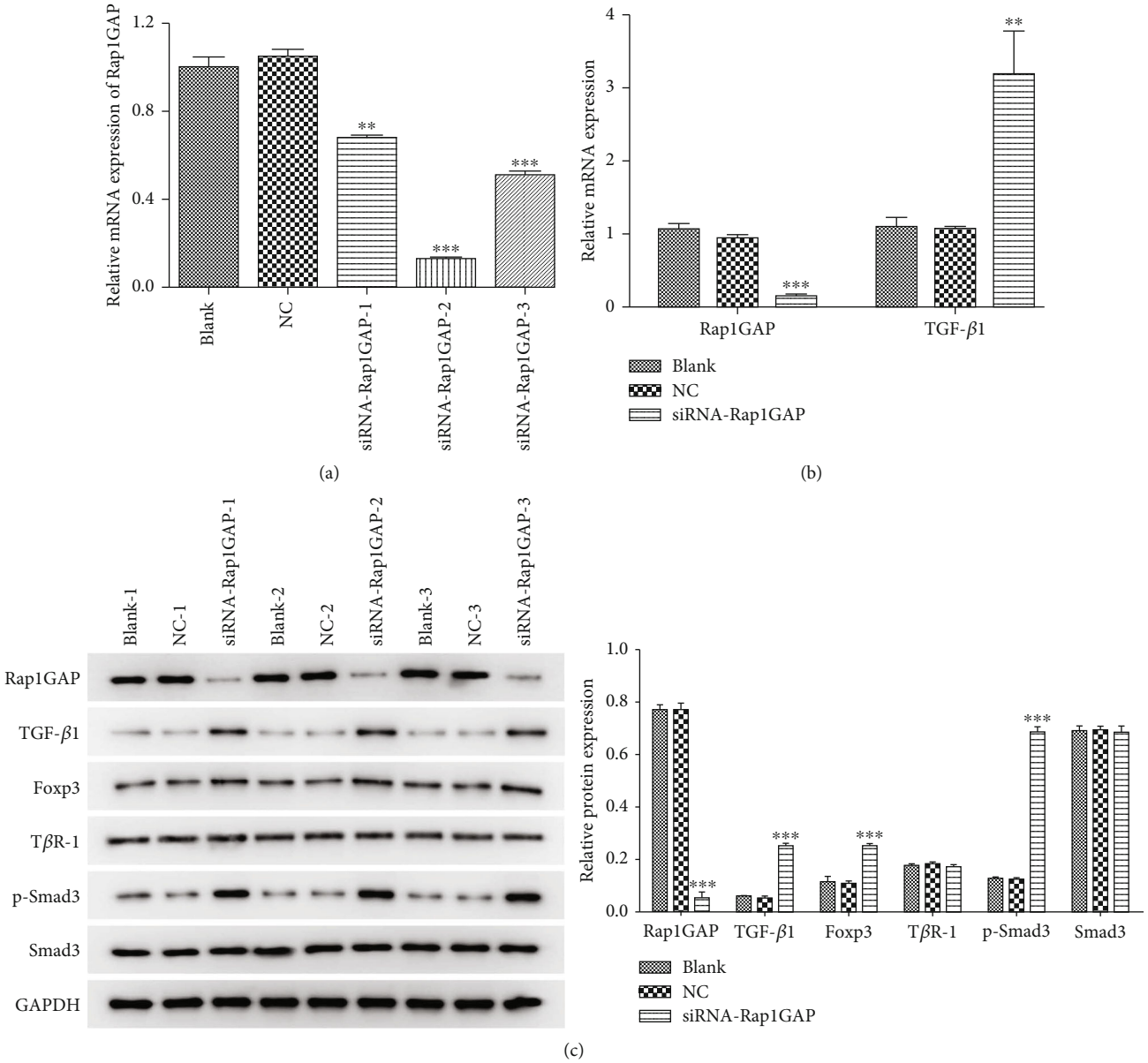

Figure 2: Continued.

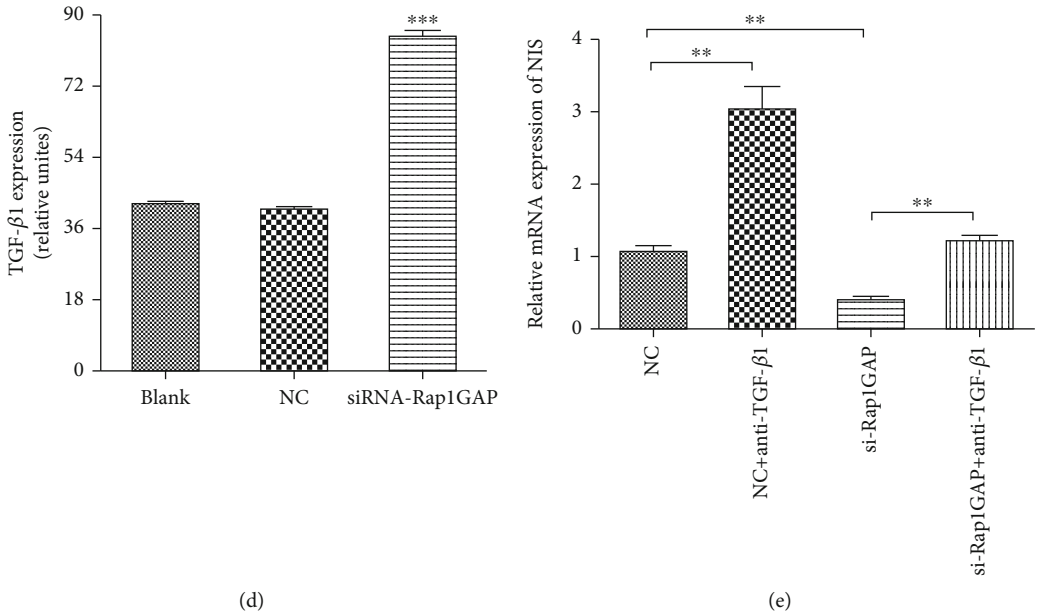

Figure 2: Expression changes in TGF-β/Smad3 pathways were detected by qRT-PCR, WB, and ELISA with knockdown of Rap1GAP. (a) The knockdown efficiencies of three Rap1GAP-siRNAs were detected by qRT-PCR. (b) The mRNA expression of TGF-β1 in the siRNA-Rap1GAP group. (c) Protein expression in TGF-β/Smad3 pathway was detected by WB. (d) The protein expression of TGF-β1 in siRNA-Rap1GAP group was detected by ELISA. (e) Anti-TGF-β1 can rescue the downregulation of NIS expression caused by siRNA-RAP1GAP. $^{**}p < 0.01$ and $^{***}p < 0.001$ compared with the blank and NC groups. Independent experiments were conducted in triplicates.

siRNA-Rap1GAP by immunofluorescence assay. As shown in Figure 3, membrane localizations of TGF-β1 and p-Smad3 were notably induced in the siRNA-Rap1GAP group.

3.3. The Deficiency Expression of Rap1GAP Affects Cell Apoptosis and Cycle. Flow cytometry analysis was performed to study the effects of Rap1GAP on cell apoptosis (Figure 4(a)) and cycle (Figure 4(b)). The results suggested that the apoptosis rate of BCPAP in the siRNA-Rap1GAP group was significantly lower than those in the blank and NC groups ($p < 0.01$). Meanwhile, the low expression of Rap1GAP resulted in a significant increase of BCPAP cell numbers in G2 phase and a significant decrease of cell numbers in S phase, thereby illustrating a G2 phase retardation of transfected BCPAP. Western analysis was used for further detect the apoptosis-related proteins. The results showed that antiapoptotic protein (bcl-2) was downregulated and apoptotic promoting protein (Bax) was upregulated, compared with the blank and NC groups ($p < 0.01$).

3.4. Knockdown of Rap1GAP Enhances the Function of Tumor Cells and Promote Tumor Growth. Transwell, wound healing, and EDU assays were finally performed to explore cell invasion, migration, and proliferation, respectively. In BCPAP with low expression of Rap1GAP, the number of invaded cells was significantly increased (Figure 5(a)). Additionally, after 24 h culture, we found that the scratch distance of transfected cells was significantly reduced (Figure 5(b)) and the proliferation ration of transfected BCPAP was significantly increased (Figure 5(c)). What is more, the weight and size of orthotopic transplantation tumor in the siRNA-Rap1GAP group were increased (Figure 6). These findings suggested that knockdown of Rap1GAP can promote cell migration, invasion, and proliferation of BCPAP and promote tumor growth.

4. Discussion

Attributed to the improvement of diagnostic level, the number of confirmed cases of PTC has increased rapidly thereby leading to a steadily rising incidence of thyroid cancer all over the world [21]. Although PTC is an indolent tumor, papillary carcinoma with an aggressive variant is highly invasive and has a tendency to dedifferentiate and may contribute to the eventual development of poorly differentiated or undifferentiated thyroid carcinoma [22]. Distal metastasis is the dominant phenotype of invasive variants, and the median survival of patients with distant metastasis was estimated to be 4.1 years, while the 10-year specific survival rate dropped to 26% [23]. Several gene mutations have been shown to be specific in PTC, and combined application with needle biopsy can improve the accuracy of PTC diagnosis [9]. Therefore, a more comprehensive understanding of the molecular mechanisms of cell invasion and metastasis, as well as the identification of predictive PTC biomarkers, can improve the diagnostic efficiency of malignant tumors and reduce the prognostic risk.

Rap1GAP is a family member of GTPase-activating proteins and is believed to be involved in cancer progression [24]. It has been reported that the expression of Rap1GAP is abundant in well-differentiated rat thyroid cells, but it is selectively reduced in tumor cell lines with mesenchymal

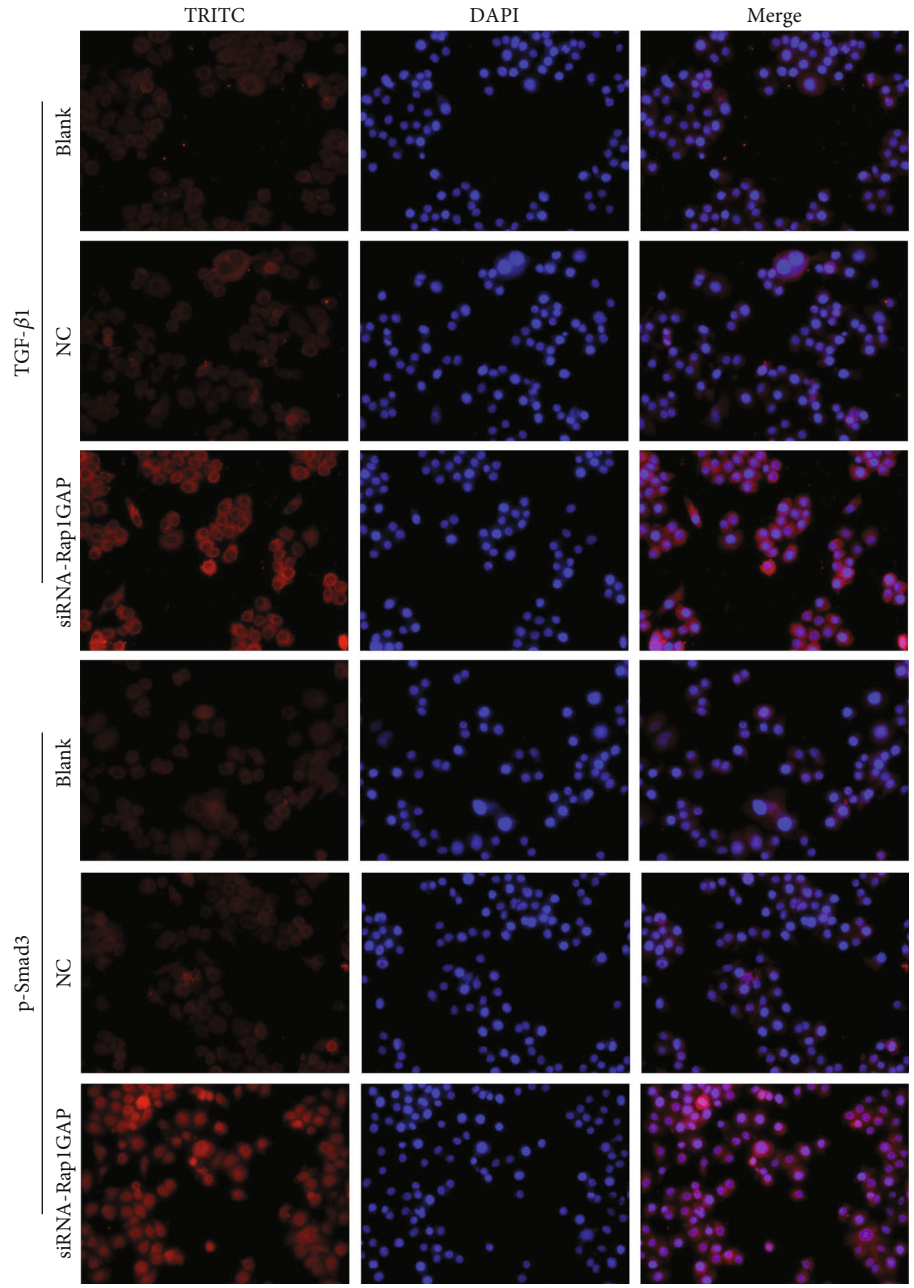

Figure 3: Immunofluorescence detection of TGF-β1 and p-Smad3 in transfected BCPAP.

morphology, and restoration of Rap1GAP expression can inhibit tumor cell migration and invasion [12]. To further explore the effect of Rap1GAP on PTC, we downregulated the expression of Rap1GAP in BCPAP using siRNA plasmids and found that the cell migration and invasion were significantly promoted ($p < 0.01$). The depletion of Rap1GAP in thyroid tumors may enhance Src kinase activity, thereby promoting skeletal remodeling and motility in cancer cells [25], which may well explain our results. Tsygankova et al. elaborated that Rap1Gap-deficient tumor cells exhibited cell-cell adhesion defects and abnormal distribution of adhesion-junction proteins [26]. Furthermore, Rap1GAP has also been identified as a more effective cell-matrix inhibitor, and overexpression of Rap1GAP in cancer cells can impair cell proliferation and migration on type IV collagen [27]. Therefore, we hypothesized that low expression of Rap1GAP in PTC cells may promote tumor invasion by altering cell-cell and cell-matrix adhesion.

To investigate the correlation of Rap1GAP and NIS in PTC cells, we experimentally confirmed that Rap1GAP silence could induce the downregulation of NIS expression in BCPAP. BRAF may play an important role in this relationship, because it is believed that the presence of BRAF V600E mutation is associated with the deletion of Rap1GAP allele and changes in protein expression [13], while hiSTONE deacetylation of NIS promoter is the basis of BRAF

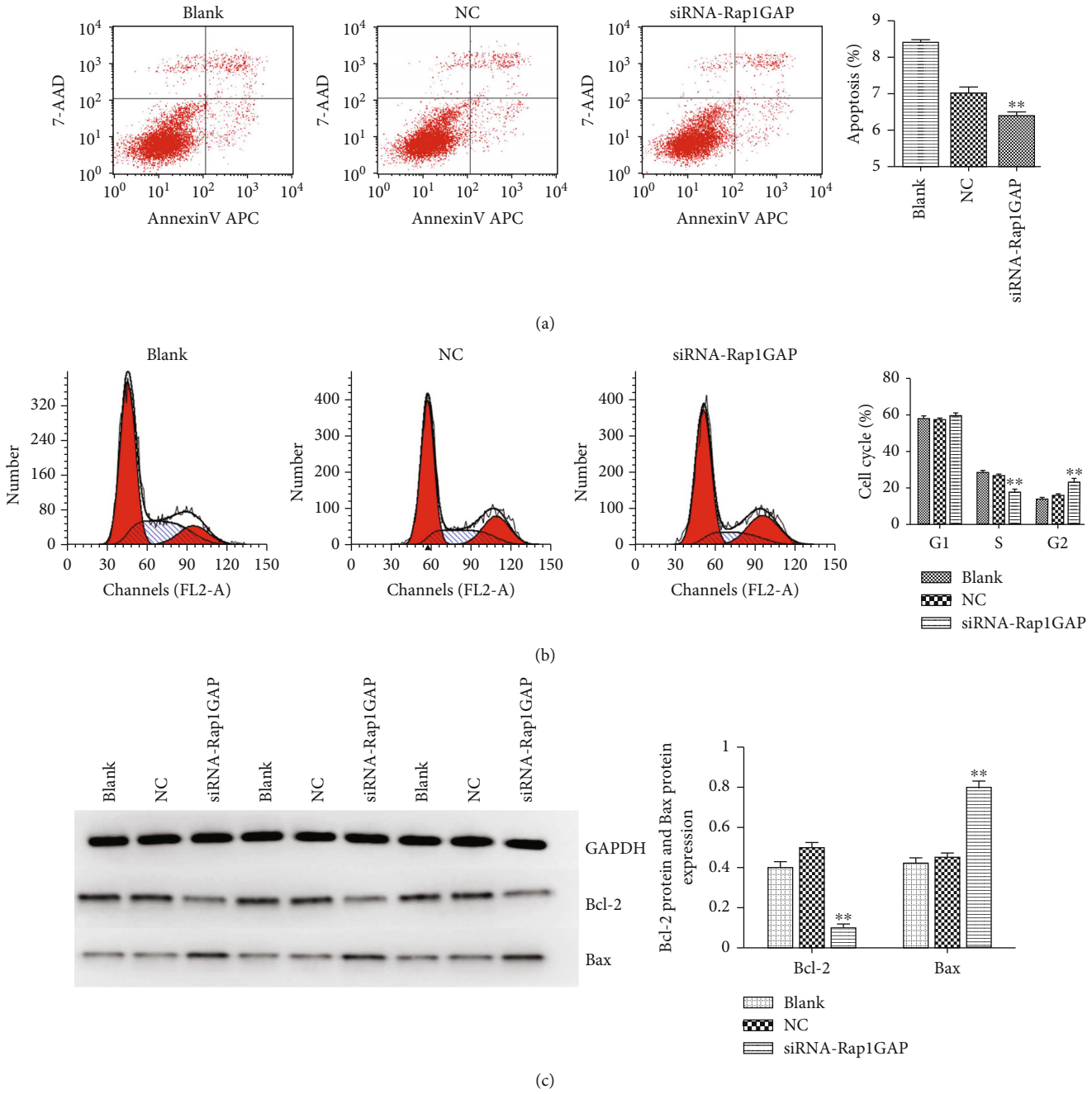

Figure 4: Flow cytometry detects cell apoptosis (a) and cycle (b) of transfected BCPAP. Western blot detects the expression levels of antiapoptotic protein (Bcl-2) and apoptotic promoting protein (Bax) (c) of transfected BCPAP. $^{**}p < 0.01$ compared with the blank and NC groups. Independent experiments were conducted in triplicates.

V600E promoting NIS silencing in thyroid cancer [28]. Additionally, in a mouse model with PTC oncogene knock-in, decreased expression of the thyroid specific gene NIS and increased expression of the epithelial-mesenchymal transition regulator TGF-β1 were detected at the same time [29]. To learn whether Rap1GAP regulates NIS expression through TGF-β1, we firstly studied the expression relationship between them and confirmed that the expression of NIS was negatively associated with the TGF-β1 concentration in BCPAP cells. In BCPAP cells transfected with siRNA-Rap1GAP, we also observed that the expression and nuclear localization of TGF-β1 and TGF-β/Smad3 pathway-related proteins including Foxp3 and p-Smad3 were significantly activated. By constructing lentivirus-mediated Foxp3 overexpression cells, a related study revealed that upregulated Foxp3 in PTC cells may significantly reduce transcription and protein levels of NIS and also activate the TGF-β1 pathway [30]. Additionally, TGF-β1 may induce the downregulation of NIS gene expression in thyroid follicular cells by activating Smad3 [31].

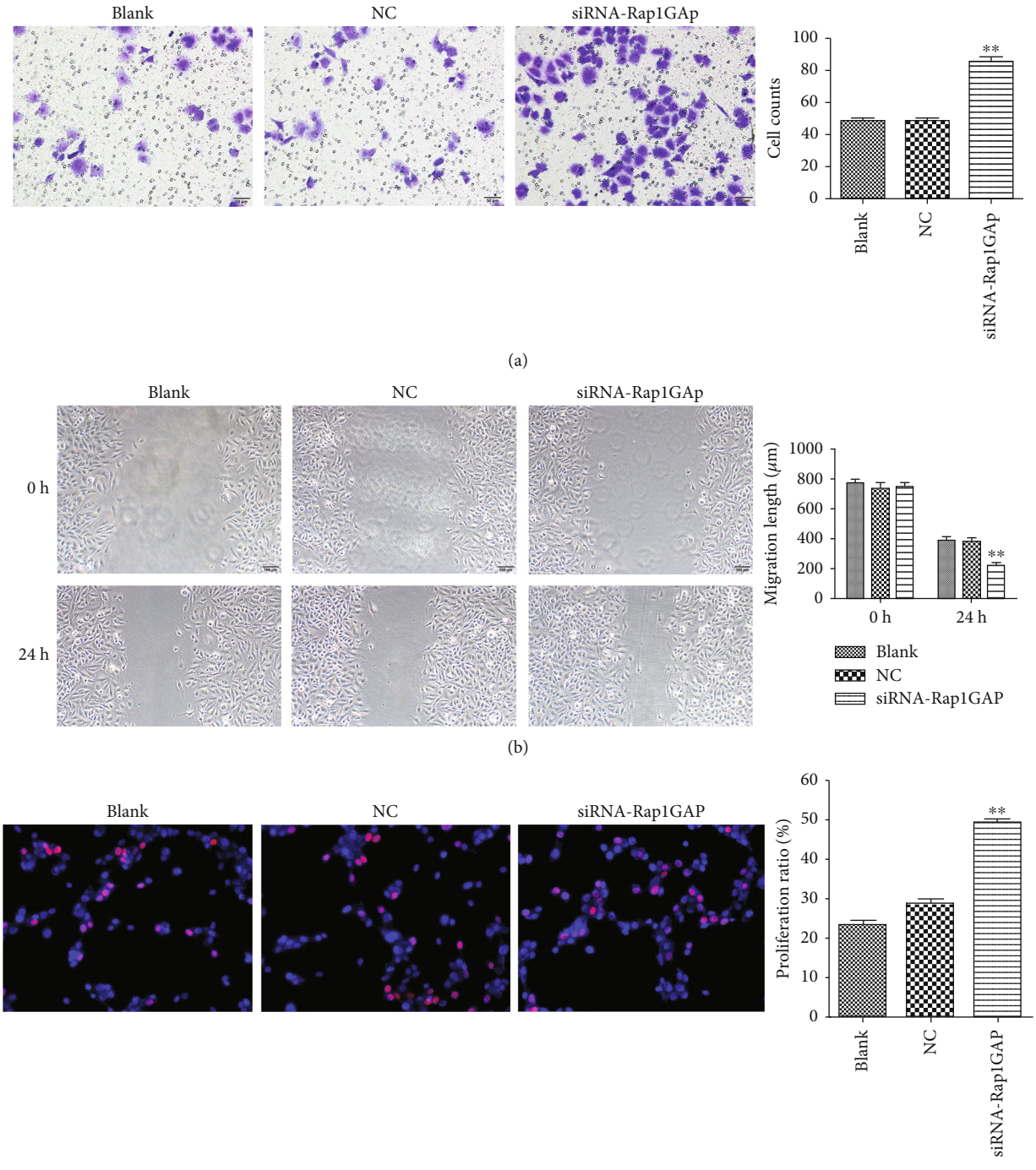

Figure 5: Cell invasion, migration, and proliferation of transfected BCPAP cells were measured by transwell (a), wound healing (b), and EDU assays (c), respectively. $^{**}p < 0.01$ compared with the blank and NC groups. Independent experiments were conducted in triplicates.

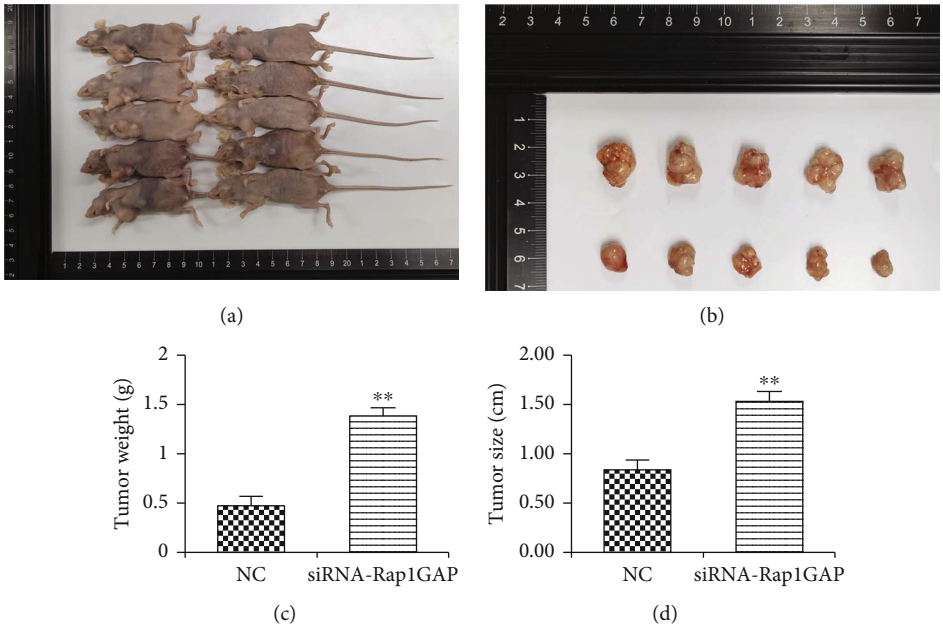

Figure 6: The mouse model of orthotopic transplanted tumor was constructed (a). Tumors removed from the mouse model (b). The weight (c) and size (d) of orthotopic transplantation tumor were measured. $^{**}p < 0.01$ compared with the NC group.

Restoration experiments in this present study further confirmed that anti-TGF-β1 could rescue the downregulation of NIS expression caused by Rap1GAP deficiency.

This study explored the regulatory relations of Rap1GAP-TGF-β/Smad3-NIS in PTC cells but only did the experiment in one cell line. Additionally, there is still a lack of valuable animal experimental results to clarify this regulatory mechanism. More cell lines and animal experiments are needed to verify this mechanism. Based on the understanding of this regulatory relationship, we will further collect tissue samples from patients to explore the potential correlation between Rap1-GAP expression and clinicopathological characteristics, so as to excavate the clinical value of Rap1GAP as a molecular marker for diagnosis and prognosis of patients with PTC.

5. Conclusion

In this present study, we found that TGF-β1 inhibited NIS expression and anti-TGF-β1 reversed the decrease in NIS expression caused by downregulation of Rap1GAP. Meanwhile, the knockdown of Rap1GAP can induce the activation of TGF-β1/Samd3 pathway and alter cell apoptosis, cycle, migration, and invasion in PTC cells. Our results provide a new perspective on the molecular regulatory mechanism of Rap1Gap in inhibiting PTC progression.

Abbreviations

PTC: Papillary thyroid cancer
Rap1GAP: Rap1 GTPase-activating protein
NIS: Sodium iodide symporter
TSH: Thyroid-stimulating hormone
TGF-β1: Transforming growth factor beta1
FBS: Fetal bovine serum
qRT-PCR: Quantitative reverse-transcription polymerase chain reaction
PAGE: Polyacrylamide gel electrophoresis
F: Forward
R: Reverse
WB: Western blotting
SDS-PAGE: Sodium dodecyl sulfate polyacrylamide gel electrophoresis
NC: Negative control
ELISA: Enzyme-linked immunosorbent assay
SD: Standard deviation.

Additional Points

Highlights. (1) TGF-β1 may inhibit the expression of NIS in BCPAP cells. (2) The downregulation of Rap1GAP can significantly reduce the expression of NIS. (3) The knockdown of Rap1GAP alters cell apoptosis, cycle, migration, invasion, and proliferation in BCPAP. (4) Anti-TGF-β1 can reverse the decrease in NIS expression caused by downregulation of Rap1GAP

Conflicts of Interest

The authors declare that no conflicts of interest exist.

Authors' Contributions

Gao Weili conceived and drafted the manuscript. Zheng Yan, Han Shuwen, Wang Yangyanqiu, Mao Jing, and Jin Yin performed the experiments. Zheng Yan, Chen Gong, and Zhou Qing analyzed the data. Zheng Yan, Wang Yangyanqiu, Han Shuwen, and Gao Weili wrote and revised the paper. All authors read and approved the paper. Zheng

Yan and Wang Yangyanqiu contributed equally to this work and should be considered co-first authors.

Acknowledgments

This work was supported by the Science and Technology Projects of Zhejiang Province (No. GF19H160010) and Medical and Health Technology Projects of Zhejiang Province (No. 2019RC282). The authors gratefully acknowledge the multiple databases, which made the data available.

References

[1] A. Coca-Pelaz, J. P. Shah, J. C. Hernandez-Prera et al., "Papillary thyroid cancer-aggressive variants and impact on management: a narrative review," *Advances in Therapy*, vol. 37, no. 7, pp. 3112–3128, 2020.

[2] K. Bergdorf, D. C. Ferguson, M. Mehrad, K. Ely, T. Stricker, and V. L. Weiss, "Papillary thyroid carcinoma behavior: clues in the tumor microenvironment," *Endocrine-Related Cancer*, vol. 26, no. 6, pp. 601–614, 2019.

[3] I. Vasileiadis, G. Boutzios, M. Karalaki, E. Misiakos, and T. Karatzas, "Papillary thyroid carcinoma of the isthmus: total thyroidectomy or isthmusectomy?," *American Journal of Surgery*, vol. 216, no. 1, pp. 135–139, 2018.

[4] E. O. Gur, S. Karaisli, S. Haciyanli et al., "Multifocality related factors in papillary thyroid carcinoma," *Asian Journal of Surgery*, vol. 42, no. 1, pp. 297–302, 2019.

[5] Y. T. Fu, H. B. Zheng, D. Q. Zhang, L. Zhou, and H. Sun, "MicroRNA-1266 suppresses papillary thyroid carcinoma cell metastasis and growth via targeting FGFR2," *European Review for Medical and Pharmacological Sciences*, vol. 22, no. 11, pp. 3430–3438, 2018.

[6] I. Reyes, N. Reyes, R. Suriano et al., "Gene expression profiling identifies potential molecular markers of papillary thyroid carcinoma," *Cancer biomarkers: section A of Disease markers*, vol. 24, no. 1, pp. 71–83, 2019.

[7] A. K. Lam, C. Y. Lo, and K. S. Lam, "Papillary carcinoma of thyroid: a 30-yr clinicopathological review of the histological variants," *Endocrine Pathology*, vol. 16, no. 4, pp. 323–330, 2005.

[8] H. Teng, F. Mao, J. Liang et al., "Transcriptomic signature associated with carcinogenesis and aggressiveness of papillary thyroid carcinoma," *Theranostics*, vol. 8, no. 16, pp. 4345–4358, 2018.

[9] K. T. Tang and C. H. Lee, "BRAF mutation in papillary thyroid carcinoma: pathogenic role and clinical implications," *Journal of the Chinese Medical Association: JCMA*, vol. 73, no. 3, pp. 113–128, 2010.

[10] M. Tamate, R. Tanaka, H. Osogami et al., "Rap1GAP inhibits tumor progression in endometrial cancer," *Biochemical and Biophysical Research Communications*, vol. 485, no. 2, pp. 476–483, 2017.

[11] T. Qiu, X. Qi, J. Cen, and Z. Chen, "Rap1GAP alters leukemia cell differentiation, apoptosis and invasion in vitro," *Oncology Reports*, vol. 28, no. 2, pp. 622–628, 2012.

[12] O. M. Tsygankova, G. V. Prendergast, K. Puttaswamy et al., "Downregulation of Rap1GAP contributes to Ras transformation," *Molecular and Cellular Biology*, vol. 27, no. 19, pp. 6647–6658, 2007.

[13] A. Nellore, K. Paziana, C. Ma et al., "Loss of Rap1GAP in papillary thyroid cancer," *The Journal of Clinical Endocrinology and Metabolism*, vol. 94, no. 3, pp. 1026–1032, 2009.

[14] M. Xu, J. Zhou, Q. Zhang et al., "MiR-3121-3p promotes tumor invasion and metastasis by suppressing Rap1GAP in papillary thyroid cancer in vitro," *Annals of translational medicine*, vol. 8, no. 19, p. 1229, 2020.

[15] S. Ravera, A. Reyna-Neyra, G. Ferrandino, L. M. Amzel, and N. Carrasco, "The sodium/iodide symporter (NIS): molecular physiology and preclinical and clinical applications," *Annual Review of Physiology*, vol. 79, pp. 261–289, 2017.

[16] A. Lakshmanan, D. Scarberry, D. H. Shen, and S. M. Jhiang, "Modulation of sodium iodide symporter in thyroid cancer," *Hormones & cancer*, vol. 5, no. 6, pp. 363–373, 2014.

[17] H. Zhang and D. Chen, "Synergistic inhibition of MEK/ERK and BRAF V600E with PD98059 and PLX4032 induces sodium/iodide symporter (NIS) expression and radioiodine uptake in BRAF mutated papillary thyroid cancer cells," *Thyroid Research*, vol. 11, no. 1, p. 13, 2018.

[18] C. Eloy, J. Santos, J. Cameselle-Teijeiro, P. Soares, and M. Sobrinho-Simões, "TGF-beta/Smad pathway and BRAF mutation play different roles in circumscribed and infiltrative papillary thyroid carcinoma," *Virchows Archiv: an international journal of pathology*, vol. 460, no. 6, pp. 587–600, 2012.

[19] A. E. Pekary and J. M. Hershman, "Tumor necrosis factor, ceramide, transforming growth factor-beta1, and aging reduce Na+/I- symporter messenger ribonucleic acid levels in FRTL-5 cells," *Endocrinology*, vol. 139, no. 2, pp. 703–712, 1998.

[20] X. Yu, H. Shen, L. Liu, L. Lin, M. Gao, and S. Wang, "Changes of sodium iodide symporter regulated by IGF-I and TGF-β1 in mammary gland cells from lactating mice at different iodine levels," *Biological Trace Element Research*, vol. 146, no. 1, pp. 73–78, 2012.

[21] A. Zembska, A. Jawiarczyk-Przybyłowska, B. Wojtczak, and M. Bolanowski, "MicroRNA expression in the progression and aggressiveness of papillary thyroid carcinoma," *Anticancer Research*, vol. 39, no. 1, pp. 33–40, 2019.

[22] J. Albores-Saavedra, D. E. Henson, E. Glazer, and A. M. Schwartz, "Changing patterns in the incidence and survival of thyroid cancer with follicular phenotype–papillary, follicular, and anaplastic: a morphological and epidemiological study," *Endocrine Pathology*, vol. 18, no. 1, pp. 1–7, 2007.

[23] M. Shoup, A. Stojadinovic, A. Nissan et al., "Prognostic indicators of outcomes in patients with distant metastases from differentiated thyroid carcinoma," *Journal of the American College of Surgeons*, vol. 197, no. 2, pp. 191–197, 2003.

[24] J. Zhao, C. Mai, D. Weng et al., "Reduced expression of Rap1-GAP as a prognostic biomarker for primary gastric cancer patients," *Cancer biomarkers: section A of Disease markers*, vol. 22, no. 3, pp. 375–384, 2018.

[25] X. Dong, W. Tang, S. Stopenski, M. S. Brose, C. Korch, and J. L. Meinkoth, "RAP1GAP inhibits cytoskeletal remodeling and motility in thyroid cancer cells," *Endocrine-Related Cancer*, vol. 19, no. 4, pp. 575–588, 2012.

[26] O. M. Tsygankova, C. Ma, W. Tang et al., "Downregulation of Rap1GAP in human tumor cells alters cell/matrix and cell/cell adhesion," *Molecular and Cellular Biology*, vol. 30, no. 13, pp. 3262–3274, 2010.

[27] L. A. Vuchak, O. M. Tsygankova, and J. L. Meinkoth, "Rap1-GAP impairs cell-matrix adhesion in the absence of effects on cell-cell adhesion," *Cell Adhesion & Migration*, vol. 5, no. 4, pp. 323–331, 2011.

[28] Z. Zhang, D. Liu, A. K. Murugan, Z. Liu, and M. Xing, "Histone deacetylation of NIS promoter underlies BRAF V600E-

promoted NIS silencing in thyroid cancer," *Endocrine-Related Cancer*, vol. 21, no. 2, pp. 161–173, 2014.

[29] R. Ma, S. Bonnefond, S. A. Morshed, R. Latif, and T. F. Davies, "Stemness is derived from thyroid cancer cells," *Frontiers in Endocrinology*, vol. 5, p. 114, 2014.

[30] S. Ma, Q. Wang, X. Ma et al., "FoxP3 in papillary thyroid carcinoma induces NIS repression through activation of the TGF-β1/Smad signaling pathway," *Tumour biology: the journal of the International Society for Oncodevelopmental Biology and Medicine*, vol. 37, no. 1, pp. 989–998, 2016.

[31] E. Costamagna, B. García, and P. Santisteban, "The Functional Interaction between the Paired Domain Transcription Factor Pax8 and Smad3 Is Involved in Transforming Growth Factor-β Repression of the Sodium/Iodide Symporter Gene," *The Journal of Biological Chemistry*, vol. 279, no. 5, pp. 3439–3446, 2004.

Hindawi
BioMed Research International
Volume 2021, Article ID 9394563, 9 pages
https://doi.org/10.1155/2021/9394563

Research Article

lncRNA SNHG15 Promotes Ovarian Cancer Progression through Regulated CDK6 via Sponging miR-370-3p

Yi Wang,[1,2] Minghong Ding,[3] Xiaoqing Yuan,[4] Ruibao Jiao,[5] Dagao Zhu,[2] Wanzhong Huang,[2] Wenxia Deng,[2] and Yulong Liu [1,6,7]

[1]*Department of Oncology, The Second Affiliated Hospital of Soochow University, Suzhou 215004, China*
[2]*Department of Oncology, Tongling People's Hospital, Tongling 244000, China*
[3]*Department of Obstetrics and Gynecology, Tongling People's Hospital, Tongling 244000, China*
[4]*Department of Pathology, Tongling People's Hospital, Tongling 244000, China*
[5]*Department of Laboratory Medicine, Tongling People's Hospital, Tongling 244000, China*
[6]*State Key Laboratory of Radiation Medicine and Protection, School of Radiation Medicine and Protection, Medical College of Soochow University, Suzhou 215123, China*
[7]*Collaborative Innovation Center of Radiological Medicine of Jiangsu Higher Education Institutions, Suzhou 215123, China*

Correspondence should be addressed to Yulong Liu; yulongliu2002@suda.edu.cn

Received 22 July 2021; Accepted 28 September 2021; Published 25 October 2021

Academic Editor: Qiang Liu

Ovarian cancer is a kind of cancer from the female genital tract; the molecular mechanism still needs to be explored. lncRNA plays a vital role in tumorigenesis and development. Our aim was to identify oncogenic lncRNAs in ovarian cancer and explore the potential molecular mechanism. SNHG15 was initially identified by using GEO datasets (GSE135886 and GSE119054) and validated by tumor tissues and the cell line, identifying that SNHG15 was upregulated in ovarian cancer. Besides, high SNHG15 indicated poor prognosis in ovarian cancer. Furthermore, knockdown SNHG15 suppresses ovarian cancer proliferation and promotes apoptosis. Mechanistically, SNHG15 promotes proliferation through upregulated CDK6 via sponging miR-370-3p. Taken together, our findings emphasize the important role of SNHG15 in ovarian cancer, suggesting that SNHG15 may be a promising target for ovarian cancer.

1. Introduction

Ovarian cancer is the leading fatal neoplasm of the female genital tract [1–3]. Ovarian cancer affects annually 295414 new patients, with approximately 184799 deaths/year [4]. Despite the rapid development of diagnosis and treatment, the 5-year survival remains poor [5, 6]. Therefore, the mechanism of ovarian cancer occurrence and new strategies of treatment still need to be explored.

Long noncoding RNAs (lncRNAs) are non-protein-coding RNAs with a length of more than 200 nucleotides [7]. With the deepening of research in recent years, people's cognition of lncRNAs has been consistently improved and a large amount of evidence suggests that lncRNA has become an indispensable participant in the development of different human tumors [8–10]; for instance, HOTAIR promotes hepatocellular carcinoma progression [11] and regulated leukemia differentiation [12]; H19 promotes glioma angiogenesis [13] and promotes leukemogenesis [14]; MEG3 inhibits prostate cancer progression [15] and regulates imatinib resistance in chronic myeloid leukemia [16]. Therefore, lncRNA may be a promising therapeutic target in treating tumors, including ovarian cancer; there is a great need to identify lncRNAs to provide a new treatment strategy for ovarian cancer.

Recently, SNHG15 was described as an oncogenic lncRNA in several cancers [17–19] but the role of SNGH15 in ovarian cancer remains unclear. Herein, SNHG15 was identified by using GEO datasets and validated by ovarian cancer tissues and we investigated the clinical value and mechanism of SNHG15 in ovarian cancer. We hope that this research may

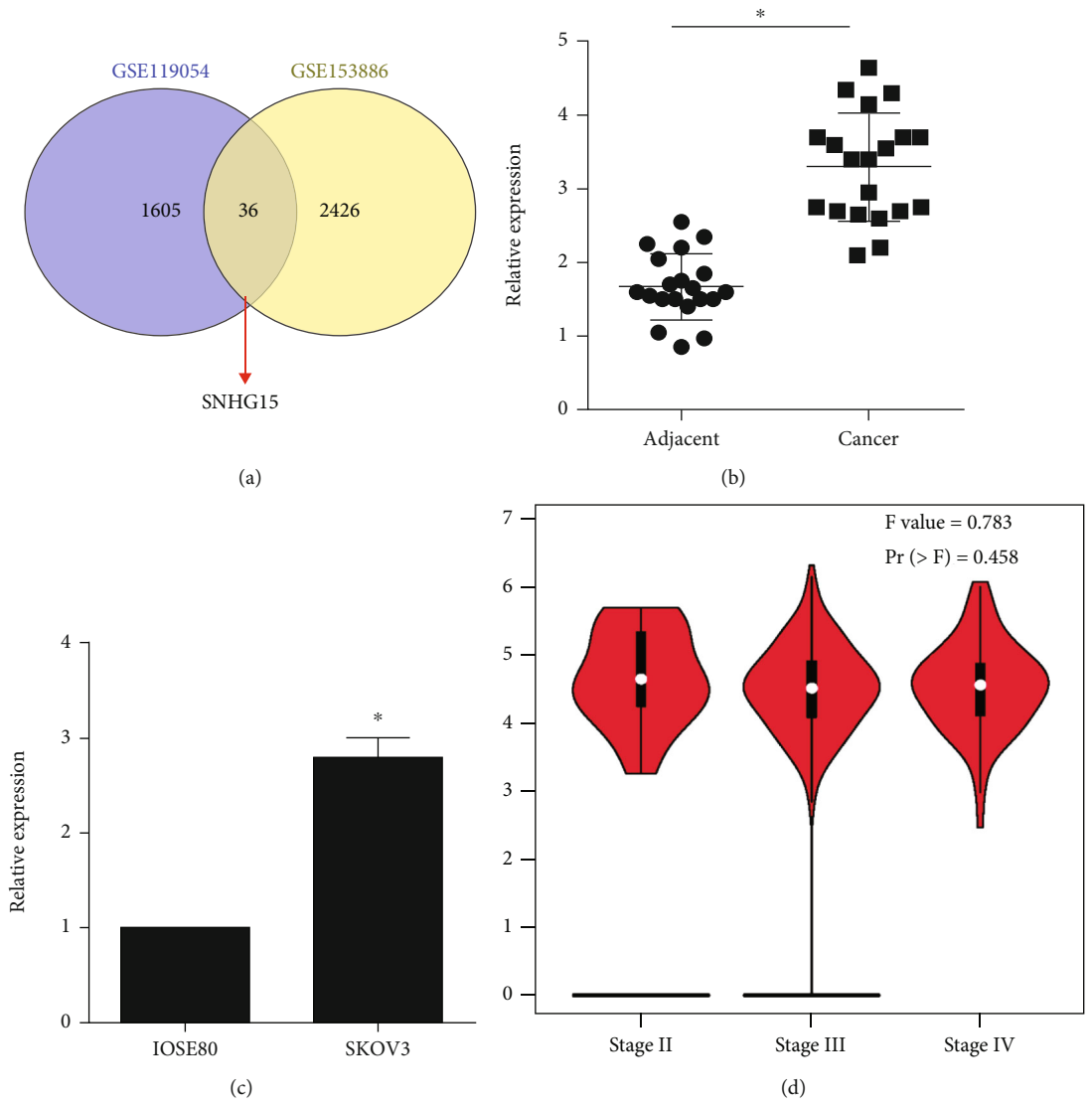

Figure 1: Continued.

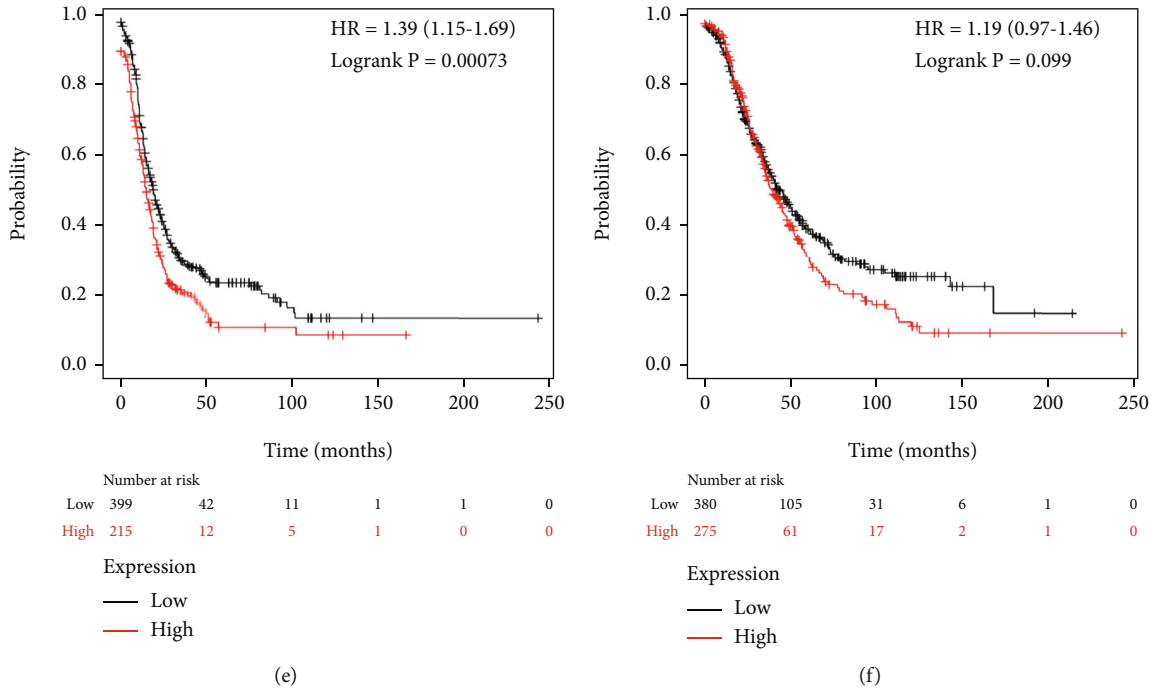

Figure 1: The identification of SNHG15 and the clinical value of SNHG15. Identification of SNHG15 by GEO datasets (a); SNHG15 upregulated in ovarian cancer tissues (b) and cancer cell line (c); GEPIA database indicated that SNHG15 did not correlate with the clinical stage in ovarian cancer (d); Kaplan-Meier plotter database indicated that SNHG15 correlated with PFS (e) but not OS (f).

provide novel ideals for clinical-targeted therapy of ovarian cancer.

2. Methods

2.1. Databases and Bioinformatics Analysis. We identified 2 datasets (GSE135886 and GSE119054) by using the keywords: "ovarian cancer and lncRNA" in the Gene Expression Omnibus (GEO) database (https://www.ncbi.nlm.nih.gov/gds/). The GEO2R tool was used to screen for differentially expressed lncRNAs (DElncRNAs) between healthy ovarian tissue and ovarian cancer tissue. DElncRNAs were selected as the following criteria:|log 2FC | >2 and P_{adj} value < 0.05.

Gene Expression Profiling Interactive Analysis (GEPIA) database (http://gepia.cancer-pku.cn) was employed to analyze the clinical significance of SNHG15.

Kaplan-Meier plotter database (http://kmplot.com/) was employed to explore the prognostic value of SNHG15 in ovarian cancer patients.

StarBase database (http://estarbase.sysu.edu.cn) was employed to identify the relationship between SNHG15, miR-370-3p, and CDK6.

2.2. Patients' Samples. Ovarian cancer and normal tissues from newly diagnosed ovarian cancer patients in our hospital from 2019 to 2021 were collected. The study was conducted according to the principles of the Declaration of Helsinki, approved by the medical ethics committee of Tongling People's Hospital, and with the written informed consent of each patient.

2.3. Cell Line Culture and Transfection. SKOV3 and IOSE80 were purchased from the Shanghai cell bank of Chinese Academy of Sciences. Cells were cultured in DMEM medium (Gibco) supplemented with 10% fetal bovine serum and cultured at 37°C in a 5% CO_2 incubator.

miRNA negative control (NC), the miR-370-3p inhibitor, si-SNHG15, and si-NC were ordered from GenePharma (Shanghai, China). Lipofectamine 2000 (Thermo Fisher Scientific Inc.) was used to transfected these into cell according to the manufacturer's protocol.

2.4. Quantitative Real-Time PCR. RNA from cells were extract by using TRIzol reagent (Invitrogen), and the PrimeScript RT reagent kit (TaKaRa, Dalian, China) was used to synthesize cDNA according to the manufacturer's protocol. qRT-PCR was performed by using TB Green PCR Mix (TaKaRa, Dalian, China). The primer sequences used were SNHG15-F: GGTGACGGTCTCAAAGTGGA, SNHG15-R: GCCTCCCAGTTTCATGGACA, GAPDH-F: GGAGCG AGATCCCTCCAAAAT, and GADPH-R: GGCTGTTGT CATACTTCTCATGG; the miRNA reverse transcription PCR and qRT-PCR primers were ordered from RiboBio Inc. (Guangzhou, Guangdong, China). The expression of lncRNA was analyzed by $2^{-\Delta\Delta Ct}$ method.

2.5. Flow Cytometry. For apoptosis, each group of cells was collected and washed twice with PBS, using an apoptosis detection kit (BD Biosciences, Bedford, MA, United States), according to the manufacturer's protocol.

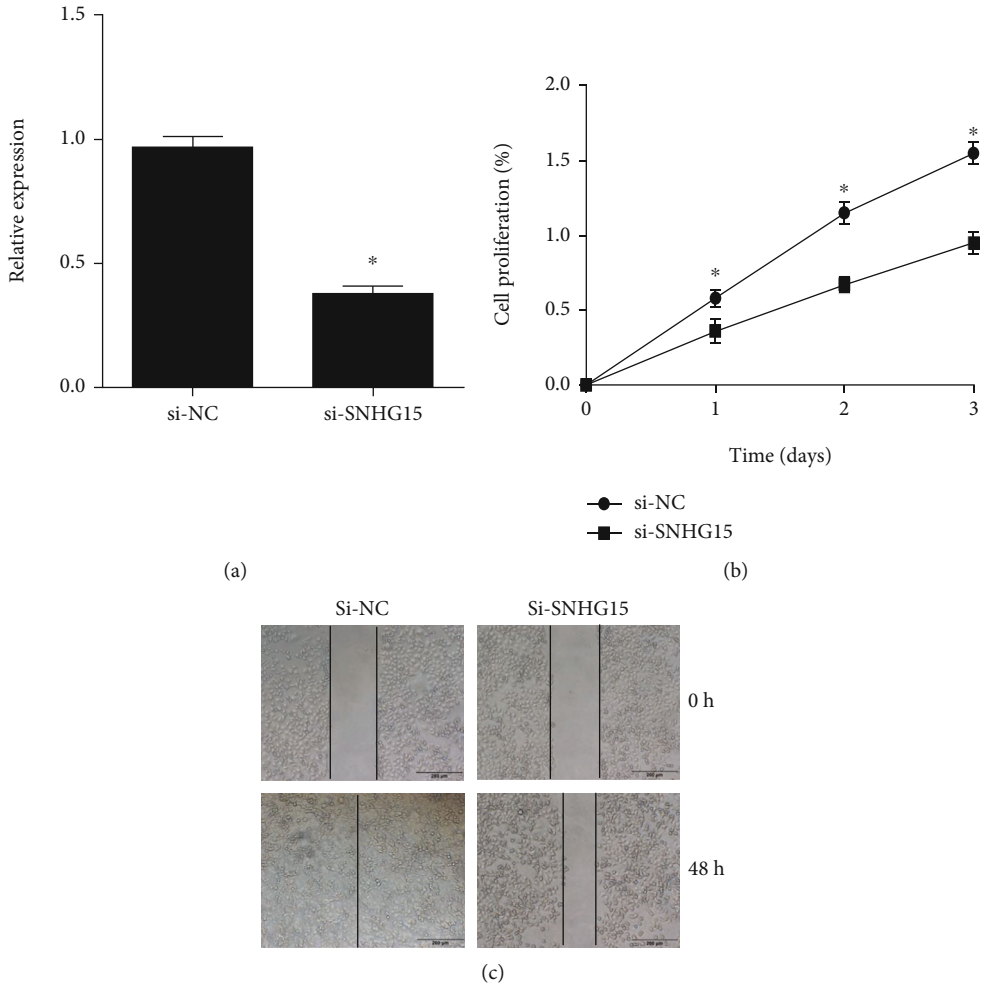

Figure 2: The impact of SNHG15 on the proliferation and migration of ovarian cancer. SNHG15 was significantly downregulated after siRNA transfection (a); SNHG15 suppressed the proliferation (b) and migration (c) of ovarian cancer cell. $^*P < 0.05$.

For cell cycle, each group of cells was collected and fixed with 70% precooled ethanol, using a cell cycle detection kit (Beyotime Institute of Biotechnology, China), according to the manufacturer's protocol.

Cell cycle and cell apoptosis were detected by CytoFLEX (Becton Dickinson, USA) and cell cycle was analyzed by Kaluza software (Kaluza® Analysis Software, Beckman Coulter).

2.6. Cell Proliferation and Scratch Assay. Each group of cells was measured at 24, 48, and 72 hours after cell transfection by CCK8 assay (Beyotime Institute of Biotechnology, China), according to the manufacturer's protocol.

Each group of cells was seeded in a 6-well plate, and when the bottom confluence reached 80%, scratch the bottom of the well with 100 μL sterile pipette tip. The healed wounds were imaged at 0 and 48 h after scratching.

2.7. Luciferase. Cells were seeded and cotransfected with SNHG15-WT/SNHG15-MT or CDK6-WT/CDK6-MT vector and NC or the miR-370-3p inhibitor using Lipofectamine 2000 in 24-well plates. Vectors are based on psicheck2 and the binding sites of miR-370-3p were constructed. 48 hours later, luminescence was detect by using the Luciferase Reporter Assay Kit (Beyotime Institute of Biotechnology, China) according to the manufacturer's protocol.

2.8. Western Blot. Cells were lysed with RIPA containing 1% PMSF (Beyotime Institute of Biotechnology, China) and then clarified by centrifugation. The proteins were electrophoresed by SDS-PAGE and then transferred into PVDF membranes. CDK6 (1 : 5000) and β-actin (1 : 3000) (Cell Signaling, Danvers, MA, USA) were the primary antibodies. Chemiluminescent signal was detected by ECL staining (Beyotime Institute of Biotechnology, China).

2.9. Statistical Analysis. All the experiment results were analyzed by GraphPad Prism 6.0 software (GraphPad Software, San Diego, CA). P value < 0.05 was considered statistically significant.

3. Results

3.1. SNHG15 Was Upregulated and Indicated Adverse Prognosis of Ovarian Cancer. To identify abnormally expressed lncRNA in ovarian cancer, we employed GSE135886 and GSE119054 from the GEO database to

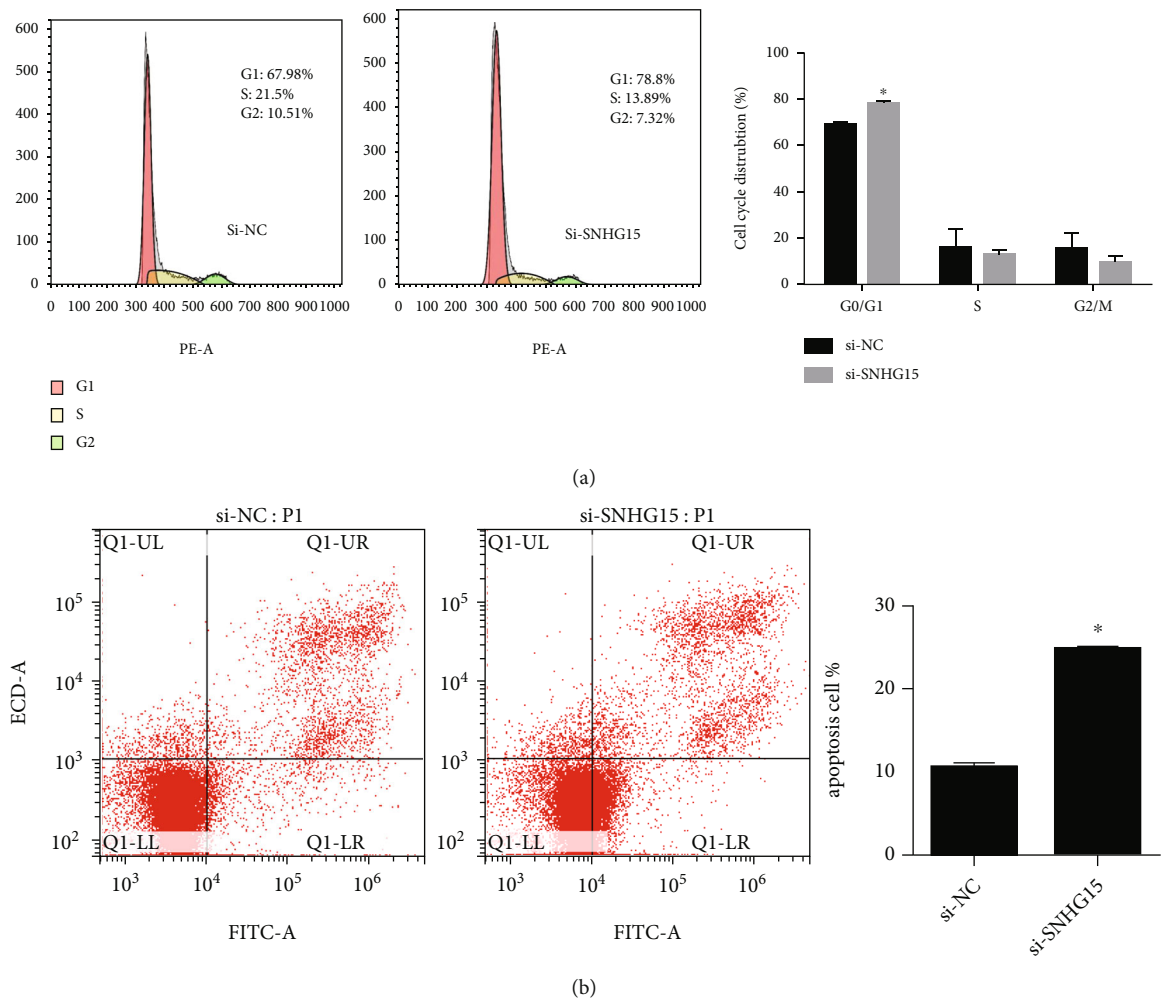

Figure 3: Effect of SNHG15 on cell cycle and apoptosis of ovarian cancer. SNHG15 knockdown induces G0/G1 arrest (a) and promotes apoptosis (b). $^*P < 0.05$.

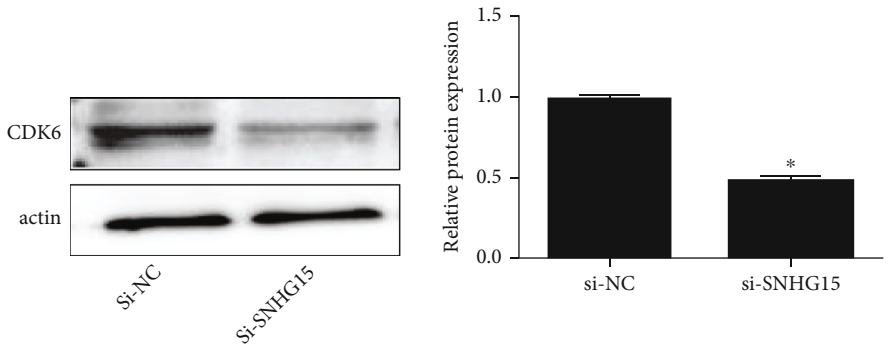

Figure 4: The impact of SNHG15 on CDK6 expression of ovarian cancer.

explore potential oncogenic lncRNA. As shown in Figure 1(a), there were 1605 lncRNAs upregulated in the GSE119054 dataset and 2426 lncRNAs upregulated in the GSE153886 dataset. There were 36 lncRNA in both datasets, and SNHG15 was among them.

To validated the aberrant expression of SNHG15, we performed qPCR to assess the SNHG15 expression in 20 patients, and highly expressed SNHG15 were observed in cancer tissues (Figure 1(b)) and SKOV3 cells (Figure 1(c)).

To evaluated the clinical significance of SNHG15, GEPIA was used to analyze the correlation between SNHG15 and the clinical stage of ovarian cancer; however, SNHG15 did not correlate with the clinical stage (Figure 1(d)). Simultaneously, we used Kaplan-Meier plotter database to explore the relationship

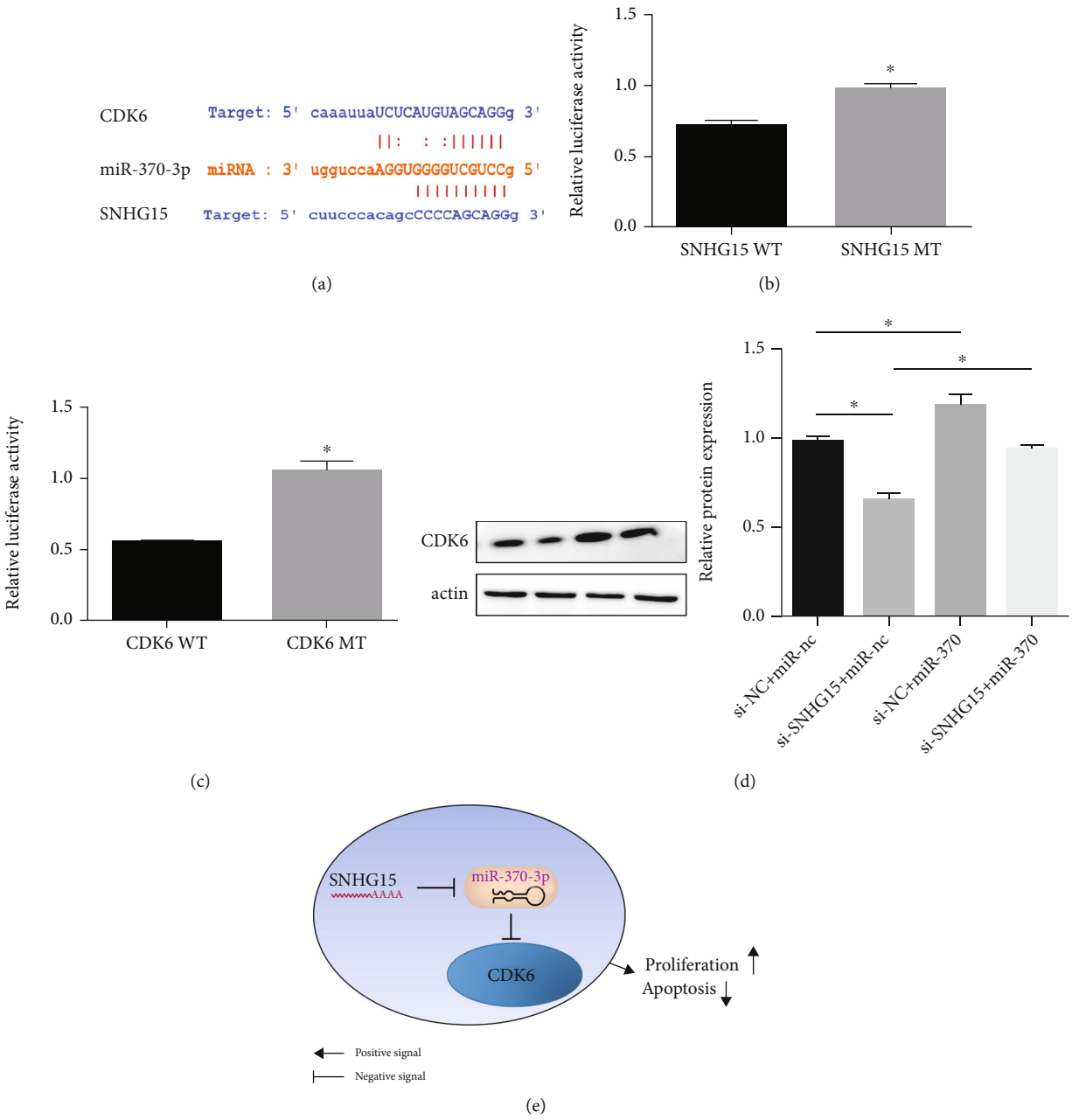

Figure 5: SNHG15 regulated CDK6 via sponging miR-370-3p. The predicted binding site of SNHG15, miR-370-3p, and CDK6 (a). The predicted binding sites of miR-370-3p to SNHG15 (b) and CDK6 (c) were confirmed by luciferase reporter assay. The miR-370-3p inhibitor restored downregulated expression of CDK6 induced by SNHG15 knockdown (d); the hypothetical mechanism of SNHG15 in ovarian cancer (e).

between SNHG15 and survival. As shown in Figure 1(e), high SNHG15 predicted poor PFS. For OS, there was a strong trend that was not statistically significant (Figure 1(f)). Above all, high SNHG15 predicted poor prognosis in ovarian cancer.

3.2. SNHG15 Knockdown Suppressed the Proliferation of Ovarian Cancer Cell. In summary, SNHG15 was upregulated and predicted poor prognosis in ovarian cancer but the mechanism of SNHG15 remains undetermined. We transfected SKOV3 cells with the specific siRNA target SNHG15 (Figure 2(a)). CCK8 assays were employed to assess the impact of SNHG15 on the proliferation of SKOV3 cell; as shown in Figure 2(b), the cell proliferation rate decreased in the si-SNHG15 group than that in si-NC group.

In addition, the scratch test was used to assess the impact of SNHG15 on the migration of SKOV3 cell, as shown in Figure 2(c); in the si-SNHG15 group, the scratch area healing rate after 48 hours was lower than that in the

si-NC group. These results indicated that SNHG15 knockdown restrained the migration and proliferation of ovarian cancer cell.

3.3. SNHG15 Knockdown Arrest Cell Cycle and Promoting Apoptosis of Ovarian Cancer Cell. Then, we investigated the impact of SNHG15 on cell cycle and apoptosis. And our results indicated that the proportion of the G0/G1 phase was higher in the si-SNHG15 group than the si-NC group (Figure 3(a)), indicating that SNHG15 knockdown induced G1/G0 phase arrest.

Besides, flow cytometry revealed an increase in apoptosis in the si-SNHG15 group than the si-NC group (Figure 3(b)), indicating that SNHG15 knockdown promoted ovarian cancer cell apoptosis.

3.4. SNHG15 Regulated CDK6 Expression. CDK6 regulated cell cycle progression under physiological and pathological conditions [20, 21], and published evidences have showed that CDK6 was important in the development of ovarian cancer [22, 23]. To demonstrate whether SHNG15 regulated CDK6 in ovarian cancer, we analyzed the CDK6 expression after SNHG15 knockdown, and in the si-SNHG15 group, CDK6 was lower than that in the si-NC group (Figure 4), indicating that SNHG15 regulated CDK6 expression in ovarian cancer.

3.5. SNHG15 Regulated CDK6 Expression via miR-370-3p. SNHG15 usually regulated the expression of target gene via miRNA in cancers [24, 25]. Thus, we used StarBase database to predict potential miRNA that interacts with SNHG15 and CDK6. miR-370-3p was suggested as a potential miRNA which interacts with SNHG15 and CDK6 (Figure 5(a)). Subsequently, we construct plasmids containing the wild-type and mutated-type binding sites of miR-370-3p in SNHG15 and 3′UTR of CDK6 for luciferase report assays. And the results of luciferase report assays showed that luciferase activity was decreased in the SNHG15 wild-type and CDK-3′UTR wild-type groups than the SNHG15 mutated-type and CDK-3′UTR mutated-type groups (Figures 5(b) and 5(c)). Lastly, rescue experiment indicated that the miR-370-3p inhibitor restored downregulated expression of CDK6 induced by SNHG15 knockdown (Figure 5(d)). To sum up, our results demonstrate that SNHG15 plays a biological role in ovarian cancer through CDK6 via miR-370-3p (Figure 5(e)).

4. Discussion

A growing body of evidences suggests the association of tumor and lncRNA, and lncRNA may be a therapeutic target for tumor [26, 27]. Herein, we initially identified that SNHG15 was upregulated in ovarian cancer based on published data, and then, we validated it in tumor tissues and cell lines. Lastly, the clinical value and mechanism of SNHG15 in ovarian cancer were investigated. The results showed that SNHG15 was upregulated and predicted poor prognosis in ovarian cancer; in addition, SNHG15 promoted cancer cell proliferation through upregulated CDK6 via inhibited mir-370-3p.

SNHG15 was firstly reported in 2012 [28]. Subsequently, SNHG15 was investigated in tumor, and the SNHG15 expression was upregulated in cancers and high SNHG15 expression predicted poor prognosis, for instance, gastric cancer [17], lung cancer [18], colorectal cancer [29], and glioma [24]. Consistent with the recent evidence raised by Zhang et al. [30], our results showed that SNHG15 was upregulated in ovarian cancer; it is noteworthy that our results were based on the GEO dataset and verified by the specimen of our own; this makes the results more reliable. In addition, the prognostic role of SNHG15 was identified by Kaplan-Meier plotter database due to our limited sample size and SNHG15 was correlated with poor PFS. Nonetheless, these results indicated that SNHG15 was highly expressed in ovarian cancer and predicted poor outcome; it can be used to stratify newly diagnosed patients and initiate individualized therapeutic methods.

According to published data, SNHG15 promotes tumor progression via serving as miRNA sponges to inhibit miRNA function, implying that in papillary thyroid carcinoma, SNHG15 controlled the YAP1-Hippo signaling pathway via miR-200-3p [25], and accelerates tumor progression in liver cancer via inhibiting miR-141-3p [31] and via sponging miR-338-3p in colorectal cancer [19]. In our study, we found that SNHG15 silencing suppresses proliferation of ovarian cancer, whilst inducing G0/G1 phase arrest and promoting apoptosis. What is more, the G1/S checkpoint regulator—CDK6—expression was downregulated, which suggests that CDK6 was the target of SNHG15. Indeed, a recent study suggests that SNHG15 targets CDK6 in glioma [24]. Then, we identified miR-370-3p as the bridge between SNHG15 and CDK6 by using online database, luciferase report assays, and rescue experiment. Taken together, our results showed that SNHG15 promoted ovarian cancer cell proliferation through upregulated CDK6 via inhibiting mir-370-3p.

5. Conclusion

In conclusion, our study suggests that SNHG15 may be used as a prognostic indicator in ovarian cancer and reveals the SNHG15/miR-370-3p/CDK6 pathway in ovarian cancer. Our findings provided a new molecular mechanism of SNHG15 in ovarian cancer and may provide theoretical basis for the development of new clinical treatment strategies.

Abbreviations

CCK8: Cell counting kit-8
DElncRNAs: Differentially expressed lncRNAs
GEO: Gene Expression Omnibus
FC: Fold change
GEPIA: Gene expression profiling interactive analysis
lncRNAs: Long noncoding RNAs
OS: Overall survival
PFS: Progression-free survival.

Data Availability

The datasets used and/or analyzed during the current study are available from the corresponding author upon reasonable request.

Consent

All individuals participating in the study obtained informed consent.

Conflicts of Interest

The authors have no conflict of interests.

Acknowledgments

The authors disclosed the receipt of the following financial support for the research: this work was supported by the Discipline Construction Promotion Project of The Second Affiliated Hospital of Soochow University (a team project of application innovation of nuclear technology in medicine) (serial number: XKTJHTD2021001) & the Priority Academic Program Development of Jiangsu Higher Education Institutions (PAPD).

References

[1] M. Gong, C. Luo, H. Meng et al., "Upregulated LINC00565 accelerates ovarian cancer progression by targeting GAS6," *Oncotargets and Therapy*, vol. Volume 12, pp. 10011–10022, 2019.

[2] B. Deb, A. Uddin, and S. Chakraborty, "miRNAs and ovarian cancer: an overview," *Journal of Cellular Physiology*, vol. 233, no. 5, pp. 3846–3854, 2018.

[3] S. Elsherif, S. Javadi, C. Viswanathan, S. Faria, and P. Bhosale, "Low-grade epithelial ovarian cancer: what a radiologist should know," *The British Journal of Radiology*, vol. 92, no. 1095, article 20180571, 2019.

[4] A. Suarez-Zaizar, E. Cardenas-Cardenas, Y. A. Barajas-Castro, and P. Cortes-Esteban, "Controversies on the treatment of ovarian cancer with dose-dense chemotherapy," *Chinese Clinical Oncology*, vol. 9, no. 4, p. 53, 2020.

[5] C. Pan, I. Stevic, V. Müller et al., "Exosomal microRNAs as tumor markers in epithelial ovarian cancer," *Molecular Oncology*, vol. 12, no. 11, pp. 1935–1948, 2018.

[6] N. Lalwani, S. R. Prasad, R. Vikram, A. K. Shanbhogue, P. C. Huettner, and N. Fasih, "Histologic, molecular, and cytogenetic features of ovarian cancers: implications for diagnosis and treatment," *Radiographics*, vol. 31, no. 3, pp. 625–646, 2011.

[7] J. J. Quinn and H. Y. Chang, "Unique features of long non-coding RNA biogenesis and function," *Nature Reviews. Genetics*, vol. 17, no. 1, pp. 47–62, 2016.

[8] Y. Chi, D. Wang, J. Wang, W. Yu, and J. Yang, "Long non-coding RNA in the pathogenesis of cancers," *Cell*, vol. 8, no. 9, p. 1015, 2019.

[9] J. Jarroux, A. Morillon, and M. Pinskaya, "History, discovery, and classification of lncRNAs," *Advances in Experimental Medicine and Biology*, vol. 1008, pp. 1–46, 2017.

[10] A. Sanchez Calle, Y. Kawamura, Y. Yamamoto, F. Takeshita, and T. Ochiya, "Emerging roles of long non-coding RNA in cancer," *Cancer Science*, vol. 109, no. 7, pp. 2093–2100, 2018.

[11] D. Cheng, J. Deng, B. Zhang et al., "LncRNA HOTAIR epigenetically suppresses miR-122 expression in hepatocellular carcinoma via DNA methylation," *eBioMedicine*, vol. 36, pp. 159–170, 2018.

[12] L. Hu, J. Liu, Y. Meng et al., "Long non-coding RNA HOTAIR regulates myeloid differentiation through the upregulation of p21 via miR-17-5p in acute myeloid leukaemia," *RNA Biology*, vol. 18, no. 10, pp. 1434–1444, 2021.

[13] Z. Z. Liu, Y. F. Tian, H. Wu, S. Y. Ouyang, and W. L. Kuang, "LncRNA H19 promotes glioma angiogenesis through miR-138/HIF-1α/VEGF axis," *Neoplasma*, vol. 67, no. 1, pp. 111–118, 2020.

[14] T. J. Zhang, J. D. Zhou, W. Zhang et al., "H19 overexpression promotes leukemogenesis and predicts unfavorable prognosis in acute myeloid leukemia," *Clinical Epigenetics*, vol. 10, no. 1, p. 47, 2018.

[15] M. Wu, Y. Huang, T. Chen et al., "LncRNA MEG3 inhibits the progression of prostate cancer by modulating miR-9-5p/QKI-5axis," *Journal of Cellular and Molecular Medicine*, vol. 23, no. 1, pp. 29–38, 2019.

[16] X. Zhou, P. Yuan, Q. Liu, and Z. Liu, "LncRNA MEG3 regulates Imatinib resistance in chronic myeloid leukemia via suppressing MicroRNA-21," *Biomolecules & Therapeutics*, vol. 25, no. 5, pp. 490–496, 2017.

[17] Z. Chen, T. Zhong, T. Li et al., "LncRNA SNHG15 modulates gastric cancer tumorigenesis by impairing miR-506-5p expression," *Bioscience Reports*, vol. 41, no. 7, 2021.

[18] B. Jin, H. Jin, H. B. Wu, J. J. Xu, and B. Li, "Long non-coding RNA SNHG15 promotes CDK14 expression via miR-486 to accelerate non-small cell lung cancer cells progression and metastasis," *Journal of Cellular Physiology*, vol. 233, no. 9, pp. 7164–7172, 2018.

[19] M. Li, Z. Bian, G. Jin et al., "LncRNA-SNHG15 enhances cell proliferation in colorectal cancer by inhibiting miR-338-3p," *Cancer Medicine*, vol. 8, no. 5, pp. 2404–2413, 2019.

[20] E. Laurenti, C. Frelin, S. Xie et al., "CDK6 levels regulate quiescence exit in human hematopoietic stem cells," *Cell Stem Cell*, vol. 16, no. 3, pp. 302–313, 2015.

[21] A. S. Tigan, F. Bellutti, K. Kollmann, G. Tebb, and V. Sexl, "CDK6–a review of the past and a glimpse into the future: from cell-cycle control to transcriptional regulation," *Oncogene*, vol. 35, no. 24, pp. 3083–3091, 2016.

[22] L. Duan, Y. Yan, G. Wang, Y. L. Xing, J. Sun, and L. L. Wang, "MuiR-182-5p functions as a tumor suppressor to sensitize human ovarian cancer cells to cisplatin through direct targeting the cyclin dependent kinase 6 (CDK6)," *Journal of BUON*, vol. 25, no. 5, pp. 2279–2286, 2020.

[23] X. Pan, Z. Guo, Y. Chen et al., "STAT3-induced lncRNA SNHG17 exerts oncogenic effects on ovarian cancer through regulating CDK6," *Molecular Therapy-Nucleic Acids*, vol. 22, pp. 38–49, 2020.

[24] Z. Li, J. Zhang, H. Zheng et al., "Modulating lncRNA SNHG15/CDK6/miR-627 circuit by palbociclib, overcomes temozolomide resistance and reduces M2-polarization of glioma associated microglia in glioblastoma multiforme," *Journal of Experimental & Clinical Cancer Research*, vol. 38, no. 1, p. 380, 2019.

[25] D. M. Wu, S. Wang, X. Wen et al., "LncRNA SNHG15 acts as a ceRNA to regulate YAP1-hippo signaling pathway by sponging miR-200a-3p in papillary thyroid carcinoma," *Cell Death & Disease*, vol. 9, no. 10, p. 947, 2018.

[26] M. M. Kumar and R. Goyal, "LncRNA as a therapeutic target for angiogenesis," *Current Topics in Medicinal Chemistry*, vol. 17, no. 15, pp. 1750–1757, 2017.

[27] A. Renganathan and E. Felley-Bosco, "Long noncoding RNAs in cancer and therapeutic potential," *Advances in Experimental Medicine and Biology*, vol. 1008, pp. 199–222, 2017.

[28] H. M. Tani and M. Torimura, "Identification of short-lived long non-coding RNAs as surrogate indicators for chemical stress response," *Biochemical and Biophysical Research Communications*, vol. 439, no. 4, pp. 547–551, 2013.

[29] M. Saeinasab, A. R. Bahrami, J. González et al., "SNHG15 is a bifunctional MYC-regulated noncoding locus encoding a lncRNA that promotes cell proliferation, invasion and drug resistance in colorectal cancer by interacting with AIF," *Journal of Experimental & Clinical Cancer Research*, vol. 38, no. 1, p. 172, 2019.

[30] J. Zhang, L. Wang, J. Jiang, and Z. Qiao, "The lncRNA SNHG15/miR-18a-5p axis promotes cell proliferation in ovarian cancer through activating Akt/mTOR signaling pathway," *Journal of Cellular Biochemistry*, vol. 121, no. 12, pp. 4699–4710, 2020.

[31] J. Ye, L. Tan, Y. Fu et al., "LncRNA SNHG15 promotes hepatocellular carcinoma progression by sponging miR-141-3p," *Journal of Cellular Biochemistry*, vol. 120, no. 12, pp. 19775–19783, 2019.

Hindawi
BioMed Research International
Volume 2021, Article ID 9623571, 12 pages
https://doi.org/10.1155/2021/9623571

Research Article

Plasma D-Dimer Level Correlates with Age, Metastasis, Recurrence, Tumor-Node-Metastasis Classification (TNM), and Treatment of Non-Small-Cell Lung Cancer (NSCLC) Patients

Jiqiang Guo,[1,2,3] Ying Gao,[1,2,3] Zhihua Gong,[2,3] Pengfei Dong,[4] Yajie Mao,[2,3] Fang Li,[2,3] Jianrong Rong,[2,3] Junping Zhang,[2,3] Yongnian Zhou,[2,3] Huijing Feng,[2,3] Hongxia Guo,[2,3] Linxia Gu,[4] Meiwen An,[1] Kaixue Wen,[2,3] and Jin Zhang[2,3]

[1]*College of Biomedical Engineering, Taiyuan University of Technology, Taiyuan, 030024, Shanxi, China*
[2]*Shanxi Bethune Hospital, Shanxi Academy of Medical Sciences, Tongji Shanxi Hospital, Third Hospital of Shanxi Medical University, Taiyuan, 030032, China*
[3]*Tongji Hospital, Tongji Medical College, Huazhong University of Science and Technology, Wuhan, 430030, China*
[4]*Department of Biomedical and Chemical Engineering and Sciences, Florida Institute of Technology, Melbourne, 32901 FL, USA*

Correspondence should be addressed to Meiwen An; meiwen_an@163.com, Kaixue Wen; wkx0322@163.com, and Jin Zhang; zhangjin_99@126.com

Received 10 May 2021; Revised 6 July 2021; Accepted 11 August 2021; Published 19 October 2021

Academic Editor: Bing Wang

Objective. This study is aimed at teasing out the correlation of plasma D-dimer (D-D) levels to age, metastasis, TNM stage (tumor-node-metastasis classification), and treatment in non-small-cell lung cancer (NSCLC) patients of different ages, to facilitate early diagnosis of hypercoagulable state, choose appropriate treatment, and use appropriate anticoagulants. Hence, thrombosis and complications caused by excessive anticoagulants can be prevented; thrombus or disseminated intravascular coagulation (DIC) and other complications in elderly patients with NSCLC can be reduced or avoided. By monitoring the level of plasma D-D in patients with NSCLC, recurrence and metastasis can be predicted in the early stage and the TNM stage can be evaluated. *Methods*. A total of 670 patients with NSCLC were selected in Shanxi Bethune Hospital from March 2014 to October 2020 as the experimental group, and 950 healthy people were selected from the physical examination center of the same hospital as the control group. The data of patients with NSCLC diagnosed for the first time without any treatment were collected and grouped based on metastasis, TNM stage, treatment, and pathological type, and the correlation with plasma D-D level was analyzed. Plasma D-D levels were measured by immunoturbidimetry on an ACL TOP 700 Automatic Coagulation Analyzer. The patients were further divided into two groups according to different treatment methods, and the differences in plasma D-D levels between patients receiving chemotherapy and those receiving targeted therapy in different treatment cycles were analyzed. The correlation between D-D levels and age in healthy controls was analyzed. The difference in D-D levels between NSCLC patients and healthy controls of the same age was analyzed. *Results*. All data of both the experimental group and the control group were normally distributed. The average age of the experimental group was 61.31 ± 6.23 (range: 36-92) years. The average age of the control group was 61.14 ± 11.12 (range: 35-85) years. There was no significant difference in gender between the experimental group and the control group ($p > 0.05$). The plasma D-D level of NSCLC patients was significantly higher than that of the healthy controls ($p < 0.05$). No significant difference in plasma D-D level was found between NSCLC patients of different genders, and the finding was similar between healthy controls of different genders ($p > 0.05$). Significant difference in the D-D level was found between the groups of 30-59 years and 60-69 years ($p < 0.05$), between groups of 60-69 years and 70-79 years ($p < 0.05$), and between 70-79 years and ≥80 years ($p < 0.05$). The plasma D-D level of patients ≤ 79 years old increased with age, but it decreased in those over 80 years old. According to Pearson correlation analysis, there was a positive correlation between the D-D level and the age of NSCLC patients under 79 years old ($p < 0.05$). The differences in D-D levels between the four age groups were statistically

significant ($p < 0.05$), showing an upward trend of the D-D level in healthy controls with the increase of age. There were statistically significant differences in D-D levels between NSCLC patients and healthy controls of the matching age group ($p < 0.05$), suggesting that NSCLC patients had significantly higher D-D levels than healthy people of the same age group. The differences in D-D levels between NSCLC patients without metastasis, NSCLC patients with metastasis, and healthy people were statistically significant ($p < 0.05$). The patients with metastasis had the highest D-D level, and healthy people had the lowest D-D level. The difference in plasma D-D levels between patients of different TNM stages was statistically significant ($p < 0.05$). Patients with an advanced TNM stage tended to have higher D-D levels. The TNM stage and D-D level of NSCLC patients changed significantly before and after treatment. An earlier stage was related to a more obvious change in D-D levels after treatment with a statistically significant difference ($p < 0.05$). A more advanced stage was associated with a smaller change in the D-D level after treatment, with no statistically significant difference ($p > 0.05$). The plasma D-D levels before and after four cycles of chemotherapy or targeted therapy were higher than those of the healthy control group, and the differences were statistically significant ($p < 0.05$). The D-D level of patients after chemotherapy was significantly lower than that before chemotherapy ($p < 0.05$), but there was no significant difference before and after targeted therapy ($p > 0.05$). The D-D level after the first cycle of chemotherapy was higher than that before chemotherapy. The level of D-D after the third and fourth cycles was significantly lower than that before chemotherapy ($p < 0.05$). No significant difference was found between the D-D level before treatment and that after four cycles of chemotherapy ($p > 0.05$). *Conclusion*. It is suggested that coagulation test indexes should be included to evaluate the treatment regimen for NSCLC patients. Most patients with NSCLC are in a hypercoagulable state, which is related to age, tumor invasion and metastasis, recurrence, and treatment. Regular monitoring of plasma D-D levels can facilitate early diagnosis of a hypercoagulable state and timely and appropriate use of anticoagulants, to avoid or reduce complications such as venous thromboembolism in NSCLC patients and to prevent the risk of bleeding caused by excessive anticoagulants. Clinicians can choose the treatment with less harm and maximum benefit for NSCLC patients based on the plasma D-D level. When in a hypercoagulable state, the body's blood viscosity increases, making it more conducive to the growth and infiltration of tumor cells. Our study shows that the recurrence and metastasis of NSCLC are related to coagulation indexes, which provides a theoretical basis for the early diagnosis and treatment of recurrent and metastatic NSCLC.

1. Introduction

Lung cancer is the most common and deadly malignant tumor worldwide. At the time of diagnosis, 80% of lung cancer patients are in the advanced stage, and the 5-year survival rate is less than 15%, posing a serious threat to human health [1, 2]. Non-small-cell lung cancer (NSCLC), the most common pathological type [3] of lung cancer, includes squamous cell carcinoma, adenocarcinoma, adenosquamous cell carcinoma, and other histological types except small-cell carcinoma and accounts for about 85% of all lung cancer cases [4]. Compared with small-cell carcinoma, NSCLC features slow growth and division, as well as late diffusion and metastasis.

The hypercoagulable state, which is common in patients with malignant tumors, can result in thrombosis, such as pulmonary embolism, and hence is a leading factor of death [5–7]. In recent years, studies have found that the disordered coagulation function may be related to the occurrence and development as well as the clinical treatment and prognosis of malignant tumors [8, 9]. Therefore, the changes in coagulation function and the necessity of early anticoagulation therapy have attracted the attention of clinicians globally [10, 11]. The complex mechanism of hypercoagulable state in patients with malignant tumors is closely related to the biological characteristics of the tumor and can lead to disordered coagulation and fibrinolysis system [12]. Tumor cells can secrete more tissue factors, promote the release of procoagulant substances, and interact with vascular endothelial cells, platelets, and monocytes, which all contribute to the hypercoagulable state. Studies have shown that fibrinogen (FIB), platelet (PLT), and cancer cells can form microthrombosis under a hypercoagulable state, so tumor cells can escape immune attack, thus leading to tumor metastasis [13, 14]. In this paper, by analyzing the characteristics of D-D levels in NSCLC patients, we retrospectively explored the correlation of D-D levels to age, metastasis, TNM stage, and treatment methods, as well as the effect of D-D levels on a hypercoagulable state in NSCLC patients.

2. Materials and Methods

2.1. Population Statistics

(1) 670 NSCLC cases and 950 healthy volunteers were selected for the investigation. All of them were in the Shanxi Bethune Hospital from March 2014 to October 2020. The NSCLC patients were diagnosed according to the World Health Organization criteria (2015 edition). And their TNM staging is based on the International Association for the Study of Lung Cancer (IASLC) and the Union for International Cancer Control (UICC) (issued in January 2017) (Table 1). Healthy volunteers mean they received physical examination without obvious heart, liver, or kidney diseases and the normal result of accessory examination

(2) NSCLC patients of inclusive and exclusive criteria: inclusive: age group: 35 to 95 years old, male or female; firstly diagnosed by pathology or cytology; expected survival life-time ≥ 3 months; without other cancers; volunteer; and no enrollment in other clinical trials. Exclusive: with severe immunodeficiency or autoimmune diseases; with chronic congestive heart failure; with a history of operation, trauma, and burn in six months; and with hormone or anticoagulant therapies

Table 1: TNM classification of non-small-cell lung cancer (8th edition).

Comprehensive staging	T stage	N stage	M stage	Number
0 stage	Tis (carcinoma in situ)	N0	M0	0
IA1 stage	T1a (mis)	N0	M0	98
IA2 stage	T1b	N0	M0	
IA3 stage	T1c	N0	M0	
IB stage	T2a	N0	M0	
IIA stage	T2b	N0	M0	
IIB stage	T1a-c	N1	M0	101
	T2a	N1	M0	
	T2b	N1	M0	
	T3	N0	M0	
IIIA stage	T1a-c	N2	M0	172
	T2a-b	N2	M0	
	T3	N1	M0	
	T4	N0	M0	
	T4	N1	M0	
IIIB stage	T1a-c	N3	M0	
	T2a-b	N3	M0	
	T3	N2	M0	
	T4	N2	M0	
IIIC stage	T3	N3	M0	
	T4	N3	M0	
IVA stage	Any T	Any N	M1a/b	299
IVB stage	Any T	Any N	M1c	
Total				670

TNM:Tumor Node Metastasis.

(3) TNM staging

(4) NSCLC patient therapy grouping

Chemotherapy group: chemotherapy regimen: on the basis of supporting treatment, pemetrexed (MTA, 500 mg/bottle, Hausen Pharmaceutical, H20093996) 500 mg/m^2 (d1) + cisplatin (DDP, 20 mg/bottle, Qilu Pharmaceutical, production batch number: 09100212) 75 mg/m^2 (d1-d5), ivgtt, was given according to the body surface area. Oral folic acid 400 μg/d was given 7 days before the first administration of pemetrexed for at least 5 days until 21 days after the last administration, and vitamin B12 1000 μg was injected intramuscularly 7 days before the beginning of the first cycle of chemotherapy, then once every 3 cycles. Dexamethasone tablets (4 mg, bid) were taken orally on the day before, the same day, and after administration to prevent skin reaction. The above chemotherapy consists of one cycle every 3 weeks, with a total of four cycles. If the disease progressed or there were serious adverse reactions, the treatment was stopped and the study was withdrawn, but the adverse reactions were recorded. Targeted drug therapy group: the targeted treatment group was treated with erlotinib (Roche Registration Ltd., H20170030 (150 mg/d)).

Table 2

(a) Comparison of the number of patients in different gender groups between the experimental group and the control group (n)

Grouping	Experience group	Control group	χ^2 value	p value
Male	358	497	0.197	0.657
Female	312	453		
Total	670	950		

(b) Comparison of the number of patients in different age groups between the experimental group and the control group (n)

Grouping (year)	Experience group	Control group	χ^2 value	p value
30-59	189	349	26.815	$p \leq 0.001$
60-69	273	283		
70-79	167	177		
≥80	41	141		
Total	670	950		

After continuous treatment for 3 weeks, the interval was 1 week for 1 cycle, and the treatment was carried out for 4 cycles.

Table 3: Internal quality control results of coagulation test items from 2014 to 2020.

Year	PT		INR		APTT		TT		FIB-C		AT-III		D-D	
	IQC	CV (%)	IQC	CV (%)	IQC	CV (%)	IQC	CV (%)	IQC	CV (%)	IQC	CV (%)	IQC	CV (%)
2020	11.05 + 0.46	4.29	1.01 + 0.05	4.14	30.29 + 0.95	3.81	14.41 + 0.78	4.62	2.85 + 0.13	4.56	102.00 + 3.89	3.44	421.00 + 20.00	4.75
2019	11.50 + 0.50	4.35	1.08 + 0.04	3.70	30.70 + 1.25	4.07	14.50 + 0.79	4.83	3.04 + 0.15	4.93	110.00 + 4.42	4.17	421.00 + 20.00	4.75
2018	11.00 + 0.50	4.50	1.02 + 0.05	4.90	30.30 + 1.20	3.96	14.80 + 0.72	4.73	3.19 + 0.13	4.08	105.00 + 4.11	3.91	386.00 + 22.00	5.70
2017	11.50 + 0.45	3.91	1.06 + 0.05	4.72	31.00 + 1.12	3.61	14.60 + 0.83	5.68	3.30 + 0.16	4.85	103.00 + 3.98	3.81	354.00 + 22.00	5.25
2016	11.50 + 0.50	4.35	1.07 + 0.06	5.59	31.08 + 1.30	4.18	14.35 + 0.66	5.53	3.29 + 0.15	4.56	108.00 + 4.22	4.16	753.00 + 23.00	3.12
2015	10.90 + 0.50	4.59	0.99 + 0.04	5.06	31.40 + 0.99	3.87	14.71 + 0.59	4.23	3.04 + 0.19	5.25	110.00 + 4.31	4.07	728.00 + 24.00	3.23
2014	11.50 + 0.66	4.74	1.06 + 0.06	5.66	30.90 + 1.56	5.05	14.63 + 0.56	3.89	2.85 + 0.19	6.67	103.00 + 3.76	4.05	739.00 + 25.00	3.34

IQC: internal quality control.

(5) Healthy volunteers of inclusive criteria

Age group: 35 to 95 years old, male or female; Negative tumor markers; Healthy (conclusion) with the normal result of accessory examination; Volunteer; No enrollment in other clinical trials.

(6) Age grouping (NSCLC cases and 950 healthy volunteers)

2.2. Methods. Plasma sample: fasting elbow venous blood was collected (containing sodium citrate anticoagulant; anticoagulant and whole blood ratio was 1 : 9) and centrifugated at 3500 r/min for 10 min ($r = 13$ cm), 25°C. NSCLC patient's blood samples were collected 12 hours before and after treatment.

Plasma PT, INR, APTT, TT, FIB-C, AT-III, and D-D were detected by an ACL TOP 700 Automatic Coagulation Analyzer. The test kit was purchased from Wofen company of Spain (modelRecombiplasTin 2G, RecombiplasTin 2G, APTT-SP, Thrombin Time, Fibrinogen-C (clauss method) XL Kit, Liquid Antithrombin, D-D HS500). The normal range of Pt was 9 s-12 s; the normal range of PTA was 80%-160%; the normal range of INR was 0.8-1.4; the normal range of APTT was 28 s-41 s; the normal range of FIB-C was 2.00 g/l-4.40 g/l; the normal range of D-D was 0-200 ng/l.

2.3. Internal Quality Control Results of Coagulation Test Items

2.3.1. Statistical Analysis. All data were analyzed by SPSS 19.0 statistical software, and the measurement data in accordance with normal distribution were analyzed by means ± standard deviation($\bar{x} \pm s$) description and comparison between groups using the t/F test. The qualitative data (or counting data) were described by percentage, and the comparison between groups was described by percentage χ^2 inspection. Pearson correlation was used to analyze the correlation. The difference was statistically significant ($p < 0.05$).

3. Results

3.1. Difference in the D-D Level between the Experimental Group and the Control Group. There were 358 male and 312 female patients in the NSCLC group. The age ranged from 36 to 92 years, with an average of 61.31 ± 6.23 years. There were 497 males and 453 females in the control group, with an average age of 60.21 ± 11.12 years. The experimental group and the control group were further divided into four age groups (30-59, 60-69, 70-79, and ≥80 years), respectively. There was no significant difference in the number of different genders between the two groups ($p > 0.05$). A significant difference was found in the number of cases of different ages between the two groups ($p < 0.05$), which was comparable. Compared with the control group, the levels of D-D (D-dimer), PT (Prothrombin Time), INR (International Normalized Ratio), and FIB-C (Fibrinogen-c) in the experimental group were significantly higher ($p < 0.05$), the level of TT (Thrombin Time) was significantly lower ($p < 0.05$), and the levels of PT% (Prothrombin Time Activity) and APTT (Activated Partial Thromboplastin Time) were significantly lower ($p > 0.05$) (Tables 2-5).

Table 4: Comparison of D-D between patients with non-small-cell lung cancer and normal people ($\bar{x} \pm s$).

Test items	Experience group	Control group	t value	p value
PT	11.36 ± 1.01	10.87 ± 0.65	4.452	$p \leq 0.001$
INR	1.05 ± 0.09	1.01 ± 0.06	4.503	$p \leq 0.001$
APTT	31.65 ± 2.71	31.46 ± 3.47	0.481	0.631
TT	13.58 ± 1.11	14.22 ± 1.22	-4.269	$p \leq 0.001$
FIB-C	4.00 ± 1.03	3.00 ± 0.55	9.282	$p \leq 0.001$
AT-III	105.00 ± 18.79	104.46 ± 11.61	0.264	0.792
D-D	647.30 ± 1404.26	120.07 ± 71.55	4.108	$p \leq 0.001$

D-D: D-dimer; TT: Thrombin Time; PT: Prothrombin Time; INR: International Normalized Ratio; PT%: Prothrombin Time Activity; APTT: Activated Partial Thromboplastin Time; FIB-C: Fibrinogen-c.

3.2. Difference in D-D Levels of Different Age Groups in the Experimental Group and the Control Group. The data of the experimental group were normally distributed. The difference in D-D level between the 30-59 age group and the 70-79 age group was statistically significant ($p < 0.05$), and no significant difference was found between the other age groups ($p < 0.05$). The D-D levels of 30-59, 60-69, and 70-79 age groups showed an overall upward trend with increasing age, but the D-D level of the ≥80 age group was lower than that of the 60-69 age group and the 70-79 age group. Pearson correlation analysis showed that the D-D levels of 30-59, 60-69, and 70-79 age groups were positively correlated to age ($p < 0.05$), indicating that in patients younger than 80 years, D-D levels presented an upward trend with the increase of age (Table 6).

The data of the control group followed a normal distribution. The between-group difference in the D-D level was statistically significant in all age groups ($p < 0.05$). Pearson correlation analysis showed a positive correlation between D-D level and age in all age groups ($p < 0.05$). The level of D-D in the control group showed an upward trend with the increase of age in the controls younger than 80 years old (Table 6).

The D-D level of the experimental group was significantly higher than that of the control group ($p < 0.05$). The D-D level in all age groups of the experimental group was significantly higher than that in all age groups of the control group. The D-D level showed an upward trend with the increase of age in subjects younger than 80 years old in both groups. However, for those older than 80 years in the experimental group, the D-D level decreased (Table 6).

3.3. Difference in D-D Levels between Patients with and without Metastasis. There were 98 patients without metastasis and 572 patients with metastasis. The D-D level of patients without metastasis was significantly higher than the control group ($p < 0.01$). Therefore, it was the D-D level

Table 5: Correlation analysis of coagulation indexes in patients with non-small-cell lung cancer.

Test items		PT	INR	PT%	APTT	TT	FIB-C	AT-III	D-D
PT	r value	1	0.998	-0.840	0.425	0.351	0.243	-0.399	0.450
	p value		$p \leq 0.001$	$p \leq 0.001$	0.019	0.057	0.196	0.002	0.013
INR	r value	0.998	1	-0.837	0.425	0.351	0.243	-0.404	0.445
	p value	$p \leq 0.001$		$p \leq 0.001$	0.019	0.057	0.195	0.002	0.014
PT%	r value	-0.840	-0.837	1	-0.355	-0.332	-0.209	0.329	-0.317
	p value	$p \leq 0.001$	$p \leq 0.001$		0.054	0.073	0.267	0.012	0.088
APTT	r value	0.425	0.425	-0.355	1	0.091	0.265	-0.128	0.116
	p value	0.019	0.019	0.054		0.632	0.042	0.501	0.543
TT	r value	0.351	0.351	-0.332	0.091	1	-0.439	-0.229	-0.120
	p value	0.057	0.057	0.073	0.632		0.001	0.022	0.529
FIB-C	r value	0.243	0.243	-0.209	0.265	-0.439	1	-0.056	0.148
	p value	0.196	0.195	0.267	0.042	0.001		0.768	0.436
AT-III	r value	-0.399	-0.404	0.329	-0.128	-0.229	-0.056	1	0.191
	p value	0.002	0.002	0.012	0.501	0.022	0.768		0.132
D-D	r value	0.450	0.445	-0.317	0.116	-0.120	0.148	0.191	1
	p value	0.013	0.014	0.088	0.543	0.529	0.436	0.132	

PT: Prothrombin Time; INR: International Normolized Ratio; PT%: Prothrombin Time Activity; APTT: Activated Partial Thromboplastin Time; TT: Thrombin Time; FIB-C: Fibrinogen-c; AT-?: Anti-Thrombin ?, D-D: D-dimer.

Table 6: Comparison of D-D levels in different age groups between the experimental group and the control group ($\bar{x} \pm s$).

Test items	Experience group D-D (ng/ml)	Control group D-D (ng/ml)	t value	p value
30-59 age group	549.07 ± 771.86	75.04 ± 36.43	3.091	0.018
60-69 age group	1058.44 ± 1626.59	108.73 ± 43.41	4.437	0.014
70-79 age group	1194.02 ± 1566.64	145.15 ± 51.70	7.497	0.001
≥80 age group	764.68 ± 879.61	245.30 ± 85.92	3.579	0.016
Total	911.35 ± 1297.27	137.95 ± 82.35	7.091	$p \leq 0.001$
F value	1.955	2.472		
p value	0.124	0.015		
r value	0.509	0.711		
p value	0.007	$p \leq 0.001$		

D-D: D-dimer.

Table 7: Comparison of D-D levels between the experimental group and the control group ($\bar{x} \pm s$).

Grouping	Experience group D-D (ng/ml)	Control group D-D (ng/ml)	t value	p value
Nonmetastasis	448.50 ± 505.17	120.07 ± 71.55	2.945	0.004
Metastasis	846.10 ± 1908.34		4.986	$p \leq 0.001$
t value	4.560			
p value	0.001			

D-D: D-dimer.

in patients with metastasis ($p < 0.01$). The D-D level of patients without metastasis was significantly higher than that of those with metastasis ($p < 0.01$) (Table 7).

ROC curves of the D-D level for predicting tumor metastasis in NSCLC patients showed an area under the curve of 0.717 (95% confidence interval, 0.603-0.831, $p < 0.001$) (Figure 1).

3.4. Difference in D-D Levels between Patients in Different TNM Stages. According to the TNM classification: 98 cases were in stage I, 101 cases in stage II, 172 cases in stage III, and 299 cases in stage IV. Compared with the D-D level of the control group, the D-D levels of the patients in all TNM stages were higher than those of the control group. And a more advanced TNM stage was related to a higher

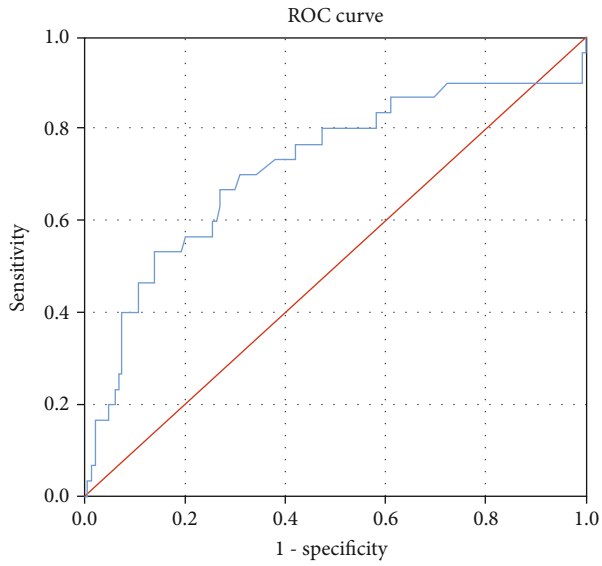

Figure 1: ROC curves of D-dimer for predicting tumor metastasis in NSCLC patients.

D-D level. There was no statistical significance between stage I patients and the control group ($p > 0.05$), but a statistically significant difference was found when comparing the D-D level of the control group with that of stages II, III, and IV patients ($p < 0.05$). There was a significant difference in the D-D level between stage I and stage II patients ($p < 0.05$) (Table 8). The D-D level of stage III patients was significantly higher than that of stage I and II patients ($p < 0.05$) (Table 8). The D-D level of stage IV patients was significantly higher than that of stage I, II, and III patients ($p < 0.05$) (Table 9). Pearson correlation analysis showed the D-D levels of patients were positively correlated with stage ($p < 0.05$), indicating that the D-D level presented an upward trend with the increase of TNM classification (Table 9).

3.5. Differences in D-D Levels of the Experimental Group with Different Treatment Methods before and after Treatment and Comparison with the Control Group. The D-D level of the experimental group after treatment (chemotherapy or targeted therapy) was significantly lower than that before treatment ($p < 0.05$) (Table 10). However, despite the type of treatment used, the D-D level after treatment was still higher than that in the control group, with a significant difference ($p < 0.05$) (Table 11).

For patients receiving chemotherapy, the D-D level before treatment was significantly higher than that of the control group ($p < 0.05$); the D-D level after treatment was significantly lower than that before treatment ($p < 0.05$) (Table 12). The D-D level at each chemotherapy cycle was lower than that before treatment, and the D-D level at the third cycle was significantly different from that before the treatment ($p < 0.05$) (Table 13). Pearson correlation analysis showed that the D-D levels of patients were negatively correlated to the cycle ($p < 0.05$), indicating that D-D levels presented a downward trend with the increase of chemotherapy cycle (Table 13). The difference in the D-D level between cycles was statistically significant ($p < 0.05$) (Table 14).

For patients receiving targeted therapy, the D-D level before treatment was significantly higher than that of the control group ($p < 0.05$) (Table 15). The D-D level decreased after treatment compared with that before the treatment, but the difference was not significant ($p > 0.05$) (Table 15). The D-D level at each treatment cycle was lower than that before the treatment. Although not significant, the difference was more obvious in the later cycle of treatment ($p > 0.05$) (Table 16). The comparison of D-D levels between the treatment cycles showed that the decrease of the D-D level was more obvious in the later cycle of treatment ($p > 0.05$) (Table 17). Pearson correlation analysis showed that the D-D levels of patients were negatively correlated to the cycle ($p < 0.05$), indicating that D-D levels presented a downward trend with the increase of targeted therapy cycles (Table 16).

4. Discussion

The incidence of NSCLC ranks first among all tumors, and it is more commonly found in the elderly [15]. However, in recent years, patients suffering NSCLC tend to be younger [16]. Due to the lack of typical clinical symptoms, NSCLC cases may have missed or delayed diagnosis. When diagnosed, they are already in the late stage. D-D, a degradation product of cross-linked fibrin, is a molecular marker that can reflect the hypercoagulable state and hyperfibrinolysis in the body. The increase of D-D often indicates active thrombosis and fibrinolysis in the body. D-D has a high negative predictive value in the exclusion of thrombotic diseases. When D-D is lower than the clinical decision level, the possibility of thrombosis can be excluded.

Studies have shown that the survival rate of malignant tumor patients without venous thromboembolism (VTE) is at least 3 times higher than that of patients with VTE, and the risk of death for tumor patients with VTE can be increased by 2-6 times [17]. The incidence of VTE in NSCLC patients is about 4%-10%. In patients with advanced NSCLC, about 10% have symptomatic VTE, and more than 50% have asymptomatic VTE [18]. VTE, a common complication and the second cause of death in NSCLC patients, is associated with a poor prognosis of NSCLC. The hypercoagulable state of blood is the underlying mechanism for VTE. Therefore, the change of coagulation function in patients with NSCLC is of great value in predicting survival and guiding treatment.

Age is often used as an important reference index. Studies on the relationship between D-D levels and age in healthy people have shown that healthy elderly people (≥60) have a significantly higher D-D level than healthy young people [19]. The increase of D-D levels in the elderly may be caused by the elevated probability of vascular sclerosis, vulnerable vascular endothelial cells, decreased inhibition of coagulation system activation, secondary hyperfibrinolysis, and increased risk of hypertension and hyperlipidemia. D-D is mainly excreted by the kidney and cleared by phagocytes.

Table 8: Comparison of the D-D level between the experimental group and the control group in different TNM classification ($\bar{x} \pm s$).

Grouping	Experience group		Control group		t value	p value
TNM classification	Number	D-D (ng/ml)	Number	D-D (ng/ml)		
I stage	98	138.35 ± 36.54	950	120.07 ± 71.55	0.71	$p > 0.05$
II stage	101	200.55 ± 155.21			2.80	$p < 0.05$
III stage	172	671.36 ± 327.49			6.30	$p < 0.05$
IV stage	299	1500.85 ± 611.02			2.33	$p < 0.05$
t value	1.955					
p value	0.124					
r value	0.773					
p value	$p \leq 0.001$					

D-D: D-dimer.

Table 9: p values of D-D level comparison between stage I and stage II in the experimental group.

	Grouping	I stage	II stage	III stage	IV stage
Grouping	D-D (ng/ml)	138.35 ± 36.54	200.55 ± 155.21	671.36 ± 327.49	1500.85 ± 611.02
I stage	138.35 ± 36.54	1	$p < 0.05$	$p < 0.05$	$p < 0.05$
II stage	200.55 ± 155.21	$p < 0.05$	1	$p < 0.05$	$p < 0.05$
III stage	671.36 ± 327.49	$p < 0.05$	$p < 0.05$	1	$p < 0.05$
IV stage	1500.85 ± 611.02	$p < 0.05$	$p < 0.05$	$p < 0.05$	1

D-D: D-dimer.

Table 10: Comparison of D-D levels between the experimental group and the control group before and after treatment (chemotherapy, targeted therapy) ($\bar{x} \pm s$).

Grouping	Experience group D-D (ng/ml)	Control group D-D (ng/ml)	t value	p value
Before treatment	1077.26 ± 1301.52	120.07 ± 71.55	10.091	$p \leq 0.001$
After treatment	669.69 ± 1014.35		7.241	$p \leq 0.001$
t value	4.256			
p value	0.013			

D-D: D-dimer.

Table 11: Comparison of D-D levels before and after chemotherapy and targeted therapy in the experimental group ($\bar{x} \pm s$).

Grouping	Chemotherapy group D-D (ng/ml)	Targeted therapy group D-D (ng/ml)	t value	p value
Before treatment	918.45 ± 1068.53	1168.54 ± 1437.67	0.294	0.863
After treatment	490.35 ± 674.18	898.49 ± 1295.33	5.131	0.011
t value	6.640	0.847		
p value	0.003	0.398		

D-D: D-dimer.

Table 12: Comparison of D-D levels between the experimental group and the control group before and after chemotherapy ($\bar{x} \pm s$).

Grouping	Chemotherapy group D-D (ng/ml)	Control group D-D (ng/ml)	t value	p value
Before chemotherapy	918.45 ± 1068.53	120.07 ± 71.55	5.450	$p \leq 0.001$
After chemotherapy	490.35 ± 674.18		0.988	0.023
t value	1.010			
p value	0.020			

D-D: D-dimer.

Table 13: Comparison of D-D levels in different chemotherapy cycles and before chemotherapy in the experimental group ($\bar{x} \pm s$).

Grouping	After chemotherapy D-D (ng/ml)	Before chemotherapy D-D (ng/ml)	t value	p value
First cycle	669.52 ± 990.73	618.45 ± 1068.53	0.255	0.732
Second cycle	497.70 ± 507.63		0.748	0.079
Third cycle	371.94 ± 284.75		1.256	0.015
Fourth cycle	247.69 ± 152.09		1.377	0.013
t value	3.763			
p value	0.042			
r value	0.785			
p value	$p \leq 0.001$			

D-D: D-dimer.

Table 14: p value of D-D level comparison between the experimental group and the chemotherapy cycle group.

	Grouping	Before chemotherapy	First cycle	Second cycle	Third cycle	Fourth cycle
Grouping	D-D (ng/ml)	918.45 ± 1068.53	669.52 ± 990.73	497.70 ± 507.63	371.94 ± 284.75	247.69 ± 152.09
Before chemotherapy	918.45 ± 1068.53	1	0.732	0.079	0.015	0.013
First cycle	669.52 ± 990.73	0.732	1	0.134	0.045	0.026
Second cycle	497.70 ± 507.63	0.079	0.134	1	0.176	0.044
Third cycle	371.94 ± 284.75	0.015	0.045	0.176	1	0.128
Fourth cycle	247.69 ± 152.09	0.013	0.026	0.044	0.128	1

D-D: D-dimer.

Table 15: Comparison of D-D levels between the experimental group and the control group before and after targeted therapy ($\bar{x} \pm s$).

Grouping	Targeted therapy group D-D (ng/ml)	Control group D-D (ng/ml)	t value	p value
Before targeted therapy	1168.54 ± 1437.67	120.07 ± 71.55	7.497	$p \leq 0.001$
After targeted therapy	898.49 ± 1295.33		0.713	0.174
t value	2.886			
p value	0.021			

D-D: D-dimer.

Table 16: Comparison of D-D levels in different targeted treatment cycles and before targeted treatment in the experimental group ($\bar{x} \pm s$).

Grouping	After targeted therapy D-D (ng/ml)	Before targeted therapy D-D (ng/ml)	t value	p value
First cycle	1018.41 ± 1353.63	1168.54 ± 1437.67	0.433	0.206
Second cycle	969.42 ± 1482.26		0.735	0.093
Third cycle	854.86 ± 1321.79		0.959	0.046
Fourth cycle	709.83 ± 825.03		1.060	0.032
t value	8.939			
p value	$p \leq 0.001$			
r value	0.887			
p value	$p \leq 0.001$			

D-D: D-dimer.

As the body's metabolic capacity declines with the increase of age, the D-D level will elevate [20]. In line with the above conclusions, the results of this study reveal the correlation between age and D-D level. With the increase of age, the D-D level shows an upward trend, which is also consistent with the conclusion of Bacon et al.'s study [21]. However, the mechanism of this increase is not clear. Studies have shown that in NSCLC patients, older age is associated with a later TNM stage, lower physical condition score, higher plasma D-D level, and shorter survival time [22]. This study demonstrates that the D-D level of elderly NSCLC patients is significantly higher than that of healthy people of all age

Table 17: p value of D-D level comparison between the experimental group and the targeted treatment group.

	Grouping	First cycle	Second cycle	Third cycle	Fourth cycle
Grouping	D-D (ng/ml)	1018.41 ± 1353.63	969.42 ± 1482.26	854.86 ± 1321.79	709.83 ± 825.03
First cycle	1018.41 ± 1353.63	1	0.657	0.369	0.129
Second cycle	969.42 ± 1482.26	0.657	1	0.544	0.185
Third cycle	854.86 ± 1321.79	0.369	0.544	1	0.319
Fourth cycle	709.83 ± 825.03	0.129	0.185	0.319	1

D-D: D-dimer.

groups, indicating that the coagulation and fibrinolysis system is activated in elderly NSCLC patients. In NSCLC patients of 50-79 years old, as age increases, the D-D level is positively correlated with age. Elderly patients have increased risk of hypertension, cardiovascular diseases, and diabetes, and the development of these diseases may damage the endothelial cells, which is conducive to the formation of intravascular thrombosis [23, 24]. And this formation is manifested by the rise of the D-D level. However, considering the weakened function of the major organs in NSCLC patients over 80 years, together with complications and other influencing factors, NSCLC patients over 80 years old are usually excluded from the study or the number of such patients enrolled is very small [25]. Hence, this study only applied Pearson correlation analysis to patients of 50-79 years old for correlation analysis.

Increasingly clinical evidence has shown obvious abnormalities in the coagulation system and significantly increased D-D levels in patients with malignant tumors, such as digestive system malignant tumor, liver cancer, colorectal cancer, gastric cancer, and breast cancer. The mechanism may be that tumor cells or necrotic surrounding tissues trigger the release of tissue factors, which activate coagulation factors X and XI in the extrinsic coagulation system and fibrinolytic system, leading to the local production of fibrinolytic enzymes, which can directly degrade the extracellular matrix and endow the tumor cells with the invading and metastatic abilities [26]. In this process, the released inflammatory mediators (such as IL and TNF-α) damage the vascular endothelial cells, resulting in the hypercoagulable state of blood [27, 28] and making tumor cells adhere to the vascular wall. The hypercoagulable state in tumor patients not only increases the risk of VTE but also promotes blood vessel distribution around the tumor, enriches the blood supply of tumor tissues, and enhances tumor progression (recurrence and metastasis) [29]. As a specific degradation product of fibrin monomers cross-linked by activator XIII and then hydrolyzed by fibrinolytic enzymes, D-D is a specific marker of fibrinolysis. Continuous increase of D-D often indicates disease progression or poor prognosis.

This study found that the D-D level in NSCLC patients was significantly higher than that in the control group, which can be explained as follows. The tissue of NSCLC patients can secrete procoagulants, and their antithrombotic ability decreases after the vascular intima is infiltrated by lung cancer tissue, both resulting in hypercoagulability in patients [30]. Cancer cells in the blood of NSCLC patients can directly elevate the D-D level, and reactive white blood cells can also increase the plasma D-D level. The TNM stage is an important index for the prognosis and treatment of tumors [31]. Our study found that the TNM stage was significantly correlated with the plasma D-D level. An advanced TNM stage was associated with increased D-D levels. The D-D level in stage III and IV patients of NSCLC was significantly higher than that in patients of stages I and II, with statistical significance ($p < 0.05$). There was no significant difference in the level of D-D between stage I and stage II patients ($p > 0.05$). The D-D level of stage III patients was significantly higher than that of stage I and II patients ($p > 0.05$). The main reason may be that the tumor infiltration of stage III and IV patients is deeper and more extensive than that of stage I and II patients and is often accompanied by lymph nodes and other distant metastases. Cancer patients often suffer complications, such as hypertension, hyperlipidemia, heart failure, and myocardial infarction, which can accelerate blood coagulation, making the D-D level higher. Therefore, monitoring D-D levels and improving the hypercoagulable state of blood in NSCLC patients of different TNM stages can facilitate the early prevention and treatment so as to increase the survival rate of patients. In addition, a majority of NSCLC patients are elderly, and elderly patients, especially those with advanced cancer, are usually bedridden for a long time, resulting in blood stasis. Therefore, NSCLC patients are more likely to suffer abnormal coagulation function and thrombosis than healthy people [32].

NSCLC is a malignant tumor with high mortality. In clinical practice, thrombolysis, anticoagulation, and other treatments usually start after obvious thrombosis appears in patients, and therefore, the curative effect is poor. Many patients die of serious thromboembolism, disseminated intravascular coagulation, and other adverse events [33]. Chemotherapy and targeted therapy, which can improve the clinical symptoms of patients, are commonly used to treat NSCLC [34]. Since VTE directly impacts the survival of NSCLC patients, and the best monitoring index of VTE is the D-D level, the effect of chemotherapy and targeted therapy on D-D levels in NSCLC patients is worth further studying.

This study found that the plasma D-D level of NSCLC patients was higher than that of healthy people, with significant differences, indicating that NSCLC patients are in a

hypercoagulable state, which can cause VTE at any time [35]. This result also suggests the necessity to monitor and control the plasma D-D level in the follow-up treatment of NSCLC patients to prevent thrombosis.

This study also found that after chemotherapy, the difference in the D-D level between two consecutive cycles was not significant, but a significant difference was found between the two cycles with a one-cycle interval, and the difference before and after treatment was also significant, indicating that chemotherapy can well control the hypercoagulable state of NSCLC patients. In patients receiving targeted therapy, the D-D level showed an overall downward trend after treatment. Although there was no significant difference in the first four cycles, the difference was increasingly obvious. Our results suggest that targeted therapy has an impact on the D-D level of NSCLC patients, but chemotherapy exerts a better effect on the improvement of hypercoagulable state in patients. In addition, heparin can be administered when necessary based on the D-D level of patients [36] in order to achieve an ideal therapeutic effect.

5. Conclusion

The plasma D-D level is conducive to the early detection and treatment of NSCLC. For NSCLC patients, blood coagulation function should be examined regularly to detect the hypercoagulable state of blood and conduct treatment timely. An older age is associated with a higher D-D level, advanced stage, and metastasis in NSCLC patients. The elevated D-D level indicates the existence of a hypercoagulable state and the activation of the secondary fibrinolytic system, which can increase the risk of VTE and disseminated intravascular coagulation. Therefore, monitoring the D-D level can help to judge and predict the disease condition. To treat NSCLC, we can use antithrombotic, low molecular weight heparin, and other preventive anticoagulants to eliminate or reduce the risk of deep venous thrombosis and other complications and to control tumor metastasis and improve the comprehensive curative effect and survival of patients.

Data Availability

Based on patient privacy, data are available from the corresponding authors on reasonable request.

Conflicts of Interest

The authors declare that they have no competing interests.

Authors' Contributions

Jiqiang Guo and Ying Gao contributed equally to this work.

Acknowledgments

The authors thank all persons who helped them gather information for patients and supported them for statistical analysis. This work is supported by the Research on Intelligent and Accurate Detection of Medical Devices in Shanxi Province (provincial key training laboratory). We thank all patients and volunteers who participated in the study and all staff in Shanxi Bethune Hospital for their help in the collection of samples.

References

[1] B. G. Han and L. K. Zhou, "Chinese expert consensus on anti-angiogenic drug therapy for advanced non-small cell lung cancer (2019 edition)," *Chinese journal of lung cancer*, vol. 22, no. 7, pp. 401–412, 2019.

[2] C. Kiyohara, K. Yoshimasu, K. Takayama, and Y. Nakanishi, "Lung cancer susceptibility: are we on our way to identifying a high-risk group?," *Future Oncology*, vol. 3, no. 6, pp. 617–627, 2016.

[3] Y. Wang and Y. Wang, "Research progress of antiangiogenic drugs in the treatment of advanced non-squamous non-small cell lung cancer," *Oncology Progress*, vol. 16, no. 10, pp. 16–21, 2018.

[4] J. Yang, Q. H. You, and F. L. Meng, "Preliminary study on the expression and function of mi R-211 in non-small cell lung cancer," *CHinese Journal of Cancer Prevention and Treatment*, vol. 25, no. 11, pp. 773–777, 2018.

[5] A. Katholing, S. Rietbrock, L. Bamber, C. Martinez, and A. T. Cohen, "Epidemiology of first and recurrent venous thromboembolism in patients with active cancer. A population-based cohort study," *Thromb Haemost*, vol. 117, no. 1, pp. 57–65, 2017.

[6] Y. Lin, Z. Liu, Y. Qiu et al., "Clinical significance of plasma D-dimer and fibrinogen in digestive cancer: a systematic review and meta-analysis," *European Journal of Surgical Oncology*, vol. 44, no. 10, pp. 1494–1503, 2018.

[7] E. Donnellan and A. A. Khorana, "Cancer and venous thromboembolic disease: a review," *The Oncologist*, vol. 22, no. 2, pp. 199–207, 2017.

[8] L.-R. Zhu, J. Li, P. Chen, Q. Jiang, and X.-P. Tang, "Clinical significance of plasma fibrinogen and D-dimer in predicting the chemotherapy efficacy and prognosis for small cell lung cancer patients," *Clinical & Translational Oncology*, vol. 18, no. 2, pp. 178–188, 2016.

[9] Y. Hisada and N. Mackman, "Cancer-associated pathways and biomarkers of venous thrombosis," *Blood*, vol. 130, no. 13, pp. 1499–1506, 2017.

[10] C. Ay and I. Pabinger, "VTE risk assessment in cancer. Who needs prophylaxis and who does not?," *Hämostaseologie*, vol. 35, no. 4, pp. 319–324, 2015.

[11] J.-J. Hung, Y.-C. Yeh, W.-J. Jeng et al., "Predictive value of the International Association for the Study of Lung Cancer/American Thoracic Society/European Respiratory Society classification of lung adenocarcinoma in tumor recurrence and patient survival," *Journal of Clinical Oncology*, vol. 32, no. 22, pp. 2357–2364, 2014.

[12] Z. Wang, J. Miao, L. Wang et al., "EGFR-mutant NSCLC presenting with stroke and massive systemic embolization as the first manifestation: case report," *BMC Neurology*, vol. 21, no. 1, 2021.

[13] K. Wakatsuki, S. Matsumoto, K. Migita et al., "Prognostic value of the fibrinogen-to-platelet ratio as an inflammatory and coagulative index in patients with gastric cancer," *Surge Today*, vol. 49, no. 4, pp. 334–342, 2019.

[14] T. Suzuki, H. Shimada, T. Nanami et al., "Hyperfibrinogenemia is associated with inflammatory mediators and poor

prognosis in patients with gastric cancer," *Surge Today*, vol. 46, no. 12, pp. 1394–1401, 2016.

[15] H. Zheng, Z. Li, and R. Zeng, "Comparison of normal reference intervals of plasma D-dimer between elderly and young people," *China Modern Medicine*, vol. 23, no. 21, pp. 140–142, 2016.

[16] X. Jiang, "Retrospective analysis of plasma D-dimer detection results in 671 tumor patients," *Chinese Journal of Health Laboratory Technology*, vol. 18, no. 12, pp. 2646-2647, 2008.

[17] C. J. Fernandes, L. T. K. Morinaga, J. L. Alves et al., "Cancer-associated thrombosis: the when, how and why," *European Respiratory Review*, vol. 28, no. 151, pp. 180–191, 2019.

[18] M. C. Vedovati, M. Ciustozzi, and C. Becattini, "Venous thromboembolism and cancer: Current and future role of direct-acting oral anticoagulants," *Thrombosis Research*, vol. 177, no. 24, pp. 33–41, 2019.

[19] J. Peng, L. Le, and H. Xinai, "Investigation and analysis of normal reference value of plasma D-dimer in healthy people," *Journal of Clinical and Experimental Medicine*, vol. 11, no. 8, pp. 626–628, 2012.

[20] G. Radhakrishna and D. Berridge, "Cancer-related venous thromboembolic disease: current management and areas of uncertainty," *Phlebology*, vol. 27, 2_suppl, pp. 53–60, 2012.

[21] S. L. Bacon, K. L. Lavoie, A. Arsenault et al., "The research on endothelial function in women and men at risk for cardiovascular disease (reward) study: methodology," *BMC Cardiovascular Disorders*, vol. 11, no. 1, p. 50, 2011.

[22] M. RIGHINI, A. PERRIER, P. D. E. MOERLOOSE, and H. BOUNAMEAUX, "D-dimer for venous thromboembolism diagnosis: 20 years later," *Thrombosis and Haemostasis*, vol. 6, no. 7, pp. 1059–1071, 2013.

[23] H. Takano, K. Nakajima, Y. Nagayoshi et al., "Clinical associations of Trousseau's syndrome associated with cerebral infarction and ovarian cancer," *Journal of Gynecologic Oncology*, vol. 29, no. 5, 2018.

[24] S. Guo, W. Lin, and C. Wu, "Analysis of related factors affecting plasma D-dimer level in elderly patients," *Tianjin Medical Journal*, vol. 41, no. 7, pp. 658–661, 2013.

[25] P. Zhang, X. Wu, and B. Ai, "Clinical observation of first-line chemotherapy in patients with advanced non-small cell lung cancer aged 80 and above," *Chinese Journal of Clinical Healthcare*, vol. 15, no. 5, pp. 538-539, 2012.

[26] C. Tieken and H. H. Versteeg, "Anticoagulants versus cancer," *Thrombosis Research*, vol. 140, Supplement 1, pp. S148–S153, 2016.

[27] W. Li, Y. Tang, Y. Song et al., "Prognostic role of pretreatment plasma D-dimer in patients with solid tumors: a systematic review and meta-analysis," *Cellular Physiology and Biochemistry*, vol. 45, no. 4, pp. 1663–1676, 2018.

[28] C. H. Liu, P. Gong, and J. Yang, "Relationship between circulating tumor cells and coagulation factors in primary lung cancer patients," *Chinese Journal of Oncology*, vol. 38, no. 5, pp. 368–371, 2016.

[29] X. Fei, H. Wang, W. Yuan, M. Wo, and L. Jiang, "Tissue factor pathway inhibitor-1 is a valuable marker for the prediction of deep venous thrombosis and tumor metastasis in patients with lung cancer," *BioMed Research International*, vol. 2017, 8 pages, 2017.

[30] M. Lous-Bou, L. B. Harrington, and C. Kabrhel, "Environmental and genetic risk factors associated with venous thromboembolism," *Seminars in Thrombosis and Hemostasis*, vol. 42, no. 8, pp. 808–820, 2016.

[31] R. Y. Wang, R. Liu, and L. J. Zhao, "Correlation analysis between FIB and D-dimer and elinicopathological features in patients with coloreetal caneer and type 2 diabetes," *Chinese journal of canc-er prevention and treatment*, vol. 24, no. 5, pp. 332–336, 2017.

[32] N. M. Kuderer, M. S. Poniewierski, and E. Culakova, "Predictors of venous thromboembolism and early mortality in lung cancer: results from a global prospective study (CANTARISK)," *The Oncologist*, vol. 23, no. 2, pp. 247–255, 2018.

[33] G. T. Gerotziafas, A. Taher, H. Abdel-Razeq et al., "A predictive score for thrombosis associated with breast, colorectal, lung, or ovarian cancer: the prospective COMPASS–Cancer-Associated thrombosis study," *The Oncologist*, vol. 22, no. 10, pp. 1222–1231, 2017.

[34] D. Yue, S. Xu, Q. Wang et al., "Erlotinib versus vinorelbine plus cisplatin as adjuvant therapy in Chinese patients with stage IIIA _EGFR_ mutation-positive non-small-cell lung cancer (EVAN): a randomised, open-label, phase 2 trial," *The lancet. Respiratory medicine*, vol. 6, no. 11, pp. 863–873, 2018.

[35] C. Gong, Z. Li, and D. Zhou, "Risk factors of lung cancer complicated with symptomatic venous thromboembolism," *Chinese Journal of Tuberculosis and Respiratory Diseases*, vol. 39, no. 6, pp. 454–458, 2016.

[36] Chinese Medical Association, oncology branch of Chinese Medical Association, and Journal of Chinese Medical Association, "Guidelines for the clinical diagnosis and treatment of lung cancer of Chinese Medical Association (2019 Edition)," *Chinese Journal of oncology*, vol. 42, no. 4, pp. 257–287, 2020.

Hindawi
BioMed Research International
Volume 2021, Article ID 9789613, 2 pages
https://doi.org/10.1155/2021/9789613

Corrigendum

Corrigendum to "Cytoreductive Surgery plus Hyperthermic Intraperitoneal Chemotherapy Improves Survival with Acceptable Safety for Advanced Ovarian Cancer: A Clinical Study of 100 Patients"

Jue Zhang,[1] Xin-bao Li,[1] Zhong-he Ji,[1] Ru Ma,[1] Wen-pei Bai,[2] and Yan Li[1]

[1]*Department of Peritoneal Cancer Surgery, Beijing Shijitan Hospital, Capital Medical University, China*
[2]*Department of Gynecology, Beijing Shijitan Hospital, Capital Medical University, China*

Correspondence should be addressed to Yan Li; liyansd2@163.com

Received 5 August 2021; Accepted 5 August 2021; Published 30 August 2021

In the article titled "Cytoreductive Surgery plus Hyperthermic Intraperitoneal Chemotherapy Improves Survival with Acceptable Safety for Advanced Ovarian Cancer: A Clinical Study of 100 Patients" [1], there was an error in Figure 2(b) where mPTS should have been mPFS and mOS should have been mPFS. The corrected Figure 2 is as below.

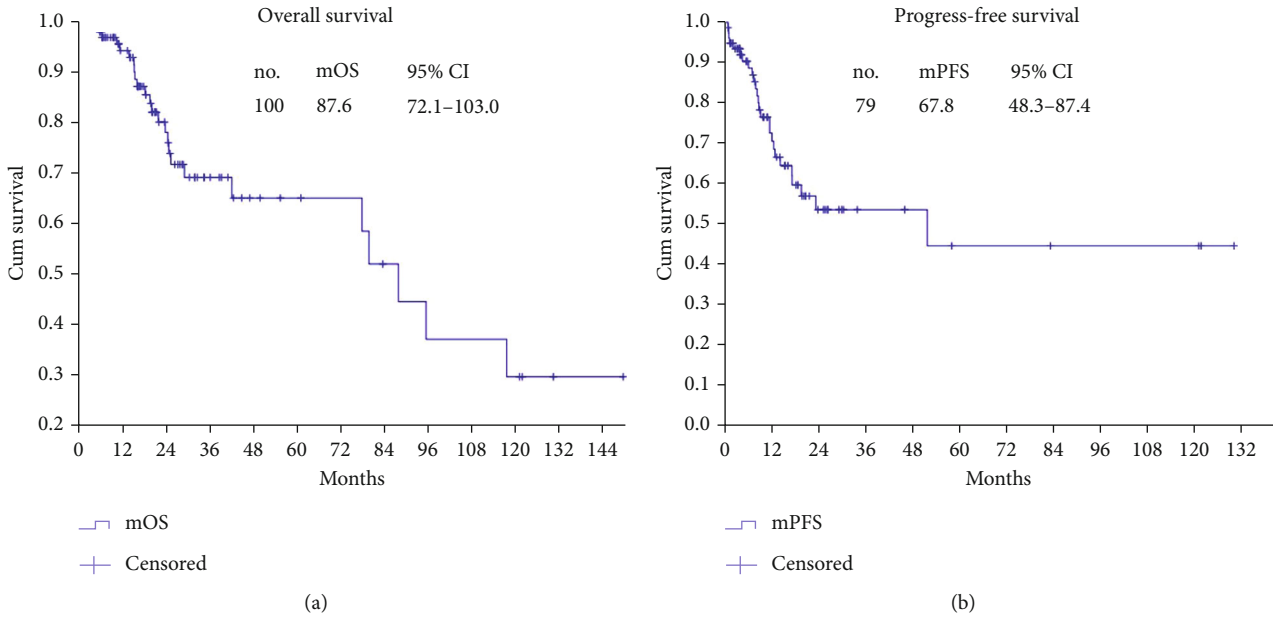

Figure 2: OS and PFS in the AOC patients. (a) OS of 100 AOC patients. (b) PFS of 79 AOC patients with complete CRS+HIPEC.

References

[1] J. Zhang, X.-b. Li, Z.-h. Ji, R. Ma, W.-p. Bai, and Y. Li, "Cytoreductive Surgery plus Hyperthermic Intraperitoneal Chemotherapy Improves Survival with Acceptable Safety for Advanced Ovarian Cancer: A Clinical Study of 100 Patients," *BioMed Research International*, vol. 2021, Article ID 5533134, 12 pages, 2021.

Hindawi
BioMed Research International
Volume 2021, Article ID 1028158, 12 pages
https://doi.org/10.1155/2021/1028158

Research Article

Development and Validation of an Autophagy-Related Signature for Head and Neck Squamous Cell Carcinoma

Chang Liu,[1] Wenling Wu,[2] Meng Xu,[1] Jinglin Mi,[1] Longjiang Xu,[3] and Rensheng Wang[1]

[1]*Department of Radiation Oncology, The First Affiliated Hospital of Guangxi Medical University, Radiation Oncology Clinical Medical Research Center of Guangxi, Nanning 530021, China*
[2]*Department of Medical Oncology, The First Affiliated Hospital of Guangxi Medical University, Nanning, Guangxi Zhuang Autonomous Region 530021, China*
[3]*Department of Pathology, The Second Affiliated Hospital of Soochow University, Suzhou, 215000 Jiangsu, China*

Correspondence should be addressed to Longjiang Xu; dbyjr0627@163.com and Rensheng Wang; 13807806008@163.com

Received 27 May 2021; Accepted 23 July 2021; Published 11 August 2021

Academic Editor: Qiang Liu

Introduction. HNSCC is the sixth most frequent type of malignant carcinoma with a low prognosis rate. In addition, autophagy is important in cancer development and progression. The purpose of this study is to investigate the potential significance of ARGs in the diagnosis and treatment of HNSCC. *Materials and Methods*. Expression data and clinical information of HNSCC samples were collected from the TCGA database, and a list of ARGs was obtained from the MSigDB. Then, we used R software to perform differential expression analysis and functional enrichment analysis. Further analysis was also performed to find out the survival-related ARGs in HNSCC, and two prognosis-related ARGs, FADD and NKX2-3, were selected to construct a prognosis prediction model. Moreover, some methods were applied to validate the prognosis prediction model. Finally, we used cell lines and clinical tissue samples of HNSCC to analyze the importance of FADD and NKX2-3. *Results*. We screened a total of 38 differentially expressed ARGs, and enrichment analysis showed that these genes were mainly involved in autophagy. Then, we selected FADD and NKX2-3 to construct a prognosis model and the risk score calculated by the model was proved to be effective in predicting the survival of HNSCC patients. Additionally, significant differences of the clinicopathological parameters could also be observed in the risk scores and the expression of NKX2-3 and FADD. The expression of FADD and NKX2-3 in cell lines and HNSCC tissue samples also showed the same trends. *Conclusions*. ARGs may be a potential biomarker for HNSCC prognosis, and targeted therapies for FADD and NKX2-3 are possible to be a new strategy of HNSCC treatment.

1. Introduction

Head and neck squamous cell carcinoma (HNSCC) is the sixth most common malignancy of the world. It arises in the epithelium cells of the upper aerodigestive tract and includes the larynx, paranasal sinuses, oral cavity, nasal cavity, and pharynx [1]. Genetic mutation, environmental exposure, viral infection, and unhealthy lifestyle are the common risk factors for HNSCC [2]. Despite a considerable expansion in our therapeutic repertoire for the management of malignancies in recent decades, mortality from HNSCC has not significantly improved. If diagnosed at the early stage, HNSCC is usually curable [3]. Predicting the prognosis of HNSCC with high accuracy is critical for improving treatment, screening, and surveillance. At present, the TNM (Tumor, Node, Metastasis) stage system is still extensively used as the prognostic indicator to monitor the HNSCC progression. However, it is common to observe significant differences in clinical outcomes among patients at the same TNM stage [4]. Therefore, the identification of novel and reliable prognostic molecular signatures is important for improving the unfavorable prognosis of patients with HNSCC [5, 6]. Additionally, it is significant to develop new therapeutic strategies, so that we could treat tumors with much more precision.

Autophagy is a common biological phenomenon and another name for it is type II programmed cell death. It is a process in order to maintain cellular homeostasis, conducting damaged or defective intracellular components [7]. Previous studies have found cell autophagy is a high conserved process. During this process, cytoplasmic materials are sequestered into double-membrane compartments and subsequently mature into autophagosomes. Then, the cargo is delivered to lysosomes, in which it is for degradation or recycling [8]. Abnormal autophagy function is intimately associated with numerous human diseases, including cancers [9]. It is stated that autophagy could promote tumor development or in some cases could inhibit the occurrence of tumor, by affecting many physiological processes [10]. Autophagy was reported by several studies that it could play a critical role in the formation of HNSCC. Also, abnormal expression of autophagy-related genes (ARGs) is also associated with poor prognosis of patients with HNSCC [10]. This means that ARGs can be used as a novel and reliable indicator of HNSCC patients. However, autophagy is a complex process with several steps. In this process, hundreds of molecular biological changes are involved, and a series of ARGs closely control it [11]. Therefore, compared with a single gene, a model which integrates several ARGs that plays important roles in HNSCC may increase the accuracy of the prediction of the prognosis for patients with HNSCC. These important ARGs could also serve as targets for HNSCC therapy.

To better investigate the influence of ARGs on the survival of clinical patients, we downloaded original gene expression data for HNSCC from the TCGA database. We then used these gene expression data, together with information we obtained from other public databases, to develop a prognostic prediction model as an indicator of overall survival (OS) for HNSCC. We also identified the genes related to clinical outcomes of HNSCC patients. Finally, we used experiments to confirm the results of our analysis, with the purpose of selecting possible targets that can be used for the clinical diagnosis and treatment of HNSCC patients.

2. Materials and Methods

2.1. Data Acquisition. The Cancer Genome Atlas (TCGA) database is a complete genome-wide gene expression database used for categorizing and detecting genomic abnormalities in a large population worldwide [12]. We downloaded the mRNA expression data and clinical information of HNSCC patients from the TCGA database, including 502 tumor tissues and 44 adjacent nontumor tissues. In addition, a total of 232 ARGs were obtained from the Molecular Signatures Database (MSigDB), by retrieving "Autophagy." The MSigDB is one of the most widely used and comprehensive databases of gene sets for performing gene set enrichment analysis [13].

2.2. Differentially Expressed ARGs and Enrichment Analysis. We analyzed the expression data by using Wilcox test methods through package limma in R [14] to choose the differentially expressed ARGs between tumor and paired nontumor tissues, and the analysis principle was the thresholds of $|\log 2 \text{ fold change (FC)}| > 2$ and adjusted p value < 0.05. Then, we draw heat map, volcano map, and box plot. Gene Ontology (GO) enrichment analysis and Kyoto Encyclopedia of Genes and Genomes (KEGG) pathway analysis were also performed to find the major biological attributes of differential expression ARGs. The visualization of the enrichment maps was performed by R through the "ClusterProfiler" packages [15].

2.3. Construction of Prognostic Signature Based on ARGs. Univariate and multivariate Cox regression analyses were applied to screen the survival-associated ARGs in HNSCC ($p < 0.05$, HR > 1). We obtained 2 prognostic ARGs, and then, based on the multivariate Cox regression, we calculated the correlation coefficient of the ARGs. According to the correlation coefficient, the survival-related prediction formulas were performed to build prognostic models. We evaluated the risk score of all HNSCC samples through the prognosis prediction model. To further assess the survival differences, we first divided the HNSCC patients into a high-risk group and a low-risk group, according to the median value of the risk score. Then, Kaplan-Meier (K-M) methods were applied to compare the high-risk and low-risk groups.

2.4. Validation of the Prognosis Prediction Model. Clinical data were extracted from HNSCC samples, and risk score was performed on these samples. Univariate and multivariate Cox regression analyses were performed to confirm the influence of risk score and other clinical characteristics on poor prognosis. Finally, the nomogram was also used to assess the prognostic value.

2.5. Cell Culture. HOK (human oral epithelial cell line), HSC-3, HSC-4, and HSC-6 (human oral squamous cell line) were purchased from the Institute of Chinese Academy of Sciences (Shanghai, China). We cultured these cells in 1640 (Gibco, USA) medium with 10% fetal bovine serum (Gibco, USA) in an incubator, which was 37°C and 5% CO_2 incubator.

2.6. RNA Extraction and RT-qPCR. Total RNA was extracted from HOK, HSC-3, HSC-4, and HSC-6 cell lines by using Trizol (Invitrogen). Subsequently, RNA concentration was measured by an ultraviolet spectrophotometer. We stored the extracted RNA samples at −80°C until use. The complementary deoxyribonucleic acids (cDNAs) were obtained by reverse transcription, and the SYBR Green method was used for PCR detection. GAPDH was used as internal references for mRNA, and the 2-$\Delta\Delta$Ct method was used to analyze the mRNA relative expression. The primer sequences of the ARGs were as follows: FADD: 5′-CGGCCTAGACCTCTTCTCCAT-3′ (forward), 5′-TGAGACTTTGAGCTGACGAGC-3′ (reverse); NKX2-3: 5′-GGAAGACGAGGGCGAGAAAT-3′ (forward), 5′-TCTAGAGACTTCTTCAGCTGGC-3′ (reverse).

2.7. HE and Immunohistochemical. We collected the tissue samples from the First Affiliated Hospital of Guangxi Medical University, which was approved by the Ethics Committee. All the paraffin-embedded sections were cut into 4 μm

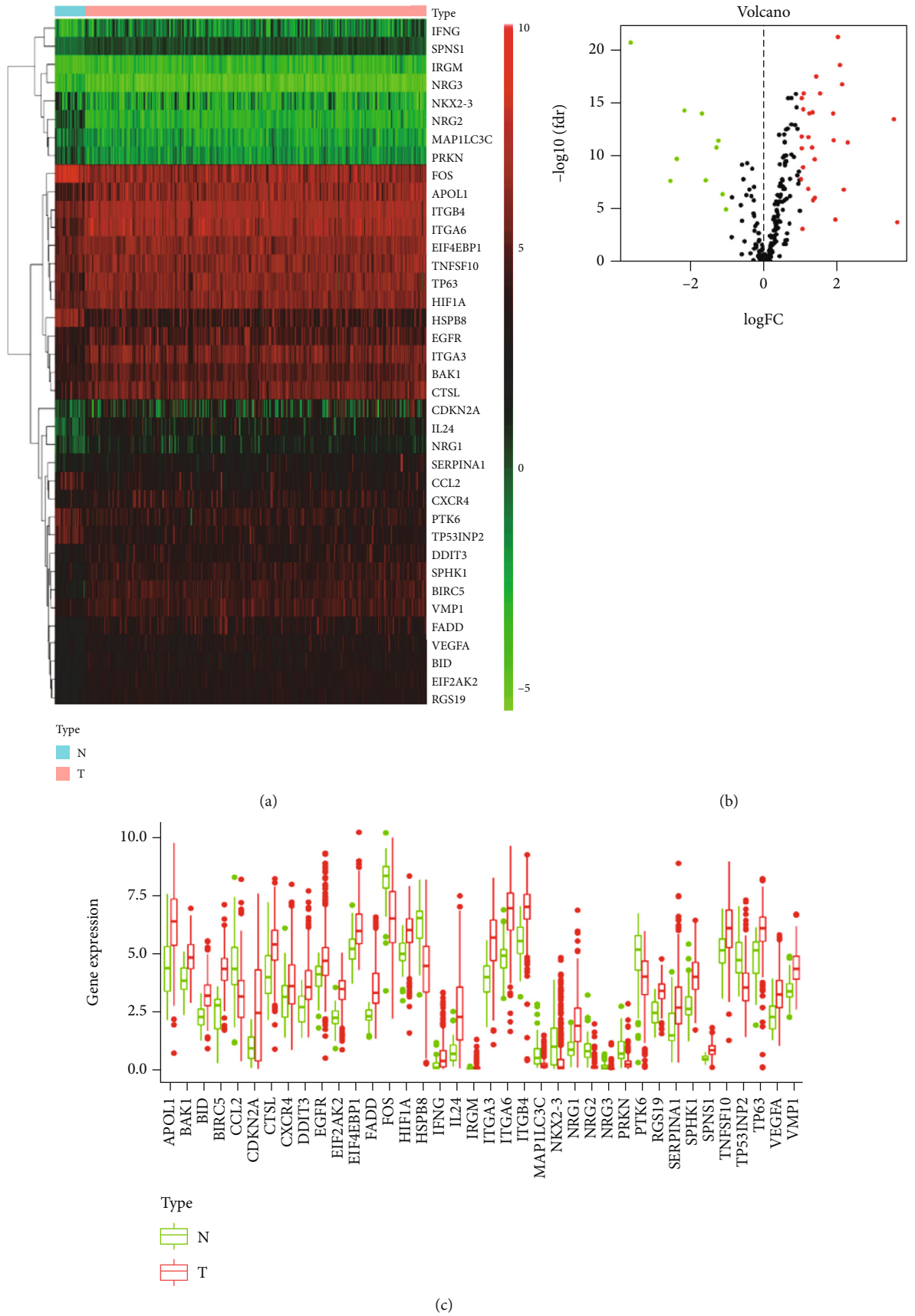

Figure 1: (a) Heat map and volcano plot showed the differentially expressed ARGs. (c) Box plot showed the differentially expressed ARG expression level between HNSCC tissues and nontumor tissues.

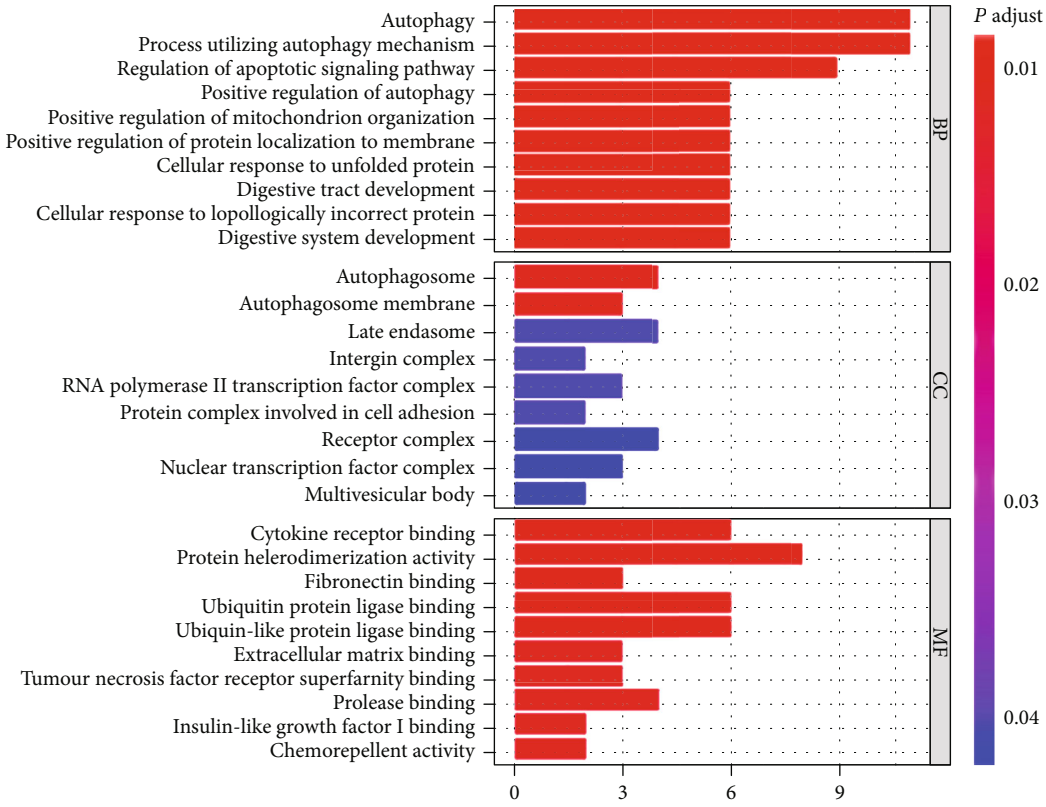

(a)

Figure 2: Continued.

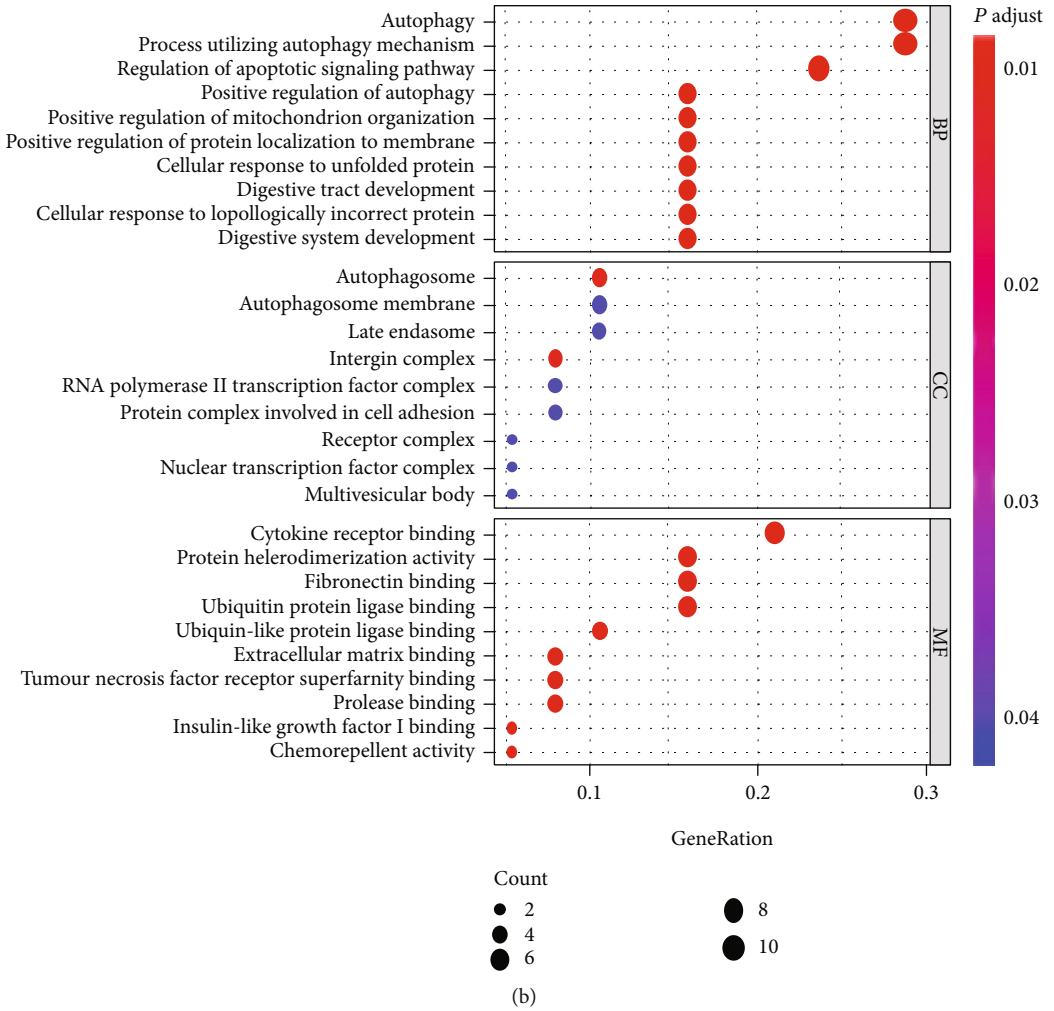

(b)

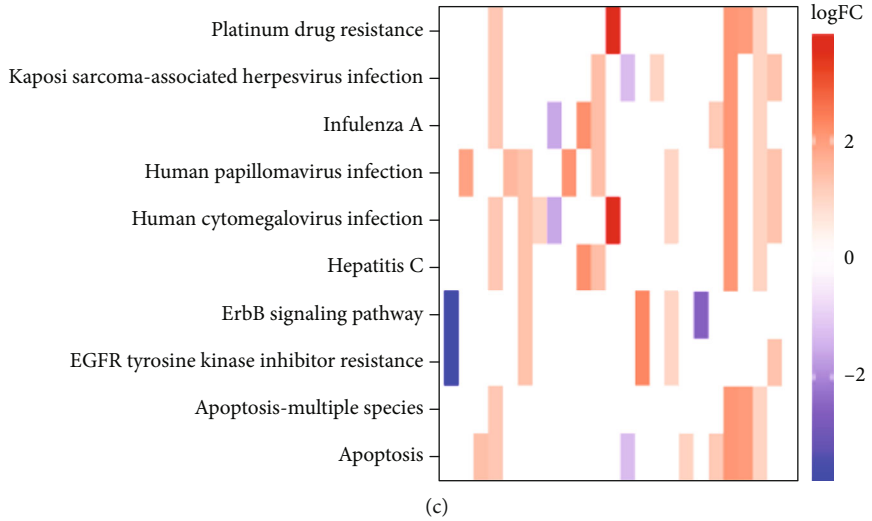

(c)

Figure 2: Continued.

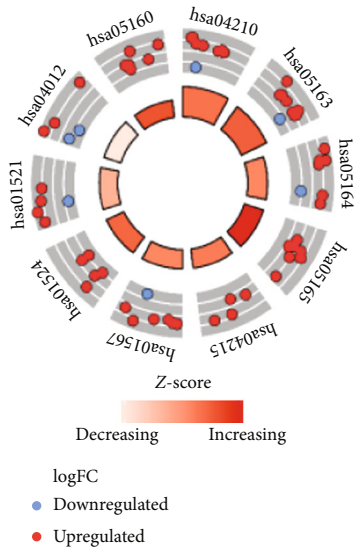

ID	Description
hsa04210	Apoptosis
hsa05163	Human cytomegalovirus infection
hsa05164	Infulenza A
hsa05165	Human papillomavirus infection
hsa04215	Apoptosis-multiple species
hsa05167	Kaposi sarcoma-associated herpesvirus infection
hsa01524	Platinum drug resistance
hsa01521	EGFR tyrosine kinase inhibitor resistance
hsa04012	ErbB signaling pathway
hsa05160	Hepatitis C

(d)

Figure 2: (a, b) Differentially expressed ARGs analyzed by GO enrichment. CC: cellular component; MF: molecular function; BP: biological process. (c, d) Enrichment of KEGG pathways of differentially expressed ARGs.

sections. The HE and IHC staining for FADD proteins were then carried out in these tissue samples. We diluted the primary antibody FADD (Bioss, Beijing) with a ratio of 1 : 50. When finished, we observed the gene expression under the microscope. Finally, we took pictures of it and the magnifications used were 100x.

2.8. Statistical Analysis. The independent sample t-test and chi-squared test were used to compare the data of two groups. Statistical significance was defined as $p < 0.05$. All statistical analyses were carried out using the IBM SPSS software (version 25).

3. Results

3.1. Identification of Differentially Expressed ARGs between HNSCC Tissues and Adjacent Nontumor Tissues. We involved a total of 502 primary HNSCC patients with gene expression data and clinical information in our study. At the same time, 232 ARGs derived from MSigDB were included in our study and there were 38 differentially expressed ARGs, including 28 upregulated (APOL1, BIRC5, VMP1, FADD, ITGB4, ITGA6, EIF4EBP1, TNFSF10, TP63, HIF1A, EGFR, ITGA3, BAK1, CTSL, CDKN2A, IL24, NGR1, SERPINA1, CXCR4, SPHK1, VEGFA, BID, EIF2AK2, RGS19, IFNG, DDIT3, SPNS1, and IRGM) and 10 downregulated ARGs (FOS, CCL2, HSPB8, PTK6, TP53INP2, NRG3, NKX2-3, NRG2, MAP1LC3C, and PRKN), with thresholds of |log 2 fold change (FC) | >2. The heat map and volcano plot showed the differentially expressed ARGs, green represented low expression, and red represented high expression (Figures 1(a) and 1(b)). Finally, the box plot was generated. We applied it for visualizing the expression level of the differentially expressed ARGs between HNSCC tissues and nontumor tissues (Figure 1(c)).

3.2. GO and KEGG Enrichment Analysis of Differentially Expressed ARGs. In order to better understand the associated mechanisms in the development of HNSCC, we functionally categorized the differentially expressed ARGs. The Gene Ontology (GO) database denotes for numerous gene annotation terms, classified based on their association with biological processes (BP), molecule function (MF), and cellular component (CC). We then used the Kyoto Encyclopedia of Genes and Genomes (KEGG) to identify functional and pathways.

Figures 2(a) and 2(b) demonstrate the top 10 BP, MF, and CC, respectively, of GO enrichment, which is mainly involved in autophagy, positive regulation of mitochondrion organization, cellular response to topologically incorrect protein, positive regulation of protein localization to a membrane, nuclear transcription factor complex, and so on. Additionally, the top 10 of KEGG enrichment are summarized in Figures 2(c) and 2(d). KEGG enrichment shows that pathways of differentially expression ARGs mainly involve pathways in apoptosis, platinum drug resistance, EGFR tyrosine kinase inhibitor resistance, and ErbB signaling pathway.

3.3. Identification of Prognostic ARGs and Construction of the Prognosis Prediction Model. Differentially expressed ARGs, which were significantly associated with survival of patients, were screened to analyze ARGs involved in HNSCC progression. As a result, we identified two ARGs, including FADD and NKX2-3, and furthermore, the prognosis prediction model was constructed by these two prognostic ARGs. The prognosis prediction model = (0.138281 ∗ FADD expression value) + (−0.449975 ∗ NKX2-3 expression value), and the calculated result was risk score.

Figures 3(a) and 3(b) demonstrate the distributions of risk score of HNSCC patients and the relationships between risk score and survival time. The abscissa represents the

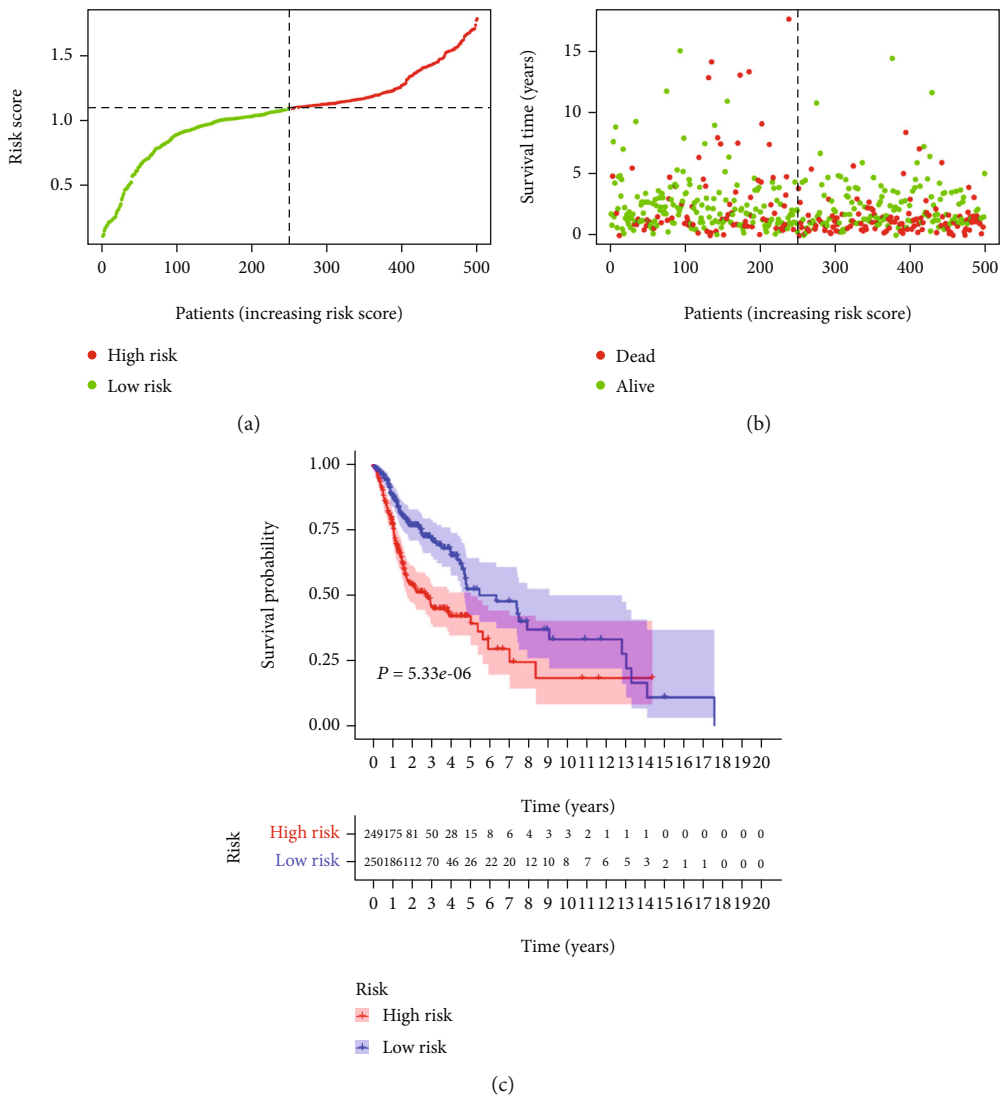

Figure 3: Construction of the prognosis prediction model.

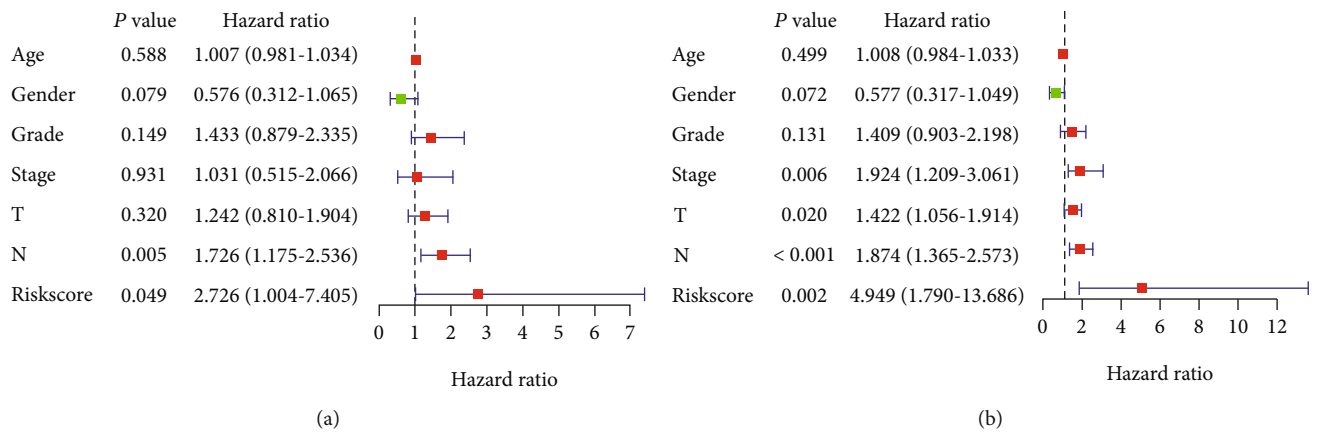

Figure 4: (a, b) Univariate and multivariate regression analysis of different clinicopathological variables (including the risk score) as independent prognostic indicators for HNSCC patients.

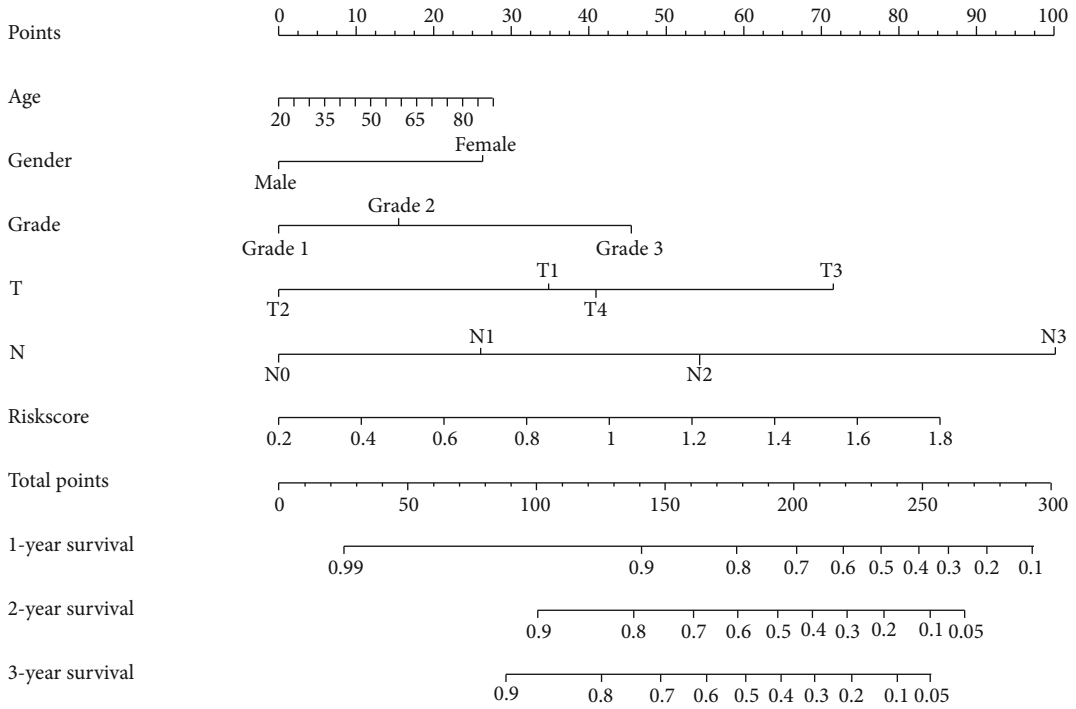

Figure 5: The nomogram was generated to predict the probability of 1-, 2-, and 3-year survival.

patients, and the risk score of the HNSCC cases in the TCGA database increases successively from left to right. The dotted line in the middle divides all the patients into the low-risk group and the high-risk group, which are shown in green and red, respectively. As can be seen from Figure 3(b), the survival time of patients decreases gradually from left to right, which means that the survival time of patients in the high-risk group is lower. To determine the role of the risk score in predicting the clinical prognosis of patients with HNSCC, a K-M survival curve was developed to analyze the differences in prognosis between the high-risk group and the low-risk group. K-M analysis showed that the survival rate was significantly lower in patients of the high-risk group than the low-risk group (Figure 3(c)).

3.4. Validation of the Risk Score Obtained by the Prognosis Prediction Model as an Independent Prognostic Indicator for HNSCC. Univariate analysis showed that risk score was significantly related to the prognosis of patients (HR = 4.949; $p = 0.002$; Figure 4(a)). Then, after adjustment for other clinicopathologic features, multivariate analysis demonstrated that risk score remained an independent prognostic indicator for HNSCC patients (HR = 2.726; $p = 0.049$; Figure 4(b)). In addition, the p values of lymph node metastasis were also less than 0.05 in univariate analysis and multivariate analysis, which could be used as independent prognostic indicators as well. In the HNSCC data downloaded from TCGA, only 2 patients had distant metastasis, so we did not include metastasis as a factor in our analysis.

3.5. Construction of Nomogram. A nomogram always integrates multiple related factors, and each factor was assigned scores in proportion to its risk contribution to survival. By adding the total score of all these predicted factors to the total subscale, we were able to evaluate the prognosis of patients with HNSCC. It is a robust tool that has been used to quantitatively determine the risk of individuals in the clinical setting. In order to better apply risk score for clinical prediction, a nomogram was generated to predict the probability of 1-, 2-, and 3-year survival. As is shown in Figure 5, we involved the risk score, together with age, gender, tumor grade, tumor stage, tumor size, and lymph node metastasis into the nomogram.

3.6. The Relationships between Clinicopathological Parameters and Prognosis Prediction Model. The risk score of the prognosis prediction model was higher in T3-4 than in T1-2 ($p = 0.01$) and higher in Stage III&IV than in Stage I&II ($p = 0.018$). No difference of risk score was observed from age, gender, and grade (Figure 6). Similarly, we also calculated the correlation between prognosis-related ARGs and clinical characteristics. FADD was upregulated in patients younger than 65 years of age. Significant differences could also be observed in the expression of NKX2-3 in age, grade, stage, and tumor size (Figure 6).

3.7. Expression of FADD and NKX2 in Cell Lines and HNSCC Tissue Samples. We detected FADD and NKX2-3 expression in oral squamous cell carcinoma cell lines HSC-3, HSC-4, and HSC-6 and human oral squamous cell line HOK by RT-qPCR. Among them, the primary site of HSC-3 is the tongue squamous epithelium, while the primary site of HSC-4 and HSC-6 is the oral squamous epithelium. The results showed that the HSC-3, HSC-4, and HSC-6 cell lines all had a higher FADD expression level compared with that in HOK (Figure 7(a)). The results

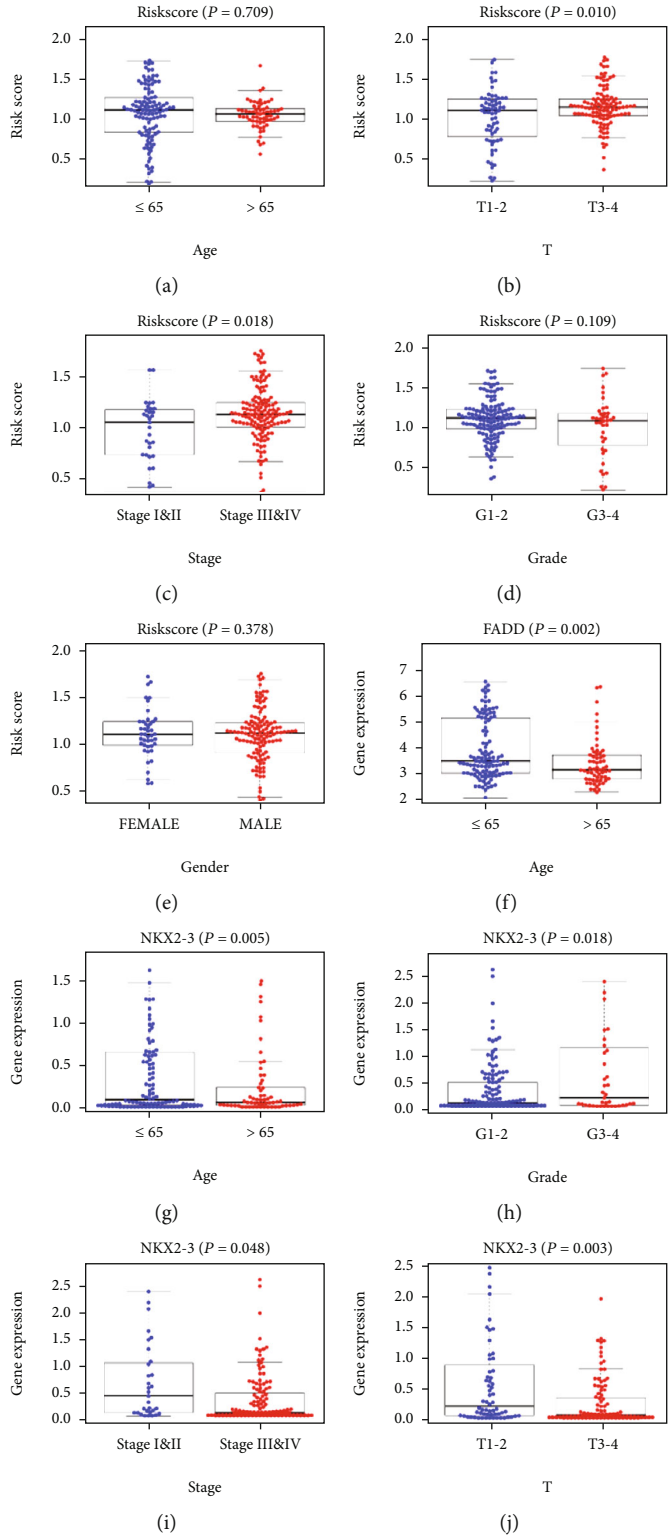

Figure 6: (a–e) Clinical correlation of risk score. (f) Clinical correlation of FADD. (g–j) Clinical correlation of NKX2-3.

were all statistically different ($p < 0.05$), and the expression trend of FADD was consistent with the trend we analyzed in HNSCC (Figure 7(a)). On the contrary, we found that NKX2-3 had a higher expression level in the human oral squamous cell line HOK than HSC-3, which was consistent with the trend in our analysis. However, the expression levels of NKX2-3 in HSC-4 and HSC-6 were different (Figure 7(b)).

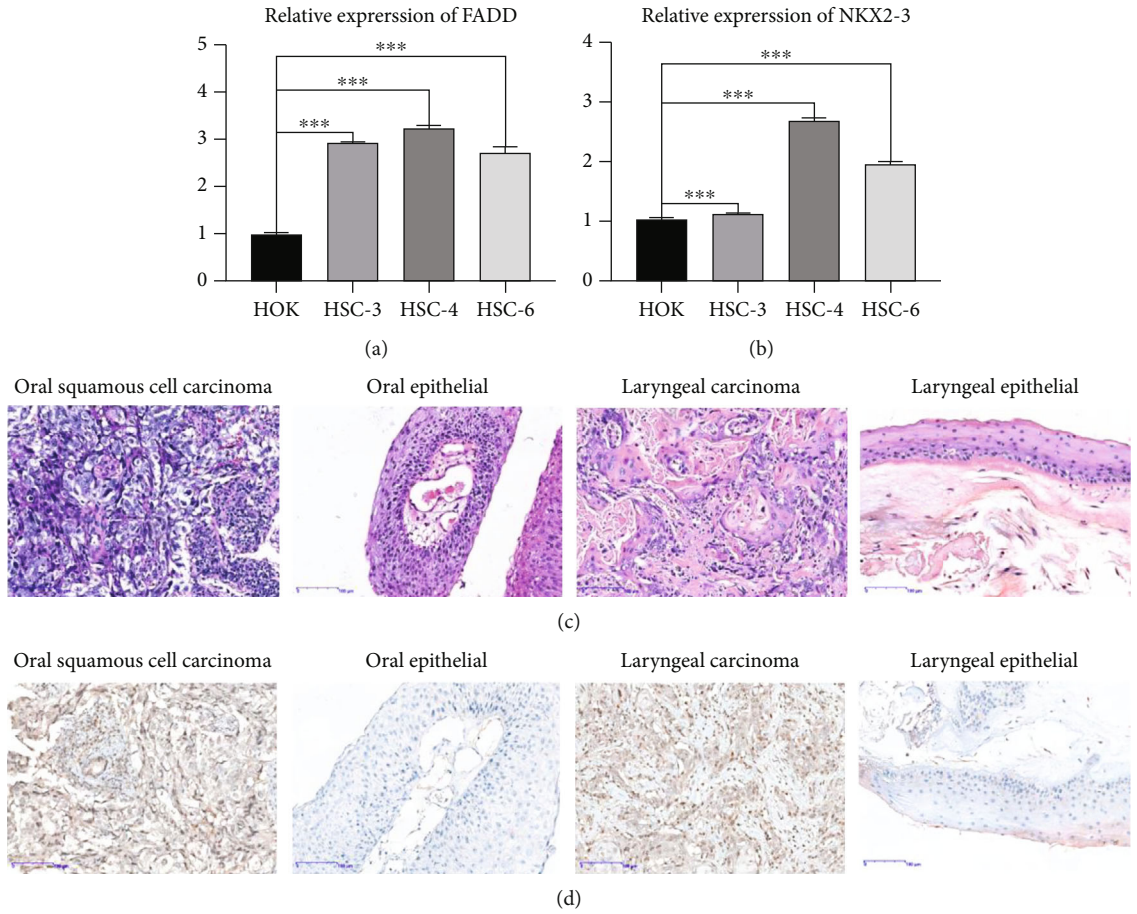

Figure 7: (a, b) RT-qPCR of FADD and NKX2-3 on HOK, HSC-3, HSC-4, and HSC-6 cells. (c, d) HE and IHC of FADD on HNSCC tissues and normal tissues.

To further clarify the potential biological function of ARGs in HNSCC transformation, we next selected FADD, which performed well in cell lines, to characterize the expression changes in clinical samples by IHC. Tissues of oral squamous cell carcinoma and laryngeal carcinoma tissues were used for detection, both of which belong to HNSCC. We also collected normal oral epithelial tissues and laryngeal epithelial tissues as control groups for detection. We first performed HE staining to observe the pathological structure of these tissues (Figure 7(c)). For IHC, the identification of the staining was semiquantitative. Based on the results, score zero represented <5% positively stained cells, score one 6%-25% cells, score two 26-50%, and score three >50% [16]. For the final score, zero was considered negative, and 1-3 as positive. Positive expression of FADD proteins was detected in the oral squamous cell carcinoma and laryngeal carcinoma tissues (Figure 7(d)). Weak positive expression of FADD was seen in the oral epithelial tissues and laryngeal epithelial tissues (Figure 7(d)). The positive percentage of FADD was 65.2% (15/23) and 25.0% (2/8) in oral squamous cell carcinoma tissues and oral epithelial tissues, respectively ($p < 0.05$). Also, approximately 66.7% (14/21) of laryngeal carcinoma tissues and 28.6% (2/7) of laryngeal epithelial tissues were positive for FADD. The results were all statistically different ($p < 0.05$).

4. Discussion

In recent decades, the prognosis of HNSCC has been relatively poor, and treatment plans have been based primarily on the TNM stage. In addition, histopathological findings, such as marginal state, perineural infiltration, and lymphovascular invasion, are also used as the basis for treatment planning [17]. Previous studies have confirmed that autophagy always plays a crucial role in each stage of tumor [18, 19]. It could play an inhibitory role in the occurrence of cancer, and meanwhile, it could also promote cancer development. In addition, it is able to regulate the response of cancer cells to various therapies and treatments [20]. Thus, we believe that autophagy is associated with the development of HNSCC, and the exploration of autophagy mechanism opens up a new perspective for studying the new methods to the diagnosis and treatment of HNSCC [21].

In our study, we first obtained all ARGs from the public databases, then identified 38 differentially expressed ARGs in HNSCC samples, and finally selected 2 ARGs that related to the prognosis of patients with HNSCC. The prognosis prediction model was developed to predict the survival of HNSCC patients. The results demonstrated that the HNSCC patients with high-risk scores always resulted in poor overall survival. To better predict the survival of patients, we

incorporated the risk score, age, gender, tumor grade, tumor stage, tumor size, and lymph node metastasis to construct a nomogram. Our results showed that the risk score has a high prognostic value and it could be used as a diagnostic biomarker. Finally, we analyzed the clinical features of two prognostic ARGs that we used to construct the prognostic model and calculate the risk score. According to our analysis and experimental results, these two genes have significant differences both in cell lines and clinical samples, which means they are closely associated with the occurrence and development of HNSCC. They are able to be used as therapeutic targets for HNSCC. Among these two ARGs, Fas-associated protein with death domain is the full name for FADD. FADD is a key adaptor protein that mediates apoptosis signal transduction [22]. Excepted for being related to apoptosis, FADD is also involved in the process of cell cycle progression, proliferation, innate immunity, tumor development, inflammation, and autophagy [23]. Therefore, during many essential cellular processes, FADD is a significant and special controller [24]. This gene is believed to be the driver gene for chromosomal region 11q13.3 amplification [25]. FADD often has a high expression trend in HNSCC. Also, a study found that high FADD expression always results in worse OS, DSS, and DFS in patients with HNSCC and thus has potential values for prognostic prediction and treatment planning development [26, 27]. A meta-analysis has found that immunohistochemical assessment of FADD could be incorporated into the prognostic evaluation of HNSCC [28]. In addition, NKX2-3 is a member of the NKX family, which is a series of the homeodomain transcription factors. NKX2-3 plays crucial roles in many biologic processes, including cell proliferation and growth, metabolic process, immune and inflammatory response, and angiogenesis [29, 30]. However, the abnormal expression of NKX2-3 is mostly seen in digestive system diseases, which has been considered as a gene related to inflammatory bowel disease and Crohn's disease [31, 32]. A study has found that NKX2-3 could regulate the Wnt signaling pathway and then play a critical role in the pathogenesis of colorectal cancer and could be a new biomarker for clinical practice, including early diagnosis and subsequent therapy [33, 34].

In this study, a prognosis prediction for HNSCC was established and it showed good predictive ability, which provided useful guidance for the prediction of individual patients. In addition, we confirmed the critical role of ARGs, including NKX2-3 and FADD, during the occurrence and development of HNSCC for the first time, which can be used as a diagnostic biomarker and a therapeutic target for HNSCC. However, there are still some limitations in our study. This is a study based on bioinformatics analysis, and the data were acquired from the public database. Thus, we need more independent cohorts to prove the effectiveness of the model we constructed. Additionally, although we did some preliminary validation on the 2 ARGs, their mechanism needs further functional experimental research and more clinical samples to verify. In conclusion, this study provides new strategies for the diagnosis, prognosis prediction, and treatment of patients with HNSCC.

Data Availability

All data included in this study are available from the corresponding author upon request.

Conflicts of Interest

The authors declared no conflict of interest.

Authors' Contributions

Chang Liu and Wenling Wu contributed equally to this work.

Acknowledgments

This study was supported by the Basic Ability Enhancement Project of Guangxi Science and Technology Cooperation and Exchange Project (GKH 159905-2-11), Central Guided Local Science and Technology Development Project (GK ZY18076006), Guangxi Science and Technology Program Project (GK AD17129013), Young Teachers in Guangxi Zhuang Autonomous Region (No. 2018KY0134), and Open Project of Suzhou Key Laboratory of Radiological Medicine and Radiation Protection (GZK1202006).

References

[1] A. Argiris, M. V. Karamouzis, D. Raben, and R. L. Ferris, "Head and neck cancer," *The Lancet*, vol. 371, no. 9625, pp. 1695–1709, 2008.

[2] A. Jou and J. Hess, "Epidemiology and molecular biology of head and neck cancer," *Oncology Research and Treatment*, vol. 40, no. 6, pp. 328–332, 2017.

[3] L. Arantes, A. C. de Carvalho, M. E. Melendez, and A. Lopes Carvalho, "Serum, plasma and saliva biomarkers for head and neck cancer," *Expert Review of Molecular Diagnostics*, vol. 18, no. 1, pp. 85–112, 2018.

[4] V. Budach and I. Tinhofer, "Novel prognostic clinical factors and biomarkers for outcome prediction in head and neck cancer: a systematic review," *The Lancet Oncology*, vol. 20, no. 6, pp. e313–e326, 2019.

[5] C. M. Glastonbury, "Head and neck squamous cell cancer: approach to staging and surveillance," in *Diseases of the Brain, Head and Neck, Spine 2020–2023. IDKD Springer Series*, pp. 215–222, Springer, Cham. Switzerland, 2020.

[6] P. Economopoulou, R. de Bree, I. Kotsantis, and A. Psyrri, "Diagnostic tumor markers in head and neck squamous cell carcinoma (HNSCC) in the clinical setting," *Frontiers in Oncology*, vol. 9, p. 827, 2019.

[7] K. G. Lyamzaev, A. V. Tokarchuk, A. A. Panteleeva, A. Y. Mulkidjanian, V. P. Skulachev, and B. V. Chernyak, "Induction of autophagy by depolarization of mitochondria," *Autophagy*, vol. 14, no. 5, pp. 921–924, 2018.

[8] S. Hernández-Tiedra, G. Fabriàs, D. Dávila et al., "Dihydroceramide accumulation mediates cytotoxic autophagy of cancer cells via autolysosome destabilization," *Autophagy*, vol. 12, no. 11, pp. 2213–2229, 2016.

[9] P. Boya, F. Reggiori, and P. Codogno, "Emerging regulation and functions of autophagy," *Nature Cell Biology*, vol. 15, no. 7, pp. 713–720, 2013.

[10] A. Tektemur, S. Ozaydin, E. Etem Onalan et al., "TRPM2 mediates distruption of autophagy machinery and correlates with the grade level in prostate cancer," *Journal of Cancer Research and Clinical Oncology*, vol. 145, no. 5, pp. 1297–1311, 2019.

[11] Z. Q. Yao, X. Zhang, Y. Zhen et al., "A novel small-molecule activator of sirtuin-1 induces autophagic cell death/mitophagy as a potential therapeutic strategy in glioblastoma," *Cell Death & Disease*, vol. 9, no. 7, p. 767, 2018.

[12] The Cancer Genome Atlas Research Network, J. N. Weinstein, E. A. Collisson et al., "The Cancer Genome Atlas pan-cancer analysis project," *Nature Genetics*, vol. 45, no. 10, pp. 1113–1120, 2013.

[13] A. Liberzon, C. Birger, H. Thorvaldsdóttir, M. Ghandi, J. P. Mesirov, and P. Tamayo, "The Molecular Signatures Database Hallmark Gene Set Collection," *Cell Systems*, vol. 1, no. 6, pp. 417–425, 2015.

[14] M. E. Ritchie, B. Phipson, D. Wu et al., "limma powers differential expression analyses for RNA-sequencing and microarray studies," *Nucleic Acids Research*, vol. 43, no. 7, article e47, 2015.

[15] G. Yu, L. G. Wang, Y. Han, and Q. Y. He, "clusterProfiler: an R package for comparing biological themes among gene clusters," *OMICS*, vol. 16, no. 5, pp. 284–287, 2012.

[16] L. Zhu, D. Yan, Y. Chen, S. Chen, N. Chen, and J. Han, "The identification of autophagy-related genes in the prognosis of oral squamous cell carcinoma," *Oral Diseases*, vol. 26, no. 8, pp. 1659–1667, 2020.

[17] C. Liu, Z. Yu, S. Huang et al., "Combined identification of three miRNAs in serum as effective diagnostic biomarkers for HNSCC," *eBioMedicine*, vol. 50, pp. 135–143, 2019.

[18] A. V. Onorati, M. Dyczynski, R. Ojha, and R. K. Amaravadi, "Targeting autophagy in cancer," *Cancer*, vol. 124, no. 16, pp. 3307–3318, 2018.

[19] A. Scrivo, M. Bourdenx, O. Pampliega, and A. M. Cuervo, "Selective autophagy as a potential therapeutic target for neurodegenerative disorders," *Lancet Neurology*, vol. 17, no. 9, pp. 802–815, 2018.

[20] N. Mizushima and B. Levine, "Autophagy in human diseases," *The New England Journal of Medicine*, vol. 383, no. 16, pp. 1564–1576, 2020.

[21] D. Glick, S. Barth, and K. F. Macleod, "Autophagy: cellular and molecular mechanisms," *The Journal of Pathology*, vol. 221, no. 1, pp. 3–12, 2010.

[22] S. Mouasni and L. Tourneur, "FADD at the crossroads between cancer and inflammation," *Trends in Immunology*, vol. 39, no. 12, pp. 1036–1053, 2018.

[23] R. Schwarzer, H. Jiao, L. Wachsmuth, A. Tresch, and M. Pasparakis, "FADD and caspase-8 regulate gut homeostasis and inflammation by controlling MLKL- and GSDMD-mediated death of intestinal epithelial cells," *Immunity*, vol. 52, no. 6, pp. 978–993.e6, 2020.

[24] L. Tourneur and G. Chiocchia, "FADD: a regulator of life and death," *Trends in Immunology*, vol. 31, no. 7, pp. 260–269, 2010.

[25] W. J. Pattje, L. J. Melchers, L. Slagter-Menkema et al., "FADD expression is associated with regional and distant metastasis in squamous cell carcinoma of the head and neck," *Histopathology*, vol. 63, no. 2, pp. 263–270, 2013.

[26] J. J. Rasamny, A. Allak, K. A. Krook et al., "Cyclin D1 and FADD as biomarkers in head and neck squamous cell carcinoma," *Otolaryngology and Head and Neck Surgery*, vol. 146, no. 6, pp. 923–931, 2012.

[27] J. L. Marín-Rubio, L. Vela-Martín, J. Fernández-Piqueras, and M. Villa-Morales, "FADD in cancer: mechanisms of altered expression and function, and clinical implications," *Cancers*, vol. 11, no. 10, p. 1462, 2019.

[28] M. Á. González-Moles, Á. Ayén, I. González-Ruiz et al., "Prognostic and clinicopathological significance of FADD upregulation in head and neck squamous cell carcinoma: a systematic review and meta-analysis," *Cancers*, vol. 12, no. 9, p. 2393, 2020.

[29] W. Yu, J. P. Hegarty, A. Berg et al., "NKX2-3 transcriptional regulation of endothelin-1 and VEGF signaling in human intestinal microvascular endothelial cells," *PLoS One*, vol. 6, no. 5, article e20454, 2011.

[30] C. Kerkhofs, S. Stevens, S. N. Faust et al., "Mutations in RPSA and NKX2-3 link development of the spleen and intestinal vasculature," *Human Mutation*, vol. 41, no. 1, pp. 196–202, 2020.

[31] W. Yu, Z. Lin, A. A. Kelly et al., "Association of a Nkx2-3 polymorphism with Crohn's disease and expression of Nkx2-3 is up-regulated in B cell lines and intestinal tissues with Crohn's disease," *Journal of Crohn's & Colitis*, vol. 3, no. 3, pp. 189–195, 2009.

[32] D. Vojkovics, Z. Kellermayer, F. Gábris et al., "Differential effects of the absence of Nkx2-3 and MAdCAM-1 on the distribution of intestinal type 3 innate lymphoid cells and postnatal SILT formation in mice," *Frontiers in Immunology*, vol. 10, p. 366, 2019.

[33] W. Yu, Z. Lin, D. M. Pastor et al., "Genes regulated by Nkx2-3 in sporadic and inflammatory bowel disease-associated colorectal cancer cell lines," *Digestive Diseases and Sciences*, vol. 55, no. 11, pp. 3171–3180, 2010.

[34] D. Vojkovics, Z. Kellermayer, B. Kajtár, G. Roncador, Á. Vincze, and P. Balogh, "Nkx2-3-a slippery slope from development through inflammation toward hematopoietic malignancies," *Biomarker Insights*, vol. 13, 2018.

Hindawi
BioMed Research International
Volume 2021, Article ID 3381957, 12 pages
https://doi.org/10.1155/2021/3381957

Research Article

ARHGEF3 Associated with Invasion, Metastasis, and Proliferation in Human Osteosarcoma

Jie Gong,[1] Wei Tang,[2] Bin Lv,[3] Shushu Zhang,[4] Tingjuan Fan,[4] Guangyu Gao,[4] Dong Chen,[1] and Yulong Liu[4,5,6]

[1]*Department of Orthopedics, Suzhou Xiangcheng People's Hospital, 1060 Huayuan Road, Suzhou 215004, China*
[2]*Department of Ultrasound, The Second Affiliated Hospital of Soochow University, Suzhou 215004, China*
[3]*Jiangxi Key Laboratory of Cancer Metastasis and Precision Treatment, The Third Affiliated Hospital of Nanchang University, Nanchang, Jiangxi, China*
[4]*Department of Oncology, The Second Affiliated Hospital of Soochow University, 1055, Sanxiang Road, Suzhou, 215004 Jiangsu, China*
[5]*State Key Laboratory of Radiation Medicine and Protection, School of Radiation Medicine and Protection, Soochow University, Suzhou 215123, China*
[6]*Collaborative Innovation Center of Radiological Medicine of Jiangsu Higher Education Institutions, Suzhou 215123, China*

Correspondence should be addressed to Dong Chen; hardy12@163.com and Yulong Liu; yulongliu2002@suda.edu.cn

Received 11 May 2021; Accepted 8 July 2021; Published 26 July 2021

Academic Editor: Qiang Liu

Background. Osteosarcoma is a malignant bone tumor composed of mesenchymal cells producing osteoid and immature bone. This study is aimed at developing novel potential prognostic biomarkers and constructing a miRNA-mRNA network for progression in osteosarcoma. *Method*. GSE70367 and GSE70414 were obtained in the Gene Expression Omnibus (GEO) database. GEO software and the GEO2R calculation method were used to analyze two gene profiles. The coexpression of differentially expressed miRNAs (DEMs) and genes (DEGs) was identified and searched for in the FunRich database for pathway and ontology analysis. Cytoscape was utilized to construct the mRNA-miRNA network. Survival analysis of identified miRNAs and mRNAs was performed by utilizing the Kaplan-Meier Plotter. Besides, expression levels of DEMs and target mRNAs were verified by performing quantitative real-time PCR (qRT-PCR) and Western blot (WB). *Results*. Six differentially expressed microRNAs (DEMs) were identified, and 8 target genes were selected after screening. By using the KM Plotter software, miRNA-124 and ARHGEF3 were obviously associated with the overall survival of patients with osteosarcoma. Furthermore, ARHGEF3 was found downregulated in osteosarcoma cells by performing qRT-PCR and WB experiments. Results also showed that downregulated ARHGEF3 may associate with invasion, metastasis, and proliferation. *Conclusions*. By using microarray and bioinformatics analysis, DEMs were selected, and a complete miRNA-mRNA network was constructed. ARHGEF3 may act as a therapeutic and prognostic target of osteosarcoma.

1. Background

Osteosarcoma (OS) is the most common primary malignant carcinoma in bone tissues, which is characterized by malignant osteogenesis and malignant osteoblast differentiation [1]. Because of its rapid progress and poor prognosis, it is the main lethal disease in adolescence. Due to the lack of effective tumor early diagnostic markers, despite the rapid development of surgery, chemotherapy, radiotherapy, and other treatment methods, the long-term survival rate of patients with metastatic diseases remains at 25-30% [2]. The prognosis of advanced patients is still worse. Its etiology is not clear, but its occurrence and development may be regulated by genetic factors [3]. Therefore, it is urgent to have a deep understanding of its basic biology to determine its prognostic biomarkers and therapeutic targets [4].

MicroRNA (miRNA) is a class of noncoding single-stranded RNA molecules with a length of about 22 nucleotides encoded by endogenous genes. They are involved in the regulation of post transcriptional gene expression in animals and

plants [5, 6]. For example, Liu and Cui found that miRNA-98-5p inhibits the progression of osteosarcoma by regulating cell cycle via targeting cell division cycle 25 expression [7]. Cai et al. found that overexpression of microRNA-206 accelerates osteosarcoma cells to proliferate and metastasize by targeting Notch3 [8]. Xu et al. also reported that downregulated microRNA-184 may reduce the cancer size of OS through regulation of the Wnt/β-catenin signaling pathway and may suffer a new method for the diagnosis and treatment of OS [9]. These findings suggest that the abnormal expression of miRNAs may be related to the occurrence and development of cancer, which may be through regulating cancer-related genes and participating in the pathogenesis of OS.

In our research, we identified differentially expressed genes and microRNAs by analyzing 1 osteosarcoma mRNA microarray dataset and 1 microRNA dataset. Our objective to identify the key genes in OS with survival, mRNA-microRNA interaction, ontology enrichment, and network analyses.

2. Methods

2.1. Microarray Data. GEO database is a database for storing chip, second-generation sequencing, and other high-throughput sequencing data. Using this database, we can retrieve some experimental sequencing data uploaded by others. In this article, GSE70367 and GSE70414 were achieved from GEO.

GSE70367, including 5 osteosarcoma cell lines and 1 human mesenchymal stem cell line (hMSC).. miRNA expression profiling research of these cell lines was conducted on an Affymetrix Multispecies miRNA-3 Array (GPL16384). Dataset GSE70414, 5 OS cell lines and 1 hMSC, was offered by the Affymetrix Human Genome U133 Plus 2.0 Array (GPL570).

2.2. Differently Expressed miRNA Analysis. GEO2R (https://www.ncbi.nlm.nih.gov/geo/geo2r/) is an interactive web tool, which permits people to compare two or more sets of samples in the GEO Series to select DEGs under different experimental situations. The results showed that it was a gene table in order of importance. GEO2R uses the GEOquery and limma R packages in the Bioconductor project to compare the processed tables provided by the original committer. In this study, GEO2R was utilized to select the DEMs and DEGs between the OS and human mesenchymal stem cells. Furthermore, $|\log 2FC| \geq 3$ and $P < 0.05$ were utilized as a cut-off criterion, and an obvious statistical difference would be thought if the statistics were up to our standards.

2.3. Functional and Pathway Enrichment Analysis. FunRich (http://www.funrich.org) is an independent software tool, mainly used for functional enrichment and interaction network analysis of genes and proteins. The analysis results can be drawn into different types of pictures. Users can not only search the default background database but also load the custom database, which can be used for function-rich analysis. Cytoscape software was utilized to carry out KEGG (Kyoto Encyclopedia of Genes and Genomes) enrichment analysis. ClueGO is a data visualization tool based on the plug-in of Cytoscape. It supports the enrichment analysis of more than ten common databases such as GO, KEGG, Reactome, and miRBase. Finally, the enrichment results are displayed in the form of a network.

2.4. Prediction of Potential DEM Target mRNAs and MicroRNA-mRNA Regulatory Network. miRNAs inhibit the expression of target genes mainly by binding to target mRNA, promoting the degradation of mRNA, or hindering its translation. Accurate and rapid prediction of miRNA target genes by bioinformatics methods can provide clues for the study of miRNA function. Upregulated and downregulated DEMs were submitted to the FunRich online program to achieve target genes. Besides, GSE70414 was obtained from the GEO database. By combining the target genes from FunRich software and differential expression analysis of GSE70414, the intersection genes between the two results were selected and the microRNA-mRNA network was constructed by utilizing Cytoscape.

2.5. Analysis of the MicroRNAs and their Association with Osteosarcoma Prognosis. The Kaplan-Meier Plotter (http://www.kmplot.com/) is an online website for survival analysis. At present, the website can carry out research on 54,675 genes and 18,674 cancer samples, involving breast cancer, lung cancer, etc.; the data types include chip data and high-throughput sequencing data, involving mRNA and miRNA, and are constantly enriched [11]. In this study, we divided OS patients into two groups (high expression and low expression) according to the expression of specific genes. The overall survival of OS patients was analyzed by the KM Plotter database.

2.6. Cell Culture and Antibodies. The human OS cell lines (MG63, 143B, U2OS, U2R) were offered by Professor Kang Tie Bang (Sun Yat-sen University Cancer Center, State Key Laboratory of Oncology in South China, Collaborative Innovation Center for Cancer Medicine, Guangzhou, China). Osteosarcoma cells and hFOB1.19 cells were cultured in Dulbecco's modified Eagle's medium (DMEM; Thermo Fisher Scientific) supplemented with 10% fetal bovine serum (FBS; Gibco) in an incubator. The incubator is at 37 degrees Celsius with 5% CO_2. Anti-β-actin and anti-ARHGEF3 (rabbit) antibodies were purchased from the Proteintech Group, Inc. (Wuhan, China).

2.7. Quantitative Real-Time PCR. Total RNA was extracted from OS cell lines and hFOB1.19 cells using TRIzol reagents (Invitrogen, Carlsbad, CA, USA) according to the manufacturer's instructions. The total RNA extracted was amplified by RT-PCR using SYBR Green Supermix (Bio-Rad Laboratories) according to the manufacturer's instructions, and mRNA levels of ARHGEF3 were detected. The results were calculated by the $2^{-\Delta\Delta Ct}$ method. We found ARHGEF3 primer pairs in previous studies, and the primer pairs are shown in Table 1. The reference group was GAPDH to avoid errors caused by factors such as sampling error, RNA quantitative error, and nonuniform amplification efficiency of each PCR system.

2.8. Protein Extraction and Western Blotting. Osteosarcoma cells and hFOB1.19 cells were collected by centrifugation and then washed with PBS. The resulting precipitate was

Table 1: The primers for quantitative real-time polymerase chain reaction with GAPDH used as the internal standard control.

	Forward	Reverse
ARHGEF3	5′-GCCAGGATCGATATGGTTGCGAAGGACTAC-3′	5′-AAGCTAGAATTCGCTCTCTCACAGGGCTGAC-3′
GAPDH	5′-TGGTATCGTGGAAGGACTCATGAC-3	5′-ATGCCAGTGAGCTTCCCGTTCAGC-3

added to the radio immunoprecipitation assay (RIPA) buffer (Thermo Fisher Scientific) and then cracked on ice for half an hour. The cracked sample was centrifuged in a 4°C centrifuge at 12,000 rpm for 20 minutes, and the supernatant was left. Bradford assay (Bio-Rad Laboratories) was used to quantify the protein. Western blot assays were performed on the total protein obtained. The protein was separated on 10% sodium dodecyl sulfate-polyacrylamide gel (SDS-PAGE) and then transferred to a polyvinylidene fluoride (PVDF) membrane (Millipore, USA). The resulting PVDF membrane was placed in 5% skimmed milk and blocked for about 1 hour. The specific antibody was then incubated overnight at 4°C, washed three times with PBST (1 × PBS with Tween) the next day, and then incubated at room temperature for 1 hour with the corresponding secondary antibody (rabbit). The strips were incubated with the secondary antibody and washed three times with PBST, and finally, autoradiography was performed with an ECL kit (Thermo Fisher Scientific).

2.9. Cell Transfection. The oe-ARHGEF3 sequence was cloned into pLKO.1 vector, and the stable system with overexpression ARHGEF3 was constructed for the next experiment. ARHGEF3 oeRNA were purchased from GenePharma Co. Ltd. (Suzhou, China). Lipofectamine 2000 and Lipofectamine® RNAiMAX were used as the transfection reagents according to the manufacturer's instructions.

2.10. Transwell Assays. Transwell chambers were placed on a 24-well plate, and osteosarcoma cells in the logarithmic growth phase were digested with trypsin and washed with PBS and serum-free medium. $1 * 10^5$ cells and serum-free medium were inoculated in the upper compartment of each well. DMEM medium containing 10% fetal bovine serum was added to the lower compartment. For cell invasion assay, 50 μl diluted matrix glue (BD Biosciences, Franklin Lakes, NJ) was added to the upper chamber and incubated at 37°C for 4-5 hours; the following operation is the same as above. The cells were cultured in a 37°C incubator for 22 hours in the migration experiment and 24 hours in the invasion experiment. The cells that have migrated or invaded are fixed, stained, and counted at a specified time.

2.11. Wound Healing Assays. Wound healing assays were constructed to measure cell migration and repair. We used a 20 UL pipette tip to line the central growth area of adherent cells cultured on a 12-well plate. The floating cells in the central part were washed with PBS, and the cells were cultured for another 24 hours. Besides, we observed and filmed the migration process 0 and 36 hours after scratch. After that, we also measured and calculated the distance between the two edges of the scratch.

3. Results

3.1. Identification of the DEGs between Osteosarcoma Cell Lines and Human Mesenchymal Stem Cells. GEO2R was utilized to analyze the miRNA and mRNA expression profiles from the GSE70367 and GSE70414. Based on the cut-off criteria ($P < 0.05$ and $|\log 2FC| \geq 2$), 36 DEMs including hsa-microRNA-1290, hsa-microRNA-124-3, hsa-microRNA-1912, hsa-microRNA-224, hsa-microRNA-31, and hsa-microRNA-21 (Figure 1) and 118 differentially expressed mRNAs were identified (Figure 2).

3.2. Screening of Potential Transcription Factors and Enrichment Analysis. Transcription factor enrichment research found HNF1A, VSX2, HOXD8, HOXA13, GFI1, BSX, HOXB7, LHX3, CRX, and ATF6 (Figure 3). To further understand the function of the selected miRNAs, FunRich was utilized to carry out GO enrichment research. The result indicated that DE-microRNAs were most enriched in the lysosome, nucleus, cytoplasm, transcription factor activity, GTPase activity, protein serine/threonine kinase activity, transport, protein targeting, and regulation of nucleobase, nucleoside, nucleotide, and nucleic acid metabolism (Figure 4). We also utilized Cytoscape and ClueGO to conduct the KEGG pathway analysis. These identified microRNAs were mainly enriched in 6 pathways including glycosphingolipid biosynthesis, retinol metabolism, AGE-RAGE signaling pathway in diabetic complications, pancreatic secretion, inflammatory mediator regulation of TRP channels, and renin secretion (Figure 5).

3.3. miRNA-mRNA Regulatory Network. By utilizing FunRich software, 1610 potential target mRNAs were obtained, and only 8 of them differentially expressed in GSE70414 (ARHGEF3, EYA2, GALNT10, KCNK2, PLD5, VAT1L, ABLIM1, and PTGFRN). To show the composition and relationship of miRNA and mRNA more clearly, we built a microRNA-mRNA network by utilizing Cytoscape software. Finally, 8 essential microRNA-mRNA pairs (microRNA-124-3 and microRNA-31) were selected which implied the vital effect of osteosarcoma (Figure 6).

3.4. Research of the MicroRNAs and Their Association with Osteosarcoma Prognosis. KM Plotter was used to research the survival of patients with osteosarcoma. By uploading 2 microRNAs we identified, we achieved 2 survival curves. The outcome demonstrated that microRNA-124 (Figure 7) were associated with prognosis of patients with OS. However, the expression of microRNA-31 may have no obvious association with the survival rate. Next, hsa-mir-124 was chosen for further study. By uploading 6 target mRNAs, the corresponding survival curve was achieved (Figure 8). The outcome indicated that the expression level of ARHGEF3 and

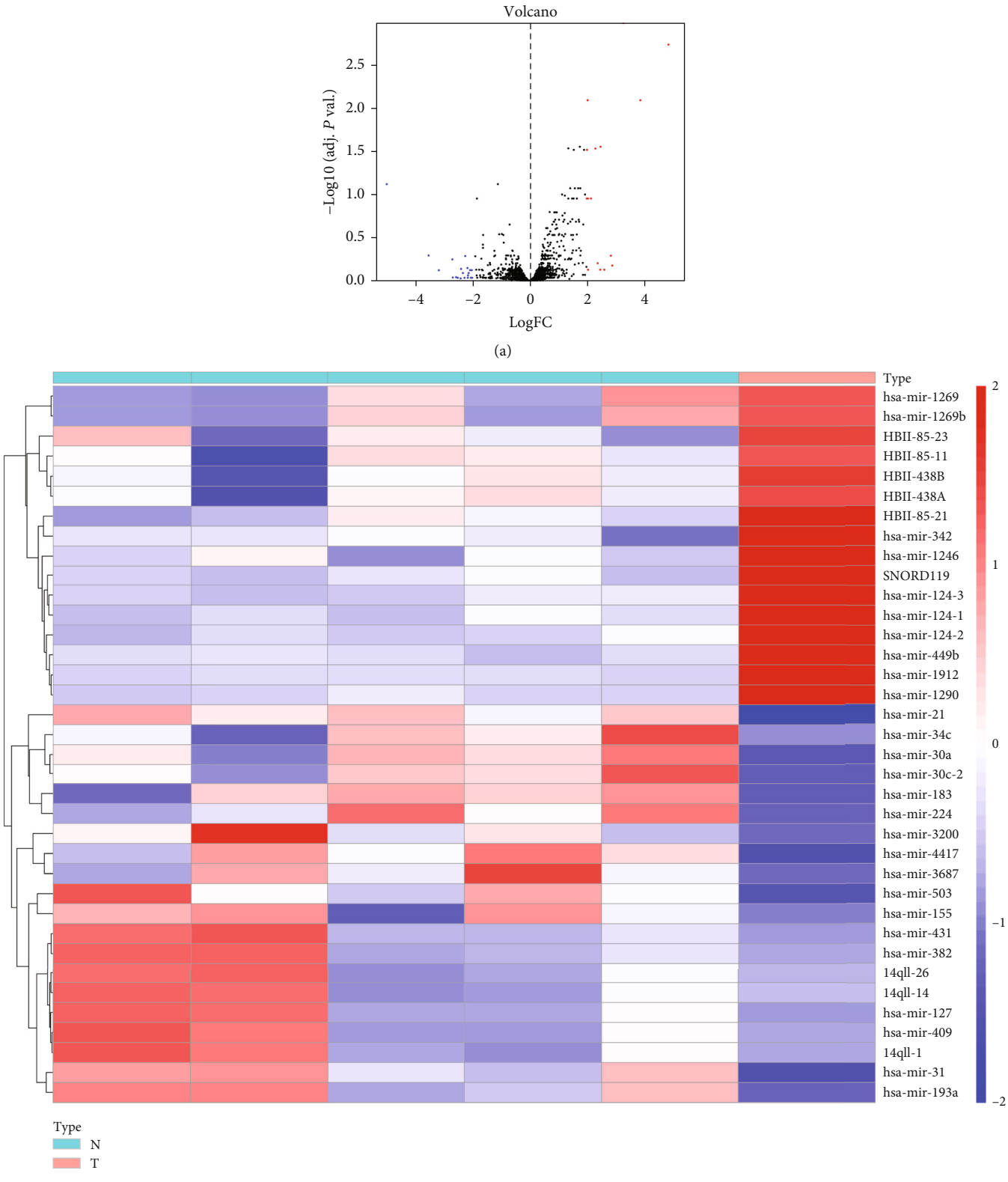

Figure 1: Heat map and volcano map of differentially expressed genes of GSE48074.

PLD5 may have an obvious association with the overall survival of patients with osteosarcoma. This indicated that the identified microRNAs and mRNAs may be potential targets.

3.5. Validation of the Expression with qRT-PCR and Western Blot. To further assess the expression of ARHGEF3, we selected four osteosarcoma cell lines to detect its mRNA level

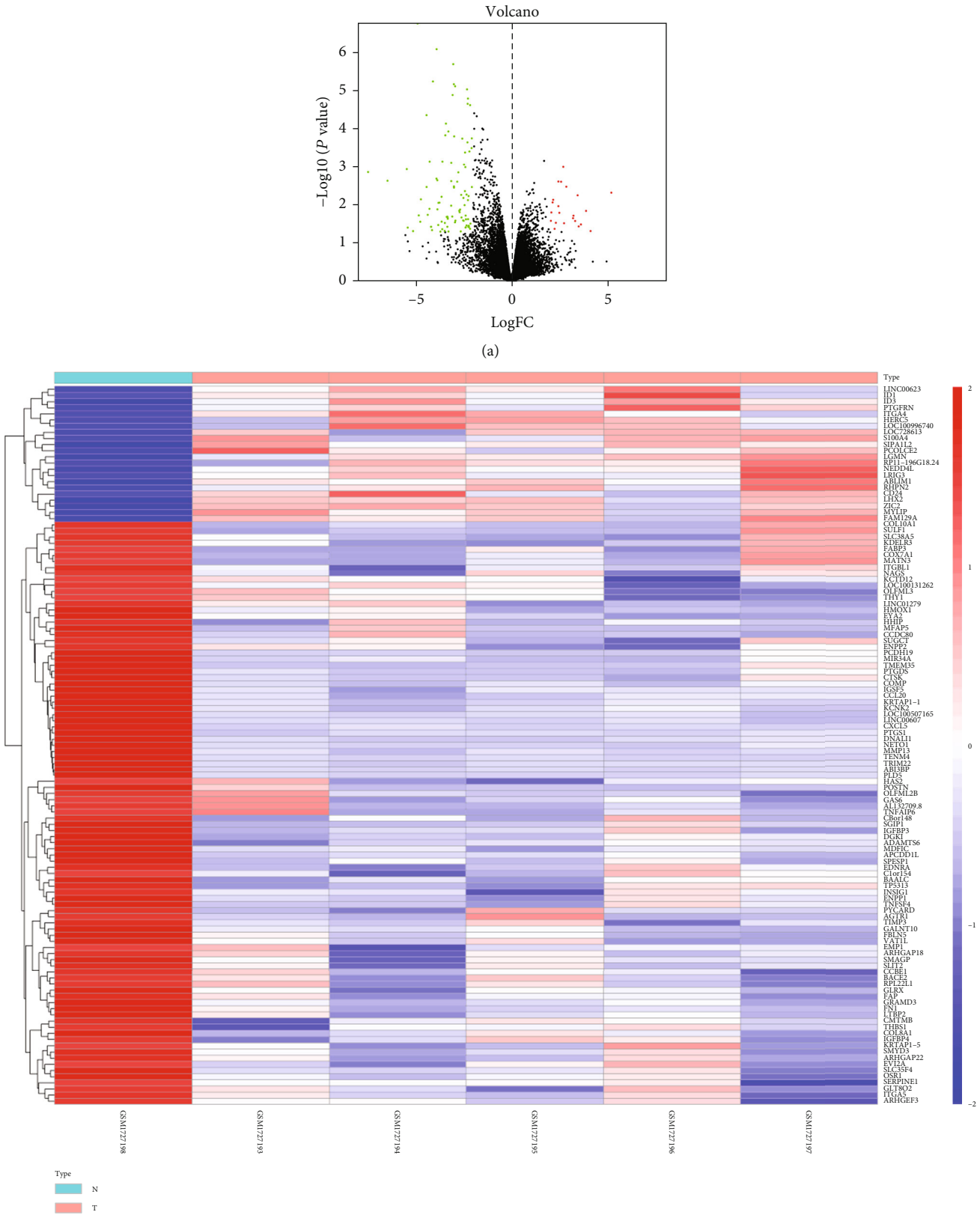

Figure 2: Heat map and volcano map of differentially expressed genes of GSE70574.

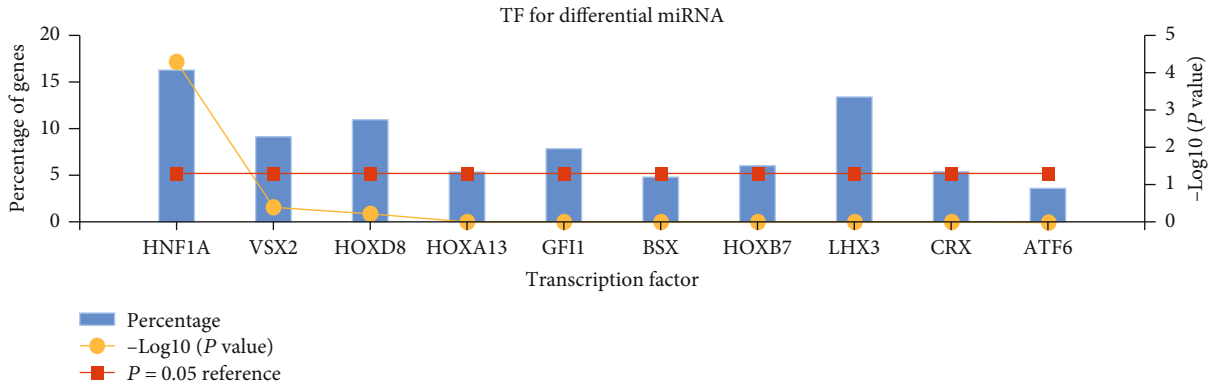

Figure 3: Identification of the potential transcription factors of DEMs by FunRich software.

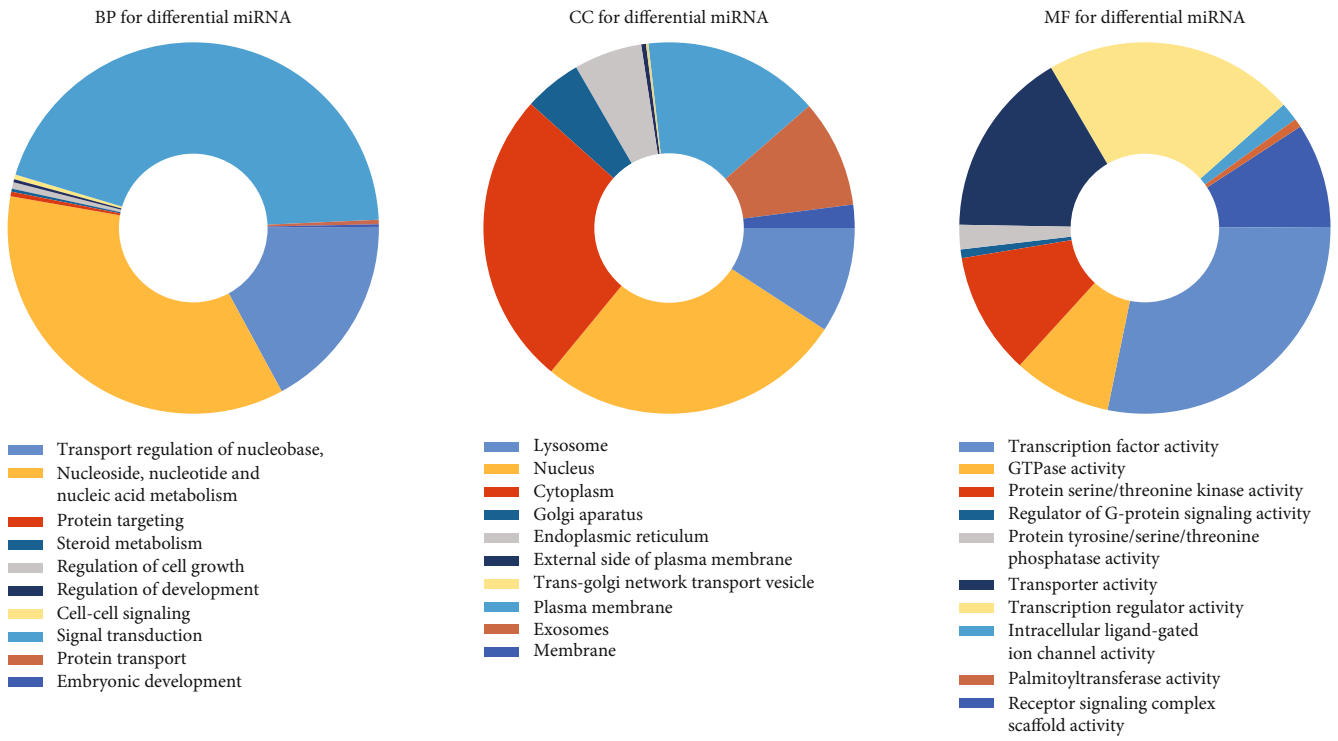

Figure 4: The top 10 of the biological process, cellular component, and molecular function of the target genes of miRNAs.

and protein expression, and the control group was the normal osteoblast hFOB1.19. Consistent with the microarray data, ARHGEF3 was highly expressed in hFOB1.19 cells and was low expressed in various osteosarcoma cell lines at both mRNA and protein levels (Figures 9(a) and 9(b)). Although the difference in the expression of other cell lines was not as significant as that of 143B cells, this result can prove to some extent that the high expression of ARHGEF3 in osteosarcoma cell lines may be associated with poor prognosis of osteosarcoma cells.

3.6. Overexpression of ARHGEF3 Inhibited the Aggressiveness of 143B Cells in the Osteosarcoma Cell Line. According to the expression level results obtained in the above experiments, we selected the cell line 143B with the lowest expression level for the next experiment. To determine the biological significance of ARHGEF3, we transfected 143B cells with oeRNA (oe-ARHGEF3) to upregulate ARHGEF3 gene expression, and the oeRNA was introduced into 143B cells by the lentiviral vector to establish stable cell lines (143B/oe-ARHGEF3 and 143B/NC). Previous studies on ARHGEF3 have found that the low expression of ARHGEF3 promotes the invasion and repair of many tumors. Therefore, to know whether ARHGEF3 has the same performance in osteosarcoma, we conducted migration, invasion, and wound healing assays. In wound healing assays, results showed that the healing rate of 143B/oe-ARHGEF3 stable cells was significantly slower than that of 143B/NC stable cells at 36 h. In the transwell experiment, we can see that compared with 143B/NC cells, 143B/oe-ARHGEF3 stable cells migrated and invaded the lower compartment in a significantly reduced number. These results indicated that overexpression ARHGEF3 could

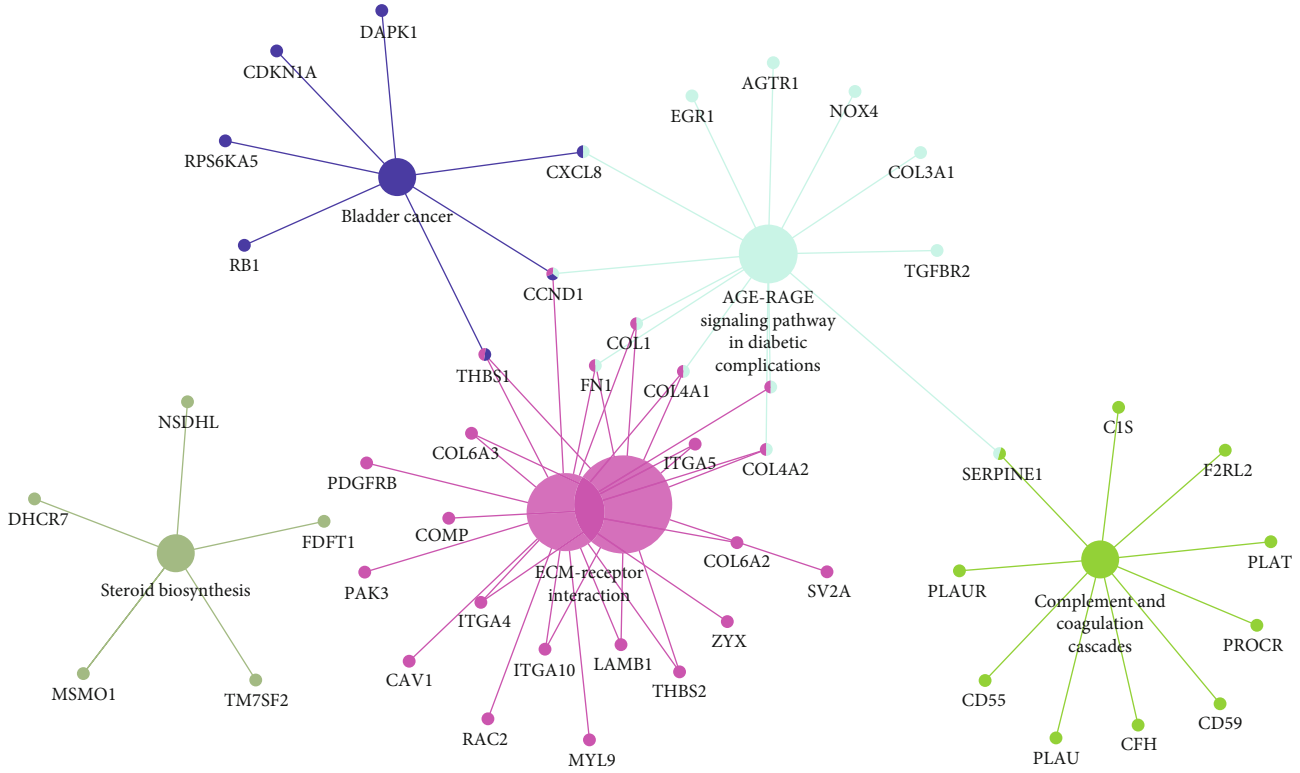

Figure 5: KEGG pathway enrichment analysis of potential target mRNAs.

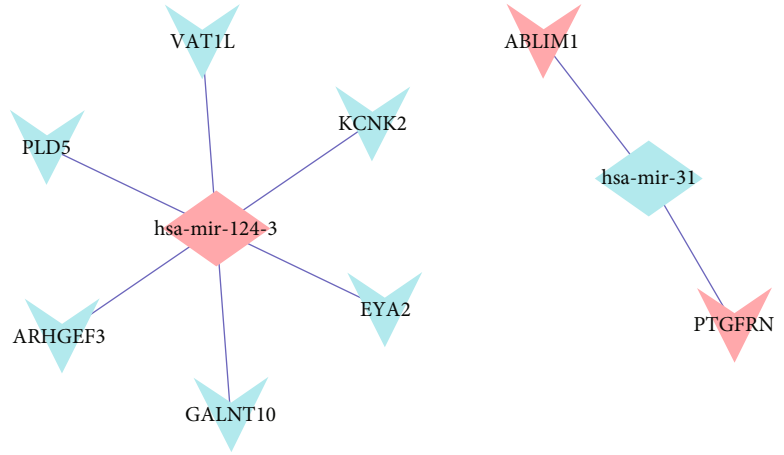

Figure 6: Identified target mRNAs and miRNA-mRNA regulatory network.

inhibit the migration, invasion, and healing of 143B cells and that high ARHGEF3 expression promoted the invasiveness of 143B cells in an osteosarcoma cell line (Figures 10 and 11).

4. Discussion

At present, much evidence shows that miRNAs and mRNAs are the key regulators of tumorigenesis, development, spread, and inhibition of tumor cell proliferation or induction of apoptosis. At the same time, a gene-targeting therapy strategy should also be considered, which is related to inhibiting the growth and metastasis of osteosarcoma [10, 11]. In our study, GSE70367 and GSE70414 were obtained in the GEO database. 6 DE-microRNAs including microRNA-1290, microRNA-124-3, microRNA-1912, microRNA-224, microRNA-31, and microRNA-21 were selected. To further learn the function of the 6 microRNAs in osteosarcoma, FunRich was utilized for further study. Transcription factor enrichment analysis demonstrated that these microRNAs were primarily associated with the HNF1A, VSX2, HOXD8, HOXA13, GFI1, BSX, HOXB7, LHX3, CRX, and ATF6. Gene Ontology enrichment analysis indicated that these miRNAs were associated with lysosome, nucleus, cytoplasm, transcription factor activity, GTPase activity, protein

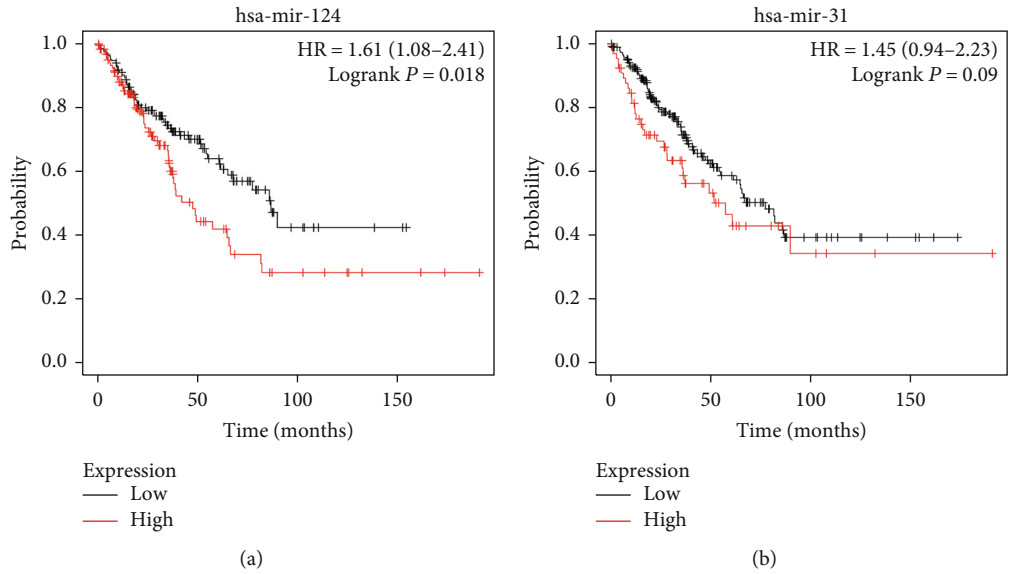

Figure 7: The association between the expression level of selected miRNAs and osteosarcoma prognosis.

serine/threonine kinase activity, transport, protein targeting, and regulation of nucleobase, nucleoside, nucleotide, and nucleic acid metabolism. This is consistent with the recognition that lysosomes and the nucleus play an important role in some common human diseases [12]. As for GTPase activity, it is a key component of many intracellular processes. The incorrect regulation of G protein is related to diseases: cancer [13–15], cardiovascular disease [16], genetic disease [17], and so on. Kyoto Encyclopedia of Genes and Genomes pathway analysis demonstrated that these identified microRNAs were mainly enriched in 6 pathways. The pathways of focal adhesion in mankind have been researched for several years. It plays an oncogenic role in cancer invasiveness and metastasis. Besides, previous research has proven the relationship between focal adhesion activation and metastasis in breast cancer [18]. Inhabiting focal adhesion could slow metastasis formation of mammary cancers [19, 20]. Therefore, it has been identified as a potential therapeutic target for aggressive breast carcinoma [21]. As for the ECM-receptor interaction pathway, Zhang et al. reported that Twist-related protein 2 may promote migration and invasion of kidney cancer cells by regulating ITGA6 and CD44 expression associated with the ECM-receptor-interaction pathway [22]. It may also involve the development of breast carcinoma [23]. However, the function of these pathways in osteosarcoma has not been described in detail yet.

The microRNA-mRNA network was constructed on the basis of FunRich and Cytoscape. Six microRNAs were identified for further study. Besides, 1610 potential target mRNAs were obtained and only 8 of them differentially expressed in GSE70414 (ARHGEF3, EYA2, GALNT10, KCNK2, PLD5, VAT1L, ABLIM1, and PTGFRN). Besides, some microRNAs have been confirmed to be associated with cancer biological behavior. For example, a previous research indicated that microRNA-1290 promoted proliferation, sphere formation, colony formation, and invasion of NSCLC [24]. It took part in the radio resistance of human cervical tumor cells and chemoresistance in hepatocellular cancer [25]. Besides, another study concluded that microRNA-1290 sensitized the Wnt pathway and added the reprogramming-related transcript factors c-Myc and Nanog in colorectal carcinoma [26]. As for hsa-mir-124-3, it is a subtype of miR-124 and highly expressed in the mammalian nervous system. Besides, it might act as a potential target for the diagnosis and treatment of hepatocellular carcinoma [27]. It was also found to improve GATA6 expression and be related to a poor prognosis in cholangiocarcinoma [28]. In osteosarcoma, it was found that the expression of miR-124 was significantly downregulated in tumor patients when compared to periostitis patients and healthy controls. The conclusion indicated that microRNA-124 was an independent prognostic indicator for OS [29]. As for hsa-mir-31, Tu et al. reported that it was induced by ultraviolet which was correlated with chronic actinic dermatitis severity, which acted as a vital role in regulating the keratinocyte permeability barrier through targeting CLDN1 [30]. It looks like a novel metastatic colorectal cancer marker whose expression level permits for the selection of patients with wild-type KRAS cancer who more possibly respond to anti-EGFR treatment [31]. In chordoma, it was found differentially expressed compared with healthy nucleus pulposus and may serve as a prognostic factor and therapeutic target [32]. By using FunRich software, 1610 potential target genes were obtained and only 8 of them differentially expressed in GSE70414 (ARHGEF3, EYA2, GALNT10, KCNK2, PLD5, VAT1L, ABLIM1, and PTGFRN). As a result, a microRNA-mRNA network was built including 2 microRNAs (microRNA-124-3 and microRNA-31) and 8 mRNAs.

ARHGEF3 (Rho Guanine Nucleotide Exchange Factor 3) is a protein coding gene. ARHGEF3-related diseases include methotrexate-related lymphoproliferation and osteoporosis. A previous study reported that overexpression of ARHGEF3

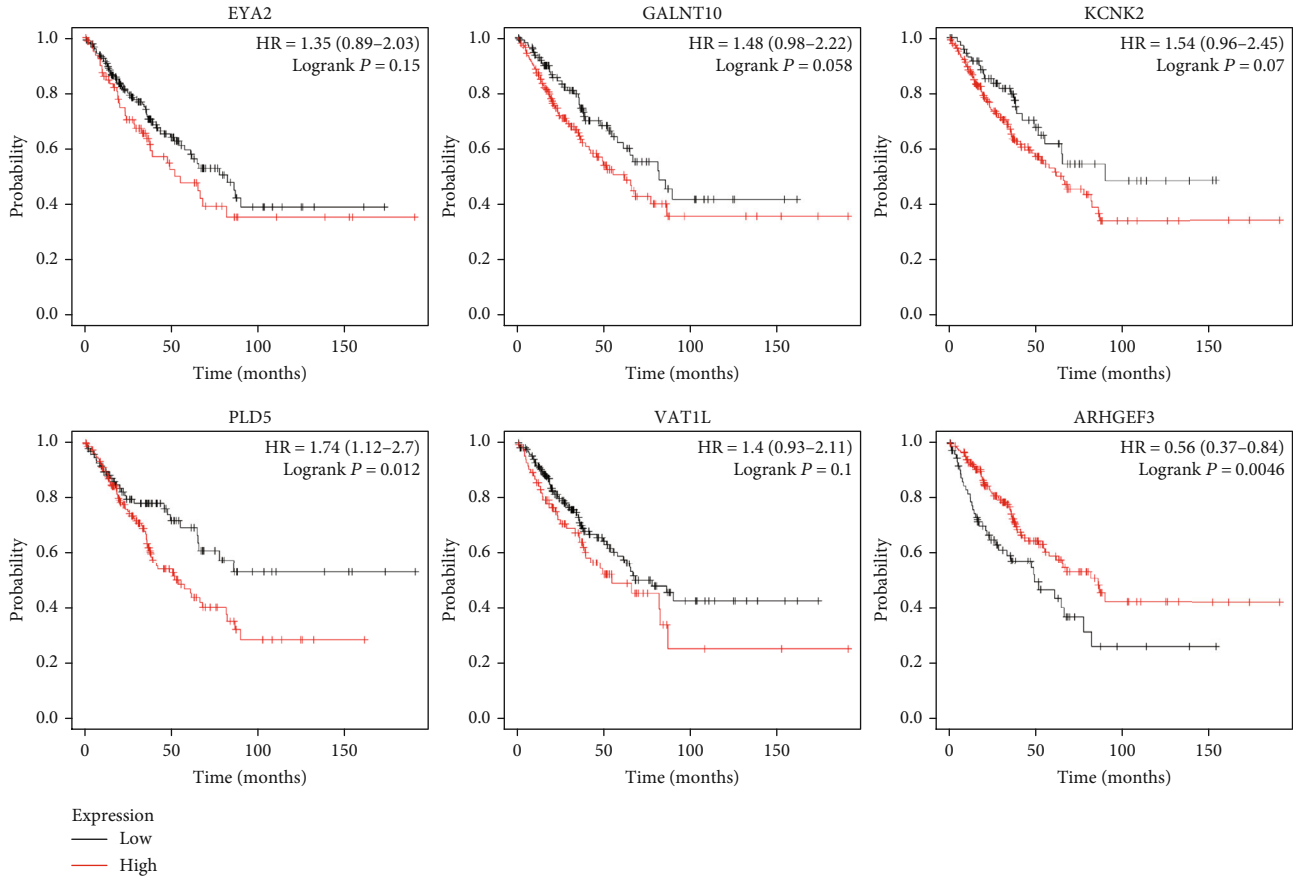

Figure 8: The association between the expression level of target mRNAs and osteosarcoma prognosis.

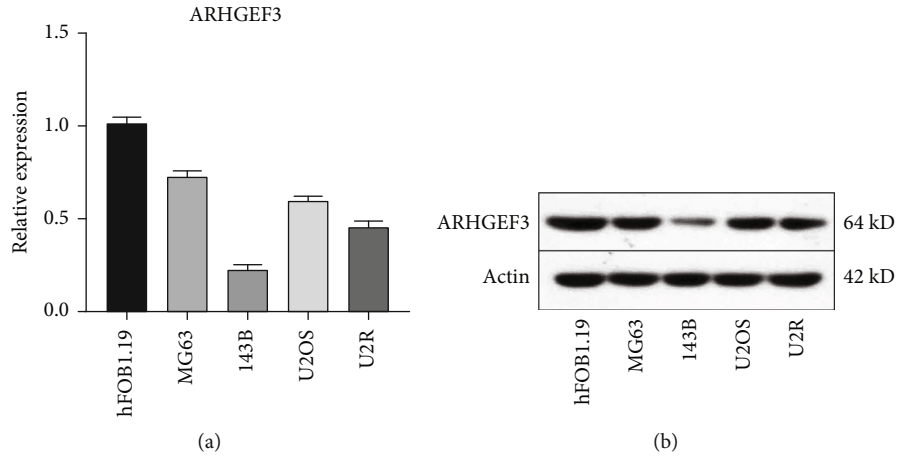

Figure 9: (a) The mRNA expression level of ARHGEF3 in various OS cell lines and osteoblastic cell lines was determined by qRT-PCR. Data are presented as mean ± SD. $^{*}P < 0.05$ vs. hFOB1.19. (b) The expression level of ARHGRF3 in hFOB1.19 and osteosarcoma cell lines (detected by Western blot).

played a vital oncogenic role in nasopharyngeal carcinoma pathogenesis by preventing cell apoptosis through the overexpression of baculoviral IAP repeat containing 8, and ARHGEF3 might be used as a new prognosis biomarker and effective therapeutic target for human NPC [33]. It also sensitizes acute myeloid leukemia differentiation via activation of RhoA signaling pathways directly regulated by small GTPase family proteins [34]. Besides, it may act as potential regulators of several mRNAs in bone cells, including TNFRSF11B, ARHGDIA, PTH1R, and ACTA2, which heavily affects osteoblast-like and osteoclast-like cells [35].

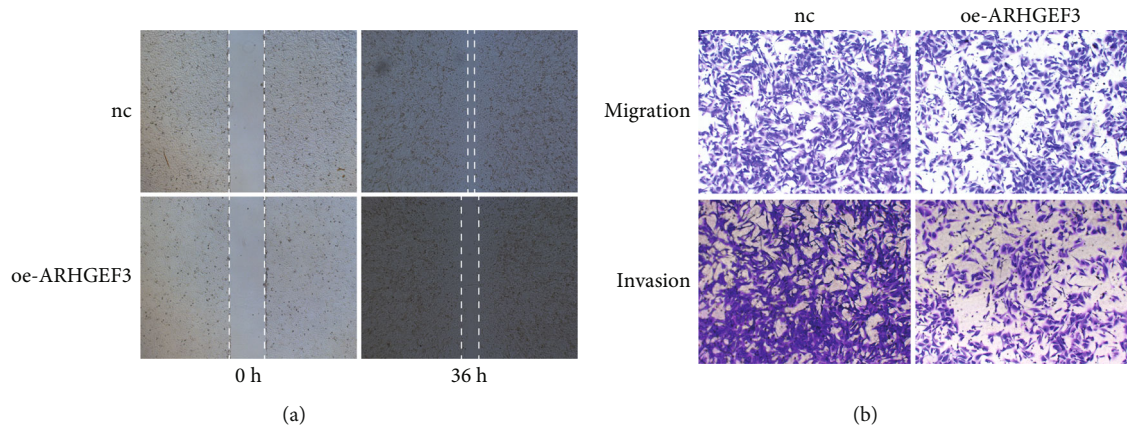

Figure 10: (a) Wound healing assays in the overexpression cell line and NC. (b) The migration and invasion assays. Measurements were in triplicate, and data were presented as the mean ± SD. $^{**}P < 0.01$ vs. hFOB1.19 (scale: 10x).

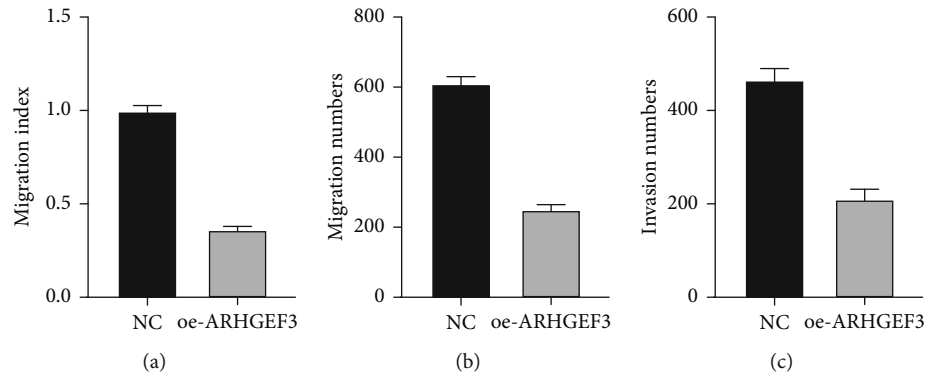

Figure 11: (a) Migration index of wound healing assays in the overexpression cell line and NC. (b) The migration numbers. (c) The invasion numbers. Measurements were in triplicate, and data were presented as the mean ± SD. $^{**}P < 0.01$ vs. hFOB1.19.

GALNT10 (Polypeptide N-Acetylgalactosaminyltransferase 10) is an enzyme that mediates the modification of proteins and lipids. It plays an important role in normal cell progression and other physiological processes. It is also a vital marker for the reason that can offer particular goals for therapeutic interventions [36]. A previous research indicated that overexpression of GALNT10 is associated with an immunosuppressive microenvironment to accelerate cancer development and predicts worse clinical results in high grade ovarian serous carcinoma patients [36]. Besides, it could also promote gastric cancer cell metastasis ability and reduce the sensitivity to 5-fluorouracil by regulating Homeobox D13 [37].

EYA2 (EYA Transcriptional Coactivator and Phosphatase 2) is a protein coding gene. Diseases related to EYA2 include syndromic microphthalmia and malignant peripheral nerve sheath tumor. A previous study reported that it can promote the invasion of human astrocytoma according to the regulation of extracellular signal-regulated kinase/matrix metalloproteinase signaling [38]. Besides, it can promote cell proliferation, invasion, and tumor progression by regulating docetaxel sensitivity and mitochondrial membrane potential, possibly through the AKT/Bcl-2 axis [39]. In lung adenocarcinoma, the expression of EYA2 was found upregulated in cancer tissues and may be involved in the progression of lung adenocarcinoma as a transcriptional activator [40].

Survival analysis demonstrated that expression of microRNA-124-3 was related to worse prognosis of patients with osteosarcoma by using KM Plotter software. Similarly, after uploading 8 miRNAs, we got the corresponding survival curves. The results indicated that upregulated ARHGEF3 and PLD5 were associated with poor overall survival. PLD5 is a protein that in humans is encoded by the phospholipase D family, member 5 genes. According to previous studies, PLD was found upregulated in many tumor cells such as triple-negative breast cancer [41], ovarian cancer [42], and colorectal cancer [43]. However, as for PLD5, according to searching the relevant literature, we did not find any evidence that it was related to the tumor. Survival analysis also indicated that hsa-mir-124 and target mRNAs (ARHGEF3 and PLD5) may have an obvious association with the prognosis of patients with osteosarcoma.

Since miRNAs generally negatively regulate target mRNAs, we chose ARHGEF3 for further study according to the survival curves. The WB and qRT-PCR results revealed that the expression level of ARHGEF3 in osteosarcoma (MG63, 143B, U2OS, and U2R) was indeed much lower than that in human osteoblasts (hFOB1.19), especially in the 143B

cell line. Therefore, we selected 143B cells to conduct the ARHGEF3 overexpression experiment and conducted Transwell assays and wound healing assays on the cells that had been overexpressed with ARHGEF3, and the results showed that ARHGEF3 overexpression does reduce the invasion and healing ability of 143B cells. In conclusion, we can infer that ARHGEF3 acts as a biomarker in OS as in other tumors.

Nowadays, with the development of precision medicine, the individual differences of treatment methods are paid more and more attention. Therefore, it is important to find novel markers and treatment ways. Our research demonstrated that microRNA-124 and ARHGEF3 were involved in the development of OS by some signaling pathways and had prognostic worth. Since our primary analysis was achieved from the GEO database by using R software, more experiments are needed to verify our conclusions and explore the mechanism.

5. Conclusion

Our research demonstrated certain mechanisms for the progression of osteosarcoma. Also, has-miR-124 and ARHGEF3 were selected as potential biomarkers of OS. However, these results need more research to prove them.

Data Availability

The datasets used and/or analyzed during the current study are available from the corresponding author on reasonable request.

Conflicts of Interest

The authors have declared that no conflicts of interests exist.

Authors' Contributions

Shushu Zhang contributed to the conception of the present study and completed the draft of the manuscript. All authors participated in the design of the study and conducted the research. Wei Tang processed and analyzed the data from the dataset. Wei Tang, Jie Gong, and Bin Lv contributed equally to this work.

References

[1] G. Maire, J. W. Martin, M. Yoshimoto, S. Chilton-MacNeill, M. Zielenska, and J. A. Squire, "Analysis of miRNA-gene expression-genomic profiles reveals complex mechanisms of microRNA deregulation in osteosarcoma," *Cancer Genetics*, vol. 204, no. 3, pp. 138–146, 2011.

[2] A. Luetke, P. A. Meyers, I. Lewis, and H. Juergens, "Osteosarcoma treatment - where do we stand? A state of the art review," *Cancer Treatment Reviews*, vol. 40, no. 4, pp. 523–532, 2014.

[3] B. Fuchs, K. Zhang, A. Schabel, M. E. Bolander, and G. Sarkar, "Identification of twenty-two candidate markers for human osteogenic sarcoma," *Gene*, vol. 278, no. 1-2, pp. 245–252, 2001.

[4] R. Gorlick, "Osteosarcoma: clinical practice and the expanding role of biology," *Journal of Musculoskeletal & Neuronal Interactions*, vol. 2, no. 6, pp. 549–551, 2002.

[5] Y. Ma, X. Pan, P. Xu et al., "Plasma microRNA alterations between EGFR-activating mutational NSCLC patients with and without primary resistance to TKI," *Oncotarget*, vol. 8, no. 51, pp. 88529–88536, 2017.

[6] S. Mishra, T. Yadav, and V. Rani, "Exploring miRNA based approaches in cancer diagnostics and therapeutics," *Critical Reviews in Oncology/Hematology*, vol. 98, pp. 12–23, 2016.

[7] X. Liu and M. Cui, "miRNA-98-5p inhibits the progression of osteosarcoma by regulating cell cycle via targeting CDC25A expression," *European Review for Medical and Pharmacological Sciences*, vol. 23, no. 22, pp. 9793–9802, 2019.

[8] W. T. Cai, P. Guan, M. X. Lin, B. Fu, B. Wu, and J. Wu, "miRNA-206 suppresses the metastasis of osteosarcoma via targeting Notch3," *Journal of Biological Regulators and Homeostatic Agents*, vol. 34, no. 3, pp. 775–783, 2020.

[9] Z. Du, F. Li, L. Wang, H. Huang, and S. Xu, "Regulatory effects of microRNA-184 on osteosarcoma via the Wnt/β-catenin signaling pathway," *Molecular Medicine Reports*, vol. 18, no. 2, pp. 1917–1924, 2018.

[10] B. Otoukesh, M. Abbasi, H. O. Gorgani et al., "MicroRNAs signatures, bioinformatics analysis of miRNAs, miRNA mimics and antagonists, and miRNA therapeutics in osteosarcoma," *Cancer Cell International*, vol. 20, no. 1, 2020.

[11] B. Xie, Y. Li, R. Zhao et al., "Identification of key genes and miRNAs in osteosarcoma patients with chemoresistance by bioinformatics analysis," *BioMed Research International*, vol. 2018, Article ID 4761064, 10 pages, 2018.

[12] A. Ballabio, "The awesome lysosome," *EMBO Molecular Medicine*, vol. 8, no. 2, pp. 73–76, 2016.

[13] A. Young, J. Lyons, A. L. Miller, V. T. Phan, I. R. Alarcon, and F. McCormick, "Chapter 1 Ras signaling and therapies," *Advances in Cancer Research*, vol. 102, pp. 1–17, 2009.

[14] D. Vigil, J. Cherfils, K. L. Rossman, and C. J. Der, "Ras superfamily GEFs and GAPs: validated and tractable targets for cancer therapy?," *Nature Reviews. Cancer*, vol. 10, no. 12, pp. 842–857, 2010.

[15] M. O'Hayre, J. Vazquez-Prado, I. Kufareva et al., "The emerging mutational landscape of G proteins and G-protein-coupled receptors in cancer," *Nature Reviews. Cancer*, vol. 13, no. 6, pp. 412–424, 2013.

[16] G. Loirand, V. Sauzeau, and P. Pacaud, "Small G proteins in the cardiovascular system: physiological and pathological aspects," *Physiological Reviews*, vol. 93, no. 4, pp. 1659–1720, 2013.

[17] E. Seixas, M. Barros, M. C. Seabra, and D. C. Barral, "Rab and Arf proteins in genetic diseases," *Traffic*, vol. 14, no. 8, pp. 871–885, 2013.

[18] M. Luo and J. L. Guan, "Focal adhesion kinase: a prominent determinant in breast cancer initiation, progression and metastasis," *Cancer Letters*, vol. 289, no. 2, pp. 127–139, 2010.

[19] M. J. van Nimwegen, S. Verkoeijen, L. van Buren, D. Burg, and B. van de Water, "Requirement for focal adhesion kinase in the early phase of mammary adenocarcinoma lung metastasis formation," *Cancer Research*, vol. 65, no. 11, pp. 4698–4706, 2005.

[20] P. P. Provenzano, D. R. Inman, K. W. Eliceiri, H. E. Beggs, and P. J. Keely, "Mammary epithelial-specific disruption of focal adhesion kinase retards tumor formation and metastasis in a

transgenic mouse model of human breast cancer," *The American Journal of Pathology*, vol. 173, no. 5, pp. 1551–1565, 2008.

[21] B. Y. Lee, P. Timpson, L. G. Horvath, and R. J. Daly, "FAK signaling in human cancer as a target for therapeutics," *Pharmacology & Therapeutics*, vol. 146, pp. 132–149, 2015.

[22] H. J. Zhang, J. Tao, L. Sheng et al., "Retracted: Twist2 promotes kidney cancer cell proliferation and invasion via regulating ITGA6 and CD44 expression in the ECM-receptor-interaction pathway," *Biomedicine & Pharmacotherapy*, vol. 81, pp. 453–459, 2016.

[23] Y. Bao, L. Wang, L. Shi et al., "Transcriptome profiling revealed multiple genes and ECM-receptor interaction pathways that may be associated with breast cancer," *Cellular & Molecular Biology Letters*, vol. 24, no. 1, 2019.

[24] G. Kim, H. J. An, M. J. Lee et al., "Hsa-miR-1246 and hsa-miR-1290 are associated with stemness and invasiveness of non-small cell lung cancer," *Lung Cancer*, vol. 91, pp. 15–22, 2016.

[25] B. Zhang, J. Chen, Z. Ren et al., "A specific miRNA signature promotes radioresistance of human cervical cancer cells," *Cancer Cell International*, vol. 13, no. 1, p. 118, 2013.

[26] J. Wu, X. Ji, L. Zhu et al., "Up-regulation of microRNA-1290 impairs cytokinesis and affects the reprogramming of colon cancer cells," *Cancer Letters*, vol. 329, no. 2, pp. 155–163, 2013.

[27] H. D. Long, Y. S. Ma, H. Q. Yang et al., "Reduced hsa-miR-124-3p levels are associated with the poor survival of patients with hepatocellular carcinoma," *Molecular Biology Reports*, vol. 45, no. 6, pp. 2615–2623, 2018.

[28] F. Tian, J. Chen, S. Zheng et al., "miR-124 targets GATA6 to suppress cholangiocarcinoma cell invasion and metastasis," *BMC Cancer*, vol. 17, no. 1, p. 175, 2017.

[29] C. Cong, W. Wang, J. Tian, T. Gao, W. Zheng, and C. Zhou, "Identification of serum miR-124 as a biomarker for diagnosis and prognosis in osteosarcoma," *Cancer Biomarkers*, vol. 21, no. 2, pp. 449–454, 2018.

[30] Y. Tu, W. Wu, Y. Guo et al., "Upregulation of hsa-miR-31-3p induced by ultraviolet affects keratinocytes permeability barrier by targeting CLDN1," *Biochemical and Biophysical Research Communications*, vol. 532, no. 4, pp. 626–632, 2020.

[31] G. Manceau, S. Imbeaud, R. Thiebaut et al., "Hsa-miR-31-3p expression is linked to progression-free survival in patients with KRAS wild-type metastatic colorectal cancer treated with anti-EGFR therapy," *Clinical Cancer Research*, vol. 20, no. 12, pp. 3338–3347, 2014.

[32] O. F. Bayrak, S. Gulluoglu, E. Aydemir et al., "MicroRNA expression profiling reveals the potential function of microRNA-31 in chordomas," *Journal of Neuro-Oncology*, vol. 115, no. 2, pp. 143–151, 2013.

[33] T. H. Liu, F. Zheng, M. Y. Cai et al., "The putative tumor activator ARHGEF3 promotes nasopharyngeal carcinoma cell pathogenesis by inhibiting cellular apoptosis," *Oncotarget*, vol. 7, no. 18, pp. 25836–25848, 2016.

[34] L. D'Amato, C. Dell'Aversana, M. Conte et al., "ARHGEF3 controls HDACi-induced differentiation via RhoA-dependent pathways in acute myeloid leukemias," *Epigenetics*, vol. 10, no. 1, pp. 6–18, 2015.

[35] B. H. Mullin, C. Mamotte, R. L. Prince, and S. G. Wilson, "Influence of ARHGEF3 and RHOA knockdown on ACTA2 and other genes in osteoblasts and osteoclasts," *PLoS One*, vol. 9, no. 5, 2014.

[36] G. Zhang, J. Lu, M. Yang, Y. Wang, H. Liu, and C. Xu, "Elevated GALNT10 expression identifies immunosuppressive microenvironment and dismal prognosis of patients with high grade serous ovarian cancer," *Cancer Immunology, Immunotherapy*, vol. 69, no. 2, pp. 175–187, 2020.

[37] G. Xu, Y. L. Wu, N. Li et al., "GALNT10 promotes the proliferation and metastatic ability of gastric cancer and reduces 5-fluorouracil sensitivity by activating HOXD13," *European Review for Medical and Pharmacological Sciences*, vol. 24, no. 22, pp. 11610–11619, 2020.

[38] Z. Wen, C. Liang, Q. Pan, and Y. Wang, "Eya2 overexpression promotes the invasion of human astrocytoma through the regulation of ERK/MMP9 signaling," *International Journal of Molecular Medicine*, vol. 40, no. 5, pp. 1315–1322, 2017.

[39] Z. Liu, L. Zhao, and Y. Song, "Eya2 is overexpressed in human prostate cancer and regulates docetaxel sensitivity and mitochondrial membrane potential through AKT/Bcl-2 signaling," *BioMed Research International*, vol. 2019, Article ID 3808432, 2019.

[40] J. T. Guo, L. H. Ding, C. Y. Liang, N. K. Zhou, and Q. N. Ye, "Expression of EYA2 in non-small cell lang cancer," *Zhonghua Zhong Liu Za Zhi*, vol. 31, no. 7, pp. 528–531, 2009.

[41] J. Gomez-Cambronero, "Lack of effective translational regulation of PLD expression and exosome biogenesis in triple-negative breast cancer cells," *Cancer Metastasis Reviews*, vol. 37, no. 2-3, pp. 491–507, 2018.

[42] S. Pignata, C. Pisano, M. Di Napoli, S. C. Cecere, R. Tambaro, and L. Attademo, "Treatment of recurrent epithelial ovarian cancer," *Cancer*, vol. 125, Supplement 24, pp. 4609–4615, 2019.

[43] S. Majdop, Y. Skornick, S. Avital, and L. Berkovich, "Phospholipase D activation mediates growth and migration of colon cancer cells interacting with cancer-associated fibroblasts," *Cellular and Molecular Biology (Noisy-le-Grand, France)*, vol. 64, no. 14, pp. 84–88, 2018.

Hindawi
BioMed Research International
Volume 2021, Article ID 9937742, 6 pages
https://doi.org/10.1155/2021/9937742

Research Article

Correlation between US-FNAC with BRAF V600E Mutation Analysis and Central Neck Lymph Node Metastasis in cN0 Papillary Thyroid Cancer

Ruoxuan Li,[1] Jiping Hao,[1] Zhao Zhu,[1] Xudong Qiao,[1] Ling Wang,[1] and Zubang Zhou[2]

[1]*Department of Ultrasound Medicine, Ninth Hospital of Xi'an, Xi'an 710054, China*
[2]*Department of Ultrasound Medicine, Gansu Provincial Hospital, Lanzhou 730000, China*

Correspondence should be addressed to Zubang Zhou; zzbxjh@126.com

Received 25 March 2021; Accepted 21 June 2021; Published 2 July 2021

Academic Editor: Bing Wang

The aim of this study was to explore the correlation between ultrasound-guided fine-needle aspiration cytology(US-FNAC) combined with BRAF V600E mutation analysis and central neck lymph node metastasis in cN0 papillary thyroid cancer, so as to provide reliable molecular evidence to use it for preoperative evaluation, operation procedure design, and postoperative follow-up planning in clinic. Specimens were obtained from 250 patients with cN0 thyroid cancer (TI-RADS≥4a, highly suspected of PTC by US-FNAC) after bilateral thyroidectomy and central neck lymph node dissection with accessible postoperative pathologic results of PTC and central neck lymph nodes and used for cytological diagnosis by H&E stain and BRAF V600E mutation detection. Single-factor analysis showed that differences between the central neck lymph node metastasis and nonmetastasis groups were statistically significant in gender, BRAF V600E mutation, and extracapsular extension. Logistic multivariate regression analysis showed significant differences in gender, BRAF V600E mutation, and extracapsular extension. Positive BRAF V600E mutations by US-FNAC, extracapsular extension, and male gender are risk factors of central neck lymph node metastasis in cN0 PTC metastatic PTC to central neck lymph node. Patients with those factors should undergo prophylactic central neck lymph node dissection.

1. Introduction

Thyroid cancer is one of the most common malignant tumors in the head and neck. According to Global Cancer Statistics 2018, thyroid cancer ranks in the ninth place in the incidence rate [1], 80%-90% [2] of which was attributable to papillary thyroid cancer (PTC), the most common subtype. Although ultrasonography is the preferred imaging examination for thyroid nodules, its sensitivity to examine central neck lymph node metastasis was low [3], while a closed correlation has been identified between metastasis to central neck lymph nodes and recurrence of cancer. Therefore, it is important to identify whether there is neck lymph nodes metastasis, especially for central neck lymph nodes before the surgery, which determines the prognosis of a patient as well as the method and range of the surgery. In this study, we enrolled 250 patients with cN0 PTC to receive ultrasound-guided fine-needle aspiration cytology (US-FNAC) combined with BRAF V600E mutation detection, so as to identify the potential application value of US-FNAC with BRAF V600E mutation detection in assessing central neck lymph node metastasis in cN0 PTC, in order to provide reliable molecular evidence to use it for preoperative evaluation, operation procedure design, and postoperative follow-up planning in the clinic.

2. Materials and Methods

2.1. Subject. We enrolled 250 patients with cN0 PTC who visited the ultrasound medicine department of Ninth Hospital of Xi'an and Gansu Provincial Hospital from Oct. 2017 to Feb. 2021, including 101 males and 149 females, aged 22-72

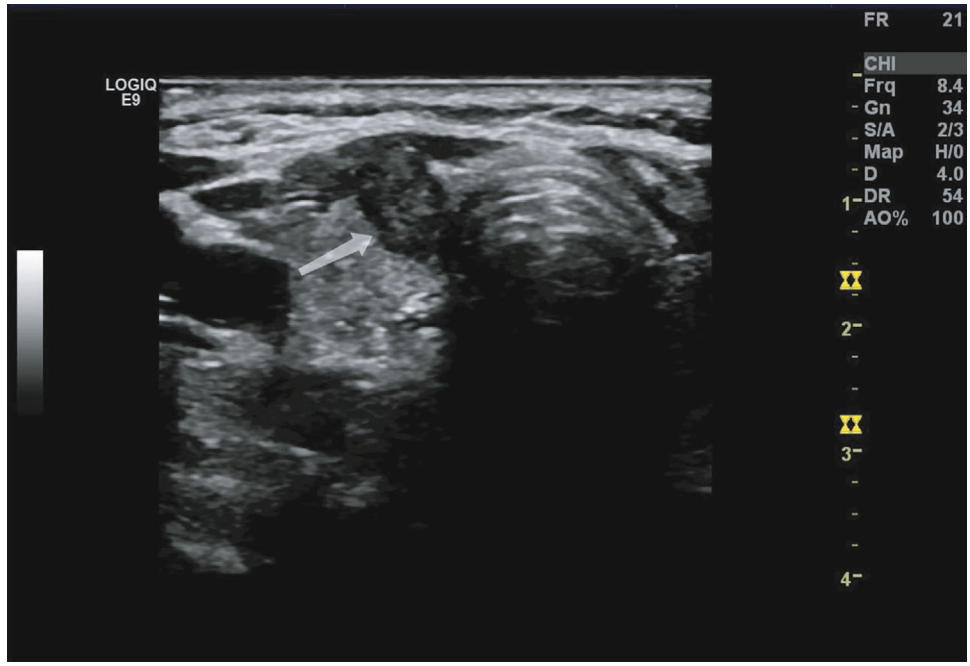

Figure 1: PTC ultrasonic image: the lesion manifests hypoecho, clear margin, inner microcalcification, a height-to-width ratio > 1, and extracapsular invasion.

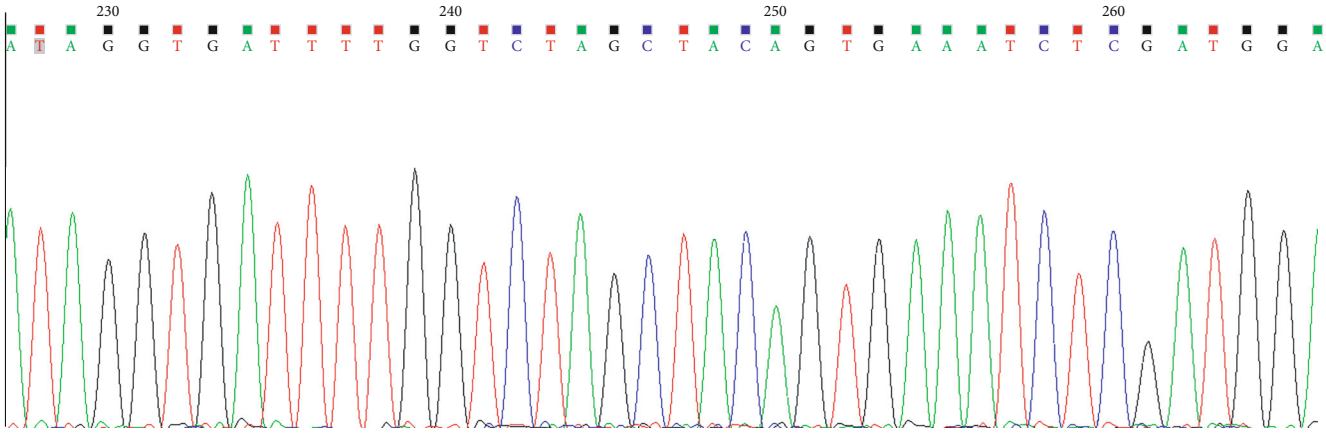

Figure 2: Negative results of US-FNAC combined with BRAF V600E mutation by PCR (no mutation).

years (average age 44.8), and divided into the metastatic group (140 cases) and nonmetastatic group (110 cases) according to the postoperative pathologic results of central neck lymph nodes. Enrollment criteria are as follows: TI-RADS≥4a, highly suspected of PTC with US-FNAC, no central neck lymph node metastasis found by all preoperative examinations, PTC diagnosed by postoperative pathology, and accessible pathologic results of central neck lymph nodes. US-FNAC procedures of all subjects were satisfactory with successful cytologic examinations and BRAF V600E mutation detections. For all patients, thyroid nodes were found for the first time, with normal thyroid function, normal past conditions, and no history of radiation exposure. All participants signed the informed consents. Patients who met all the above criteria were enrolled in this study.

2.2. Instruments and Methods

2.2.1. Instruments. Instruments are as follows: Color Doppler Ultrasound GE LOGIQ E9, linear array probe 9 L, 6 ~ 8 MHz, aspiration biopsy needle, CL type,23G × 50 mm. The BRAF gene mutation detection kit (PCR sequencing) (produced by Da An Gene Co., Ltd. of Sun Yat-sen University) was used.

This study assessed thyroid nodes according to TI-RADS in ATA guidelines, where the malignant signs include hypoechoic or extreme hypoechoic, unclear margin, a height-to-width ratio > 1, microcalcification (≤2 mm in diameter with punctate hyperechoic foci in this study), thyroid extracapsular invasion (an interrupted echo band of thyroid capsule caused by malignant nodule invasion, or an indistinct echo band of thyroid capsule without normal tissue between the

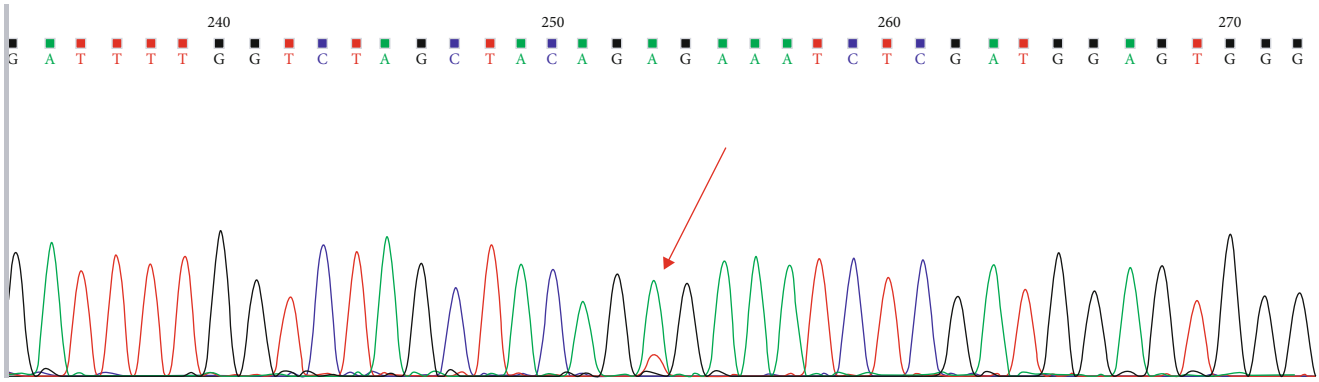

Figure 3: Positive results of US-FNAC combined with BRAF V600E mutation by PCR (see mutation site indicated by the arrow).

malignant nodule and the capsule in ultrasound imaging), and neck lymph node metastasis, see Figure 1.

2.2.2. US-FNAC and BRAF V600E Mutation Detection. Biopsies were obtained from the node of TI-RADS≥4a; if multiple lesions, biopsies were obtained from the one most highly suspected of malignancy. US-FNAC was performed by skillful senior doctors. All participants underwent necessary examinations before puncture to make sure no contraindications for puncture and signed informed consents of invasive examinations. Patients were asked to lie on their back with neck hyperextension to sufficiently expose the puncture sites. After routine disinfection and laying towel, 5 ml lidocaine was used for local anesthesia. Under the guidance of ultrasound, the needle was inserted into the suspicious node repeatedly to acquire enough tissue, part of it was used for cytological diagnosis, and the rest stored in a pathological sample bottle at 2°C-8°C. After DNA extraction, BRAF V600E gene mutation was detected by real-time fluorescent quantitative polymerase chain reaction (PCR) (see Figures 2 and 3). After the postoperative pathologic results obtained, the BRAF V600E gene mutation results in the metastasis group and the nonmetastasis group were observed, and differences and correlations in BRAF V600E mutation, clinical manifestations, and ultrasonic features in the two groups were analyzed.

2.3. Statistical Analysis. All statistical analyses were performed using SPSS 25.0 software. χ^2 test was used for enumeration data and single-factor analysis. Multivariate logistic regression analysis was used for relative risk factors with a two-sided test. P values of less than 0.05 were regarded as statistically significant.

3. Results

3.1. Clinical Presentations and Ultrasound Image of Patients with cN0 PTC. In the 250 typical PTC patients, 40.4% males and 59.6% females, aged 22-72 with 115 cases < 45 years old and 135 cases ≥ 45 years old where there were 112 cases with multiple lesions and 138 cases with single lesion and 114 cases with lesions ≥ 10 mm in diameter and 136 cases less than 10 mm. In addition, there were 129 cases with positive

Table 1: Correlation between central neck lymph node metastasis and clinical presentations and ultrasonic features.

	Central neck lymph node metastasis	No central neck lymph node metastasis	χ^2	P
Gender				
Female	100	49	18.489	≤0.001
Male	40	61		
Age				
<45	58	57	2.677	0.102
≥45	82	53		
Tumor diameter				
<10 mm	76	60	0.002	0.967
≥10 mm	64	50		
Tumor number				
Single	82	56	1.462	0.227
Multiple	58	54		
BRAF V600E mutations				
Negative	92	29	38.193	≤0.001
Positive	48	81		
Extracapsular invasion				
No	106	39	40.987	≤0.001
Yes	34	71		
Height-to-width ratio				
<1	54	50	1.201	0.273
>1	86	60		
Microcalcification				
No	87	62	0.854	0.355
Yes	53	48		
Margin				
Unclear	85	66	0.013	0.909
Clear	55	44		

Table 2: Assignment description.

Factor	Variable	Assignment description
Central neck lymph node metastasis	Y	0: no central neck lymph node metastasis; 1: central neck lymph node metastasis
Gender	X_1	0: female; 1: male
BRAF V600E mutation	X_2	0: negative; 1: positive
Extracapsular invasion	X_3	0: no; 1: yes

Table 3: Multivariate analysis of risk factors of central neck lymph node metastasis.

	β	Standard error	Wald	P	OR	95% CI
Gender	0.941	0.309	9.282	0.002	2.564	(1.399,4.698)
BRAF V600E mutation	1.345	0.313	18.422	≤0.001	3.836	(2.076,7.089)
Extracapsular invasion	1.084	0.315	11.867	0.001	2.956	(1.595,5.476)

results of US-FNAC combined with BRAF V600E mutation detection while 121 cases negative, 140 cases with central neck lymph node metastasis while 110 cases without, 99 cases where ultrasound images showed clear margins while 151 cases with indistinct margins; 146 cases with a height-to-width ratio > 1 and 104 cases with a height-to-width ratio < 1; 101 cases with microcalcification while 149 cases without, and 105 cases with malignant extracapsular invasion while 145 cases without.

3.2. Correlation between Neck Lymph Node Metastasis and Clinical Presentations and Ultrasonic Features in cN0 PTC Patients. The single-factor analysis showed statistically significant differences in gender ($\chi^2 = 18.489$, $P \leq 0.001$), BRAF V600E mutation ($\chi^2 = 38.193$, $P \leq 0.001$), and extracapsular invasion ($\chi^2 = 40.987$, $P \leq 0.001$) between the central neck lymph node metastasis group and the no central neck lymph node metastasis group (see Table 1). No significant differences were found in the other variants, so gender, BRAF V600E mutation, and extracapsular invasion were enrolled into the subsequent multivariate logistic regression analysis.

According to the results of multivariate logistic regression analysis, central neck lymph node metastasis was significantly influenced by gender ($P = 0.002$), BRAF V600E mutation ($P \leq 0.001$), and extracapsular invasion ($P = 0.001$) (see Tables 2 and 3).

4. Discussion

Preoperative determination of neck lymph node metastasis in PTC patients is closely related to the patient condition assessment and prognosis. There have been a large body of research on the diagnostic efficiency of ultrasound in neck lymph node metastasis where it is reported that the sensitivity of two-dimensional ultrasound in the diagnosis of central neck lymph node metastasis is only 12.1% [4], and there were about 60% of PTC patients whose neck lymph node metastasis had not been found before the operation [5]. However, views on surgical methods remain divided, i.e., whether prophylactic neck lymph node dissection is needed. In the 2015 American Thyroid Association Management Guidelines for Adult Patients with Thyroid Nodules and Differentiated Thyroid Cancer, prophylactic neck lymph node dissection is not recommended for patients with T1, T2, and cN0 stages [6], while it is still controversial whether the operation scheme is applicable to all patients. For example, Chinese scholars like Liu et al. [7] believed that there was still a lack of evidence to routinely perform such operation for all patients. However, Hwang and Orlof [8] believed that routine central neck lymph node dissection could block the metastasis of thyroid cancer to the lateral neck lymph nodes, so as to improve the prognosis. Nevertheless, prophylactic neck lymph node dissection may lead to multiple complications, such as recurrent laryngeal nerve injury and temporary or permanent hypoparathyroidism. Therefore, it is of great significance to identify neck lymph node metastasis in PTC patients before operation, especially the central neck lymph nodes, so as to reduce surgery-caused trauma, develop a scientific follow-up system, and improve patients' quality of life.

In recent years, there have been many studies on biomarkers of PTC, particularly in BRAF gene [9]. However, it has always been controversial whether there is a correlation between BRAF V600E mutation and neck lymph node metastasis. For example, Cohen et al. [10] found that BRAF V600E mutation is closely related to neck lymph node metastasis in PTC patients, while Hong et al. [11] believed that BRAF V600E gene mutation detection results of FNAC-obtained thyroid node samples could not effectively predict central neck lymph node metastasis and thyroid extracapsular invasion in PTC patients. In this study, we have done a single-factor analysis of central neck lymph node metastasis, clinical manifestations, and ultrasonic features in PTC patients of the cN0 stage, which showed that central neck lymph node metastasis is related to gender, BRAF V600E mutation, and extracapsular invasion. Further, multivariate logistic regression analysis of all above risk factors showed that central neck lymph node metastasis was significantly influenced by gender, BRAF V600E mutation, and extracapsular invasion in ultrasonic images. Among them, analysis in BRAF V600E mutation showed that the β value of 0.941

indicated that BRAF V600E gene mutation had a positive effect on neck lymph node metastasis, and OR of 3.836 indicates that with positive BRAF V600E gene mutations, the risk of central neck lymph node metastasis was 3.836 times higher than negative mutations with other independent factors unchanged. Similarly, we found that the risk of central neck lymph node metastasis in male patients was 2.564 times higher than that in female, and the risk in patients with thyroid extracapsular invasion was 2.956 times higher than that in patients with intact capsule, suggesting that BRAF V600E mutation was not the only cause of central neck lymph node metastasis, so that it cannot be used independently to predict the risk of central neck lymph node metastasis but can just be used as a reference indicator of neck lymph node metastasis. Therefore, other independent indicators to predict the risk of central neck lymph node metastasis in patients cN0 stage PTC should be found to improve the assessment of metastasis risks, which is consistent with the findings of Hong et al. [11] and Zhang et al. [12]. In our previous study [13], we found that female gender, BRAF V600E gene mutation, and extracapsular invasion were risk factors for central neck lymph node metastasis in PTC patients, and logistic regression analysis showed that central neck lymph node metastasis was caused by BRAF V600E gene mutation and extracapsular invasion in combination, which is slightly different from the results of this study, due to the expanded sample size of the latter. Meanwhile, the PTC patients enrolled in this study were not limited to those with classic PTC pathological types and were all in the cN0 stage, while in the previous study, the sample size was smaller, PTC pathology enrolled were all classic types, and patients were those with no central neck lymph node metastasis only found by preoperative ultrasound examination.

5. Conclusion

Comprehensive and systemic evaluations are needed by taking US-FNAC combined with BRAF V600E mutation detection, extracapsular invasion in ultrasonic images, and gender into consideration for patients with thyroid nodes of TI-RADS≥4a, highly suspected of malignancy, and without neck lymph node metastasis by all preoperative examinations to assess the risk of central neck lymph node metastasis so as to avoid adverse effects caused by excessive surgery. Male patients with BRAF V600E mutation and extracapsular invasion have a higher risk of central neck lymph node metastasis, so prophylactic central neck lymph node dissection should be performed at the same time of lesion resection.

6. Limitations

The study still has limitations that patients enrolled were of a single race (all Chinese Han nationality), while a previous report [14] has found that BRAF V600E mutation may be related to race in PTC patients. Therefore, subsequent studies should enroll patients of multiple nationalities to further explore the correlation between US-FNAC combined with BRAF V600E mutation detection and central neck lymph node metastasis in patients with cN0 PTC.

Data Availability

The data used to support the findings of this study are available from the corresponding author upon request.

Conflicts of Interest

The authors declare no conflict of interest.

Acknowledgments

The authors thank Zhihai Li and Hua Yang for providing a loving and caring environment for scientific research and writing. They also thank Xiaohang Yang for the help and love in difficulties.

References

[1] F. Bray, J. Ferlay, I. Soerjomataram, R. L. Siegel, L. A. Torre, and A. Jemal, "Global cancer statistics 2018: GLOBOCAN estimates of incidence and mortality worldwide for 36 cancers in 185 countries," *CA: a Cancer Journal for Clinicians*, vol. 68, no. 6, pp. 394–424, 2018.

[2] L. Siegel Rebecca, D. Miller Kimberly, and J. Ahmedin, "Cancer statistics, 2015," *CA: a Cancer Journal for Clinicians*, vol. 60, no. 5, pp. 277–300, 2015.

[3] Y. J. Choi, J. S. Yun, S. H. Kook, E. C. Jung, and Y. L. Park, "Clinical and imaging assessment of neck lymph node metastasis in papillary thyroid carcinomas," *World Journal of Surgery*, vol. 34, no. 7, pp. 1494–1499, 2010.

[4] C. H. Park, C. M. Song, Y. B. Ji et al., "Significance of the extracapsular spread of metastatic lymph nodes in papillary thyroid carcinoma," *Clinical and experimental otorhinolaryngology*, vol. 6, no. 3, pp. 289–294, 2015.

[5] S. P. Sun, Y. Zhang, Z. Q. Cui et al., "Clinical application of carbon nanoparticle lymph node tracer in the VI region lymph node dissection of differentiated thyroid cancer," *Genetics and Molecular Research*, vol. 13, no. 2, pp. 3432–3437, 2014.

[6] B. R. Haugen, E. K. Alexander, K. C. Bible et al., "2015 American Thyroid Association management guidelines for adult patients with thyroid nodules and differentiated thyroid cancer: the American Thyroid Association guidelines task force on thyroid nodules and differentiated thyroid cancer," *Thyroid*, vol. 26, no. 1, pp. 1–133, 2016.

[7] W. Liu, R. C. Cheng, and Y. J. Su, "Surgical planning and rational analysis of cN0 papillary thyroid carcinoma for 2015 American Thyroid Association management guidelines for adult patients with thyroid nodules and differentiated thyroid cancer," *Chinese Journal of Practical Surgery*, vol. 37, no. 5, pp. 568–571+576, 2017.

[8] H. S. Hwang and L. A. Orloff, "Efficacy of preoperative ultrasound in the detection of neck lymph node metastasis from thyroid cancer," *Laryngoscope*, vol. 76, no. 1, pp. 131–136, 2012.

[9] E. K. Choi, A. Chong, J. M. Ha, C. K. Jung, J. H. O, and S. H. Kim, "Clinicopathological characteristics including BRAF V600E mutation status and PET/CT findings in papillary thyroid carcinoma," *Clinical Endocrinology*, vol. 87, no. 1, pp. 73–79, 2017.

[10] Y. Cohen, M. Xing, E. Mambo et al., "BRAF mutation in papillary thyroid carcinoma," *Journal of the National Cancer Institute*, vol. 95, no. 8, pp. 625–627, 2003.

[11] Y. Hong, Z. Luo, Q. Wen et al., "Use of the BRAF V600E mutation in fine-needle aspirations of thyroid nodules," *Chinese Journal of Ultrasonography*, vol. 24, no. 8, pp. 671–674, 2015.

[12] Y. Zhang, Y. Luo, Y. Zhang et al., "Correlation between Ultrasound-guided Fine-needle Aspiration Combined with BRAF ^{V600E} Detection and Invasive Pathological Features of Papillary Thyroid Cancer," *Acta Academiae Medicinae Sinicae*, vol. 41, no. 4, pp. 517–523, 2019.

[13] R. Li, Z. Zhou, and J. Xie, "Application of ultrasound-guided fine-needle aspiration combined with BRAF V600E mutation detection and ultrasound features in estimating central neck lymph nodes metastasis of classic papillary thyroid cancer," *Chinese Journal of Ultrasonography*, vol. 28, no. 12, pp. 1056–1060, 2019.

[14] T. Xi, C. Hu, J. Zhao et al., "BRAF V600E mutation in papillary thyroid carcinoma," *Chinese Journal of Clinical Oncology*, vol. 39, no. 11, pp. 785–787, 2012.

Hindawi
BioMed Research International
Volume 2021, Article ID 5533134, 12 pages
https://doi.org/10.1155/2021/5533134

Research Article

Cytoreductive Surgery plus Hyperthermic Intraperitoneal Chemotherapy Improves Survival with Acceptable Safety for Advanced Ovarian Cancer: A Clinical Study of 100 Patients

Jue Zhang,[1] Xin-bao Li,[1] Zhong-he Ji,[1] Ru Ma,[1] Wen-pei Bai,[2] and Yan Li[1]

[1]*Department of Peritoneal Cancer Surgery, Beijing Shijitan Hospital, Capital Medical University, China*
[2]*Department of Gynecology, Beijing Shijitan Hospital, Capital Medical University, China*

Correspondence should be addressed to Yan Li; liyansd2@163.com

Received 24 January 2021; Revised 28 March 2021; Accepted 17 May 2021; Published 23 June 2021

Academic Editor: Qiang Liu

Background. The mainstay of treatment for advanced ovarian cancer is debulking surgery followed by chemotherapy that includes carboplatin and paclitaxel, but the prognosis is poor. This study is aimed at evaluating the efficacy and safety of cytoreductive surgery plus hyperthermic intraperitoneal chemotherapy (CRS+HIPEC) as first-line surgical treatment in patients with advanced ovarian cancer (AOC). *Methods*. FIGO stage III/IV AOC patients underwent CRS+HIPEC as first-line surgical treatment at our center from December 2007 to January 2020. The primary endpoint was survival, and the secondary endpoint was safety. *Results*. Among 100 patients, the median Karnofsky performance status (KPS) score was 80 (50-100), median peritoneal cancer index (PCI) was 19 (1-39), median completeness of cytoreduction (CC) score was 1 (0-3), number of organ regions removed was 4 (3-9), number of peritoneal regions removed was 4 (1-9), and number of anastomoses was 1 (0-4). The median follow-up was 36.8 months; 75 (75.0%) patients were still alive, and 25 (25.0%) had died. The median overall survival (mOS) was 87.6 (95% CI: 72.1-103.0) months, and the 1-, 2-, 3-, 4-, and 5-year survival rates were 94.1%, 77.2%, 68.2%, 64.2%, and 64.2%, respectively. Univariate analysis showed that better mOS correlated with an age ≤, KPS ≥ 80, ascites ≤ 1000 ml, PCI < 19, and CC score 0-1. Multivariate Cox analysis showed that CC was an independent factor for OS; patients who underwent CRS with a CC score 0-1 had a mPFS of 67.8 (95% CI: 48.3-87.4) months. The perioperative serious adverse event and morbidity rates were 4.0% and 2.0%, respectively. *Conclusions*. CRS+HIPEC improves survival for AOC patients with acceptable safety at experienced high-volume centers. Stringent patient selection and complete CRS are key factors for better survival.

1. Introduction

The majority of patients with ovarian cancer (OC) are diagnosed with advanced disease that has spread beyond the ovaries to cause peritoneal metastasis (PM), and this advanced stage accounts for the highest mortality of all gynecologic cancers [1]. The fatal manifestation of cancer dissemination on the omentum, peritoneum, and mesentery leads to refractory ascites, progressive intestinal obstruction, and intractable abdominal pain associated with early death and a miserable quality of life for such patients [2, 3]. Even after the standard treatment of optimal debulking surgery followed by intravenous platinum/taxane-based chemotherapy for advanced ovarian cancer (AOC) [4, 5], 75% of patients still develop recurrence and present with PM [6], which is the most difficult obstacle to improving AOC treatment.

Over the past three decades, aggressive cytoreductive surgery (CRS) plus hyperthermic intraperitoneal chemotherapy (HIPEC) has been developed as a comprehensive treatment package integrating multivisceral resections to remove macroscopic residual tumors, and HIPEC has been used to treat residual cancer cells after CRS [7, 8].

Bakrin et al. [9] report a multicenter retrospective cohort study included 566 patients, 92 patients with primary EOCPM, and 474 patients with recurrent EOCPM, which

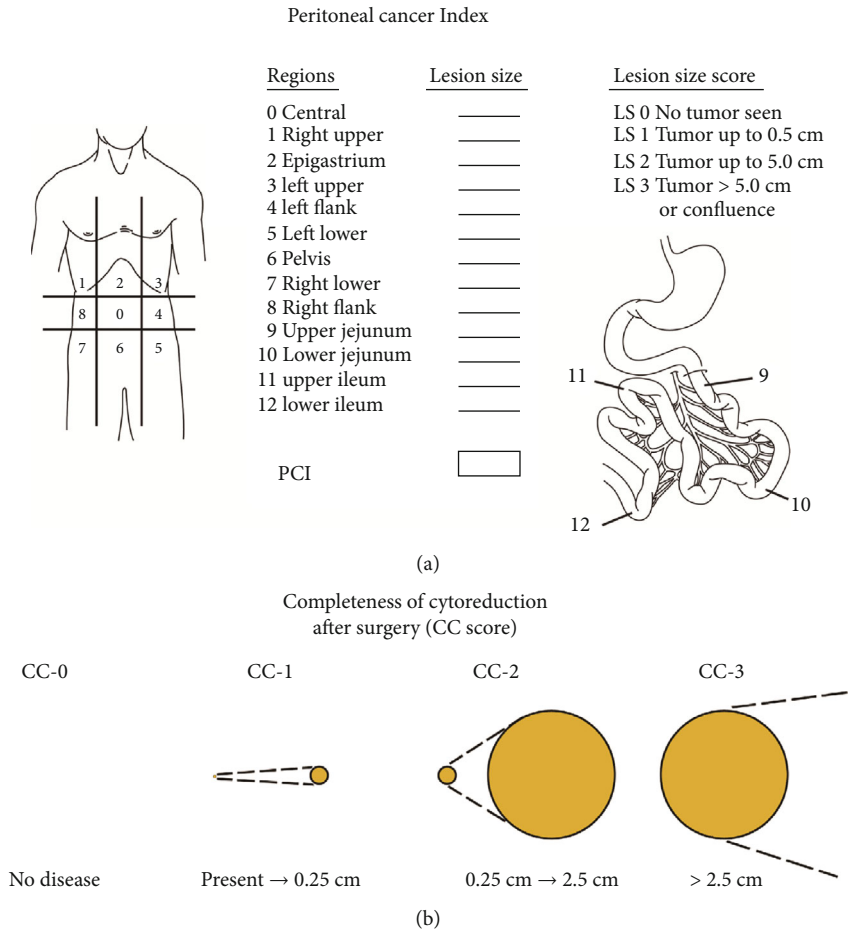

Figure 1: Graphical representation of PCI and CC score according to the Sugarbaker [8].

the CRS+HIPEC as first-line treatment. The median overall survivals (mOSs) were 35.4 months and 45.7 months for advanced and recurrent EOC, respectively. van Driel et al. [10] report a first RCT to compare the efficacy and safety of CRS+HIPEC and CRS groups, and the results showed the survival gain in the CRS+HIPEC group. Although CRS+HIPEC is considered one of several acceptable options for patients with stage III/IV OC by the National Comprehensive Cancer Network (NCCN) guidelines [11], there is currently limited evidence from clinical studies to definitively determine the efficacy and safety of standard operation programs and patient selection criteria.

A retrospective analysis was conducted in this study to assess the efficacy and safety of CRS+HIPEC as a front-line surgical regimen in 100 patients with AOC.

2. Methods and Materials

2.1. Patient Selection. From December 1, 2007, to January 1, 2020, 100 patients diagnosed with FIGO stage III/IV OC underwent CRS+HIPEC as a first-line surgery strategy at our center. Informed consent was obtained from all patients, and the study was approved by the institutional review board and the ethics committee.

The main inclusion criteria were as follows: (1) no history of PM-related surgery; (2) peripheral white blood cell count $\geq 3,500/mm^3$ and platelet count $\geq 8,000/mm^3$; (3) acceptable liver function, with bilirubin $\leq 2 \times$ the upper limit of normal (ULN) and aspartic aminotransferase (AST) and alanine aminotransferase (ALT) $\leq 2 \times$ ULN; (4) acceptable renal function, with serum creatinine (Scr) ≤ 1.5 mg/dl; (5) adequate cardiovascular and pulmonary function and function of other major organs that could tolerate major operation; and (6) Karnofsky performance status (KPS) ≥ 50.

The major exclusion criteria were as follows: (1) history of PM-related surgery; (2) any lung, liver, or prominent retroperitoneal lymph node metastases found during preoperative assessment; (3) imaging examination showing obvious contractures of the mesentery; (4) serum bilirubin level $> 3 \times$ ULN and ALT/AST $\geq 2 \times$ ULN; (5) liver enzymes $> 3 \times$ ULN; (6) Scr > 1.5 mg/dl; (7) KPS score < 50; and (8) absence of peritoneal metastasis.

2.2. Preoperative Evaluation. Patients were evaluated according to the Chinese expert consensus [12] of CRS+HIPEC, which included the following: (1) physical examination: serum tumor marker levels including carbohydrate antigen 125 (CA 125, normal range: 0-35 U/mL), carbohydrate antigen 199 (CA 19-9, normal range: 0-

Table 1: Demographic and clinical characteristics of 100 AOC patients.

Items	Value
Clinical characteristics	
Age (median, range) (y)	58.5 (28-87)
KPS score (median, range)	80 (50-100)
History of chemotherapy (*n*, %)	
Yes	52 (52.0)
No	48 (48.0)
Histopathology (*n*, %)	
Serous carcinoma	91 (91.0)
Other types	9 (9.0)
Cycles of SC before surgery (median, range)	3 (0-45)
Cycles of IPC before surgery (median, range)	1 (0-9)
Cycles of SC after surgery (median, range)	4 (0-26)
Cycles of IPC after surgery (median, range)	6 (0-8)
SC before surgery (*n*, %)	48 (48)
IPC before surgery (*n*, %)	16 (16)
SC after surgery (*n*, %)	76 (76)
IPC after surgery (*n*, %)	46 (46)
CRS+HIPEC relevant parameters	
Organ regions resected (*n*, %)	
1-3 resections	39 (39.0)
>4 resections	61 (61.0)
Peritoneal regions resected (*n*, %)	
0-3 resections	37 (37.0)
4-6 resections	40 (40.0)
>6 resections	23 (23.0)
Number of anastomosis (*n*, %)	
0-1	34 (34.0)
≥1	66 (66.0)
PCI score (*n*, %)	
≤19	53 (53.0)
>19	47 (47.0)
CC score (*n*, %)	
0-1	79 (79.0)
2-3	21 (21.0)
Lymph node dissection (*n*, %)	
Pelvic lymph node	100 (100)
Abdominal aortic lymph node	68 (68)
Iliac lymph nodes	100 (100)
Fluid output volume at surgery (median, range)	
Blood loss (ml)	550 (0-3,000)
Urine output (ml)	1,500 (300-4,500)
Ascites (ml)	270 (0-8,000)
≤1000 (*n*, %)	68 (68.0)
>1000 (*n*, %)	32 (32.0)
Fluid intake volume at surgery (median, range)	
Plasma (ml)	600 (0-4,000)
RBC (U)[a]	2 (0-12.0)
Other fluids (ml)[b]	6,735 (100-13,950)
CRS+HIPEC duration (median, range) (min)	600 (80-910)
Stay in hospital (median, range) (d)	27 (0-120)

[a]1 U = 200 ml. [b]Including crystalloid, colloidal fluid injection volume.

37 U/mL), and carcinoembryonic antigen (CEA, normal range: 0-5 ng/mL); (2) imaging examination: abdominopelvic multidetector computed tomography (CT) plus multiplanar reconstruction to evaluate gastrointestinal motility, intestinal obstruction, and mesenteric contracture; and (3) cytology: cytological examination of ascites or exfoliating cells from peritoneal washing fluid.

2.3. CRS+HIPEC Procedures. All CRS+HIPEC procedures were conducted by a designated team focusing on PM treatment. Briefly, abdominal exploration was performed through a midline xiphoid-to-pubis incision after administering general anesthesia, and the peritoneal cancer index (PCI) was evaluated and recorded. Then, maximal CRS was performed, including curative or palliative resection of the primary tumor with acceptable margins an any involved adjacent structures, lymphadenectomy, and peritoneal resection, and then, the completeness of cytoreduction (CC) score was calculated.

Open HIPEC was implemented with each drug dissolved in 3 L of heated saline at 43 ± 0.5°C, and the duration of HIPEC was 60 min with a flow rate of 400 mL/min. The HIPEC regimens included docetaxel (DTX) 120 mg + cisplatin (DDP) 120 mg, DTX 120 mg + mitomycin C (MMC) 30 mg for patients with high-risk factors for renal dysfunction, and DTX 120 mg only for patients with a single kidney and/or impaired renal function confirmed by laboratory tests.

After the operation, the patients were transferred to the intensive care unit for recovery and then to the ward when they stabilized.

2.4. Postoperative Chemotherapy. Adjuvant chemotherapy was delivered within 6 to 8 weeks after CRS+HIPEC, including platinum/taxane-based systematic chemotherapy (SC) and perioperative intraperitoneal chemotherapy (IPC) through the IPC port once every 4 to 6 weeks. DDP 100 mg/m^2 and paclitaxel/DTX 100 mg/m^2 were administered.

2.5. Follow-Up. All patients were regularly followed up once every 3 months for the first 2 years, every 6 months for years 3 to 5, and every year thereafter to obtain detailed information on disease status. The most recent follow-up was performed on January 1, 2020, and no patients have been lost.

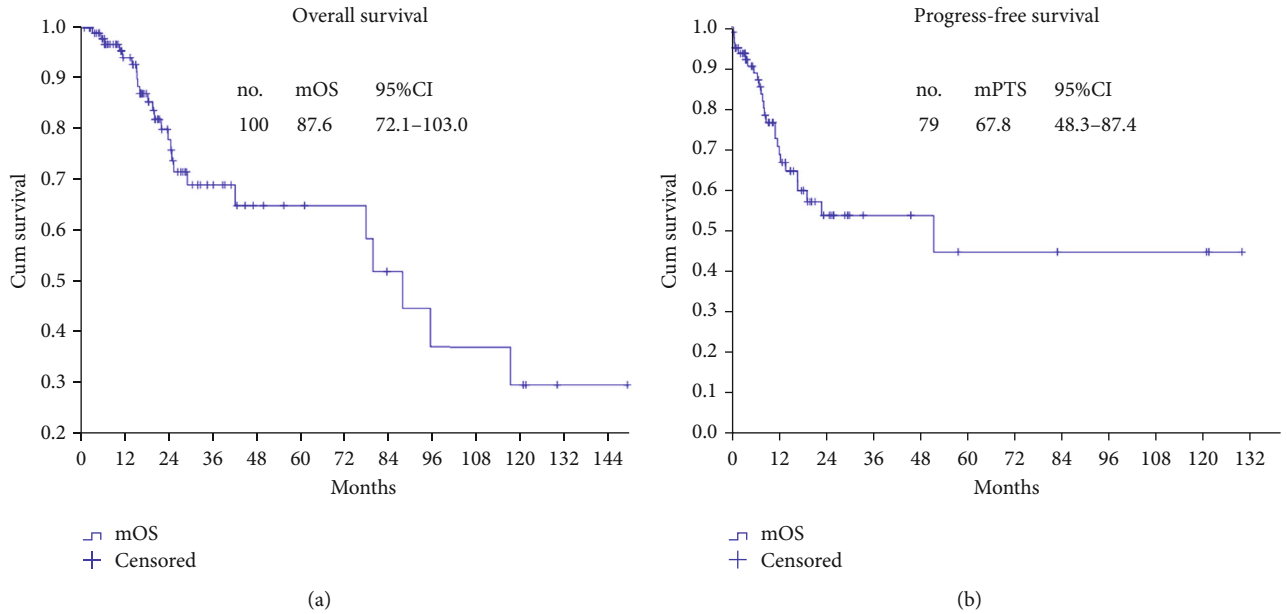

Figure 2: OS and PFS in the AOC patients. (a) OS of 100 AOC patients. (b) PFS of 79 AOC patients with complete CRS+HIPEC.

2.6. Study Parameters. (1) Clinicopathological characteristics: age, history of adjuvant therapy, KPS score, and preoperative tumor markers; (2) CRS+HIPEC-related parameters: duration of surgery, number of organs and peritoneal resected, number of anastomotic stoma, HIPEC regimens, PCI, CC score, and intraoperative volume; (3) survival: survival status, median overall survival (mOS), and median progression-free disease (mPFS); and (4) adverse events

2.7. Study Endpoints and Definition. (1) The primary endpoints of this study were OS and PFS. OS was defined as the time interval from the first surgery to tumor-related death or last follow-up. PFS was calculated from the date of surgery until the last follow-up that met the following criteria: the patients who underwent surgery-based curative comprehensive treatment developed any clinical manifestations, the CA 125 level rose again after surgery, medical imaging discovered any mass in the operation field, and the biopsy confirmed the diagnosis. (2) The secondary endpoints were perioperative serious adverse events (SAEs), which were defined as complications directly attributable to the treatment within 30 days of CRS+HIPEC and were evaluated based on the National Cancer Institute Common Terminology Criteria for Adverse Events version 4.0 [11]. (3) The PCI, according to Sugarbaker's criteria [8], is a standardized intraoperative staging system to determine the PM burden. The abdomen was divided into 13 areas, which included 9 sections of the abdominal cavity and 4 sections of the upper ileum, lower ileum, upper jejunum, and lower jejunum. The size of intraperitoneal nodules in each area was quantified. A score of 0 indicates that no malignant deposits are visualized; a score of 1 signifies that tumor nodules ≤ 0.5 cm are present; a score of 2 indicates that tumor nodules between 0.5 and 5.0 cm are present; a score of 3 signifies that tumor nodules > 5.0 cm in any dimension are present, and a confluence or layering of the tumor is scored as 3. The maximum score is 39. (4) The CC score was defined as follows: a CC score of 0 indicates no visible residual peritoneal disease after CRS, a CC score of 1 indicates less than 2.5 mm of residual disease, a CC score of 2 indicates a residual tumor between 2.5 mm and 2.5 cm, and a CC score of 3 indicates more than 2.5 cm of residual tumor or the presence of a sheet of unresectable tumor nodules [8] (Figure 1)

3. Statistics Analysis

The patient information was systematically integrated into a prospectively established database. Data analysis was conducted using the Statistical Package for Social Sciences version 24.0 (SPSS, Inc., Chicago, IL). Descriptive data are expressed as medians [range or 95% confidence intervals (CIs)] for quantitative variables and as numbers (percentage) for qualitative data. The hypothesis test was performed by the χ^2 test or Fisher's exact test. The Kaplan-Meier method was used to compare median survival with the log-rank test, and multivariate Cox regression analysis was performed to determine the independent predictors. The factors with $P < 0.05$ in the univariate analysis were included in the multivariate analysis model. A two-sided $P < 0.05$ was considered statistically significant.

4. Results

4.1. Characteristics of the AOC Patients. In total, 100 AOC patients were treated with 106 CRS+HIPEC procedures, including 6 patients who each underwent 2 CRS+HIPEC procedures due to tumor recurrence. The median age was 58.5 (28-87) years, and the median KPS score was 80 (50-100); according to histopathological classification, 91 (91/100, 91.0%) patients had serous adenocarcinoma, and 9 (9/100, 9.0%) patients had other types of tumors. For the areas of surgical excision, the median number of organ

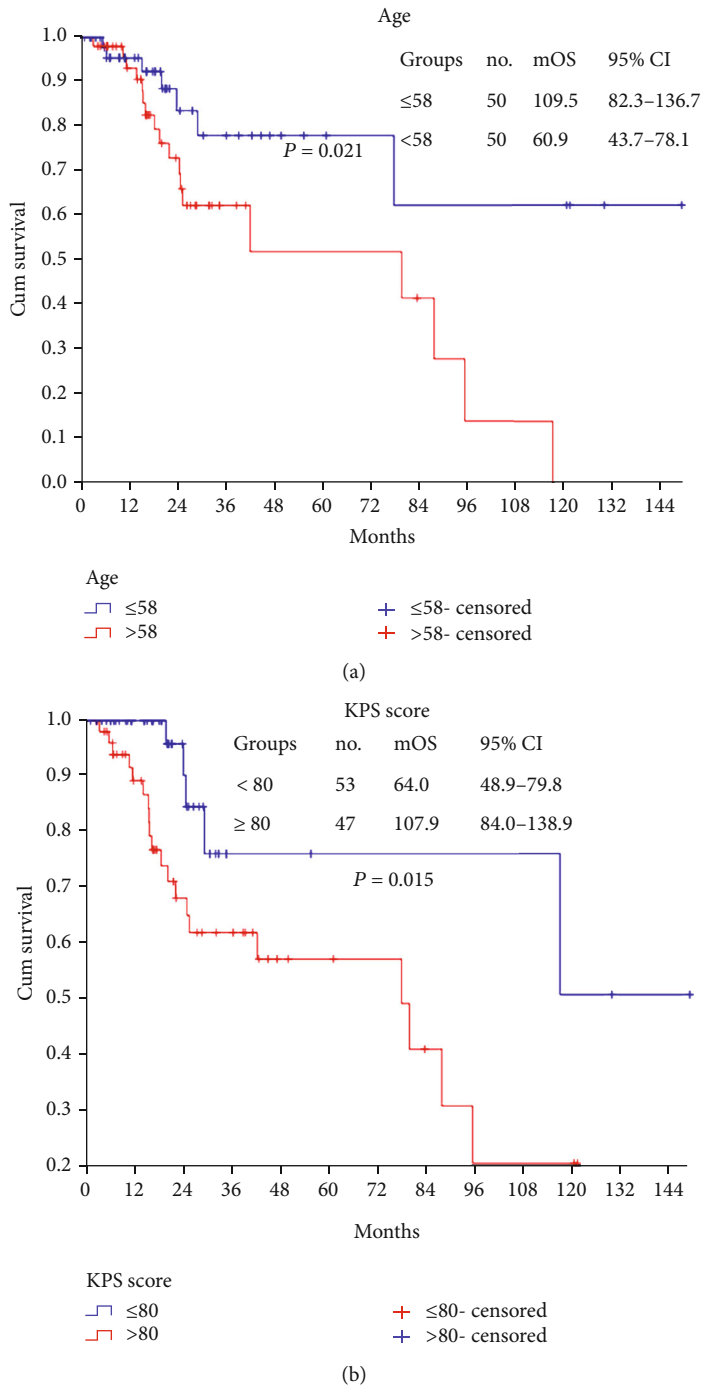

Figure 3: Continued.

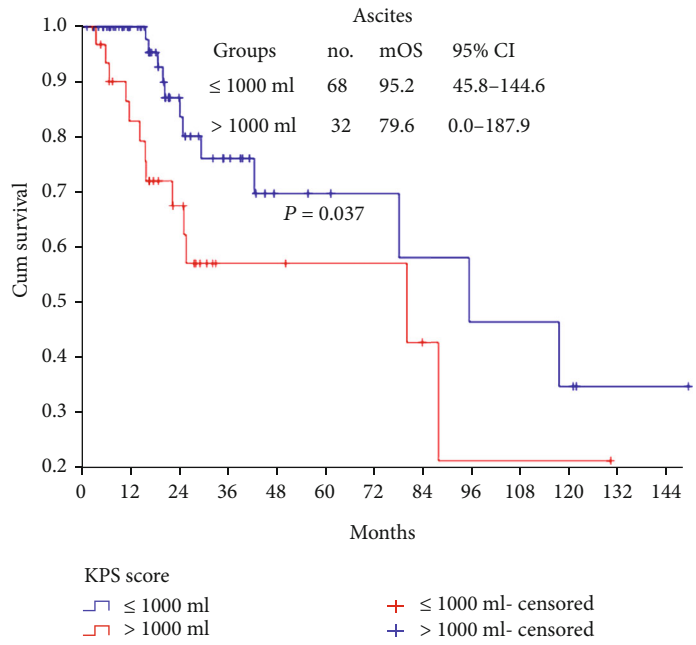

(c)

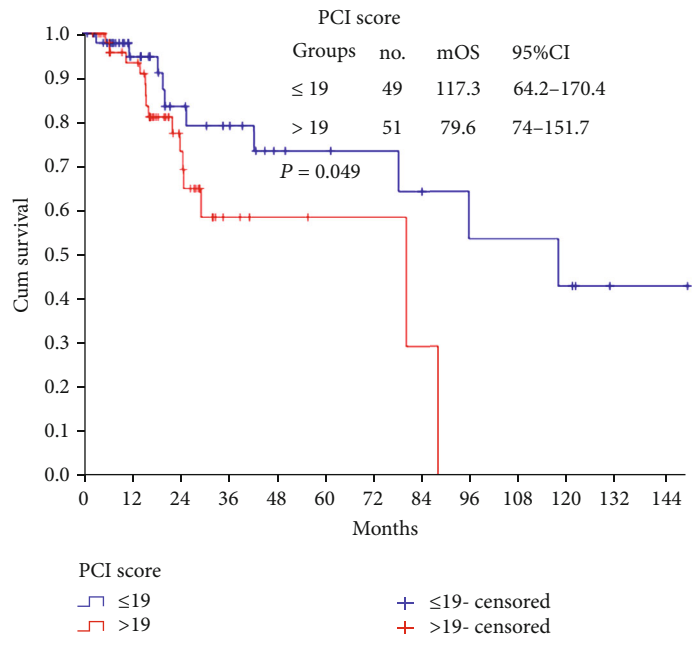

(d)

Figure 3: Continued.

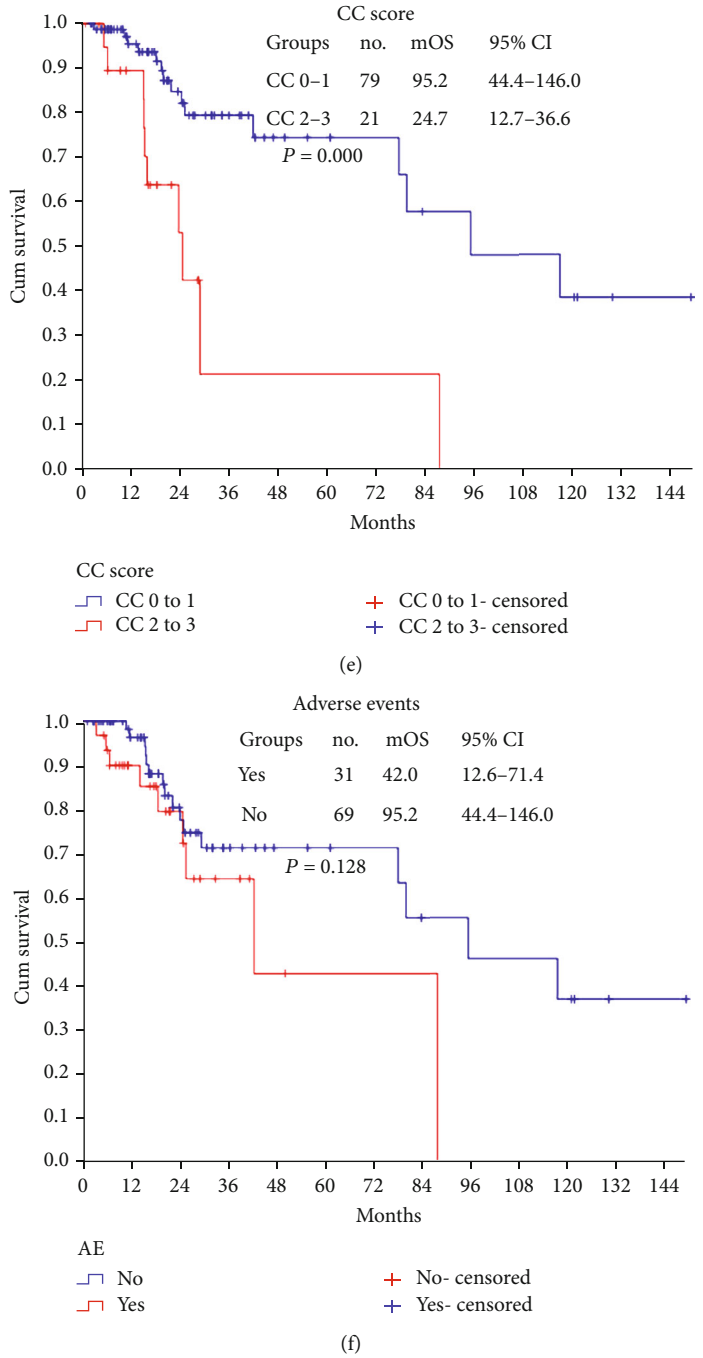

Figure 3: Overall survival of 100 AOC patients with correlation factors. (a) Age; (b) KPS score; (c) ascites; (d) PCI score; (e) CC score; (f) adverse events.

Table 2: Univariate and multivariate analyses on predictors of OS for 100 AOC patients.

Variables	Univariate analysis				Multivariate analysis			
	χ^2	P	HR	95% CI	χ^2	P	HR	95% CI
CC score (CC 2-3 *vs.* CC 0-1)	11.4	<0.001	4.2	1.8-9.8	6.8	0.009	3.2	1.3-7.5
Age (>58 y *vs.* ≤58 y)	4.8	0.021	2.7	1.1-6.5				
KPS score (≥80 *vs.* <80)	5.0	0.015	0.3	0.1-0.9				
PCI score (>19 *vs.* ≤19)	3.8	0.049	2.5	1.0-6.0				
Ascites (>1000 ml *vs.* ≤1000 ml)	4.2	0.037	2.3	1.0-5.0				

CI: confidence interval; HR: hazard ratio.

Table 3: Major clinicopathological features of 4 patients with OS over 10 years.

No	Age (y)	KPS score	Histopathology	CRS	HIPEC	PCI score	CC score	Recurrence	Survival status	OS (mo)
1	41	100	High-grade serous carcinoma	Hysterectomy and resection of bilateral ovarian/fallopian tubes, pelvic lymphadenectomy, ascending colon resection, sigmoidectomy, left and right diaphragmatic peritoneum, greater/lesser omentectomy, round ligament of liver resection, right paracolic sulci peritoneum, mesenteric fulguration	DDP120 mg + DTX 120 mg	19	1	No	Survival	149.2
2	52	90	High-grade serous carcinoma	Hysterectomy and resection of bilateral ovarian/fallopian tube, pelvic lymphadenectomy, greater/lesser omentectomy	MMC 40 mg	13	1	No	Survival	129.9
3	49	80	High-grade serous carcinoma	Hysterectomy and resection of bilateral ovarian/fallopian tube, pelvic lymphadenectomy, sigmoidectomy, cholecystectomy, greater/lesser omentectomy	DDP120 mg + DTX 120 mg	11	1	No	Survival	121.5
4	32	80	High-grade serous carcinoma	Hysterectomy and resection of bilateral ovarian/fallopian tubes, pelvic lymphadenectomy, greater/lesser omentectomy	DDP120 mg + DTX 120 mg	15	1	No	Survival	120.9

MMC: mitomycin C; DDP: cisplatin; DTX: docetaxel; y: year; mo: months.

resections was 4 (3-9), and the number of peritoneal resections was 4 (1-9). Regarding adjuvant therapies, preoperatively, SC was applied in 48 (48/100, 48.0%) cases, and IPC was applied in 16 (16/100, 16.0%) cases; postoperatively, SC was applied in 76 (76/100, 76.0%) cases, and IPC was applied in 46.0 (46/100, 46.0%) cases. The clinicopathological characteristics are listed in Table 1.

4.2. Efficacy. The median follow-up was 36.8 (0.8-159.3) months. At the time of analysis, 25 (25/100, 25%) patients had died, and 75 (75/100, 75.0%) patients were alive; the mOS was 87.6 (95% CI: 72.1-103.0) months, and the 1-, 2-, 3-, 4-, and 5- year survival rates were 94.1%, 77.2%, 68.2%, 64.2%, and 64.2%, respectively (Figure 2).

4.3. Univariate and Multivariate Analyses for Predictors of OS. A univariate analysis identified 5 covariates indicative of improved survival, including age ≤ 58 years (Figure 3(a), $P = 0.021$), KPS score ≥ 80 (Figure 3(b), $P = 0.015$), ascites ≤ 1000 ml (Figure 3(c), $P = 0.037$), PCI ≤ 19 (Figure 3(d), $P = 0.049$), and CC score 0-1 (Figure 3(e), $P < 0.001$) (Table 2). Multivariate Cox regression analysis identified the CC score as the only independent predictor for better survival. Compared with a CC score of 2-3, a CC score of 0-1 was approximately 3.2 times ($P = 0.009$, HR = 3.2, 95%, and CI: 1.3-7.5) more likely to indicate improved survival (Table 2).

4.4. Special Analysis of Four Patients with an OS of over 10 Years. At the time of analysis, there were 4 (4/100, 4.0%) patients with an OS of over 10 years and without any evidence of tumor recurrence; their OS durations were 149.2, 129.9, 121.5, and 120.9 months. The detailed clinical course of these four patients is listed in Table 3.

4.5. Adverse Events. Adverse events (AEs) from grades I to V occurred in 31 (31/100, 31.0%) patients, including anemia and hypoproteinemia in 5 (5/100, 5.0%) patients, urinary fistula in 4 (4/100, 4.0%) patients, ileus in 4 (4/100, 4.0%) patients, respiratory infection in 4 (4/100, 4.0%) patients, deep vein thrombosis (DVT) in 3 (3/100, 3.0%) patients, wound infection in 3 (3/100, 3.0%) patients, renal dysfunction in 2 (2/100, 2.0%) patients, and urinary tract infection in 2 (2/100, 2.0%) patients. Grades III to V SAEs occurred in 4 (4/100, 4.0%) patients, including 2 (2/100, 2.0%) patients who died within 30 days of acute renal failure, 1 (1/100, 1.0%) patient with blood loss, and 1 (1/100, 1.0%) patient with ascending colon leakage. The detailed information is listed in Table 4.

4.6. Survival Analysis of Patients with CC Scores of 0-1. A subgroup analysis was conducted. Seventy-nine (79/100, 79.0%) AOC patients achieved CC scores of 0-1, the mPFS was 67.8 (95% CI: 48.3-87.4) months (Figure 2(b)), and the mOS was 95.2 (95% CI: 44.4-146.0) months (Figure 3(e)).

Table 4: Adverse events rate of 100 AOC patients.

Items	*n*, %
SAE (grades III-V)	4 (4.0)
Perioperative mortality	2 (2.0)
Blood loss	1 (1.0)
Colon leakage	1 (1.0)
AE (grades I-II)	27 (27.0)
Anemia and hypoproteinemia	5 (5.0)
Urinary fistula	4 (4.0)
Ileus	4 (4.0)
Respiratory infection	4 (4.0)
DVT	3 (3.0)
Wound infection	3 (3.0)
Renal dysfunction	2 (2.0)
Urinary tract infection	2 (2.0)

AE: adverse event; SAE: serious adverse event; DVT: deep venous thrombosis.

5. Discussion

The treatment of AOC remains an open and critical question. Despite clinical remission after palliative surgery and platinum/taxane-based systematic chemotherapy [5, 13, 14], the overall survival of patients with PM is very limited. At present, PM is no longer regarded as a form of systemic and widespread metastasis but a locoregional spread of abdominopelvic malignancies [15]. Accordingly, an integrated treatment strategy of CRS+HIPEC has been developed by pioneering oncologists and has become a standard treatment for malignant mesothelioma of the peritoneum and pseudomyxoma peritoneum and selected patients with colorectal cancer [16–19]. Gradually, the efficacy of CRS+HIPEC has been supported and promoted by various cancer centers for patients with AOC [20–22], but valuable new information and evidence, which could help in the process of selecting patients, formulating HIPEC regimens, normalizing standard surgical procedures, and evaluating safety, are urgently needed.

We aimed to investigate the efficacy and safety of CRS+HIPEC as a first-line surgery strategy in100 patients with AOC. In essence, by comparing long-term survival, we were able to evaluate whether CRS+HIPEC, as a comprehensive therapy strategy, can be a suitable for the routine treatment for AOC. The results showed that the mOS was 87.6 months, and the 1-, 3-, and 5-year survival rates were 94.1%, 68.2%, and 64.2%, respectively. Complete CRS was achieved in 79.0% of patients, and the mPFS was 67.8 months. Of special note are four patients with high-grade serous disease who achieved an OS > 10 years and were disease-free at the time of the most recent follow-up. The multimodality approach following traditional therapy achieved a mOS of 50 months and a mPFS of 3 to 4 months, 5-year survival rates of over 30%, and a relapse rate of 75%. Our results indicated that CRS+HIPEC significantly prolongs the survival of patients with AOC compared to traditional treatment.

van Driel et al. [10] reported the first large-sample randomized controlled trial (RCT) on CRS+HIPEC in primary stage III OC in 2018. A total of 245 patients with newly diagnosed AOC (stage III), fallopian tube carcinoma, and

Table 5: Previously published studies for AOC patients with complete CRS in recent 5 years.

No.	Author	Year	No. (%)	mOS (mo)	mPFS (mo)	SAE (%)	Mortality (%)
1	Coccolini et al. [31]	2015	54 (100.0)	32.9	12.5	35.2	5.6
2	Kocic et al. [32]	2016	28 (96.8)	51.0	19.0	NA	NA
	Sun et al. [33]	2016	28 (60.9)	79.5	8.5	10.0	0.0
3	Manzanedo et al. [34]	2017	59 (97.0)	NA	17.0	NA	NA
4	Magge et al. [35]	2017	68 (90.6)	41.8	13.3	NA	NA
5	Pavlov et al. [2]	2017	112 (97.0)	40.3	26.7	9.5	0.8
6	Di Giorgio et al. [36]	2017	371 (72.6)	52.4	16.6	17.4	0.0
7	Mendivil et al. [24]	2017	68 (100.0)	33.8	25.1	0.0	0.0
8	Mercier et al. [16]	2018	155 (92.5)	69.3	30.3	NA	NA
9	van Driel et al. [10]	2018	106 (87.0)	45.7	14.2	27.0	0.0
10	This study	2019	79 (79.0)	95.2	67.8	4.0	2.0

NA: not available; mo: months.

primary peritoneal carcinoma were treated with CRS+HIPEC (DDP 100 mg, 40°C, and 90 min) following neoadjuvant chemotherapy. The mOS was 45.7 months for 106 (87.0%) patients with CC scores of 0-1, and the SAE rate was 27.0%. In our study, a mOS of 87.6 months and a mPFS of 67.8 months were achieved, and these results were better than those in previous studies. Two points deserve special attention. First, our patients underwent radical resection with strict surgical procedures to strive for complete CRS. This leaves a minimal residual tumor burden after surgery. Second, complete and nearly complete CRS was immediately followed by HIPEC with drug combinations at a temperature of 43°C. The synergistic effects of DDP, DTX, hyperthermia, and radical resection could produce significantly better survival benefits not comparable to those of any other treatment modalities applied individually.

The more extensive surgery to minimize tumor burden led to the success of CRS+HIPEC, which is an independent prognostic factor for patients with AOC [23]. In recent years, CRS+HIPEC has also been evaluated in the settings of primary AOC in several studies with variable results, showing that the mOS after complete CRS that achieves a CC score of 0-1 was 32.9 to 79.5 months, and the 5-year survival rate was 12.0 to 66.0% [9, 23–27] (Table 5). Our study also showed favorable survival for patients with CC scores 0-1 who had a mOS of 95.2 months, and the 1-, 3-, and 5-year survival rates were 95.4%, 78.7%, and 73.8%, respectively. Additionally, the multivariate Cox regression analysis identified the CC score as an independent factor for better survival, which is in accordance with the literature reports. In addition, compared with a CC score of 2-3, a CC score 0-1 was approximately 3.2 times more likely to indicate improved survival. All of these results indicated that complete CRS was key to better survival.

As such, every attempt should be made to achieve complete CRS, which means a high risk for AEs and mortality. The safety of CRS+HIPEC has been fully verified, with a perioperative mortality rate of 0 to 10.0% and an incidence of SAEs of 22.0% to 28.0% [18, 34–37]. In our experience, the incidence of grades I to V AEs was 31.0%, and 4.0% of patients developed SAEs, with a perioperative mortality rate of 2.0%, which is similar to that in literature reports. Although we observed no significant differences in patient survival, the mOS of patients without AEs was 53.2 months longer than that of patients with AEs (Figure 3(f)). Hence, further studies are necessary to confirm that AEs may have a detrimental impact on survival.

Apart from its retrospective design, the limitations of this study are the use of single-center cohort with a short median follow-up, but the results showed a tendency towards long survival and safety benefits for AOC patients who underwent CRS+HIPEC as an upfront surgery strategy at experienced high-volume peritoneal cancer centers.

6. Conclusions

In summary, this study has provided evidence that CRS+HIPEC, as a preferred surgical strategy, could prolong the survival of AOC patients, especially for those with a KPS score > 80, low PCI, and complete CRS. Therefore, strict patient selection and complete CRS in specialized peritoneal cancer centers are key factors for better survival.

Abbreviations

OC: Ovarian cancer
PC: Peritoneal carcinoma
AOC: Advanced ovarian cancer
CRS: Cytoreductive surgery
HIPEC: Hyperthermic intraperitoneal chemotherapy
ULN: Upper limit of normal
ALT: Alanine aminotransferase
AST: Aspartic aminotransferase
Scr: Serum creatinine
KPS: Karnofsky performance status
CA 125: Carbohydrate antigen 125
CA 199: Carbohydrate antigen 199
CEA: Carcinoembryonic antigen
CT: Computed tomography
DTX: Docetaxel
MMC: Mitomycin C
DDP: Cisplatin

SC: Systematic chemotherapy
IPC: Intraperitoneal chemotherapy
OS: Overall survival
PFS: Progress-free survival
AEs: Adverse events
SAEs: Serious adverse events
PCI: Peritoneal cancer index
CC: Completeness of cytoreduction
CIs: Confidence intervals.

Data Availability

The datasets used and analyzed during the current study are available from the corresponding author on reasonable request.

Ethical Approval

The protocol of this prospective investigation was granted by the Institutional Review Board at Beijing Shijitan Hospital (code number 2019054). All methods were performed in accordance with the relevant guidelines and regulations or Declaration of Helsinki as patients were involved.

Consent

Written informed consent was obtained from all subjects or, if subjects are under 18, from a parent and/or legal guardian.

Disclosure

This manuscript has been presented as a preprint in http://Researchsquare.com.

Conflicts of Interest

The authors declare that they have no competing interests.

Acknowledgments

This study was supported by the grants supporting Beijing Municipal Administration of Hospitals' Ascent Plan (DFL20180701), Special Fund for the Capital Characteristic Clinical Medicine Development Project (Z161100000516077), Beijing Municipal Grant for Medical Talents Group on Peritoneal Surface Oncology (2017400003235J007), Key Discipline Development Fund of Beijing Shijitan Hospital affiliated to the Capital Medical University (2016fmzlwk), Beijing Natural Science Foundation (7172108), Health Science Promotion Project of Beijing (2018-TG-27), and Hubei Provincial Natural Science Foundation of China (2017CFB177). Thanks for the support of journal of Cancer Research and Clinic (a domestic journal of China), in which the data from this article was published on November, 2020, issue 32 (8): 574-578. With the permission and authorization of the journal, we updated the data and translated it into English and submitted to the journal of Biomed Research International.

References

[1] L. A. Torre, B. Trabert, C. E. DeSantis et al., "Ovarian cancer statistics, 2018," *CA: a Cancer Journal for Clinicians*, vol. 68, no. 4, pp. 284–296, 2018.

[2] M. J. Pavlov, M. S. Ceranic, S. M. Latincic, P. V. Sabljak, D. M. Kecmanovic, and P. H. Sugarbaker, "Cytoreductive surgery and hyperthermic intraperitoneal chemotherapy for the treatment of advanced epithelial and recurrent ovarian carcinoma: a single center experience," *International Journal of Hyperthermia*, vol. 34, no. 5, pp. 564–569, 2018.

[3] W. F. Morano, M. Khalili, D. S. Chi, W. B. Bowne, and J. Esquivel, "Clinical studies in CRS and HIPEC: trials, tribulations, and future directions- a systematic review," *Journal of Surgical Oncology*, vol. 117, no. 2, pp. 245–259, 2018.

[4] J. GOH, G. R. MOHAN, R. LADWA, S. ANANDA, P. A. COHEN, and S. BARON-HAY, "Frontline treatment of epithelial ovarian cancer," *Asia-Pacific Journal of Clinical Oncology*, vol. 11, Suppl 6, pp. 1–16, 2015.

[5] D. M. Provencher, C. J. Gallagher, W. R. Parulekar et al., "OV21/PETROC: a randomized gynecologic cancer intergroup phase II study of intraperitoneal versus intravenous chemotherapy following neoadjuvant chemotherapy and optimal debulking surgery in epithelial ovarian cancer," *Annals of Oncology*, vol. 29, no. 2, pp. 431–438, 2018.

[6] P. Cascales-Campos, V. López-López, J. Gil et al., "Hyperthermic intraperitoneal chemotherapy with paclitaxel or cisplatin in patients with stage III-C/IV ovarian cancer. Is there any difference?," *Surgical Oncology*, vol. 25, no. 3, pp. 164–170, 2016.

[7] G. S. Kireeva, G. I. Gafton, K. D. Guseynov et al., "HIPEC in patients with primary advanced ovarian cancer: is there a role? A systematic review of short- and long-term outcomes," *Surgical Oncology*, vol. 27, no. 2, pp. 251–258, 2018.

[8] P. H. Sugarbaker, "Cytoreductive surgery and perioperative intraperitoneal chemotherapy for the treatment of advanced primary and recurrent ovarian cancer," *Current Opinion in Obstetrics & Gynecology*, vol. 21, no. 1, pp. 15–24, 2009.

[9] N. Bakrin, J. M. Bereder, E. Decullier et al., "Peritoneal carcinomatosis treated with cytoreductive surgery and hyperthermic intraperitoneal chemotherapy (HIPEC) for advanced ovarian carcinoma: a French multicentre retrospective cohort study of 566 patients," *European Journal of Surgical Oncology*, vol. 39, no. 12, pp. 1435–1443, 2013.

[10] W. J. van Driel, S. N. Koole, K. Sikorska et al., "Hyperthermic intraperitoneal chemotherapy in ovarian cancer," *The New England Journal of Medicine*, vol. 378, no. 3, pp. 230–240, 2018.

[11] NCCN guidelines, *Ovarian cancer*, NCCN, America, 2019, org/patients/survey/.

[12] Y. Li, Y. F. Zhou, H. Liang et al., "Chinese expert consensus on cytoreductive surgery and hyperthermic intraperitoneal chemotherapy for peritoneal malignancies," *World Journal of Gastroenterology*, vol. 22, no. 30, pp. 6906–6916, 2016.

[13] H. Yao and J. Ma, "Dendrimer-paclitaxel complexes for efficient treatment in ovarian cancer: study on OVCAR-3 and HEK293T cells," *Acta Biochimica Polonica*, vol. 65, no. 2, pp. 219–225, 2019.

[14] M. Petrillo, L. P. Anchora, G. Scambia, and A. Fagotti, "Cytoreductive surgery plus platinum-based hyperthermic intraperitoneal chemotherapy in epithelial ovarian cancer: a promising integrated approach to improve locoregional control," *The Oncologist*, vol. 21, no. 5, pp. 532–534, 2016.

[15] P. H. Sugarbaker, "Peritoneal metastases from gastrointestinal cancer," *Current Oncology Reports*, vol. 20, no. 8, p. 62, 2018.

[16] the PSOGI Working Group, the BIG-RENAPE Working Group, F. Mercier, N. Bakrin et al., "Peritoneal carcinomatosis of rare ovarian origin treated by cytoreductive surgery and hyperthermic intraperitoneal chemotherapy: a multi-institutional cohort from PSOGI and BIG-RENAPE," *Annals of Surgical Oncology*, vol. 25, no. 6, pp. 1668–1675, 2018.

[17] on behalf of the RENAPE Network, B. Malgras, E. Gayat et al., "Impact of combination chemotherapy in peritoneal mesothelioma hyperthermic intraperitoneal chemotherapy (HIPEC): the RENAPE study," *Annals of Surgical Oncology*, vol. 25, no. 11, pp. 3271–3279, 2018.

[18] C. Q. Huang, Y. Min, S. Y. Wang et al., "Cytoreductive surgery plus hyperthermic intraperitoneal chemotherapy improves survival for peritoneal carcinomatosis from colorectal cancer: a systematic review and meta-analysis of current evidence," *Oncotarget*, vol. 8, no. 33, pp. 55657–55683, 2017.

[19] Y. Wang, F. Ren, P. Chen, S. Liu, Z. Song, and X. Ma, "Effects of cytoreductive surgery plus hyperthermic intraperitoneal chemotherapy (HIPEC) versus cytoreductive surgery for ovarian cancer patients: a systematic review and meta-analysis," *European Journal of Surgical Oncology*, vol. 45, no. 3, pp. 301–309, 2019.

[20] M. Deraco, S. Sinukumar, R. A. Salcedo-Hernández et al., "Clinico-pathological outcomes after total parietal peritonectomy, cytoreductive surgery and hyperthermic intraperitoneal chemotherapy in advanced serous papillary peritoneal carcinoma submitted to neoadjuvant systemic chemotherapy- largest single institute experience," *European Journal of Surgical Oncology*, vol. 45, no. 11, pp. 2103–2108, 2019.

[21] R. Pozzar, L. M. Baldwin, B. A. Goff, and D. L. Berry, "Patient, physician, and caregiver perspectives on ovarian cancer treatment decision making: lessons from a qualitative pilot study," *Pilot Feasibility Stud.*, vol. 4, no. 1, p. 91, 2018.

[22] K. Jaaback, N. Johnson, and T. A. Lawrie, "Intraperitoneal chemotherapy for the initial management of primary epithelial ovarian cancer," *Cochrane Database of Systematic Reviews*, vol. 1, article CD005340, 2016.

[23] D. Biacchi, F. Accarpio, L. Ansaloni et al., "Upfront debulking surgery versus interval debulking surgery for advanced tubo-ovarian high-grade serous carcinoma and diffuse peritoneal metastases treated with peritonectomy procedures plus HIPEC," *Journal of Surgical Oncology*, vol. 120, no. 7, pp. 1208–1219, 2019.

[24] A. A. Mendivil, M. A. Rettenmaier, L. N. Abaid et al., "Consolidation hyperthermic intraperitoneal chemotherapy for the treatment of advanced stage ovarian carcinoma: a 3 year experience," *Cancer Chemotherapy and Pharmacology*, vol. 80, no. 2, pp. 405–410, 2017.

[25] R. A. Cowan, R. E. O'Cearbhaill, O. Zivanovic, and D. S. Chi, "Current status and future prospects of hyperthermic intraoperative intraperitoneal chemotherapy (HIPEC) clinical trials in ovarian cancer," *International Journal of Hyperthermia*, vol. 33, no. 5, pp. 548–553, 2017.

[26] M. Markman, "Hyperthermic intraperitoneal chemotherapy in ovarian cancer: where do we go from here?," *The Oncologist*, vol. 21, no. 5, pp. 529–531, 2016.

[27] A. Bhatt and O. Glehen, "The role of cytoreductive surgery and hyperthermic intraperitoneal chemotherapy (HIPEC) in ovarian cancer: a review," *Indian Journal of Surgical Oncology*, vol. 7, no. 2, pp. 188–197, 2016.

[28] M. Ba, H. Long, X. Zhang et al., "Hyperthermic intraperitoneal perfusion chemotherapy and cytoreductive surgery for controlling malignant ascites from ovarian cancer," *International Journal of Gynecological Cancer*, vol. 26, no. 9, pp. 1571–1579, 2016.

[29] P. A. Cascales-Campos, J. Gil, E. Gil et al., "Treatment of microscopic disease with hyperthermic intraoperative intraperitoneal chemotherapy after complete cytoreduction improves disease-free survival in patients with stage IIIC/IV ovarian cancer," *Annals of Surgical Oncology*, vol. 21, no. 7, pp. 2383–2389, 2014.

[30] P. Cascales Campos, J. Gil, and P. Parrilla, "Morbidity and mortality outcomes of cytoreductive surgery and hyperthermic intraperitoneal chemotherapy in patients with primary and recurrent advanced ovarian cancer," *European Journal of Surgical Oncology*, vol. 40, no. 8, pp. 970–975, 2014.

[31] F. Coccolini, L. Campanati, F. Catena et al., "Hyperthermic intraperitoneal chemotherapy with cisplatin and paclitaxel in advanced ovarian cancer: a multicenter prospective observational study," *Journal of Gynecologic Oncology*, vol. 26, no. 1, pp. 54–61, 2015.

[32] M. Kocic, S. Nikolic, M. Zegarac et al., "Prognostic factors and outcomes of cytoreductive surgery combined with hyperthermic intraperitoneal chemotherapy in patients with advanced ovarian cancer - a single tertiary institution experience," *Journal of BUON*, vol. 21, no. 5, pp. 1176–1183, 2016.

[33] J. H. Sun, Z. H. Ji, Y. Yu et al., "Cytoreductive surgery plus hyperthermic intraperitoneal chemotherapy to treat advanced/recurrent epithelial ovarian cancer: results from a retrospective study on prospectively established database," *Translational Oncology*, vol. 9, no. 2, pp. 130–138, 2016.

[34] I. Manzanedo, F. Pereira, E. Pérez-Viejo et al., "Hyperthermic intraoperative intraperitoneal chemotherapy (HIPEC) with primary or secondary cytoreductive surgery in the treatment of advanced epithelial ovarian cancer," *Minerva Ginecologica*, vol. 69, no. 2, pp. 119–127, 2017.

[35] D. Magge, L. Ramalingam, Y. Shuai et al., "Hyperthermic intraperitoneal chemoperfusion as a component of multimodality therapy for ovarian and primary peritoneal cancer," *Journal of Surgical Oncology*, vol. 116, no. 3, pp. 320–328, 2017.

[36] A. di Giorgio, P. de Iaco, M. de Simone et al., "Cytoreduction (peritonectomy procedures) combined with hyperthermic intraperitoneal chemotherapy (HIPEC) in advanced ovarian cancer: retrospective Italian multicenter observational study of 511 cases," *Annals of Surgical Oncology*, vol. 24, no. 4, pp. 914–922, 2017.

[37] National cancer institute, "Common terminology critertia for adverse events (CTCAE) v5.0," 2017, https://ctep.cancer.gov/protocolDevelopment/electronic_applications/ctc.htm#ctc_50.

Hindawi
BioMed Research International
Volume 2021, Article ID 1728352, 10 pages
https://doi.org/10.1155/2021/1728352

Research Article

LncRNA H19 Upregulation Participates in the Response of Glioma Cells to Radiation

Yanbei Kuang[1,2,3,4], **Zhitong Bing**[1,2,3,4], **Xiaodong Jin**[1,2,3,4] and **Qiang Li**[1,2,3,4]

[1]*Institute of Modern Physics, Chinese Academy of Sciences, Lanzhou 730000, China*
[2]*Key Laboratory of Heavy Ion Radiation Biology and Medicine of Chinese Academy of Sciences, Lanzhou 730000, China*
[3]*Key Laboratory of Basic Research on Heavy Ion Radiation Application in Medicine, Gansu Province, Lanzhou 730000, China*
[4]*University of Chinese Academy of Sciences, Beijing 100049, China*

Correspondence should be addressed to Xiaodong Jin; jinxd@impcas.ac.cn and Qiang Li; liqiang@impcas.ac.cn

Received 11 April 2021; Accepted 16 May 2021; Published 1 June 2021

Academic Editor: Ning Cao

Previous studies have indicated that radiation resistance of glioma is one of the leading causes of radiotherapy failure. Mounting evidence suggests that long non-coding RNA (lncRNA) plays an important role in regulating radiosensitivity of cancer cells via implicating in various cell processes. However, the underlying mechanisms remain unclear and need further study, especially at the molecular level. We found that the expression level of lncRNA H19 was elevated by radiation, and then, the modulation of H19 affected the resistant of glioma cells to X-rays. Dual-luciferase reporter analyses showed that H19 was transcriptionally activated by CREB1 in glioma cells after irradiation. In addition, both flow cytometry and 5-ethynyl-2′-deoxyuridine (EdU) assay suggested that H19 was involved in the cell cycle arrest, apoptosis, and DNA synthesis to modulate the radiation response of glioma cells and influenced their radioresistance. Therefore, H19 might play a crucial role in enhancing the radioresistance of glioma.

1. Introduction

Glioma is the most prevalent and malignant primary brain tumor in the central nervous system (CNS), and its incidence ranks first among intracranial tumors, accounting for 25.5% of all CNS primary tumors and 80.8% of all CNS malignant tumors [1, 2]. The World Health Organization (WHO) divides gliomas from WHO grade I to WHO grade IV according to the degree of malignancy, among which grade IV glioma is mainly glioblastoma (GBM) [3]. GBM is one of the tumors with a very high mortality rate. Almost all GBM patients receiving treatment will relapse, and the median survival is only about 15 months [4]. Surgery is the principal treatment for glioma patients, in combination with radiotherapy and chemotherapy [5, 6]. Although radiotherapy is an aggressive treatment to shrink tumor volume or prevent tumor relapse after surgical treatment [7, 8], the radiotherapy efficacy is still limited by many factors such as the radioresistance of cancer cells. The radioresistance of glioma is one of the most leading causes of radiotherapy failure.

Emerging evidence has shown that long non-coding RNAs (lncRNAs) more than 200 nt in length play a powerful role in molecular regulation of cancer cells involving in various aspects [9]. H19 is a 2.3-kb lncRNA encoded by the H19 gene located on the chromosome 11p15.5 as an imprinting gene with maternal expression. Many glioma-related studies assumed that H19-derived miR-675 participates in diverse cellular processes including cell invasion [10], proliferation [11, 12], migration [11, 12], cell cycle [11], hypoxia tumor microenvironment [13], and development of glioma [14]. Besides, it has been reported that the H19 expression in glioma tissues is higher than that in para-carcinoma tissues and associated with poor prognosis of glioma patients [15]. Li et al. found that H19 downregulation could enhance the sensitivity of GBM cells to chemotherapy drug temozolomide [16]. Furthermore, acting as a sponge of miRNAs and modulating miRNA action upon target mRNAs is another mechanism by which H19 functions as a modulator. Chen et al. observed that H19 promoted glioma cell proliferation and invasion by sponging of miR-152 [17]. Meanwhile, some

researchers hold that H19 plays a key role in regulating the radiosensitivity of cancer cells. H19 promoted the radioresistance of cardiac carcinoma cells via interacting with miR-130a-3p and miR-17-5p [18]. However, another study reported that the suppressed H19 and overexpressed miR-193a-3p level tended to significantly increase the resistance of hepatocellular carcinoma cells to radiation [19]. Few studies have explored whether H19 is involved in the regulation of radioresistance in glioma cells.

cAMP response element binding protein 1 (CREB1) is an important transcription factor belonging to the basic leucine zipper (bZIP) family [20]. It has been found to regulate the transcription of many growth factors and stress response molecules [21]. CREB1 plays essential roles in tumorigenesis via involving in the activation of multitudinous pathway [21, 22]. Researches on the most targets of CREB1 were limited to protein-coding genes [23, 24]; however, the non-coding targets need more exploration.

In this study, we explored whether radiation-induced CREB1 directly activates H19 transcription, and then, the depletion of H19 reduced the radioresistance of glioma cells, aiming at providing a novel target for radiotherapeutic intervention against glioma.

2. Materials and Methods

2.1. Cells. Human glioma cells lines T98G (WHO grade IV), U87 (WHO grade IV), U251 (WHO grade IV), and human embryonic kidney cell line 293T were acquired from the Chinese Academy of Sciences Cell Resource Centre (Shanghai, China). T98G, U251, and 293T cells were cultured in DMEM containing 10% foetal bovine serum (Bailing Bio, Lanzhou, China), while MEM with 10% foetal bovine serum was used for U87 cell culture.

2.2. Irradiation. Irradiation was performed using an X-ray machine (PXi, North Branford, CT, USA) operated at 225 kVp and a dose rate of 2.0 Gy/min at room temperature.

2.3. Plasmids and siRNAs. siRNAs (RiboBio, China) and their corresponding negative controls were transiently transfected using riboFECT™ CP Reagent (RiboBio, China) at a final concentration of 50 nM. Each plasmid was transfected by FuGENE® 6 (Promega, USA) at 2.5 μg per 35 mm Petri dish. Overexpressing CREB1 plasmid and its corresponding negative control LentiCMV-IL2-hCD87, pGL3-based construct containing the H19 promoter and its corresponding negative control pGL3, and Renilla luciferase plasmid were purchased from Sangon, Shanghai, China. The target sequences of siRNAs used in this study were as follows:

siRNA-H19: CCTCTAGCTTGGAAATGAA
siRNA-CREB1: GCTCGAGAGTGTCGTAGAA

2.4. Bioinformatics Analysis. The Chinese Glioma Genome Atlas (CGGA) and The Cancer Genome Atlas (TCGA) database were adopted to analyse the relationship between the H19 expression and the prognosis of glioma patients.

2.5. RNA Extraction and Real-Time PCR. Total RNA was extracted utilizing TRIzol reagent (CWBIO, China). cDNA was obtained via PrimeScript RT Mix reagent (Takara, China). Real-time PCR was conducted with Quantity Nova SYBR Green PCR Master Mix (QIAGEN, Germany), and β-actin was used as an internal reference. All procedures were completed in the QuanStudio 5 Real-time PCR system (Therom Lifetech ABI, USA). The primers of H19 were as follows:

Fw: 5′TCCTGAACACCTTAGGCTGG3′
Rev: 5′TGATGTTGGGCTGATGAGGT3′

2.6. Dual-Luciferase Reporter Assay. 293T cells were cotransfected with the corresponding plasmid according to the experimental design and a Renilla luciferase plasmid as internal reference for 24 h. The reporter activity was tested using the Dual-luciferase-reporter Gene Assay Kit (Beyotime, China).

2.7. Colony Formation Assay. After transfection for 24 h, an appropriate number of cells undergoing different transfection were seeded in 6-well plate and placed in an incubator. When the cells adhered to the wall, they were irradiated with X-rays at 0, 1, 2, 4, and 6 Gy. Keeping culture for two weeks, cell colonies were stained with crystal violet for 15 min. Colonies with more than 50 cells were regarded as survivors. Cell survival data were fitted using the linear-quadratic (LQ) model.

2.8. Flow Cytometry. Cells were collected at the indicated time points after irradiation. The percentage of apoptosis was detected according to the protocol of Annexin V Apoptosis Detection Kit I (BD Biosciences, USA). The analysis of cell cycle was also completed through flow cytometry. After being harvested and fixed in 70% ice-cold ethanol at -20°C for 48 hours, the cells were stained for 20 minutes on ice with PBS containing 100 μg/mL RNase, 0.2% Triton X-100, and 50 μg/mL PI (Sigma-Aldrich, USA).

2.9. 5-Ethynyl-2′-Deoxyuridine (EdU) Assay. DNA synthesis in cells was detected using the Cell-Light EdU DNA Cell Proliferation Kit (RiboBio, China) according to the reagent instructions. Images were taken, and the cells were counted in five randomly chosen visual fields under a microscope (BX51, Olympus, Japan).

2.10. Western Blot Analysis. RIPA buffer (Beyotime, China) supplemented with protease inhibitor (Roche, Switzerland) was used to perform the protein extraction. Antibodies against CREB1 (12208-1-AP, Proteintech, China) and β-actin (20536-1-AP, Proteintech, China) were purchased for use in the present study.

2.11. Statistics. Data are represented as the mean ± standard deviation (SD). One-way ANOVA and Student's t-test were performed for comparisons between groups. $p < 0.05$ and $p < 0.01$ were considered statistically significant and statistically extremely significant, respectively.

3. Results

3.1. Positive Associations between High H19 Expression and Radioresistance of Glioma. As a first attempt to investigate whether H19 has an impact on the radioresistance of glioma, we first searched for relevant clinical data to analyse their relationship. Shown in Figure 1(a) is the dataset of the Cancer Genome Atlas (TCGA) database. The patients with GBM were divided into two subgroups, radioresistant and radiosensitive, respectively. The H19 expression was significantly higher in the radioresistant patients in contrast to the radiosensitive counterparts. In addition, Kaplan–Meier analysis of the Chinese Glioma Genome Atlas (CGGA) databases indicated a significant relationship between H19 overexpression and primary or recurrent glioma patients' survival rates (Figure 1(b)). These results suggested that the high expression of H19 in patients with GBM was correlated with poor prognosis. To confirm that H19 plays a key role in the radiosensitivity of glioma, we further examined the H19 background level in T98G, U87, and U251 cells using real-time PCR and compared the radioresistance of these cell lines through performing a colony formation assay. As shown in Figure 1(c), in T98G cells, the expression of H19 was several hundred fold higher than those in U87 and U251 cells. As expected, when being compared between cell lines, T98G cell line was the most resistant to radiation while the other two cell lines were more radiosensitive in a similar degree. Collectively, these results suggested a strong correlation between H19 level and the radioresistance of glioma.

3.2. Radiation Induced the Expression of H19 and Downregulation of H19 Increased the Radiosensitivity of Glioma Cells. According to the aforementioned experimental results, we should investigate whether H19 participates in the radiation response and regulates the radioresistance of glioma cells. Therefore, we harvested cells at different time points after irradiation and observed the changes in the H19 expression. As shown in Figure 2(a), the H19 expression was significantly upregulated in all the three cell lines after irradiation compared to the unirradiated groups. Then, we modified the expression of H19 and observed the changes in the radioresistance of glioma cells. The efficiency of knocking down H19 was shown in SF. As shown in Figure 2(b), H19 downregulation caused a conspicuous increase in the radiosensitivity of glioma cells, and consistent trends were observed in all the three cell lines. Thus, the data demonstrated that the augment of H19 caused by radiation participated in the radiosensitivity regulation of glioma cells and downregulation of H19 increased the radiosensitivity of glioma cells.

3.3. Downregulation of H19 Promoted Cell Cycle Arrest and Apoptosis after Irradiation. The above data prompted us to explore how H19 regulates the radiosensitivity of glioma cells, especially through which pathway. Since irradiation induced the increase of H19, we intended to restrain this upregulation via siRNA and survey the changes in cell cycle and apoptosis. Cycle arrest was detected by flow cytometry at 24 h postirradiation. Compared with the siRNA-control group, an increasing percentage of G2/M phase cells was observed in the siRNA-H19 group of the three cell lines (Figure 3(a)), accompanied by a decrease in the proportion of G0/G1 and S phase cells. Besides, apoptosis rate analysis was conducted at 72 h postirradiation (Figure 3(b)). Our results indicated that cell apoptosis was significantly induced at 72 h after irradiation. The rate of apoptosis was dramatically increased in all siRNA-H19 groups when compared to the respective siRNA-control group in glioma cell lines. These results showed that H19 suppression might regulate the radiosensitivity of glioma cells via enhancing cell cycle arrest and apoptosis.

3.4. Downregulation of H19 Reduced DNA Synthesis after Irradiation. DNA synthesis situation was investigated using the EdU assay. As shown in Figures 4(a)–4(c), glioma cells transfected with siRNA-H19 exhibited no differences compared to the siRNA-control group in DNA synthesis. However, when cells were exposed to irradiation, the DNA synthesis obviously decreased in the siRNA-H19 + IR group compared with the siRNA-control+IR group. The evidence from the EdU incorporation assay supported that H19 could modulated the radiosensitivity of glioma cells, because repression of H19 could inhibit DNA replication activity after irradiation.

3.5. H19 Was a Direct Transcriptional Target of CREB1. We used the RegRNA2.0 database to predict the proteins which could bind to H19 and found that CREB1 is one of them. Therefore, first we detected the CREB1 expression following irradiation. As shown in Figure 5(a), high expression of CREB1 persisted for several days starting at 6 h after irradiation. Then, we depleted the expression level of CREB1 and found the CREB1 downregulation caused an increase in the radiosensitivity of glioma cells (Figure 5(b)). CREB1 and H19 had a positive correlation relationship in expression and function. Next, we silenced CREB1 and explored the changes of the H19 expression in T98G cells after irradiation. As shown in Figure 5(c), there was no obvious difference in the H19 expression in the siRNA-control and siRNA-CREB1 groups at 24 h postirradiation. However, at 48 h postirradiation, radiation-induced H19 augment was markedly attenuated by transfection with siRNA-CREB1. Therefore, CREB1 downregulation would reduce the H19 expression level after irradiation. It is tempting to speculate that CREB1 could activate the transcription of H19 when cells received irradiation. Hence, we conducted a dual-luciferase reporter assay to investigate whether CREB1 could mediate the H19 expression at the transcriptional level. We examined the genomic promoter regions of H19 in JASPAR. Two potential binding sites named P1 and P2 were found within the promoter of H19 (Figure 5(d)), respectively, located at -1638 to -1627 kb and -1605 to -1594 kb of H19. DNA fragments containing wild-type P1 and P2 sites (H19 promoter) or, respectively, mutational P1 (H19 Mut P1) and P2 (H19 Mut P2) site were cloned into the promoter region of a firefly luciferase reporter plasmid (pGL3). The three generated plasmids (Figure 5(d)) were used in the subsequent experiments. The

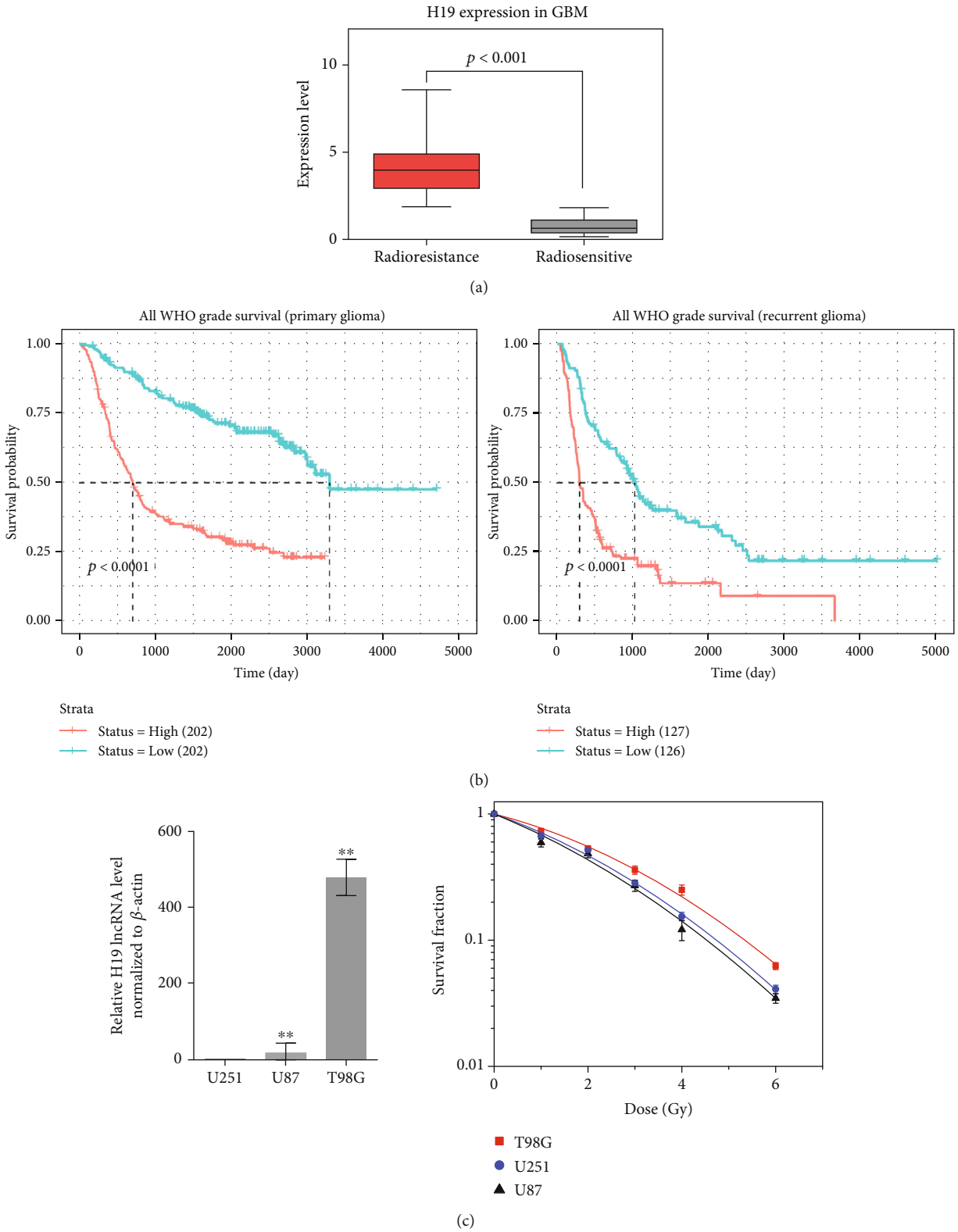

Figure 1: High expression of H19 positively correlates with the radioresistance of glioma. (a) Gene set analysis of H19 expression in patients with GBM who received radiotherapy using the TCGA database. (b) Kaplan-Meier analysis of H19 expression in primary and recurrent glioma patients using the CGGA database. (c) Real-time PCR analysis of H19 expression in T98G, U87 and U251 cells ($n = 3$) and clonogenic survival data of T98G, U87 and U251 cells after irradiation with X-rays ($n = 3$). $^{*}p < 0.05$; $^{**}p < 0.01$ compared with the control group.

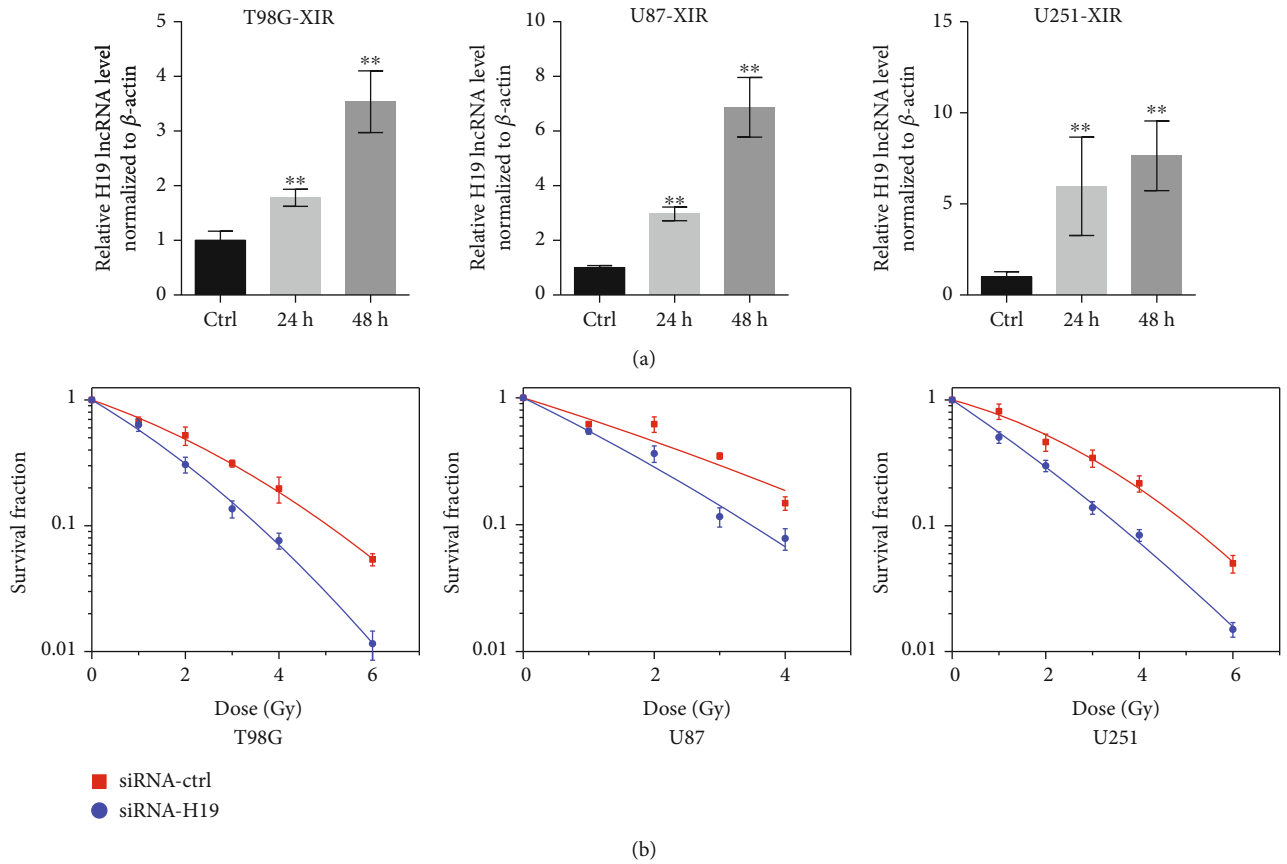

Figure 2: Radiation induced the expression of H19, and downregulation of H19 increased the radiosensitivity of glioma cells. (a) Real-time PCR analysis of the H19 expression in T98G, U87, and U251 cells at 24 h and 48 h postirradiation ($n = 3$). (b) Clonogenic survival data of T98G, U87, and U251 cells transfected with siRNA-ctrl or siRNA-H19 after irradiation with X-rays ($n = 3$). $^{*}p < 0.05$; $^{**}p < 0.01$ compared with the control group.

results, as shown in Figure 5(e), indicated that the luciferase activity of the group cotransfected CREB1 overexpression plasmid (OE-CREB1) and H19 Promoter plasmid is significantly higher than the other control groups, suggesting that the P1 and P2 sites were responsible for the transcription of H19. To confirm this deduction, we transfected Mut P1 or Mut P2 to rescue luciferase expression. As expected, the increase of the OE-CREB1 + H19 promoter group in luciferase expression was markedly attenuated by the mutation of P1 or P2 sites (Figure 5(f)). In addition, the efficiency of siRNA-CREB1 and overexpressing CREB1 was shown in SF. Thus, the data above demonstrated that H19 was transcriptionally activated by CREB1.

4. Discussion

This study articulated the upregulation mechanism of H19 in glioma cells exposed to X-rays and indicated that H19 might exert an influence on radiosensitivity of glioma cells through apoptosis, cell cycle arrest, and DNA synthesis.

Previous studies reported that there is a positive correlation between the high expression of H19 and the poor prognosis in glioma patients [15]. The findings from our study (Figure 1(b)) are consistent with the previous results. H19 indeed acts as an enhancer of tumorigenesis and development in glioma. In respect to radiosensitivity, the results of the cell level validation (Figure 1(c)) were consistent with the bioinformatics analysis (Figure 1(a)). The H19 expression in T98G cells was much higher than the other two cell lines, and T98G cells were the most resistant to X-rays. Although H19 level in U87 cells was 18-fold higher than that in U251 cells, they had a similar radiation resistance as shown in Figure 1(c). We suppose that the radioresistance of glioma cells is determined not only by H19 but also by the entire genetic background, but the significant role of H19 cannot be denied.

The increase of H19 after irradiation (Figure 2(a)) indicated that H19 participated in the response of glioma cells to X-rays. Concretely, H19 suppression promoted G2/M arrest and apoptosis compared to the control group (Figure 3). The augment of G2/M arrest means that it took longer time for the siRNA-H19 group to resume cell cycle progression after irradiation compared with the control group, suggesting that DNA damage repair was more severely blocked in the siRNA-H19 group. Besides, the siRNA-H19 group had a higher rate of apoptosis indeed, indicating that more irreparable damages occurred in cells when H19 was downregulated. Nonetheless, the mechanisms underlying cell cycle arrest and apoptosis enhancement by H19 downregulation remain further investigation.

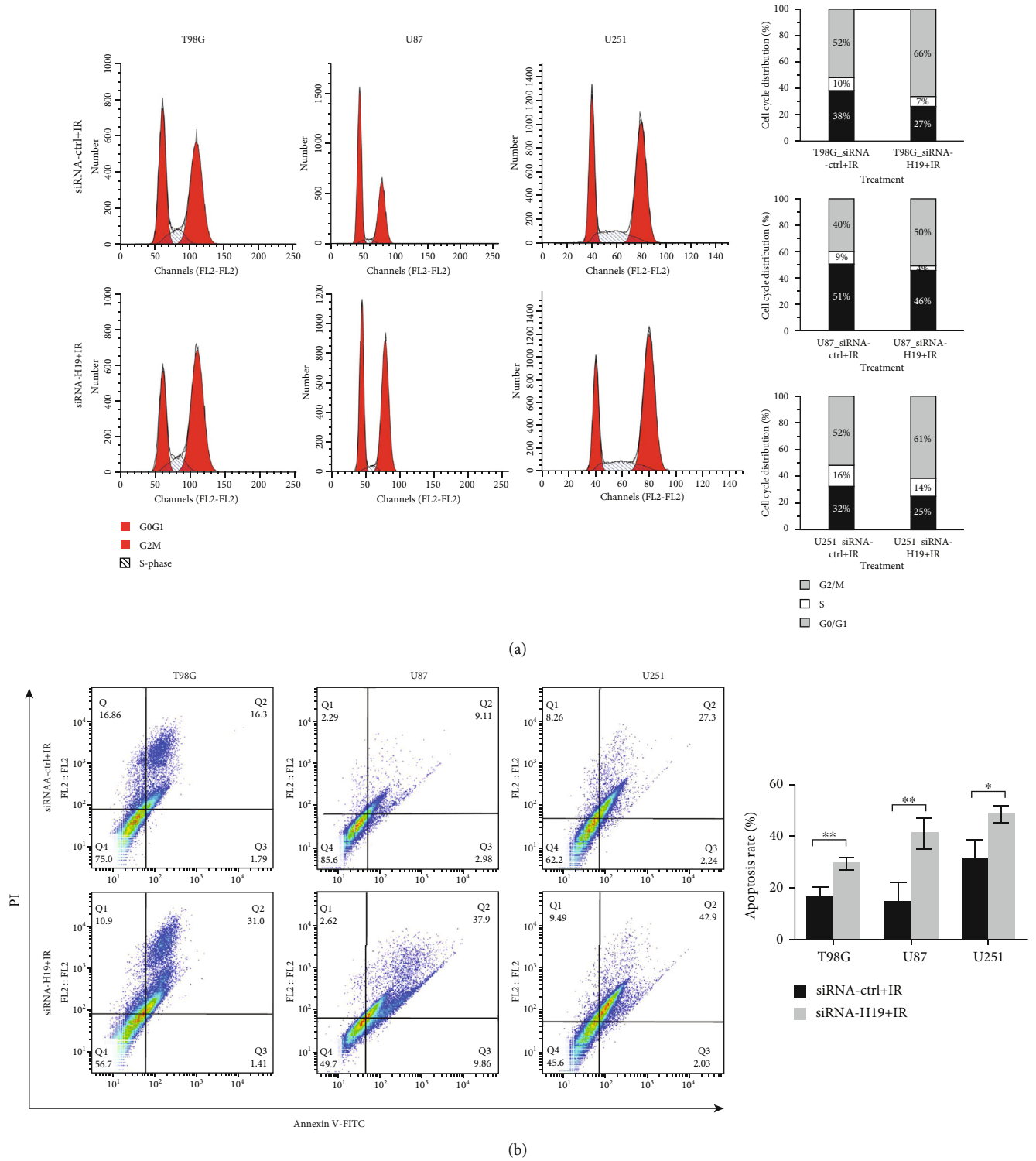

Figure 3: The effects of H19 downregulation on glioma cell cycle and apoptosis after irradiation. (a) Cell cycle distribution in T98G, U87, and U251 cells transfected with siRNA-ctrl or siRNA-H19 at 24 h postirradiation. (b) Cell apoptosis assay in T98G, U87, and U251 cells transfected with siRNA-ctrl or siRNA-H19 at 72 h postirradiation.

However, we have conducted a preliminary research (data not shown). Our results define p21 acting as a downstream molecule of H19 in glioma cells, and p21 could modulate radiation-caused G2/M arrest and apoptosis [25]. Future studies are needed to refine this point. Of course, there is a considerable body of existing researches regarding the modulation of H19 to cell cycle and apoptosis through other pathways. H19 inhibits the apoptosis process via the downregulation of proapoptotic factor Bax as well as tumor suppressor factor p53 [26]. Besides, H19 contacts with the

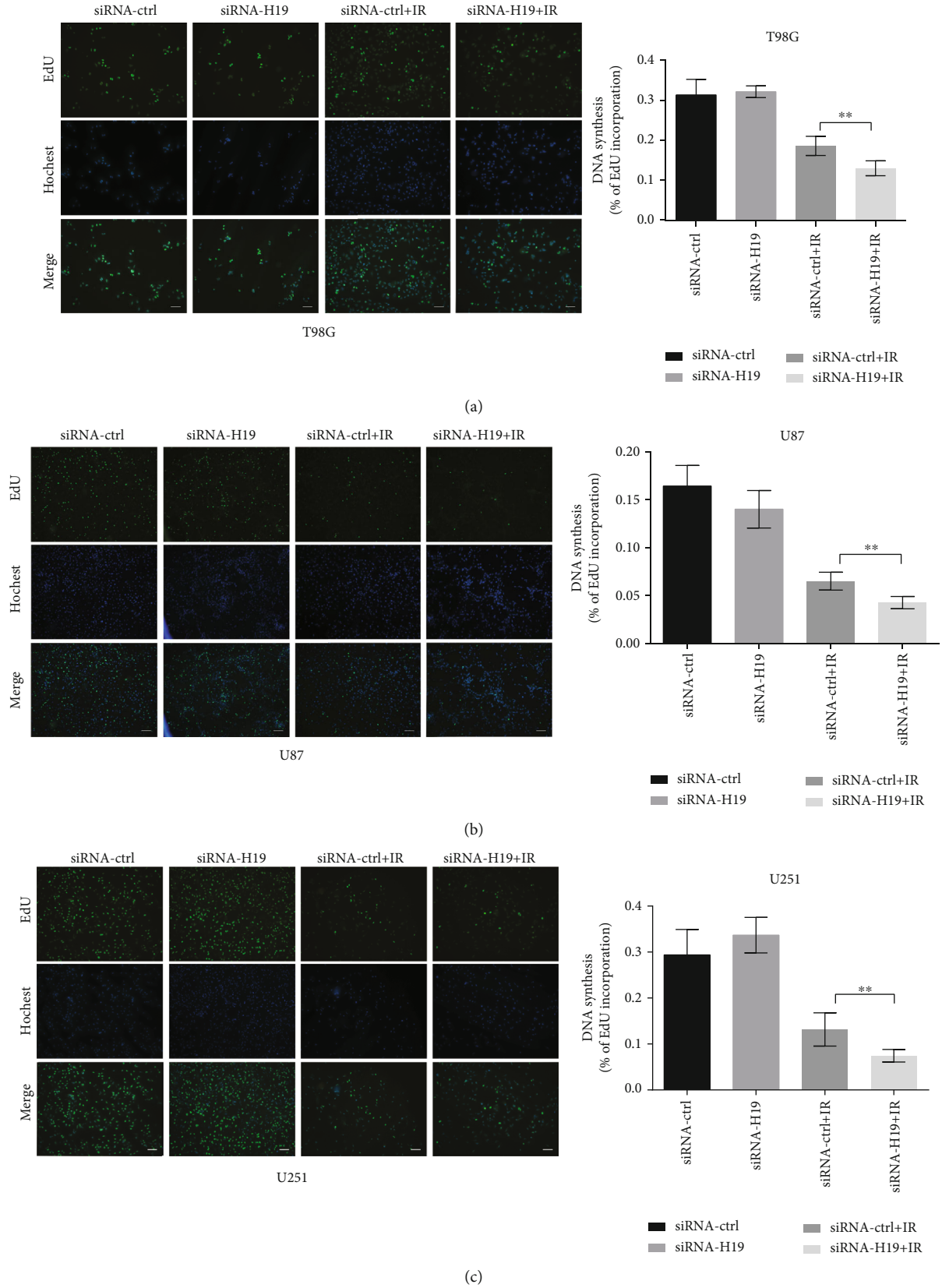

Figure 4: The effects of H19 downregulation on DNA synthesis. (a–c) DNA synthesis analysis of T98G, U87, and U251 cells transfected with siRNA-control or siRNA-H19 at 24 h postirradiation based on the EdU assay (scale bars, 50 μm, $n = 5$). $^{*}p < 0.05$; $^{**}p < 0.01$ compared with the control group.

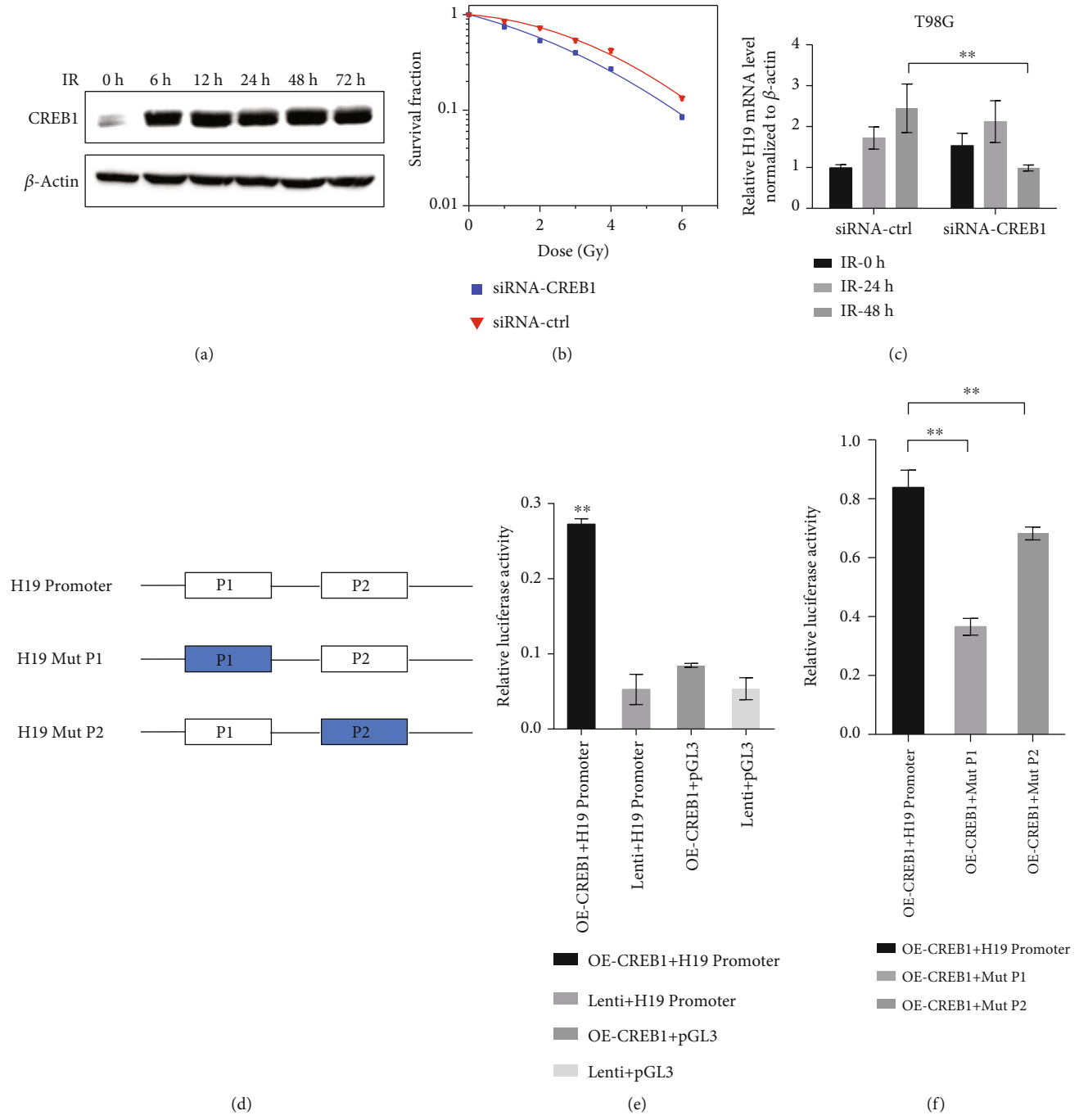

Figure 5: H19 is a direct transcriptional target of CREB1. (a) The expression of CREB1 in T98G cells at different time points after irradiation. (b) Clonogenic survival assay of T98G cells after transfection with siRNA-ctrl or siRNA-CREB1 and irradiation with X-rays ($n = 3$). (c) Real-time PCR analysis of H19 expression in T98G cells transfection with siRNA-ctrl or siRNA-CREB1 and irradiation with X-rays ($n = 3$). (d) Schematic illustration of firefly luciferase reporter plasmids. (e, f) Relative luciferase activity in 293T cells co-transfected with the indicated reporter constructs and Renilla luciferase plasmid ($n = 3$). Lenti is the vector of OE-CREB1 and pGL3 is the vector of H19 Promoter. $^{*}p < 0.05$; $^{**}p < 0.01$ compared with the control group.

apoptosis process and cell cycle depending on the regulation to miR-138 and SOX4 [27], miR-675 [28], miRNA-107 [29], YAP1 [30], and Ras/Raf/MEK/ERK cascade [31]. Therefore, the molecular mechanisms underlying the H19 cellular functions are complex.

Regarding the transcriptional activation of H19, the action mechanism for CREB1 has been well-documented in this study. According to Figure 5(f), P1 and P2 both had transcriptional modulatory activity, and P1 site appeared to play a more important role than P2. Furthermore, as shown in Figure 5(c), H19 level in the siRNA-CREB1 groups at 24 h postirradiation was still increased compared to the time point of 0 h after irradiation. This phenomenon can be explained by the fact that other transcriptional

factors could also promote the H19 expression according to our results (data not shown). Therefore, the upregulation of H19 postirradiation is of great importance for radiation response in glioma cells.

This study elucidated the mechanism of H19's transcriptional activation after irradiation and identified H19 as a potential target to improve the radiotherapy efficacy of glioma. Apart from these, H19 has the potential to act as a biomarker for the prediction of glioma patients' radiosensitivity.

5. Conclusion

In conclusion, the present study verified that radiation-induced CREB1 directly activated H19 transcription and upregulated H19 participated in radioresistance regulation of glioma cells via several cellular process, including apoptosis and G2/M phase arrest and DNA synthesis. Thus, our data indicated that H19 plays a key role in regulating the radiosensitivity of glioma cells.

Data Availability

The datasets generated during and/or analysed during the current study are available from the corresponding author on reasonable request.

Conflicts of Interest

The authors declare no conflicts of interest.

Acknowledgments

This work was jointly supported by the National Key Research Program of China (Grant Nos. 2018YFC0115700 and 2018YFC0115702), the National Natural Science Foundation of China (Grant Nos. 11875299 and U1532264), the Key Deployment Project of Chinese Academy of Sciences (Grant No. KFZD-SW-222), and the National Natural Science Foundation of Chinese Academy of Engineering Physics (Grant No. U1730133).

Supplementary Materials

Supplemental Figure: (a) The siRNA effect of H19 was detected at 24 h and 48 h post-transfection using real-time PCR. (b) The siRNA and overexpression effect of CREB1 at the protein level were determined 24 h post-transfection using western blotting. $^{*}p < 0.05$; $^{**}p < 0.01$ compared with the control group. *(Supplementary Materials)*

References

[1] Q. T. Ostrom, G. Cioffi, H. Gittleman et al., "CBTRUS statistical report: primary brain and other central nervous system tumors diagnosed in the United States in 2012-2016," *Neuro-Oncology*, vol. 21, Supplement 5, pp. v1–v100, 2019.

[2] Q. T. Ostrom, H. Gittleman, P. Liao et al., "CBTRUS statistical report: primary brain and other central nervous system tumors diagnosed in the United States in 2010-2014," *Neuro-Oncology*, vol. 19, Supplement 5, pp. v1–v88, 2017.

[3] A. Rousseau, K. Mokhtari, and C. Duyckaerts, "The 2007 WHO classification of tumors of the central nervous system - what has changed?," *Current Opinion in Neurology*, vol. 21, no. 6, pp. 720–727, 2008.

[4] M. R. Gilbert, M. Wang, K. D. Aldape et al., "Dose-dense temozolomide for newly diagnosed glioblastoma: a randomized phase III clinical trial," *Journal of Clinical Oncology*, vol. 31, no. 32, pp. 4085–4091, 2013.

[5] F. Allahdini, A. Amirjamshidi, M. Reza-Zarei, and M. Abdollahi, "Evaluating the prognostic factors effective on the outcome of patients with glioblastoma multiformis: does maximal resection of the tumor lengthen the median survival?," *World Neurosurgery*, vol. 73, no. 2, pp. 128–134, 2010.

[6] M. A. Vogelbaum, "Does extent of resection of a glioblastoma matter?," *Clinical Neurosurgery*, vol. 59, pp. 79–81, 2012.

[7] P. Cantero-Munoz, M. A. Urien, and A. Ruano-Ravina, "Efficacy and safety of intraoperative radiotherapy in colorectal cancer: a systematic review," *Cancer Letters*, vol. 306, no. 2, pp. 121–133, 2011.

[8] M. K. Thompson, P. Poortmans, A. J. Chalmers et al., "Practice-changing radiation therapy trials for the treatment of cancer: where are we 150 years after the birth of Marie Curie?," *British Journal of Cancer*, vol. 119, no. 4, pp. 389–407, 2018.

[9] Y. Qu, H. Y. Tan, Y. T. Chan, H. Jiang, N. Wang, and D. Wang, "The functional role of long noncoding RNA in resistance to anticancer treatment," *Therapeutic Advances in Medical Oncology*, vol. 12, 2020.

[10] Y. Shi, Y. Wang, W. Luan et al., "Long non-coding RNA H19 promotes glioma cell invasion by deriving miR-675," *PLoS One*, vol. 9, no. 1, article e86295, 2014.

[11] C. Li, B. Lei, S. Huang et al., "H19 derived microRNA-675 regulates cell proliferation and migration through CDK6 in glioma," *American Journal of Translational Research*, vol. 7, no. 10, pp. 1747–1764, 2015.

[12] Y. Zheng, X. Lu, L. Xu, Z. Chen, Q. Li, and J. Yuan, "MicroRNA-675 promotes glioma cell proliferation and motility by negatively regulating retinoblastoma 1," *Human Pathology*, vol. 69, pp. 63–71, 2017.

[13] A. Lo Dico, V. Costa, C. Martelli et al., "MiR675-5p acts on HIF-1α to sustain hypoxic responses: a new therapeutic strategy for glioma," *Theranostics*, vol. 6, no. 8, pp. 1105–1118, 2016.

[14] J. X. Pan, T. N. Chen, K. Ma, S. Wang, C. Y. Yang, and G. Y. Cui, "A negative feedback loop of H19/miR-675/VDR mediates therapeutic effect of cucurmin in the treatment of glioma," *Journal of Cellular Physiology*, vol. 235, no. 3, pp. 2171–2182, 2020.

[15] N. Guan, R. Wang, W. S. Guo, Y. J. Lai, Y. D. Zhang, and Y. Y. Cheng, "Long non-coding RNA H19 regulates the development of gliomas through the Wnt/β-catenin signaling pathway," *European Review for Medical and Pharmacological Sciences*, vol. 23, no. 10, pp. 4243–4253, 2019.

[16] W. Li, P. Jiang, X. Sun, S. Xu, X. Ma, and R. Zhan, "Suppressing H19 modulates tumorigenicity and stemness in U251 and U87MG glioma cells," *Cellular and Molecular Neurobiology*, vol. 36, no. 8, pp. 1219–1227, 2016.

[17] L. Chen, Y. Wang, J. He, C. Zhang, J. Chen, and D. Shi, "Long noncoding RNA H19 promotes proliferation and invasion in human glioma cells by downregulating miR-152," *Oncology Research*, vol. 26, no. 9, pp. 1419–1428, 2018.

[18] J. Jia, X. Zhang, D. Zhan et al., "lncRNA H19 interacted with miR-130a-3p and miR-17-5p to modify radio-resistance and

chemo-sensitivity of cardiac carcinoma cells," *Cancer Medicine*, vol. 8, no. 4, pp. 1604–1618, 2019.

[19] H. Ma, L. Yuan, W. Li, K. Xu, and L. Yang, "The lncRNA H19/miR-193a-3p axis modifies the radio-resistance and chemotherapeutic tolerance of hepatocellular carcinoma cells by targeting PSEN1," *Journal of Cellular Biochemistry*, vol. 119, no. 10, pp. 8325–8335, 2018.

[20] A. J. Shaywitz and M. E. Greenberg, "CREB: a stimulus-induced transcription factor activated by a diverse array of extracellular signals," *Annual Review of Biochemistry*, vol. 68, no. 1, pp. 821–861, 1999.

[21] Y. T. Siu and D. Y. Jin, "CREB–a real culprit in oncogenesis," *The FEBS Journal*, vol. 274, no. 13, pp. 3224–3232, 2007.

[22] D. B. Shankar, J. C. Cheng, K. Kinjo et al., "The role of CREB as a proto-oncogene in hematopoiesis and in acute myeloid leukemia," *Cancer Cell*, vol. 7, no. 4, pp. 351–362, 2005.

[23] A. Maureira, R. Sanchez, N. Valenzuela et al., "The CREB transcription factor controls transcriptional activity of the human RIC8B gene," *Journal of Cellular Biochemistry*, vol. 117, no. 8, pp. 1797–1805, 2016.

[24] H. Mylroie, O. Dumont, A. Bauer et al., "PKCε-CREB-Nrf2 signalling induces HO-1 in the vascular endothelium and enhances resistance to inflammation and apoptosis," *Cardiovascular Research*, vol. 106, no. 3, pp. 509–519, 2015.

[25] Y. Kuang, J. Kang, H. Li et al., "Multiple functions of p21 in cancer radiotherapy," *Journal of Cancer Research and Clinical Oncology*, vol. 147, no. 4, pp. 987–1006, 2021.

[26] B. Alipoor, S. N. Parvar, Z. Sabati, H. Ghaedi, and H. Ghasemi, "An updated review of the H19 lncRNA in human cancer: molecular mechanism and diagnostic and therapeutic importance," *Molecular Biology Reports*, vol. 47, no. 8, pp. 6357–6374, 2020.

[27] H. Si, P. Chen, H. Li, and X. Wang, "Long non-coding RNA H19 regulates cell growth and metastasis via miR-138 in breast cancer," *American Journal of Translational Research*, vol. 11, no. 5, pp. 3213–3225, 2019.

[28] C. Liu, Z. Chen, J. Fang, A. Xu, W. Zhang, and Z. Wang, "H19-derived miR-675 contributes to bladder cancer cell proliferation by regulating p53 activation," *Tumour Biology*, vol. 37, no. 1, pp. 263–270, 2016.

[29] J. Cui, J. Mo, M. Luo et al., "c-Myc-activated long non-coding RNA H19 downregulates miR-107 and promotes cell cycle progression of non-small cell lung cancer," *International Journal of Clinical and Experimental Pathology*, vol. 8, no. 10, pp. 12400–12409, 2015.

[30] L. Zhang, X. Song, X. Li, C. Wu, and J. Jiang, "Yes-associated protein 1 as a novel prognostic biomarker for gastrointestinal cancer: a meta-analysis," *BioMed Research International*, vol. 2018, Article ID 4039173, 10 pages, 2018.

[31] L. Li, G. D. Zhao, Z. Shi, L. L. Qi, L. Y. Zhou, and Z. X. Fu, "The Ras/Raf/MEK/ERK signaling pathway and its role in the occurrence and development of HCC," *Oncology Letters*, vol. 12, no. 5, pp. 3045–3050, 2016.

Hindawi
BioMed Research International
Volume 2021, Article ID 9951405, 13 pages
https://doi.org/10.1155/2021/9951405

Research Article

miR-942-5p Inhibits Proliferation, Metastasis, and Epithelial-Mesenchymal Transition in Colorectal Cancer by Targeting CCBE1

Lin Zhou,[1] **Qing Chen**,[2] **Jie Wu**,[1] **Jian Yang**,[3] **Huancai Yin**,[4] **Jingjing Tian**,[4] **Lian Gong**,[1] **DanDan Kong**,[1] **and Min Tao**[1]

[1]*Department of Oncology, The First Affiliated Hospital of Soochow University, Suzhou, Jiangsu 215006, China*
[2]*Department of Oncology, Jingjiang People's Hospital, Jingjiang, Jiangsu 214504, China*
[3]*Department of General Surgery, The First Affiliated Hospital of Soochow University, Suzhou, Jiangsu 215006, China*
[4]*CAS Key Lab of Bio-Medical Diagnostics, Suzhou Institute of Biomedical Engineering and Technology, Chinese Academy of Sciences, Suzhou, Jiangsu 215163, China*

Correspondence should be addressed to Min Tao; taomin@suda.edu.cn

Received 16 March 2021; Revised 3 April 2021; Accepted 15 April 2021; Published 29 April 2021

Academic Editor: Qiang Liu

Although colorectal cancer (CRC) is common, there is a paucity of information regarding its molecular pathogenesis. Studies have shown that miRNAs play pivotal roles in the development and progression of CRC. There is a need to further investigate the biological functions of miRNAs in CRC. In particular, it has been reported that miR-942-5p exhibits tumor-suppressive properties. Thus, we analyzed the functional significance of miR-942-5p in CRC and the underlying molecular mechanisms. We found that miR-942-5p was downregulated in CRC tissues and cells. Cell Counting Kit-8, EdU, and colony formation assays revealed that the overexpression of miR-942-5p by mimics inhibited the proliferation of CRC cells. Use of the miR-942-5p inhibitor effectively enhanced the proliferative potential of CRC cells. Further, *in vivo* xenograft experiments confirmed these results. Increased expression of miR-942-5p suppressed the invasion, migration, and epithelial-mesenchymal transition of CRC cell lines, while decreased miR-942-5p expression had the opposite effect. CCBE1, a secretory molecule for lymphangiogenesis, was established as a downstream target of miR-942-5p, and its expression was inversely correlated with the expression of miR-942-5p in CRC cells. Additionally, cotransfection of the miR-942-5p inhibitor with si-CCBE1 into CRC cells reversed the effects induced by miR-942-5p overexpression. In conclusion, we confirmed that miR-942-5p exerts oncogenic actions in CRC by targeting CCBE1 and identified miR-942-5p as a potential clinical biomarker for CRC diagnosis and therapy.

1. Introduction

Colorectal cancer (CRC) is a prevalent disease worldwide [1]. Approximately 1.8 million new CRC cases are diagnosed globally each year, along with more than 881,000 mortalities [2]. Most fatalities occur in the malignant stage of this disease as the result of tumor recurrence and distant metastasis [3, 4]. Therefore, in order to improve CRC diagnosis and treatment, it is important to identify new trigger genes for CRC and to understand the underlying molecular mechanisms.

MicroRNAs (miRNAs) are a class of noncoding RNA molecules [5]. Studies have shown that miRNAs play essential roles in gene regulation. They bind to the 3′-UTRs of mRNAs, thereby regulating the expression of genes and guiding posttranscriptional inhibition [5]. miRNAs also facilitate tumor growth, invasion, and immune escape by regulating the expression of target mRNAs [6]. Previous studies have shown that miRNAs may be the first choice for noninvasive screening of CRC because they are well suited for early detection [7–9]. The antitumor effects of miR-942-5p in gastric,

cervical, and other tumors have been documented [10, 11]. However, the mechanism of action of miR-942-5p in CRC has not been elucidated yet.

The gene-encoding collagen and calcium-binding epidermal growth factor domain-containing protein 1 (CCBE1) is located in the 18q21.32 region of the human chromosome and encodes a highly conserved protein with an EGF-like domain [12]. CCBE1 is a secretory molecule for lymphangiogenesis that stimulates angiogenesis and the germination of venous endothelial cells [13]. In breast and lung cancers, CCBE1 has been shown to be a potential tumor suppressor [14, 15], while in gastrointestinal stromal tumors (GISTs), CCBE1 enhances tumor angiogenesis [16]. High expression of CCBE1 is associated with tumor invasiveness and poor CRC prognosis. CCBE1 promotes CRC lymphangiogenesis and lymphatic metastasis by regulating transforming growth factor-β [12, 17, 18]. However, the role of CCBE1 in CRC is still not fully understood.

Our study was aimed at measuring the expression of miR-942-5p in CRC tissues and in adjacent normal tissues and at investigating the potential mechanism of action of miR-942-5p. Ultimately, our findings indicated that miR-942-5p suppressed cell proliferation and epithelial-mesenchymal transition (EMT) and induced metastasis of CRC by targeting CCBE1.

2. Materials and Methods

2.1. CRC Tissue Specimens. In total, 35 paired CRC tissues were collected from the First Affiliated Hospital of Soochow University from July 2018 to July 2019. Samples were collected according to the Institutional Review Board-approved protocol of the First Affiliated Hospital of Soochow University, and each patient signed an informed consent form.

2.2. Database Analysis. The miR-942-5p expression data and related clinical information were obtained from TCGA database (https://cancergenome.nih.gov/) and analyzed using R (3.5.1).

2.3. Cell Cultures. Human CRC cell lines (LoVo, HCT116, SW480, SW1116, SW620, and HT29) and HEK-293T cells were sourced from the Biological Sciences Cell Bank of Shanghai Institutes (Shanghai, China). Normal colon epithelial cells (NCM460) were obtained from ATCC (Manassas, VA, USA). Cell lines were cultured in Dulbecco's modified Eagle's medium or Roswell Park Memorial Institute medium supplemented with 10% fetal bovine serum (FBS). All cell lines were cultivated at 37°C in a 5% CO_2 atmosphere.

2.4. qRT-PCR. Total RNA from CRC cells and tissues was isolated using a TRIzol reagent (Beyotime, China). The miR-942-5p primers were designed by Sangon Biotech (Shanghai, China). qRT-PCR was performed using the miDETECT A Track™ miRNA qRT-PCR Starter Kit (RiboBio, China). The reaction conditions were as follows: 95°C for 10 min and 50 cycles of 95°C for 2 s, 60°C for 20 s, and 70°C for 10 s. The mRNA primers were designed by Sangon Biotech, and qRT-PCR was performed using the Eva Green PCR kit in a LightCycler 96 qPCR cycle (Roche, Basel, Switzerland). The reaction conditions were as follows: 95°C for 30 s, 50 cycles at 95°C for 10 s, and 60°C for 30 s. Relative mRNA and miRNA levels were quantified using the $2^{-\Delta\Delta Ct}$ method [19]. Human U6 and β-actin gene fragments were amplified as internal controls. The primer sequences were as follows: miR-942-5p, 5′-CCGTCTTCTCTGTTTTGGC CATGTG-3′; U6, 5′-GAAGGATGACACGCAAATTCG-3′ ; CCBE1, forward 5′-AGGCGACACTCCACAGT-3′ and reverse 5′-GATTAGTGGTCG CTATATT-3′; β-actin, forward 5-CTCACCATGGATGATGATATCGC-3 and reverse 5-AGGAATCCTTCTGACCCATGC-3′.

2.5. Cell Transfection. miR-942-5p mimics, miR-942-5p mimic NC, miR-942-5p inhibitor, and miR-942-5p inhibitor NC were purchased from RiboBio and transfected into cells at a final concentration of 100 nM. Transfection was performed using Lipofectamine 2000 (Invitrogen). Small interfering RNAs (siRNAs) for CCBE1 (si-CCBE1) were obtained from RiboBio. The CCBE1 siRNA sequences were 5′-GCCAUGAGAAGUCUGAGAA-3′ and the nontargeted siRNA sequences were 5′-UUGGAGCGUGCGUAAG UAU-3′.

2.6. Cellular Proliferation and Growth Assay. After transfection, the cells were inoculated at 5×10^3 cells per well in 96-microwell microplates. Cell viability was quantified after 24, 48, 72, 96, and 120 h of cultivation using the Cell Counting Kit-8 (CCK-8) (Biosharp, Shanghai). Absorbance was measured using an enzyme standard instrument (wavelength, 450 nm).

In the clonogenic survival assay, cells were inoculated in 6-well plates at a concentration of 800 cells/well and maintained for 14 days in fresh complete medium. Colonies were fixed for 20-30 min with paraformaldehyde and stained with crystal violet solution for 20 min. Colonies larger than 10 cells were imaged.

2.7. EdU. EdU was determined using the BeyoClick EdU-555 cell proliferation test kit (Beyotime, China). HCT116 and LoVo cells were transfected with miRNA mimics and inhibitors, respectively. Negative controls were inoculated into 24-well culture plates. Cells were cultured in media containing 10% FBS for 48 h and then fixed with 4% paraformaldehyde. Cells were incubated in 50 mM EdU solution for 2 h before staining with DAPI. Cells were stained using Hoechst solution, and their DNA content was visualized using a fluorescence microscope.

2.8. Wound-Healing Assay. LoVo and HCT116 human CRC cells (3×10^4 per well) were plated in 24-well plates as a monolayer. At 48 h posttransfection, the cells were scratched using a 10 μL pipette tip. Scratch healing was monitored and imaged using a microscope at 0 and 48 h after scratching.

2.9. Transwell Invasion Assay. The experiment was performed in 24-well Transwell plates with 8 μM chamber inserts (Corning, USA). Forty-eight hours posttransfection, cells were plated into the upper chamber in 100 μL serum-

free medium (3×10^5). 600 μL of fresh complete medium was added to the lower chamber of a 24-well plate. The cells were incubated for 48 h, after which the top membrane surface cells were removed by wiping. Cells that had invaded the lower chamber were fixed using paraformaldehyde for 30 min, stained with 0.1% crystal violet for 20 min, imaged, and counted under a microscope.

2.10. Tumor Formation Assay in Nude Mouse Models. To establish the CRC xenograft model, 0.1 mL (2×10^7 cells/mL) of LoVo cell suspensions was subcutaneously injected into the left side of four-week-old nude mice. Transplanted mice were randomly allocated into two groups of five mice each, after 10 days. Mice in each group were injected with 1 nmol agomiR-942-5p or agomiR-NC every two days. The injections were performed seven times. Four-week-old nude mice received a subcutaneous injection of 0.1 mL of HCT116 cell suspensions (2×10^7 cells/mL) into their right side. Transplanted mice were randomly allocated into two groups of five mice each, after 10 days. Mice in each group were injected with 2 nmol antagomir miR-942-5p or antagomir NC every two days. The injections were performed seven times. The growth of the subcutaneous tumors was evaluated every six days after transplantation. Tumor dimensions were measured using a caliper, and tumor volumes were calculated using the formula length $\times$ width$^2 \times 0.5$. After 18 days, the mice were sacrificed, and the weight of the subcutaneous tumor was recorded.

2.11. Western Blotting. Cells were lysed in 500 μL radio immunoprecipitation assay lysis buffer (Beyotime, China). The samples were run on 10% polyacrylamide-sodium dodecyl sulfate gels and transferred onto polyvinylidene difluoride membranes by electroblotting. The membranes were sealed in skim milk and then incubated with anti-E-cadherin antibody (1 : 1000, 60335-1-Ig, Proteintech), anti-N-cadherin antibody (1 : 1000, 66219-1-Ig, Proteintech), anti-vimentin antibody (1 : 1000, YM6529, ImmunoWay), anti-CCBE1 antibody (1 : 1000, YN1730, ImmunoWay), and anti-β-actin (1 : 1000, CST, USA).

2.12. Dual-Luciferase Reporter Assay. Plasmid vectors containing the 3′-UTR of CCBE1 with either a wild-type or a mutant version of the predicted target site were cloned into the psiCHECK-2 reporter vector. The HEK-293T and LoVo cell lines were seeded in 24-well plates at a density of 2×10^6 cells/well. Cells were then cotransfected with the luciferase reporter construct and miRNA mimics using the Lipofectamine 2000 reagent. After 48 h of incubation, luciferase reporter activity was analyzed using the Dual-Luciferase® Reporter Assay System (Beyotime, China).

2.13. Statistical Analysis. Statistical analyses were performed using SPSS 18.0 software (IBM). Quantitative data is presented as mean ± standard deviation. Statistical differences among groups were determined using Student's t-test or one-way ANOVA. The Pearson correlation coefficient was calculated to assess the association between miR-942-5p expression and CCBE1 expression. Statistical significance was set at $P < 0.05$.

3. Results

3.1. Downregulation of miR-942-5p in CRC Tissues and Cell Lines Predicts Poor Survival. CRC tissues showed significantly lower miR-942-5p expression levels than those of adjacent normal tissues (Figure 1(a)). Furthermore, miR-942-5p was also underexpressed in CRC cell lines compared with the NCM460 cell line (Figure 1(b)). To confirm the effect of miR-942-5p on CRC prognosis, we obtained expression data from TCGA database. The results indicated that miR-942-5p levels were positively and significantly associated with patient survival time ($P = 0.018$) and progression-free survival time ($P = 0.022$) in colon adenocarcinoma (COAD) (Figures 1(c) and 1(d)). Similarly, in rectal adenocarcinoma (READ), miR-942-5p levels were positively and significantly associated with patient survival time ($P = 0.002$) and progression-free survival time ($P = 0.001$) (Figures 1(e) and 1(f)). These results suggest that miR-942-5p levels are significantly downregulated in CRC tissues and cells.

3.2. miR-942-5p Inhibits CRC Cell Proliferation In Vitro and In Vivo. To uncover the biological significance of miR-942-5p in CRC cells, LoVo and HCT116 cells were transfected with miRNA mimics and inhibitors, respectively. CCK-8 assays showed that overexpression of miR-942-5p inhibited the growth rates of LoVo cells, while inhibition of miR-942-5p significantly enhanced HCT116 cell proliferation (Figure 2(a)). Colony formation assays demonstrated that overexpression of miR-942-5p repressed the proliferation of LoVo cells. In contrast, silencing of miR-942-5p expression enhanced the growth of HCT116 cell colonies (Figure 2(b)). Compared to the mimic-NC-transduced cells, DNA synthesis in miR-942-5p-transduced cells was significantly inhibited (Figure 2(c)), while DNA synthesis in HCT116 cells transfected with the miR-942-5p inhibitor was significantly enhanced (Figure 2(d)). To evaluate the *in vivo* function of miR-942-5p, a nude mouse model for studying tumor formation was used. It was observed that miR-942-5p overexpression significantly suppressed tumor growth in the nude mouse model, while inhibition of miR-942-5p promoted tumor growth in the nude mouse model (Figure 2(e)).

3.3. miR-942-5p Regulates the Invasion, Migration, and EMT of CRC Cells. To investigate the underlying role of miR-942-5p on CRC cell invasion and migration, Transwell assays and wound-healing experiments were performed. As shown in Figure 3(a), cells overexpressing miR-942-5p exhibited significantly weaker cell invasion than those of the control. In contrast, silencing of miR-942-5p enhanced the invasive ability of HCT116 cells (Figure 3(b)). Figures 3(c) and 3(d) show that the overexpression of miR-942-5p reduced the migration distance of LoVo cells. However, this effect was reversed upon miR-942-5p knockdown in HCT116 cells. Additionally, overexpression of miR-942-5p resulted in increased E-cadherin expression and decreased levels of N-cadherin and vimentin proteins (Figure 3(e)). Downregulation of miR-

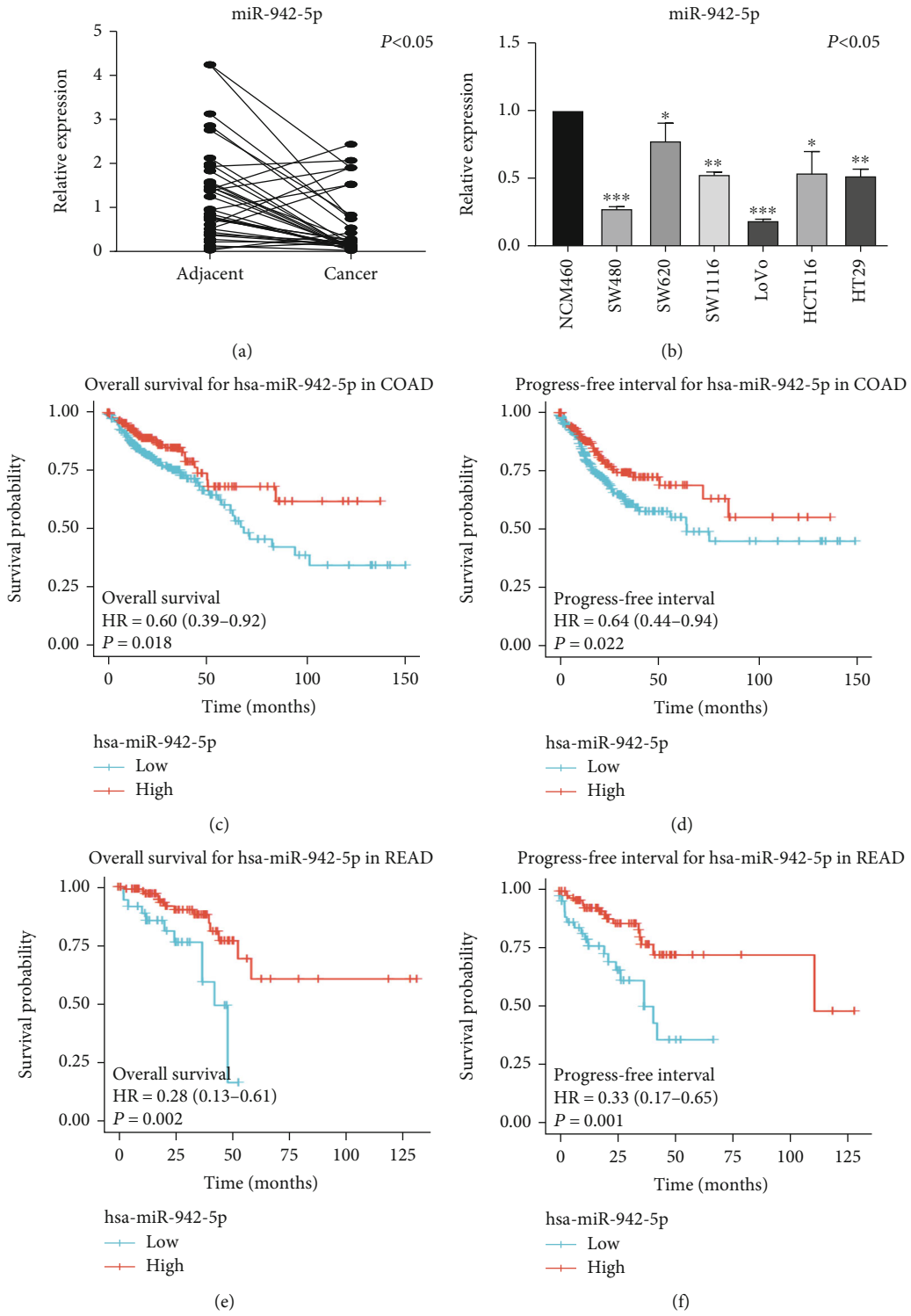

Figure 1: miR-942-5p was downregulated in CRC and was a prognostic indicator for CRC. (a) Detection of miR-942-5p in 35 pairs of CRC tissues and adjacent normal tissues was assessed by qRT-PCR. miR-942-5p in tumor tissues was markedly downregulated compared to the corresponding adjacent tissues. (b) miR-942-5p expression in six CRC cells and normal human colon mucosal epithelial cell line. (c, d) Overall survival and progress-free interval analysis on the basis of miR-942-5p in COAD was illustrated by the TCGA database. (e, f) Overall survival and progress-free interval analysis on the basis of miR-942-5p in READ was illustrated by the TCGA database.

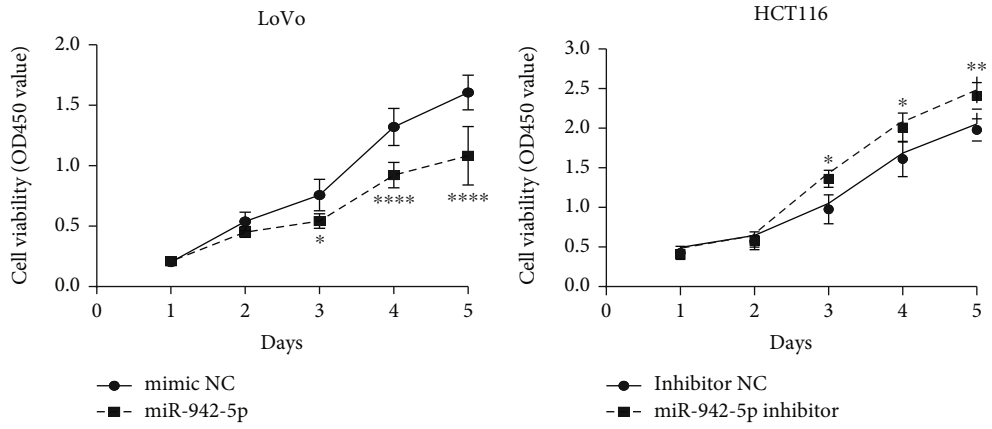

(a)

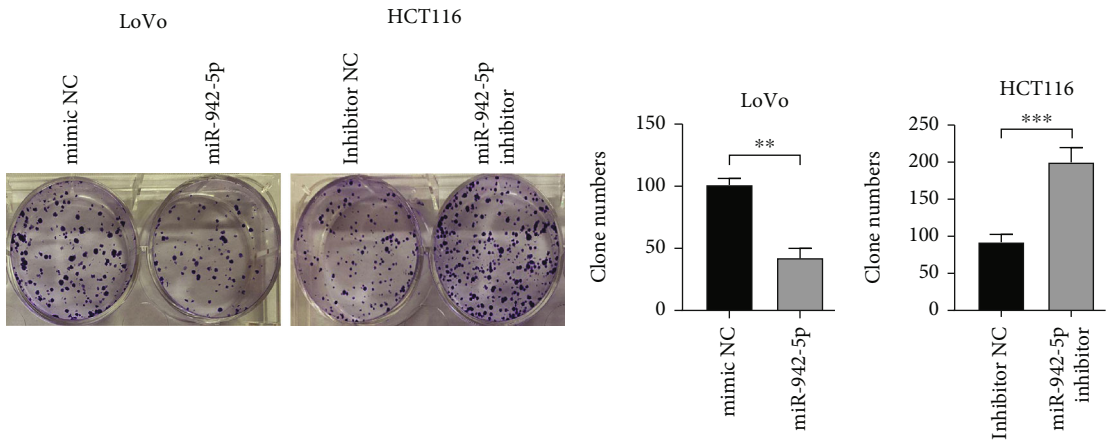

(b)

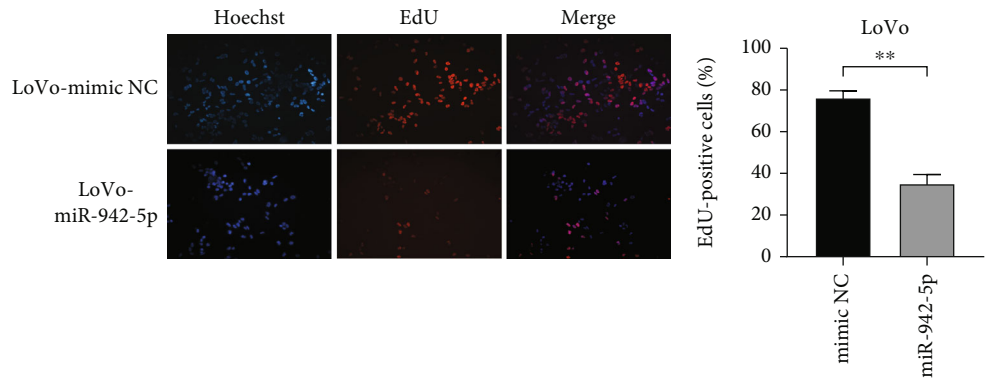

(c)

Figure 2: Continued.

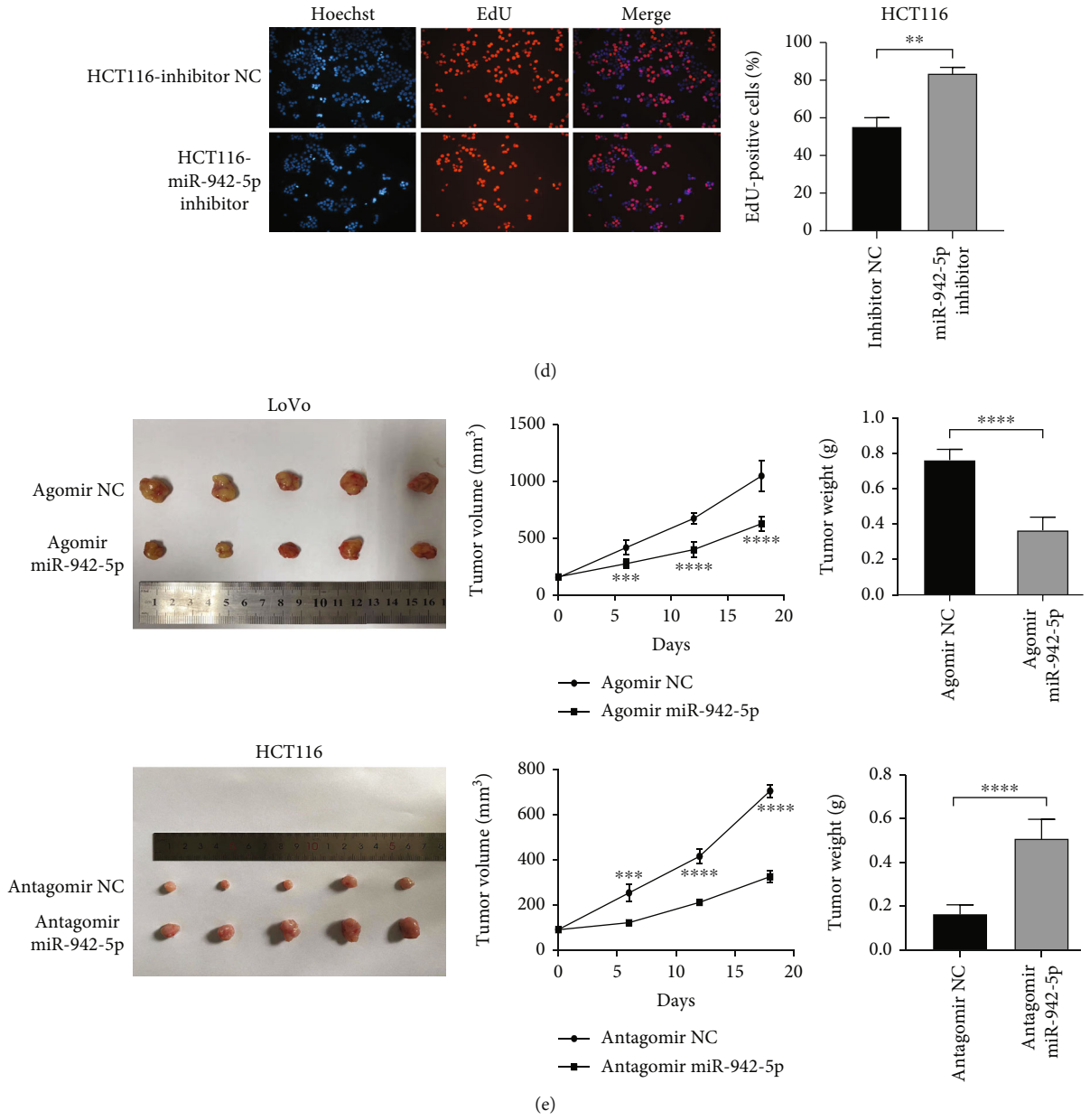

Figure 2: miR-942-5p represses CRC cell growth *in vitro* and *in vivo*. (a) The number of cells was determined by CCK-8 assays to detect the cell viability. (b) The colony-forming ability of transduced HCT116 cells and LoVo cells was measured by colony formation assay. (c, d) The effect of miR-942-5p on DNA synthesis was identified by EDU analysis. (e) To observe the effect of miR-942-5p on tumor formation in nude mice, the xenograft model of nude mice was established. $^{*}P < 0.05$, $^{**}P < 0.01$, $^{***}P < 0.001$, and $^{****}P < 0.0001$.

942-5p resulted in decreased E-cadherin protein levels and increased levels of N-cadherin and vimentin proteins (Figure 3(f)). The above results demonstrate that miR-942-5p regulates the invasion, migration, and EMT of CRC cells.

3.4. miR-942-5p Directly Targets CCBE1 and Suppresses Its Expression. To further delineate the mechanism of miR-942-5p in CRC, we used TargetScan to predict the potential targets of miR-942-5p. Bioinformatic analyses predicted that CCBE1 is a potential target of miR-942-5p (Figure 4(a)). Overexpression of miR-942-5p decreased the relative luciferase activity of the CCBE1 reporter construct, which contained the 3′-UTR of CCBE1 (Figure 4(b)). Figure 4(c) shows that the expression of CCBE1 in CRC tissues was significantly higher than that in the adjacent tissues. There was a strong inverse correlation between CCBE1 expression and miR-942-5p expression in CRC tissues. Furthermore, the expression of CCBE1 was significantly higher in CRC cells than in NCM460, and there was a significant negative correlation between the expression of CCBE1 and that of miR-942-5p in CRC cells (Figure 4(d)). CCBE1 expression levels in miR-942-5p-transduced and NC-transduced cells were determined by qRT-PCR. The results showed that miR-942-5p expression was inversely correlated with CCBE1 levels (Figure 4(e)). Moreover, the upregulation of miR-942-5p suppressed CCBE1 protein

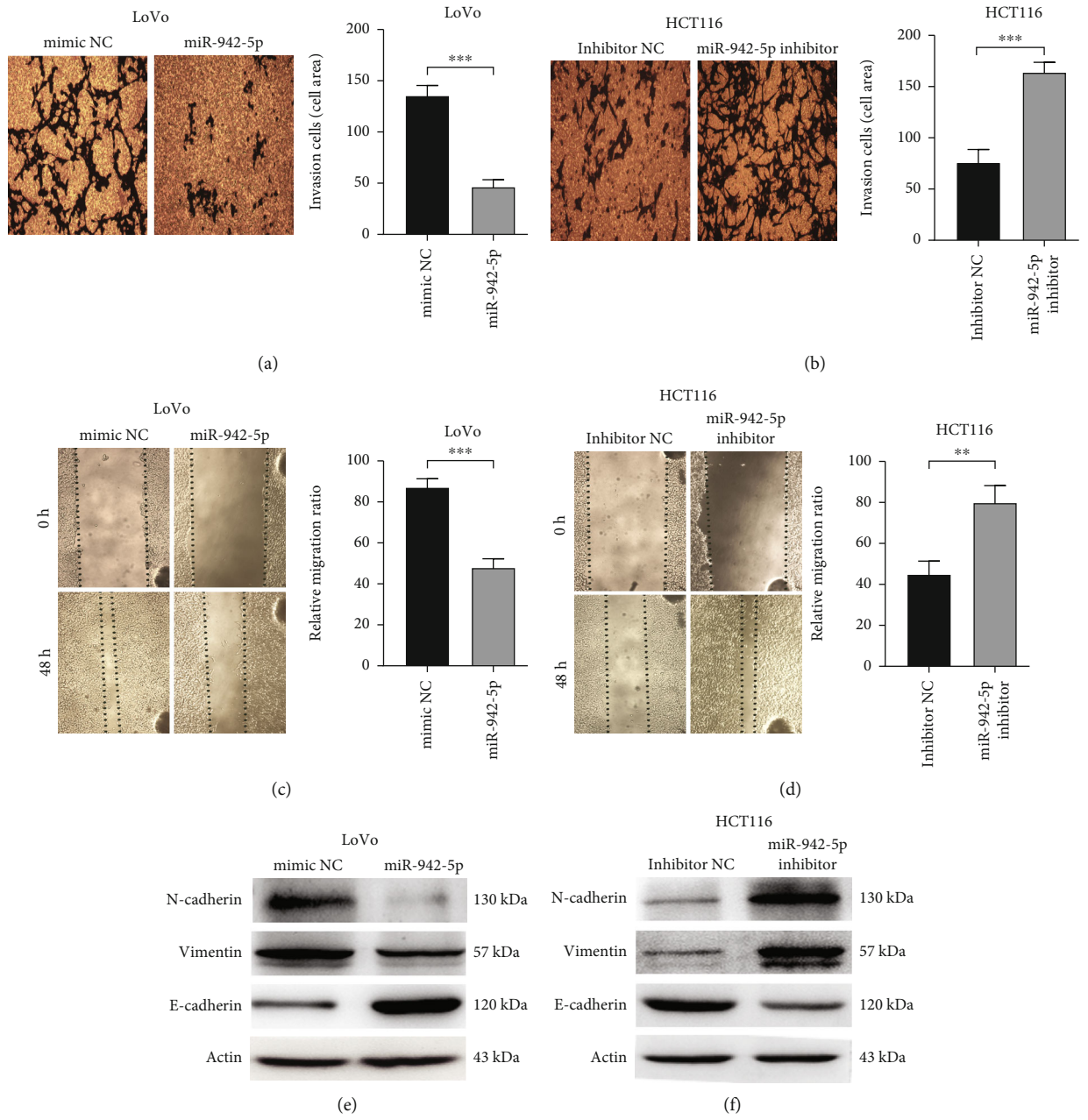

FIGURE 3: miR-942-5p inhibited the invasion and migration of CRC cells. (a, b) Transwell assay was used to evaluate the effect of miR-942-5p expression on the invasion ability of CRC cells. $^{***}P < 0.001$. (c, d) Wound-healing assay was used to evaluate the effect of miR-942-5p expression on cell migration capacity. $^{**}P < 0.01$ and $^{***}P < 0.001$. (e, f) The protein levels of N-cadherin, E-cadherin, and vimentin was determined by Western blot assays.

levels, whereas miR-942-5p inhibition enhanced CCBE1 protein levels (Figure 4(f)).

3.5. miR-942-5p Represses Cell Proliferation by Directly Targeting CCBE1 in CRC. To determine whether miR-942-5p participates in the regulation of CRC cell functions by targeting CCBE1, a series of functional restoration assays were performed. First, we cotransfected HCT116 cells with si-CCBE1 and an miR-942-5p inhibitor. Western blot analysis demonstrated that when miR-942-5p levels were suppressed by the miR-942-5p inhibitor, the protein levels of CCBE1 in HCT116 cells increased. After cotransfection with si-CCBE1 and miR-942-5p inhibitors, CCBE1 levels were significantly reduced (Figure 5(a)). Cell proliferation experiments revealed that inhibition of CCBE1 by si-CCBE1 reversed the effect of the miR-942-5p inhibitor, leading to a decrease in cell viability (Figure 5(b)). The wound-healing and cell invasion assays revealed that si-CCBE1 partially reversed the migration- and invasion-promoting effects of the miR-942-5p inhibitor (Figures 5(c) and 5(d)). At the same time, si-CCBE1 partially reversed the EMT-promoting effect of miR-942-5p in CRC cells (Figure 5(e)). These findings indicate that miR-942-5p may directly target gene CCBE1 to regulate the viability, motility, and EMT of CRC cells.

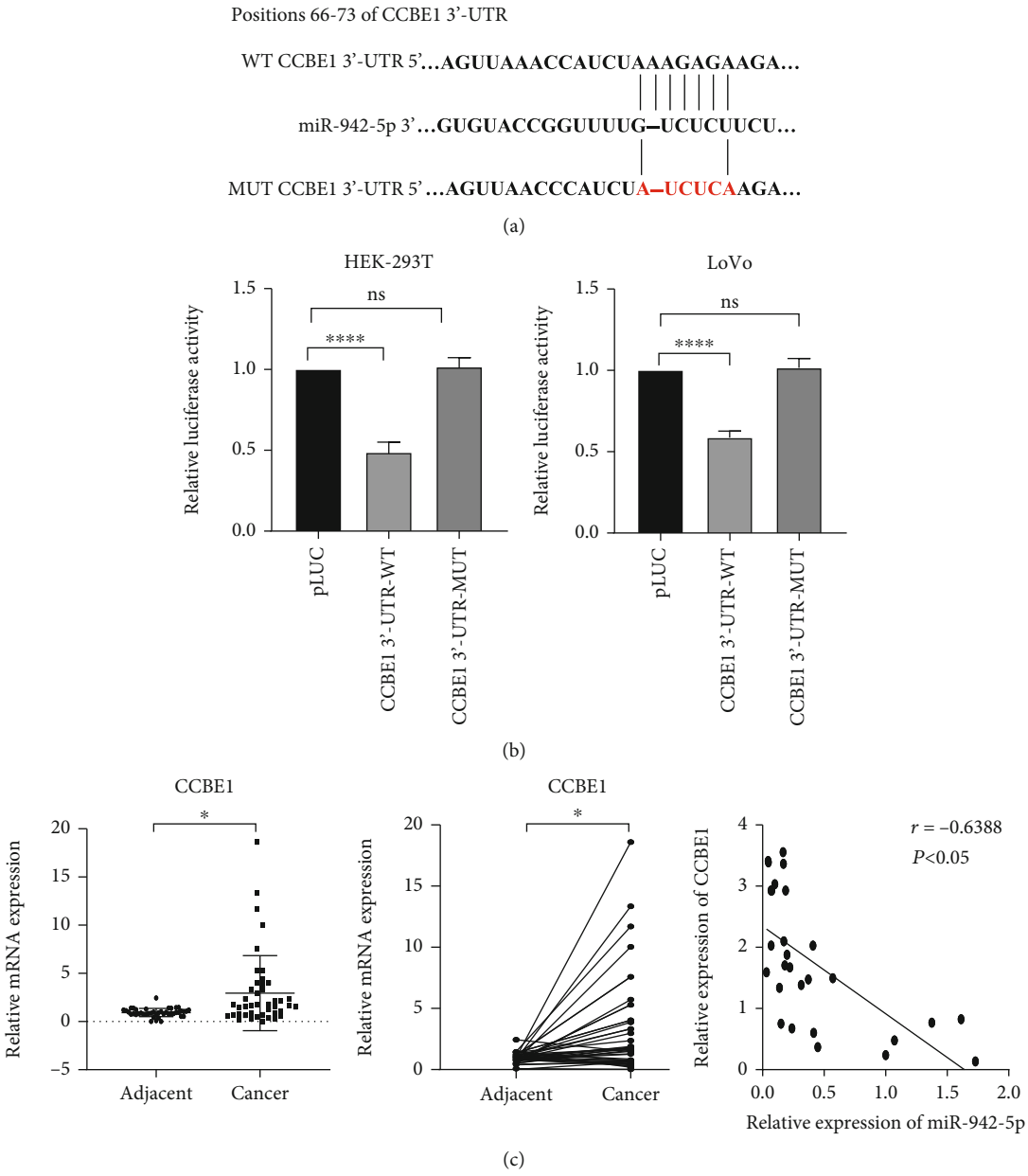

Figure 4: Continued.

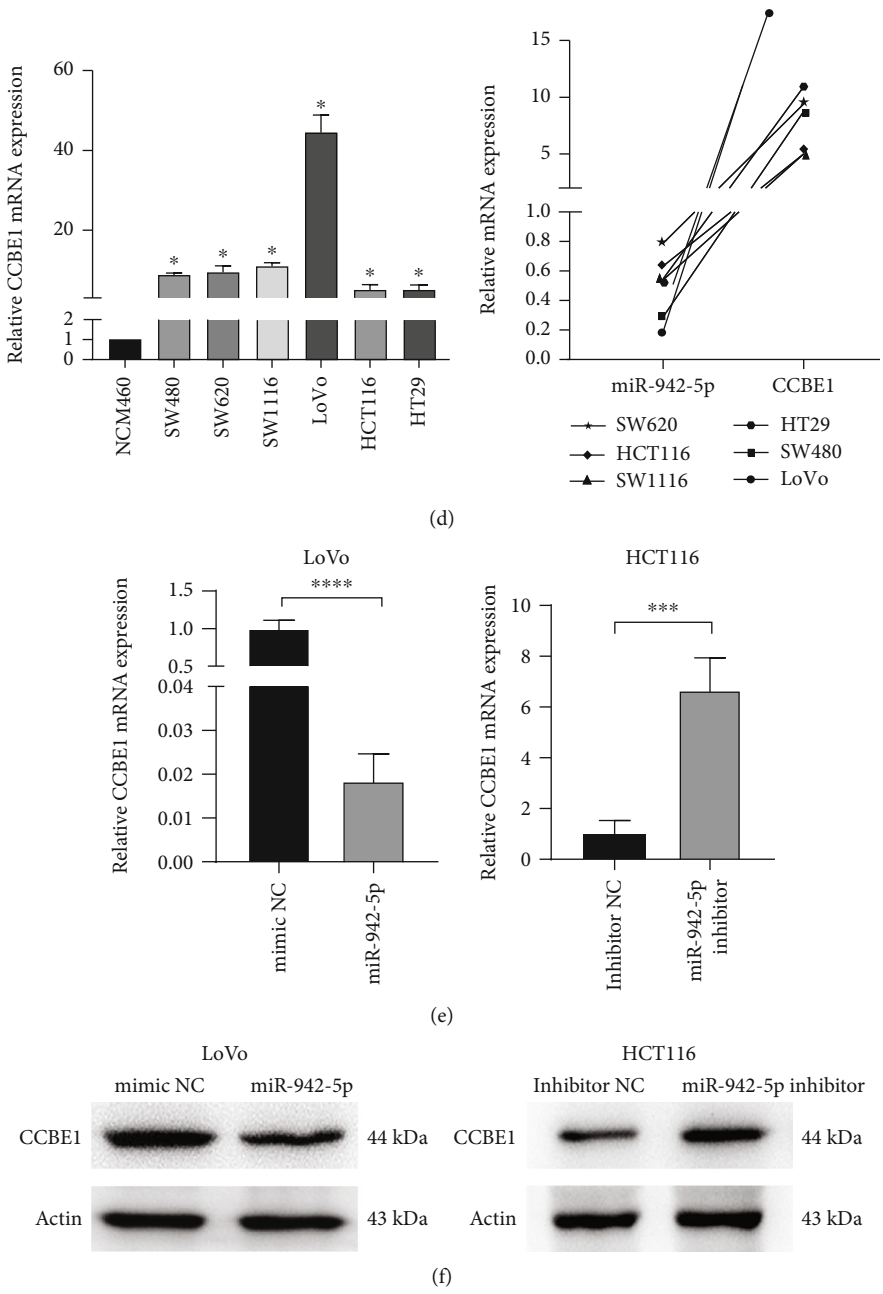

Figure 4: CCBE1 was overexpressed in CRC and its level inversely correlated with miR-942-5p. (a) The putative miR-942-5p binding sites in the CCBE1 3′-UTR. (b) Luciferase reporter was carried out in HEK-293T and LoVo cells cotransduced with miR-942-5p mimics and wild-type or mutant-type 3′-UTR CCBE1 reporter plasmids. $^{****}P < 0.0001$. (c) qRT-PCR was used to detect the relative expression of CCBE1 in CRC tissues matched with adjacent tumor tissues ($n = 35$). $^{*}P < 0.05$. The correlation between CCBE1 and miR-942-5p was evaluated by Pearson correlation coefficient. $r = -0.6388$, $P < 0.05$. (d) qRT-PCR was used to detect the relative expression of CCBE1 in CRC cells matched with NCM460. $^{*}P < 0.05$. In CRC cells, there is a negative correlation between CCBE1 and miR-942-5p. (e) qRT-PCR was used to detect the relative expression of CCBE1 in miR-942-5p-transduced LoVo cells and miR-942-5p inhibitor HCT116 cells. $^{***}P < 0.001$ and $^{****}P < 0.0001$. (f) The levels of CCBE1 protein in miR-942-5p-transduced LoVo and miR-942-5p inhibitor HCT116 cells were evaluated by Western blot.

4. Discussion

Most miRNAs are located in fragile sites or in cancer-related regions of the genome. In normal cells, an equilibrium is maintained between tumor-promoting miRNA factors and tumor-suppressing miRNAs, resulting in a normal expression phenotype. However, in malignant cells, tumor-promoting miRNA expression levels are higher than those of tumor-suppressing miRNAs, leading to increased expression of oncogenes and/or inhibition of tumor suppressor genes [20]. This imbalance leads to the occurrence and development of human cancer, a disorder characterized by

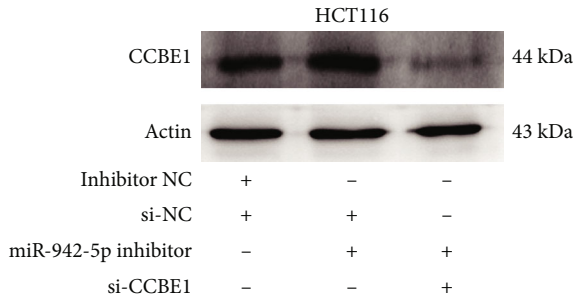

(a)

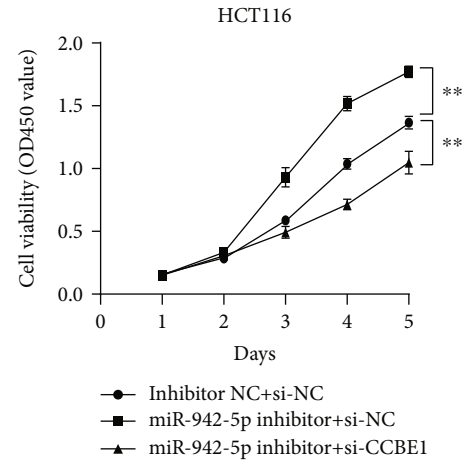

(b)

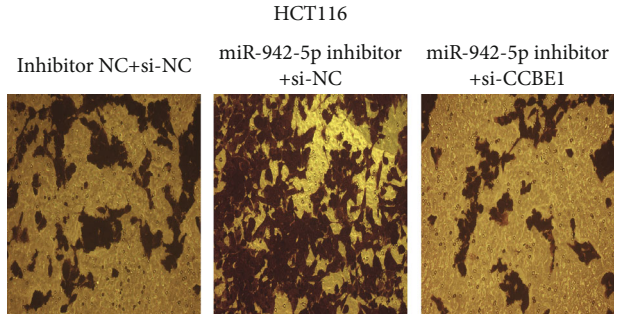

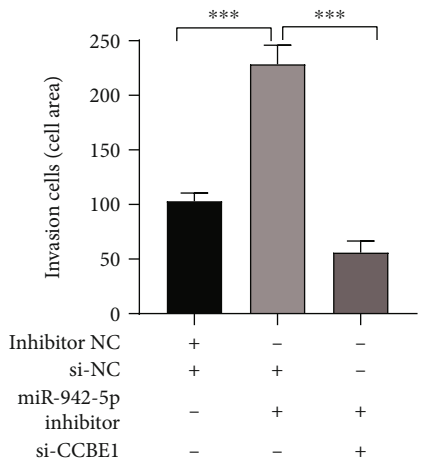

(c)

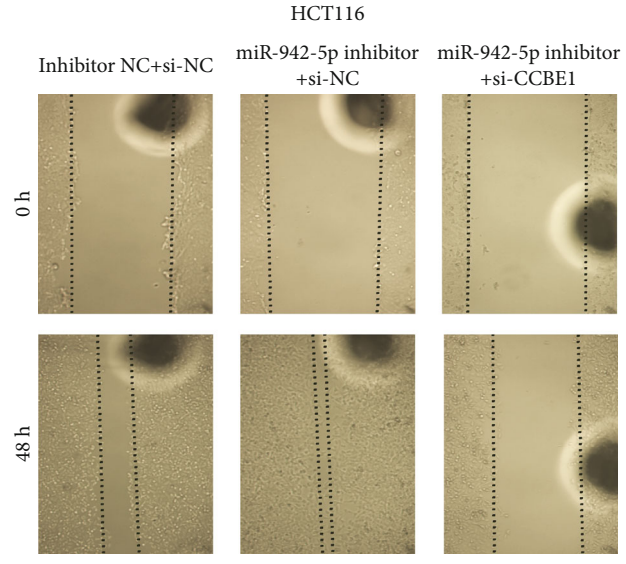

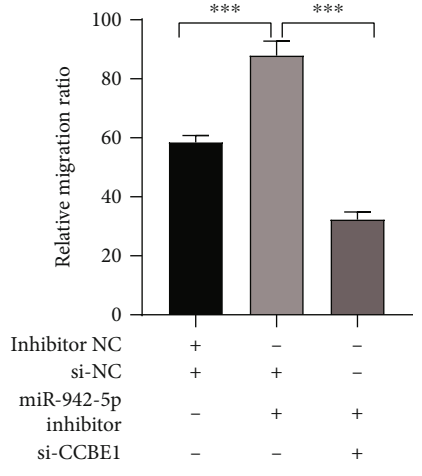

(d)

Figure 5: Continued.

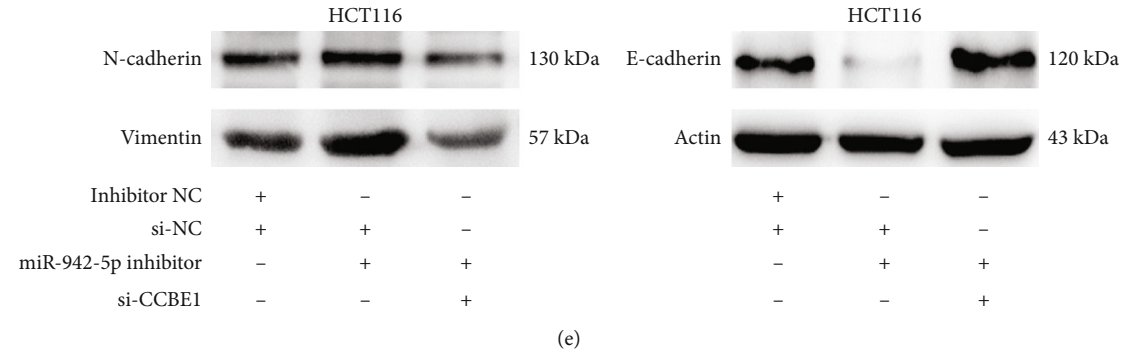

(e)

Figure 5: miR-942-5p downregulation inhibited CRC cell proliferation, invasion, and migration via targeting CCBE1. HCT116 cells were cotransfected with the miR-942-5p and/or si-CCBE1 for 48 h. (a) Western blot was used to analyze the proteins levels of CCBE1. (b) The CCK-8 was used to evaluate the cell viability of HCT116 cells. $^{**}P < 0.01$. (c) Transwell assay was used to evaluate the invasive ability of CRC cells. $^{***}P < 0.001$. (d) Wound-healing assay was used to evaluate the cell migration capacities. $^{***}P < 0.001$. (e) The protein levels of N-cadherin, E-cadherin, and vimentin were determined by Western blot assays.

epigenetic defects, chromosomal abnormalities, and biogenesis defects in the miRNA pathway [21]. miRNAs also play a pivotal role in angiogenesis, causing distant tumor metastasis [22].

In the present study, we focused on the functions and molecular mechanisms of miR-942-5p in CRC cells. We observed that miR-942-5p expression was significantly decreased in CRC tissues and cells. In *in vitro* experiments, miR-942-5p knockdown enhanced cellular proliferation, spreading, invasion, and EMT, while upregulating miR-942-5p reduced cell viability. This suggests that miR-942-5p acts as a tumor suppressor in CRC. Studies have shown that miR-942-5p affects EMT by regulating AKT1 expression in cervical cancer [10, 23]. EMT is a biological process in which malignant tumor cells with epithelial characteristics acquire the ability to infiltrate and invade. During EMT, epithelial cells undergo extensive changes leading to cell separation, extracellular matrix reorganization, and increased cellular motility and invasive capability [24]. Moreover, transcription factors affecting EMT and its regulated genes enhance carcinogenesis, promoting the occurrence of tumors, establishment of precancerous lesions, accumulation of genetic alterations, escape from immunosurveillance, and ability to resist treatment [25]. In the EMT process, the cellular phenotype changes. The epithelial phenotype of cancer cells, including E-cadherin expression, is lost, and the cells acquire interstitial phenotypes, characterized by N-cadherin and vimentin expression [26–28]. Notably, overexpression of miR-942-5p causes increased levels of E-cadherin and decreased levels of N-cadherin and vimentin [29]. Decreased expression of miR-942-5p has the opposite effect. In summary, abnormal expression of miR-942-5p may play a crucial role in CRC development.

CCBE1 was originally identified in the chromosomal region of 18q21-qTER in breast and prostate cancer cell lines [14]. CCBE1 stimulates angiogenesis and lymphangiogenic budding from the venous endothelium and could be an independent regulator of these processes [30]. In addition, the CCBE1 gene is associated with primary systemic lymphatic dysplasia and is therefore a target gene for its treatment [12]. CCBE1 expression is closely associated with tumor progression. Overexpression of CCBE1 in CRC cells promotes lymphangiogenesis and the proteolytic decomposition of vascular endothelial growth factor C (VEGFC) [18]. High expression of CCBE1 in rectal cancer is associated with tumor occurrence and differentiation, lymph node metastasis, and poor prognosis [17]. Similarly, research has shown that CCBE1 expression is associated with poor survival in patients with CRC. Therefore, CCBE1 can be used as an independent and effective biomarker for the prognosis of postoperative patients with CRC [12]. Moreover, microRNAs that regulate CCBE1 expression in CRC have not yet been reported. Our findings suggest that CCBE1 is an miR-942-5p target. CCBE1 levels were inversely associated with miR-942-5p levels in CRC cells. Furthermore, downregulation of CCBE1 was able to reverse the growth-enhancing effects of the miR-942-5p inhibitor on CRC cells. These results indicate that miR-942-5p mediates its antitumor effects by inhibiting CCBE1 function in CRC cells.

5. Conclusion

miR-942-5p acts as a tumor suppressor gene in CRC. We demonstrated that miR-942-5p expression decreased in CRC and that miR-942-5p suppressed the proliferation and metastasis of cancer cells. In addition, miR-942-5p inhibited metastasis and EMT by targeting CCBE1. miR-942-5p may be an effective target for the development of CRC therapies. However, the molecular mechanisms through which miR-942-5p affects CRC pathogenesis remain to be further explored.

Data Availability

The data presented in this work are freely accessible to any other concerned researchers or students.

Ethical Approval

The study conformed to the provisions of the Declaration of Helsinki (as revised in 2013). The research protocol was approved by the Ethics Committee of the First Affiliated

Hospital of Soochow University (IRB no. 2017213). All animal experiments were approved by the Animal Research Ethics Committee of Soochow University (IRB no. A201809059).

Consent

All patients had provided written informed consent prior to obtaining the samples.

Conflicts of Interest

The authors declare that they have no conflicts of interest.

Authors' Contributions

Lin Zhou and Qing Chen contributed equally to this work.

Funding

This research work was supported by grants from the National Natural Science Foundation of China (81772645, 81902385), the Natural Science Foundation of the Jiangsu Higher Education Institutions of China (18KJB320025), and the Suzhou Institute of Biomedical Engineering and Technology of the Chinese Academy of Sciences (Y851401105).

References

[1] R. L. Siegel, K. D. Miller, S. A. Fedewa et al., "Colorectal cancer statistics, 2017," *CA: A Cancer Journal for Clinicians*, vol. 67, no. 3, pp. 177–193, 2017.

[2] F. Bray, J. Ferlay, I. Soerjomataram, R. L. Siegel, L. A. Torre, and A. Jemal, "Global cancer statistics 2018: GLOBOCAN estimates of incidence and mortality worldwide for 36 cancers in 185 countries," *CA: A Cancer Journal for Clinicians*, vol. 68, no. 6, pp. 394–424, 2018.

[3] J. Taieb, T. André, and E. Auclin, "Refining adjuvant therapy for non-metastatic colon cancer, new standards and perspectives," *Cancer Treatment Reviews*, vol. 75, pp. 1–11, 2019.

[4] G. Yothers, M. J. O'Connell, C. J. Allegra et al., "Oxaliplatin as adjuvant therapy for colon cancer: updated results of NSABP C-07 trial, including survival and subset analyses," *Journal of Clinical Oncology*, vol. 29, no. 28, pp. 3768–3774, 2011.

[5] G. C. Shukla, J. Singh, and S. Barik, "MicroRNAs: processing, maturation, target recognition and regulatory functions," *Molecular and Cellular Pharmacology*, vol. 3, no. 3, pp. 83–92, 2011.

[6] J. Hayes, P. P. Peruzzi, and S. Lawler, "MicroRNAs in cancer: biomarkers, functions and therapy," *Trends in Molecular Medicine*, vol. 20, no. 8, pp. 460–469, 2014.

[7] J. Thomas, M. Ohtsuka, M. Pichler, and H. Ling, "MicroRNAs: clinical relevance in colorectal cancer," *International Journal of Molecular Sciences*, vol. 16, no. 12, pp. 28063–28076, 2015.

[8] A. O. Fadaka, A. Pretorius, and A. Klein, "Biomarkers for stratification in colorectal cancer: microRNAs," *Cancer Control*, vol. 26, article 1073274819862784, 2019.

[9] H. Fan, X. Liu, W. W. Zheng, Z. H. Zhuang, and C. D. Wang, "MiR-150 alleviates EMT and cell invasion of colorectal cancer through targeting Gli 1," *European Review for Medical and Pharmacological Sciences*, vol. 21, no. 21, pp. 4853–4859, 2017.

[10] R. Ou, L. Mo, H. Tang et al., "circRNA-AKT1 sequesters miR-942-5p to upregulate AKT1 and promote cervical cancer progression," *Molecular Therapy - Nucleic Acids*, vol. 20, pp. 308–322, 2020.

[11] J. Lu, Y.-h. Wang, X.-y. Huang et al., "circ-CEP85L suppresses the proliferation and invasion of gastric cancer by regulating NFKBIA expression via miR-942-5p," *Journal of Cellular Physiology*, vol. 235, no. 9, pp. 6287–6299, 2020.

[12] Y. R. Zhao, H. Liu, L. M. Xiao, C. G. Jin, Z. P. Zhang, and C. G. Yang, "The clinical significance of CCBE1 expression in human colorectal cancer," *Cancer Management and Research*, vol. 10, pp. 6581–6590, 2018.

[13] L. Le Guen, T. Karpanen, D. Schulte et al., "Ccbe1 regulates Vegfc-mediated induction of Vegfr3 signaling during embryonic lymphangiogenesis," *Development*, vol. 141, no. 6, pp. 1239–1249, 2014.

[14] A. Mesci, X. Huang, S. Taeb et al., "Targeting of CCBE1 by miR-330-3p in human breast cancer promotes metastasis," *British Journal of Cancer*, vol. 116, no. 10, pp. 1350–1357, 2017.

[15] P. Li, Z. Cong, Y. Qiang et al., "Clinical significance of CCBE1 expression in lung cancer," *Molecular Medicine Reports*, vol. 17, no. 2, pp. 2107–2112, 2018.

[16] G. A. Tian, C. C. Zhu, X. X. Zhang et al., "CCBE1 promotes GIST development through enhancing angiogenesis and mediating resistance to imatinib," *Scientific Reports*, vol. 6, no. 1, article 31071, 2016.

[17] L. Zhang and F. J. Liu, "Expression of SLP-2 gene and CCBE1 are associated with prognosis of rectal cancer," *European Review for Medical and Pharmacological Sciences*, vol. 21, no. 6, pp. 1214–1218, 2017.

[18] J. Song, W. Chen, X. Cui et al., "CCBE1 promotes tumor lymphangiogenesis and is negatively regulated by TGFβ signaling in colorectal cancer," *Theranostics*, vol. 10, no. 5, pp. 2327–2341, 2020.

[19] K. J. Livak and T. D. Schmittgen, "Analysis of Relative Gene Expression Data Using Real-Time Quantitative PCR and the $2^{-\Delta\Delta C}{}_{T}$ Method," *Methods*, vol. 25, no. 4, pp. 402–408, 2001.

[20] U. Zaheer, M. Faheem, I. Qadri et al., "Expression profile of microRNA: an emerging hallmark of cancer," *Current Pharmaceutical Design*, vol. 25, no. 6, pp. 642–653, 2019.

[21] G. A. Calin and C. M. Croce, "MicroRNA signatures in human cancers," *Nature Reviews. Cancer*, vol. 6, no. 11, pp. 857–866, 2006.

[22] G. P. Nagaraju, A. S. Madanraj, S. Aliya et al., "MicroRNAs as biomarkers and prospective therapeutic targets in colon and pancreatic cancers," *Tumour Biology*, vol. 37, no. 1, pp. 97–104, 2016.

[23] F. Yang, C. Shao, K. Wei et al., "miR-942 promotes tumor migration, invasion, and angiogenesis by regulating EMT via BARX2 in non-small-cell lung cancer," *Journal of Cellular Physiology*, vol. 234, no. 12, pp. 23596–23607, 2019.

[24] Y. Zhang and R. A. Weinberg, "Epithelial-to-mesenchymal transition in cancer: complexity and opportunities," *Frontiers of Medicine*, vol. 12, no. 4, pp. 361–373, 2018.

[25] M. P. Stemmler, R. L. Eccles, S. Brabletz, and T. Brabletz, "Non-redundant functions of EMT transcription factors," *Nature Cell Biology*, vol. 21, no. 1, pp. 102–112, 2019.

[26] L. D. M. Derycke and M. E. Bracke, "N-cadherin in the spotlight of cell-cell adhesion, differentiation, embryogenesis,

invasion and signalling," *The International Journal of Developmental Biology*, vol. 48, no. 5-6, pp. 463–476, 2004.

[27] R. A. Battaglia, S. Delic, H. Herrmann, and N. T. Snider, "Vimentin on the move: new developments in cell migration," *F1000Research*, vol. 7, article 1796, 2018.

[28] F. van Roy and G. Berx, "The cell-cell adhesion molecule E-cadherin," *Cellular and Molecular Life Sciences*, vol. 65, no. 23, pp. 3756–3788, 2008.

[29] Ranković, Zidar, Žlajpah, and Boštjančič, "Epithelial-mesenchymal transition-related microRNAs and their target genes in colorectal cancerogenesis," *Journal of Clinical Medicine*, vol. 8, article 1603, 2019.

[30] F. L. Bos, M. Caunt, J. Peterson-Maduro et al., "CCBE1 is essential for mammalian lymphatic vascular development and enhances the lymphangiogenic effect of vascular endothelial growth factor-c in vivo," *Circulation Research*, vol. 109, no. 5, pp. 486–491, 2011.

Hindawi
BioMed Research International
Volume 2021, Article ID 5575704, 20 pages
https://doi.org/10.1155/2021/5575704

Research Article

Expression Pattern and Prognostic Value of EPHA/EFNA in Breast Cancer by Bioinformatics Analysis: Revealing Its Importance in Chemotherapy

Zheng Liang[1], **Xu Wang**[2], **Kaiti Dong**[1], **Xinhua Li**[1], **Chenge Qin**[1] and **Huifang Zhou**[1]

[1]*Department of Otorhinolaryngology, Tianjin Medical University General Hospital, Tianjin 300052, China*
[2]*Department of Breast Oncology, Key Laboratory of Breast Cancer Prevention and Therapy (Ministry of Education), Key Laboratory of Cancer Prevention and Therapy, Tianjin, National Clinical Research Center for Cancer, Tianjin's Clinical Research Center for Cancer, Tianjin Medical University Cancer Institute and Hospital, Tianjin 300060, China*

Correspondence should be addressed to Zheng Liang; liangzheng01@tmu.edu.cn

Received 17 February 2021; Revised 26 March 2021; Accepted 10 April 2021; Published 23 April 2021

Academic Editor: Qiang Liu

The activities of the ephrin family in breast cancer (BrCa) are complex. Family A receptors (EPHA) and ligands (EFNA) can act as oncogenes or tumor suppressors and are implicated in chemoresistance. Here, we examined the expression pattern and prognostic value of the EPHA/EFNA family in patients with breast cancer, including patients with different subtypes or different chemotherapy cohorts. In the UALCAN database, the mRNA expression of EPHA1, EPHA10, EFNA1, EFNA3, and EFNA4 was significantly higher, whereas that of EPHA2, EPHA4, EPHA5, and EFNA5 was significantly lower in breast cancer tissues than in paracancerous tissues. The transcriptional levels of EPHA/EFNA family members were correlated with intrinsic subclasses of breast cancer. The relationship between EPHA/EFNA and the clinicopathological parameters of BrCa was analyzed using bc-GenExMiner V4.5. EPHA1, EPHA2, EPHA4, EPHA7, EFNA3, EFNA4, and EFNA5 were upregulated in estrogen receptor- (ER-) and progesterone receptor- (PR-) negative tumors, whereas EPHA3, EPHA6, and EFNA1 were upregulated in ER- and PR-positive tumors. EPHA1, EPHA2, EFNA3, and EFNA4 mRNA expression was significantly higher in human epidermal growth factor receptor 2- (HER2-) positive tumors than in HER2-negative tumors. Triple-negative status was positively correlated with EPHA1, EPHA2, EPHA4, EPHA7, EFNA3, EFNA4, and EFNA5 and negatively correlated with EPHA3 and EPHA10 mRNA expression. Genetic alterations of EPHA/EFNA in breast cancer varied from 1.1% to 10% for individual genes, as determined by the cBioPortal database. The Kaplan–Meier plotter indicated that high EphA7 mRNA expression was associated with poor overall survival (OS) and recurrence-free survival (RFS), especially in the HER2 and luminal A subtypes. EFNA4 was predicted to have poor OS and RFS in breast cancers, especially in luminal B, basal-like subtype, and patients treated with adjuvant chemotherapy. High EPHA3 expression was significantly associated with better OS and RFS, especially in the luminal A subtype, but with poor RFS in BrCa patients receiving chemotherapy. Our findings systematically elucidate the expression pattern and prognostic value of the EPHA/EFNA family in BrCa, which might provide potential prognostic factors and novel targets in BrCa patients, including those with different subtypes or treated with chemotherapy.

1. Introduction

Breast cancer is the most commonly diagnosed female cancer and the cause of 685,000 cancer mortality in 2020 worldwide [1]. Tumor recurrence and metastasis contribute to the high death rate [2]. Despite extensive research into the treatment of BrCa, chemotherapy resistance is an important issue limiting the efficacy of treatment. Novel biomarkers to predict prognosis or the sensitivity to chemotherapy are urgently needed.

Receptor tyrosine kinases (RTKs) play an important role in a variety of cellular processes in cancer [3]. Ephrins, also

known as ephrin ligands, and Eph receptors (Ephs), which are RTKs, are key regulators of physiological and pathological processes involved in development and disease, such as cellular motility, cell repulsion, and cell adhesion [4]. The Ephrin family consists of multiple Ephs and ephrins. Both receptors and ligands are membrane-bound proteins that require direct cell-cell interaction for activation. Eph/ephrin signal transduction occurs not only in the receptor-expressing cell but also in the ligand-expressing cell via bidirectional signaling [5]. The ligands can have a glycosylphosphatidylinositol anchor (A type) or a membrane-spanning protein domain (B type). The receptors are also categorized as A or B according to the type of ligand they bind to. Ephrin family A includes ten receptors named EPHA (1–10) and five ligands designated as EFNA (1–5) [6]. The interaction between ligands and receptors via bidirectional signaling and its involvement in cancer biology are mediated by complex processes [7, 8]. Several Ephrin A (EPHA/EFNA) family members are overexpressed or downregulated in a variety of tumors, suggesting that they act as oncogenes or as tumor suppressors according to the cellular context [9]. Ephrin A family members that are overexpressed in cancer including EFNA1 in melanoma [10]; EPHA2 in prostate cancer [11], nasopharyngeal carcinoma [12], and squamous-cell carcinoma of the head and neck [13]; and EPHA3 in non-small-cell lung cancer [14]. EPHA7 acts as a tumor suppressor in follicular lymphoma and is a potential therapeutic target [15]. EphA2 expression levels are associated with the invasiveness and aggressive behavior of BrCa [16]. The role of EPHA/EFNA as tumor suppressors in breast carcinogenesis was also demonstrated by targeting EPHA2 [17]. EPHA2 regulates the sensitivity to paclitaxel in nasopharyngeal carcinoma via the phosphoinositide 3-kinase/Akt signaling pathway [18]. Cisplatin chemotherapy-induced ERK1/2-RSK1/2-EphA2-GPRC5A signaling is related to acquired chemoresistance in ovarian cancer [19]. Previous findings indicate that EPHA/EFNA family members may serve as biomarkers for predicting prognosis or the response to treatment, which prompted us to analyze the expression pattern and prognostic role of the EPHA/EFNA family in BrCa.

Online databases provide access to a wealth of information, such as microarray RNA chips from the Gene Expression Omnibus (GEO) [20] and RNA sequences from The Cancer Genome Atlas (TCGA) [21]. In this study, we compared the transcriptional levels of EPHA/EFNA in BrCa and paracancerous tissues using the UALCAN database [22]. The relationship between members of the EPHA/EFNA family and clinicopathologic characteristics of BrCa patients was analyzed using breast cancer gene expression miner (bc-GenExMiner) v4.5 [23, 24]. Genetic alterations of EPHA/EFNA family members, including mutations and putative copy number alterations (CNAs), were analyzed in cBioPortal [25]. Moreover, the association of EPHA/EFNA gene expression with clinical outcomes was assessed in patients with BrCa, including patients with different subtypes or those undergoing chemotherapy, using the Kaplan–Meier plotter database [26].

2. Methods and Materials

2.1. Gene Expression Analysis in UALCAN. UALCAN (http://ualcan.path.uab.edu/) is an online comprehensive and interactive platform based on RNA-seq data and clinical information from TCGA database [22]. In this study, UALCAN was used to investigate the transcriptional levels of EPHA/EFNA family members in primary BrCa tissues and their association with the subtype.

2.2. Analysis of the Relationship between EPHA/EFNA and Clinicopathologic Characteristics in Bc-GenExMiner. Bc-GenExMiner v4.5 (http://bcgenex.centregauducheau.fr/BC-GEM), a statistical mining tool of published BrCa transcriptomic data, was used to evaluate the relationship between EPHA/EFNA family members and the clinicopathologic characteristics of BrCa patients, including age, nodal status, estrogen receptor (ER) status, progesterone receptor (PR) status, human epidermal growth factor receptor 2 (HER2) status, lymph node status, triple-negative tumors, and P53 status (sequence). Information on ER, PR, HER2, lymph node status, and pathological grade was not available for all 3,996 patients.

2.3. Genetic Alterations Analysis in cBioPortal. OncoPrint is a feature of cBioPortal, an open-source web application that allows researchers to explore and analyze cancer genomic datasets (http://www.cbioportal.org/) [27, 28]. In this study, genetic alterations of EPHA/EFNA family members including mutations and putative CNAs were analyzed. A total of 1084 tumor samples with RNA-seq data on cBioPortal were included in the study.

2.4. The Prognostic Value of EPHA/EFNA mRNA Expression in BrCa Patients including Those with Different Subtypes and Undergoing Chemotherapy. The Kaplan–Meier plotter is an online database that facilitates predicting the effect of gene expression on survival in cancer. Sources for the database include GEO, EGA (European Genome-Phenome Archive), and TCGA. This platform, which contains gene expression information and survival data of BrCa patients, was used to perform a meta-analysis to verify the prognostic value of EPHA/EFNA family members for predicting overall survival (OS) and relapse-free survival (RFS). Additional analyses were restricted to cohorts according to subtype and including the patients treated with chemotherapy. Kaplan–Meier survival plots were used to compare the prognosis of all cohorts. Hazard ratios (HRs), 95% confidence intervals (CIs), and log-rank P values were calculated and displayed online.

2.5. Statistical Analysis. The differential mRNA expression of EPHA/EFNA in BrCa tissues was compared by Student's t -test. The log-rank test was used to compare Kaplan-Meier survival plots. A P value of <0.05 was considered statistically significant.

3. Results

3.1. Transcriptional Levels of EPHA/EFNA in BrCa. To evaluate the expression pattern of EPHA/EFNA in BrCa, the

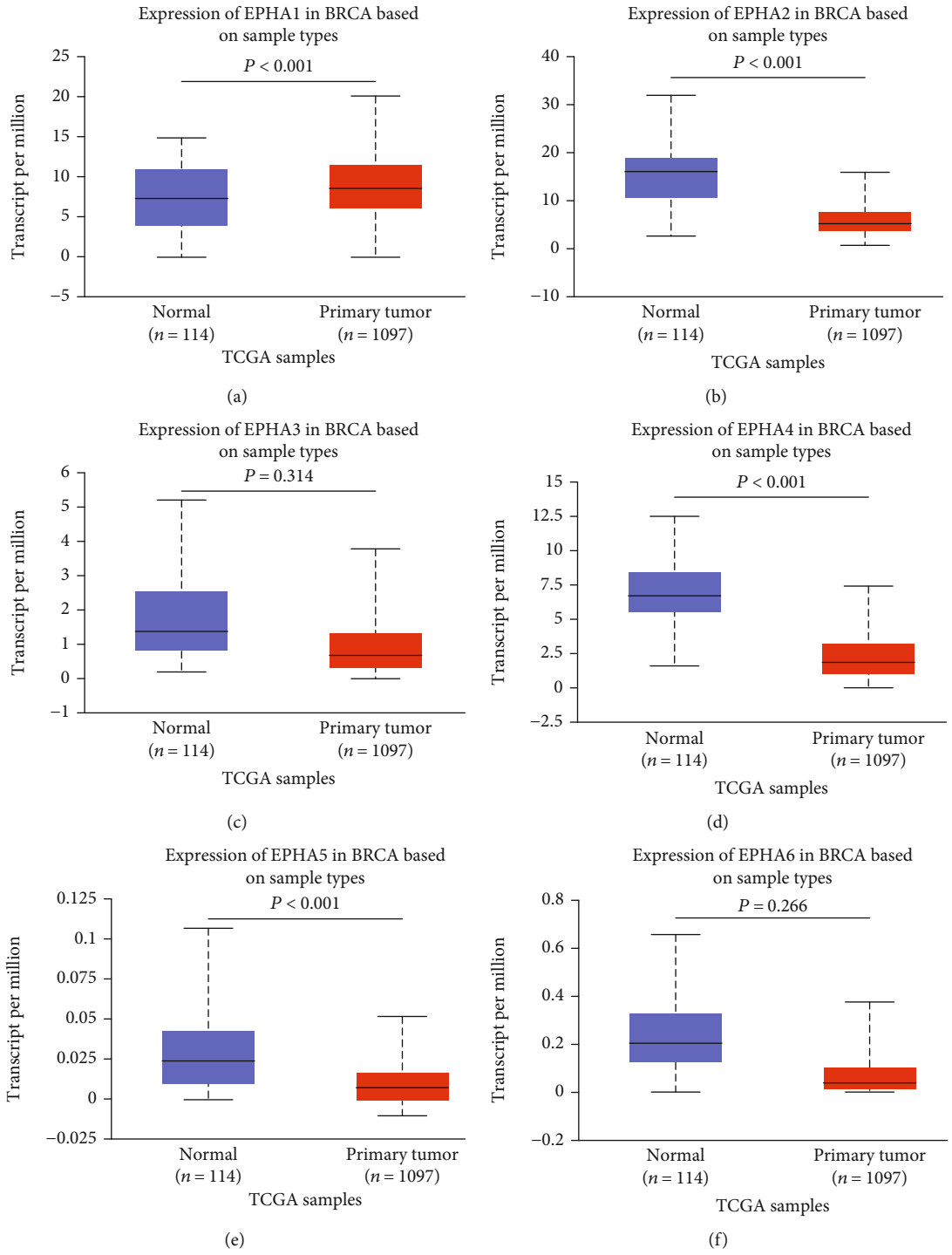

Figure 1: Continued.

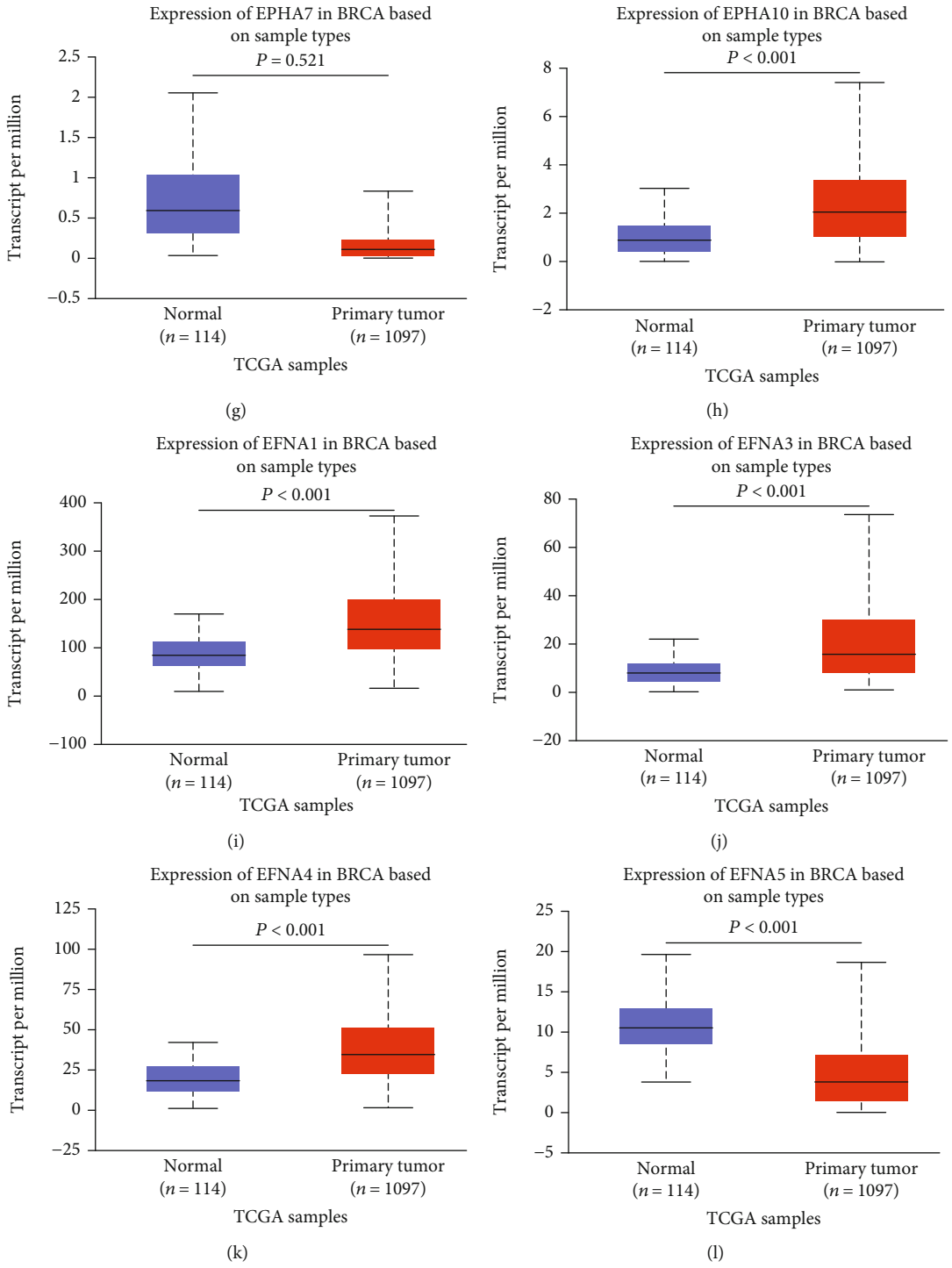

Figure 1: Transcriptional levels of EPHA/EFNA in breast cancer and paracancerous tissues from the TCGA dataset based on data mining via UALCAN. The transcriptional levels of EPHA1, EPHA10, EFNA1, EFNA3, and EFNA4 (a, h, i, j, and k) were upregulated, whereas the transcriptional levels of EPHA2, EPHA4, EPHA5, and EFNA5 (b, d, e, and l) were downregulated in breast cancer tissues compared with paracancerous tissues. The transcriptional levels of EPHA3, EPHA6, and EPHA7 (c, f, and g) did not differ significantly between breast cancer and paracancerous tissues.

transcriptional levels of EPHA/EFNA family members were compared between BrCa and paracancerous tissues using the UALCAN database. As shown in Figure 1, EPHA2 (Figure 1(b), $P < 0.001$), EPHA4 (Figure 1(d), $P < 0.001$), and EPHA5 (Figure 1(e), $P < 0.001$) expression was significantly lower in BrCa tissues than in paracancerous tissues. EPHA1 (Figure 1(a), $P < 0.001$) and EPHA10 (Figure 1(h), $P < 0.001$) expression was significantly higher in BrCa than in paracancerous tissues (Figure 1(f), $P < 0.001$). The expression of EPHA3 (Figure 1(c), $P = 0.314$), EPHA6 (Figure 1(f),

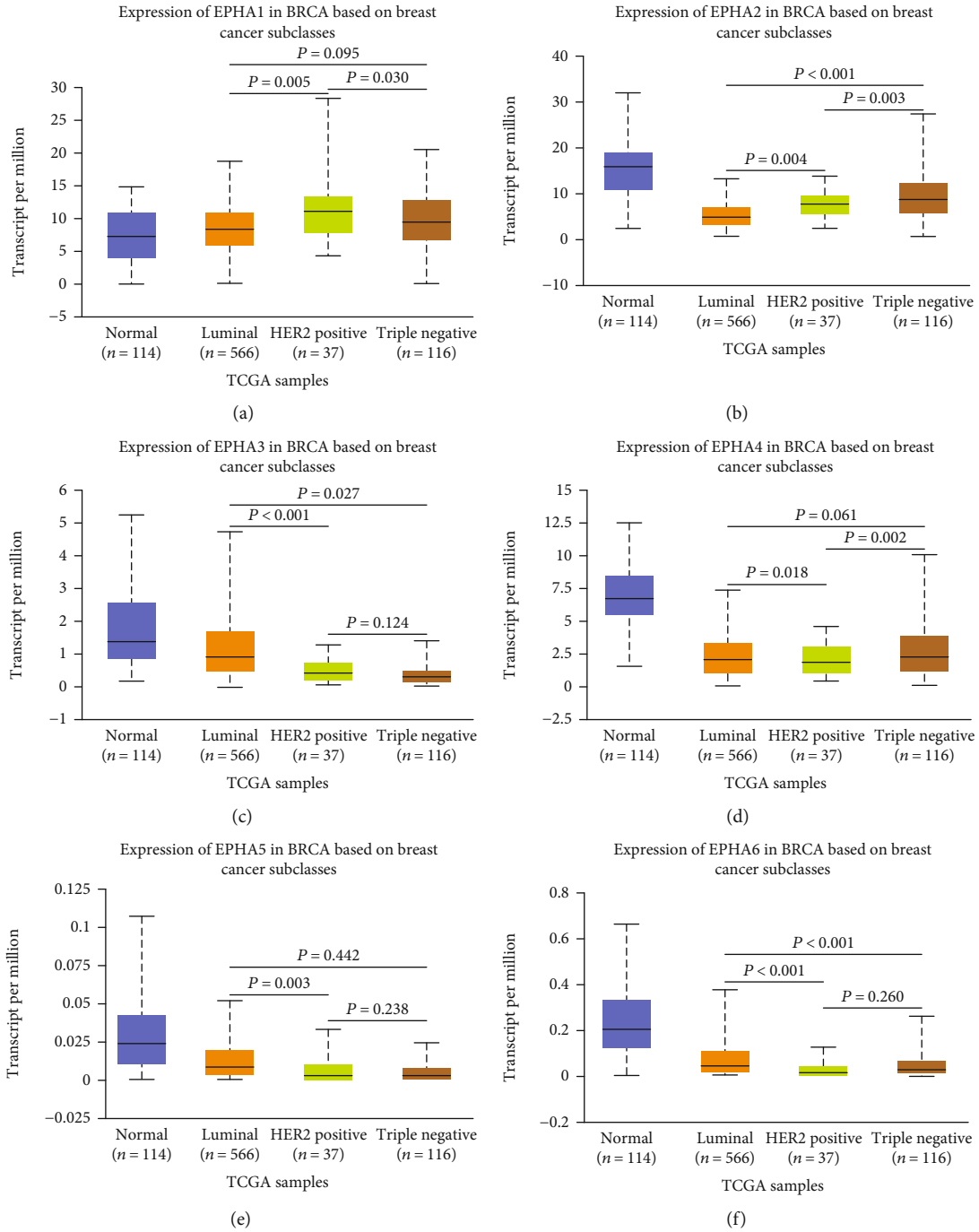

Figure 2: Continued.

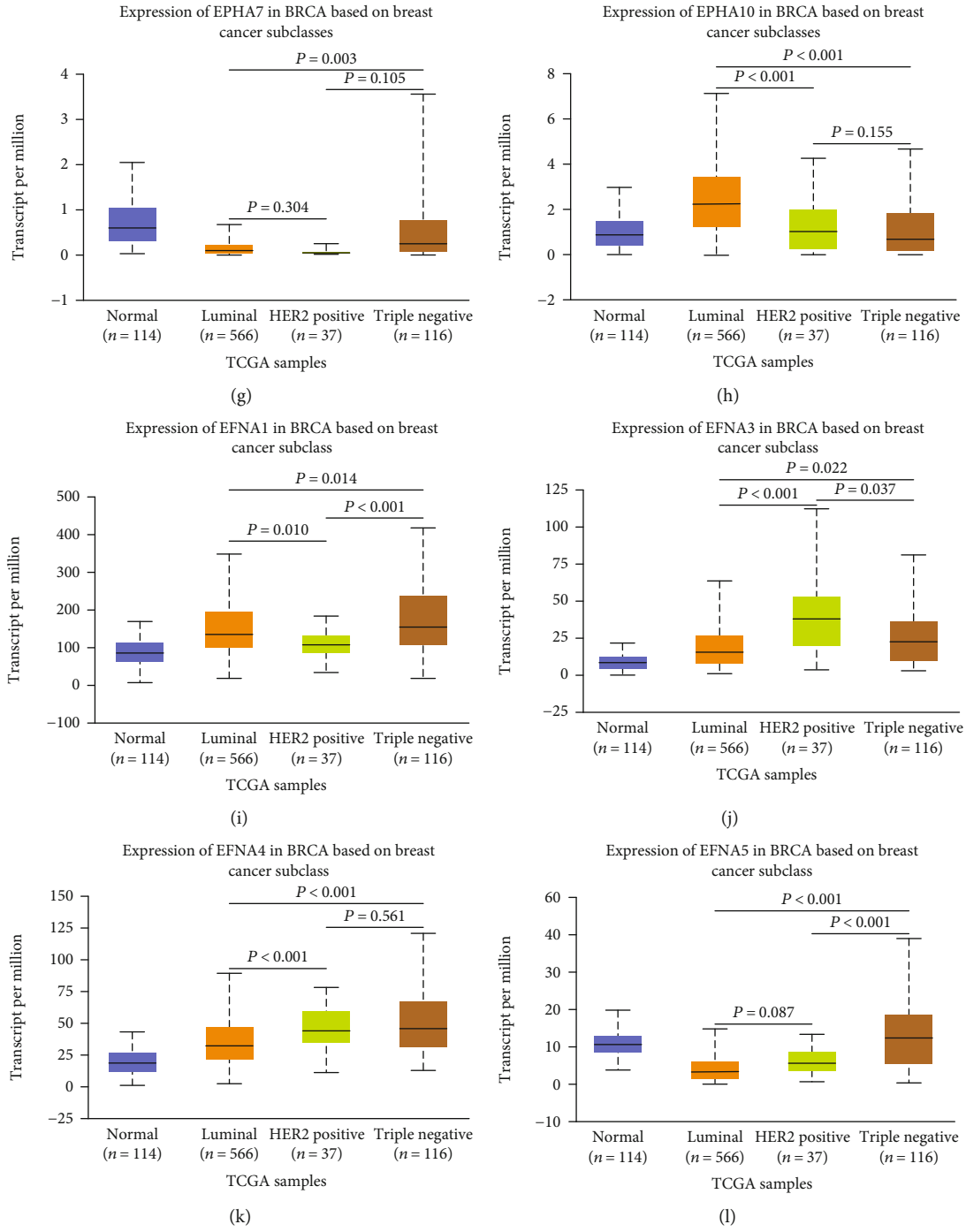

FIGURE 2: The transcriptional level of EPHA/EFNA in breast cancer patients with different subtypes. HER2-positive and triple-negative breast cancer patients tended to express lower levels of EPHA3, EPHA5, EPHA6, and EPHA10 mRNA. The highest mRNA expression of EPHA3, EPHA5, EPHA6, and EPHA10 was found in the luminal subtype. The highest mRNA expression of EFNA was detected in triple-negative tissues except EFNA3, and the lowest mRNA expression of EFNA was detected in the luminal subtype, except for EFNA1.

$P = 0.266$), and EPHA7 (Figure 1(g), $P = 0.521$) did not differ significantly between BrCa and paracancerous tissues. Analysis of EFNA expression showed that the transcriptional levels of EFNA1 (Figure 1(i), $P < 0.001$), EFNA3 (Figure 1(j), $P < 0.001$), and EFNA4 (Figure 1(k), $P < 0.001$) were significantly higher in BrCa than in paracancerous tissues, whereas the transcriptional level of EFNA5 (Figure 1(l), $P < 0.001$) was significantly lower in BrCa than in paracancerous tissues. EPHA8 and EFNA2 were expressed at markedly low levels according to the UALCAN database, and they were not included in the analysis.

3.2. Transcriptional Levels of EPHA/EFNA in Different BrCa Subtypes. The classification of BrCa into subtypes is helpful

Table 1: Association between EPHA/EFNA mRNA expression and clinicopathological features of patients with breast cancer.

(a)

Parameters	EPHA1	EPHA2	EPHA3	EPHA4	EPHA5	EPHA6
Age (years)	0.2250			0.3583	0.8373	0.1242
>51						
≤51		0.0002	<0.0001			
Nodal status	0.9075		0.6126	0.5222	0.9379	0.2129
Negative		0.0142				
Positive						
ER (IHC)					0.2271	
Negative	<0.0001	<0.0001		<0.0001		
Positive			<0.0001			0.0015
PR (IHC)					0.2851	
Negative	<0.0001	<0.0001		<0.0001		
Positive			<0.0001			0.0066
HER2 (IHC)			0.1385	0.7082	0.4015	
Negative						0.0031
Positive	<0.0001	<0.0001				
Triple-negative status					0.0924	0.4042
Not			<0.0001			
TNBC	<0.0001	<0.0001		<0.0001		
P53 sequence				0.2714	0.5513	
Wild type			<0.0001			0.0035
Mutated	<0.0001	<0.0001				

(b)

Parameters	EPHA7	EPHA10	EFNA1	EFNA3	EFNA4	EFNA5
Age (years)	0.0577	0.0878				
>51			<0.0001	0.0092		
≤51					0.0003	<0.0001
Nodal status	0.9157	0.7342	0.4045		0.6819	0.7867
Negative						
Positive				0.0482		
ER (IHC)						
Negative	<0.0001			<0.0001	<0.0001	<0.0001
Positive		<0.0001	<0.0001			
PR (IHC)		0.5102				
Negative	0.0046			<0.0001	<0.0001	<0.0001
Positive			<0.0001			
HER2 (IHC)	0.9010	0.9299				0.5285
Negative			<0.0001			
Positive				<0.0001	<0.0001	
Triple-negative status			0.3715			
Not		0.0333				
TNBC	0.0002			<0.0001	<0.0001	<0.0001
P53 sequence	0.4840	0.1113				
Wild type			0.0206			
Mutated				<0.0001	<0.0001	<0.0001

for predicting the therapeutic response and prognosis of patients [29]. Here, we analyzed the transcriptional levels of EPHA/EFNA family members according to BrCa subtype using the UALCAN database. As shown in Figure 2, EPHA3, EPHA5, EPHA6, and EPHA10 mRNA levels were low in HER2-positive and triple-negative BrCa patients, whereas other EPHA family members did not show this trend. EPHA3, EPHA5, EPHA6, and EPHA10 were expressed at high levels in the luminal subtype (Figures 2(c), 2(e), 2(f), and 2(h)). The highest mRNA expression levels of EFNA were detected in triple-negative tissues except EFNA3, whereas the luminal subtype showed the lowest EFNA mRNA levels (Figures 2(i)–2(l)) except EFNA1. Taken together, these findings indicate that the transcriptional levels of EPHA/EFNA family members are correlated with intrinsic subclasses in BrCa patients.

3.3. Association between EPHA/EFNA mRNA Expression and the Clinicopathological Features of Patients with BrCa. We used bc-GenExMiner v4.5 to examine the relationship between EPHA/EFNA and the clinicopathologic characteristics of patients. For the age parameter, EPHA2 ($P = 0.0002$), EPHA3 ($P < 0.0001$), EFNA4 ($P = 0.0003$), and EFNA5 ($P < 0.0001$) were expressed at high levels in patients aged ≤51 years (Table 1). EFNA1 ($P < 0.0001$) and EFNA3 ($P = 0.0092$) were expressed at high levels in older patients, whereas the mRNA expression levels of the other EPHA/EFNA family members were not significantly correlated with age. EPHA2 ($P = 0.0142$) mRNA was higher in BrCa patients with negative lymph nodes than in those with positive lymph nodes, whereas EFNA3 ($P = 0.0482$) showed the opposite trend. The mRNA expression of the other EPHA/EFNA family members was not significantly associated with nodal status. ER- and PR-negative patients had higher levels of EPHA1 ($P < 0.0001$), EPHA2 ($P < 0.0001$), EPHA4 ($P < 0.0001$), EPHA7 ($P < 0.0001$ and =0.0046, respectively), EFNA3 ($P < 0.0001$), EFNA4 ($P < 0.0001$), and EFNA5 ($P < 0.0001$). On the other hand, EPHA3 ($P < 0.0001$), EPHA6 ($P < 0.0015$ and =0.0066, respectively), and EFNA1 ($P < 0.0001$) were higher in ER- and PR-positive patients. The EPHA10 mRNA level was higher in ER-positive patients ($P < 0.0001$) but not significantly associated with PR status ($P = 0.5102$). EPHA5 mRNA expression was not significantly associated with ER ($P = 0.2271$) and PR ($P = 0.2851$) status. EPHA1, EPHA2, EFNA3, and EFNA4 ($P < 0.0001$, all) mRNA levels were significantly higher in the HER2-positive group than in the HER2-negative group. Only EPHA6 ($P = 0.0031$) and EFNA1 ($P < 0.0001$) were significantly increased in the HER2-negative group. The mRNA expression of the other EPHA/EFNA family members was not associated with HER2 status. Triple-negative status was positively correlated with the mRNA expression of EPHA1 ($P < 0.0001$), EPHA2 ($P < 0.0001$), EPHA4 ($P < 0.0001$), EPHA7 ($P = 0.0002$), EFNA3 ($P < 0.0001$), EFNA4 ($P < 0.0001$), and EFNA5 ($P < 0.0001$) and negatively correlated with EPHA3 ($P < 0.0001$) and EPHA10 ($P = 0.0333$). The mRNA expression of the other EPHA/EFNA family members was not associated with triple-negative status. P53 mutant status (sequence) was positively correlated with EPHA1, EPHA2, EFNA3, EFNA4, and EFNA5 ($P < 0.0001$ for all) and P53 wild-type status was positively correlated with EPHA3 ($P < 0.0001$), EPHA6 ($P = 0.0035$), and EFNA1 ($P = 0.0206$) mRNA expression. The mRNA expression of the other EPHA/EFNA family members was not associated with P53 mutant status.

3.4. Genetic Alterations of EPHA/EFNA in BrCa. Different kinds of genetic alterations, such as missense mutations, amplification, and deep deletions, regulate cancer-related gene expression and participate in oncogenesis. We speculated that genetic alterations may regulate the transcriptional levels of EPHA/EFNA. To investigate mutations and CNAs of the EPHA/EFNA family in BrCa, the OncoPrint feature of cBioPortal (http://www.cbioportal.org) was used to investigate the proportion and percentage of specimens with genetic alterations in EPHA/EFNA. The frequency of alterations in these genes among BrCa samples varied from 1.1% to 10% for individual genes as shown in Figure 3.

3.5. The Prognostic Value of EPHA/EFNA mRNA Expression in BrCa Patients. The prognostic value of the mRNA expression of 12 EPHA/EFNA family members in BrCa patients was examined using the Kaplan–Meier plotter. High mRNA expression of EPHA7 (Figure 4(g), HR = 1.49, 95% CI: 1.09–2.05, $P = 0.012$) and EFNA4 (Figure 4(k), HR = 1.31, 95% CI: 1.04–1.64, $P = 0.02$) was associated with poor OS. EPHA6 mRNA expression (Figure 4(f), HR = 1.34, 95% CI: 0.98–1.84, $P = 0.067$) was moderately associated with poor OS. High mRNA expression of EPHA3 (Figure 4(c), HR = 0.71, 95% CI: 0.57–0.89, $P = 0.0023$) and EPHA4 (Figure 4(d), HR = 0.72, 95% CI: 0.52–0.99, $P = 0.045$) was significantly associated with better OS. The mRNA expression levels of the other EPHA/EFNA family members were not significantly correlated with OS.

Regarding RFS, high mRNA expression of EPHA7 (Figure 5(g), HR = 1.21, 95% CI: 1.04–1.42, $P = 0.014$), EFNA3 (Figure 5(j), HR = 1.17, 95% CI: 1.04–1.33, $P = 0.01$), and EFNA4 (Figure 5(k), HR = 1.28, 95% CI: 1.14–1.44, $P < 0.0001$) was associated with worse RFS. High mRNA expression of other EPHA/EFNA family members was significantly associated with better RFS except EFNA1. The RFS curves are shown in Figure 5 (EPHA1: HR = 0.68, 95% CI: 0.61–0.76, $P < 0.0001$; EPHA2: HR = 0.8, 95% CI: 0.72–0.89, $P < 0.0001$; EPHA3: HR = 0.78, 95% CI: 0.7–0.87, $P < 0.0001$; EPHA4: HR = 0.74, 95% CI: 0.62–0.87, $P = 0.00036$; EPHA5: HR = 0.72, 95% CI: 0.61–0.86, $P = 0.00019$; EPHA6: HR = 0.82, 95% CI: 0.69–0.97, $P = 0.019$; EPHA10: HR = 0.61, 95% CI: 0.52–0.71, $P < 0.0001$; and EFNA5: HR = 0.74, 95% CI: 0.66–0.82, $P < 0.0001$).

3.6. The Prognostic Value of EPHA/EFNA mRNA Expression in BrCa Patients with Different Subtypes. To further analyze the effect of EPHA/EFNA according to the BrCa subtype, the prognostic value of EPHA/EFNA family members was assessed in BrCa patients with different molecular subtypes, including basal-like, luminal A, luminal B, and HER2+ subtypes according to the 2011 St. Gallen criteria [30]. Because OS data were lacking for some patients, this analysis was

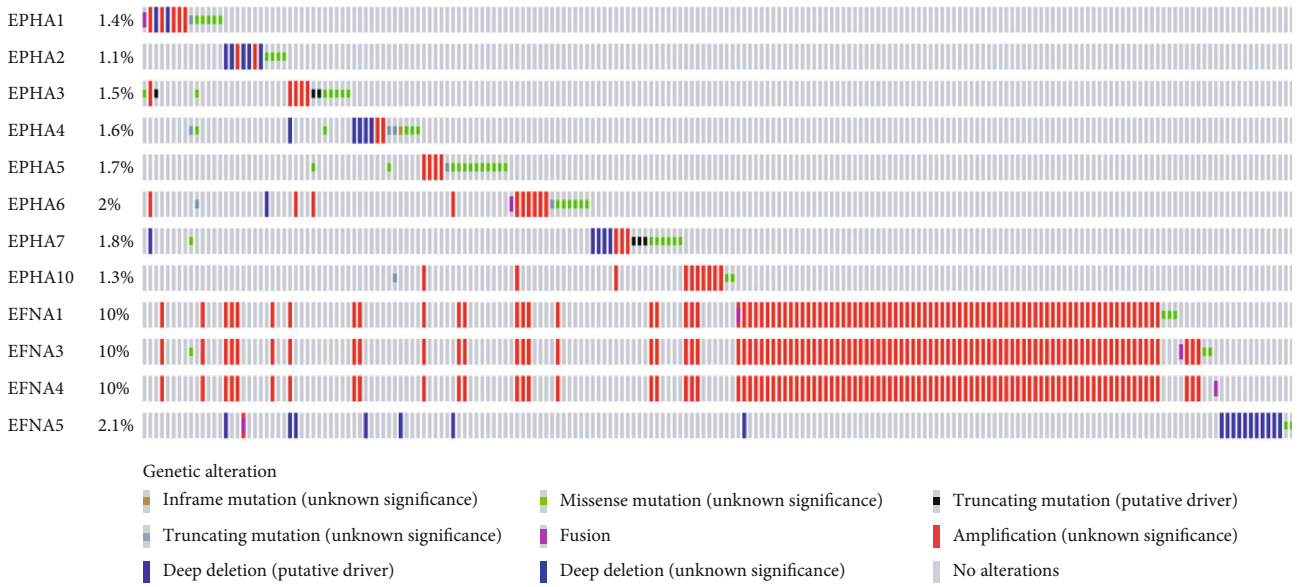

Figure 3: EPHA/EFNA family gene alteration analysis in invasive breast carcinoma. OncoPrint represents the distribution and percentages of samples with different types of alterations in the EPHA/EFNA family. The right part of the figure without alterations was not included.

limited to RFS. In the basal-like subtype, high mRNA expression of EFNA1 (HR = 1.36, 95% CI: 1.06–1.76, $P = 0.016$) and EFNA4 (HR = 1.53, 95% CI: 1.16–2.01, $P = 0.022$) predicted an unfavorable RFS, whereas high mRNA expression levels of EPHA1 (HR = 0.61, 95% CI: 0.48–0.79, $P = 0.0001$), EPHA4 (HR = 0.69, 95% CI: 0.49–0.96, $P = 0.0029$), EPHA5 (HR = 0.45, 95% CI: 0.29–0.68, $P = 0.00015$), EPHA7 (HR = 0.68, 95% CI: 0.49–0.95, $P = 0.022$), and EFNA5 (HR = 0.69, 95% CI: 0.54–0.89, $P = 0.0037$) were correlated with better RFS. The remaining EPHA/EFNA members were not associated with prognosis in basal-like BrCa. (Table 2).

In the luminal A subtype, high mRNA expression levels of EPHA1 (HR = 0.63, 95% CI: 0.53–0.75, $P < 0.0001$), EPHA2 (HR = 0.61, 95% CI:0.51–0.72, $P < 0.0001$), EPHA3 (HR = 0.73, 95% CI: 0.61–0.87, $P = 0.00046$), EPHA4 (HR = 0.69, 95% CI: 0.54–0.88, $P = 0.0026$), EPHA10 (HR = 0.54, 95% CI: 0.42–0.7, $P < 0.0001$), EFNA3 (HR = 0.81, 95% CI: 0.68–0.96, $P = 0.017$), EFNA4 (HR = 0.72, 95% CI: 0.6–0.86, $P = 0.00036$), and EFNA5 (HR = 0.61, 95% CI: 0.51–0.73, $P < 0.0001$) were associated with better RFS, whereas the high mRNA expression level of EPHA7 (HR = 1.49, 95% CI: 1.16–1.91, $P = 0.0016$) was associated with unfavorable RFS. The remaining EPHA/EFNA members were not associated with prognosis in luminal A BrCa.

In the luminal B subtype, high mRNA expression levels of EPHA1 (HR = 0.63, 95% CI: 0.52–0.76, $P < 0.0001$), EPHA2 (HR = 0.76, 95% CI: 0.63–0.93, $P = 0.0067$), EPHA4 (HR = 0.57, 95% CI: 0.42–0.79, $P = 0.00047$), EPHA5 (HR = 0.66, 95% CI: 0.48–0.89, $P = 0.0068$), EPHA6 (HR = 0.61, 95% CI: 0.45–0.85, $P = 0.0026$), EPHA10 (HR = 0.55, 95% CI: 0.4–0.75, $P = 0.00012$), and EFNA5 (HR = 0.67, 95% CI: 0.55–0.83, $P = 0.00015$) were associated with better RFS, whereas high mRNA expression levels of EFNA1 (HR = 1.38, 95% CI: 1.09–1.75, $P = 0.0065$), EFNA3 (HR = 1.39, 95% CI: 1.1–1.76, $P = 0.0057$), and EFNA4 (HR = 1.29, 95% CI: 1.05–1.6, $P = 0.016$) were associated with worse RFS. The remaining EPHA/EFNA members were not associated with prognosis in luminal B BrCa.

In HER2+ BrCa patients, high mRNA expression levels of EPHA1 (HR = 0.55, 95% CI: 0.37–0.8, $P = 0.0019$), EPHA6 (HR = 0.53, 95% CI: 0.29–0.94, $P = 0.028$), and EFNA5 (HR = 0.66, 95% CI: 0.45–0.97, $P = 0.033$) were correlated with better RFS. Only high mRNA expression of EPHA7 (HR = 2.32, 95% CI: 1.45–3.72, $P = 0.00031$) was associated with worse RFS. The remaining EPHA/EFNA members were not associated with prognosis in HER2-overexpressing BrCa. These results indicate that EPHA/EFNA may serve as potential prognostic predictors in BrCa patients with different subtype.

3.7. The Prognostic Value of EPHA/EFNA mRNA Expression in BrCa Patients Treated with Chemotherapy. The prognostic value of EPHA/EFNA expression was analyzed in BrCa patients receiving different chemotherapy regimens, including adjuvant chemotherapy, neoadjuvant chemotherapy, and no chemotherapy. As shown in Table 3, high expression of EPHA2 (HR = 1.49, 95% CI: 1.08–2.06, $P = 0.016$), EPHA3 (HR = 1.55, 95% CI: 1.12–2.15, $P = 0.008$), EPHA4 (HR = 1.95, 95% CI: 1.2–3.18, $P = 0.0064$), EFNA3 (HR = 1.96, 95% CI: 1.44–2.65, $P < 0.001$), and EFNA4 (HR = 1.4, 95% CI: 1.02–1.93, $P = 0.037$) and low expression of EPHA5 (HR = 0.43, 95% CI: 0.25–0.93, $P = 0.002$), EPHA6 (HR = 0.51, 95% CI: 0.27–0.95, $P = 0.03$), and EPHA10 (HR = 0.48, 95% CI: 0.29–0.8, $P = 0.0043$) were significantly correlated with poor RFS in BrCa patients treated with adjuvant chemotherapy. High expression levels of EPHA3 (HR = 1.95, 95% CI: 1–3.8, $P = 0.048$) and EPHA10 (HR = 2.43, 95% CI: 1.16–5.9, $P = 0.016$) and low expression of EPHA1 (HR = 0.39, 95% CI: 0.22–0.68, $P < 0.001$),

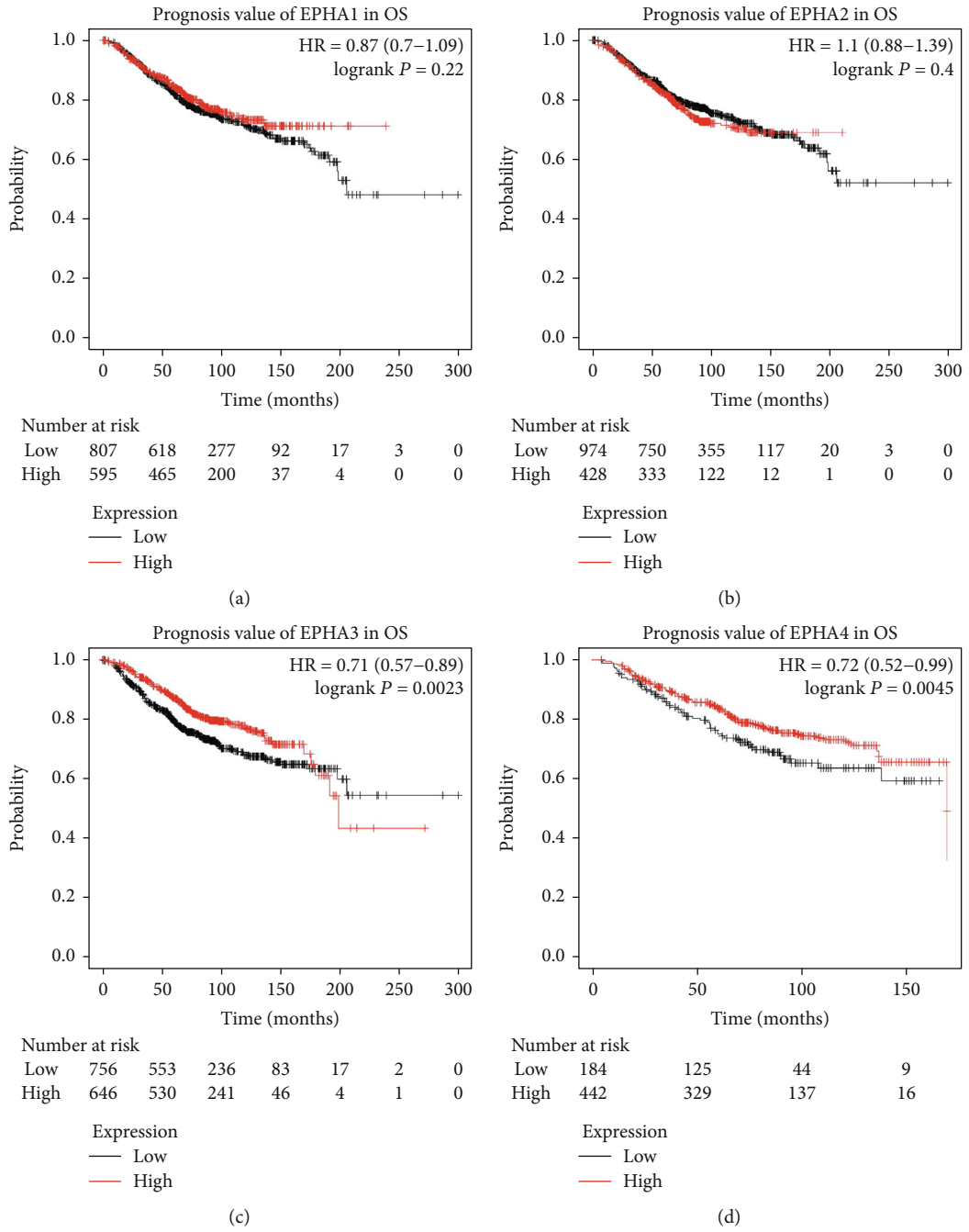

Figure 4: Continued.

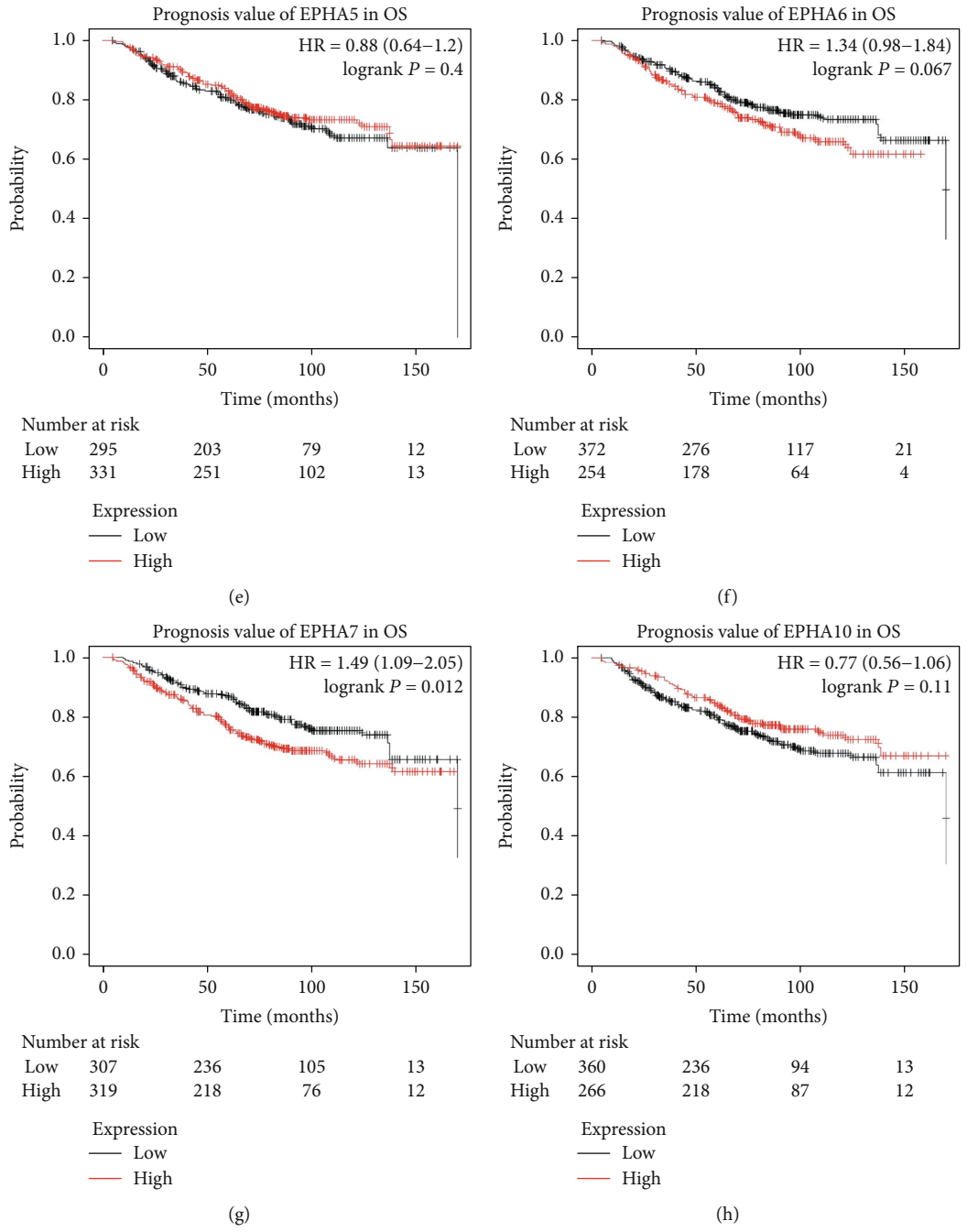

Figure 4: Continued.

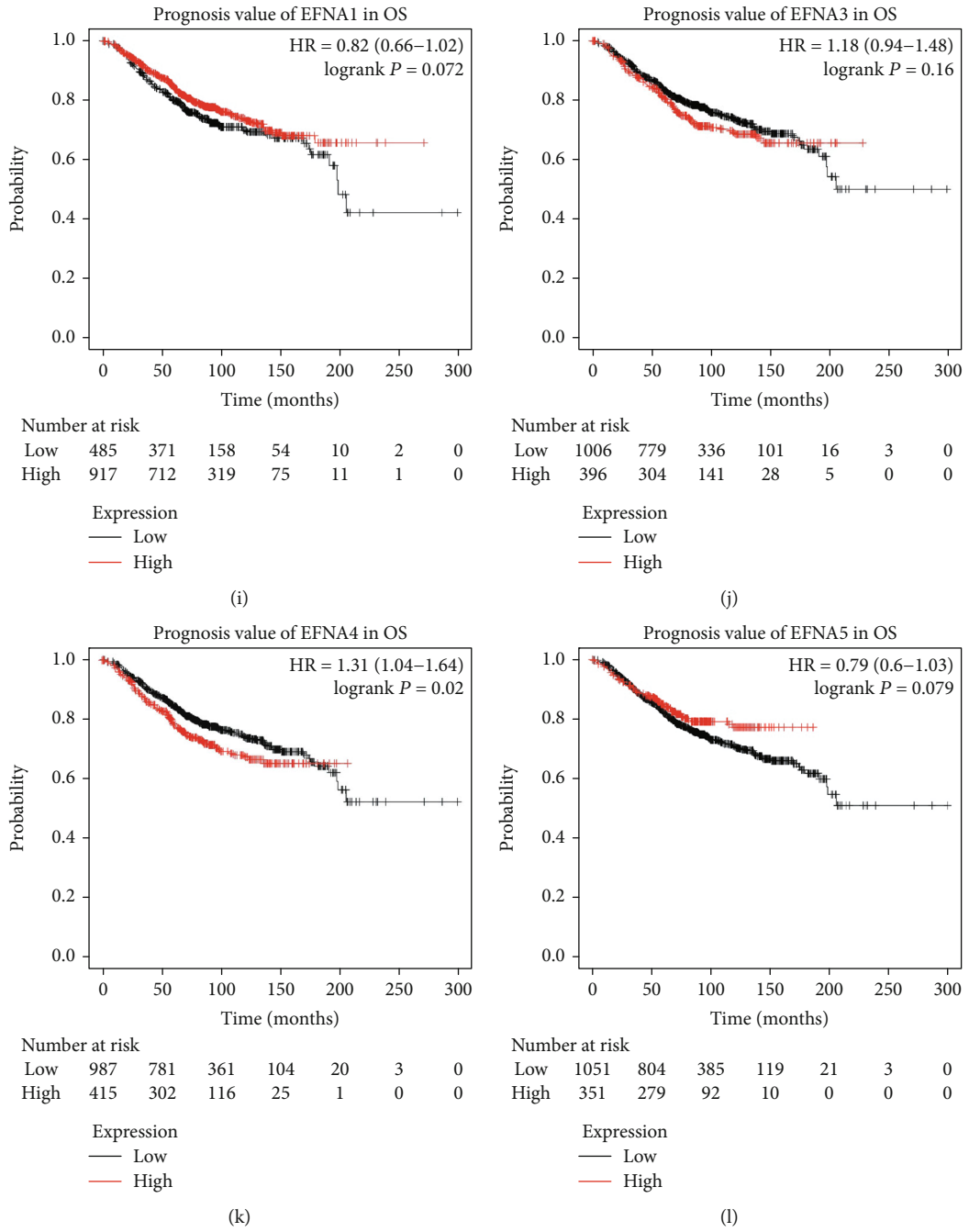

Figure 4: Survival analyses of EPHA/EFNA in breast cancer (overall survival (OS) in the Kaplan–Meier plotter). High mRNA expression of EPHA7 (g) and EFNA4 (k) was associated with poor OS. EPHA6 (f) expression was moderately associated with poor OS. High mRNA expression of EPHA3 (c) and EPHA4 (d) was significantly associated with better OS. The mRNA expression levels of the other EPHA/EFNA family members were not significantly correlated with OS.

EPHA2 (HR = 0.55, 95% CI: 0.31–0.97, $P = 0.037$), and EPHA5 (HR = 0.34, 95% CI: 0.16–0.77, $P = 0.004$) were significantly correlated with poor RFS in BrCa patients treated with neoadjuvant chemotherapy. These results indicate that EPHA/EFNA may serve as potential prognostic factors in BrCa patients treated with chemotherapy, suggesting that these genes are potential targets for the treatment of BrCa.

4. Discussion

The activities of the EPHA/EFNA family in BrCa are complex and paradoxical. The expression and prognostic value of EPHA/EFNA in BrCa have not been extensively investigated. In the present study, two cancer databases were used to analyze the transcriptional levels of EPHA/EFNA family

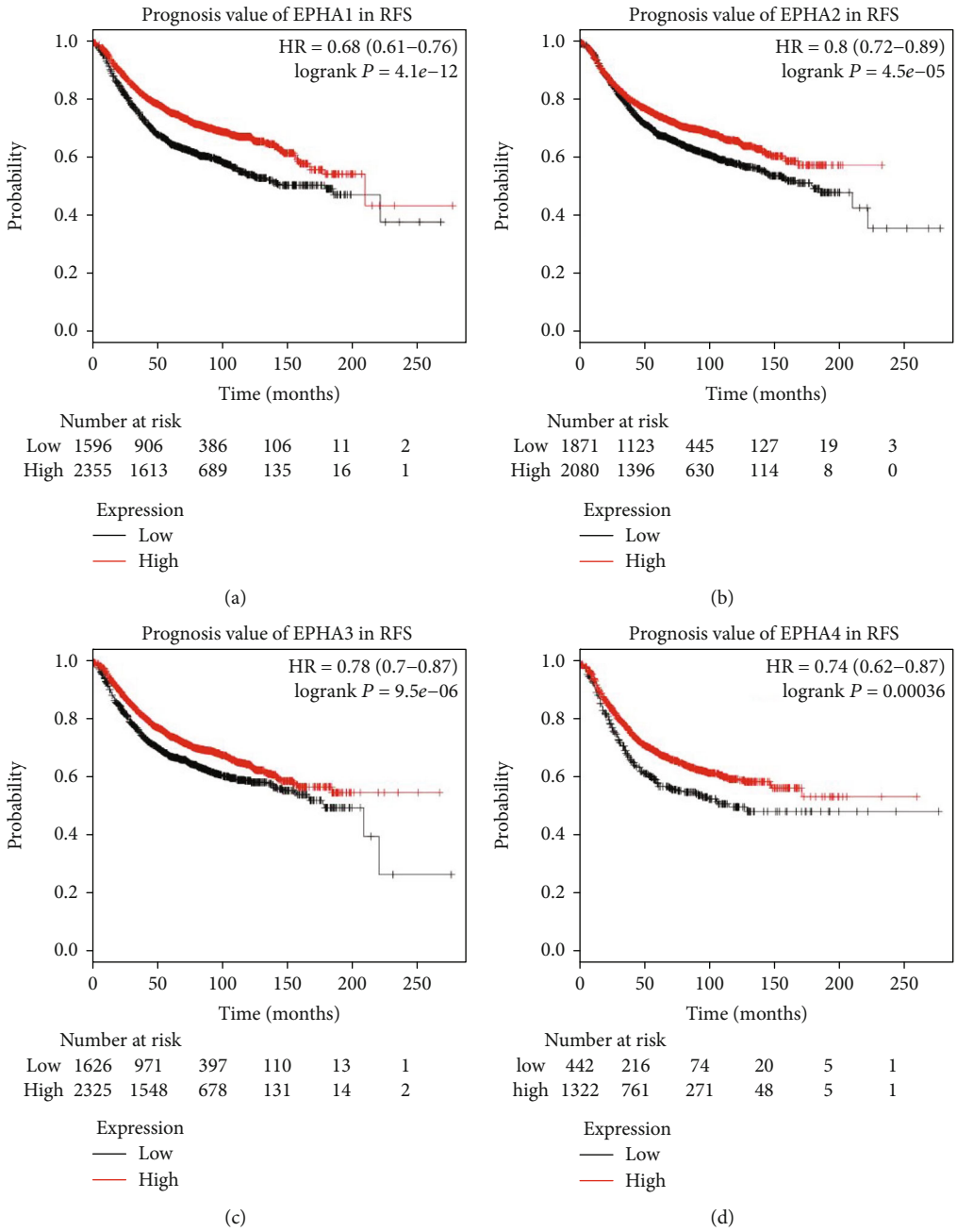

Figure 5: Continued.

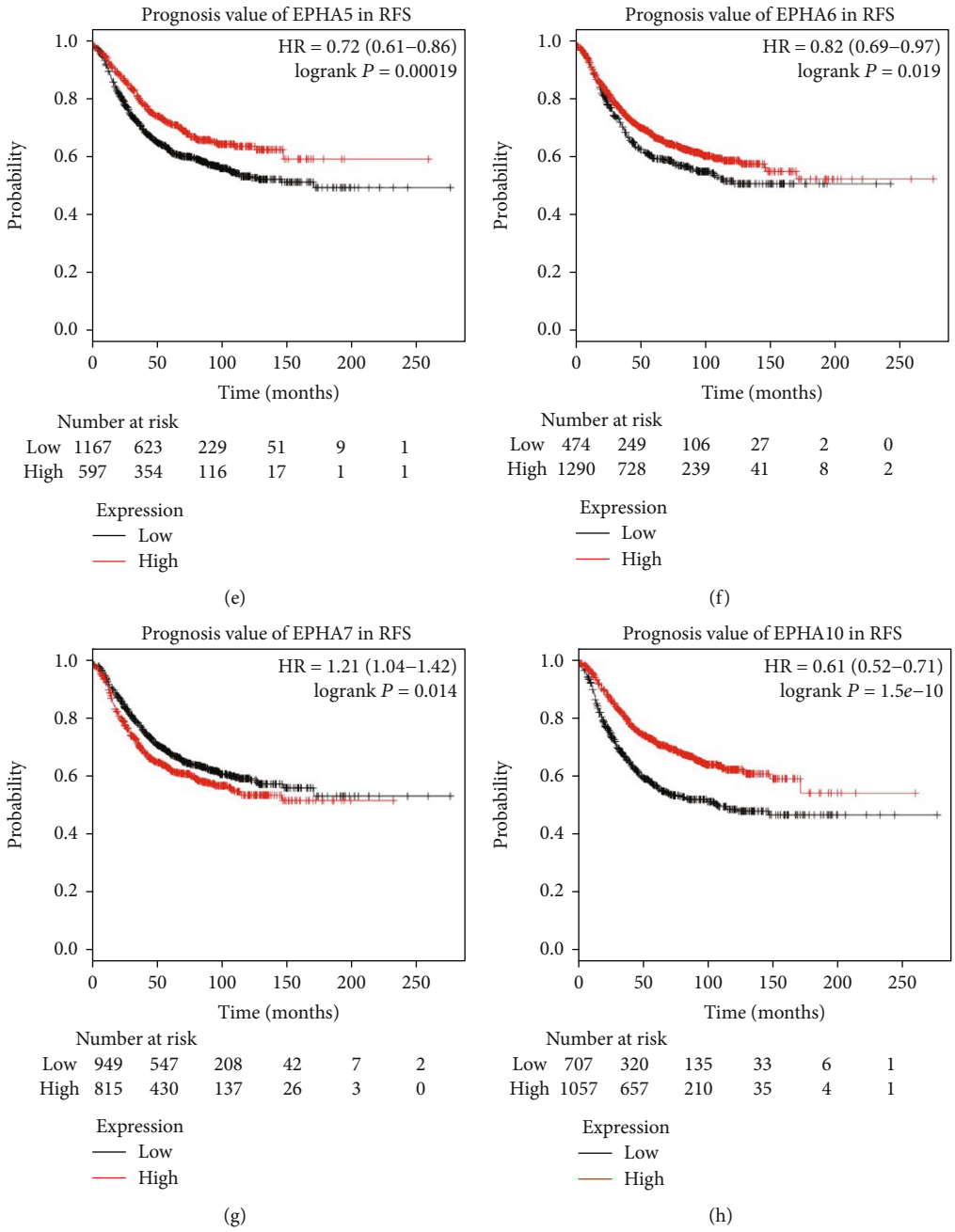

Figure 5: Continued.

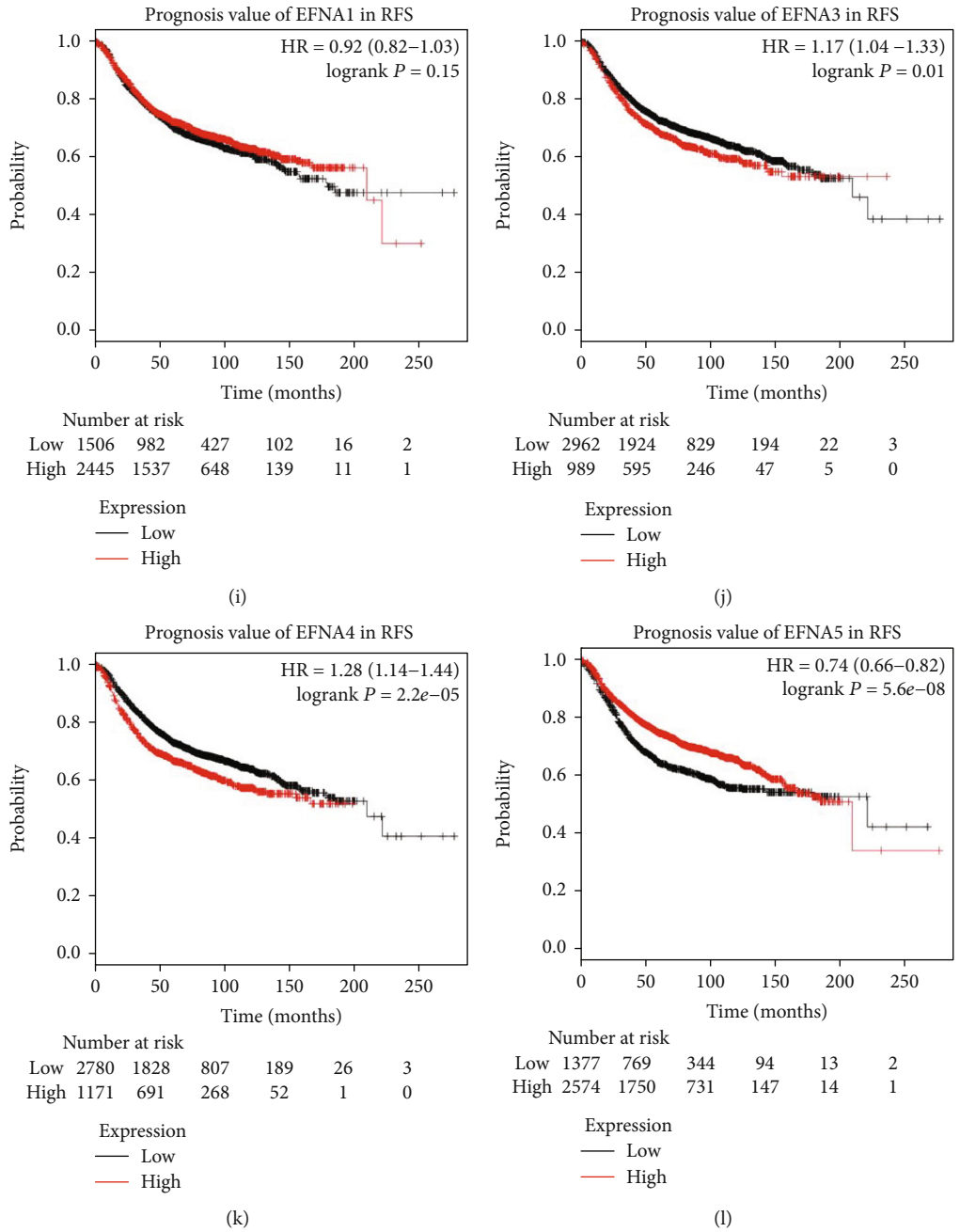

Figure 5: Survival analyses of the EPHA/EFNA in breast cancer (recurrence-free survival (RFS) in the Kaplan–Meier plotter). High mRNA expression of EPHA7 (g), EFNA3 (j) and EFNA4 (k) was associated with worse RFS. High mRNA expression of other EPHA/EFNA family members was significantly associated with better RFS except EFNA1.

members in BrCa and paracancerous tissues, as well as their association with the BrCa subtype and clinicopathological features. The genetic alterations of EPHA/EFNA family members, including mutations and putative CNAs, were analyzed using cBioPortal. The Kaplan–Meier plotter was used to analyze the association between the expression levels of EPHA/EFNA and OS or RFS in BrCa patients, as well as RFS in different BrCa subtypes, including patients undergoing chemotherapy. The results may be valuable in identifying new BrCa biomarkers for predicting prognosis or sensitivity to chemotherapy and suggest that EPHA and EFNA play both oncogenic and tumor suppressor roles in BrCa.

Expression analysis showed that the transcriptional levels of EPHA2, EPHA4, and EPHA5 were significantly lower in BrCa tissues than in nontumor tissues and EPHA1 and EPHA10 were significantly upregulated in BrCa tissues. Brantley et al. investigated EPHA/EFNA protein expression in BrCa and found that EPHA2, EPHA4, and EPHA7 were significantly upregulated in BrCa samples relative to normal controls. The discrepancy between the protein and mRNA

Table 2: Prognostic values of EPHA/EFNA mRNA expression for RFS in different BrCa intrinsic subtypes.

Subclasses	*N*	HR (95% CI)	*P*
EPHA1			
Basal like	618	0.61 (0.48–0.79)	0.0001
Luminal A	1,933	0.63 (0.53–0.75)	<0.0001
Luminal B	1,149	0.63 (0.52–0.76)	<0.0001
HER2 positive	251	0.55 (0.37–0.8)	0.0019
EPHA2			
Basal like	618	0.84 (0.65–1.09)	0.19
Luminal A	1,933	0.61 (0.51–0.72)	<0.0001
Luminal B	1,149	0.76 (0.63–0.93)	0.0067
HER2 positive	251	0.669 (0.42-1.03)	0.068
EPHA3			
Basal like	618	0.85 (0.65–1.11)	0.23
Luminal A	1,933	0.73 (0.61–0.87)	0.00046
Luminal B	1,149	1.21 (0.96–1.52)	0.1
HER2 positive	251	0.74 (0.5–1.08)	0.11
EPHA4			
Basal like	360	0.69 (0.49–0.96)	0.029
Luminal A	841	0.69 (0.54–0.88)	0.0026
Luminal B	407	0.57 (0.42–0.79)	0.00047
HER2 positive	156	0.74 (0.46–1.18)	0.21
EPHA5			
Basal like	360	0.45 (0.29–0.68)	0.00015
Luminal A	841	0.77 (0.59–1.01)	0.059
Luminal B	407	0.66 (0.48–0.89)	0.0068
HER2 positive	156	0.74 (0.46–1.19)	0.21
EPHA6			
Basal like	360	0.78 (0.53–1.15)	0.21
Luminal A	841	1.18 (0.91–1.52)	0.21
Luminal B	407	0.61 (0.45–0.85)	0.0026
HER2 positive	156	0.53 (0.29–0.94)	0.028
EPHA7			
Basal like	360	0.68 (0.49–0.95)	0.022
Luminal A	841	1.49 (1.16–1.91)	0.0016
Luminal B	407	0.84 (0.61–1.15)	0.27
HER2 positive	156	2.32 (1.45–3.72)	0.00031
EPHA10			
Basal like	360	0.71 (0.49–1.02)	0.064
Luminal A	841	0.54 (0.42–0.7)	<0.0001
Luminal B	407	0.55 (0.4–0.75)	0.00012
HER2 positive	156	1.28 (0.75–2.2)	0.37
EFNA1			
Basal like	618	1.36 (1.06–1.76)	0.016
Luminal A	1,933	0.89 (0.73–1.07)	0.21
Luminal B	1,149	1.38 (1.09–1.75)	0.0065
HER2 positive	251	1.45 (0.91–2.33)	0.12
EFNA3			
Basal like	618	1.29 (0.97–1.73)	0.082
Luminal A	1,933	0.81 (0.68–0.96)	0.017
Luminal B	1,149	1.39 (1.1–1.76)	0.0057
HER2 positive	251	1.43 (0.96–2.14)	0.081
EFNA4			
Basal like	618	1.53 (1.16–2.01)	0.0022
Luminal A	1,933	0.72 (0.6–0.86)	0.00036
Luminal B	1,149	1.29 (1.05–1.6)	0.016
HER2 positive	251	0.82 (0.51–1.3)	0.39
EFNA5			
Basal like	618	0.69 (0.54–0.89)	0.0037
Luminal A	1,933	0.61 (0.51–0.73)	<0.0001
Luminal B	1,149	0.67 (0.55–0.83)	0.00015
HER2 positive	251	0.66 (0.45–0.97)	0.033

levels of EPHA2 may be due to the fact that high levels of EPHA2 in tumor cells are the result of increased protein stability [31]. In certain malignant breast cell models, EPHA2 protein levels are 50- to 500-fold higher despite comparable levels of EphA2 mRNA [32, 33]. Discrepancies in EPHA2 expression may also result from the inclusion of both invasive and noninvasive breast tumors in the TCGA database. The mRNA level of EPHA2 is higher in invasive tumors than in normal breast cells; however, EPHA2 expression is lower in noninvasive breast tumors than in normal breast cells [34]. In this study, EFNA was upregulated in BrCa tissues except for EFNA5. EPHA2 is the dominant and the best characterized EPHA receptor in the BrCa. The role of EPHA2 in breast tumor progression is controversial, and conflicting data on the clinical significance of EPHA2 have been reported in different studies [35, 36]. For example, data show that EPHA2 is overexpressed in BrCa clinical samples; however, there is also evidence that EPHA2 acts as a tumor suppressor in breast carcinogenesis [17]. The malignant behavior of EPHA2 is mediated by ligand-independent signaling, and its antioncogenic properties are attributed to ligand-dependent signaling [37]. The crosstalk between EphA2 and BrCa oncogenic pathways promotes tumor cell malignancy in ligand-independent signaling [38, 39]. We found an inverse correlation between EPHA2 and the mRNA expression of A-type ligands in the database, as shown by the downregulation of EPHA2 and EFNA overexpression in BrCa cells. Ligand upregulation in the tumor indicates that the ligand-dependent pathway is dominant in the database. Downregulation of the EPHA2 receptor by the ephrin ligand may involve ligand-mediated receptor internalization. In general, EPHA2 negatively regulates tumor growth and migration after canonical ligand-induced EPHA2 signaling, which inhibits the AKT-mTORC1 and MAPK pathways [17]. The interaction between EPHA2 and its ligand activates a negative feedback pathway mediated by growth factor-activated RAS signaling [40]. EFNA1 is upregulated in noninvasive breast cells, thereby inhibiting invasiveness, whereas EFNA1 is downregulated in invasive tumors, allowing EPHA2 to participate in invasion [34].

Table 3: Prognostic value of EPHA/EFNA mRNA expression for RFS in BrCa patients undergoing chemotherapy.

Chemotherapies	Cases of RFS	HR	95% CI	*P* value
EPHA1				
Adjuvant chemotherapy	594	1.28	0.94–1.73	0.11
Neoadjuvant chemotherapy	223	0.39	0.22–0.68	<0.001
Nonchemotherapy	1,873	0.82	0.69–0.97	0.023
EPHA2				
Adjuvant chemotherapy	594	1.49	1.08–2.06	0.016
Neoadjuvant chemotherapy	223	0.55	0.31–0.97	0.037
Nonchemotherapy	1,873	0.8	0.66–0.98	0.029
EPHA3				
Adjuvant chemotherapy	594	1.55	1.12–2.15	0.008
Neoadjuvant chemotherapy	223	1.95	1–3.8	0.048
Nonchemotherapy	1,873	0.71	0.58–0.87	0.001
EPHA4				
Adjuvant chemotherapy	255	1.95	1.2–3.18	0.0064
Neoadjuvant chemotherapy	111	0.76	0.35–1.65	0.48
Nonchemotherapy	243	1.57	0.91–2.71	0.1
EPHA5				
Adjuvant chemotherapy	255	0.43	0.25–0.93	0.002
Neoadjuvant chemotherapy	111	0.34	0.16–0.77	0.004
Nonchemotherapy	243	0.69	0.39–1.22	0.2
EPHA6				
Adjuvant chemotherapy	255	0.51	0.27–0.95	0.03
Neoadjuvant chemotherapy	111	1.9	0.9–3.99	0.086
Nonchemotherapy	243	0.7	0.39–1.24	0.22
EPHA7				
Adjuvant chemotherapy	255	0.64	0.4–1.03	0.065
Neoadjuvant chemotherapy	111	1.86	0.82–4.23	0.13
Nonchemotherapy	243	1.42	0.82–2.46	0.21
EPHA10				
Adjuvant chemotherapy	255	0.48	0.29–0.8	0.0043
Neoadjuvant chemotherapy	111	2.43	1.16–5.9	0.016
Nonchemotherapy	243	0.62	0.35–1.11	0.1
EFNA1				
Adjuvant chemotherapy	594	0.82	0.6–1.11	0.2
Neoadjuvant chemotherapy	223	0.73	0.42–1.26	0.25
Nonchemotherapy	1,873	0.82	0.69–0.97	0.02
EFNA3				
Adjuvant chemotherapy	594	1.96	1.44–2.65	<0.001
Neoadjuvant chemotherapy	223	1.34	0.77–2.32	0.3
Nonchemotherapy	1,873	1.2	1–1.44	0.05
EFNA4				
Adjuvant chemotherapy	594	1.4	1.02–1.93	0.037
Neoadjuvant chemotherapy	223	0.71	0.41–1.23	0.22
Nonchemotherapy	1,873	0.86	0.73–1.02	0.077
EFNA5				
Adjuvant chemotherapy	594	0.85	0.6–1.19	0.34
Neoadjuvant chemotherapy	223	0.63	0.35–1.14	0.12
Nonchemotherapy	1,873	0.78	0.64–0.95	0.012

We also compared the differential transcriptional levels of EPHA/EFNA family members according to the different intrinsic subtypes of BrCa. The results showed differences in the expression patterns between the BrCa subtypes. EPHA3, EPHA5, EPHA6, and EPHA10 were expressed at the highest levels in luminal tissues, whereas HER2-positive and triple-negative tissues tended to express lower levels of EPHA3, EPHA5, EPHA6, and EPHA10. The highest mRNA expression levels of EFNA were found in triple-negative tissues except EFNA3, whereas the lowest mRNA expression levels of EFNA were found in the luminal subtype except EFNA1. Analysis of the bc-GenExMiner database showed that EPHA1, EPHA2, EPHA4, EPHA7, EFNA3, EFNA4, and EFNA5 were upregulated in ER- and PR-negative patients and positively correlated with triple-negative status. Consistent with this, some studies have shown that EPHA2 overexpression in BrCa is negatively correlated with ER and PR status [32, 41, 42]. EPHA2 overexpression decreases estrogen dependence and tamoxifen sensitivity [43], and EPHA2 is preferentially expressed in the basal-like phenotype [44]. In contrast, EPHA2 expression is also negatively regulated by ERα [41] and wild-type p53 [45]. The correlation of EPHA2 with HER2-positive status in the present study is consistent with the results of previous studies [39, 46], and EPHA2 is associated with resistance to trastuzumab therapy [47].

Analysis of the other EPHA/EFNA family members showed that EPHA1 was significantly upregulated in BrCa tissues compared to paracancerous tissues. A previous report showed that EPHA1 downregulation is associated with the invasiveness of breast carcinoma cells [34]. Consistent with the present profiling analyses, EPHA4 expression is associated with basal-like BrCa [48] and EPHA5 has been reported to act as a tumor suppressor, which may be related to abrrant promoter methylation [49]. Liu et al. [50] showed that EPHA7 mRNA was downregulated in BrCa specimens and loss of EPHA7 expression is more common in high-grade, early TNM-stage patients, without lymph node metastasis and correlation with negative HER2 status. Correspondingly, the present data also found downregulation of EPHA7 expression in BrCa specimens. EPHA10 is the only kinase-deficient Eph receptor [51]. The present data indicate that

EPHA10 is upregulated in BrCa tissues, which is similar with a previous study showing that EPHA10 expression is significantly lower in invasive than in noninvasive breast tumors, and is absent in normal cells [34]. Similar with the previous study, the present data showed EFNA4 was upregulated in TNBC [52]. EFNA4 is required for proper differentiation and polarization of mammary epithelial cells, signifying a biologic basis for the overexpression of EFNA4 in BrCa [53].

The most common cancer-related genetic alteration is the DNA CNAs. The OncoPrint feature of cBioPortal was used to determine the frequency of genetic alterations in the EPHA/EFNA family. The results showed that EPHA/EFNA was not frequently amplified. This finding suggests that the EPHA/EFNA family does not affect BrCa survival through DNA alterations, whereas it may affect BrCa through alterations of the interaction network. The copy-gain frequency of EFNA1, EFNA3, and EFNA4 accounts for a large proportion of BrCa samples, which may explain the significant upregulation of EFNA1, EFNA3, and EFNA4 in BrCa tissues from UALCAN.

The Kaplan–Meier plotter is a survey of public microarray data repositories of survival from 3955 patients with BrCa. Besides, in general patients, we analyzed the prognostic value of EPHA/EFNA mRNA in different BrCa subtypes and in BrCa patients treated with chemotherapy. Large-scale expression profiling studies revealed a negative association between the overexpression of EPHA2, EPHA4, and EPHA7 and overall and disease-free survival in BrCa [54]. Consistent with this report and its positive correlation with the triple-negative (TNBC) status in the bc-GenExMiner, the Kaplan–Meier plotter indicated that high EPHA7 mRNA expression predicted a poor OS and RFS in BrCa, especially in the HER2+ and luminal A subtypes. EFNA4 was associated with poor OS and RFS in BrCa, which is consistent with its positive correlation with the TNBC status. In particular, EFNA4 was associated with poor RFS in luminal B and basal-like subtypes and in BrCa patients treated with adjuvant chemotherapy. High mRNA expression of EPHA3 was significantly associated with better OS and RFS, especially in the luminal A subtype, which is consistent with its negative correlation with the TNBC status. However, in patients receiving adjuvant chemotherapy and neoadjuvant chemotherapy, EPHA3 is a risk factor. These results suggest that EPHA3, EPHA7 and EFNA4 are involved in BrCa development and could predict the prognosis of patients with BrCa in various subtypes and in those receiving different chemotherapy regimens. BrCa is a heterogeneous disease with subtype-dependent histopathological and clinical significance. In the subgroup analysis, the triple-negative (basal-like) subtype is a unique subtype of BrCa with a poor prognosis and more likely to develop chemoresistance [55]. In this study, we showed that low expression of EPHA1, EPHA4, EPHA5, and EPHA7 and high expression of EFNA1, EFNA4, and EFNA5 predicted an unfavorable prognosis in basal-like patients. Although we found that high mRNA expression of EPHA2 was associated with a longer RFS in patients with BrCa, it was a risk factor in the cohort receiving adjuvant chemotherapy. In fact, the RSK1/2-EphA2-GPRC5A oncogenic signaling association with platinum chemotherapy resistance has been reported in recent study [19] . Furthermore, in clinical practice, these biomarkers coupled with the specific role of EPHA/EFNA signaling in cancer could promote targeted therapeutics, as reported before [52, 56].

The present study has several limitations that should be addressed in future studies. First, mRNA levels are not always indicative of a functional protein and thus may not fully represent the protein expression of EPHA/EFNA [25]. Future studies should include protein detection techniques to accurately assess the protein levels. Second, the function of EPHA3 and EFNA7 in BrCa has not been studied in BrCa and needs to be investigated in the future. Third, multivariate analysis could not be used in the database to correct the associations between different clinicopathological features.

In conclusion, we showed that the EPHA/EFNA family is widely expressed in BrCa tumor cells. EPHA/EFNA were identified as prognostic factors and potential targets for BrCa, which may improve our understanding of the complexity and heterogeneity of BrCa at the molecular level. The present results may help develop tools to accurately predict prognosis and design customized therapies.

Abbreviations

EPHA: Ephrin A
HR: Hazard ratio
BrCa: Breast cancer
KM plotter: Kaplan–Meier plotter
RFS: Relapse-free survival
RTK: Tyrosine kinase receptor
CI: Confidence interval
ER: Estrogen receptor
PR: Progesterone receptor
HER2: Human epidermal growth factor receptor 2
SPSS: Statistical product and service solutions
OS: Overall survival.

Data Availability

The data used to support the findings of this study are included within the article.

Conflicts of Interest

The authors declare no potential conflicts of interest.

Authors' Contributions

ZL conceived and designed the study, analyzed the data, and wrote the manuscript. XW conceived and designed the study. ZL and KD performed the statistical analysis and analyzed the data. XL and CQ participated in data preparation, analysis, and figure preparation. ZHF revised the final manuscript. All authors have read and approved the manuscript for publication.

Acknowledgments

This study was financially supported by the Natural Science Foundation of Tianjin City, China (Grant no. 17JCYBJC25600), and the project of the Tianjin Health Bureau (grant no. 2014KZ124).

References

[1] H. Sung, J. Ferlay, R. Siegel, I. Soerjomataram, A. Jemal, and F. Bray, "Global cancer statistics 2020: GLOBOCAN estimates of incidence and mortality worldwide for 36 cancers in 185 countries," *CA: a Cancer Journal for Clinicians*, pp. 1–41, 2021.

[2] D. A. Berry, K. A. Cronin, S. K. Plevritis et al., "Effect of screening and adjuvant therapy on mortality from breast cancer," *The New England Journal of Medicine*, vol. 353, no. 17, pp. 1784–1792, 2005.

[3] Z. Du and C. M. Lovly, "Mechanisms of receptor tyrosine kinase activation in cancer," *Molecular Cancer*, vol. 17, no. 1, p. 58, 2018.

[4] E. M. Lisabeth, G. Falivelli, and E. B. Pasquale, "Eph receptor signaling and ephrins," *Cold Spring Harbor Perspectives in Biology*, vol. 5, no. 9, 2013.

[5] E. B. Pasquale, "Eph-ephrin bidirectional signaling in physiology and disease," *Cell*, vol. 133, pp. 38–52, 2008.

[6] Eph Nomenclature Committee, "Unified nomenclature for Eph family receptors and their ligands, the ephrins," *Cell*, vol. 90, no. 3, pp. 403-404, 1997.

[7] E. B. Pasquale, "Eph receptors and ephrins in cancer: bidirectional signalling and beyond," *Nature Reviews. Cancer*, vol. 10, no. 3, pp. 165–180, 2010.

[8] C.-T. J. Kou and R. P. Kandpal, "Differential expression patterns of Eph receptors and Ephrin ligands in human cancers," *BioMed Research International*, vol. 2018, Article ID 7390104, 23 pages, 2018.

[9] B. Mosch, B. Reissenweber, C. Neuber, and J. Pietzsch, "Eph receptors and ephrin ligands: important players in angiogenesis and tumor angiogenesis," *Journal of Oncology*, vol. 2010, Article ID 135285, 12 pages, 2010.

[10] D. J. Easty, S. P. Hill, M. Y. Hsu et al., "Up-regulation of ephrin-A1 during melanoma progression," *International Journal of Cancer*, vol. 84, no. 5, pp. 494–501, 1999.

[11] J. Walker-Daniels, K. Coffman, M. Azimi et al., "Overexpression of the EphA2 tyrosine kinase in prostate cancer," *Prostate*, vol. 41, no. 4, pp. 275–280, 1999.

[12] Y.-P. Xiang, T. Xiao, Q. G. Li et al., "Y772 phosphorylation of EphA2 is responsible for EphA2-dependent NPC nasopharyngeal carcinoma growth by Shp2/Erk-1/2 signaling pathway," *Cell Death & Disease*, vol. 11, no. 8, p. 709, 2020.

[13] Y. Liu, X. Zhang, Y. Qiu et al., "Clinical significance of EphA2 expression in squamous-cell carcinoma of the head and neck," *Journal of Cancer Research and Clinical Oncology*, vol. 137, no. 5, pp. 761–769, 2011.

[14] R. Govindan, L. Ding, M. Griffith et al., "Genomic landscape of non-small cell lung cancer in smokers and never-smokers," *Cell*, vol. 150, no. 6, pp. 1121–1134, 2012.

[15] E. Oricchio, G. Nanjangud, A. L. Wolfe et al., "The Eph-receptor A7 is a soluble tumor suppressor for follicular lymphoma," *Cell*, vol. 147, no. 3, pp. 554–564, 2011.

[16] J. Walker-Daniels, A. R. Hess, M. J. C. Hendrix, and M. S. Kinch, "Differential regulation of EphA2 in normal and malignant cells," *The American Journal of Pathology*, vol. 162, no. 4, pp. 1037–1042, 2003.

[17] L. W. Noblitt, D. S. Bangari, S. Shukla et al., "Decreased tumorigenic potential of EphA2-overexpressing breast cancer cells following treatment with adenoviral vectors that express EphrinA1," *Cancer Gene Therapy*, vol. 11, no. 11, pp. 757–766, 2004.

[18] Y. Wang, Y. Liu, G. Li et al., "Ephrin type-A receptor 2 regulates sensitivity to paclitaxel in nasopharyngeal carcinoma via the phosphoinositide 3-kinase/Akt signalling pathway," *Molecular Medicine Reports*, vol. 11, no. 2, pp. 924–930, 2015.

[19] L. Moyano-Galceran, E. A. Pietilä, S. P. Turunen et al., "Adaptive RSK-EphA2-GPRC5A signaling switch triggers chemotherapy resistance in ovarian cancer," *EMBO Molecular Medicine*, vol. 12, no. 4, article e11177, 2020.

[20] T. Barrett, S. E. Wilhite, P. Ledoux et al., "NCBI GEO: archive for functional genomics data sets—update," *Nucleic Acids Research*, vol. 41, no. D1, pp. D991–D995, 2012.

[21] The Cancer Genome Atlas Research Network, J. N. Weinstein, E. A. Collisson et al., "The Cancer Genome Atlas Pan-Cancer analysis project," *Nature Genetics*, vol. 45, no. 10, pp. 1113–1120, 2013.

[22] D. S. Chandrashekar, B. Bashel, S. A. H. Balasubramanya et al., "UALCAN: a portal for facilitating tumor subgroup gene expression and survival analyses," *Neoplasia*, vol. 19, no. 8, pp. 649–658, 2017.

[23] P. Jézéquel, M. Campone, W. Gouraud et al., "bc-GenExMiner: an easy-to-use online platform for gene prognostic analyses in breast cancer," *Breast Cancer Research and Treatment*, vol. 131, no. 3, pp. 765–775, 2012.

[24] P. Jezequel, J. S. Frenel, L. Campion et al., "bc-GenExMiner 3.0: new mining module computes breast cancer gene expression correlation analyses," *Database*, vol. 2013, article bas060, 2013.

[25] J. Mei, L. Hao, X. Liu et al., "Comprehensive analysis of peroxiredoxins expression profiles and prognostic values in breast cancer," *Biomarker Research*, vol. 7, no. 1, p. 16, 2019.

[26] B. Győrffy, A. Lanczky, A. C. Eklund et al., "An online survival analysis tool to rapidly assess the effect of 22,277 genes on breast cancer prognosis using microarray data of 1,809 patients," *Breast Cancer Research and Treatment*, vol. 123, no. 3, pp. 725–731, 2010.

[27] E. Cerami, J. Gao, U. Dogrusoz et al., "The cBio cancer genomics portal: an open platform for exploring multidimensional cancer genomics data," *AACR.*, vol. 2, no. 5, pp. 401–404, 2012.

[28] J. Gao, B. A. Aksoy, U. Dogrusoz et al., "Integrative analysis of complex cancer genomics and clinical profiles using the cBioPortal," *Science Signaling*, vol. 6, no. 269, p. pl1, 2013.

[29] W. Goto, S. Kashiwagi, K. Takada et al., "Significance of intrinsic breast cancer subtypes on the long-term prognosis after neoadjuvant chemotherapy," *Journal of Translational Medicine*, vol. 16, no. 1, p. 307, 2018.

[30] A. Goldhirsch, W. C. Wood, A. S. Coates et al., "Strategies for subtypes–dealing with the diversity of breast cancer: highlights of the St Gallen International Expert Consensus on the Primary Therapy of Early Breast Cancer 2011," *Annals of Oncology*, vol. 22, no. 8, pp. 1736–1747, 2011.

[31] J. Walker-Daniels, D. J. Riese, and M. S. Kinch, "c-Cbl-dependent EphA2 protein degradation is induced by ligand binding," *Molecular Cancer Research*, vol. 1, no. 1, pp. 79–87, 2002.

[32] D. P. Zelinski, N. D. Zantek, J. C. Stewart, A. R. Irizarry, and M. S. Kinch, "EphA2 overexpression causes tumorigenesis of

mammary epithelial cells," *Cancer Research*, vol. 61, no. 5, pp. 2301–2306, 2001.

[33] N. D. Zantek, J. Walker-Daniels, J. Stewart et al., "MCF-10A-NeoST: a new cell system for studying cell-ECM and cell-cell interactions in breast cancer," *Clinical Cancer Research*, vol. 7, no. 11, pp. 3640–3648, 2001.

[34] B. P. Fox and R. P. Kandpal, "Invasiveness of breast carcinoma cells and transcript profile: Eph receptors and ephrin ligands as molecular markers of potential diagnostic and prognostic application," *Biochemical and Biophysical Research Communications*, vol. 318, no. 4, pp. 882–892, 2004.

[35] M. Pan, "Overexpression ofEphA2gene in invasive human breast cancer and its association with hormone receptor status," *Journal of Clinical Oncology*, vol. 23, 16_suppl, p. 9583, 2005.

[36] K. Ogawa, R. Pasqualini, R. A. Lindberg, R. Kain, A. L. Freeman, and E. B. Pasquale, "The ephrin-A1 ligand and its receptor, EphA2, are expressed during tumor neovascularization," *Oncogene*, vol. 19, no. 52, pp. 6043–6052, 2000.

[37] H. Miao, D. Q. Li, A. Mukherjee et al., "EphA2 mediates ligand-dependent inhibition and ligand-independent promotion of cell migration and invasion via a reciprocal regulatory loop with Akt," *Cancer Cell*, vol. 16, no. 1, pp. 9–20, 2009.

[38] D. M. Brantley-Sieders, G. Zhuang, D. Hicks et al., "The receptor tyrosine kinase EphA2 promotes mammary adenocarcinoma tumorigenesis and metastatic progression in mice by amplifying ErbB2 signaling," *The Journal of Clinical Investigation*, vol. 118, no. 1, pp. 64–78, 2008.

[39] G. Zhuang, D. Brantley-Sieders, D. Hicks, W. Fang, Y. Hwang, and J. Chen, "Interactions of EphA2 and HER2 promote tumor progression and anti-HER2 resistance," *AACR.*, vol. 68, 2008.

[40] M. Macrae, R. M. Neve, P. Rodriguez-Viciana et al., "A conditional feedback loop regulates Ras activity through EphA2," *Cancer Cell*, vol. 8, no. 2, pp. 111–118, 2005.

[41] D. P. Zelinski, N. D. Zantek, J. Walker-Daniels, M. A. Peters, E. J. Taparowsky, and M. S. Kinch, "Estrogen and Myc negatively regulate expression of the EphA2 tyrosine kinase," *Journal of Cellular Biochemistry*, vol. 85, no. 4, pp. 714–720, 2002.

[42] A. A. Kamat, D. Coffey, W. M. Merritt et al., "EphA2 overexpression is associated with lack of hormone receptor expression and poor outcome in endometrial cancer," *Cancer*, vol. 115, no. 12, pp. 2684–2692, 2009.

[43] M. Lu, K. D. Miller, Y. Gokmen-Polar, M. H. Jeng, and M. S. Kinch, "EphA2 overexpression decreases estrogen dependence and tamoxifen sensitivity," *Cancer Research*, vol. 63, no. 12, pp. 3425–3429, 2003.

[44] F. Huang, K. Reeves, X. Han et al., "Identification of candidate molecular markers predicting sensitivity in solid tumors to dasatinib: rationale for patient selection," *Cancer Research*, vol. 67, no. 5, pp. 2226–2238, 2007.

[45] M. Dohn, J. Jiang, and X. Chen, "Receptor tyrosine kinase EphA2 is regulated by p53-family proteins and induces apoptosis," *Oncogene*, vol. 20, no. 45, pp. 6503–6515, 2001.

[46] V. M. Youngblood, L. C. Kim, D. N. Edwards et al., "The Ephrin-A1/EPHA2 signaling axis regulates glutamine metabolism in HER2-positive breast cancer," *Cancer Research*, vol. 76, no. 7, pp. 1825–1836, 2016.

[47] G. Zhuang, D. M. Brantley-Sieders, D. Vaught et al., "Elevation of receptor tyrosine kinase EphA2 mediates resistance to trastuzumab therapy," *Cancer Research*, vol. 70, no. 1, pp. 299–308, 2010.

[48] I. Y. Hachim, M. Villatoro, L. Canaff et al., "Transforming growth factor-beta regulation of ephrin type-A receptor 4 signaling in breast cancer cellular migration," *Scientific Reports*, vol. 7, no. 1, p. 14976, 2017.

[49] D. Y. Fu, Z. M. Wang, B. L. Wang et al., "Frequent epigenetic inactivation of the receptor tyrosine kinase EphA5 by promoter methylation in human breast cancer," *Human Pathology*, vol. 41, no. 1, pp. 48–58, 2010.

[50] Z. Liu, Q. Zhang, X. Li, and Z. Tao, "Aberrant expression of receptor tyrosine kinase EphA7 in breast cancers," *International Journal of Clinical and Experimental Pathology*, vol. 9, no. 7, pp. 7352–7358, 2016.

[51] K. K. Murai and E. B. Pasquale, "'Eph'ective signaling: forward, reverse and crosstalk," *Journal of Cell Science*, vol. 116, no. 14, pp. 2823–2832, 2003.

[52] M. Damelin, A. Bankovich, A. Park et al., "Anti-EFNA4 calicheamicin conjugates effectively target triple-negative breast and ovarian tumor-initiating cells to result in sustained tumor regressions," *Clinical Cancer Research*, vol. 21, no. 18, pp. 4165–4173, 2015.

[53] A. Burleigh, S. McKinney, J. Brimhall et al., "A co-culture genome-wide RNAi screen with mammary epithelial cells reveals transmembrane signals required for growth and differentiation," *Breast Cancer Research*, vol. 17, no. 1, p. 4, 2015.

[54] D. M. Brantley-Sieders, A. Jiang, K. Sarma et al., "Eph/ephrin profiling in human breast cancer reveals significant associations between expression level and clinical outcome," *PLoS One*, vol. 6, no. 9, article e24426, 2011.

[55] S. Boichuk, A. Galembikova, A. Sitenkov et al., "Establishment and characterization of a triple negative basal-like breast cancer cell line with multi-drug resistance," *Oncology Letters*, vol. 14, no. 4, pp. 5039–5045, 2017.

[56] J. W. Lee, H. D. Han, M. M. K. Shahzad et al., "EphA2 immunoconjugate as molecularly targeted chemotherapy for ovarian carcinoma," *Journal of the National Cancer Institute*, vol. 101, no. 17, pp. 1193–1205, 2009.

Hindawi
BioMed Research International
Volume 2021, Article ID 5526327, 7 pages
https://doi.org/10.1155/2021/5526327

Research Article

The Prognostic Significance of Hsp70 in Patients with Colorectal Cancer Patients: A PRISMA-Compliant Meta-Analysis

Guangyu Gao,[1] **Songtao Liu**,[2] **Zhen Yao**,[1] **Yanyan Zhan**,[1] **Wenyue Chen**,[1] **and Yulong Liu**[1,3,4]

[1]*Department of Nuclear Accident Medical Emergency, The Second Affiliated Hospital of Soochow University, Suzhou 215004, China*
[2]*Department of Ultrasound, The Second Affiliated Hospital of Soochow University, Suzhou 215004, China*
[3]*State Key Laboratory of Radiation Medicine and Protection, School of Radiation Medicine and Protection, Soochow University, Suzhou 215123, China*
[4]*Collaborative Innovation Center of Radiological Medicine of Jiangsu Higher Education Institutions, Suzhou 215123, China*

Correspondence should be addressed to Yulong Liu; yulongliu2002@suda.edu.cn

Received 1 February 2021; Revised 31 March 2021; Accepted 6 April 2021; Published 16 April 2021

Academic Editor: Ning Cao

Background. Hsp70 (heat shock protein 70) plays a key role in carcinogenesis and cancer progression. However, the relationship between the Hsp70 expression level and the colorectal cancer patient survival is unknown. This study is aimed at investigating the relationship between Hsp70 and the prognosis of colorectal carcinoma patients. *Methods*. PubMed, Web of Science, and Embase were used for systematic computer literature retrieval. Stata SE14.0 software was used for quantitative meta-analysis. Besides, data was extracted from selected articles. Relationships between Hsp70 expression level and prognosis were further studied. The hazard ratios (HRs) and 95% confidence intervals (95% CIs) were also computed. *Results*. A total of 11 potentially eligible studies with 2269 patients were identified in 10 tumors from PubMed, Web of Science, and Embase. Hsp70 overexpression was associated with poor overall survival (OS) and disease-free survival (DFS) in colorectal carcinoma patients (HRs, 0.65 (95% CI: 0.52-0.78) and 0.77 (95% CI: 0.23-1.32), respectively). *Conclusions*. Hsp70 overexpression can predict poor survival in colorectal cancer patients.

1. Introduction

Colorectal cancer (CRC) is a serious health problem worldwide. The response and overall survival of advanced colorectal cancer patients are very poor compared with the early stage. While colorectal cancer can be treated through surgery, tumor recurrence develops in about 25% to 40% of patients [1]. Surgical tumor resection is the major treatment method for local advanced colorectal cancer. However, there is no effective treatment for metastatic tumors, especially those that cannot be surgically removed and those with poor chemotherapy and radiotherapy effects [2].

Hsps are well-maintained molecules overexpressed in cells subjected to various stress stimuli (heat shock or disruption of homeostasis). Hsps act as molecular chaperones assisting protein folding in normal metabolic conditions and promoting protein repair and stabilization during molecular stress [3]. Hsps are essential in cellular defense against carcinogenesis [4]. Their tumorigenesis role includes oncogenic protein stabilization, programmed cell death, replicative senescence inhibition, tumor angiogenesis induction, invasion, and metastasis activation [5]. Interestingly, most Hsp70 expression studies are based on colorectal cancer cell lines and xenografts and not actual biopsy samples [6].

Studies have shown that Hsp70 expression is upregulated in various carcinoma tissues and could be a potential biomarker [7]. Besides, previous studies have reported that Hsp70 overexpression is associated with poor survival in some cancers, including breast carcinoma [8–10], esophageal adenocarcinoma [11], non-small-cell lung cancer [12],

prostate cancer [13, 14], gastric cancer [15, 16], leukemia [17], hepatocellular carcinoma [18, 19], pancreatic cancer [20], and colon cancer [21–23]. However, no study has reported the relationship between the Hsp70 expression level and prognosis of colorectal cancer patients. Therefore, in this study, the relationship between Hsp70 and the prognosis of colorectal carcinoma patients was investigated.

2. Methods

2.1. Literature Retrieval. Studies published between July 9, 1989 and July 9, 2020 were downloaded from PubMed, Web of Science, and Embase. Text word and MeSH strategy were used for the retrieval. The following terms were used: heat shock protein 70 OR Hsp70 AND colorectal AND cancer OR carcinoma OR malignant OR neoplasm OR tumor. Besides, the reference lists of the retrieved studies were manually screened for additional literature retrieval.

2.2. Selection Criteria. Two researchers independently extracted the studies. The inclusion criteria were as follows: (a) studies showing the relationship between the Hsp70 expression level and OS or DFS in colorectal carcinoma, (b) studies describing the relationship between clinicopathological parameters and Hsp70 expression levels in human carcinoma tissues, (c) studies grouping patients (two groups) based on Hsp70 expression level, and (d) if hazard ratios and 95% confidence intervals could be calculated. The exclusion criteria were as follows: (a) studies with insufficient information to compute hazard ratios and 95% confidence intervals or (b) letters, case reports, expert opinions, and reviews or (c) *in vitro* or animal studies. Besides, only English researches were included.

2.3. Data Extraction. Two authors (GY and ZY) extracted data from identified articles that complied with the standards, and a third researcher resolved different opinions. The first author, country, year of publication, tumor type, sample size, study design, cut-off value, follow-up time, methods used, and the outcome were recorded. Hazard ratios with 95% confidence intervals for overall survival or disease-free survival were also determined. Engauge Digitizer version 4.1 was used to calculate prognosis after drawing the Kaplan-Meier curves [24].

2.4. Statistical Methods. The prognostic value of the Hsp70 expression level in colorectal cancer patients was determined by estimating the hazard ratios between the upregulated and downregulated Hsp70 tissue groups for overall survival or disease-free survival. The 95% confidence intervals and the heterogeneity were also calculated and evaluated based on P value and I^2. Furthermore, $I^2 > 50\%$ indicated significant heterogeneity. The random-effects model was used to determine the total hazard ratios. A fixed-effects model was used when $I^2 \leq 50\%$ (moderate heterogeneity). The Stata 14.0 software was used for all data analyses.

3. Results

3.1. Included Studies and Characteristics. The research procedure is shown in Figure 1. A total of 1085 articles were selected after screening Web of Science, Embase, and PubMed. A total of 890 studies were excluded after the title and abstract search. Moreover, 142 articles were excluded since they did not meet the inclusion criteria. Another 42 records had insufficient data for HR calculation. Finally, 11 articles with 2269 patients were used [21–23, 25–32]. The 11 articles had a sample size of 167 to 256 (average 206) (Table 1). Besides, the 11 articles were published between 2009 and 2020 from various countries, including Hungary (4), Korea (2), and Britain, Greece, and Jordan (1 each). Most articles used immunohistochemistry (IHC) to determine the Hsp70 expression level.

3.2. High Hsp70 Expression Is Associated with Poor OS. Systematic meta-analysis was used to assess the relationship between the Hsp70 expression level and OS in colorectal cancer patients. Meta-analysis of nine articles with 1917 colorectal cancer patients showed that Hsp70 expression was significantly associated with OS (HR 0.65; 95% CI: 0.52-0.78; Figure 2), indicating that Hsp70 overexpression is associated with poor survival. A fixed-effects model was used since no significant heterogeneity was found ($I^2 = 0\%$) in the identified studies.

3.3. High Hsp70 Expression Is Associated with Poor DFS. The relationship between Hsp70 expression and disease-free survival of 352 cancer patients was also investigated (Figure 3). A fixed-effects model was used since there was no significant heterogeneity ($I^2 = 0$). The upregulated Hsp70 was associated with poor disease-free survival (HR = 0.77, 95% CI: 0.23-1.32).

3.4. Publication Bias. Begg's and Egger's tests were used to evaluate the publication bias via funnel plot symmetry estimation. There was no significant asymmetry of the funnel plots. Therefore, this study has no significant publication bias [33] (Figures 4 and 5). A sensitivity analysis was also conducted to verify the credibility of hazard ratios for overall survival. There were no significant impacts on HRs after excluding any one study, suggesting result reliability (Figure 6).

4. Discussion

In recent years, potential prognostic biomarkers have been identified to improve the efficacy and survival rate. However, the prognosis of most cancers is relatively low. Therefore, high/positive tissue Hsp70 expression could be associated with the prognosis of colorectal carcinoma patients. Furthermore, previous studies have concluded that Hsp70 expression has biological and clinical significance. However, various cancers have different results. Hsp70 is significantly upregulated in gastric, breast, and prostate carcinoma compared with the normal tissues. In contrast, some articles have indicated that Hsp70 is significantly downregulated in cancer tissues compared with normal tissues in malignant

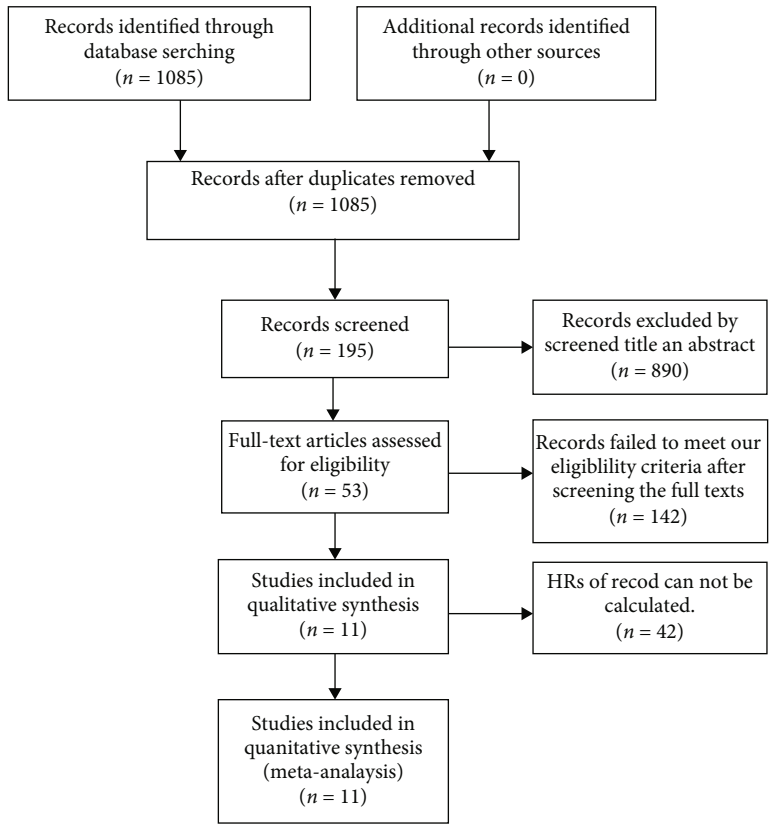

Figure 1: The flow chart of the selection process in the meta-analysis.

Table 1: Main characteristics of the 11 studies in the meta-analysis.

Study	Country	Year	Sample	Study design	Sizes	Cut-off value	Gender (female/male)	Follow-up time (month)	Tumor stage (I/II/III/IV)	Outcome	Method	NOS
Dundas, S. et al.	Britain	2005	CRC	R	231	25%	NA	0-120	NA	OS	IHC	7
Graf, L. et al.	Hungary	2018	CRC	R	232	20%	112/120	0-60	NA	OS	IHC	7
Jubran, R. et al.	Hungary	2017	CRC	R	227	NR	121/106	0-60	30/40/60/97	OS	IHC	8
Kocsis, J. et al.	Hungary	2009	CRC	R	178	NR	89/88	33 (24-44)	25/26/60/67	OS	IHC	9
Kocsis, J. et al.	Hungary	2010	CRC	R	254	NR	NA	33.0 (23.5–43.5)	80/60/110/4	OS	IHC	8
Lazaris, A. et al.	Greece	1997	CRC	R	128	25%	NA	44.76 (0-222.36)	NA	OS	IHC	9
Jogi, A. et al.	Sweden	2009	CRC	R	196	25%	NA	0-60	NA	OS	IHC	8
Shotar, A. et al.	Jordan	2005	CRC	R	215	20%	112/103	6.88 (0.64-17.05)	40/32/79/64	OS	IHC	8
Sun, X. et al.	Sweden	1997	CRC	R	256	20%	122/134	0-156	NA	OS	IHC	7
Kim, J. et al.	Korea	2014	CRC	R	167	25%	NA	29 (0-120)	NA	DFS	IHC	9
Oh, H. et al.	Korea	2017	CRC	R	185	NR	90/95	51.1 (3.1-57.1)	NA	DFS	IHC	9

Abbreviation: CRC: colorectal cancer; R: retrospective analysis; NR: not report; OS: overall survival; DFS: disease-free survival; IHC: immunohistochemistry; NA: not available; NOS: Newcastle-Ottawa Scale.

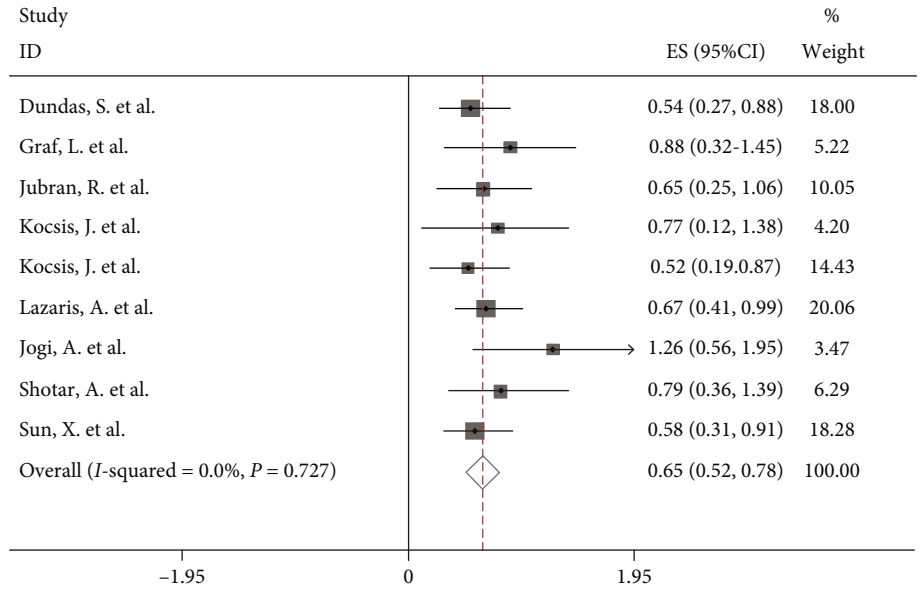

Figure 2: The relationship between Hsp70 expression and overall survival (OS) in human colorectal cancer.

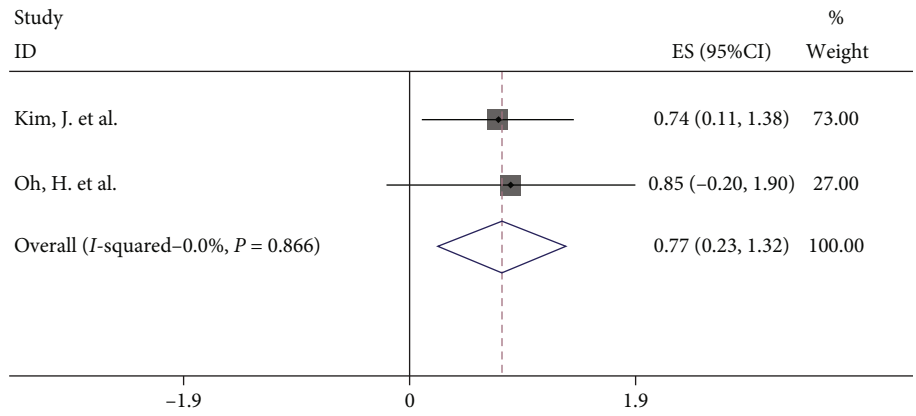

Figure 3: Forest plot indicating the association between Hsp70 expression and DFS.

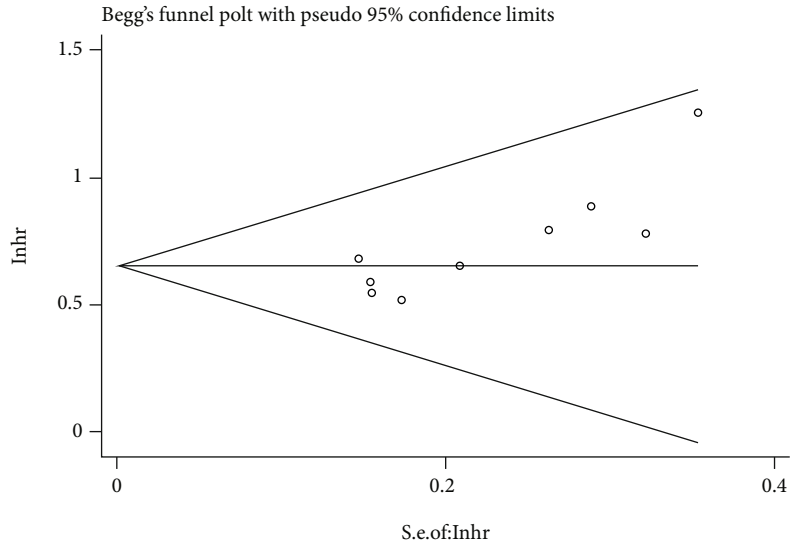

Figure 4: Begg and Egger tests of OS.

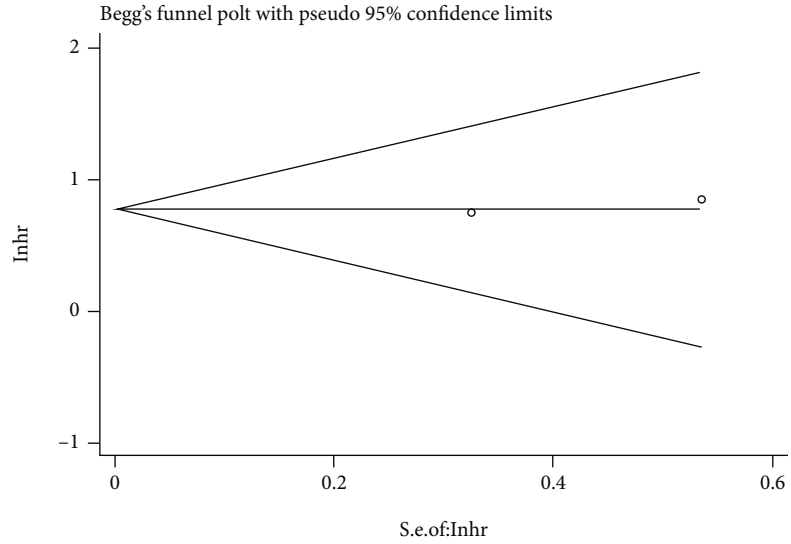

Figure 5: Begg and Egger tests of DFS.

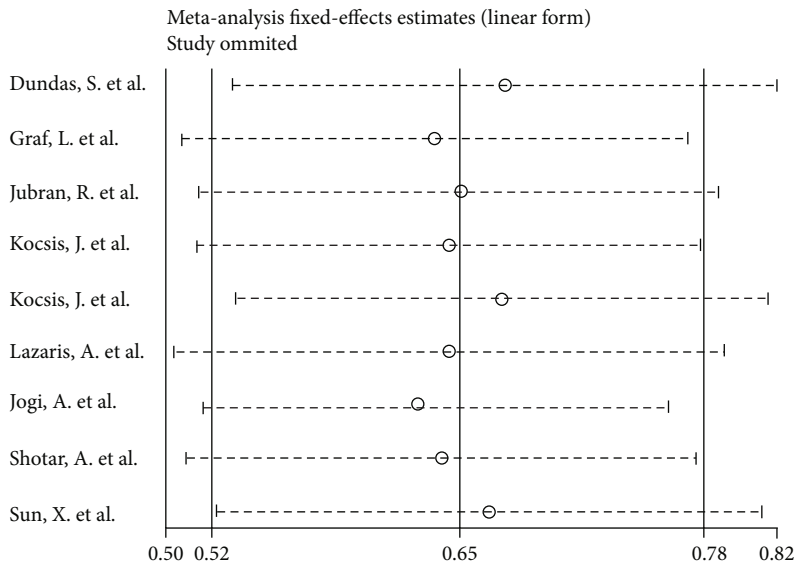

Figure 6: Sensitivity analysis evaluating the impact of each research.

melanoma, colon cancer, and urothelial bladder cancer. The different results could be due to the various interactions between Hsp70 and other human gene products in different organs. Recent articles have verified that Hsp70 overexpression is associated with poor survival in breast cancer, colorectal cancer, melanoma, gastric cancer, hepatocellular carcinoma, non-small-cell lung cancer, ovarian cancer, and testicular cancer. Besides, Hsp70 overexpression is not associated with esophageal adenocarcinoma and esophageal squamous cell cancer, while it is associated with better survival in urinary bladder cancer and pancreatic cancer. Sun et al. reported no significant relationships between Hsp with sex or age of patients, tumor site, Duke's stage, growth pattern, or differentiation [34]. Shotar also reported that there is no significant relationship between the HSP70 and p53 expressions [30]. Similarly, Kocsis et al. reported that mortalin blood analysis, mortalin, and sHSP70 have a high prognostic value at the TNM stage and can identify colorectal cancer patients at high risk of poor survival [29]. Oh et al. also reported that the dominant intensity score-based Hsp70 IHC interpretation can be an effective method for MSI-H-prognostic stratification (a high level of microsatellite instability) in colorectal cancer [22]. In this study, the prognostic value and clinicopathologic significance of Hsp70 in colorectal carcinoma patients were assessed. This study can help understand the tumor generation process and the treatment value of Hsp70 in colorectal cancer. The meta-analysis included 2269 tumor patients from 11 articles (Hungary (4), Korea (2), and Britain, Greece, and Jordan (1 each)). A fixed-effects model was used for heterogeneity examination. The combined HRs indicated that Hsp70 overexpression was associated with the poor prognosis of colorectal carcinoma

patients. Hsp70 overexpression was also related to poor DFS. However, a large study should be conducted to verify these results.

Notably, this study has several limitations. First, some survival statistics from digital computer technology should be carefully considered. Besides, non-English articles were excluded. Second, only 11 articles with 2269 patients were included. There were no enough articles for subgroup analyses on disease-free survival. Third, different studies had different definitions of Hsp70 expression. Therefore, more researches are needed for more inclusive conclusions.

5. Conclusion

Hsp70 overexpression is significantly associated with poor overall survival and disease-free survival in colorectal carcinoma patients. Several such studies can provide mechanistic, pathophysiological, and epidemiological evidence complementing the findings of the current clinical trials on Hsp70 inhibitors.

Abbreviations

Hsp70: Heat shock protein 70
CI: Confidence intervention
Embase: Excerpta Medica database
HR: Hazard ratio
OS: Overall survival
DFS: Disease-free survival
CRC: Colorectal cancer.

Data Availability

All data included in this study are available from the corresponding author upon request.

Conflicts of Interest

The authors declare that they have no conflict of interest.

Authors' Contributions

All authors confirmed result accuracy. Guangyu Gao, Zhen Yao, and Nanping Lin conceived and designed the study; acquired, analyzed, and interpreted the data; and drafted the article. Yingchao Wang revised the article while Xiaolong Liu and Jingfeng Liu critically revised it. The report was finally approved. Songtao Liu and Guangyu Gao equally contributed to this work.

Acknowledgments

The authors thank Dr. Yulong Liu for the support.

References

[1] S. R. Steele, G. J. Chang, S. Hendren et al., "Practice guideline for the surveillance of patients after curative treatment of colon and rectal cancer," *Diseases of the Colon and Rectum*, vol. 58, no. 8, pp. 713–725, 2015.

[2] J. D. Vogel, C. Eskicioglu, M. R. Weiser, D. L. Feingold, and S. R. Steele, "The American Society of Colon and Rectal Surgeons clinical practice guidelines for the treatment of colon cancer," *Diseases of the Colon and Rectum*, vol. 60, no. 10, pp. 999–1017, 2017.

[3] H. Wang, M. S. Tan, R. C. Lu, J. T. Yu, and L. Tan, "Heat Shock Proteins at the Crossroads between Cancer and Alzheimer's Disease," *BioMed Research International*, vol. 2014, Article ID 239164, 9 pages, 2014.

[4] M. C. Diehl, M. O. Idowu, K. Kimmelshue, T. P. York, L. W. Elmore, and S. E. Holt, "Elevated expression of nuclear Hsp90 in invasive breast tumors," *Cancer Biology & Therapy*, vol. 8, no. 20, pp. 1952–1961, 2009.

[5] R. Moradi-Marjaneh, M. Paseban, and M. Moradi Marjaneh, "Hsp70 inhibitors: implications for the treatment of colorectal cancer," *IUBMB Life*, vol. 71, no. 12, pp. 1834–1845, 2019.

[6] E. Turrini, E. Catanzaro, M. G. Muraro et al., "Hemidesmus indicus induces immunogenic death in human colorectal cancer cells," *Oncotarget*, vol. 9, no. 36, pp. 24443–24456, 2018.

[7] D. T. Dimas, C. D. Perlepe, T. N. Sergentanis et al., "The prognostic significance of Hsp70/Hsp90 expression in breast cancer: a systematic review and meta-analysis," *Anticancer Research*, vol. 38, no. 3, pp. 1551–1562, 2018.

[8] A. Kalogeraki, E. Giannikaki, M. Tzardi et al., "Correlation of heat shock protein (HSP70) expression with cell proliferation (MIB1), estrogen receptors (ER) and clinicopathological variables in invasive ductal breast carcinomas," *Journal of Experimental & Clinical Cancer Research*, vol. 26, no. 3, pp. 367-368, 2007.

[9] A. Lazaris, E. B. Chatzigianni, D. Panoussopoulos, G. N. Tzimas, P. S. Davaris, and B. Golematis, "Proliferating cell nuclear antigen and heat shock protein 70 immunolocalization in invasive ductal breast cancer not otherwise specified," *Breast Cancer Research and Treatment*, vol. 43, no. 1, pp. 43–51, 1997.

[10] D. R. Ciocca, G. M. Clark, A. K. Tandon, S. A. Fuqua, W. J. Welch, and W. L. McGuire, "Heat shock protein hsp70 in patients with axillary lymph node-negative breast cancer: prognostic implications," *Journal of the National Cancer Institute*, vol. 85, no. 7, pp. 570–574, 1993.

[11] H. K. Söderström, J. T. Kauppi, N. Oksala et al., "Overexpression of HSP27 and HSP70 is associated with decreased survival among patients with esophageal adenocarcinoma," *World Journal of Clinical Cases*, vol. 7, no. 3, pp. 260–269, 2019.

[12] J. Sun, S. L. Che, J. J. Piao, M. Xu, L. Y. Chen, and Z. H. Lin, "Mortalin overexpression predicts poor prognosis in early stage of non-small cell lung cancer," *Tumour Biology*, vol. 39, no. 3, p. 1010428317695918, 2017.

[13] S. Kumar, S. Gurshaney, Y. Adagunodo et al., "Hsp70 and gama-Semino protein as possible prognostic marker of prostate cancer," *Frontiers in Bioscience (Landmark edition)*, vol. 23, pp. 1987–2000, 2018.

[14] A. Glaessgen, S. Jonmarker, A. Lindberg et al., "Heat shock proteins 27, 60 and 70 as prognostic markers of prostate cancer," *APMIS*, vol. 116, no. 10, pp. 888–895, 2008.

[15] E. Zhai, W. Liang, Y. Lin et al., "HSP70/HSP90-organizing protein contributes to gastric cancer progression in an autocrine fashion and predicts poor survival in gastric cancer," *Cellular Physiology and Biochemistry*, vol. 47, no. 2, pp. 879–892, 2018.

[16] A. Kimura, K. Ogata, B. Altan et al., "Nuclear heat shock protein 110 expression is associated with poor prognosis and

hyperthermo-chemotherapy resistance in gastric cancer patients with peritoneal metastasis," *World Journal of Gastroenterology*, vol. 23, no. 42, pp. 7541–7550, 2017.

[17] K. Klikova, I. Pilchova, A. Stefanikova, J. Hatok, D. Dobrota, and P. Racay, "The role of heat shock proteins in leukemia," *Klinická Onkologie*, vol. 29, no. 1, pp. 29–38, 2016.

[18] C. Wang, Y. Zhang, K. Guo et al., "Heat shock proteins in hepatocellular carcinoma: molecular mechanism and therapeutic potential," *International Journal of Cancer*, vol. 138, no. 8, pp. 1824–1834, 2016.

[19] L. Jiang, D. L. Kwong, Y. Li et al., "HBP21, a chaperone of heat shock protein 70, functions as a tumor suppressor in hepatocellular carcinoma," *Carcinogenesis*, vol. 36, no. 10, pp. 1111–1120, 2015.

[20] X. Cui, Z. Li, J. Piao et al., "Mortalin expression in pancreatic cancer and its clinical and prognostic significance," *Human Pathology*, vol. 64, pp. 171–178, 2017.

[21] L. Gráf, L. Barabás, B. Madaras et al., "High serum Hsp70 level predicts poor survival in colorectal cancer: results obtained in an independent validation cohort," *Cancer Biomarkers*, vol. 23, no. 4, pp. 539–547, 2018.

[22] H. J. Oh, J. H. Kim, T. H. Lee et al., "Dominant high expression of wild-type HSP110 defines a poor prognostic subgroup of colorectal carcinomas with microsatellite instability: a whole-section immunohistochemical analysis," *APMIS*, vol. 125, no. 12, pp. 1076–1083, 2017.

[23] J. H. Kim, K. J. Kim, Y. Y. Rhee et al., "Expression status of wild-type HSP110 correlates with HSP110 T17 deletion size and patient prognosis in microsatellite-unstable colorectal cancer," *Modern Pathology*, vol. 27, no. 3, pp. 443–453, 2014.

[24] M. K. Parmar, V. Torri, and L. Stewart, "Extracting summary statistics to perform meta-analyses of the published literature for survival endpoints," *Statistics in Medicine*, vol. 17, no. 24, pp. 2815–2834, 1998.

[25] R. Jubran, J. Kocsis, N. Garam et al., "Circulating mitochondrial stress 70 protein/mortalin and cytosolic Hsp70 in blood: risk indicators in colorectal cancer," *International Journal of Cancer*, vol. 141, no. 11, pp. 2329–2335, 2017.

[26] P. Rozenberg, J. Kocsis, M. Saar, Z. Prohaszka, G. Fust, and Z. Fishelson, "Elevated levels of mitochondrial mortalin and cytosolic HSP70 in blood as risk factors in patients with colorectal cancer," *International Journal of Cancer*, vol. 133, no. 2, pp. 514–518, 2013.

[27] K. Bauer, U. Nitsche, J. Slotta-Huspenina et al., "High HSP27 and HSP70 expression levels are independent adverse prognostic factors in primary resected colon cancer," *Cellular Oncology (Dordrecht)*, vol. 35, no. 3, pp. 197–205, 2012.

[28] J. Kocsis, T. Mészáros, B. Madaras et al., "High levels of acute phase proteins and soluble 70 kDa heat shock proteins are independent and additive risk factors for mortality in colorectal cancer," *Cell Stress & Chaperones*, vol. 16, no. 1, pp. 49–55, 2011.

[29] J. Kocsis, B. Madaras, E. K. Toth, G. Fust, and Z. Prohaszka, "Serum level of soluble 70-kD heat shock protein is associated with high mortality in patients with colorectal cancer without distant metastasis," *Cell Stress & Chaperones*, vol. 15, no. 2, pp. 143–151, 2010.

[30] A. M. Shotar, "P53 and heat shock protein 70 expressions in colorectal adenocarcinoma," *Saudi Medical Journal*, vol. 26, no. 10, pp. 1602–1606, 2005.

[31] S. R. Dundas, L. C. Lawrie, P. H. Rooney, and G. I. Murray, "Mortalin is over-expressed by colorectal adenocarcinomas and correlates with poor survival," *The Journal of Pathology*, vol. 205, no. 1, pp. 74–81, 2005.

[32] A. C. Lazaris, G. E. Theodoropoulos, P. S. Davaris et al., "Heat shock protein 70 and HLA-DR molecules tissue expression. Prognostic implications in colorectal cancer," *Diseases of the Colon and Rectum*, vol. 38, no. 7, pp. 739–745, 1995.

[33] W. G. Melsen, M. C. Bootsma, M. M. Rovers, and M. J. Bonten, "The effects of clinical and statistical heterogeneity on the predictive values of results from meta-analyses," *Clinical Microbiology and Infection*, vol. 20, no. 2, pp. 123–129, 2014.

[34] X. F. Sun, H. Zhang, J. Carstensen, A. Jansson, and B. Nordenskjold, "Heat shock protein 72/73 in relation to cytoplasmic p53 expression and prognosis in colorectal adenocarcinomas," *International Journal of Cancer*, vol. 74, no. 6, pp. 600–604, 1997.

Hindawi
BioMed Research International
Volume 2021, Article ID 5524486, 14 pages
https://doi.org/10.1155/2021/5524486

Research Article

Identification of Key miRNAs in the Treatment of Dabrafenib-Resistant Melanoma

Guangyu Gao,[1] Zhen Yao,[1] Jiaofeng Shen,[2] and Yulong Liu[1,3,4]

[1]*Department of Nuclear Accident Medical Emergency, The Second Affiliated Hospital of Soochow University, Suzhou 215004, China*
[2]*Department of Oncology, The Second Affiliated Hospital of Soochow University, Suzhou 215004, China*
[3]*State Key Laboratory of Radiation Medicine and Protection, School of Radiation Medicine and Protection, Soochow University, Suzhou 215123, China*
[4]*Collaborative Innovation Center of Radiological Medicine of Jiangsu Higher Education Institutions, Suzhou 215123, China*

Correspondence should be addressed to Jiaofeng Shen; jfshenzz@163.com and Yulong Liu; yulongliu2002@suda.edu.cn

Received 27 January 2021; Revised 13 February 2021; Accepted 11 March 2021; Published 7 April 2021

Academic Editor: Qiang Liu

Dabrafenib resistance is a significant problem in melanoma, and its underlying molecular mechanism is still unclear. The purpose of this study is to research the molecular mechanism of drug resistance of dabrafenib and to explore the key genes and pathways that mediate drug resistance in melanoma. GSE117666 was downloaded from the Gene Expression Omnibus (GEO) database and 492 melanoma statistics were also downloaded from The Cancer Genome Atlas (TCGA) database. Besides, differentially expressed miRNAs (DEMs) were identified by taking advantage of the R software and GEO2R. The Database for Annotation, Visualization, and Integrated Discovery (DAVID) and FunRich was used to perform Gene Ontology (GO) and Kyoto Encyclopedia of Genes and Genomes (KEGG) pathway enrichment analysis to identify potential pathways and functional annotations linked with melanoma chemoresistance. 9 DEMs and 872 mRNAs were selected after filtering. Then, target genes were uploaded to Metascape to construct protein-protein interaction (PPI) network. Also, 6 hub mRNAs were screened after performing the PPI network. Furthermore, a total of 4 out of 9 miRNAs had an obvious association with the survival rate ($P < 0.05$) and showed a good power of risk prediction model of over survival. The present research may provide a deeper understanding of regulatory genes of dabrafenib resistance in melanoma.

1. Introduction

By 2018, 1,762,450 new tumor patients are been made definite diagnosed and 606,880 among them died in the United States [1]. Of them, melanoma is the most aggressive type of skin tumor, takes up 10% of all skin cancers, but causes more than 80% of skin carcinoma-related deaths [2]. In 2019, approximately 96,480 individuals may be diagnosed with melanoma, and 7230 may have died of the disease. Although the overall incidence of cancer has declined in men and remained stable in women, the incidence of cutaneous melanoma in the United States has continued to rise over the past decade [1]. Based on conventional chemotherapy, melanoma does not respond well to treatment, leading to a 5-year survival rate of only 15% [3]. Molecular changes associated with sun exposure [4] or DNA methylation [5] are thought to be related to the development of melanoma. Besides, the mitogen-activated protein kinase (MAPK) pathway and gene mutations in the MEK/RAS/RAF/ERK have been found [6] and have offered new drug treatment targets. Among the second generation of selective BRAFV600E inhibitors, dabrafenib is the first drug authorized for the targeted treatment of unresectable melanoma [7]. Although the efficacy and tumor control effect of BRAF inhibitors are significant, the persistence of the efficacy is limited due to drug resistance, and signs of disease progression can be seen within 6-8 months after the start of treatment [8, 9].

microRNA (miRNA) is a highly conserved and short noncoding RNA molecule that occurs naturally in plant and animal genomes. They usually bind to the untranslated $17'$-mRNA by regulating the length of the utr-3 region. Studies have shown that thousands of human protein-coding

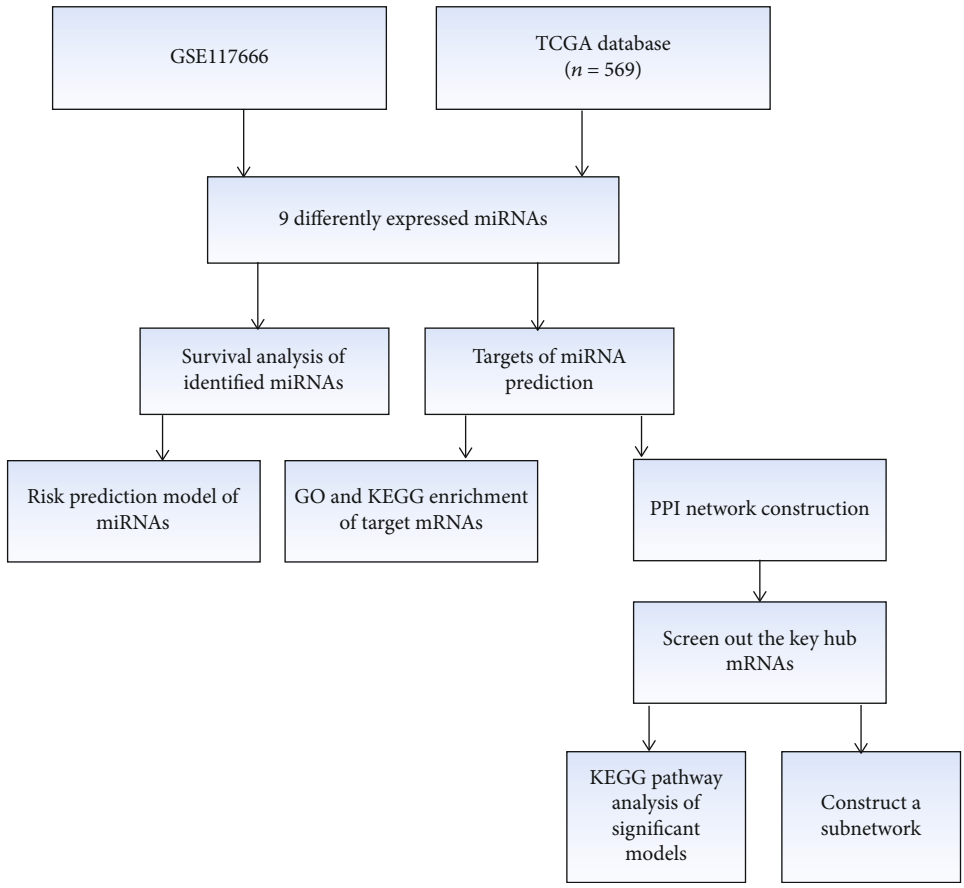

Figure 1: Flow chart of this study. GO: Gene Ontology; miRNA: microRNA; mRNA: messenger RNA; PPI: protein-protein interaction; KEGG: Enriched Kyoto Encyclopedia of Genes and Genomes.

genes are regulated by miRNAs, indicating that miRNAs are the "main regulators" of many important biological processes [10]. Although miRNA has only 20 nucleotides, it plays an important role in gene expression by regulating a large number of target genes [11]. For example, Zhang et al. found that miR-129-5p can suppress lung cancer cell viability and invasion, which may occur via the modulating of MCRS1, E-cadherin, and vimentin expression [12]. Zhang et al. found that low miR-133 expression was a common event and correlated with worse clinical outcomes in acute myeloid leukemia, suggesting that serum miR-133 might serve as a promising indicator for the early detection and prognosis evaluation of AML [13]. Xu et al. also reported that miRNA-100 inhibits human bladder urothelial carcinogenesis by directly targeting mTOR [14]. Besides, different mechanisms of BRAF inhibitor resistance in melanoma have been described: epigenetic [15], genomic [16], and phenotypic [17] transformation produces many changes leading to acquired, internal, or adaptive resistance. However, it still needs to be further explored.

In the current study, microarray data for GSE117666 and melanoma sample data in the TCGA database facilitated the investigation of differently expressed miRNAs in dabrafenib-sensitive and dabrafenib-resistant melanoma. The functions of the target mRNAs were assessed by using GO annotation, KEGG, PPI network, and the relationship between dabrafenib-resistant miRNAs and the overall survival of patients with cancer. In summary, we performed this study to find the key miRNAs and mRNAs of medicine resistance and to discover potential new tumor therapy targets to reduce dabrafenib resistance.

Table 1: Key differently expressed miRNAs of joint screening from GSE117666 and TCGA database.

ID	*P* value	Log FC
hsa-miR-509p	0.000011	-5.21303
hsa-miR-146a	0.000033	5.17469
hsa-miR-514b	0.000108	-3.48325
hsa-miR-584	0.000121	3.317673
hsa-miR-510	0.000138	-2.69851
hsa-miR-503	0.000901	-2.30348
hsa-miR-513a	0.001138	2.818463
hsa-miR-126	0.001620	-2.45363
hsa-miR-508	0.019126	-2.10383

2. Materials and Methods

2.1. Microarray Data. The GEO (https://www.ncbi.nlm.nih.gov/gds) database is a gene expression database created and maintained by NCBI. It was founded in 2000 and

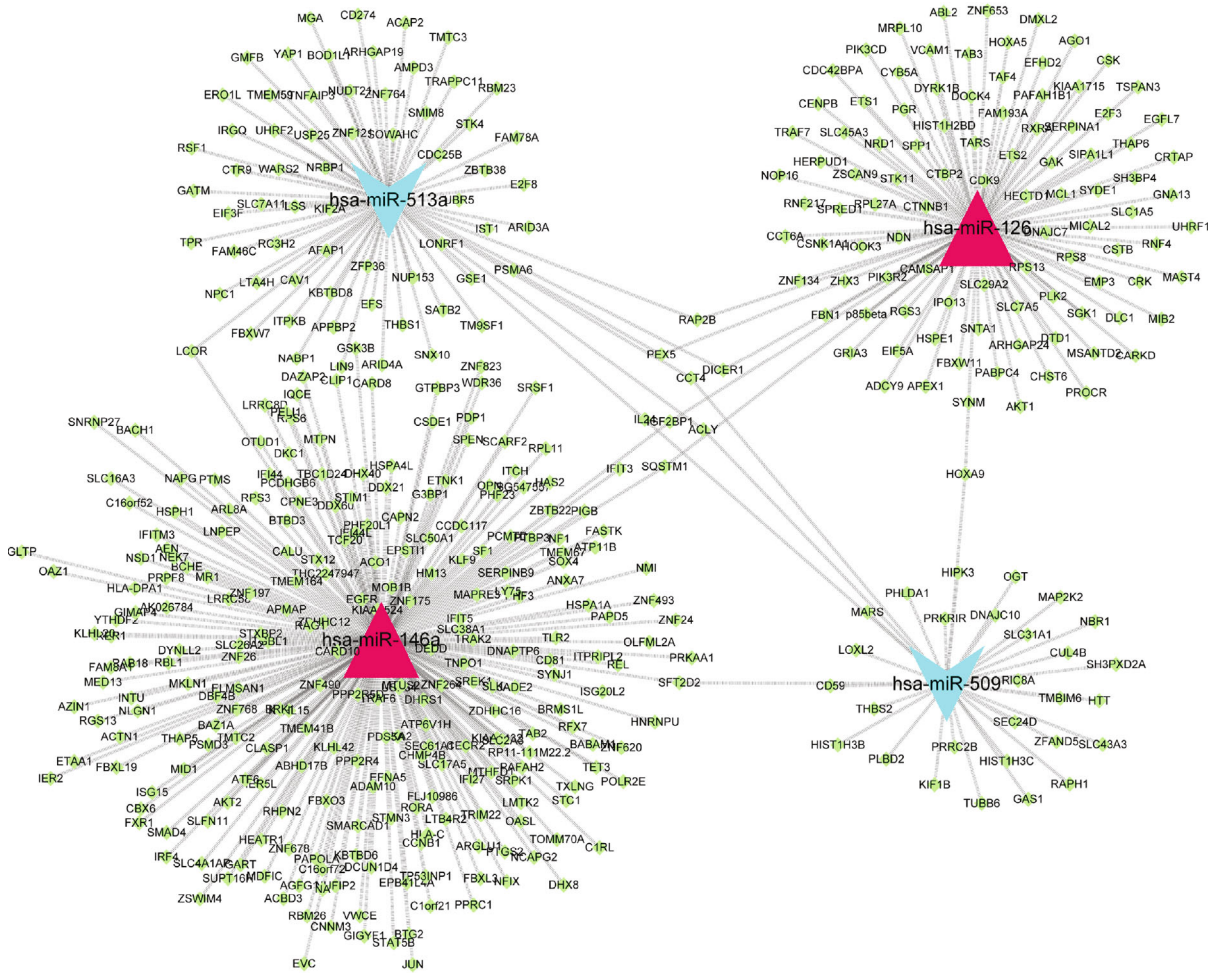

Figure 2: The interactions between differentially expressed miRNAs and target mRNAs.

contains high-throughput gene expression data submitted by research institutions around the world. In our research, gene expression profile data (GSE117666) was obtained from GEO. Three dabrafenib-resistant melanoma cells and three dabrafenib-sensitive cell lines were included. The array data were acquired from the Affymetrix Multispecies miRNA-3 Array [GPL16384; transcript (gene) version]. Besides, the flow of this study is shown in Figure 1.

2.2. DEMs Analysis. We used the R software to compare the two groups of samples. Furthermore, $|\log 2FC| \geq 2$ and $P < 0.05$ were set up as cut-off criteria, and if the statistics according to our criteria, obvious statistical differences will be considered [18].

2.3. Targets of miRNA Prediction. DEMs were achieved by the method mentioned above. miRWalk1.0 (http://mirwalk.umm.uni-heidelberg.de/) is a fully documented, freely available database that provides the largest set of predictive, experimentally proven miRNA target interactions in a variety of novel ways.

2.4. Functional and Pathway Enrichment Analysis. KEGG pathway analysis and GO functional analysis of the DEGs we identified were performed by using FunRich software. It is a stand-alone software tool used mainly for functional enrichment and interaction network analysis of genes and proteins. Besides, the results of the analysis can be depicted graphically in the form of Venn, Bar, Column, Pie, and Doughnut charts. GO analysis was divided into the cellular component (CC), biological process (BP), and molecular function (MF), and a P value < 0.05 was thought that there was a statistical difference. We also used ClueGO for KEGG pathway analysis. It is a Cytoscape plug-in that visualizes the nonredundant biological terms for large clusters of genes in a functionally grouped network. The identifiers can be uploaded from a text file or interactively from a network of Cytoscape.

2.5. Protein-Protein Interaction Network Analysis. To analyze the connection among proteins, target mRNAs were uploaded to Search Tool for the Retrieval of Interacting Genes (STRING, https://string-db.org/), a database covering 9,643,763 proteins from 2,031 organisms, and the result whose minimum interaction score was 0.4 was visualized in Cytoscape [19]. Furthermore, the Molecular Complex Detection (MCODE) was used to find obvious modules based on the constructed PPI networks with the criteria of degree

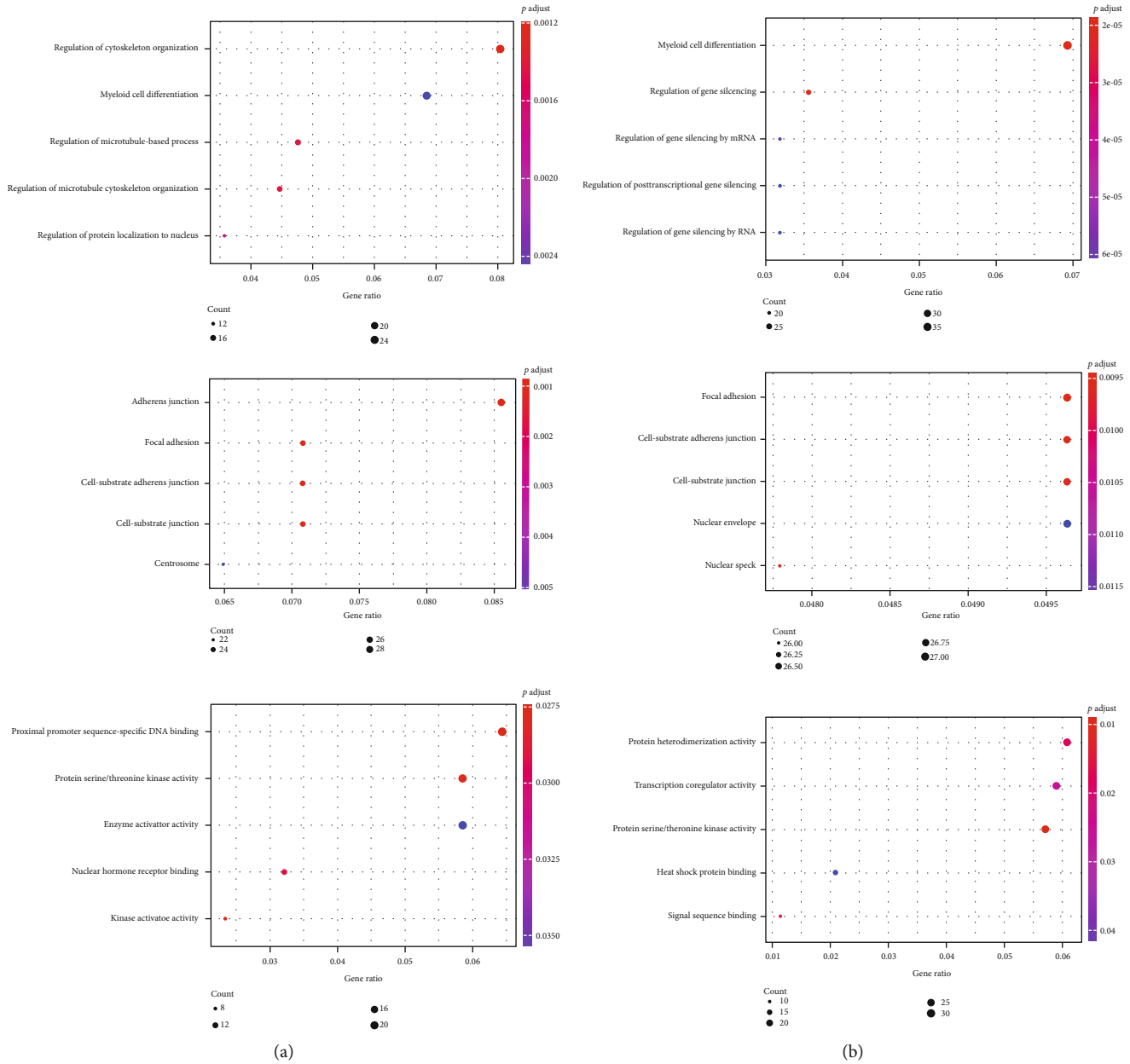

Figure 3: Differentially expressed mRNAs analyzed by GO enrichment. CC: cellular component; MF: molecular function; BP: biological process.

cut-off = 2, node density cut-off = 0.1, and node score cut-off = 0.2, and hub genes were exported.

2.6. Analysis of mRNAs Expression in Melanoma. Hub gene expression in melanoma tissues and normal tissues was extracted from the human protein atlas (http://www.proteinatlas.org). The Human Protein Atlas is a Swedish-based program initiated in 2003 to map all the human proteins in cells, tissues, and organs using an integration of various omics technologies, including antibody-based imaging, mass spectrometry-based proteomics, transcriptomics, and systems biology. Gene expressions we selected were determined through analysis of TCGA databases, which are available through TCGAportal (http://www.tcgaportal.org).

2.7. Analysis of the miRNAs and Their Relationship with Melanoma Prognosis. The Kaplan-Meier Plotter (http://www.kmplot.com/) is capable to assess the effect of 54k genes (mRNA, miRNA, protein) on survival in 21 cancer types including breast ($n = 6{,}234$), ovarian ($n = 2{,}190$), lung ($n = 3{,}452$), and gastric ($n = 1{,}440$) cancer. Sources for the databases include GEO, EGA, and TCGA. The primary purpose of the tool is a meta-analysis-based discovery and validation of survival biomarkers. [20]. Each miRNA that was selected would then be entered into the online tool to evaluate the survival of patients with melanoma. Meanwhile, we extracted HRs with 95% CI of every identified miRNA and draw a Forest plot using the Stata 14.0 software.

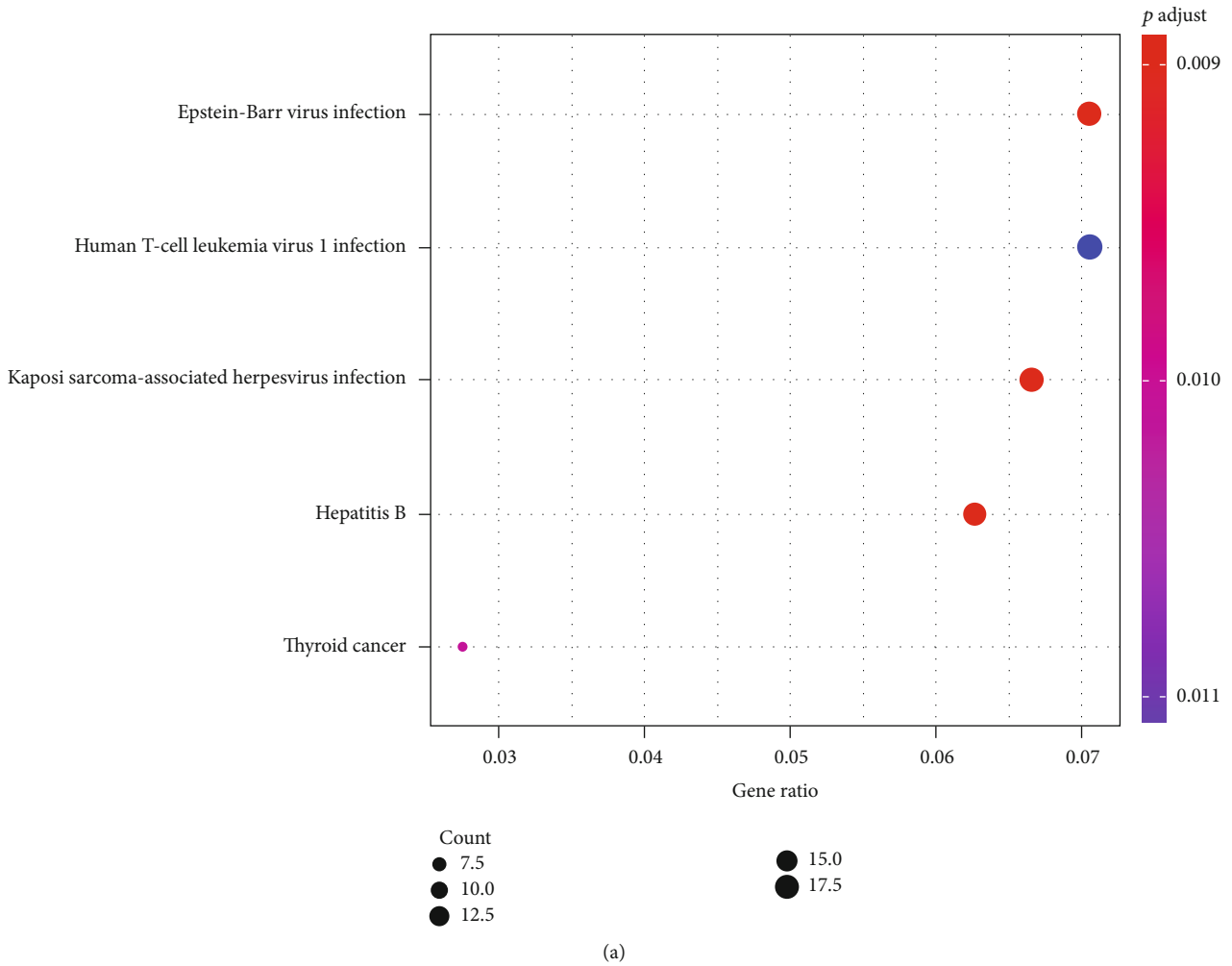

(a)

Figure 4: Continued.

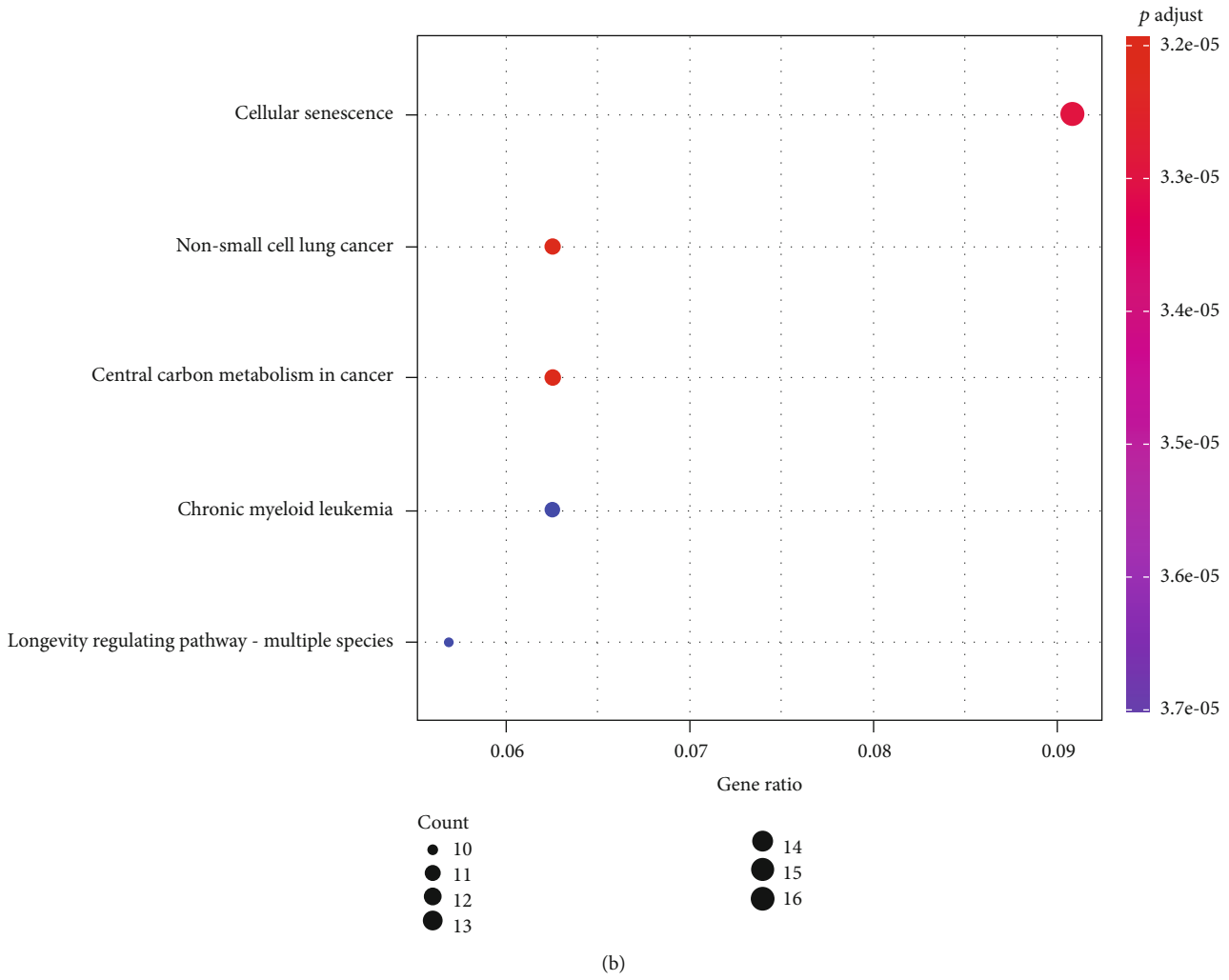

(b)

Figure 4: KEGG pathway enriched by up- and downregulated mRNAs.

2.8. Independent Prognostic Ability of the miRNA Signature. To learn more about the association between identified miRNAs and the prognosis of melanoma patients, we performed a risk prediction model. 492 melanoma statistics were also downloaded from the TCGA database. The 3-year and 5-year AUC dependent on the ROC curve was calculated using the "survivalROC" software package to evaluate the predictive ability of the identified miRNAs. A block diagram was drawn to show the risk score of the model.

3. Results

3.1. Identification of the miRNAs between Dabrafenib Sensitive and Dabrafenib Resistant Melanoma Cells. The R software was used to research the gene expression profiles from the GSE117666. It highlighted the DEGs between GSM3305847, GSM3305851, GSM3305852 (dabrafenib-sensitive), GSM33305848, GSM3305849, and GSM3305850 (acquired dabrafenib-resistant) melanoma cells. According to the cut-off criteria ($P < 0.05$ and $|\log 2FC| \geq 2$), 30 DEMs were selected. After researching 492 samples of the TCGA database, 72 DEMs were identified and 9 of them exist in both filter results which were consisted of 6 downregulated and 3 upregulated miRNAs. The result is shown in Table 1.

3.2. Target Prediction and GO Analysis. The target mRNAs of those 9 DEMs were downloaded from two miRNA target prediction websites (targetscan and miRDB). 872 mRNAs were identified after filtering. The network between miRNAs (2 upregulated miRNAs and 2 downregulated miRNAs) and target mRNAs was shown in Figure 2. To learn more about the function of these mRNAs, these mRNAs were uploaded into FunRich to perform GO and KEGG analysis. In the CC ontology, DEGs were enriched in "Cytoplasm", "Plasma membrane", and "Nucleus". In the BP ontology, DEGs were enriched in "Transport", "Cell growth and/or maintenance", and "Regulation of nucleobase, nucleoside, nucleotide, and nucleic acid metabolism". In the MF ontology, DEGs were enriched in "Protein serine/threonine kinase activity",

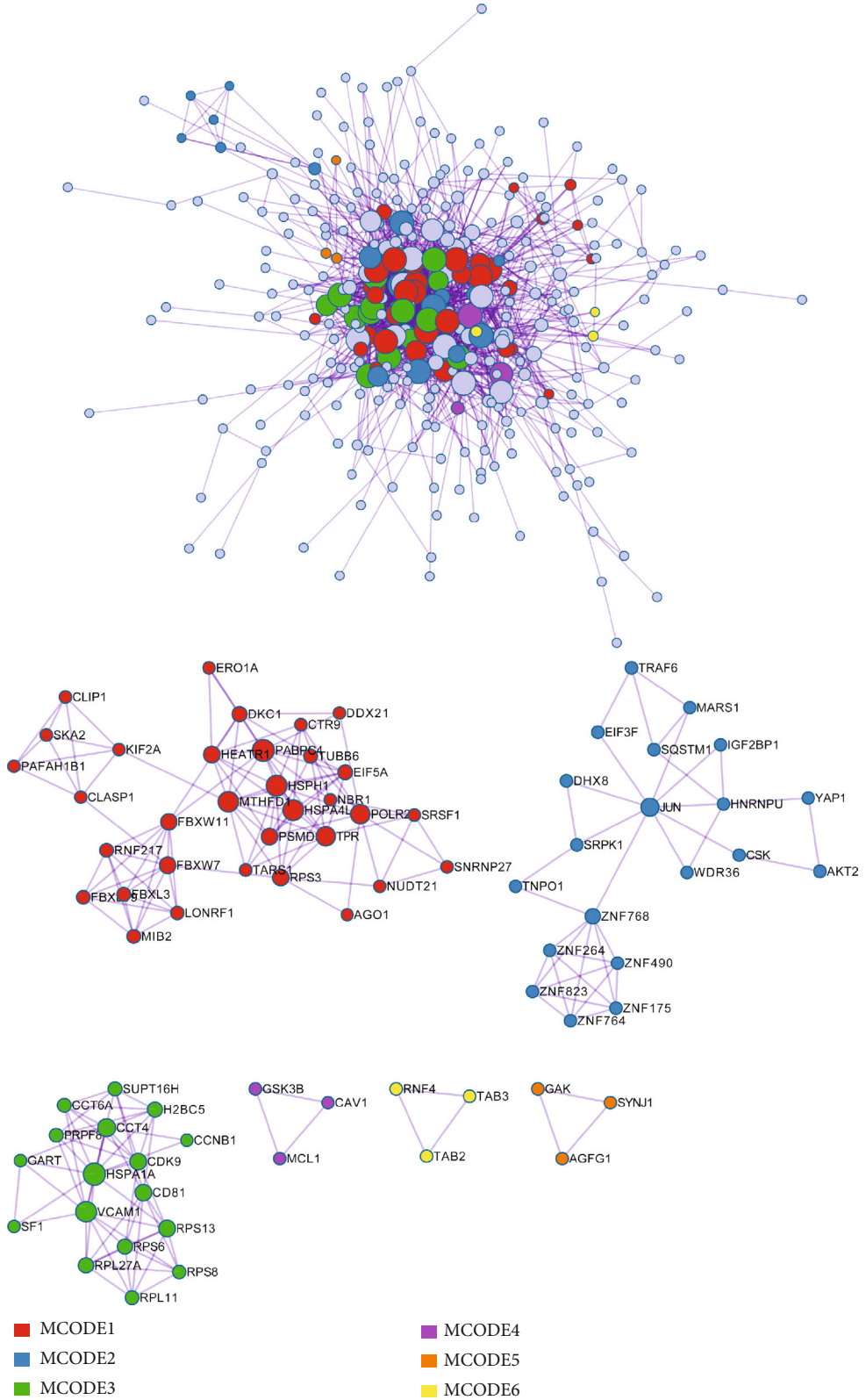

Figure 5: PPI network and identification of MCODEs.

Table 2: KEGG enrichment analysis of hub target mRNAs.

MCODE	ID	Description	Log10(*P*)
MCODE_1	hsa05165	Separation of sister chromatids	-8.2
MCODE_2	hsa04722	Osteoclast differentiation	-5.4
MCODE_3	hsa04919	Infectious disease	-10.1
MCODE_4	hsa04218	Positive regulation of apoptotic signaling pathway	-6.4
MCODE_5	hsa05163	Clathrin-mediated endocytosis	-6.7
MCODE_6	hsa05205	Intracellular receptor signaling pathway	-5.8

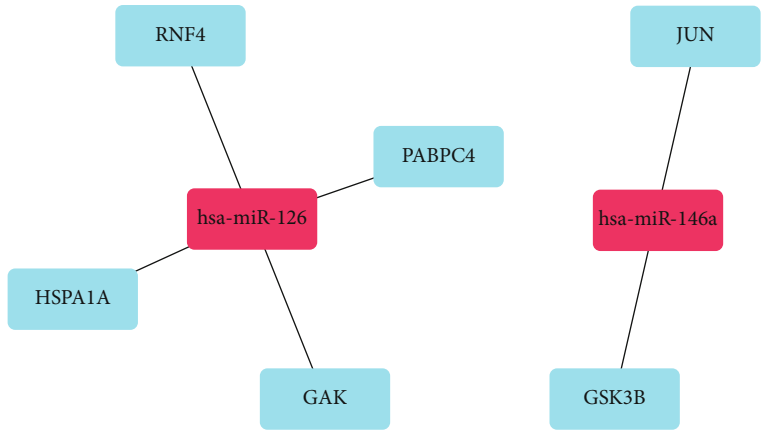

Figure 6: miRNA mRNA regulatory pairs from the 6 hub miRNA targets and their regulated miRNAs.

"Cell adhesion molecule activity", and "Guanyl-nucleotide exchange factor activity" (Figure 3).

3.3. KEGG Pathways of DEMs. By using ClueGO, we identified several KEGG significant enriched pathways. DEMs were enriched in "Pathways in cancer", "Proteoglycans in cancer", "microRNAs in cancer", "Wnt signaling pathway", "Central carbon metabolism in cancer, and "Cytokine-cytokine receptor interaction" (Figure 4).

3.4. Construction of a Protein-Protein Interaction (PPI) Network. 872 genes were inputted into the Metascape website to get interactive data. Then, if the combined score was ≥0.7, we would choose identified mRNAs to build a PPI network (Figure 5). In the PPI network, 6 modules, including PABPC4, JUN, HSPA1A, GSK3B, RNF4, and GAK were identified. The outcomes of the KEGG pathway between modules were related to "Separation of Sister Chromatids", "Osteoclast differentiation", "Infectious disease", "Positive regulation of apoptotic signaling pathway", "Clathrin-mediated endocytosis", and "Intracellular receptor signaling pathway" (Table 2). Based on the 6 key mRNAs and target miRNAs, we performed a miRNA-mRNA network (Figure 6), and it may provide a series of promising treatment targets and enlightened us on the further investigations of the molecular mechanisms.

3.5. Analysis of the Expression of the Key Genes in Normal Tissues and Melanoma Tissues. Based on the human protein atlas, the expression of target genes was researched. PABPC4, HSPA1A, and GSK3B were identified from 6 key mRNAs. After entering them into the database, we found that three mRNAs have a positive strong expression in melanoma samples and a negative weak expression in normal samples (Figure 7).

3.6. Analysis of the miRNAs and Their Relationship with Melanoma Prognosis. The Kaplan-Meier Plotter was utilized to study the prognosis of patients with melanoma-related to miRNAs we selected. After uploaded 9 miRNAs, we got 9 survival graphs. The results indicated that overexpression of hsa-miR-510, hsa-miR-503, and hsa-miR-513a (Figure 8) was related to improved overall survival in patients with melanoma. However, the expression level of hsa-miR-509, hsa-miR-146a, hsa-miR-514b, hsa-miR-584, hsa-miR-126, and hsa-miR-508 may have no obvious association with the OS. The forest plot showed in more detail the relationship between miRNAs expression and the survival and prognosis of patients (Figure 9). This suggested that the identified miRNAs may be potential targets for dabrafenib resistance in melanoma.

3.7. Evaluation of the 9-miRNA Signature for over Survival. The AUC of 3 years survival for the 9-miRNA signature

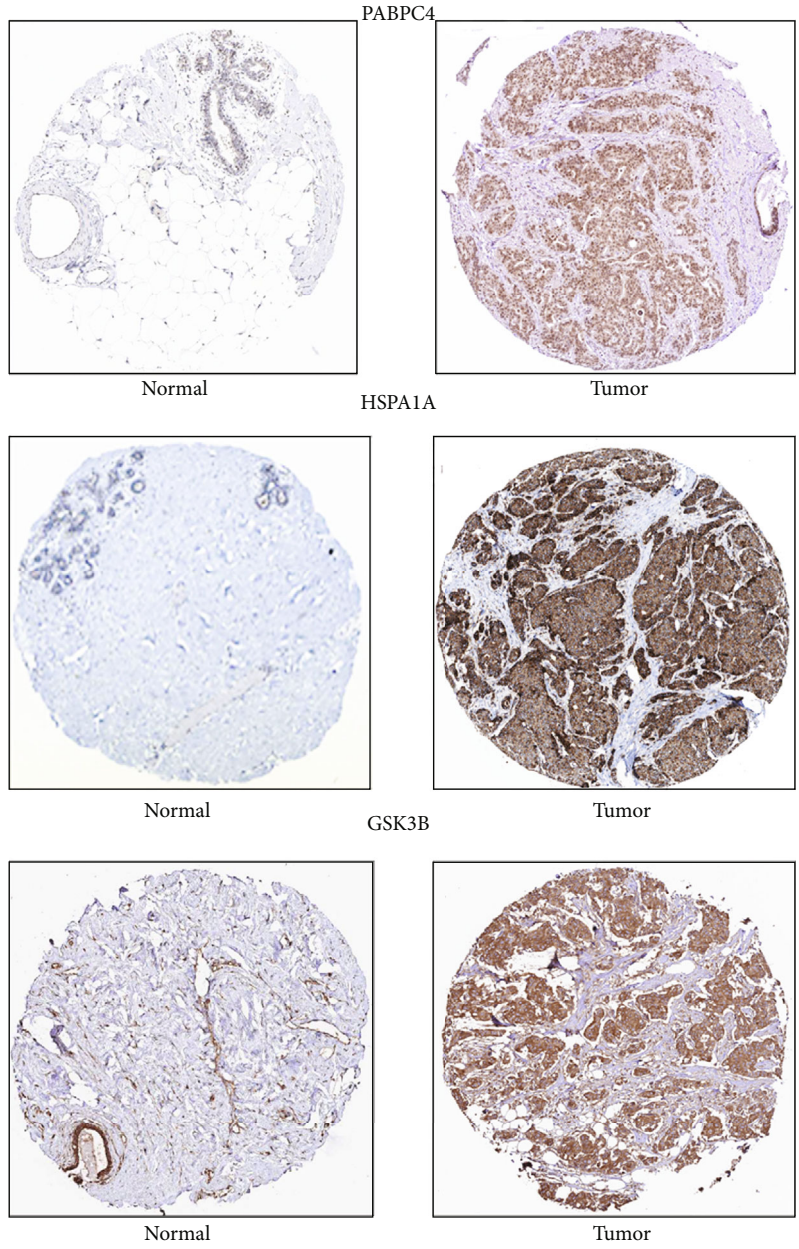

Figure 7: Genes expression of in human melanoma specimens. PABPC4, HSPA1A, and GSK3B expression in normal tissue and melanoma specimens.

achieved 0.809 and the AUC of 5 years survival achieved 0.981, which proved that the model has good performance in predicting the survival risk of melanoma patients. Besides, the box diagram also proves our conclusion (Figure 10).

4. Discussion

In recent years, the incidence and mortality of malignant melanoma are increasing year by year. Compared with other solid tumors, the age of death is lower. In addition to early surgical resection, malignant melanoma lacks specific treatment and has a poor prognosis. Therefore, the early diagnosis and treatment of malignant melanoma are extremely important. In this article, GSE117666 and 492 melanoma statistics from the TCGA database were downloaded for further study. Melanoma statistics from the TCGA database were searched from the GEO and TCGA database. 9 DEMs (hsa-miR-510, hsa-miR-503, hsa-miR-513a, hsa-miR-509, hsa-miR-146a, hsa-miR-514b, hsa-miR-584, hsa-miR-126, and hsa-miR-508) were selected by combining two screening results. Among them, certain miRNAs have been shown to affect tumor proliferation, migration, and prognosis. For example, a previous

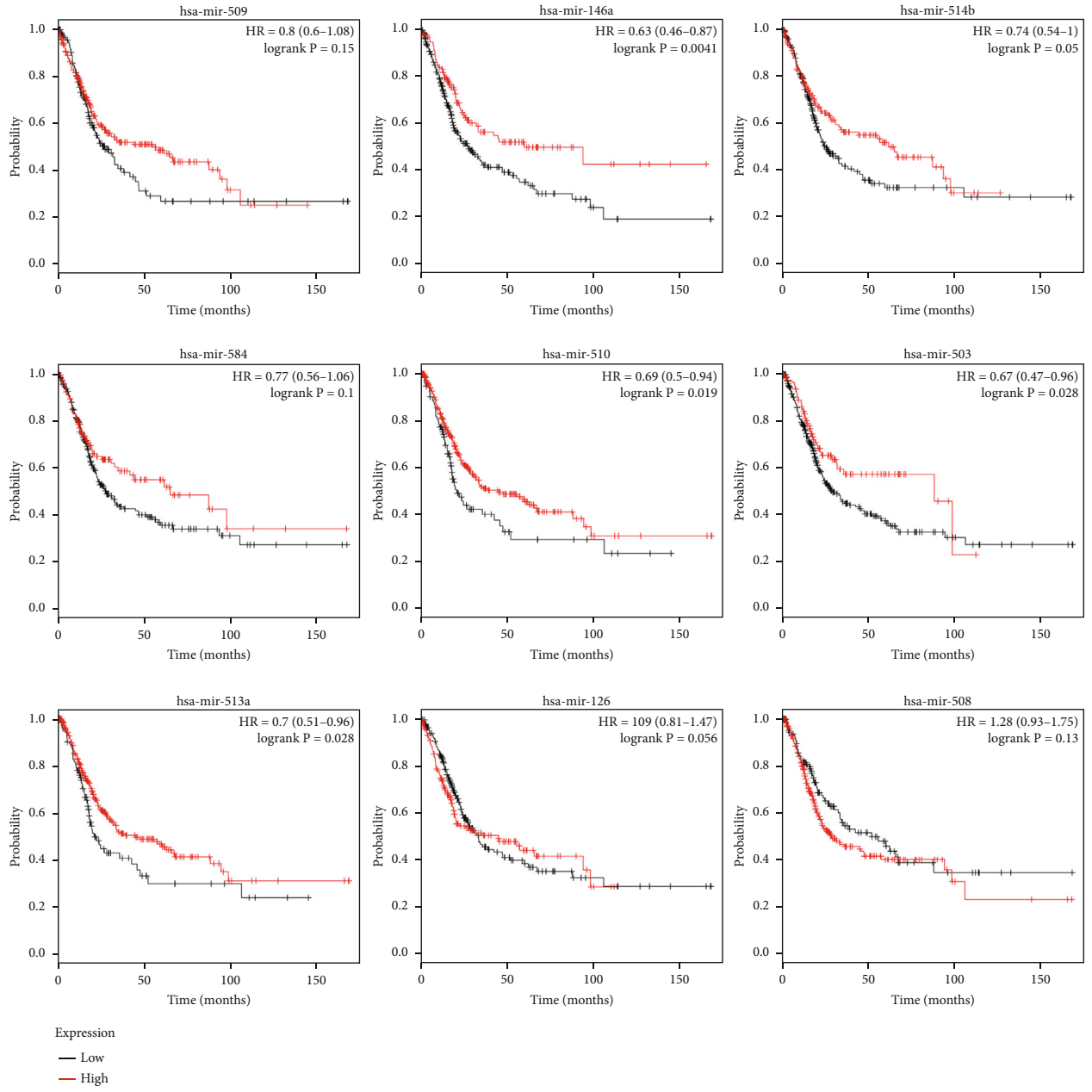

Figure 8: The association between miRNAs and melanoma prognosis.

study reported miR-510 promotes thyroid cancer cell proliferation, migration, and invasion through suppressing lncRNA SNHG15 [21]; it also serves as a prognostic biomarker, or as a potential therapeutic target, in cutaneous melanoma patients [22]. hsa-miR-146a controls Immune Response in the Melanoma Microenvironment and may provide a new therapeutic strategy to improve the current management of patients with melanoma [23]. Another study also reported hsa-miR-126 downregulation contributes to dabrafenib acquired resistance in melanoma by upregulating ADAM9 and VEGF-A [24]. Besides, it may play a tumor suppressor role by directly regulating ADAM9 and MMP7 in melanoma [25].

To understand the regulatory mechanism of the 9 miRNAs in melanoma, we chose the intersection of two screening results from MiRWalk. 872 mRNAs were identified after filtering. Function annotation indicated that these miRNAs were primarily related to "Cytoplasm", "Plasma membrane", "Nucleus", "Transport", "Cell growth and/or maintenance", "Regulation of nucleobase, nucleoside, nucleotide and nucleic acid metabolism", "Protein serine/threonine kinase activity", "Cell adhesion molecule activity", and "Guanyl-nucleotide exchange factor activity". KEGG pathway analysis of DEGs revealed involvement in "Pathways in cancer", "Proteoglycans in cancer", "microRNAs in cancer", "Wnt signaling pathway", "Central

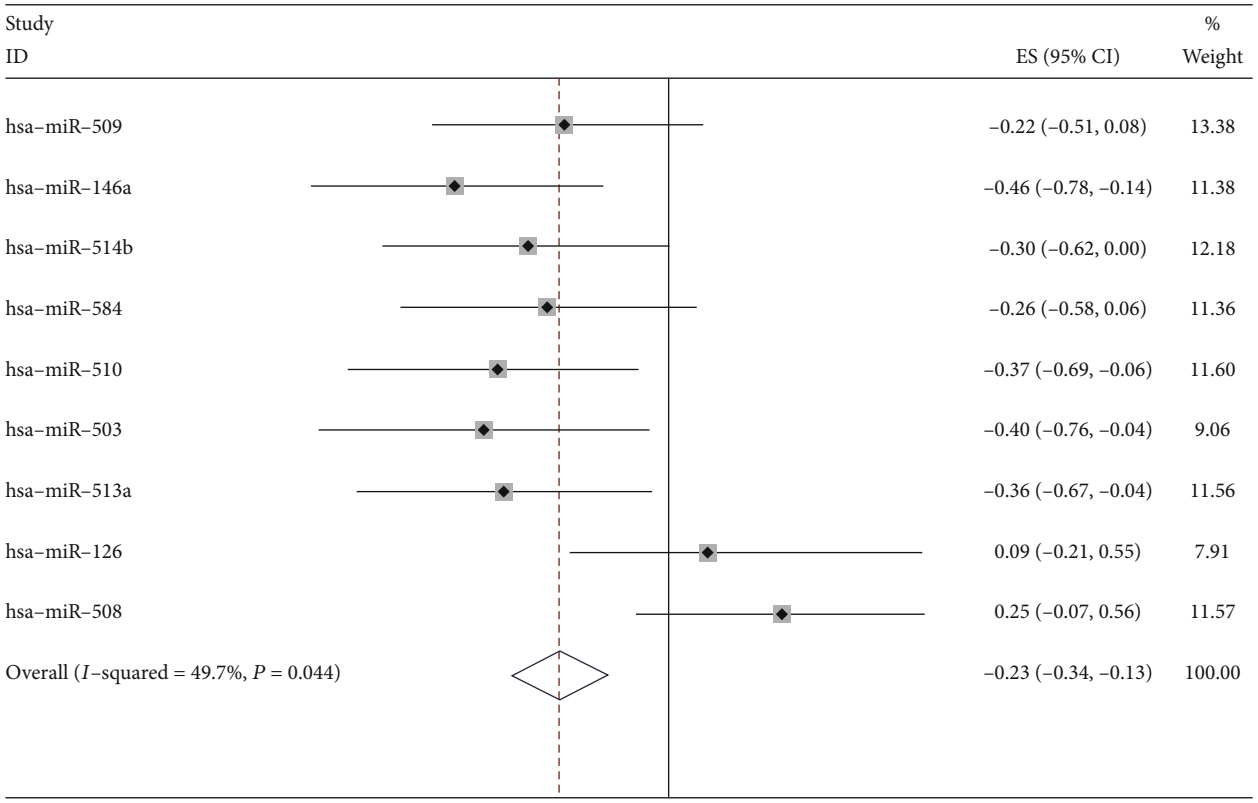

Figure 9: Forest plot demonstrating the association between identified miRNAs expression and the survival of humans with melanoma.

carbon metabolism in cancer", and "Cytokine-cytokine receptor interaction". According to previous studies, these signaling pathways participate in a diverse array of important cellular processes, including the survival, proliferation, differentiation, and activation of different cell types [26–28].

Besides, PPI network analysis indicated that 6 hub genes including PABPC4 (Poly(A) Binding Protein Cytoplasmic 4), JUN (Jun Proto-Oncogene, AP-1 Transcription Factor Subunit), HSPA1A (Heat Shock Protein Family A (Hsp70) Member 1A), GSK3B (Glycogen Synthase Kinase 3 Beta), RNF4 (Ring Finger Protein 4), and GAK (cyclin G associated kinase) may be used as new targets in dabrafenib-resistant melanoma which had higher degrees of interaction. PABPC4, a protein kinase, may be a valuable source of biomarkers for response to docetaxel-resistance prostate cancer therapy [29]. As for HSPA1A, a kind of inducible heat shock protein promotes tumor cell growth and survival [30]. It also adjusts the transfer process, including EMT and migration, and seems to be destroyed by the Hsp70-dependent heterocomplexes of E-cadherin/catenins, which act as an anchor between neighboring cells [31]. GSK3B, glycogen synthase kinase 3, was identified as novel tivantinib targets [32]. It is also related to the regulation of melanogenesis, and drug inhibition can increase melanogenesis through Wnt/beta-catenin pathway activation [33]. As for RNF4, it is a SUMO-targeted ubiquitin ligase that stabilizes a specific group of oncoproteins. It enhances tumor protein activity and acts as a positive feedback agonist for Wnt and Notch pathways. RNF4 is also necessary for the survival of cancer cells, and its overexpression is related to the poor prognosis of some cancer patients [34]. GAK (Cyclin G Associated Kinase), a protein expressed ubiquitously in various tissues, is identified as the off-target responsible for intracellular melanin accumulation. It also represents a new possible target for the prevention and treatment of irregular pigmentation by the melanogenic biosynthetic pathway [35].

Furthermore, the relationship between the 9 miRNAs and the overall survival curves for patients with melanoma revealed that overexpression of hsa-miR-510, hsa-miR-503, and hsa-miR-513a was related to improved overall survival. However, the expression level of hsa-miR-509, hsa-miR-146a, hsa-miR-514b, hsa-miR-584, hsa-miR-126, and hsa-miR-508 may have no significant relationship with the overall survival of patients. Meanwhile, evaluation of the 9-miRNA signature for overall survival by the ROC curve displayed better predictive ability.

At present, with the development of targeted therapy, more and more attention has been paid to tumor drug resistance. Therefore, it is necessary to find new biomarkers and treatment methods for patients with drug resistance. Our findings concluded that these miRNAs may act as an important role in dabrafenib-resistant melanoma. However, all of our data are obtained from GEO

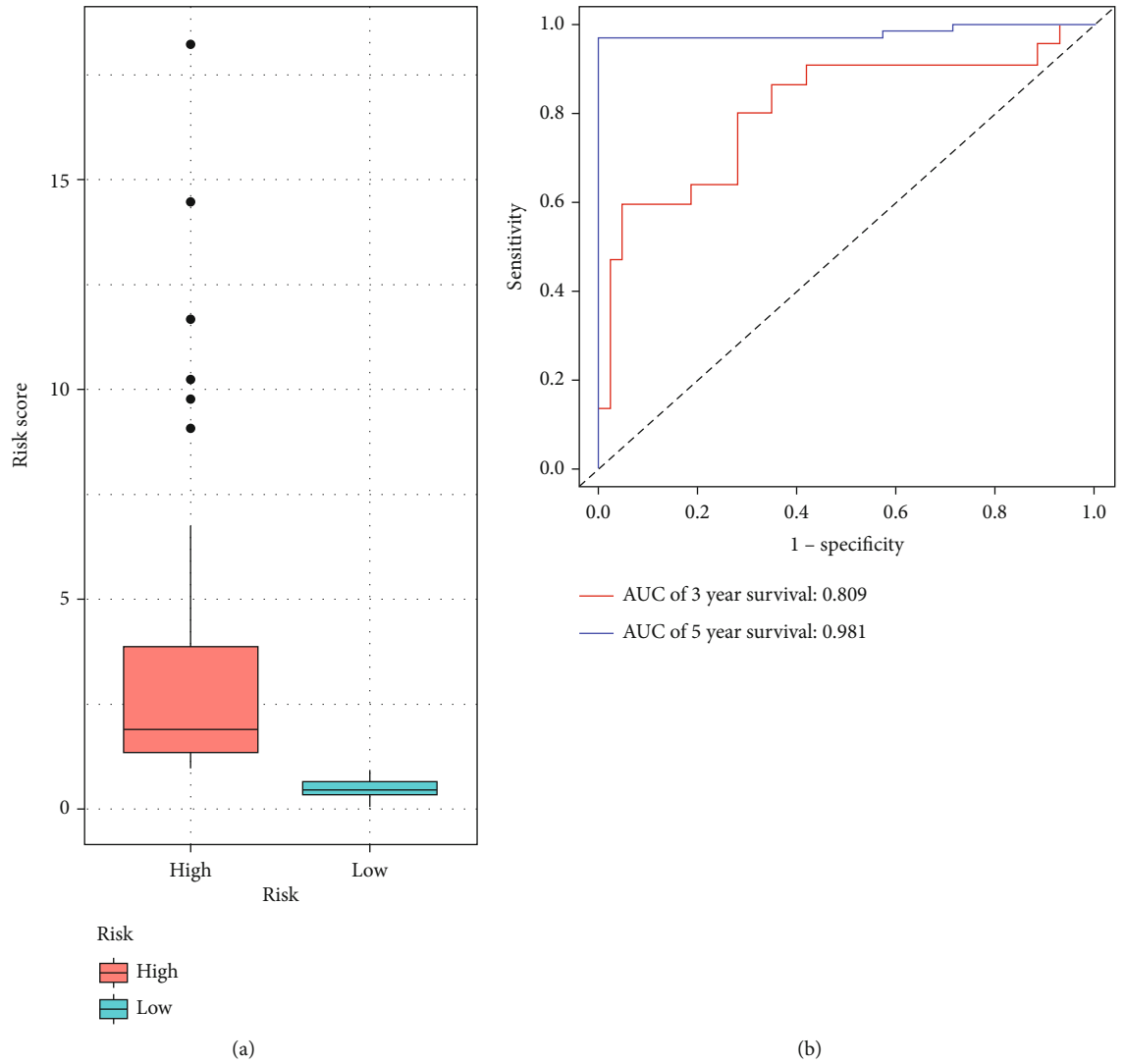

Figure 10: Risk prediction model of 9 identified miRNAs. (a) Box diagram of the risk score. (b) The AUC of 3 years and 5 years curve.

and TCGA database through bioinformatics analysis, and the number of relevant samples is limited; further data analysis and clinical trials are needed to verify.

5. Conclusion

Our study not only explored certain mechanisms of dabrafenib-resistance in melanoma but also constructed a significant 9-miRNA risk prediction model for overall survival. Bioinformatics methods were used to select the DEMs in dabrafenib-resistant melanoma cells. These findings significantly improve the understanding of the cause and underlying molecular events in melanoma, and the candidate genes and pathways could be used as therapeutic targets.

Data Availability

All data included in this study are available from the corresponding author upon request.

Conflicts of Interest

The authors declared no conflicts of interest.

Authors' Contributions

Guangyu Gao and Zhen Yao contributed equally to this work.

Acknowledgments

This manuscript has been released as a preprint at https://www.researchsquare.com/article/rs-18505/v1?redirect=/article/rs-18505. The authors disclosed receipt of the following financial support for the research, authorship, and/or publication of this article. This work was supported by the Priority Academic Program Development of Jiangsu Higher Education Institutions (PAPD).

References

[1] R. L. Siegel, K. D. Miller, and A. Jemal, "Cancer statistics, 2019," *CA: a Cancer Journal for Clinicians*, vol. 69, no. 1, pp. 7–34, 2018.

[2] M. L. Bonnelykke-Behrndtz and T. Steiniche, *Ulcerated melanoma: aspects and prognostic impact*, W. H. Ward and J. M. Farma, Eds., Cutaneous Melanoma: Etiology and Therapy, Brisbane (AU), 2017.

[3] H. Herrscher and C. Robert, "Immune checkpoint inhibitors in melanoma in the metastatic, neoadjuvant, and adjuvant setting," *Current Opinion in Oncology*, vol. 32, no. 2, pp. 106–113, 2020.

[4] S. A. V. E. R. I. O. CANDIDO, V. E. N. E. R. A. N. D. O. RAPISARDA, A. N. D. R. E. A. MARCONI et al., "Analysis of the B-RafV600E mutation in cutaneous melanoma patients with occupational sun exposure," *Oncology Reports*, vol. 31, no. 3, pp. 1079–1082, 2014.

[5] L. Falzone, R. Salemi, S. Travali et al., "MMP-9 overexpression is associated with intragenic hypermethylation of MMP9 gene in melanoma," *Aging (Albany NY)*, vol. 8, no. 5, pp. 933–944, 2016.

[6] M. Bernardo-Faura, S. Massen, C. S. Falk, N. R. Brady, and R. Eils, "Data-derived modeling characterizes plasticity of MAPK signaling in melanoma," *PLoS Computational Biology*, vol. 10, no. 9, article e1003795, 2014.

[7] A. Hauschild, J. J. Grob, L. V. Demidov et al., "Dabrafenib in BRAF-mutated metastatic melanoma: a multicentre, open-label, phase 3 randomised controlled trial," *Lancet*, vol. 380, no. 9839, pp. 358–365, 2012.

[8] J. Larkin, P. A. Ascierto, B. Dréno et al., "Combined vemurafenib and cobimetinib inBRAF-Mutated melanoma," *The New England Journal of Medicine*, vol. 371, no. 20, pp. 1867–1876, 2014.

[9] G. V. Long, D. Stroyakovskiy, H. Gogas et al., "Combined BRAF and MEK inhibition versus BRAF inhibition alone in melanoma," *The New England Journal of Medicine*, vol. 371, no. 20, pp. 1877–1888, 2014.

[10] D. S. Morera, M. S. Hennig, A. Talukder et al., "Hyaluronic acid family in bladder cancer: potential prognostic biomarkers and therapeutic targets," *British journal of cancer.*, vol. 117, no. 10, pp. 1507–1517, 2017.

[11] P. Ren, F. Gong, Y. Zhang, J. Jiang, and H. Zhang, "MicroRNA-92a promotes growth, metastasis, and chemoresistance in non-small cell lung cancer cells by targeting PTEN," *Tumour Biology*, vol. 37, no. 3, pp. 3215–3225, 2016.

[12] Y. Zhang, J. An, W. Lv, T. Lou, Y. Liu, and W. Kang, "miRNA-129-5p suppresses cell proliferation and invasion in lung cancer by targeting microspherule protein 1, E-cadherin and vimentin," *Oncology Letters*, vol. 12, no. 6, pp. 5163–5169, 2016.

[13] Z. Z. Zheng, Y. P. Ma, R. H. Wu et al., "Serum miR-133 as a novel biomarker for predicting treatment response and survival in acute myeloid leukemia," *European Review for Medical Pharmacological Sciences*, vol. 24, no. 2, pp. 777–783, 2020.

[14] C. Xu, Q. Zeng, W. Xu et al., "miRNA-100 inhibits human bladder urothelial carcinogenesis by directly targeting mTOR," *Molecular Cancer Therapeutics*, vol. 12, no. 2, pp. 207–219, 2013.

[15] M. Vizoso, H. J. Ferreira, P. Lopez-Serra et al., "Epigenetic activation of a cryptic _TBC1D16_ transcript enhances melanoma progression by targeting EGFR," *Nature Medicine*, vol. 21, no. 7, pp. 741–750, 2015.

[16] L. Lin, A. J. Sabnis, E. Chan et al., "The Hippo effector YAP promotes resistance to RAF- and MEK-targeted cancer therapies," *Nature Genetics*, vol. 47, no. 3, pp. 250–256, 2015.

[17] A. Roesch, "Tumor heterogeneity and plasticity as elusive drivers for resistance to MAPK pathway inhibition in melanoma," *Oncogene*, vol. 34, no. 23, pp. 2951–2957, 2015.

[18] L. Li, G. Wang, N. Li, H. Yu, J. Si, and J. Wang, "Identification of key genes and pathways associated with obesity in children," *Experimental and Therapeutic Medicine*, vol. 14, no. 2, pp. 1065–1073, 2017.

[19] B. Zhao, Z. Baloch, Y. Ma et al., "Identification of potential key genes and pathways in early-onset colorectal cancer through bioinformatics analysis," *Cancer Control*, vol. 26, no. 1, p. 1073274819831260, 2019.

[20] N. Ikeda, Y. Nakajima, T. Tokuhara et al., "Clinical significance of aminopeptidase N/CD13 expression in human pancreatic carcinoma," *Clinical Cancer Research*, vol. 9, no. 4, pp. 1503–1508, 2003.

[21] Y. Liu, J. Li, M. Li, F. Li, Y. Shao, and L. Wu, "microRNA-510-5p promotes thyroid cancer cell proliferation, migration, and invasion through suppressing SNHG15," *Journal of Cellular Biochemistry*, vol. 120, no. 7, 2019.

[22] T. Lu, S. Chen, L. Qu, Y. Wang, H. D. Chen, and C. He, "Identification of a five-miRNA signature predicting survival in cutaneous melanoma cancer patients," *PeerJ*, vol. 7, article e7831, 2019.

[23] J. Mastroianni, N. Stickel, H. Andrlova et al., "miR-146a controls immune response in the melanoma microenvironment," *Cancer Research*, vol. 79, pp. 183–195, 2019.

[24] S. Caporali, A. Amaro, L. Levati et al., "miR-126-3p down-regulation contributes to dabrafenib acquired resistance in melanoma by up-regulating ADAM9 and VEGF-A," *Journal of Experimental & Clinical Cancer Research*, vol. 38, no. 1, 2019.

[25] N. Felli, F. Felicetti, A. M. Lustri et al., "miR-126&126* restored expressions play a tumor suppressor role by directly regulating ADAM9 and MMP7 in melanoma," *PLoS One*, vol. 8, 2013.

[26] J. E. Schoenhals, T. R. Cushman, H. B. Barsoumian et al., "Anti-glucocorticoid-induced tumor necrosis factor-related protein (GITR) therapy overcomes radiation-induced treg immunosuppression and drives abscopal effects," *Frontiers in Immunology*, vol. 9, p. 2170, 2018.

[27] T. Okamoto, "Parkinson's disease: amantadine, zonisamide, dabrafenib," *Brain Nerve*, vol. 71, pp. 953–959, 2019.

[28] L. Kofler, C. Berg, K. Kofler et al., "Simultaneous targeted therapy for metastatic melanoma and hepatitis C," *Journal der Deutschen Dermatologischen Gesellschaft*, vol. 18, no. 1, pp. 42-43, 2019.

[29] P. Kharaziha, D. Chioureas, D. Rutishauser et al., "Molecular profiling of prostate cancer derived exosomes may reveal a predictive signature for response to docetaxel," *Oncotarget*, vol. 6, no. 25, pp. 21740–21754, 2015.

[30] M. Klink, M. Nowak, M. Kielbik et al., "The interaction of HspA1A with TLR2 and TLR4 in the response of neutrophils induced by ovarian cancer cells in vitro," *Cell Stress & Chaperones*, vol. 17, no. 6, pp. 661–674, 2012.

[31] P. Kasioumi, P. Vrazeli, P. Vezyraki et al., "Hsp70 (HSP70A1A) downregulation enhances the metastatic ability

of cancer cells," *International Journal of Oncology*, vol. 54, pp. 821–832, 2018.

[32] L. L. Remsing Rix, B. M. Kuenzi, Y. Luo et al., "GSK3 alpha and beta are new functionally relevant targets of tivantinib in lung cancer cells," *ACS Chemical Biology*, vol. 9, pp. 353–358, 2013.

[33] B. Bellei, E. Flori, E. Izzo, V. Maresca, and M. Picardo, "GSK3β inhibition promotes melanogenesis in mouse B16 melanoma cells and normal human melanocytes," *Cellular Signalling*, vol. 20, no. 10, pp. 1750–1761, 2008.

[34] M. Diefenbacher and A. Orian, "Stabilization of nuclear oncoproteins by RNF4 and the ubiquitin system in cancer," *Molecular & Cellular Oncology*, vol. 4, article e1260671, 2016.

[35] B. Bellei, A. Pitisci, E. Migliano, G. Cardinali, and M. Picardo, "Pyridinyl imidazole compounds interfere with melanosomes sorting through the inhibition of cyclin G-associated kinase, a regulator of cathepsins maturation," *Cellular Signalling*, vol. 26, no. 4, pp. 716–723, 2014.

Hindawi
BioMed Research International
Volume 2021, Article ID 5582648, 11 pages
https://doi.org/10.1155/2021/5582648

Research Article

Cediranib Induces Apoptosis, G1 Phase Cell Cycle Arrest, and Autophagy in Non-Small-Cell Lung Cancer Cell A549 In Vitro

Menghuan Guo,[1,2] **Zhiyuan Liu**,[3] **Jing Si**,[2,4] **Jinhua Zhang**,[2,4] **Jin Zhao**,[5] **Zhong Guo**,[5] **Yi Xie**,[2,4] **Hong Zhang**,[2,4] **and Lu Gan**[2,4]

[1]*School of Pharmacy, Lanzhou University, Lanzhou, Gansu 730000, China*
[2]*Advanced Energy Science and Technology Guangdong Laboratory, Huizhou, Guangdong 516029, China*
[3]*Gansu Key Laboratory of Environmental Friendly Composites and Biomass Utilization, College of Chemical Engineering, Northwest Minzu University, Lanzhou, Gansu 730030, China*
[4]*Institute of Modern Physics, Chinese Academy of Sciences, Lanzhou 730000, China*
[5]*Medical College of Northwest Minzu University, Lanzhou, Gansu 730030, China*

Correspondence should be addressed to Hong Zhang; zhanghong@impcas.ac.cn and Lu Gan; ganl@impcas.ac.cn

Received 9 February 2021; Revised 1 March 2021; Accepted 11 March 2021; Published 30 March 2021

Academic Editor: Ning Cao

Lung cancer remains the leading cause of cancer death worldwide. Late diagnosis, chemoresistance, and metastasis are the main reasons for the high mortality rate of lung cancer. Therefore, the development of other treatments is urgent. Cediranib (CED), a vascular endothelial growth factor receptor (VEGFR) kinase inhibitor, shows promising antitumour activities in various cancers including lung cancer. Here, we explored the effects and the underlying molecular mechanism of CED on non-small-cell lung cancer (NSCLC) cell line A549 cells in vitro. Our results show that CED could inhibit A549 cell proliferation and cloning formation. Meanwhile, G1 phase cell cycle arrest was also found, as featured by the increased proportion of G1 phase cells as well as the reduction of G1 phase relative proteins CDK4/cyclin D1 and CDK2/cyclin E. Moreover, the ratio of LC3-II/LC3-I was elevated significantly in CED-treated groups compared with the controls. Furthermore, the expression of p-Akt, p-P38, p-Erk1/2, and p-mTOR proteins was decreased obviously in the treatment groups. These results suggest that CED could induce apoptosis and G1 phase cell cycle arrest in A549 cells. Meanwhile, CED may induce autophagy through MAPK/Erk1/2 and Akt/mTOR signal pathway in A549 cells.

1. Introduction

Lung cancer is one of the most common malignancies and ranks the 1st in both incidence and mortality, with approximately 2.09 million new cases and 1.76 million deaths in the world in 2018 according to the Internal Agency for Research on Cancer. NSCLC accounts for approximately 80-85% of all lung cancers, and the 5-year survival rate for NSCLC patients was less than 15% currently [1, 2]. Approximately 80% patients with NSCLC develop metastases within 2 years after the diagnosis of NSCLC. Early diagnosis of lung cancer before clinical symptoms is an effective means to reduce cancer mortality, and the use of low-dose CT scans contributes to a 20% reduction in lung cancer mortality according to National Lung Screening Trial [3]. Unfortunately, over 60% of patients are diagnosed with lung cancer in the advanced stages [4]. In recent years, VEGFR inhibitors such as Ramucirumab have improved the prognosis of patients with NSCLC [5], suggesting that VEGFR inhibitor is a new strategy for NSCLC treatment.

The VEGF pathway plays an essential role in angiogenesis. It was reported that high levels of VEGF were correlated with NSCLC. Meanwhile, VEGFR is upregulated in metastatic prostate cancer, and VEGF-D, VEGFR2, and VEGFR3 are related to advanced-stage prostate disease [6]. Moreover, high VEGF-C expression predicts an adverse prognosis in pediatric and adult acute myeloid leukemia [7]. VEGF signaling affects tumour progress mainly in three ways. First,

VEGF ligands interact with VEGFR tyrosine kinases on the surface of endothelial cells, which we refer to as "canonical" VEGF signaling. It appears to be a common form to induce cell proliferation, migration, and vascular morphogenesis [8]. HIF-1 expression is elevated under hypoxia condition, and elevated HIF-1 subsequently promotes autocrine VEGF in tumour cells. The secreted VEGF binds to specific receptors on the surface of tumour cells, such as neuropilin-1 and Flt-1, and affects cell survival and migration through the activation of downstream signaling pathways such as PI3K/Akt signaling [9–11]. This is the second pathway by which VEGF maintains its own development, also known as the autocrine pathway. Meanwhile, a line of evidence presented that VEGFR tyrosine kinases can be activated in an independent manner through Src kinases or alternative "ligands" such as Gal3 and Gall, and this is considered to be "noncanonical" VEGF signaling [12–14]. Therefore, at least 3 strategies, including VEGF inhibitor, VEGFR inhibitor, and VEGFR tyrosine kinase inhibitor, have been applied to inhibit the VEGF signal pathway.

CED, a highly potent VEGFR1, VEGFR2, and VEGFR3 tyrosine kinase inhibitor, has shown promising antitumour activity in prostate cancer [15], glioblastoma [16], metastatic breast cancer [17], and renal cell carcinoma [18] *in vitro*, *in vivo*, and in clinical trials. MFOLFOX6 in combination with CED can prolong progression-free survival in patients with metastatic colorectal cancer [19]. There is evidence that CED-cisplatin cotreatment can reduce tumour dissemination and prolong the survival of mice bearing ovarian cancer [19]. Besides, antitumour activities of CED in lung cancer rely on the inhibitory activity against the VEGFR family and the platelet-derived growth factor receptor- (PDGFR-) related kinases c-Kit, PDGFR-α, and PDGFR-β [21]. Many studies have shown that CED has beneficial effects on lung cancer [21, 22]. Devery et al. have found that VEGFR2 protein and mRNA are elevated in 9/25 NSCLC cell lines and is closely correlated with cancer angiogenesis. VEGFR2 is expressed in both squamous cells and adenocarcinoma cells, but not in normal lung epithelial cells [22]. Meanwhile, administration of CED can rapidly reduce the perfusion of Calu-3 cancers (stromal vessel phenotype), leading to acute hypoxia in lung cancer [23]. Additionally, low baseline VEGFR2 and VEGFR3 were predictive for both overall survival and progression-free survival in CED-treated NSCLC patients. Furthermore, combined MEK inhibitor selumetinib with VEGFR inhibitor CED in lung cancer results in decreased cell proliferation, metastasis, and angiogenesis. However, the mechanism remains to be explored [24]. In the present study, we aimed to validate the underlying molecular mechanisms of CED in A549 cells.

2. Materials and Methods

2.1. Materials. The human NSCLC cell line A549 (p53 wild-type) was provided by the Cell Bank of Chinese Academy of Sciences (Shanghai, China). CED (purity > 99.58%) was purchased from MedChemExpress (New Jersey, USA). CED was dissolved in dimethyl sulfoxide (DMSO) at a concentration of 10 mM and stored at -80°C.

Fetal bovine serum (FBS) was purchased from Gibco (Carlsbad, CA, USA). Mouse anti-microtubule-associated protein B-light chain 3 (LC3B) was purchased from Cell Signaling Technology (Billerica, USA). Rabbit anti-GAPDH, mouse anti-mTOR, and rabbit anti-p-mTOR were purchased from Invitrogen (California, USA). Rabbit anti-VEGFR2, rabbit anti-VEGFR3, rabbit anti-P38, rabbit anti-p-P38, rabbit anti-Erk1/2, and rabbit anti-p-Erk1/2 were acquired from GeneTex (Taiwan, China). Rabbit Anti-CDK4, rabbit anti-cyclin D1, rabbit anti-CDK2, and rabbit anti-cyclin E were purchased from Abcam (Cambridge, England).

Cell counting kit-8 (CCK-8) was obtained from Yeasen Biotech (Shanghai, China). Antifade mounting medium with 4′,6-diamidino-2-phenylindole was obtained from Vector Laboratories (Shanghai, China). Annexin V-FITC/PI double staining was purchased from Becton, Dickinson and Company (New Jersey, USA).

2.2. Cell Culture. The human NSCLC cell line A549 was maintained in RPMI-1640 medium, which is supplemented with 10% FBS. Cells were incubated at 37°C in a 5% CO_2 humid environment. The cells were replaced with fresh medium every other day and plated at an appropriate density according to experimental needs.

2.3. Cell Viability Assay. CCK-8 was used to determine the proper concentrations of CED in A549 cells. The cells were incubated in 96-well plates at a density of 6000 per well with 200 μl complete medium. After 24 h, cells were treated with an increasing dose of CED (0 μM, 3 μM, 6 μM, 9 μM, 12 μM, and 15 μM) for 24 h, 48 h, and 72 h, respectively. 0.15% DMSO, the same DMSO concentration as the 15 μM group, was used to test the toxic effects of DMSO on the cells. Subsequently, CCK-8 solution (20 μl) was added to the cell culture sample and further incubated for 1 h at 37°C. The absorbance of each well was measured at 450 nm by using a microplate reader (Tecan infinite 200 M, Männedorf, Switzerland).

2.4. Colony-Forming Assay. A colony-forming assay was applied to detect cell survival activity in vitro. Briefly, cells were seeded onto the 60 mm dish at proper density with 2 ml culture media 24 h before treatment with different concentrations of CED (0 μM, 3 μM, 6 μM, and 9 μM). After incubating with CED for 48 h, the cells are digested and resuspended and then were incubated in a 60 mm dish for 10~14 days with drug-free medium. Colonies were fixed with 4% paraformaldehyde for 20 min followed by dyeing with 1% crystal violet for 15 min at room temperature. The colonies consisting of more than 50 cells were counted under a light microscope.

2.5. Cell Apoptosis Assay. The cells treated with CED for 48 h were digested with EDTA-free trypsin. Then, digested cells were washed with PBS followed by resuspending in 150 μl binding buffer. 5 μl propidium iodide (PI) and 5 μl Annexin V-FITC were added and incubated for 15 min at room temperature under dark condition. Cell apoptosis at each stage was detected on a flow cytometer FlowSight (Washington,

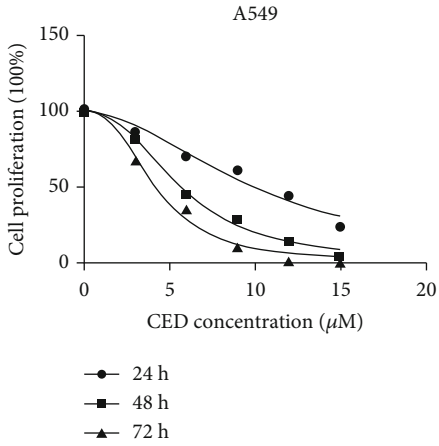

(a)

LC_x of cediranib			
A549	LC_{30}	LC_{50}	LC_{70}
24 h	6.85	10.51	14.18
48 h	3.92	6.45	8.97
72 h	3.44	4.99	6.54

(b)

Figure 1: CED significantly inhibited A549 cell viability. (a) CCK-8 assay revealed the viability of A549 cells affected by CED. (b) LC_{30}, LC_{50}, and LC_{70} of CED in A549 cells for 24 h, 48 h, and 72 h. The data represent the mean ± SD.

USA) and analyzed by IDEAS Application v6.0 software. Each sample was collected at least 10,000 events.

2.6. Cell Cycle Assay. Cells were treated with different concentrations of CED for 48 h and then were digested with trypsin followed by fixing with 75% ethanol at -20°C. After overnight incubation, cells were resuspended and rehydrated in PBS for 15 min. Subsequently, cells were resuspended in 150 μl DNA Staining Solution for 20 min under dark condition. The cell cycle was detected by flow cytometry and analyzed by FlowJo-V10 software. At least 20,000 events were examined per sample.

2.7. Immunofluorescence. A549 cells were seeded on the slices in 35 mm dishes and incubated overnight. Then, cells were treated with different concentrations of CED for 48 h. Subsequently, slices were fixed with 4% paraformaldehyde after washing with phosphate-buffered saline (PBS) for 3 times. 0.25% TritonX-100 was added to permeabilize the cells for 15 min. After washing with PBS for 3 times, the cells were blocked with 5% BSA for 70 min at room temperature (RT). After blocking, the cells were incubated with primary antibody against LC3B at 4°C overnight and then incubated with secondary antibody at room temperature for 1.5 h. Finally, cells were counterstained with DAPI for 5 min in the dark. Images were captured using a laser scanning confocal microscope (Carl Zeiss AG, Germany).

2.8. Western Blot Analysis. Cells were incubated in different concentrations of CED. After 48 h, the cells were washed with PBS and then lysed with Lysis Buffer (RIPA: PMSF = 100 : 1) on ice for 30 min. A BCA protein assay kit was used to detect the concentration of protein. The total proteins were separated by sodium dodecyl sulfate-polyacrylamide gel electrophoresis at 20 μg per gel lane, followed by transfer to a PVDF membrane. The membrane was blocked for 1 h, followed by incubation with primary antibodies against CDK4, cyclin D1, CDK2, cyclin E, LC3B, Akt, p-Akt, P38, p-P38, Erk1/2, p-Erk1/2, mTOR, and p-mTOR overnight at 4°C. Then, the membranes were washed and then incubated with secondary antibodies. Density values of target protein bands were detected by using an ECL kit from Yeasen Biotech (Shanghai, China). GAPDH was used to normalize the results.

2.9. Statistical Analysis. The experiments were totally repeated for three times, and data were presented as the mean ± SD. Statistical significance was evaluated using one-way analysis of variance (ANOVA) with the LSD (L) post hoc test in SPSS 16.0 (IBM SPSS Statistics 20.0, Armonk, NY). Origin8.0 (Origin Lab, Northampton, MA) software was used to plot the figures.

3. Results

3.1. CED Inhibited A549 Cell Proliferation. In order to investigate the effect of CED on cell viability, the cells were treated with different concentrations of CED for 24 h, 48 h, and 72 h, respectively. The CCK-8 assay showed that CED could markedly inhibit the growth of A549 cells in a concentration- and time-dependent manner. The Bliss method was used to calculate the lethal concentrations (LC_x) of CED. Our data showed that LC_{30}, LC_{50}, and LC_{70} of CED in A549 cells for 48 h were 3.92 μM, 6.45 μM, and 8.97 μM, respectively (Figure 1). The cell proliferation rate of A549 cells after 24 h of CED treatment was significantly higher than that of 48 h. Therefore, A549 cells were treated with CED for 48 h for the subsequent experiments. The following concentrations 0 μM, 3 μM, 6 μM, and 9 μM which can cover LC_{30}, LC_{50}, and LC_{70} of CED were selected. 0.15% DMSO had no toxic effect on cells, so the subsequent experiments did not examine the effect of DMSO on A549 cells alone.

3.2. CED Inhibited A549 Cell Colony Formation. We observed that the ability of cell clone formation decreased with the increase of drug concentration. The clone survival rate of the 3 μM-, 6 μM-, and 9 μM-treated groups was 92.4%, 89.6%, and 67.7%, respectively. Cell viability reduced

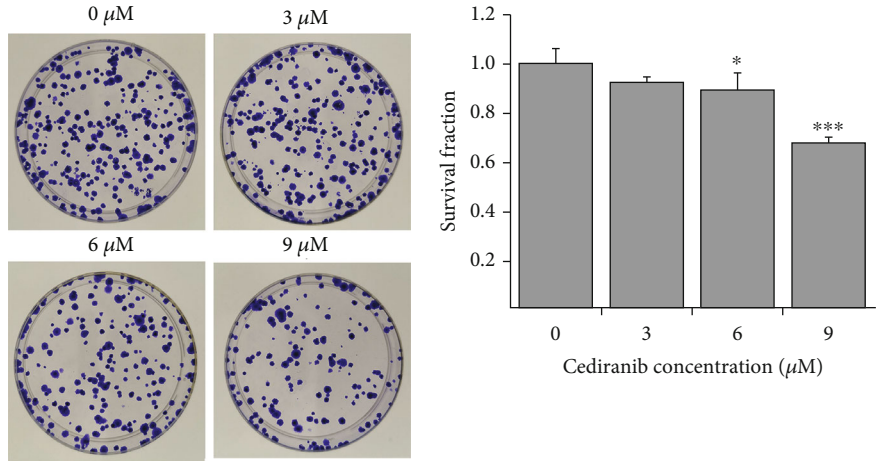

Figure 2: CED treatment could inhibit A549 cell colony formation. (a) Representative pictures of colony-forming potential of A549 cells in different treatment groups. (b) Cell survival fraction bar chart was performed with cell clone formation assay. Cells were treated with the indicated concentration of CED for 48 h and then plated for survival. All experiments were performed in triplicate. The data represent the mean ± SD. $^{*}p < 0.05$ and $^{***}p < 0.001$ (vs. control group).

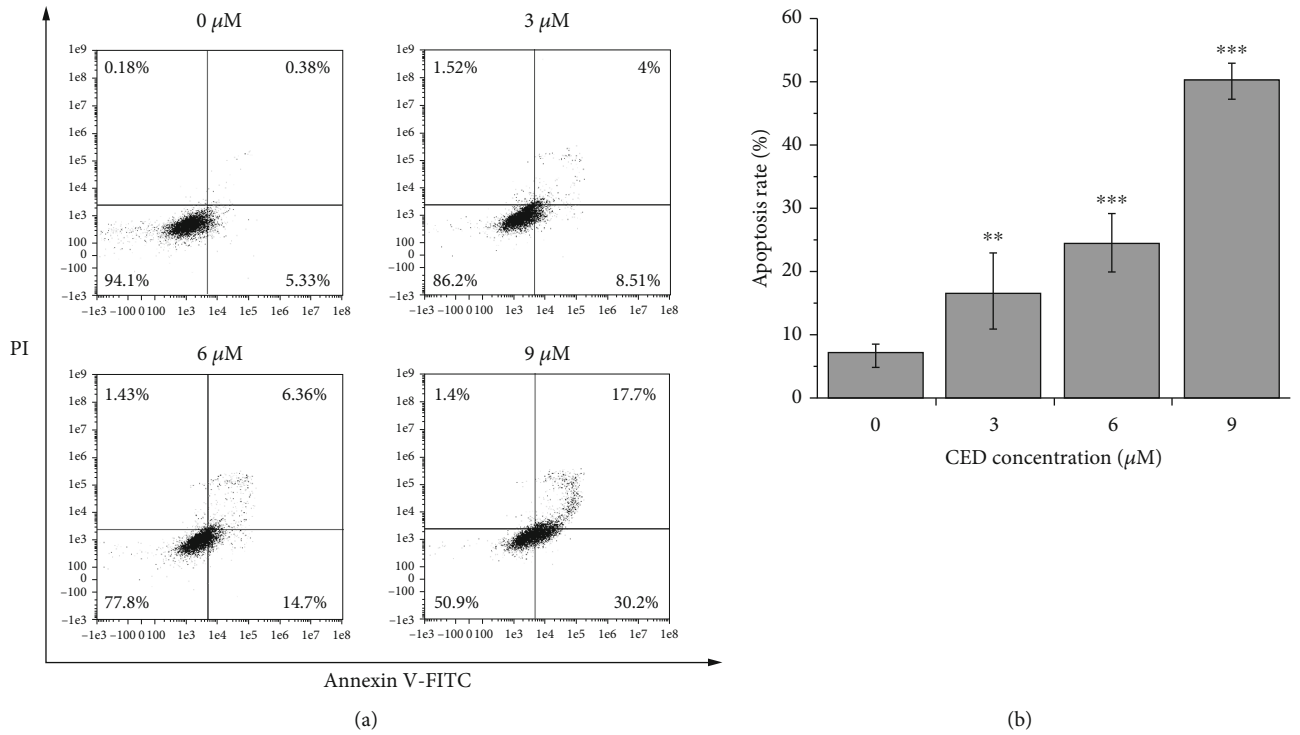

Figure 3: CED treatment for 48 h induced cell apoptosis in A549 cells. (a) Cell apoptosis assay was investigated with flow cytometry. (b) Percentages of apoptotic rate and cell population were calculated. All experiments were performed in triplicate. All data are representative of three independent experiments. $^{**}p < 0.01$ and $^{***}p < 0.001$ compared with controls.

approximately 10.4% ($p < 0.05$) and 32.34% ($p < 0.001$) after treatment with 6 μM and 9 μM CED for 48 h compared with the controls (Figure 2). However, there was no statistical significance in the 3 μM-treated group compared with the controls.

3.3. CED Induced A549 Cell Apoptosis. To further explore whether the decrease of cell survival rate induced by CED is implicated in apoptosis, an Annexin V-FITC/PI double staining assay was used to detect the apoptosis of A549 cells. As shown in Figure 3, our results indicated that cell apoptosis was significantly induced after 48 h of CED treatment. The apoptosis rate was positively correlated with the dose. The apoptosis rates were 12.51%, 21.06%, and 47.9%, respectively, after 3 μM, 6 μM, and 9 μM CED treatment, compared with 7.59% in the control group. Moreover, cells treated with

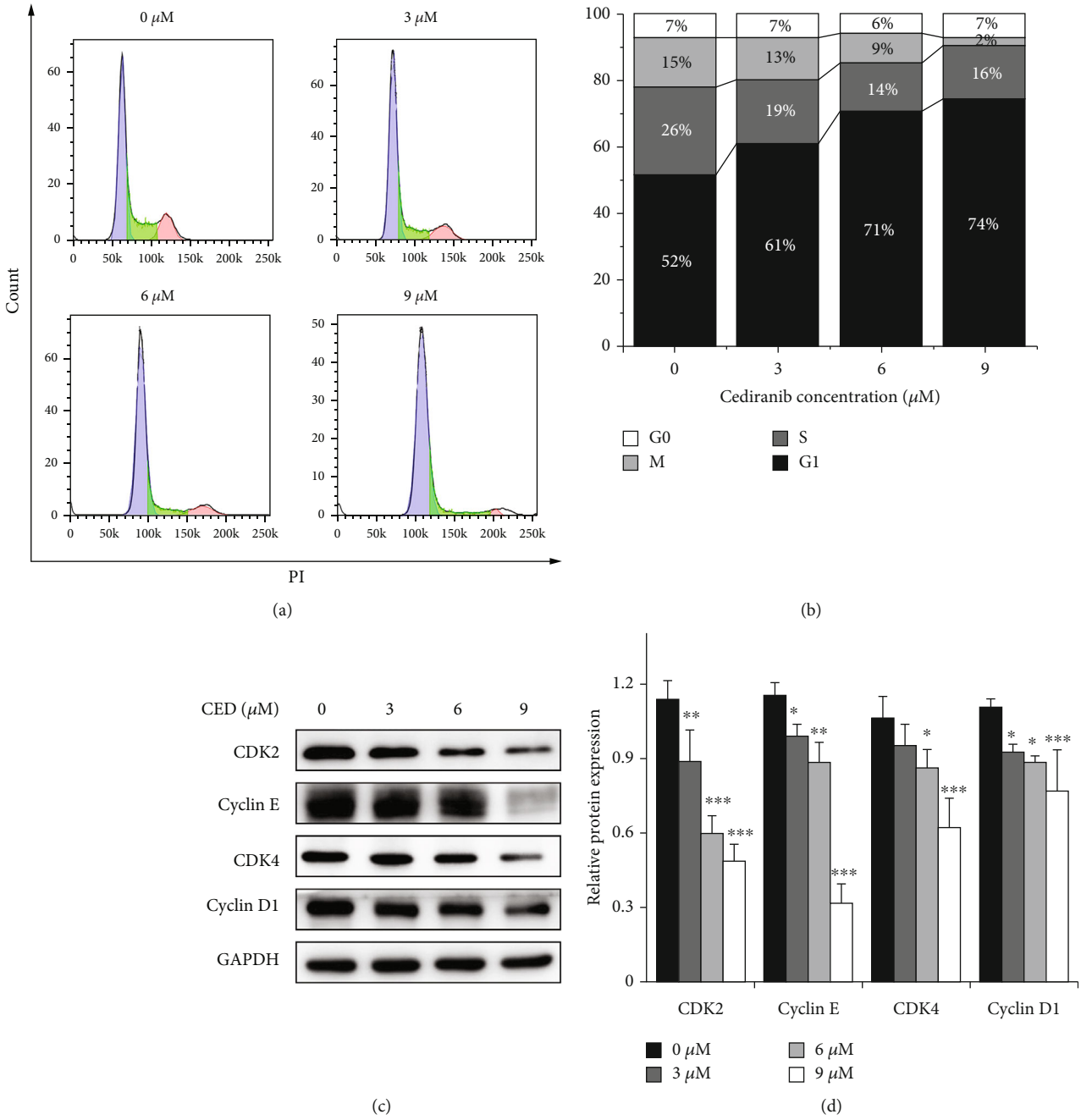

Figure 4: CED treatment induced G1 phase arrest in A549 cells after 48 h. (a) Cell cycle distribution in A549 cells pretreated with the indicated concentration of CED at the time point of 48 h. DNA content of cells stained with PI was detected using flow cytometry. (b) The percentage of the cell population in each phase was quantitatively analyzed after exposure to the indicated CED for 48 h. (c) After CED treatment, G1 phase relative proteins CDK2, cyclin E, CDK4, and cyclin D1 were detected by western blot analysis. (d) Quantitative analysis of CDK2, cyclin E, CDK4, and cyclin D1 proteins was represented by column graphs. Bars represented the mean ± SD from three independent experiments. $^{*}p < 0.05$, $^{**}p < 0.01$, and $^{***}p < 0.001$ (vs. control group).

3 μM, 6 μM, and 9 μM CED induced 2.34-fold ($p < 0.01$), 3.44-fold ($p < 0.001$), and 7.04-fold ($p < 0.001$) apoptosis compared with the controls.

3.4. CED Induced A549 Cell Cycle Arrest in G1 Phase. Cell cycle arrest was analyzed by flow cytometry after treatment with CED for 48 h. Compared with the control group, an increasing percentage of G1 phase cells was observed at all doses (Figures 4(a) and 4(b)), accompanied by a decrease in the percentage of S and G2/M phase cells. The proportion of G1 phase cells in the 3 μM, 6 μM, and 9 μM groups were 61%, 71%, and 74%, respectively, and were observably higher than that of the controls (52%). The positive correlation between G1 phase retardation

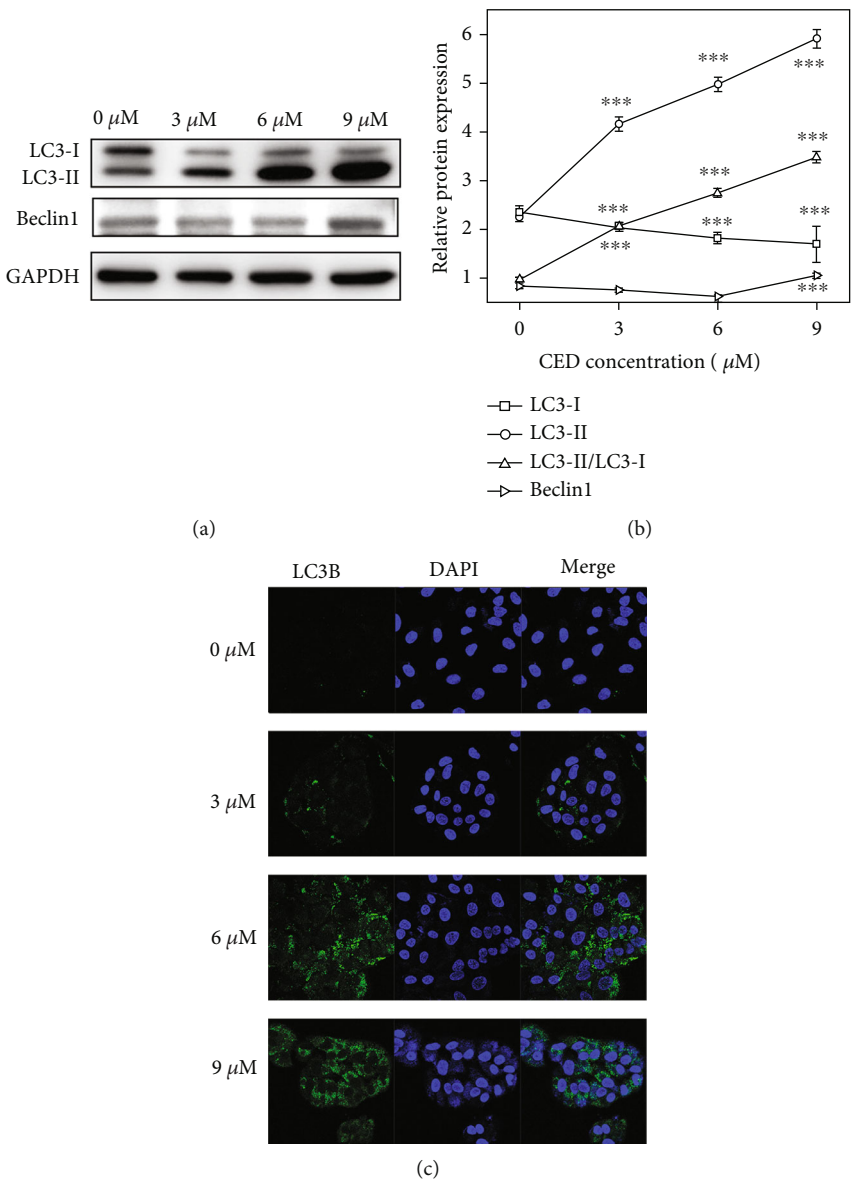

Figure 5: CED treatment activated autophagy in A549 cells. (a) A549 cells from indicated treatment groups were incubated for 48 h, and autophagy relative proteins (LC3B and Beclin1) were detected using western blot. (b) Quantitative analysis of Beclin1, LC3-I, and LC3-II proteins in A549 cells by western blot analysis. (c) The localization of LC3B protein in A549 cells supplemented with CED was determined by fluorescent microscopy. All data are representative of three independent experiments. The data are expressed as the mean ± SD. $^{***}p < 0.001$ (vs. control group).

and concentration suggests that CED may suppress the proliferation of A549 cells by inducing G1 phase cell cycle arrest. Furthermore, CED significantly affected the expression of G1 phase-related proteins CDK2, cyclin E, CDK4, and cyclin D1. As shown in Figures 4(c) and 4(d), CED could remarkably inhibit the growth of A549 cells in a concentration-dependent manner. The expression of cell cycle-related proteins was significantly decreased in the 6 μM- and 9 μM CED-treated groups. 3 μM CED treatment can also slightly decrease cell cycle-related proteins cyclin E, cyclin D1, and CDK2. However, there was no significant difference in the expression of CDK4 protein compared with the control group.

3.5. CED Induced A549 Cell Autophagy. Under physiological conditions, autophagy is at a low level. When the body is under stress, cells degrade and recycle their intracellular components by inducing autophagy [25]. We tested whether CED could induce autophagy in A549 cells using a western blot assay and fluorescence microscopy. Rat microtubule-associated protein light chain 3 (LC3), a homologue of yeast Atg8, is an essential component of autophagy. The transition from LC3-I to LC-3II, which relies on the Atg7/Atg3 ubiquitin-like system, has been recognized as a marker of autophagy [26]. Therefore, protein levels of LC3-I and LC3-II in CED-treated cells were detected using GAPDH as a control. The expression of Beclin1, an autophagy marker protein,

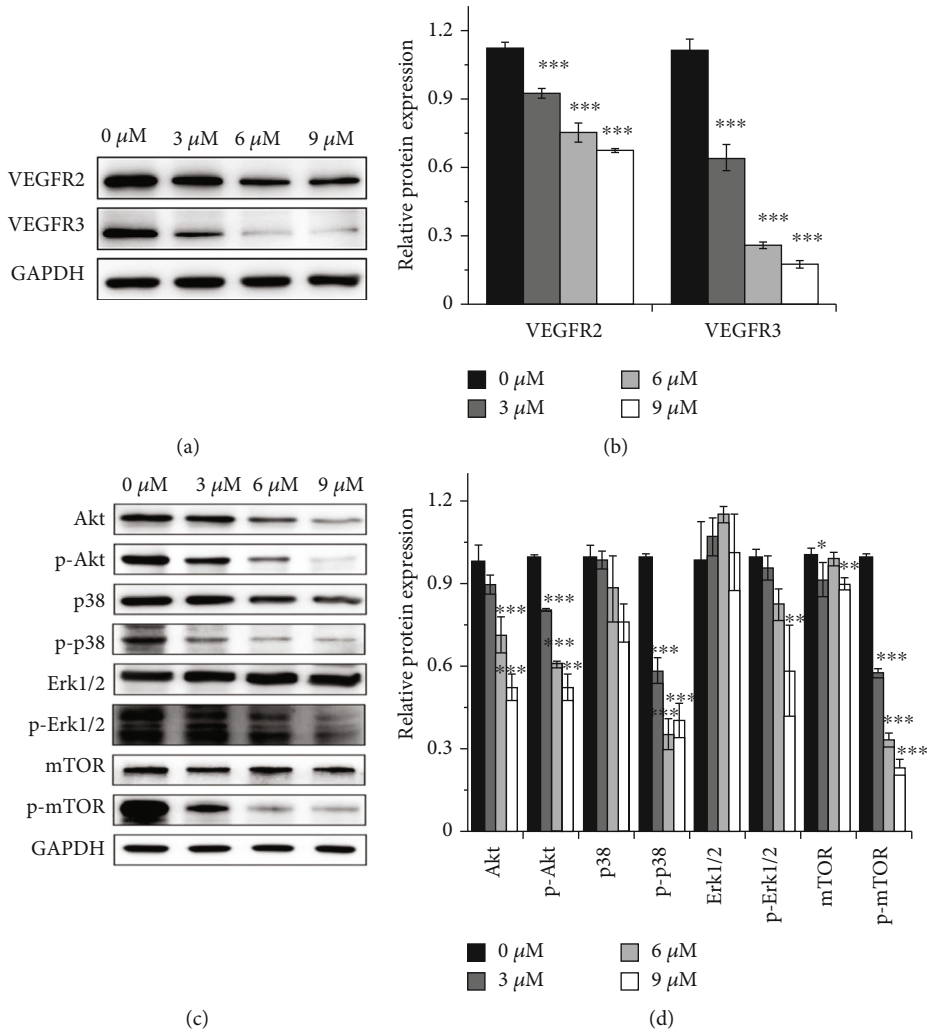

Figure 6: Effect of CED on proteins involved in VEGFR/Akt/mTOR and VEGFR/MAPK pathway in A549 cells after 48 h treatment. (a, c) Representative western blot images. (b, d) Quantitative analysis of the expression of VEGFR2, VEGFR3, Akt, p-Akt, p-38, p-p38, Erk, p-Erk, mTOR, and p-mTOR, as represented by column graphs. GAPDH was used as a control. All data are representative of three independent experiments. The data are expressed as the mean ± SD. $^{*}p < 0.05$, $^{**}p < 0.01$, and $^{***}p < 0.001$ (vs. control group).

was also detected. Our data shows that Beclin1 was upregulated in the 9 μM group. Compared with the controls, CED treatment strongly increased LC3-II and decreased LC3-I proteins in a dose-dependent manner (Figures 5(a) and 5(b)). Additionally, an increase in the ratio of LC3-II/LC3-I was clearly observed (2.14-fold ($p < 0.001$), 2.86-fold ($p < 0.001$), and 3.64-fold ($p < 0.001$), respectively, for 3 μM, 6 μM, and 9 μM CED treatment *vs.* the controls). Moreover, confocal microscopic (LSCM) biomedical images showed that the application of CED dramatically accumulated LC3B puncta in 6 μM and 9 μM groups while LC3B puncta in the 3 μM group seems weak (Figure 5(c)).

3.6. CED Suppressed Akt/mTOR and MAPK Signal Pathway. In order to elucidate the role of CED in cancer therapies, we examined the representative proteins in VEGFR, Akt/mTOR, and MAPK signal pathways by western blot. Our data demonstrated that the expression of VEGFR2 and VEGFR3 was consistently downregulated after CED treatment (Figures 6(a) and 6(b)). Phosphorylated Akt (p-Akt), phosphorylated p38 (p-p38), and phosphorylated mTOR (p-mTOR) were also inhibited by CED in all doses while phosphorylated Erk1/2 (p-Erk1/2) was only significantly decreased in the 9 μM group (Figures 6(c) and 6(d)). In addition, p38, Erk1/2, and mTOR had no change in all groups. Meanwhile, we found that CED can reduce Akt expression in the 6 μM group and the 9 μM group. These data suggested that CED may induce autophagy and G1 phase cell cycle arrest through suppressing MAPK and Akt/mTOR signal pathways. However, whether the inhibition of MAPK and Akt/mTOR signal pathways is related to the reduction of VEGFR2 and VEGFR3 needs further study.

4. Discussion

Lung cancer is one of the most common malignant tumours which severely endanger human health and life with the highest morbidity and incidence. Drug resistance

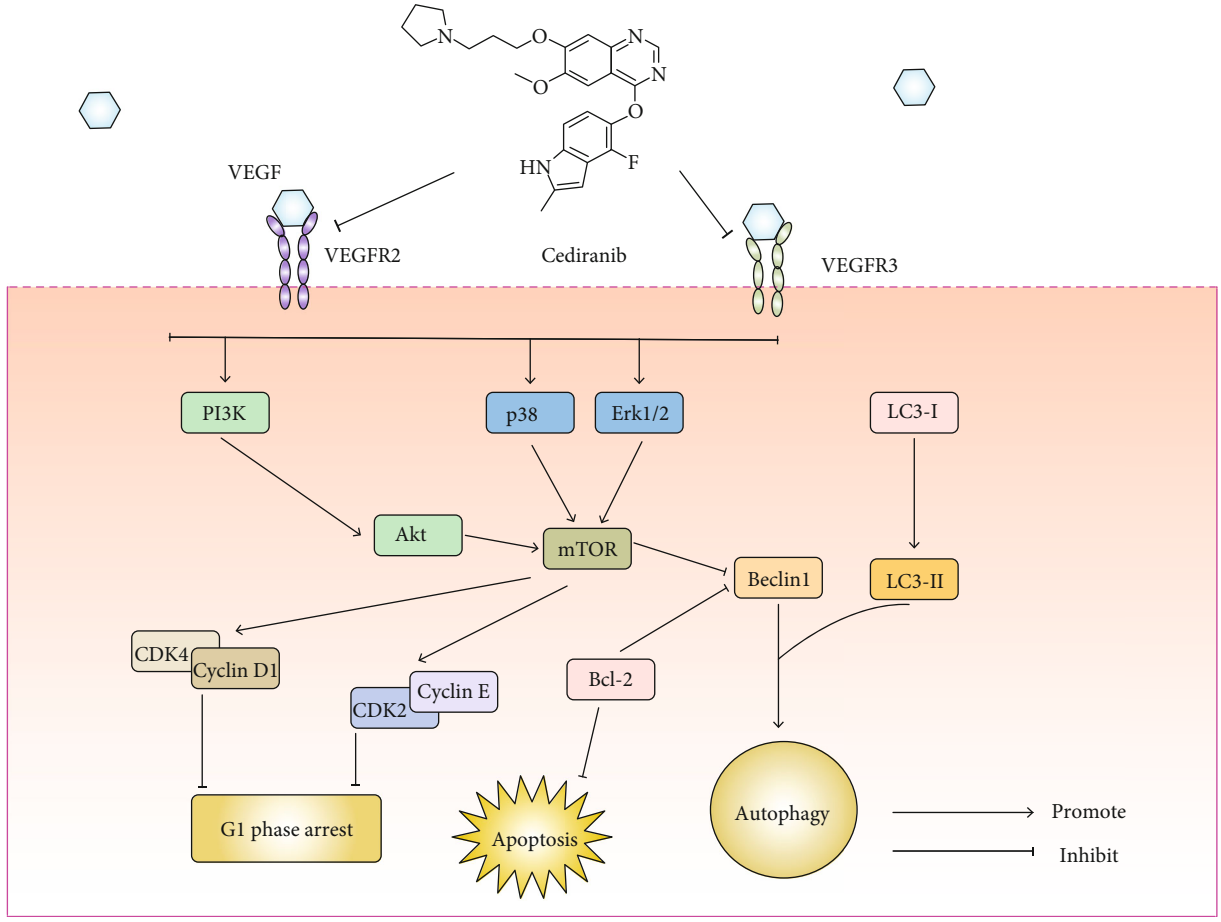

Figure 7: Schematic depicting the effect of CED on cell survival and the underlying mechanism. CED inhibits the expression of VEGFR2/3 and suppresses MAPK/Erk1/2 and Akt/mTOR signaling pathways in A549 cells. This eventually leads to apoptosis, G1 phase cell cycle arrest, and autophagy, as featured by the decrease of G1 phase relative proteins CDK4/cyclin D1 and CDK2/cyclin E and the increase of autophagy relative proteins LC3-II and Beclin1.

remains the obstacle to lung cancer treatment. Therapies targeting VEGFR signaling, such as Apatinib, Ramucirumab, and Axitinib, show promising effects on suppressing the proliferation and angiogenesis of gastric cancer, osteosarcoma, head and neck cancer, and NSCLC [27–30]. CED is a VEGFR tyrosine kinase inhibitor and shows anticancer potential against various types of tumours [31]. Our findings demonstrate that CED inhibited cell proliferation and clonal formation while inducing apoptosis, G1 phase cell cycle arrest, and autophagy in A549 cells. Figure 7 systematically depicts the effect of CED on cell survival and the underlying mechanism.

Apoptosis is a kind of programmed cell death, occurring under either physiological or pathological conditions such as normal cell turnover, immune reaction, and radiation/chemical-induced cell death [32]. Inducing cancer cell apoptosis is the ultimate goal of cancer therapies. The mechanism of apoptosis is divided into two main pathways: the intrinsic pathway (mitochondrial pathway) and the extrinsic pathway (death receptor pathway). In addition, there is an additional pathway that involves T-cell mediated cytotoxicity and perforin-granzyme-dependent cell killing [32, 33]. Annexin V/PI double staining indicated that CED can strongly induce apoptosis in A549 cells. However, potential mechanisms of apoptosis induction need to be further explored.

Cell cycle progression, which provides an opportunity for damage repair and stopping their transmission to the daughter cells, is principally modulated through cyclin-dependent kinase (CDKs) [35]. Cyclins form complexes with their specificity CDKs and act as their regulatory subunit [35]. Reversing the repressing transcription of many genes, which are essential for cells to exit from the G1 phase, is required for the cyclin D/CDK4/6 complex. CDK2 together with cyclin E governs the G1/S transition and the progression of the S phase [37].

We used flow cytometry to detect the cell cycle, and the results showed that CED could increase the proportion of G1 phase cells while decreasing the proportion of S and G2/M phase cells. The later protein quantification also discovered the decreased expression of CDK4, cyclin D, CDK2, and cyclin E. Our data indicated that CED could inhibit the transition of G1 to S phase and induce G1 phase cell cycle arrest in A549 cells.

Autophagy is an innate self-regulating process that removes dysfunctional or superfluous proteins and

organelles with the help of digestive enzymes in lysosomes [38]. LC3-II and Beclin1 are representative markers of autophagy. The elevated LC3-II and Beclin1 in treated groups were confirmed by western blot, suggesting that CED could induce autophagy in A549 cells.

It is worth noting that autophagy is a double-edged sword. On one hand, autophagy helps cells adapt to changing living conditions and recycling cytoplasm. On the other hand, autophagy or autophagy-relevant proteins may lead to apoptosis, necrosis, pyroptosis, or "autophagic-cell death" once autophagy degrades the cytoplasm excessively [39]. Meng has found that autophagy inhibitor in combination with VEGFR2 inhibitor Apatinib can further inhibit papillary thyroid carcinoma cell proliferation and induce PARP/Bcl-2-mediated apoptosis [40]. Gefitinib is an EGFR-TKI. Evidence suggests that autophagy contributed to Gefitinib resistance in NSCLC cells [41]. Therefore, the role of autophagy in tumour therapy is worth further exploring.

In order to meet the need for rapid proliferation, tumour cells promote angiogenesis by secreting proangiogenic factors such as PDGF, TGF, and VEGF family. Among them, the VEGF family is the most important factor for angiogenesis. After activating by VEGF, VEGFR dimerizes themselves and then recruits specific downstream signal transduction mediators to trigger signal transduction, following by the activation of downstream signaling pathways such as the PI3K/Akt/mTOR signal pathway and MAPK signal pathway [42, 43]. Earlier researches have reported that mTOR is a common effect factor of Akt and MAPK signal pathway and suppressed autophagic activity by combining with the positive autophagy regulator Atg1/ULK1 complexes [44]. Beclin1 is a key molecule that initiates nucleation of autophagy isolation vesicles. Under normal conditions, Beclin1 binds to Bcl-2 through the BH3 domain, and they are inactivated by each other. Ser/Thr kinases such as Akt could regulate autophagy and apoptosis by phosphorylating Beclin1 within its BH3, which reduces its inhibitory interaction with Bcl-2 or Bcl-XL [44].

According to our data, CED treatment results in the activation of autophagy flux through the Akt and MAPK signal pathway, as featured by the reduction of p-Akt, p-mTOR, p-38, and p-Erk1/2 and the accumulation of LC3-II and Beclin1. CED relieved the inhibition effect of mTOR on autophagy.

Simultaneously, mTOR was reported to act as a positive regulator of the cell cycle. Inactivation of mTOR can induce G0/G1 phase cell cycle arrest by downregulating S6K1 and 4E-BP1 [45]. Meanwhile, previous studies have found that microRNA-646 [46] and microRNA-99a [47] could induce G1 phase cell cycle arrest by downregulating mTOR signals, while overexpression of mTOR reversed the inhibitory effect of microRNA-646 on cell cycle progression. The role of mTOR in CED-induced G1 phase cell cycle arrest is complicated, and extensive exploration is needed.

5. Conclusion

In conclusion, this study verified that CED effectively suppressed cell viability and induced apoptosis, autophagy, and G1 phase cell cycle arrest in A549 cells. Meanwhile, CED may induce autophagy and G1 phase cell cycle arrest through the Akt/mTOR signal pathway and MAPK pathway.

Data Availability

The data used to support the findings of this study are available from the corresponding authors upon request.

Conflicts of Interest

No potential conflict of interest was reported by the authors.

Authors' Contributions

Menghuan Guo and Zhiyuan Liu as co-first authors.

Acknowledgments

This work was supported by the grants from the Ministry of Science and Technology National Key R&D Project (No. 2018YFE0205100), the National Natural Science Foundation of China (Nos. 81960337 and 12065001), the Fundamental Research Funds for the Central Universities (No. 31920160048), and the Science and Technology Plan Project of Chengguan district (2019RCCX0071).

References

[1] T. Akhurst, "Staging of non-small-cell lung cancer," *PET clinics*, vol. 13, no. 1, pp. 1–10, 2018.

[2] F. R. Hirsch, G. V. Scagliotti, J. L. Mulshine et al., "Lung cancer: current therapies and new targeted treatments," *Lancet*, vol. 389, no. 10066, pp. 299–311, 2017.

[3] D. R. Aberle, A. M. Adams, C. D. Berg et al., "Reduced lung-cancer mortality with low-dose computed tomographic screening," *The New England Journal of Medicine*, vol. 365, no. 5, pp. 395–409, 2011.

[4] B. C. Bade and C. S. Dela Cruz, "Lung Cancer 2020: Epidemiology, Etiology, and Prevention," *Clinics in Chest Medicine*, vol. 41, no. 1, pp. 1–24, 2020.

[5] E. B. Garon, T. E. Ciuleanu, O. Arrieta et al., "Ramucirumab plus docetaxel versus placebo plus docetaxel for second-line treatment of stage IV non-small-cell lung cancer after disease progression on platinum-based therapy (REVEL): a multicentre, double-blind, randomised phase 3 trial," *Lancet*, vol. 384, no. 9944, pp. 665–673, 2014.

[6] V. Kaushal, P. Mukunyadzi, R. A. Dennis, E. R. Siegel, D. E. Johnson, and M. Kohli, "Stage-specific characterization of the vascular endothelial growth factor axis in prostate cancer: expression of lymphangiogenic markers is associated with advanced-stage disease," *Clinical Cancer Research*, vol. 11, 2 Part 1, pp. 584–593, 2005.

[7] H. J. de Jonge, P. J. Valk, N. J. Veeger et al., "High VEGFC expression is associated with unique gene expression profiles and predicts adverse prognosis in pediatric and adult acute myeloid leukemia," *Blood*, vol. 116, no. 10, pp. 1747–1754, 2010.

[8] M. Medinger, N. Esser, U. Zirrgiebel, A. Ryan, J. M. Jürgensmeier, and J. Drevs, "Antitumor and antiangiogenic activity

of cediranib in a preclinical model of renal cell carcinoma," *Anticancer Research*, vol. 29, no. 12, pp. 5065–5076, 2009.

[9] J. Fan, V. G. Ponferrada, T. Sato et al., "Crim1 maintains retinal vascular stability during development by regulating endothelial cell Vegfa autocrine signaling," *Development*, vol. 141, no. 2, pp. 448–459, 2014.

[10] A. M. Mercurio, R. E. Bachelder, R. C. Bates, and J. Chung, "Autocrine signaling in carcinoma: VEGF and the alpha6beta4 integrin," *Seminars in Cancer Biology*, vol. 14, no. 2, pp. 115–122, 2004.

[11] B. M. Lichtenberger, P. K. Tan, H. Niederleithner, N. Ferrara, P. Petzelbauer, and M. Sibilia, "Autocrine VEGF signaling synergizes with EGFR in tumor cells to promote epithelial cancer development," *Cell*, vol. 140, no. 2, pp. 268–279, 2010.

[12] S. H. Hsieh, N. W. Ying, M. H. Wu et al., "Galectin-1, a novel ligand of neuropilin-1, activates VEGFR-2 signaling and modulates the migration of vascular endothelial cells," *Oncogene*, vol. 27, no. 26, pp. 3746–3753, 2008.

[13] N. D'Haene, S. Sauvage, C. Maris et al., "VEGFR1 and VEGFR2 involvement in extracellular galectin-1- and galectin-3-induced angiogenesis," *PLoS One*, vol. 8, no. 6, article e67029, 2013.

[14] Z. G. Jin, H. Ueba, T. Tanimoto, A. O. Lungu, M. D. Frame, and B. C. Berk, "Ligand-independent activation of vascular endothelial growth factor receptor 2 by fluid shear stress regulates activation of endothelial nitric oxide synthase," *Circulation Research*, vol. 93, no. 4, pp. 354–363, 2003.

[15] J. Kendrew, R. Odedra, A. Logié et al., "Anti-tumour and anti-vascular effects of cediranib (AZD2171) alone and in combination with other anti-tumour therapies," *Cancer Chemotherapy and Pharmacology*, vol. 71, no. 4, pp. 1021–1032, 2013.

[16] T. E. Peterson, N. D. Kirkpatrick, Y. Huang et al., "Dual inhibition of Ang-2 and VEGF receptors normalizes tumor vasculature and prolongs survival in glioblastoma by altering macrophages," *Proceedings of the National Academy of Sciences of the United States of America*, vol. 113, no. 16, pp. 4470–4475, 2016.

[17] T. T. Batchelor, D. G. Duda, E. di Tomaso et al., "Phase II study of cediranib, an oral pan-vascular endothelial growth factor receptor tyrosine kinase inhibitor, in patients with recurrent glioblastoma," *Journal of Clinical Oncology*, vol. 28, no. 17, pp. 2817–2823, 2010.

[18] J. Ledermann, A. Embleton, F. Raja et al., "Cediranib in patients with relapsed platinum-sensitive ovarian cancer (ICON6): a randomised, double-blind, placebo-controlled phase 3 trial," *The Lancet*, vol. 387, pp. 1066–1074, 2016.

[19] E. Heath, L. Heilbrun, H. Mannuel et al., "Phase II, multicenter, randomized trial of docetaxel plus prednisone with or without cediranib in men with chemotherapy-naive metastatic castrate-resistant prostate cancer," *The Oncologist*, vol. 24, no. 9, pp. 1149–e1807, 2019.

[20] A. Decio, M. Cesca, F. Bizzaro et al., "Cediranib combined with chemotherapy reduces tumor dissemination and prolongs the survival of mice bearing patient-derived ovarian cancer xenografts with different responsiveness to cisplatin," *Clinical and Experimental Hypertension*, vol. 32, no. 7, pp. 647–658, 2015.

[21] S. R. Brave, K. Ratcliffe, Z. Wilson et al., "Assessing the activity of cediranib, a VEGFR-2/3 tyrosine kinase inhibitor, against VEGFR-1 and members of the structurally related PDGFR family," *Molecular Cancer Therapeutics*, vol. 10, no. 5, pp. 861–873, 2011.

[22] A. M. Devery, R. Wadekar, S. M. Bokobza, A. M. Weber, Y. Jiang, and A. J. Ryan, "Vascular endothelial growth factor directly stimulates tumour cell proliferation in non-small cell lung cancer," *International Journal of Oncology*, vol. 47, no. 3, pp. 849–856, 2015.

[23] Y. Jiang, D. Allen, V. Kersemans et al., "Acute vascular response to cediranib treatment in human non-small-cell lung cancer xenografts with different tumour stromal architecture," *Lung Cancer*, vol. 90, no. 2, pp. 191–198, 2015.

[24] O. Takahashi, R. Komaki, P. D. Smith et al., "Combined MEK and VEGFR inhibition in orthotopic human lung cancer models results in enhanced inhibition of tumor angiogenesis, growth, and metastasis," *Clinical Cancer Research*, vol. 18, no. 6, pp. 1641–1654, 2012.

[25] Y. Ichimura, T. Kirisako, T. Takao et al., "A ubiquitin-like system mediates protein lipidation," *Nature*, vol. 408, no. 6811, pp. 488–492, 2000.

[26] J. Wu, Y. Dang, W. Su et al., "Molecular cloning and characterization of rat LC_3A and LC_3B –Two novel markers of autophagosome," *Biochemical and Biophysical Research Communications*, vol. 339, no. 1, pp. 437–442, 2006.

[27] Z. Zhang, W. Yang, F. Ma et al., "Enhancing the chemotherapy effect of apatinib on gastric cancer by co-treating with salidroside to reprogram the tumor hypoxia micro-environment and induce cell apoptosis," *Drug Delivery*, vol. 27, no. 1, pp. 691–702, 2020.

[28] Z. Tian, X. Niu, and W. Yao, "Receptor tyrosine kinases in osteosarcoma treatment: which is the key target?," *Frontiers in Oncology*, vol. 10, p. 1642, 2020.

[29] R. S. Herbst, H. T. Arkenau, J. Bendell et al., "Phase 1 expansion cohort of ramucirumab plus pembrolizumab in advanced treatment-naive NSCLC," *Journal of Thoracic Oncology*, vol. 16, no. 2, pp. 289–298, 2021.

[30] P. L. Swiecicki, E. L. Bellile, C. V. Brummel, J. C. Brenner, and F. P. Worden, "Efficacy of axitinib in metastatic head and neck cancer with novel radiographic response criteria," *Cancer*, vol. 127, no. 2, pp. 219–228, 2021.

[31] C. A. Heckman, T. Holopainen, M. Wirzenius et al., "The tyrosine kinase inhibitor cediranib blocks ligand-induced vascular endothelial growth factor receptor-3 activity and lymphangiogenesis," *Cancer Research*, vol. 68, no. 12, pp. 4754–4762, 2008.

[32] S. Elmore, "Apoptosis: a review of programmed cell death," *Toxicologic Pathology*, vol. 35, no. 4, pp. 495–516, 2007.

[33] T. Kaufmann, A. Strasser, and P. J. Jost, "Fas death receptor signalling: roles of Bid and XIAP," *Cell Death and Differentiation*, vol. 19, no. 1, pp. 42–50, 2012.

[34] G. Pistritto, D. Trisciuoglio, C. Ceci, A. Garufi, and G. D'Orazi, "Apoptosis as anticancer mechanism: function and dysfunction of its modulators and targeted therapeutic strategies,," *Aging (Albany NY)*, vol. 8, no. 4, pp. 603–619, 2016.

[35] M. Malumbres and M. Barbacid, "Cell cycle, CDKs and cancer: a changing paradigm," *Nature Reviews Cancer*, vol. 9, no. 3, pp. 153–166, 2009.

[36] E. A. Musgrove, C. E. Caldon, J. Barraclough, A. Stone, and R. L. Sutherland, "Cyclin D as a therapeutic target in cancer," *Nature Reviews Cancer*, vol. 11, no. 8, pp. 558–572, 2011.

[37] I. Sanchez and B. Dynlacht, "New insights into cyclins, CDKs, and cell cycle control," *Seminars in Cell & Developmental Biology*, vol. 16, no. 3, pp. 311–321, 2005.

[38] C. W. Wang and D. J. Klionsky, "The molecular mechanism of autophagy," *Molecular Medicine*, vol. 9, no. 3-4, pp. 65–76, 2003.

[39] A. Kuma, M. Komatsu, and N. Mizushima, "Autophagy-monitoring and autophagy-deficient mice," *Autophagy*, vol. 13, no. 10, pp. 1619–1628, 2017.

[40] X. R. Meng, *Mechanism of VEGFR2 inhibitor apatinib regulates apoptosis and autophagy in thyroid papillary carcinoma*, Tianjin Medical University, 2014.

[41] V. Noronha, V. M. Patil, A. Joshi et al., "Gefitinib versus gefitinib plus pemetrexed and carboplatin chemotherapy in *EGFR*-mutated lung cancer," *Journal of Clinical Oncology*, vol. 38, no. 2, pp. 124–136, 2020.

[42] C. Viallard and B. Larrivée, "Tumor angiogenesis and vascular normalization: alternative therapeutic targets," *Angiogenesis*, vol. 20, no. 4, pp. 409–426, 2017.

[43] M. Kowanetz and N. Ferrara, "Vascular endothelial growth factor signaling pathways: therapeutic perspective," *Clinical Cancer Research*, vol. 12, no. 17, pp. 5018–5022, 2006.

[44] G. Mariño, M. Niso-Santano, E. H. Baehrecke, and G. Kroemer, "Self-consumption: the interplay of autophagy and apoptosis," *Nature Reviews Molecular Cell Biology*, vol. 15, no. 2, pp. 81–94, 2014.

[45] D. C. Fingar, C. J. Richardson, A. R. Tee, L. Cheatham, C. Tsou, and J. Blenis, "mTOR controls cell cycle progression through its cell growth effectors S6K1 and 4E-BP1/eukaryotic translation initiation factor 4E," *Molecular and Cellular Biology*, vol. 24, no. 1, pp. 200–216, 2004.

[46] Y. L. Song, M. Z. Pan, and A. L. Wang, "MicroRNA-646 inhibits proliferation and cell cycle progression of nasopharyngeal carcinoma cells by targeting mTOR," *European Review for Medical and Pharmacological Sciences*, vol. 23, no. 20, pp. 8905–8912, 2019.

[47] L. Cui, H. Zhou, H. Zhao et al., "MicroRNA-99a induces G1-phase cell cycle arrest and suppresses tumorigenicity in renal cell carcinoma," *BMC Cancer*, vol. 12, no. 1, p. 546, 2012.